Understanding the consequences of deficient Glutamine-fructose-6-phosphate transaminase 1 (GFPT1) expression in Congenital Myasthenic Syndromes (CMS) and elucidating new therapeutic strategies

Stephen Henry Holland

Thesis submitted to the University of Ottawa
in partial Fulfillment of the requirements for the
Doctorate in Philosophy degree in Cellular and Molecular Medicine

Department of Cellular and Molecular Medicine
Faculty of Medicine
University of Ottawa

Dedication:

This doctoral thesis is dedicated to patients with congenital myasthenic syndromes and their families. It's also dedicated to my family and friends who have helped push me through this doctoral program. Thank you.

Acknowledgements:

I have many people in my life that I would like to acknowledge for their continued support during my PhD/academic journey. I would like to take the opportunity to highlight them below:

To my wife, Alexa - You have stood by me through every chapter of my academic journey, one that neither of us could have imagined when we first met in high school. What began as a shared dream has grown into a life filled with milestones: we got engaged, married, and welcomed our beautiful daughter Audrey into this world. Through all of this you have been my unwavering source of strength, my biggest cheerleader, and my constant reminder what truly matters. Thank you for your endless patience and encouragement, especially during the long nights, weekends, and countless moments when my research demanded more than I could give elsewhere. You made sacrifices, big and small, so that I could chase this dream, and I will never forget that. Your belief in me never wavered, even when I doubted myself, or faced burnout. You kept me grounded, reminded me to breathe, and celebrate every victory as if it were your own. This achievement is as much yours as it is mine. I wouldn't be here today without your love, your resilience, and your faith in us. For all that you have done and all that you are, I am forever grateful.

To my daughter Audrey - You are just 1.5 years old right now, blissfully unaware of what your Dad has been working towards all these years. One day, when you're old enough to understand, I want you to know that this achievement isn't just mine, it is ours. You came into this world during the final stretch of this PhD journey, and though you were only here for a short part, you made it the most meaningful chapter of all. When you grow up, I hope you carry with you the same values that guided me: perseverance, curiosity, and the belief that hard work can truly pay off. You can be anything that you want to be if you put your mind to it, whether that's in science, art, or something we can't even imagine yet. Never let anyone tell you otherwise. Thank you for your endless gummy smiles (now filled with teeth), your laughter, and those warm cuddle that reminded me why I was doing all of this for. You gave

me perspective when deadlines loomed and hope when experiments failed. I can't wait to see the person that you become, the dreams you choose, and the life that you build. And also, so you know, if you ever choose the path of science, the Lochmüller lab, and CHEO Research Institute will always be the place where your curiosity is welcome. But no matter what you choose, I'll be your biggest supporter, just as you've unknowingly been mine.

To my family – Thank you for your unwavering support in my pursuit of science. From the very beginning, none of us could have imagined that this journey would lead to a PhD in Cellular and Molecular Medicine. Yet here we are and you have all played a special part in this journey. To my parents, Henry and Sue: thank you for instilling in a strong work ethic and an insatiable curiosity. Those values have been my compass through every challenge and triumph. Your sacrifices, understanding, and constant encouragement made it possible for me to attend university and chase this dream. I am endlessly grateful for everything you have done to provide me with this opportunity. To my brothers, Daniel and Joseph: your strength and encouragement helped me cross this finish line. That you for the countless conversations, for listening when I needed to vent, and for always cheering me on from the sidelines. Your belief in me has meant more than you know. To my Nan, Willma: even though the science behind this thesis may have sounded like another language, your excitement and pride in my accomplishments have always touched my heart. Your joy reminded me why these milestones matter. Each of you have plated an instrumental role in supporting this chapter of my academic life. This achievement is not mine alone it belongs to all of you. Thank you for being my foundation and inspiration.

To my supervisor, Dr. Hanns Lochmüller – I am forever grateful for your incredible guidance and support over the years. Your knowledge and passion for research in neuromuscular disorders has been truly inspiring. Thank you for dedicating so much time over these past six years to teach, mentor, and challenge me. You have not only shared your expertise but also instilled in me the same excitement and

curiosity for science that drives your own work. Your encouragement and belief in my potential have shaped me into the scientist I am today. I could not have asked for a better mentor.

To our research associate, Dr. Sally Spendiff – Thank you for being a constant source of wisdom and encouragement, both in science and in life. Your willingness to engage in endless discussions, entertain my wild ideas, and then help me refocus when needed has been invaluable. You've pushed me to think critically, to refine my approach, and to strive for excellence in every experiment. Beyond the lab, your support and perspective have helped me navigate the challenges of this PhD with resilience. I am deeply grateful for your guidance and for always believing in me.

To the members of the Lochmüller lab – Thank you for being there every step of the way. From past to present members, each one of you has made a lasting contribution to my PhD journey. Whether it was providing humour during the tough moments, helping with experimental approaches, or simply chatting about life, I valued every one of you. This lab is truly fortunate to have a such a great community. I'd like to extend a special thank you to all members to helped on my thesis project (Kaela O'Connor, Kelly Ho, Daniel O'Neil, Ricardo Carmona-Martinez). I'd also like to thank Dr. Haley Geerstma (for your proteomics help and GraphPad troubleshooting), Dr. Romane Idoux, Dr. Kiran Polvarapu, Dr. Rachel Thompson, Dr. Emily O'Connor, Dr. Anu Varghese, Ofosu Adjei-Afriyie, Alexa Derksen, Katerina Palacek, Caroline Part, Malaichamy Sivasankar, Josh Zeldin, Dr. Emily Freeman, Jarred Lau, Aoife Reilly, Emilie Hill-Smith, Laura Thompson, and Tamara Burgess. I'd also like to thank Dr. Xiao Xiang, and Dr. Huy Dung Hoang for all your guidance and support throughout this PhD as well.

To all contributors to my project – Thank you for helping me complete the necessary experiments to reach this goal:

- **Dr. Andreas Roos –** Your support and positivity gave me confidence, especially during times of doubt. Thank you for providing proteomic insights in all aspects of my project. I am incredibly grateful.
- **Dr. Anne Schanzer –** Thank you for providing your expertise on sciatic nerve pathology.
- **Dr. Bart Thomson and Dr. Henning Richter –** Thank you for providing your expertise and analysis of sciatic nerve morphology, using an AI-assisted program.
- **Dr. Rashmi Kothary –** Thank you for access to the laser capture microdissection microscope. Beyond being an amazing tool, our discussions with you and your research group were a highlight of my PhD.
- **Dr. Stephen Baird** – Thank you for access to the OPERA for automated image collection and for helping me set-up my analysis for the serglycin project.

To the CHEO Research Institute For nearly eight years, from summer student to PhD candidate, you've provided me a place to learn, grow, and create lasting memories. To all past and present members — thank you for your support and dedication to science. A few special shoutouts: Keith Wilson - Thank you for our weekly chats on politics and football, and for your friendship; Lynn Kyte - The backbone of the CHEO RI — thank you for your support with events, ordering, and giving me a space to vent about the Ottawa Senators. All senior PIs (Dr. Tommy Alain, Dr. Tyson Garber, Dr. Zakia Djoud, Dr. Izabella Pena, Dr. Alex MacKenzie, Dr. Cowan, Dr. Bob Korneluk, and Dr. Shawn Beug – I appreciate all the guidance over the past 8 years; commenting on my projects throughout this academic journey. From celebrating my marriage to the arrival of my daughter Audrey - this place has been truly special because of the people here. Thank you all!

To my thesis advisory committee: Dr. Rashmi Kothary, Dr. Alex MacKenzie, and Dr. Alexandre Blais - thank you for your ongoing guidance and encouragement throughout my academic journey. It has

been a long journey starting in the first month of the COVID-19 pandemic. Thank you for sharing your curiosity in my research project and providing input on direction. Thank you!

To the Ottawa Science Policy Network, Support Our Science, and all our partners: In April 2024, we achieved something remarkable by helping secure a major investment for Canadian science, scholarships, and postdoctoral funding. Outside of my PhD work, we came together to make meaningful change. Thank you for your dedication. We've made great strides, but there's still more work ahead! A special thank you to Dr. Jeff Kinder from the Institute for Society and Science Policy for helping me network and approach science policy in a positive way, coming from a background in STEM.

To my friends: You've helped shape who I am today. I can list you all, but you all know who you are - Thank you for your constant encouragement as I've reached the end of this academic chapter. Your support means the world to me, and I can't wait to celebrate the next stage of this journey with you all.

Funding/Acknowledgements

I would like to thank all the funding sources that supported both my research and academic journey, including the **2020 Dr. Alex MacKenzie CHEO Research Institute Trainee Award**, the **2021 Ontario Graduate Scholarship**, the **2022 Queen Elizabeth II Award in Science and Technology**, the **2024 Dr. Eric Poulin Centre for Neuromuscular Disease STaR Award**, and the **University of Ottawa Admissions Scholarship**. These awards, in addition to laboratory funding, played a vital role in financing my doctoral degree. It has been a privilege to benefit from this generosity, and I am deeply grateful for your support.

In addition, I was privileged to receive the **2022 World Muscle Society Elsevier Poster Award** at the World Muscle Society Conference in Halifax, Nova Scotia. Lastly, I was fortunate to receive a **travel scholarship** for the 2025 15th annual Myasthenia Gravis Foundation of America conference in The Hague, Netherlands. Most recently I received the **Bronze Prize** at the Ottawa Hospital Research Institute Research Day. Beyond this my work with Support Our Science was recognized in the "Nature's 10, a list of people who shaped science in 2024", where we increased the Federal budget funding for graduate student scholarships and postdoctoral fellowships. We also increased grant funding in Budget 2024.

Abstract

Congenital myasthenic syndromes (CMS) are early-onset, inheritable neuromuscular disorders caused by mutations in proteins required for neuromuscular junction (NMJ) development, maintenance, function, and motor endplate organization. Clinically, CMS are heterogeneous but typically manifest as fatigable weakness affecting facial, bulbar, ocular, respiratory, limb, and/or girdle muscles, with severity ranging from transient to permanent impairment depending on the underlying genetic defect. More than 40 genes have been implicated in CMS pathogenesis. Among these, *glutamine–fructose-6-phosphate transaminase 1* (GFPT1) encodes the rate-limiting enzyme of the hexosamine biosynthetic pathway (HBP). Biallelic GFPT1 mutations cause a limb-girdle-predominant CMS, yet the molecular basis of disease and effective treatments remain poorly understood. We hypothesized that GFPT1 deficiency generates a hypoglycosylated cellular environment that impairs neuromuscular function.

Using integrated biochemical, proteomic, and functional analyses, we define the molecular consequences of GFPT1 deficiency. We demonstrate that GFPT1-CMS is a bona fide glycosylation disorder marked by impaired N-linked glycosylation and altered protein O-GlcNAcylation. Notably, we identify the first mis-glycosylated peptide in GFPT1-CMS, located within the δ-subunit of the acetylcholine receptor (AChR), providing direct evidence that reduced HBP flux disrupts glycoprotein maturation essential for NMJ transmission. Building on this mechanistic insight, we establish two metabolic strategies that restore glycosylation: galactose supplementation, which partially rescues muscle protein glycosylation, normalizes NMJ and skeletal muscle morphology, and improves behavioral outcomes; and AMDH2 knockdown, which increases O-GlcNAcylation in GFPT1-deficient cellular models.

Collectively, this work defines the first molecular signature of mis-glycosylation in GFPT1-CMS, establishes two therapeutic strategies to restore glycan homeostasis, and identifies serglycin as a potential biomarker. These discoveries advance the mechanistic understanding of glycosylation-dependent

neuromuscular disease and lay the groundwork for targeted therapeutic development in GFPT1-CMS and related disorders.

Table of Contents:

List of Figures:

Chapter 2 Figures

Chapter 3 Figures

Chapter 4 Figures

List of Tables:

List of Abbreviations:

AAV	Adeno-associated virus
ACh	Acetylcholine
AChE	Acetylcholinesterase
AChR	Acetylcholine Receptors
AChRα	Alpha-subunit of the acetylcholine receptors
AChRβ	Beta-subunit of the acetylcholine receptors
AChRγ	Gamma-subunit of the acetylcholine receptors
AChRδ	Delta-subunit of the acetylcholine receptors
AChRε	Epsilon-subunit of the acetylcholine receptors
AGRN	Agrin
ALG13	UDP-N-Acetylglucosaminyltransferase Subunit
ALG14	UDP-N-Acetylglucosaminyltransferase Subunit
ALG2	Alpha-1,3/1,6-Mannosyltransferase
ALS	Amyotrophic lateral Sclerosis
AMDHD2	Amidohydrolase Domain Containing 2
AMPK	Adenosine monophosphate-activated protein kinase
ATF4	Activating Transcription Factor 4
CDG	Congenital Disorder of Glycosylation
CDG-1j	Congenital Disorder of Glycosylation Type 1j
CHAT	Choline O-Acetyltransferase
CHCHD10	Coiled-Coil-Helix-Coiled-Coil-Helix Domain Containing 10
CHRNA1	Alpha-subunit of the acetylcholine receptors
CHRNB1	Beta-subunit of the acetylcholine receptors
CHRND	Gamma-subunit of the acetylcholine receptors
CHRNE	Delta-subunit of the acetylcholine receptors
CHRNG	Epsilon-subunit of the acetylcholine receptors
CK	Creatine kinase
CMS	Congenital myasthenic syndromes
CMT	Charcot-Marie-Tooth Disease
CNS	Central nervous system
Col13A1	Collagen Type XIII Alpha 1 Chain
COLGALT1-CDG	Collagen Beta(1-O)Galactosyltransferase 1-CDG
COLQ	Collagen Like Tail Subunit Of Asymmetric Acetylcholinesterase
COPI/II	Coat protein complex 1 and 2
DAD1	Defender Against Cell Death 1
DAG1	Dystroglycan 1
DPAGT1	Dolichyl-Phosphate N-Acetylglucosaminephosphotransferase 1
DHPRs	Dihyropyridine receptors
DLO	Dolichol
DMAPP	Dimethylallyl pyrophosphate
DNA	Deoxyribonucleic acid
DOK7	Downstream kinase 7
Dol-P	Dolichol-phosphate
Dol-P-P	Dolichol-diphosphate
DOLPP1	Dolichyldiphosphatase 1
DPAGT1	Dolichol-phosphate N-acetylglucosaminephosphotransferase 1

DUF	Domain of unknown function
ER	Endoplasmic reticulum
ERAD	Endoplasmic reticulum associated degradation
ERK	Mitogen-Activated Protein Kinase 1
EVs	Extracellular vesicles
EXT1	Exostosin Glycosyltransferase 1
EXT2	Exostosin Glycosyltransferase 2
GAG	Glycosaminoglycan
Gal-1-P	Galactose-1-phosphate
GALE	Galactose-4'epimerase
GALK	Galactokinase
GalNAc	N-acetylgalactosamine
GALT	Galactose-1-phosphate uridylytransferase
GATase	Glutaminase Domina of GFPT1
GFPT1	Glutamine-fructose-6-phosphate transaminase 1
GFPT1-L	Long isoform of Glutamine-fructose-6-phosphate transaminase 1
Glc-1-P	Glucose-1-phosphate
GlcNAc	N-acetylglucosamine
GLUT2	Glucose transporter type 2
GMPPB	GDP-mannose pyrophosphorylase B
GNPNAT	Glucosamine-phosphate N-acetyltransferase
HA	Hyaluronan
HBP	Hexosamine biosynthetic pathway
LAMA5	Laminin Subunit Alpha 5
LAMB2	Laminin Subunit Beta 2
LEMS	Lambert-Eaton myasthenic syndrome
LC3	Microtubule Associated Protein 1 Light Chain 3
LC3-II	Microtubule Associated Protein 1 Light Chain 3-II
LRP4	Lipoprotein-related protein receptor 4
MG	Myasthenia gravis
mTOR	Mammalian target of rapamycin
MuSK	Muscle-specific kinase
MYO9A	Myosin IXA
NMD	Neuromuscular disease
NMJ	Neuromuscular junction
OGA	O-GlcNAcase
OGT	O-GlcNAc transferase
OST	Oligosaccharyltransferase
OST4	Oligosaccharyltransferase complex subunit 4
PD	Parkinson's Disease
PGM1	Phosphoglucomutase 1
PGM3	Phosphoglucomutase 3
PKA	Protein kinase A
PMM2	Phosphomannomutase 2
POFUT1	Protein O-Fucosyltransferase 1
POGLUT1	Protein O-Glucosyltransferase 1
PREPL	Prolyl Endopeptidase Like
PRKCSH	PRKCSH Beta Subunit Of Glucosidase II
PTM	Post-translational modification

PTPN11	Protein Tyrosine Phosphatase Non-Receptor Type 11
PURA	Purine Rich Element Binding Protein A
RAPSYN	Receptor Associated Protein Of The Synapse
RNA	Ribonucleic Acid
RNS	Repetitive nerve stimulation
RPH3A	Rabphilin 3A
RyR1	Ryanodine receptor
SERCA	Sarcoplasmic/endoplasmic reticulum Ca^{+2}-ATPase
SGLT1	Sodium-glucose linked transporter type 1
SIS1/SIS2	Sugar isomerase domain 1 and 2
SLC18A3	Solute Carrier Family 18 Member A3
SLC25A1	Solute Carrier Family 25 Member A1
SLC39A8	Solute Carrier Family 39 Member A8
SLC5A7	Solute Carrier Family 5 Member A7
SMA	Spinal muscular atrophy
SNAP25	Synaptosome Associated Protein 25
SQSTM1	Sequesterome/P62
SR	Sarcoplasmic reticulum
SYB1	Synaptobrevin
SYT2	Synaptotagmin 2
TEFM	Transcription Elongation Factor, Mitochondrial
TFEB	Transcription factor EB
TMEM165	Transmembrane Protein 165
TMEM258	Transmembrane Protein 258
TPR	Tetratricopeptide repeat
UDP-Gal	Uridine diphosphate galactose
UDP-GalNAc	Uridine diphosphate N-acetylgalactosamine
UDP-GlcNAc	Uridine diphosphate N-acetylglucosamine
ULK1	Unc-51 Like Autophagy Activating Kinase 1
UNC13A	Unc-13 Homolog A
UPR	Unfolded protein response
VAMP1	Vesicle Associated Membrane Protein 1
XBP1	X-Box Binding Protein 1
XBP1s	X-Box Binding Protein 1 (Spliced)

List of Manuscripts:

1. **Holland SH**, R. Carmona-Martinez, K. O'Connor, D. O'Neil, A. Roos, S. Spendiff, H. Lochmüller. A Deficiency in Glutamine-Fructose-6-Phosphate Transaminase 1 (Gfpt1) in Skeletal Muscle Results in Reduced Glycosylation of the Delata Subunit of the Nicotinic Acetylcholine Receptor (AChRδ). *Biomolecules.*2024; 14(10):1252. https://doi.org/10.3390/biom14101252.

2. **Holland SH**, R. Carmona-Martinez, D. O'Neil, K. Ho, K. O'Connor, Y. Azuma, A. Roos, S. Spendiff, H. Lochmüller. Galactose treatment rescues neuromuscular junction transmission in glutamine-fructose-6-phosphate transaminase 1 (Gfpt1) deficient mice. *Human Molecular Genetics*, 2025;, ddaf140, https://doi.org/10.1093/hmg/ddaf140

3. **Holland SH,** R. Carmona-Martinez, A. Hentschel, K. O'Connor, D. O'Neil, S. Baird, A. Roos, S. Spendiff, H. Lochmüller. Hexosamine biosynthetic pathway disruption by GFPT1 loss drives coordinated defects in glycosylation, autophagy, and trafficking. *Submitted. Biomolecules.* **2026. https://doi.org/10.3390/biom16070966**

List of Reviews:

1. Pugliese. A, **SH. Holland**, C. Rodolico, H. Lochmüller, S. Spendiff. Presynaptic Congenital Myasthenic Syndromes: Understanding Clinical Phenotypes through In Vivo Models. *Journal of Neuromuscular Disorders.* 2023; 10(5):731-759. https://doi.org/10.3233/JND-221646. PMID: 37212067; PMCID: PMC10578258.

List of Appended Papers:

1. Laframboise, S. J., T. Bailey, A. Dang, M. Rose, Z. Zhou, M. D. Berg, **S. Holland**, S. Aftab Abdul, K. O'Connor, D. M. Boucher, G. Fairman, J. Deng, K. Shaw, N. Noblett, A. D'Addario, M.

Empey, K. Sinclair. Analysis of financial challenges faced by graduate students in Canada. *Biochemistry and Cell Biology.* 2023; 101(4). https://doi.org/10.1139/bcb-2023-0021.

2. Bailey, T., **S. Holland**, M. Rose, S. Laframboise, A. D'Addario, K. Sinclair, M. Makoum. International Mobility of Canadian Graduate Students: An investigation into Brain Drain. Submitted as a book chapter to University of Ottawa Institute for Science, Society, and Policy (ISSP) in *Confluences.* Accepted. Publish Date expected 2025.
3. **Holland, S**., M. Rose, A. D'Addario, C. O'Dwyer, V. Vasilyeva, K. Sinclair, T. Bailey, L. Elsakka. Funding in Decline: Analysis of Provincial Support for Ontario Graduate Students. Submitted. *FACETS*. January 2026.

Introduction

Scientific discovery is driven by the need to understand the mechanisms that govern human health and disease. In neuromuscular research, the integration of clinical observation with molecular biology has enabled major advances in diagnosing, treating and understanding inherited muscle disorders. This thesis investigates the molecular basis of *GFPT1*-related congenital myasthenic syndrome, with the aim of clarifying disease mechanisms and identifying potential therapeutic targets. Using molecular, cellular and translational approaches, this work addresses key unanswered questions with implications for both patient care and the broader biology of congenital myasthenic syndromes (CMS).

1.1 The Neuromuscular Junction and Disease

The neuromuscular junction (NMJ) is a specialized synapse that enables communication between motor neurons and skeletal muscle fibers, allowing voluntary muscle contraction. It comprises of three main components: the presynaptic motor nerve terminal, the postsynaptic muscle fiber and the terminal Schwann cell that contributes to synaptic maintenance[1] . The intricate and organized architecture ensures efficient neurotransmission essential for motor function.

Impaired NMJ formation or function underlies a wide range of neuromuscular disorders. CMS are inherited conditions caused by mutation affecting glycosylation-related, mitochondrial, presynaptic, synaptic, or postsynaptic proteins that disrupt synaptic transmission[1–3]. Autoimmune diseases such as myasthenia gravis (MG) and Lambert-Eaton myasthenic syndromes, in which autoantibodies target critical synaptic components and cause fluctuating muscle weakness further illustrate NMJ vulnerability [4,5,6].

NMJ dysfunction is also increasingly recognized in degenerative conditions including spinal muscular atrophy (SMA) [7], amyotrophic lateral sclerosis (ALS) [8], and Parkinson's disease (PD) [9], where motor neuron loss leads to secondary synaptic pathology. Similarly, impaired axonal myelination in

Charcot-Marie-Tooth disease (CMT) compromises neurotransmission, while postsynaptic remodeling is observed in muscular dystrophies and systemic conditions such as cancer cachexia.

Collectively, these conditions highlight the NMJ as a central determinant of neuromuscular health and a common site of pathology across diverse disorders. Understanding the molecular mechanisms that govern NMJ stability and plasticity is therefore essential for developing targeted therapeutic strategies.

1.2 Neurotransmission and Skeletal Muscle Contraction

Efficient skeletal muscle contraction requires precise 1:1 transmission of an action potential from the motor neuron to the muscle fiber [10]. When a nerve impulse reaches the presynaptic terminal, voltage-gated calcium (Ca^{+2}) channels open, allowing Ca^{+2} influx that triggers synaptic vesicle fusion [10]. Acetylcholine (ACh), packaged into vesicles by the vesicular acetylcholine transporter (SLC18A3), is released into the synaptic cleft and binds to nicotinic acetylcholine receptors (AChRs) on the postsynaptic membrane [10]. ACh activation allows sodium (Na^{+}) influx and potassium (K^{+}) efflux generating 30 to 40 mV endplate potential (EPP) (Figure 1) [11]. Once threshold is reached, a muscle action potential is initiated and propagates along the sarcolemma and into the transverse (T-) tubules [11]. Voltage-sensitive dihydropyridine receptors (DHPRs) mechanically activate ryanodine receptors (RyR1) on the sarcoplasmic reticulum (SR), triggering rapid Ca^{+2} release that initiates contraction [11].

Muscle relaxation is similarly well coordinated. ACh is rapidly hydrolyzed by acetylcholinesterase (AChE) into choline and acetate, terminating receptor activation and preventing further depolarization [12]. Ca^{+2} release from the SR stops, and Ca^{+2}-ATPase (SERCA) pumps actively returns Ca^{+2} to the SR in an ATP-dependent manner [11]. Adenosine triphosphate (ATP) is also required to detach myosin heads from actin, enabling full relaxation. As cytosolic Ca^{+2} levels fall, tropomyosin recovers actin binding sites returning the muscle fiber to its resting state [11].

Any disruption in this tightly regulated process, including neurotransmitter release, receptor activation, ion flux, or Ca^{+2} handling, can impair neurotransmission and lead to muscle weakness, features characteristic of CMS and other neuromuscular and neurodegenerative disorders.

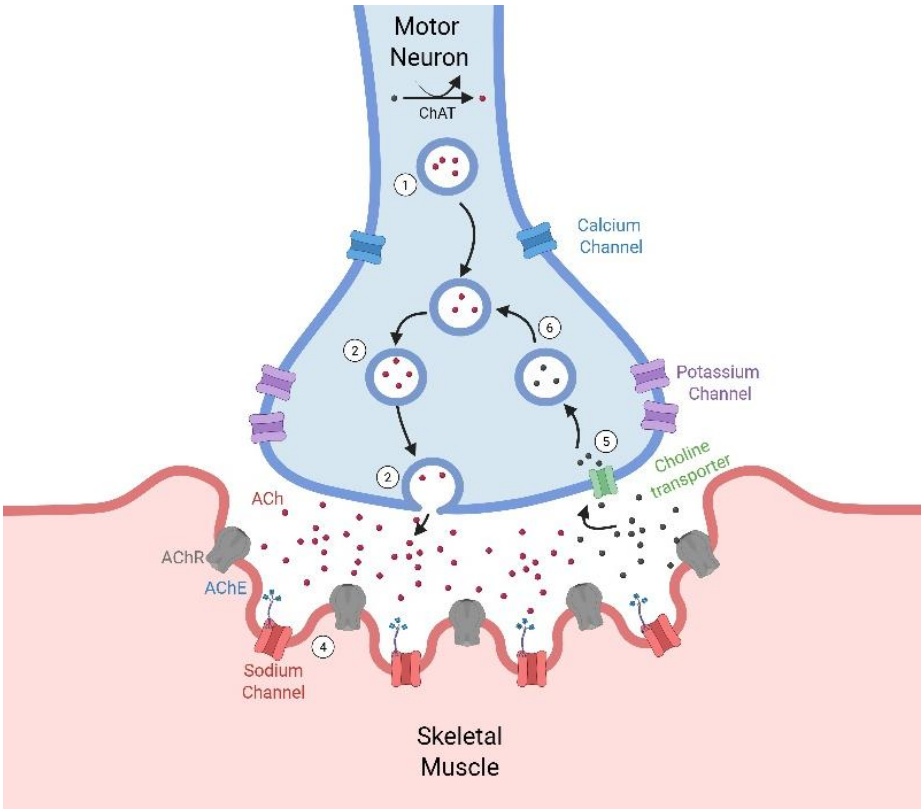

Figure 1: Neurotransmission and muscular contraction: 1) an action potential propagates along the axon of the motor neuron this leads to the opening of voltage-gated Ca^{+2} channels, at the same time, ACh is packaged into vesicles within the motor neuron. This generates a pool of vesicles containing ACh. 2) Calcium influx activates the movement of these vesicles towards the presynaptic membrane, where it interacts with SNARE complexes tethering these vesicles towards the presynaptic nerve terminal. 3) Exocytosis occurs, releasing ACh into the synaptic cleft. 4) ACh binds to AChRs located on the post-synaptic muscle membrane opening these channels allowing for the influx of Na^{+} and efflux of K^{+2} resulting in a depolarization. This depolarization travels across the muscle membrane, towards the T-Tubules resulting in a muscular contraction. 5) AChE cleaves ACh from the AChR and metabolizes ACh into acetyl-CoA and choline. This results in a conformational shift in the AChR closing the pore, blocking ion flux, leading to muscular relaxation. Choline is recycled by the choline transporter at the motor neuron. 6) Choline is packaged into vesicles brought back to the be recycled into ACh. Figure was created in BioRender.

1.3 NMJ Development and Maturation

NMJ development is highly coordinated process, much of which has been characterized in mice during embryogenesis. Motor neurons and skeletal muscle fibers differentiate at distinct times, and by

embryonic day (E) 12-13.5, motor neurons reach the central region of the muscle fibers where AChR clusters have already formed [13,14]. These early AChR clusters arise independently of innervation through a process known as pre-pattering, and initially appear along a central band of the muscle fiber [15].

As development proceeds, incoming motor axons contract multiple AChR clusters within this band. Axons that fail to form stable synapses retract, while successful contacts are maintained [16]. By E18.5, individual muscle fibers are commonly innervated by several motor neurons, a transient developmental state that is refined postnatally (Figure 2). Following birth, typically between postnatal day (P) 7-9, this poly-neuronal innervation is eliminated in favor of a single dominant motor axon per muscle fiber [17].

Synapse elimination is driven by competitive interactions: axons providing stronger or more effective synaptic input persist, whereas weaker input withdraws. Retraction of losing axons produces characteristic retraction bulbs at their distal ends, which are engulfed by the terminal Schwann cell [18]. These retraction bulbs can contain vesicles, disorganized neurofilaments, microtubules, and damaged mitochondria [19]. This coordinated interaction among muscle fibers, motor neurons, and Schwan cells establishes the mature mono-innervated NMJ architecture required for precise neuromuscular function (Figure 2).

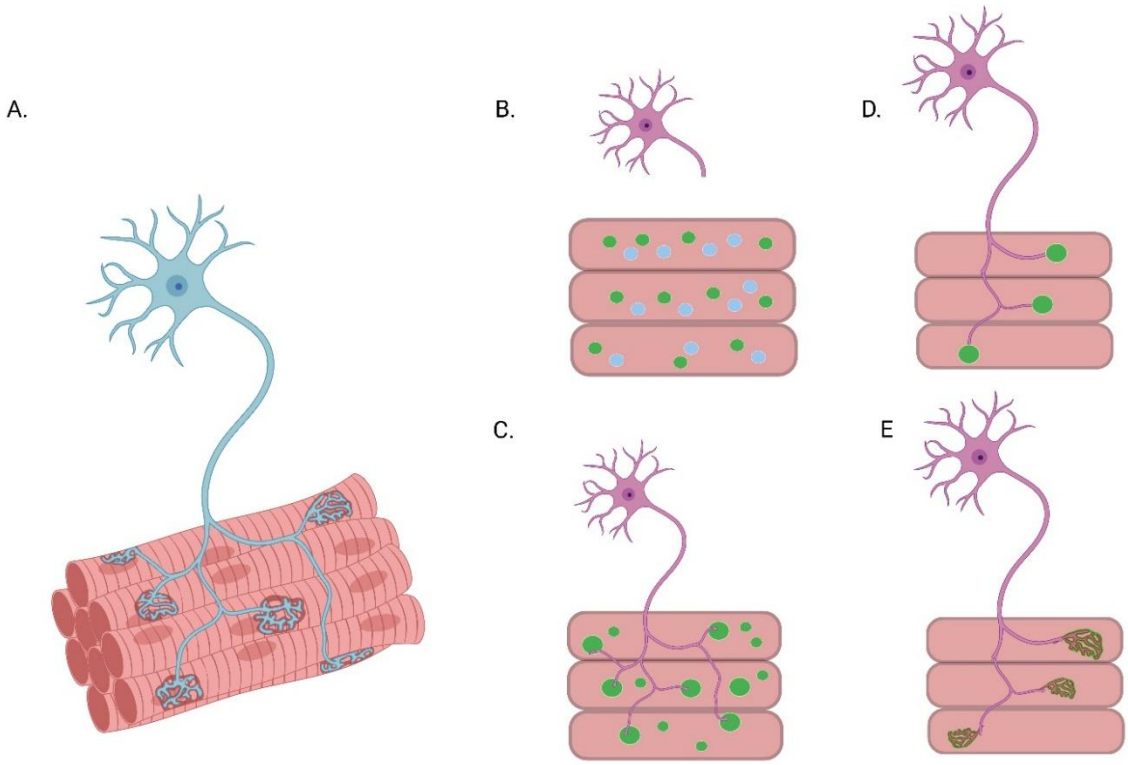

Figure 2: NMJ assembly during development. A) NMJs are formed on individual muscle fibers, this mono-innervation allows for complete control of the muscle contraction, working in unison to support movement. **B)** During embryonic development, motor neurons and muscle fibers grow independently from one another. AChRs clusters are formed and localized at the muscle membrane. C) As the motor neuron branches, it interacts with these AChR clusters. Multiple motor neuron branches interact with the individual muscle fibers, termed polyinnervation. D) As development continues, synaptic pruning, or selection of the stronger innervate motor neuron occurs. Innervations that are not deemed the strongest are broken, and the motor nerve terminal is retracted from the muscle fiber and engulfed by the terminal Schwann cell. E) the mono-innervated NMJ is formed and developed ready to contribute to neurotransmission. Images created in BioRender.

During NMJ maturation, the AChR undergoes significant developmental changes. The postsynaptic AChR is a pentameric ligand gated ion channel composed of four subunits, alpha (α), beta (β), gamma (γ), and delta (δ). In fetal muscle, the receptor adopts a $\alpha 2\beta\gamma\delta$ stoichiometry [20–22]. Around birth, the γ-subunit is downregulated, and replaced by the epsilon (ε) subunit generating the adult isoform (Figure 3) [20–22].

This subunit switch profoundly alters receptor function. Incorporation of the γ-subunit reduces ACh affinity by ~30-fold and produces receptors with lower conductance (40 pS vs 60 pS), longer mean open time (7.9 ms vs 4.1 ms), and reduced calcium permeability [23]. These features are thought to support NMJ maturation by enhancing ion flux during early development when quantal release is limited. AChRs contain two ACh- binding sites αγ/ε or αδ [23]. Interestingly the αγ site displays ~35 fold higher ligand affinity than αε or αδ [23]. Additional conserved residues contributing to ligand binding include: αY93, αW139, αY190, αY198, γW55, εW55, and δW57 [23]. The subunit switch begins between E17-E19 in mice, and is initiated at synapse-specific subsynaptic nuclei [21].

In humans, this developmental switch occurs earlier during the second to third trimester and the γ-subunit, while downregulated, remains detectable at low levels in synaptic regions throughout life [23,24]. In humans, biallelic mutations to CHRNE (AChRε) are the most common cause of CMS, whereas in mice, loss of ε-subunit results in severe neuromuscular dysfunction and early lethality [25,26]. These findings underscore the essential role of the ε-subunit in stabilizing and maintaining the mature NMJ.

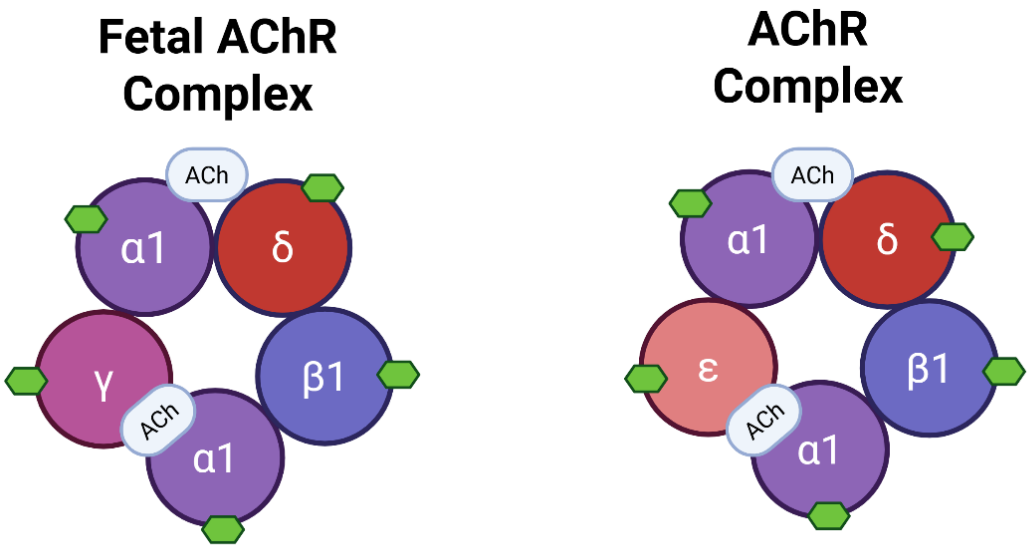

Figure 3: The nicotinic acetylcholine receptor structure: The AChR is a pentameric transmembrane protein channel composed of *α2βγδ* in fetal muscle, and *α2βεδ* in adult muscle. Each receptor contains two ACh binding sites located at the interface between α1 and their neighbouring ε/γ and δ subunits. When ACh is released from the presynaptic vesicle it binds to the AChR opening the receptor pore. This

allows sodium (Na^+) ions to influx and potassium (K^+) to efflux, generating an endplate potential that triggers muscle fiber depolarization and subsequent muscle contraction. Indeed, to stabilize this receptor complex, highly conserved glycosylation sites have been identified on each subunit (green hexagons). Image created in BioRender.

Following incorporation of the adult AChR isoform, the postsynaptic membrane undergoes further specialization to support efficient neurotransmission. Voltage-gated sodium channels ($Na_V1.4$) accumulate within the postsynaptic folds, amplifying the depolarization and ensuring reliable initiation of muscle action potentials [27]. In parallel, subsynaptic nuclei and mitochondria undergo spatial reorganization, contributing to the characteristic pretzel like morphology of mature NMJs [28,29]. Subsynaptic nuclei upregulate NMJ-specific genes required for synaptic stability and AChR maintenance, while mitochondrial enrichment provides the ATP necessary for both presynaptic vesicle cycling and postsynaptic contractile activity [28].

1.4 Acetylcholine Receptors Clustering and NMJ Maintenance

AChR clustering occurs through the Agrin-MuSK-LRP4-Dok7 pathway (Figure 4). During synaptogenesis, motor neurons release agrin into the synaptic cleft, where it binds to postsynaptic low-density lipoprotein-related protein receptor 4 (LRP4) [30]. Agrin-LRP4 interaction recruits muscle-specific kinase (MuSK), forming a receptor complex that induces MuSK autophosphorylation [31]. MuSK is a receptor tyrosine kinase containing four immunoglobulin-like domains (Ig1 to Ig4), and a cysteine-rich frizzled-like domain [32–34]. LRP4 binds to MuSK at Ig1 and Ig4 initiates its activation and triggers downstream signaling required for AChR clustering [34].

Activated MuSK recruits downstream kinase 7 (DOK7), an intracellular adaptor protein essential for MuSK dimer stabilization and phosphorylation [35]. Without DOK7, MuSK activity is insufficient to drive AChR clustering: DOK7 knockout ($Dok7^{-/-}$) mice completely lack AChR aggregates, underscoring its indispensable role [36–38]. Conversely, Dok7 overexpression can initiate ectopic AChR clustering, although these clusters remain structurally immature without additional anchoring mechanisms [39]. The MuSK-Ig1

domain also recruits ColQ, the collagen tail subunit that anchors acetylcholinesterase (AChE) at the synapse [40]. ColQ binding can restrict agrin signaling, thereby contributing to the spatial refinement of AChR activation.

Rapsyn, a postsynaptic scaffolding protein, provides the structural anchoring necessary to stabilize and maintain clustered AChRs [31]. It contains a tetratricopeptide repeat motif that mediates protein-protein interactions and links AChRs to the cytoskeleton [41,42]. In Rapsn$^{-/-}$ mice, AChRs fail to cluster despite normal MuSK activation indicating that Rapsyn is essential for forming functional synapses [41,42]. Together, these, coordinated interactions, Agrin-LRP4 binding, MuSK activation, DOK7 mediated phosphorylation, and Rapsyn dependent scaffolding establish the molecular architecture required for efficient postsynaptic differentiation.

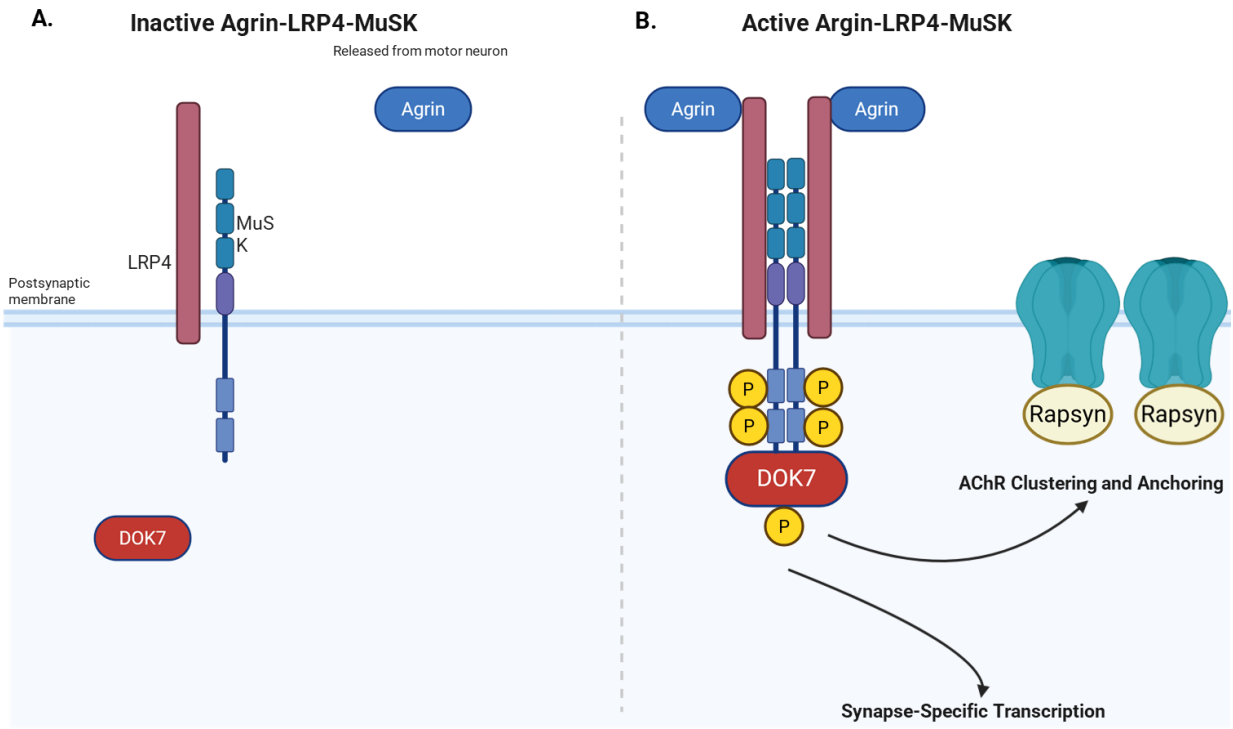

Figure 4: The Agrin-LRP4-MuSK Pathway at the NMJ: A) Agrin is a proteoglycan released from the motor neuron, which is the first step of the AChR clustering pathway. **B)** When Agrin is released into the NMJ, it binds with LRP4 which recruits MuSK, a receptor tyrosine kinase which dimerizes and phosphorylates DOK7. DOK7 recruits RAPSYN, a scaffolding protein which stabilizes and anchors AChRs in the post-synaptic muscle membrane. This activation of DOK7 and RAPSYN enables gene expression from sub-synaptic nuclei which aid NMJ remodeling and maturation. The clustering of AChR

at the postsynaptic membrane increases the probability of ACh interacting with AChR, initiating muscular contractions. Image created in BioRender.

The NMJ is not a static structure; it undergoes continuous remodeling to preserve synaptic integrity and to ensure effective neurotransmission. At the presynaptic terminal, sustained neurotransmission depends on efficient synaptic vesicle replenishment, ACh trafficking and active zone organization [10]. Proteins such as synaptophysin, SNAP25, and synaptotagmin coordinate vesicle docking and fusion, while Agrin and laminin-β2 secreted from the nerve terminal contribute to long-term synaptic stabilization [10].

Postsynaptically, AChRs must remain tightly clustered at high density within the endplate to ensure reliable signal transmission [17]. Disruption of clustering, anchoring, or turnover pathways leads to dispersal and impaired synaptic efficacy.

Terminal Schwan cells are essential for NMJ maintenance. They provide trophic support, modulate synaptic plasticity, secrete extracellular matrix (ECM) components, and respond dynamically to injury [19]. Their actions help stabilize synaptic architecture and facilitate repair [19]. The NMJ's high energetic demands are met by abundant subsynaptic mitochondria, which support ATP for vesicle recycling, ion transport, and muscle contraction while buffering intracellular Ca^{+2} [29]. Mitochondrial dysfunction, common in ageing and neuromuscular disease impairs these processes and contributes to synaptic degeneration [43,44].

Together, these presynaptic, postsynaptic, glial and metabolic processes form a dynamic system essential for NMJ stability. Perturbations in any component can compromise synaptic function and lead to progressive muscle weakness, a hallmark of CMS.

1.5 Congenital Myasthenic Syndromes (CMS)

CMS are a heterogenous group of rare, inherited disorders characterized by impaired signal transmission at the NMJ [1]. Clinically CMS presents with fatigable muscle weakness affecting multiple

muscle groups including limb-girdle, distal, proximal, respiratory, ocular, facial, and bulbar muscles [1,10,26]. Symptom severity varies widely, ranging from mild functional limitations to life-threatening respiratory crises, depending on the specific genetic defect [1,10,45].

To date, approximately 40 genes have been implicated in CMS pathogenesis, encoding proteins for NMJ neurotransmission, structural maintenance, and motor endplate modification [2]. These genes are typically classified according to the localization of their protein products within the NMJ: presynaptic, postsynaptic, synaptic and endplate-associated modifiers [1,2,45]. Recently, a novel CMS subtype has been linked to mitochondrial dysfunction, highlighting the importance of energy metabolism in synaptic stability (Summarized in Figure 5) [29].

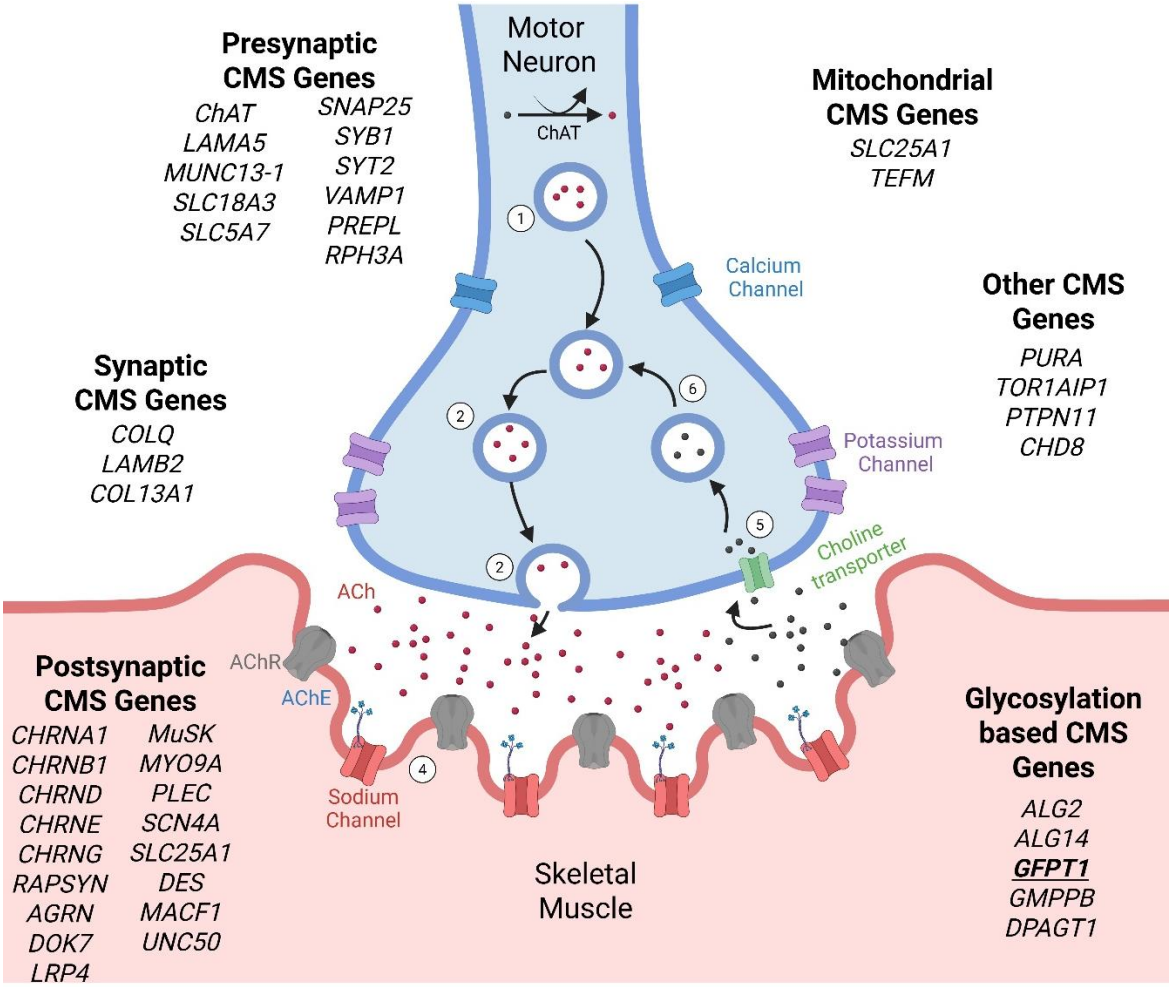

Figure 5: CMS-causative genes: To date mutation to approximately 40 genes have been associated with a CMS phenotype. This has been subdivided into 5 main categories focusing on localization or function.

Thes include presynaptic, synaptic, postsynaptic, glycosylation-based, and mitochondrial subtypes. There are four outstanding CMS genes that are deemed other as they do not belong in any individual group. Image created in BioRender.

Presynaptic CMS accounts for approximately 5-10% of all CMS cases and typically presents earlier and with greater severity than postsynaptic forms [10]. They arise from defects in ACh synthesis, vesicle packaging, and release, most commonly due to mutations to choline acetyltransferase (*ChAT*), with additional genes including: *SLC5A7, CHAT, SLC18A3, SNAP25, VAMP1/SYB1, SYT2, UNC13A, MYO9A, PREPL, LAMA5, RPH3A,* and *SLC25A1*[1,2,45]. Postsynaptic CMS involve impaired AChR expression or altered AChR channel kinetics, often caused by mutations in AChR subunits, particularly *CHRNE*, the most common cause among all diagnosed patients [46,47]. Alterations in channel kinetics give rise to fast-channel and slow-channel CMS subtypes [1,48–50]. Fast channel CMS is characterized by reduced AChR channel opening time, limiting postsynaptic depolarization and impairing action potential propagation [1,2,51]. Conversely, slow-channel CMS results from prolonged depolarization, impairing muscle repolarization and recovery [1,2,48]. Biallelic mutations in *AGRN, RAPSN, DOK7, MUSK,* and *LRP4*, reduce receptor density and compromise NMJ stability.

Synaptic CMS are rare and typically involve defects in ECM components essential for AChE anchoring, most notably *COLQ*, leading to prolonged ACh signaling and endplate dysfunction [6,52–54]. Lastly, recently described mitochondrial CMS, reflects the energetic dependence of synaptic transmission and includes mutation in *TEFM* [55] and *SLC25A1* [56–59], which impair ATP production needed for neurotransmission and AChR maintenance.

Together, these subtypes illustrate the mechanistic diversity of CMS and provide a framework for understanding glycosylation-related forms, which disrupt NMJ structure and receptor expression through impaired protein processing.

1.6 Glycosylation-based CMS

A fourth major CMS subgroup involves defects in protein glycosylation, a process essential for proper folding, stability and localization of NMJ proteins. These glycosylation-based CMS genes include glutamine-fructose-6-phosphate transaminase 1 (*GFPT1*), dolichol-phosphate N-acetylglucosaminephosphotransferase-1 (*DPAGT1*) [60–64], GDP-mannose pyrophosphorylase B (*GMPPB*) [65,66], α-1,3/1,6-mannosyltransferase (*ALG2*) [67,68], and UDP-N-acetylglucosaminyltransferase subunit 14 (*ALG14*) [67]. These enzymes are positioned during early protein glycosylation and are summarized in Figure 6.

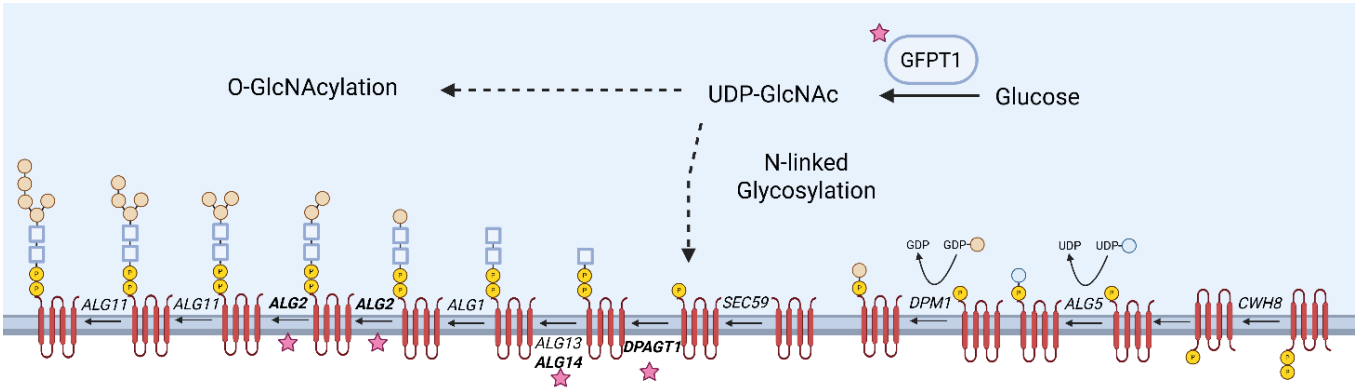

Figure 6: Summary of the five glycosylation-based CMS genes: There are currently five (5) CMS genes linked to protein glycosylation. *GFPT1, DPAGT1, ALG2* and *ALG14* are shown above as key enzymatic steps for early N-linked glycosylation and protein O-GlcNAcylation. *GFPT1* produces the necessary precursor for O- and N-linked glycosylation. *DPAGT1, ALG2* and *ALG14* are key components of the early dolichol synthesis step of N-linked glycosylation creating the first glycan assembly chain in the ER lumen. Not presented is *GMPPB*, an essential enzymatic step in protein mannosylation, forming GDP-mannose. CMS genes are marked with a red star. Image created in BioRender.

1.6.1 *DPAGT1*-CMS

DPAGT1 catalyzes the first step of the biosynthetic pathway for N-linked glycosylation oligosaccharides (Figure 6 and Figure 7) [61]. Mutations to *DPAGT1* cause two distinct disorders: CMS and *DPAGT1*-CDG (CDG type 1j). CMS-associated mutations cluster predominately within the glycosyltransferase domain and typically cause a limb-girdle pattern of weakness with minimal ocular or bulbar involvement [69]. Tubular aggregates are common on muscle biopsy and occasionally cardiac

abnormalities such as hypokinetic cardiomyopathy are described [70]. Partial therapeutic benefit has been reported with pyridostigmine and salbutamol [60,63,64,69].

DPAGT1 is also implicated in congenital disorder of glycosylation (CDG-1j), a severe multisystemic disorder with profound hypotonia, intractable seizures, microcephaly, exotropia and encephalopathy [69,71]. Both conditions involve hypoglycosylation, though the specific mechanism leading to NMJ dysfunction in *DPAGT1*-CMS remains unsolved [62].

1.6.2 GMPPB-CMS

GMPPB produces GDP-mannose, an essential donor for multiple glycosylation pathways (Figure 7) [65]. *GMPPB*-CMS typically present with classical myasthenic symptoms but is distinguished from other CMS through high serum creatine kinase levels often exceeding 500 U/L [65]. Mutations in *GMPPB* are associated with CMS, CDG, secondary dystroglycanopathies and limb-girdle muscular dystrophy [65,66,72]. Pathology reflects hypo-mannosylation of α-dystroglycan, compromising NMJ structure and leading to fatigable weakness of variable severity [65,66,72]. Individuals have reported a beneficial response to pyridostigmine and salbutamol [65].

1.6.3 ALG2/ALG14-CMS

ALG2 catalyses the early steps of the N-linked glycosylation pathway by adding α1,3 and α1,6-linked mannose residues to $Man_1GlcNAc_2$-PP-Dol, forming the first branched tri-mannosyl glycan intermediate [68,73]. Biallelic mutations to *ALG2* cause two disease subtypes: *ALG2*-CDG, and *ALG2*-CMS. In *ALG2*-CDG patients exhibit multisystemic involvement, including iris colobomas, unilateral cataract, infantile spasms, and severe developmental delay [74]. In contrast, *ALG2*-CMS patients present with pronounced hypotonia, proximal muscle weakness and feeding difficulties [67,68,75]. Muscle biopsies often reveal the presence of tubular aggregates, and occasional ragged red fibers, suggesting mitochondrial involvement [67]. Pathogenic variants such as p.Val68Gly reduce ALG2 protein levels, impairing protein

glycosylation [67]. Treatment responses vary, but pyridostigmine, 3,4-DAP, salbutamol, or ephedrine offer some benefit [67,68,76].

ALG14 forms a heterodimeric complex with ALG13 and DPAGT1 to facilitate early N-linked glycosylation [77]. ALG14 contains the ER-localization domain essential for the heterodimeric complex to attach to the ER mediating its enzymatic activity [77]. Pathogenic variants in *ALG14*-CMS such as pArg104* have been associated with non-sense mediated decay of ALG14 due to truncation, impairing protein glycosylation, with a mild disease course [67]. Missense mutations such as p.Val197Gly and p.Gly145Arg cause a severe disease with hypotonia, joint contractures, ptosis, swallowing and respiratory failure, and CNS involvement, including delayed myelination and seizures [76]. ALG14 knockdown has been shown to reduce the cell surface expression of AChR, similar to DAPGT1, and ALG2, thus highlighting a potential pathomechanism for disease [67].

1.6.4 GFPT1-CMS

GFPT1 serves as the rate-limiting enzyme of the hexosamine biosynthetic pathway (HBP) which generates UDP-GlcNAc, a critical substrate for different protein glycosylation pathways (Figure 7). *GFPT1*-CMS typically presents as a limb-girdle pattern of muscle weakness beginning in early childhood and progresses slowly throughout life [78–83,83–86]. Unlike other CMS subtypes, ocular, bulbar and facial muscles are usually spared [78–83,83–86]. Muscle biopsies frequently reveal tubular aggregates, with occasional rimmed vacuoles and ragged red fibers [78–83,83–86]. In addition, electron microscopy has demonstrated that in *GFPT1*-CMS patients a reduction of postsynaptic junctional folds is present [78–83,83–86]. Biallelic mutations to Gfpt1 result in a reduction in protein expression and/or enzymatic activity, impairing HBP flux [83,87,88]. However, recent studies have shown that Gfpt1 patient-derived myoblasts do not have any significant changes of total N-linked glycosylation levels [88]. Most recently, efforts have been directed to expand the phenotypic spectrum of *GFPT1*-CMS patients. A study of five Brazilian patients from two unrelated families harbouring the pathogenic variant c.41G>A (p.Arg41Gln) revealed

proximal muscle weakness in upper limbs, distal weakness in lower limbs consistent with food dorsiflexion weakness [89]. Weakness of distal leg muscles highlights a broader spectrum of disorders than originally recognized which may contribute to misdiagnosis [78,89]. In addition, patients may have atypical features for *GFPT1*-CMS such as neonatal onset epilepsy, cognitive impairment and leukoencephalopathy [78,86,89,90]. *GFPT1*-CMS has been associated with the most severe degree of fat infiltration into the muscle fibers, compared to other glycosylation-based CMS cases [78,86]. Interestingly there is also variability within known *GFPT1*-CMS variants such as c.322G>A (p.Arg111His) which presents in one case with classical limb girdle myasthenia, but in another case with dysmorphic features, hyperextensible joints, features of metabolic myopathy, and a strong positive AChR antibody within the serum, suggesting potential modifiers of disease may cause phenotypic variability [86].

Within human skeletal muscle GFPT1 undergoes alternative splicing to produce a long isoform (GFPT1-L) containing a 54-bp insertion in exon 9[1]. Pathogenic variants have been detected within GFPT1-L (c686-2A>G, c.686dupC, c.706>T, c.719G>A) which introduce a premature stop codon, reducing GFPT1 enzymatic activity [79–81,91]. These variants may disrupt NMJ integrity through impaired glucose metabolism, a mechanism supported by NMJ fragmentation and reduced AChE expression in diabetic mouse models [79–81,91–94], though it remains speculative. Clinically, pyridostigmine, 3,4-DAP and salbutamol provide partial benefit, but disease progression often continues, highlighting the need for novel therapies [78–83,83–86].

1.7 Protein Glycosylation

Glycosylation is a widespread post-translational modification (PTM) involving the covalent attachment of oligosaccharides to proteins[95–98]. Glycosylation is essential for proper protein folding, stability, trafficking, and function. The major glycosylation pathways relevant to neuromuscular biology including N-linked glycosylation, O-linked glycosylation, and O-GlcNAcylation, the latter serving as a dynamic regulatory modification particularly important in skeletal muscle and motor neurons [99].

Glycosylation occurs within the endoplasmic reticulum (ER) and Golgi apparatus (GA), where an array of glycosyltransferases and glycosides coordinate glycan assembly and maturation [95,96]. Defects in this process disrupt the structure and function of key synaptic proteins and contribute to a variety of congenital disorders, including several CMS subtypes [95,96]. This section focuses on two major glycosylation pathways: N-linked glycosylation and O-GlcNAcylation.

1.7.1 N-linked glycosylation

N-linked glycosylation is a highly conserved PTM initiated in the ER and completed in the Golgi apparatus. The process is comprised of three major phases: 1) Glycan chain biosynthesis; 2) Transfer of the glycan to the target protein; and 3) Dolichol regeneration and recycling [100,101].

The pathway initiates with the synthesis of dolichol (Dol), a long-chain polyisoprenoid lipid that acts as the membrane-embedded scaffold for precursor glycan chain [101]. Dol is generated from isopentenyl pyrophosphate (IPP) and dimethylallyl pyrophosphate (DMAPP) through the mevalonate pathway on cytoplasmic face of the ER [101]. Following the initial assembly of the DLO, seven sugar residues are added to dolichol pyrophosphate (PP-Dol) on the cytoplasmic face of the ER lumen. Once the intermediate $Man_5GlcNAc_2$-PP-Dol is formed, it is translocated into the ER lumen by the ER membrane transporter, RFT1 [101,102]. Within the lumen, additional glycosyltransferases extend the glycan by adding four mannose and three glucose resides, producing the mature $Glc_3Man_9GlcNAc_2$-PP-dolichol precursor. This is summarized in Figure 7.

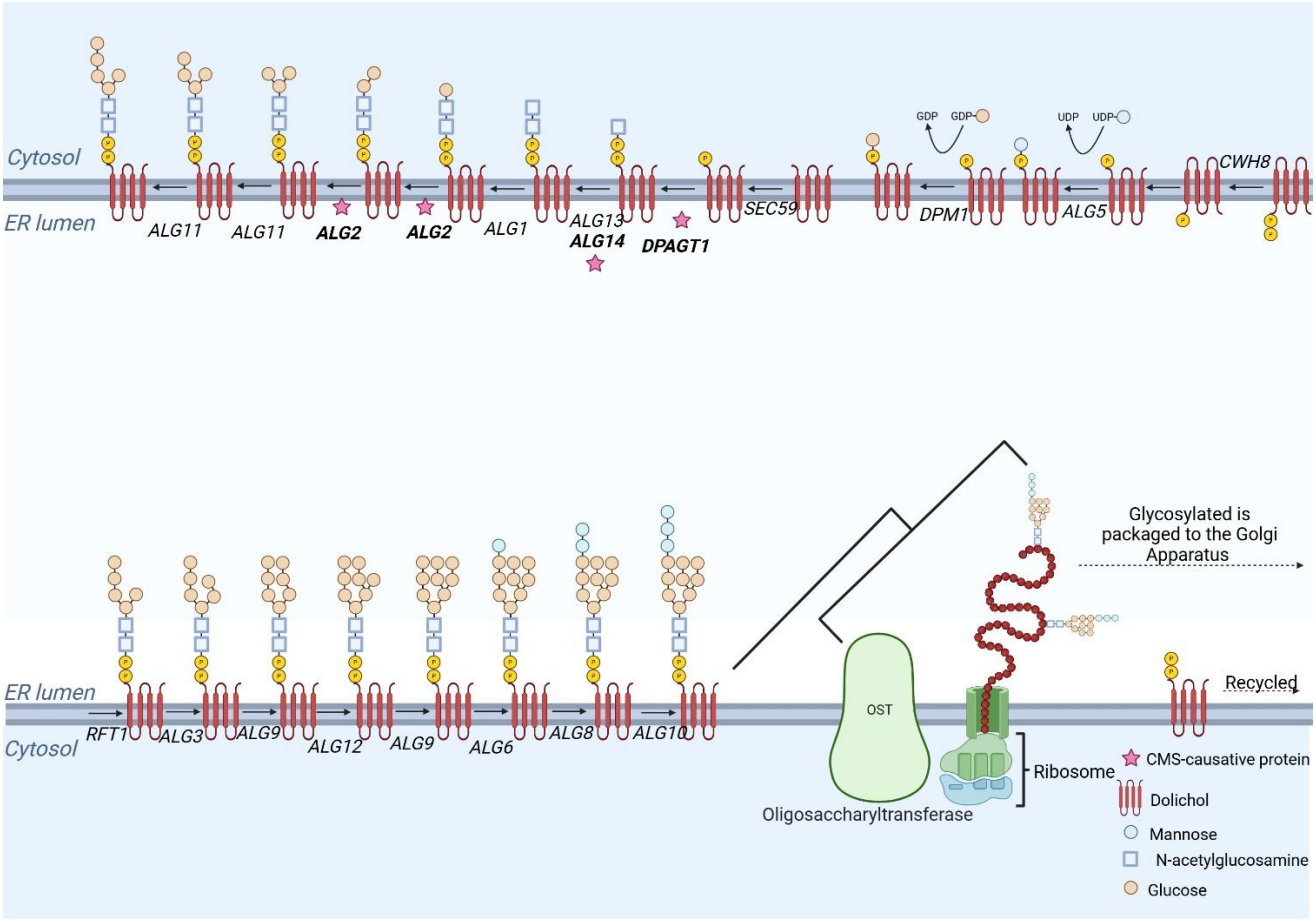

Figure 7: Schematic representation of N-linked glycosylation in the ER: Dolichol-linked oligosaccharide assembly mediated by ALG and accessory enzymes, transfer to nascent polypeptide by OST, and subsequent glycoprotein is packaged towards the Golgi for further processing. Implicated CMS genes within the N-linked glycosylation pathway are highlighted with a red star. Image created in BioRender.

The completed glycan is transferred to asparagine residues within the consensus Asn-X-Ser/Thr motif by the oligosaccharyltransferase (OST) complex. OST exists in two isoforms, defined by their catalytic subunits STT3A and STT3B [103,104]. STT3A primarily transfers fully assembled glycans and is critical for co-translational glycosylation, whereas, STT3B can transfer incomplete glycans lacking terminal glycose residues, enable partial PTMs of proteins [105]. Both complexes share core subunits proteins (RPN1, RPN2, TMEM258, DAD1, OST48, OST4) but differ in accessory proteins: DC2 and KCP2 for STT3A; TUSC3 and MAGT1 for STT3B [103,104]. Mutations to STT3A and STT3B have been associated with CDGs [105].

After glycan transfer, the nascent glycoprotein undergoes initial folding and quality control in the ER before trafficking to the GA for further maturation. Simultaneously, dolichol recycling begins: DOLPP1 dephosphorylates Dol-PP to regenerate Dol-P, allowing it to re-enter the glycan assembly cycle [100]. Impaired dolichol recycling disrupts N-linked glycan production and perturb ER homeostasis, resulting in CDG pathogenesis [100,106].

The ER quality control machinery, especially the calnexin/calreticulin cycle, ensures that only properly folded glycoproteins proceed forward [107]. Misfolded or incompletely glycosylated proteins are retained and targeted for ER-associated degradation (ERAD) [108]. Persistent defects in glycosylated proteins such in *DPAGT1-, ALG2-, ALG14-, GMPPB-,* and *GFPT1*-CMS can overwhelm these pathways triggering the unfolded protein response (UPR) and activate ER stress [109]. Disrupted proteostasis may impair NMJ stability by reducing the availability of essential synaptic proteins and triggering maladaptive stress signaling.

The core, DLO-derived glycan serves as a scaffold for all mature N-linked glycan. As glycoproteins enter the GA via COP-II coated vesicles, they encounter a series of glycosidases and glycosyltransferases that remodel the glycan by adding residues such as GlcNAc, mannose, glucose, fucose, galactose, and sialic acids [110,111]. These modifications diversify glycan structure and fine-tune protein function, trafficking and stability.

1.7.2 O-GlcNAcylation and the Hexosamine Biosynthetic Pathway

O-GlcNAcylation, first described in 1984, is a unique and reversible modification involving the addition of a single N-acetylglucosamine (GlcNAc) moiety to serine or threonine residues [112,113]. Unlike canonical glycosylation, it often occurs in the cytoplasm and nucleus, functioning as a nutrient-sensing regulatory modification linking metabolism to signaling pathways [114,115]. The donor substrate, UDP-GlcNAc, is produced through the hexosamine biosynthetic pathway (HBP) (Figure 8). Approximately 2-

5% of cellular glucose enters the HBP [116]. After glucose is converted to glucose-6-phosphate and then fructose-6-phosphate, the rate limiting enzyme, GFPT1, catalyzes the formation of glucosamine-6-phosphate [83,87,116]. This step is tightly regulated through feedback inhibition from UDP-GlcNAc [83,87,116]. Subsequent reactions include: glucosamine-phosphate N-acetyltransferase (GNPNAT) catalyzes acetyl-CoA and glucosamine-6-phosphate to generate N-acetylglucosamine-6-phosphate (GlcNAc-6P) and CoA; GlcNAc phosphomutase (PGM3/AGM1)-mediates the isomerization of GlcNAc-6P to GlcNAc-1-phosphate (GlcNAc-1P). For the last step, UDP-GlcNAc is produced through the enzymatic reaction of UDP-N-acetylglucosamine pyrophosphate (UAP1/AGX1) [116]. UDP-GlcNAc produced by the HBP feeds directly into O-GlcNAcylation, N-linked glycosylation, and other glycan pathways, positioning GFPT1 as a critical metabolic regulator.

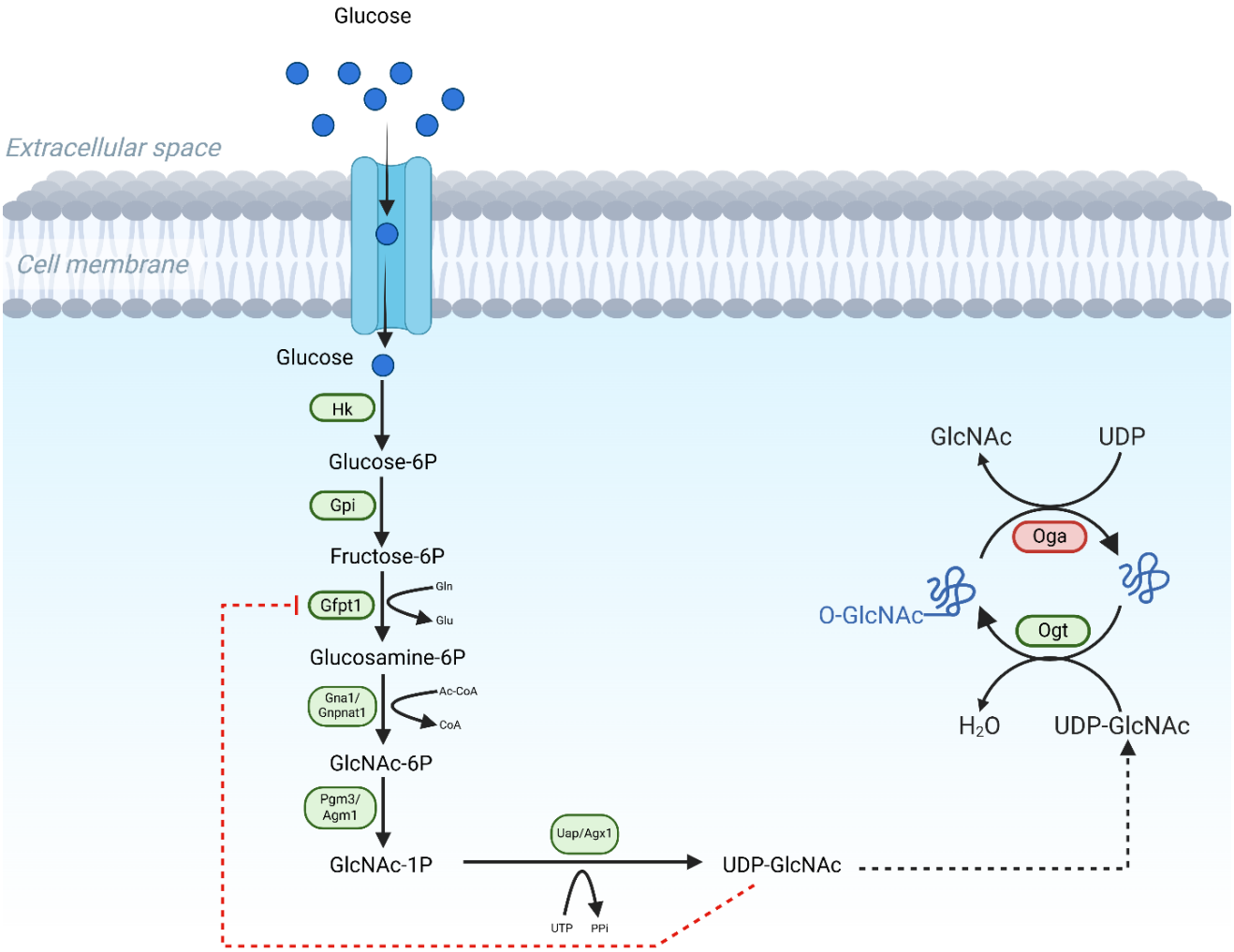

Figure 8: The hexosamine biosynthetic pathway (HBP) channels ~2–5% of cellular glucose into the production of UDP-GlcNAc, the essential donor substrate for N-linked glycosylation, O-linked glycosylation, and O-GlcNAcylation. Its rate-limiting enzyme, GFPT1, converts fructose-6-phosphate and glutamine into glucosamine-6-phosphate, thereby controlling HBP flux and UDP-GlcNAc availability. UDP-GlcNAc fuels O-GlcNAcylation, a reversible intracellular modification added by O-GlcNAc transferase (OGT) and removed by O-GlcNAcase (OGA). Together, the HBP and GFPT1 integrate nutrient status with glycosylation and signaling, positioning O-GlcNAcylation as a key regulator of metabolic and cellular homeostasis. Image created in BioRender.

The dynamic cycling of O-GlcNAc is mediated by two enzymes: O-GlcNAc transferase (OGT), which adds the GlcNAc moiety, and O-GlcNAcase (OGA), which removes it [115] (Figure 9). Unlike many PTMs, OGT does not require a strict consensus sequence; instead, substrate recognition is mediated by its N-terminal tetratricopeptide repeat (TPR) domain, which acts as a scaffold for protein interactions [114,116]. The substrate specificity of OGA is less well defined, but is thought to involve recognition of the sugar moiety rather than the surrounding peptide sequence [116]. Together OGT and OGA regulate thousands of proteins, integrating nutrients status with cellular signalling.

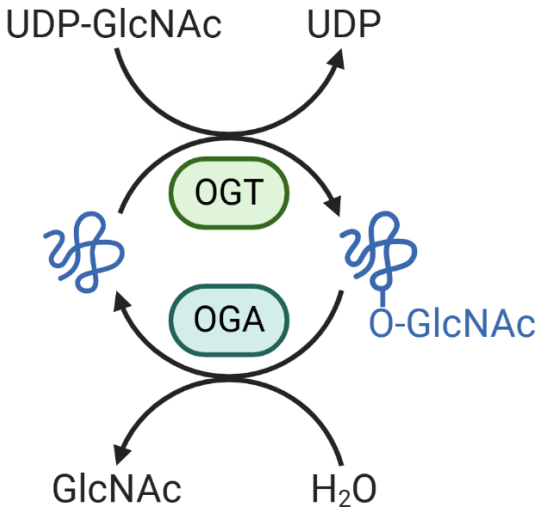

Figure 9: The process of O-GlcNAcylation: O-GlcNAcylation is a reversible protein modification produced from the hexosamine biosynthetic pathway (HBP). Its responsible for producing the necessary glycosylation substrate called UDP-GlcNAc. UDP-GlcNAc can be processed by oligotransferase (OGT), which adds GlcNAc to proteins at serine and threonine residues. The enzyme O-GlcNAc glycanase (OGA), removes the GlcNAc moiety from proteins. These proteins work in tandem to control downstream signalling cascades, to activate or repress protein activity. Image created in BioRender.

In 2021, the human O-GlcNAcome was mapped, identifying more than 5000 proteins and 7000 modification sites [117–119]. Most modified proteins localize to the cytoplasm, nucleus, and mitochondria, consistent with the function of O-GlcNAc [117–119]. In skeletal muscle, O-GlcNAcylation is emerging as a critical regulator of contractile function [120]. Major sarcomeric proteins including myosin, actin, tropomyosin, troponin, and myosin light chain are O-GlcNAcylated, suggesting direct control over calcium sensitivity, cytoskeletal organization, and mechanical performance [117,118,120].

Beyond muscle, O-GlcNAcylation broadly shapes cellular physiology, influencing stress responses, neurodegeneration, metabolic regulation and cancer progression [114,116]. Its interplay with phosphorylation allows it to modulate numerous signaling pathways, contributing to both physiological adaptation and pathology. Dysregulation of O-GlcNAcylation is implicated in diabetic myopathy, cachexia, sarcopenia, Alzheimer's disease and tumorigenesis, underscoring its relevance across diverse tissues. A deeper understanding of these mechanisms may reveal new therapeutic strategies for muscle related and metabolic disorders.

1.8 The Molecular Biology of GFPT1

The HBP is a critical metabolic signaling route that generates UDP-GlcNAc, the essential precursor for multiple protein glycosylation pathways. Its rate-limiting enzyme, glutamine-fructose-6-phosphate transaminase (GFPT), exists as two isoenzymes: GFPT1 (681aa) and GFPT2 (682aa), and share a 76% sequence homology [121]. GFPT1 is expressed in high abundance within heart, placenta, skeletal muscle, kidney, pancreas and testis while, GFPT2 is expressed primarily in the central nervous system [121].

In humans, alternative splicing of GFPT1 generates an insertion of 18 amino acids within exon 9, producing the long isoform (GFPT1-L) [81,109]. This isoform is restricted to skeletal and cardiac muscle and displays distinct enzymatic properties, including greater sensitivity to UDP-GlcNAc mediated feedback inhibition and reduced affinity for fructose-6-phosphate [109]. GFPT1-L splicing is governed by

RNA-binding proteins such as SRSF1, RBFOX1/2, and hnRNP H/F [109]. GFPT1-L is hypothesized to have evolved to fine-tune HBP flux to support energy production, insulin-mediated glucose uptake, and NMJ maintenance [109]. Notably, mice lack GFPT1-L.

Structurally GFPT1 is comprised of two major domains: 1) N-terminal glutaminase domain (GATase), responsible for enzymatic activity, the hydrolysis of L-glutamine to L-glutamate and ammonia, and; 2) C-terminal isomerase domain which uses the ammonia to convert fructose-6-phosphate into D-glucosamine-6-phosphate (SIS1 and SIS2) [121]. This is summarized below in Figure 10.

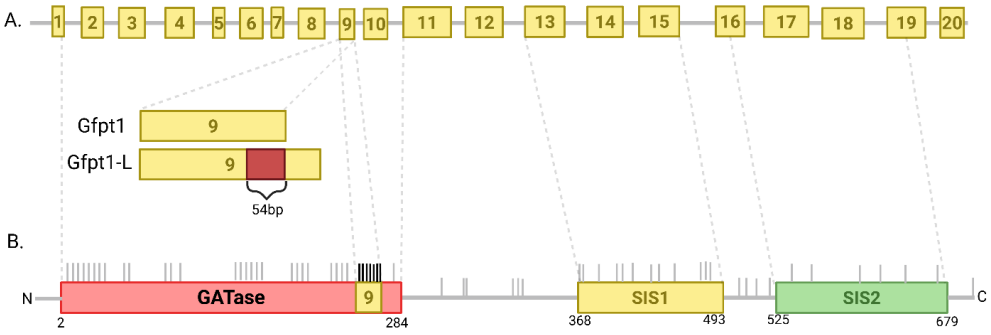

Figure 10: GFPT1 genomic structure and domain maps correlated with *GFPT1*-CMS variants. A) The genomic structure of human Gfpt1, consisting of 20 exons and one alternative splicing event that inserts a 54bp within exon 9, termed Gfpt1-L. Exons 1 through 11 encodes the GATase domain, while exons 13 to 15, and 16 to 19 encode the SIS1 and SIS2 domains respectively. B) The protein domain map for GFPT1 with known *GFPT1*-CMS variants indicated with grey vertical lines. No phenotype-genotype or localization of *GFPT1*-CMS variants exist. Notably, GFPT1-L exists as an 18aa inclusion within the GATase domain which harbour several known *GFPT1*-CMS variants. Image created in BioRender.

GFPT1 expression and activity are regulated through allosteric factors, and PTMs. Excess UDP-GlcNAc binds to the C-terminal isomerase domain of GFPT1, exerting classical feedback inhibition, while glucosamine-6-phosphte competes with fructose-6-phosphate at the active site. A mutation in the catalytic region (G451E) abolishes UDP-GlcNAc feedback inhibition and increases HBP flux in model systems such as N2a cells and *C. elegans* [122].

GFPT1 is also regulated by phosphorylation at Ser205, Ser235, and S243. At Ser205, protein kinase A (PKA) stabilizes inter-domain interactions preventing UDP-GlcNAc-mediated inhibition [123]. The

phosphorylation at Ser235 by PKA occurs without altering enzymatic activity, its hypothesized to impact enzymatic stability [121,124]. The phosphorylation at Ser243 by AMPK reduces GFPT1 activity, correlating with decreased O-GlcNAcylation under energy stress [121,125]. Conversely, mTORC2 phosphorylation at Ser243 promotes adaptation to glutamine depletion, restoring metabolic balance [126]. In neuromuscular disorders, modulation of GFPT1 via PTMs remains unexplored, representing a potential regulatory axis for disease mechanisms.

Beyond PTMs, GFPT1 expression is transcriptionally regulated by XBP1 and Sp1. Sp1 serves as a member of the Sp/KLF family, activates GFPT1 transcription via GC-rich promotor elements and responds to glucose levels [127]. Sp1 itself is O-GlcNAcylated, which inhibits its activity, forming a feedback loop linking UDP-GlcNAc abundance to GFPT1 expression [128]. XBP1, generated during the UPR, upregulates GFPT1 during nutrient or ER stress [108]. UPR signaling through ATF4 and elF2α phosphorylation further enhances HBP flux and global O-GlcNAcylation to support proteostasis and downstream gene regulation [108].

GFPT1 occupies a central metabolic position, linking glucose utilization, amino acid metabolism and cellular signaling [116]. By determining HBP flux, GFPT1 regulates the availability of UDP-GlcNAc for N-linked glycosylation, O-linked glycosylation, and O-GlcNAcylation. Pathways that influence insulin signaling, mTOR activity, nutrient sensing, and muscle contractile function [116]. This metabolic integration positions GFPT1 as a key regulator of skeletal muscle homeostasis and underscores the importance of understanding its regulation when investigating the mechanisms that underlie *GFPT1*-CMS.

1.9 Diagnosis and Treatment of CMS

1.9.1 Diagnosis of CMS

Diagnosing CMS remains challenging due to its broad phenotypic spectrum and overlap with other neuromuscular disorders [1]. Most CMS subtypes follow an autosomal recessive inheritance pattern, making family history an unreliable diagnostic tool. However, rare autosomal dominant cases exist, including slow-channel CMS, and *de novo* hemi-allelic variants in *PURA, PTPN11, SNAP25* and *SYT2* [45]. Considerable genotype-phenotype variability further complicates diagnosis, as individuals carrying variants such as ε1267delG variant in *CHRNE* or diverse *GMPPB*-CMS mutations may present with markedly different disease severity [65,129,130]. Expanding phenotypes in glycosylation-related CMS, including *GFPT1*- and *DPAGT1*-CMS, also blur traditional clinical boundaries, hence the need for genetic biomarker approaches [60,64,69,70,78,86,89,90].

Clinically, CMS often presents with fatigable muscle weakness confirmed by a decremental response on repetitive nerve stimulation (RNS) during clinical electrophysiology [1–3,45]. However, a definitive diagnosis requires genetic confirmation, typically through whole-exome or whole-genome sequencing. Despite advances in sequencing, ~40% of suspected CMS cases remain genetically unresolved [131]. Misdiagnosis is also common, particularly as MG, which shares hallmark features of fatigable weakness [1,4]. Unlike CMS, MG is caused by autoantibodies targeting NMJ proteins such as AChR, MuSK, or LRP4 [132]. These diagnostic challenges underscore the need for improved tools beyond electrophysiology and sequencing, particularly biomarkers capable of predicting disease severity, treatment response can accompany genetic detection for an earlier diagnosis.

1.9.2 Treatment of CMS: The need for more therapeutic strategies

Although several therapeutic approaches exist for CMS, no drug is currently licensed specifically for its treatment. Most interventions rely on off-label use of medications, and their efficacy varies depending

on the underlying genetic defect. Importantly, inappropriate treatment selection can exacerbate symptoms or cause adverse effects [131,133,134]. A summary of current and emerging strategies is provided in Figure 11.

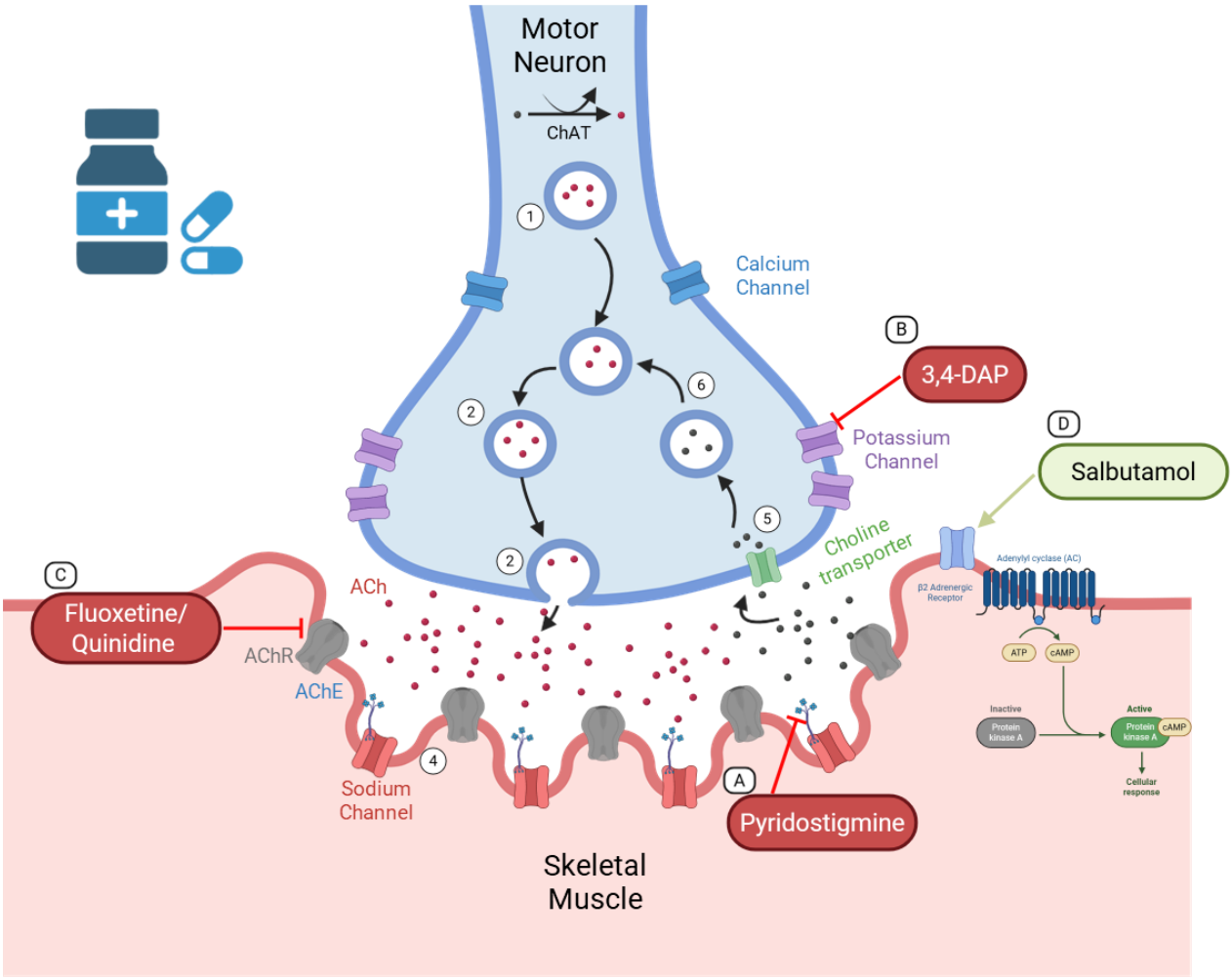

Figure 11: Summary of treatment strategies for CMS patients (NMJ): CMS patients have access to several treatment strategies that are off label which can be used for corrective care. A) AChE inhibitors such as pyridostigmine block AChE activity prolonging interaction between ACh and AChR. B) 3-4 DAP is a presynaptically active compound which blocks potassium channels prolonging the action potential and increases ACh release. C) Open AChR channel blockers such as fluoxetine and quinidine selectively inhibit AChRs in their open state. D) β2 adrenergic receptor agonists such as ephedrine and salbutamol are believed to stabilize NMJ structure through the cAMP-PKA signalling pathway.

AChE inhibitors such as pyridostigmine remains the first-line therapy for many CMS subtypes [1,45,133,134]. By inhibiting AChE, pyridostigmine prolongs ACh availability in the synaptic cleft, enhancing

postsynaptic activation. Gastrointestinal side effects (ex. nausea, abdominal discomfort, diarrhea) may occur but can be mitigated with antimuscarinic agents such as propantheline [135]. Importantly, pyridostigmine is contraindicated in slow-channel CMS, and *ColQ*-CMS where excessive AChR opening exacerbates receptor desensitization [135].

Potassium channel blockers, notably 3,4-diaminopyridine (3,4-DAP), enhance presynaptic ACh release by prolonging the action potential [134,136]. Despite demonstrating efficacy, global shortages of 3,4-DAP highlight the need for alternative therapies.

Open-channel blockers such as fluoxetine and quinidine selectively inhibit AChRs in their open state, reducing pathological depolarization in slow-channel CMS. These drugs are effective for slow-channel CMS and *ColQ*-CMS, but are contraindicated in others [131,137].

β2-adrenergic agonists, including ephedrine and salbutamol, were initially adopted from MG therapy [1,131,134]. These drugs appear to improve NMJ stability via a cAMP-PKA-dependent mechanism [138]. Preclinical models show that salbutamol enhances AChR distribution, synaptic area, and endplate organization [138]. A recent systematic review reported partial improvement in 93.6% of CMS patients, particularly in fatigue, respiratory function and feeding [139]. Symptoms such as hypotonia, ophthalmoplegia, and developmental delay were less responsive [139]. Notably, isolated cases of *CHAT*- or *DPAGT1*-CMS show no benefit, though sample size was limited to 1 patient per subtype [139]. In combinational therapeutic approaches the clinical efficacy drops to 44%, indicating that this therapy may not be as effective in severe or refractory cases of CMS [139]. Nevertheless, salbutamol remains an effective treatment strategy that has been implemented across CMS subtypes.

Emerging therapeutic options exist for CMS patients that could be included in glycosylation-based CMS patients. Gene therapy using adeno-associated virus (AAV) vectors has demonstrated promising preclinical results [39]. AAV-mediate delivery of *DOK7* [39], *COLQ* [140], *CHAT* [141], and *CHRNE*[142] restored

NMJ structure and improved muscle function in corresponding CMS mouse models. Engineered agrin fragments, such as NT1564, which retain only LRP4-binding domain, improve NMJ integrity and prolong survival in agrin loss-of-function models [143]. Another approach is the use of CIC1 inhibitors (NMD670), which increase the resting membrane potential and enhance neuromuscular transmission [5]. In addition, MuSK agonist antibodies (ARGX-119), which bind the MuSK frizzled-like domain, promote MuSK dimerization, and induce postsynaptic differentiation [36,144]. ARGX-119 rescues *Dok7*-CMS neonatal lethality, prevents disease release in mice, and has shown safety and pharmacodynamic activity in a first-in-human study [145]. A phase 1B clinical trail in *DOK7*-CMS is currently has been completed.

For glycosylation-based CMS, AChE inhibitors and 3,-4 DAP remain a mainstay of treatment, with occasional use of salbutamol for *GFPT1-, DPAGT1-, ALG2-, ALG14-* and *GMPPB*-CMS patients [63,65–68,78]. However, long-term efficacy is limited, and access to these medications remains challenging, underscoring the need for novel therapeutic strategies.

1.10 Congenital Disorders of Glycosylation (CDGs)

To date, more than 150 subtypes of CDG have been identified, representing a broad group of inborn errors of metabolism caused by defects in glycan synthesis (type I) or glycan processing/attached (type II) [146]. The most prevalent from is phosphomannomutase-2 deficiency (*PMM2*-CDG), typically inherited in a autosomal recessive manner, although autosomal dominant variants exist in *EXT1/EXT2*-, *GANAB*-, *PRKCSH*-, *POGLUT1*-, *POFUT1*-CDG [75,147]. Given the ubiquitous role of glycosylation, CDGs exhibit high clinical heterogeneity and generally multisystemic with prominent neurological involvement [148]. Approximately 20% of patients develop cardiac manifestation, including cardiomyopathy, arrhythmias, structural defects, and pericardial effusion [146,148]. Without intervention, progressive multisystem deterioration can lead to a premature mortality. [146,148].

Management of CDG is largely supportive, but several subtypes benefit from targeted metabolic therapies [115,149]. Monosaccharide supplementation has proven to be effective in specific N-linked glycosylation disorders such as mannose in *MPI*-CDG, galactose in *PGM1*-CDG, *SLC35A2*-CDG, *SLC39A8*-CDG, and *TMEM165*-CDG, and fucose *SLC35C1*-CDG [149]. In these conditions, supplementation can improve endocrine function, normalize liver enzymes, correct abnormal glycosylation, and in some cases reduce seizure severity [149]. Galactose therapy is particularly effective, oral administration (1g/kg/day) markedly improves glycosylation and clinical outcomes in nearly all reported *PGM1*-CDG cases, with similar benefit in *TMEM165*-CDG and *SLC39A8*-CDG patients [150–153]. This treatment strategy bypasses defective steps in glycan biosynthesis and highlights a mechanism-based therapeutic approach potentially relevant to glycosylation-based CMS.

therapying addition, CDGs have been targets for organ transplantation to prevent multisystem failure targeting the liver and heart [154]. Pharmacological chaperones represent another avenue, stabilizing partially functional mutant enzymes to restore proper folding and glycan processing. This strategy has shown promise in *PMM2*-CDG where variants such as R141H occurs in 80% of cases [155,156]. Acetazolamide therapy in *PMM2*-CDG patients showed improved clinical severity, motor cerebellar function and coagulation, as many chaperones can cross the blood-brain barrier essential for treatment of the neurological involvement of many CDGs [157,157].

CDGs share several pathogenic features with glycosylation-related CMS including inherited defects in glycan processing and neuromuscular involvement. However, while CMS primarily affects neuromuscular transmission, CDGs typically manifest as multisystemic disorders. Notably, some genes such as *DPAGT1* can give rise to both phenotypes: *DPAGT1*-CDG (CDG-Ij) results in a multisystem disorder with developmental delay, seizures and dysmorphic features, whereas *DPAGT1*-CMS presents with isolated neuromuscular weakness [69]. Similarly, GMPPB mutations can produce either a CMS phenotype or a broader dystroglycanopathy spectrum, depending on residual enzymatic function [66,72].

Importantly, as *GFPT1*-CMS disorders are being diagnosed, an expanded symptomatic feature list is being described, atypical from fatigable muscle weakness [78,86,90]. Therefore, glycosylation-based CMS disorders, may blend into CDG diagnoses with a multi-systemic disease.

1.11 Galactose metabolic pathway: Leloir Pathway

Galactose is a monosaccharide, hexose molecule which serves as an epimer of glucose, differing at the fourth carbon position hydroxyl group. Chemically, galactose is present as two enantiomers: *dexter (*D)- and *laevusor* (L)- galactose, with the structural confirmation of L-galactose, not naturally occurring. Galactose is naturally occurring and obtained through the diet mainly as a source of lactose, a disaccharide of galactose and glucose found in milk, and other foods such as cereals, fruit, vegetables, and honey [158]. Once ingested, galactose is absorbed by sodium-glucose linked transporter type 1 (SGLT1) in the intestinal lumen and is transported in the blood stream through glucose transporter type 2 (GLUT2) channels [159]. Galactose is then metabolized into three main pathways: 1) the Leir pathway – metabolizes galactose into precursors for glycosylation (Figure 13); 2) Oxidation of galactose to galactonate, which is further processed by the pentose phosphate pathway – producing xylulose; 3) and reduction of galactose to galactitol which is excreted [159].

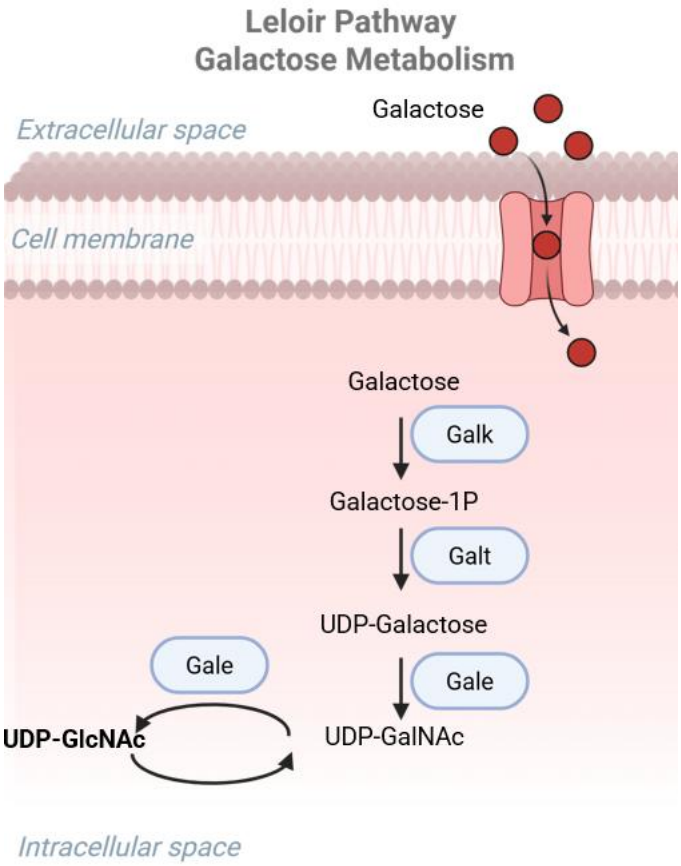

Figure 12: The metabolism schematic for galactose in skeletal muscle. The Leloir pathway converts dietary galactose into glucose-1-phosphate for entry into central metabolism. Galactose is first phosphorylated by galactokinase (GALK) to form galactose-1-phosphate, which is then exchanged with UDP-glucose by galactose-1-phosphate uridylyltransferase (GALT) to generate UDP-galactose. UDP-galactose 4-epimerase (GALE) interconverts UDP-galactose and UDP-glucose, completing the cycle and supplying substrates for glycosylation pathways. This pathway provides essential UDP-galactose for glycan synthesis and underlies the therapeutic rationale for galactose supplementation in select glycosylation disorders.

The Leloir pathway consists of a three-stage enzymatic process which produces the precursors for protein glycosylation. Galactose is converted into galactose-1-phosphate (Gal-1-P) by galactokinase (*GALK)* [159,160]. Galactose-1-phosphate uridylyltransferase (*GALT*) takes Gal-1-P and uridine diphosphate-glucose (UDP-Glc) into glucose-1-phosphate (Glc-1-P) and uridine diphosphate-galactose (UDP-Gal) [159,160]. Finally, UDP-galactose 4'epimerase (*GALE*) converts UDP-Gal to UDP-Glc, and UDP-GalNAc to UDP-GlcNAc, building blocks for protein glycosylation [159,160].

Deficiency to key proteins involved in galactose absorption, metabolism or glycosylation correspond to different CDGs including *galactosemia type 1* (GALT-deficiency)*, type 2* (GALK-deficiency), *type 3* (GALE-deficiency), *type 4* (GALM-deficiency), *PGM1*-CDG, *SLC35A2*-CDG, B*4GALT1*-CDG, *COLGALT1*-CDG, *SLC39A8*-CDG, and *TMEM165*-CDG [149,161,162]. As such, galactose metabolism is a key component of health and disease progression, thus utilization of the Leloir pathway, may benefit *GFPT1*-CMS patients.

1.12 An overview of intracellular trafficking of proteins

Intracellular trafficking is a fundamental process that enables eukaryotic cells to maintain organization, coordinate signaling and preserve protein homeostasis. Proteins and lipids are continuously transported between membrane-bound organelles through highly regulated pathways that ensure each molecule reaches its correct subcellular destination. These systems govern essential functions including secretion, membrane turnover, receptor recycling, autophagy and organelle biogenesis [113,163–165].

The secretory pathway is the major route by which newly synthesized proteins are folded, modified, sorted and delivered to the plasma membrane or extracellular space [166]. This system begins in the ER, where nascent polypeptides undergo folding, quality control, disulfide bond formation, and glycosylation [110,111,167]. Successful export from the ER requires correct folding and engagement with the machinery that concentrates cargo into COPII-coated vesicles at the ER exit sites [168]. Following ER export, cargo enters the Golgi apparatus, a series of cisternae that act as a central processing hub. The Golgi performs sequential glycan maturation, proteolytic processing, sulfation, glycosylation and sorting into specialized vesicles [169]. COPI-coated vesicles mediate retrograde trafficking from the Golgi back to the ER to recycle chaperones, SNAREs, and mis-sorted proteins, preserving protein homeostasis [170]. Within the trans-Golgi network, cargo is sorted into vesicles destined for the plasma membrane, lysosomes, or the extracellular matrix [169]. The fidelity of this system is essential, as even subtle defects in ER export, glycan maturation, or vesicle budding can impair secretion and membrane composition.

Complementing secretion are endocytic pathways that internalize proteins, lipids and extracellular material. Catherin-mediated endocytosis is a predominant route for receptor internalization, nutrient update, and synaptic vesicle recycling [171]. Internalized cargo enters the early endosome, which serves as a major sorting compartment [171]. Proteins can be recycled back to the plasma membrane, trafficked to the Golgi via retrograde pathways, or directed toward degradation through late endosome and lysosomes [172,173]. Recycling pathways are particularly important for surface receptors whose abundance and localization must be dynamically regulated [174]. These include neurotransmitter receptors, nutrient transporters, immune receptors, adhesion molecules and many signaling receptors. The balance between endocytosis, recycling, and degradation determines the sensitivity and stability of many signaling systems.

Intracellular trafficking is tightly coupled to proteostasis, the integrating network controlling protein synthesis, folding, modification and degradation. The ER provides the first checkpoint, ensuring that only properly folded proteins exit the Golgi, while misfolded proteins are retained and degraded through ER-associated degradation (ERAD) [108]. When folding capacity is exceeded, the unfolded protein response (UPR) is activated to restore balance by attenuating translation, upregulating chaperones, and enhancing degradative pathways [108]. Glycosylation plays a critical role in this process. Proper N-glycan maturation and O-linked modifications promote correct folding, chaperone management, and quality control [98]. Defects in glycosylation can impair ER exit, promote misfolded protein accumulation, and activate UPR signaling, which may eventually lead to apoptosis or chronic cellular stress if unresolved. Trafficking also intersects with autophagy, which requires membrane supply, vesicle tethering and lysosomal fusion, all dependent on tight regulation of vesicle formation and transport.

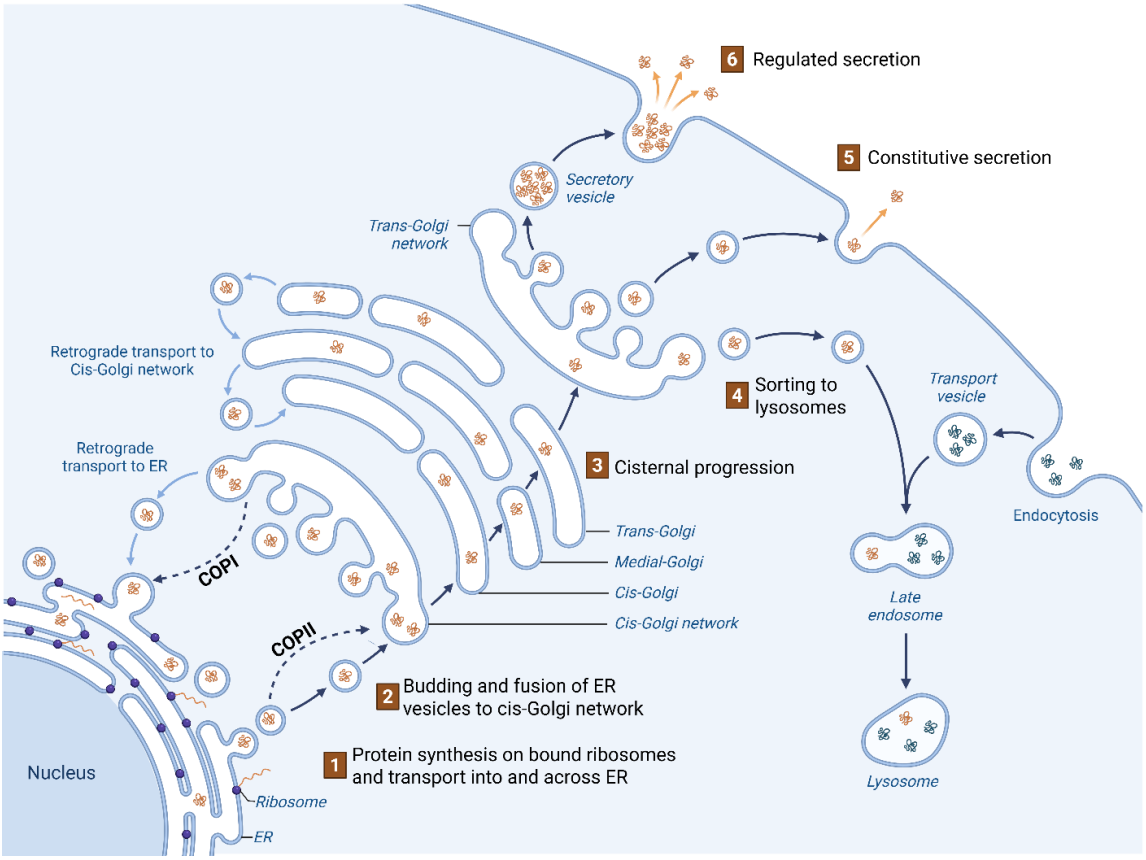

Figure 13: Overview of trafficking and protein secretion: Newly synthesized proteins enter the endoplasmic reticulum (ER) co-translationally, where they undergo folding and quality control before export in COPII-coated vesicles to the cis-Golgi network. Cargo progresses through the Golgi apparatus via cisternal maturation, undergoing post-translational modifications and sorting within the trans-Golgi network. From the trans-Golgi, proteins are directed toward constitutive secretion, regulated secretion, or lysosomal targeting through transport vesicles. Retrograde COPI-mediated trafficking maintains ER–Golgi homeostasis by recycling resident proteins and trafficking machinery. Endocytosed material enters the endosomal system and is either recycled or delivered to lysosomes for degradation, highlighting the integration of secretory and endolysosomal pathways in maintaining cellular proteostasis.

The UPR (summarized in Figure 14) is an adaptive networked activated by the accumulation of misfolded or unfolded proteins in the ER. It is mediated by three transmembrane stress sensors (IRE1, PERK and ATF6) that are maintained in an inactive state under basal conditions by the ER chaperone BiP [108]. Upon ER stress, BiP disengagement triggers sensor activation. IRE1 initiates unconventional splicing of *Xbp1* mRNA, producing the active transcription factor *XBP1s*, which promotes expression of chaperones, ER-associated degradation components, and lipid biosynthesis genes to expand ER capacity [108]. PERK attenuates global protein synthesis through phosphorylation of elf2α while selectively

inducing stress-adaptive genes such as *ATF4* [108]. ATG6, following ER stress, traffics to the Golgi where it is proteolytically cleaved to release a transcriptionally active fragment that upregulates ER folding and quality-control machinery [108]. Together, these pathways coordinate a transient reduction in secretory load with enhanced protein folding and degradation; however, chronic or unresolved UPR activation can promote maladaptive responses and contribute to tissue pathology[108,175,176].

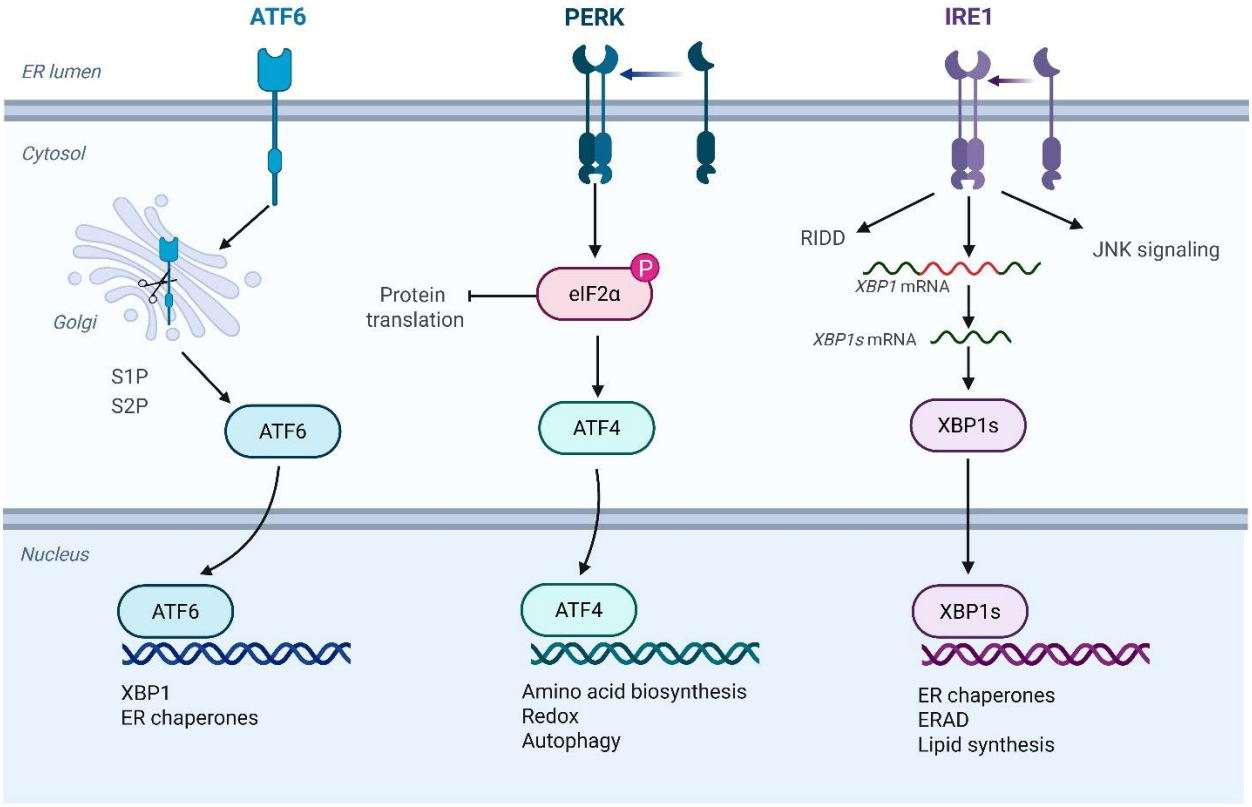

Figure 14: Overview of the Unfolded Protein Response Pathways: ER stress caused by accumulation of misfolded proteins activate the UPR through three ER-resident sensors: IRE1, PERK, and ATF6. Upon dissociation from the chaperone BiP, IRE1 promotes splicing of *Xbp1* mRNA to generate XBP1s, which induces genes involved in ER-associated degradation and ER expansion. PERK phosphorylates elF2α, transiently reducing global protein synthesis while enabling expression of stress-adaptive factors such as ATF4. ATF6 translocates to the Golgi where it is proteolytically cleaved to release a transcription factor that upregulates ER folding and quality-control machinery. Collectively, these pathways function to restore ER homeostasis or, if stress prolonged, contribute to pathological outcomes.

While trafficking is essential in all cells, some tissues depend on it to an exceptional degree. Secretory cells, neurons, and muscle fibers rely on continuous, high-capacity trafficking to sustain

communication and structural integrity [177,178]. In skeletal muscle, for example, secretion maintains the extracellular matrix, supports membrane repair, and supplies synaptic factors required for NMJ stability. Muscle fibers also possess extensive endomembrane networks including transverse tubules, sarcoplasmic reticulum and Golgi outposts, all of which require coordinated trafficking to maintain function during contraction and regeneration [11,179]. Any disturbance to these pathways can destabilize muscle structure, impair contraction and compromise synaptic signaling.

A growing number of genetic disorders arise from impaired intracellular trafficking. Mutations in components of the secretory pathway, coat proteins, cargo receptors, SNAREs, and cytoskeletal transport machinery lead to CDGs, and immune dysfunction [96]. Defects in glycosylation, ER quality control or lysosomal function often converge on common pathological themes: ER stress, protein aggregation, impaired secretion, and defective autophagy [96,164,178]. These shared mechanisms underscore centrality of trafficking to cellular homeostasis. In muscle, dystroglycanopathies, inclusion body myopathies and GNE myopathy, arise from trafficking defects contributing to ECM assembly, reduced receptor availability, unstable sarcolemma, and accumulation of undegraded cargo [180–184]. In addition, limb/girdle associated CMS (LGMD-CMS) contain tubular aggregate formations within skeletal muscle of unknown origin [62,64,78,83,85,185–187]. These aggregates may be a sign of impaired trafficking particularly in *GFPT1*-CMS.

Since intracellular trafficking interfaces with glycosylation, ER homeostasis, autophagy and secretion, it represents a critical node in the maintenance of proteostasis. Understanding how trafficking pathways integrate with metabolic signaling and protein quality control systems is essential for elucidating the mechanisms of diseases driven by defects in glycosylation or secretory function. In contexts where the supply of glycan precursors is disrupted, such as impaired HBP flux, trafficking defects may emerge as early events that drive pathological changes across multiple organelles and cellular systems. Investigating these connections provides insight into how metabolic shape organelle

communication and proteome stability, and can reveal biomarkers, therapeutic targets, and mechanisms that unify diverse clinical features.

1.13 Autophagy and its implications in skeletal muscle health

Autophagy, derived from the Greek words *auto* (self) and *phagy* (eating), is a highly conserved cellular process that mediates the degradation and recycling of intracellular components through lysosomal pathways [164]. This mechanism is essential for maintaining cellular homeostasis, particularly under stress conditions such as nutrient deprivation, oxidative damage, or organelle dysfunction [165]. In skeletal muscle, autophagy plays a critical role in proteostasis and organelle quality control, supporting the high metabolic demands of this tissue [188,189].

Autophagy can occur in a non-selective manner or through a selective pathway that targets specific substrates. These include mitophagy (removal of damaged mitochondria), aggrephagy[165] (clearance of protein aggregates), and ER-phagy (degradation of portions of endoplasmic reticulum), each using dedicated adaptors to link ubiquitinated cargo for degradation . Dysregulation of autophagic flux has been implicated in numerous diseases including neurodegeneration, cancer, and muscular disorders, and is increasingly being recognized as a therapeutic target [164,165].

The process begins with inhibition of mTORC1, a central negative regulator of autophagy, which permits the activation of the ULK1 complex (ULK1, ATG13, ATG101, and FIP200) [190,191]. This complex initiates the formation of the phagophore, a cup-shaped isolation membrane that originates from sources such as the ER, mitochondria, or plasma membrane [192]. Structural and biochemical studies how that these proteins assemble through a tripeptide interaction that are crucial for autophagosome biogenesis, positioning this complex as a central signal-integration node for downstream nutrient and energy status [190,192]. This ULK1 complex recruits class III PI3K (VPS34) complex (Beclin-1, VPS34, VPS15, and ATG14), which produces phosphatidylinositol-3-phosphate (PI3P) to nucleate phagophore assembly

and recruit PI3P-biding effectors [193,194]. Distinctly VSP34 complexes between autophagosome initiation and endo-lysosomal trafficking, respectively [194].

After the phagosome has formed, elongation occurs, which requires two ubiquitin like conjugation systems. First, ATG12-ATG5-ATG16L1 assemble a E3-like enzymatic complex [195]. Second, LC3/ATG8 is processed and lipidated to LC3-II (LC3-PE) by ATG7 (E1-like) and ATG3 (E2-like), decorating both sides of the membrane and serving as a docking platform for cargo receptors such as p62/SQSTM1 [195,196]. Biochemical reconstitution and structural studies reveal how the curvature of the phagosome, ATG14, and ATG3 membrane interactions promote LC3-II formation, a key step of autophagosome assembly [197].

Beyond the acute signaling, autophagic capacity is transcriptionally bolstered by transcription factor EB (TFEB), the master regulator of autophagy-lysosome gene network [198,199]. During stress, TFEB dephosphorylates and translocates to the nucleus, upregulating genes for autophagosome formation, lysosome biogenesis, fusion, and degradation [198,199]. TFEB activity is modulated by kinases (ERK and mTORC1) and the ubiquitin-protease pathway aligning with cellular clearance and capacity with metabolic needs [198,199].

Once the autophagosome is fully formed, it undergoes maturation and fuses with lysosomes to form the autolysosome, where cargo degradation occurs. This fusion is regulated by SNARE proteins, Rab GTPases, and lysosomal membrane proteins such as LAMP1 and LAMP2, which maintain lysosomal integrity and facilitate fusion [200,201]. The inner autophagosome membrane and its contents are degraded by lysosomal hydrolases, and the resulting macromolecules are recycled back into the cytoplasm [202]. The term autophagic flux refers to the dynamic process encompassing the autophagosome formation, cargo delivery, lysosomal fusion, and degradation. This serves as the complete process from initiation to degradation is tightly regulated and essential for cellular adaptation and survival [202]. Disruption at any stage can lead to accumulation of autophagosomes, impaired clearance of damaged components, and

pathological consequences, particularly in post-mitotic tissues like skeletal muscle. This pathway is summarized in Figure 15:

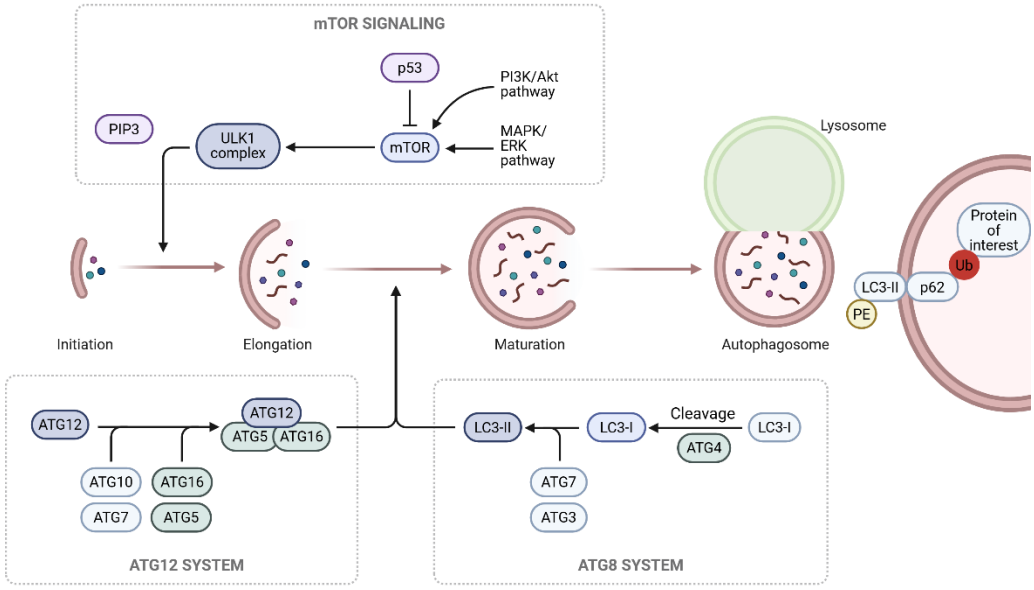

Figure 15: Autophagy is initiated when mTORC1 inhibition activates the ULK1 complex (ULK1–ATG13–ATG101–FIP200), which nucleates the phagophore and recruits the class III PI3K complex (Beclin-1–VPS34–VPS15–ATG14) to generate PI3P and direct membrane assembly. Phagophore elongation requires the ATG12–ATG5–ATG16L1 complex and LC3 lipidation (LC3-II), which decorates the membrane and enables cargo recruitment through receptors such as p62/SQSTM1. Autophagic capacity is transcriptionally reinforced by TFEB, which translocates to the nucleus under stress to upregulate autophagy–lysosome genes. Mature autophagosomes fuse with lysosomes through SNARE proteins, Rab GTPases, and LAMP1/2, forming autolysosomes where cargo is degraded and recycled. Collectively, this process, termed autophagic flux, spans initiation to lysosomal breakdown and is essential for cellular homeostasis, with disruptions causing autophagosome accumulation and impaired clearance

Beyond general muscle maintenance, autophagy plays a specialized role at the NMJ, where synaptic integrity depends on efficient clearance mechanisms. The NMJ is highly susceptible to age-related degeneration and stress-induced remodelling, a process in which autophagy is increasingly recognized as a key regulator [198]. In both presynaptic motor neurons and postsynaptic muscle fibers, autophagy removes synaptic debris, preserving synaptic transmission and structural stability [198,201]. Declining autophagic flux at the NMJ has been associated with age-related sarcopenia and neurodegenerative

conditions such as ALS [188]. Moreover, TFEB, has been implicated in NMJ maintenance, through the enhancement of myokine secretion of prosaposin and cathepsin B, and regulates gene expression involved in synaptic transmission, plasticity [203].

Impairment to the HBP and thus, protein glycosylation may perturb protein trafficking and ER homeostasis. In muscle, loss of the Gfpt1-L isoform activates ER stress and the unfolded protein response (UPR) pathway raising the possibility of secondary autophagic defects [109]. Notably, several autophagic and lysosomal proteins (LAMP1/LAMP2, ATG9) are glycosylated; glycosylation defects can impair lysosomal function and flux in storage disorders and are predicted to alter ATG9 lipid reorientation and autophagosome formation [172,173,201,204]. The presence of tubular aggregates, further supports a connection with impaired proteostasis and clearance [78]. Therefore, investigating autophagic flux in *GFPT1*-CMS may provide critical insights into disease pathogenesis and identify potential therapeutic targets.

1.14 Statement of research problem, rationale and objectives

The overall understanding of the role of *GFPT1* at the NMJ remains elusive. Current CMS treatment strategies show partial benefit, with worsening effect over time. As such, there is a need to better understand the role of *GFPT1* in CMS pathogenesis and to determine new therapeutic strategies for *GFPT1*-CMS patients. To promote this research, I hypothesized that:

1) **Deficiency of *Gfpt1* corresponds to a hypo-glycosylation environment at the NMJ resulting in the dysfunction of proteins involved with neurotransmission and NMJ maintenance**
2) **Deficiency of *Gfpt1* corresponds to an impairment in glycosylation which can be rescued by metabolic supplementation or HBP regulation.**
3) **Loss of *Gfpt1* results into an accumulation of misfolded proteins within the skeletal muscle due to dysfunctional autophagic flux, a potential cause for tubular aggregates within the skeletal muscle fiber.**

1.14.1 Objectives

Our objectives to this study are as follows:

1) To confirm *GFPT1*-CMS corresponds to a glycosylation disorder impacting proteins essential for NMJ neurotransmission and maintenance. This objective will confirm whether Gfpt1 is indeed a glycosylation disorder. In addition, elucidate if proteins at the NMJ are hypo-glycosylated corresponding to NMJ impairment.
2) Identify novel treatment strategies *GFPT1*-CMS patients. Confirming our objective #1, we can elucidate novel treatment strategies to bypass the defective glycosylation pathway using monosaccharides, and knockdown of enzymes which negatively regulate *Gfpt1*.
3) Elucidate pathomechanisms of *GFPT1*-CMS beyond a glycosylation deficiency. Confirming our objective #1 and #2, we can determine individual pathways that are mis-regulated in our *Gfpt1*-deficient models to further understand how *Gfpf1* is essential for muscle health.

References

1. Finsterer, J. Congenital myasthenic syndromes. *Orphanet J. Rare Dis.* **14**, 57 (2019).
2. Ohno, K., Ito, M. & Ohkawara, B. Review of 40 genes causing congenital myasthenic syndromes. *J. Hum. Genet.* 1–10 (2025) doi:10.1038/s10038-025-01355-9.
3. Beeson, D. Chapter 5 - Congenital myasthenic syndromes. in *Handbook of Clinical Neurology* (ed. Hanna, M. G.) vol. 203 69–88 (Elsevier, 2024).
4. Barnett, C., Herbelin, L., Dimachkie, M. M. & Barohn, R. J. Measuring Clinical Treatment Response in Myasthenia Gravis. *Neurol. Clin.* **36**, 339–353 (2018).
5. Skov, M. *et al.* The ClC-1 chloride channel inhibitor NMD670 improves skeletal muscle function in rat models and patients with myasthenia gravis. *Sci. Transl. Med.* **16**, eadk9109 (2024).
6. Ginebaugh, S. P., Badawi, Y., Tarr, T. B. & Meriney, S. D. Neuromuscular Active Zone Structure and Function in Healthy and Lambert-Eaton Myasthenic Syndrome States. *Biomolecules* **12**, 740 (2022).
7. Rossor, A. M. *et al.* Loss of BICD2 in muscle drives motor neuron loss in a developmental form of spinal muscular atrophy. *Acta Neuropathol. Commun.* **8**, 34 (2020).
8. Verma, S. *et al.* Neuromuscular Junction Dysfunction in Amyotrophic Lateral Sclerosis. *Mol. Neurobiol.* **59**, 1502–1527 (2022).
9. Iyer, S. R., Shah, S. B. & Lovering, R. M. The Neuromuscular Junction: Roles in Aging and Neuromuscular Disease. *Int. J. Mol. Sci.* **22**, 8058 (2021).
10. Pugliese, A., Holland, S. H., Rodolico, C., Lochmüller, H. & Spendiff, S. Presynaptic Congenital Myasthenic Syndromes: Understanding Clinical Phenotypes through In vivo Models. *J. Neuromuscul. Dis.* 1–29 (2023) doi:10.3233/JND-221646.
11. Wang, Z. & Raunser, S. Structural Biochemistry of Muscle Contraction. *Annu. Rev. Biochem.* **92**, 411–433 (2023).

12. Wu, J. *et al.* In-depth analysis of acetylcholinesterase: Recent advances in structure, function and assays. *Biochem. Eng. J.* **226**, 109974 (2026).

13. Ferraro, E., Molinari, F. & Berghella, L. Molecular control of neuromuscular junction development. *J. Cachexia Sarcopenia Muscle* **3**, 13–23 (2012).

14. Rodríguez Cruz, P. M., Cossins, J., Beeson, D. & Vincent, A. The Neuromuscular Junction in Health and Disease: Molecular Mechanisms Governing Synaptic Formation and Homeostasis. *Front. Mol. Neurosci.* **13**, 610964 (2020).

15. Yang, X. *et al.* Patterning of muscle acetylcholine receptor gene expression in the absence of motor innervation. *Neuron* **30**, 399–410 (2001).

16. Tapia, J. C. *et al.* Pervasive synaptic branch removal in the mammalian neuromuscular system at birth. *Neuron* **74**, 816–829 (2012).

17. Tintignac, L. A., Brenner, H.-R. & Rüegg, M. A. Mechanisms Regulating Neuromuscular Junction Development and Function and Causes of Muscle Wasting. *Physiol. Rev.* **95**, 809–852 (2015).

18. Ertürk, A., Hellal, F., Enes, J. & Bradke, F. Disorganized microtubules underlie the formation of retraction bulbs and the failure of axonal regeneration. *J. Neurosci. Off. J. Soc. Neurosci.* **27**, 9169–9180 (2007).

19. Alhindi, A. *et al.* Terminal Schwann cells at the human neuromuscular junction. *Brain Commun.* **3**, fcab081 (2021).

20. Missias, A. C., Chu, G. C., Klocke, B. J., Sanes, J. R. & Merlie, J. P. Maturation of the acetylcholine receptor in skeletal muscle: regulation of the AChR gamma-to-epsilon switch. *Dev. Biol.* **179**, 223–238 (1996).

21. Yumoto, N., Wakatsuki, S. & Sehara-Fujisawa, A. The acetylcholine receptor γ-to-ε switch occurs in individual endplates. *Biochem. Biophys. Res. Commun.* **331**, 1522–1527 (2005).

22. Li, H., Teng, J. & Hibbs, R. E. Structural switch in acetylcholine receptors in developing muscle. *Nature* **632**, 1174–1180 (2024).

23. Cetin, H., Beeson, D., Vincent, A. & Webster, R. The Structure, Function, and Physiology of the Fetal and Adult Acetylcholine Receptor in Muscle. *Front. Mol. Neurosci.* **13**, (2020).

24. Allen, N. M. *et al.* The emerging spectrum of fetal acetylcholine receptor antibody-related disorders (FARAD). *Brain* **146**, 4233–4246 (2023).

25. Cossins, J. *et al.* A mouse model of AChR deficiency syndrome with a phenotype reflecting the human condition. *Hum. Mol. Genet.* **13**, 2947–2957 (2004).

26. Krenn, M. *et al.* The clinical and molecular landscape of congenital myasthenic syndromes in Austria: a nationwide study. *J. Neurol.* **270**, 909–916 (2023).

27. Caldwell, J. h. Clustering of sodium channels at the neuromuscular junction. *Microsc. Res. Tech.* **49**, 84–89 (2000).

28. Ohkawara, B. *et al.* Transcriptome profile of subsynaptic myonuclei at the neuromuscular junction in embryogenesis. *J. Neurochem.* **168**, 342–354 (2024).

29. O'Connor, K., Spendiff, S., Lochmüller, H. & Horvath, R. Mitochondrial Mutations Can Alter Neuromuscular Transmission in Congenital Myasthenic Syndrome and Mitochondrial Disease. *Int. J. Mol. Sci.* **24**, 8505 (2023).

30. Zong, Y. & Jin, R. Structural mechanisms of the agrin-LRP4-MuSK signaling pathway in neuromuscular junction differentiation. *Cell. Mol. Life Sci. CMLS* **70**, 3077–3088 (2013).

31. Apel, E. D., Glass, D. J., Moscoso, L. M., Yancopoulos, G. D. & Sanes, J. R. Rapsyn is required for MuSK signaling and recruits synaptic components to a MuSK-containing scaffold. *Neuron* **18**, 623–635 (1997).

32. Barik, A., Xiong, W. & Mei, L. MuSK: A Kinase Critical for the Formation and Maintenance of the Neuromuscular Junction. in *Protein Kinase Technologies* (ed. Mukai, H.) 203–217 (Humana Press, Totowa, NJ, 2012). doi:10.1007/978-1-61779-824-5_11.

33. Stiegler, A. L., Burden, S. J. & Hubbard, S. R. Crystal Structure of the Frizzled-like Cysteine-rich Domain of the Receptor Tyrosine Kinase MuSK. *J. Mol. Biol.* **393**, 1–9 (2009).

34. Xie, T. *et al.* Structural insights into the assembly of the agrin/LRP4/MuSK signaling complex. *Proc. Natl. Acad. Sci.* **120**, e2300453120 (2023).

35. Yamanashi, Y., Higuchi, O. & Beeson, D. Dok-7/MuSK signaling and a congenital myasthenic syndrome. *Acta Myol.* **27**, 25–29 (2008).

36. Oury, J. *et al.* Mechanism of disease and therapeutic rescue of Dok7 congenital myasthenia. *Nature* **595**, 404–408 (2021).

37. Hamuro, J. *et al.* Mutations Causing DOK7 Congenital Myasthenia Ablate Functional Motifs in Dok-7 *. *J. Biol. Chem.* **283**, 5518–5524 (2008).

38. Zhang, S. *et al.* A mutation in DOK7 in congenital myasthenic syndrome forms aggresome in cultured cells, and reduces DOK7 expression and MuSK phosphorylation in patient-derived iPS cells. *Hum. Mol. Genet.* **32**, 1511–1523 (2022).

39. Huang, Y.-T. *et al.* Long-term muscle-specific overexpression of DOK7 in mice using AAV9-tMCK-DOK7. *Mol. Ther. Nucleic Acids* **33**, 617–628 (2023).

40. Uyen Dao, T. M. *et al.* The collagen ColQ binds to LRP4 and regulates the activation of the Muscle-Specific Kinase–LRP4 receptor complex by agrin at the neuromuscular junction. *J. Biol. Chem.* **299**, 104962 (2023).

41. Habes, M., Hénault, C. M. & Baenziger, J. E. Rapsyn-acetylcholine receptor interactions: structural models inform mechanisms of clustering at the neuromuscular junction. *Biophys. Rev.* https://doi.org/10.1007/s12551-025-01386-8 (2025) doi:10.1007/s12551-025-01386-8.

42. Chen, P.-J., Valenzuela, I. M.-P. y, Aittaleb, M. & Akaaboune, M. AChRs Are Essential for the Targeting of Rapsyn to the Postsynaptic Membrane of NMJs in Living Mice. *J. Neurosci.* **36**, 5680–5685 (2016).

43. Lessard, L. E. R. *et al.* Mitochondrial disorders are associated with morphological neuromuscular junction defects. *Neuromuscul. Disord.* **45**, 105235 (2024).

44. Marra, F. *et al.* An Overview of Mitochondrial Protein Defects in Neuromuscular Diseases. *Biomolecules* **11**, 1633 (2021).

45. Ohno, K., Ohkawara, B., Shen, X.-M., Selcen, D. & Engel, A. G. Clinical and Pathologic Features of Congenital Myasthenic Syndromes Caused by 35 Genes—A Comprehensive Review. *Int. J. Mol. Sci.* **24**, 3730 (2023).

46. Maselli, R. A. *et al.* Congenital myasthenic syndrome associated with epidermolysis bullosa caused by homozygous mutations in PLEC1 and CHRNE. *Clin. Genet.* **80**, 444–451 (2011).

47. Della Marina, A. *et al.* Blood biomarker fingerprints in a cohort of patients with CHRNE-related congenital myasthenic syndrome. *Acta Neuropathol. Commun.* **13**, 29 (2025).

48. Finsterer, J. Slow-Channel Congenital Myasthenic Syndrome Due to the Novel Variant c.1396G_A in CHRNA1 That Responds Favorably to 3,4-Diaminopyridine: A Case Report. *Cureus* **16**, e73601.

49. Durmus, H. *et al.* CONGENITAL MYASTHENIC SYNDROMES IN TURKEY: CLINICAL CLUES AND PROGNOSIS WITH LONG TERM FOLLOW-UP. *Neuromuscul. Disord. NMD* **28**, 315–322 (2018).

50. Engel, A. G., Shen, X.-M., Selcen, D. & Sine, S. New horizons for congenital myasthenic syndromes. *Ann. N. Y. Acad. Sci.* **1275**, 54–62 (2012).

51. Palace, J. *et al.* Clinical features in a series of fast channel congenital myasthenia syndrome. *Neuromuscul. Disord.* **22**, 112–117 (2012).

52. Shapira, Y. A. *et al.* Three novel *COLQ* mutations and variation of phenotypic expressivity due to G240X. *Neurology* **58**, 603–609 (2002).

53. Dusl, M. *et al.* Congenital myasthenic syndrome caused by novel COL13A1 mutations. *J. Neurol.* **266**, 1107–1112 (2019).

54. Mutations in LAMB2 causing a severe form of synaptic congenital myasthenic syndrome | Journal of Medical Genetics. https://jmg.bmj.com/content/46/3/203.

55. Van Haute, L. *et al.* TEFM variants impair mitochondrial transcription causing childhood-onset neurological disease. *Nat. Commun.* **14**, 1009 (2023).

56. Chaouch, A. *et al.* Mutations in the Mitochondrial Citrate Carrier SLC25A1 are Associated with Impaired Neuromuscular Transmission. *J. Neuromuscul. Dis.* **1**, 75–90 (2014).

57. Balaraju, S. *et al.* Congenital myasthenic syndrome with mild intellectual disability caused by a recurrent SLC25A1 variant. *Eur. J. Hum. Genet.* **28**, 373–377 (2020).

58. Zhao, Y. *et al.* Congenital myasthenic syndrome in China: genetic and myopathological characterization. *Ann. Clin. Transl. Neurol.* **8**, 898–907 (2021).

59. Li, W. *et al.* A case report of an intermediate phenotype between congenital myasthenic syndrome and D-2- and L-2-hydroxyglutaric aciduria due to novel SLC25A1 variants. *BMC Neurol.* **20**, 278 (2020).

60. Basiri, K. *et al.* Clinical features in a large Iranian family with a limb-girdle congenital myasthenic syndrome due to a mutation in DPAGT1. *Neuromuscul. Disord.* **23**, 469–472 (2013).

61. Belaya, K. *et al.* Identification of DPAGT1 as a new gene in which mutations cause a congenital myasthenic syndrome. *Ann. N. Y. Acad. Sci.* **1275**, 29–35 (2012).

62. Belaya, K. *et al.* Mutations in DPAGT1 Cause a Limb-Girdle Congenital Myasthenic Syndrome with Tubular Aggregates. *Am. J. Hum. Genet.* **91**, 193–201 (2012).

63. vanden Brande, L. *et al.* Pathogenic DPAGT1 variants in limb-girdle congenital myasthenic syndrome (LG-CMS) associated with tubular aggregates and ORAI1 hypoglycosylation. *Neuropathol. Appl. Neurobiol.* **50**, e12952 (2024).

64. Finlayson, S. *et al.* Clinical features of congenital myasthenic syndrome due to mutations in DPAGT1. *J. Neurol. Neurosurg. Psychiatry* **84**, 1119–1125 (2013).

65. Belaya, K. *et al.* Mutations in GMPPB cause congenital myasthenic syndrome and bridge myasthenic disorders with dystroglycanopathies. *Brain* **138**, 2493–2504 (2015).

66. Rodríguez Cruz, P. M. *et al.* Clinical features of the myasthenic syndrome arising from mutations in GMPPB. *J. Neurol. Neurosurg. Psychiatry* **87**, 802–809 (2016).

67. Cossins, J. *et al.* Congenital myasthenic syndromes due to mutations in ALG2 and ALG14. *Brain* **136**, 944–956 (2013).

68. Ehrstedt, C., Liu, W.-W., Frykholm, C., Beeson, D. & Punga, A. R. Novel pathogenic ALG2 mutation causing congenital myasthenic syndrome: A case report. *Neuromuscul. Disord.* **32**, 80–83 (2022).

69. Özsoy, Ö. *et al.* DPAGT1-CDG: Report of Two New Pediatric Patients and Brief Review of the Literature. *Mol. Syndromol.* **14**, 322–330 (2023).

70. Cheli, M., Brugnoni, R., Gibertini, S., Mantegazza, R. & Maggi, L. Novel DPAGT1 Gene Mutation in Two Twins with Congenital Myasthenic Syndrome and a Review of the Literature. *J. Neuromuscul. Dis.* **10**, 449–458 (2023).

71. Wu, X. *et al.* Deficiency of UDP-GlcNAc:Dolichol Phosphate N-Acetylglucosamine-1 Phosphate Transferase (DPAGT1) causes a novel congenital disorder of Glycosylation Type Ij. *Hum. Mutat.* **22**, 144–150 (2003).

72. Liu, Z. *et al.* GMPPB-congenital disorders of glycosylation associate with decreased enzymatic activity of GMPPB. *Mol. Biomed.* **2**, 13 (2021).

73. Dean, N. Alg1, Alg2, and Alg11 Mannosyltransferases of the Endoplasmic Reticulum. in *Handbook of Glycosyltransferases and Related Genes* 1239–1247 (Springer, Tokyo, 2014). doi:10.1007/978-4-431-54240-7_14.

74. Thiel, C. *et al.* A new type of congenital disorders of glycosylation (CDG-Ii) provides new insights into the early steps of dolichol-linked oligosaccharide biosynthesis. *J. Biol. Chem.* **278**, 22498–22505 (2003).

75. Monies, D. M. *et al.* Clinical and pathological heterogeneity of a congenital disorder of glycosylation manifesting as a myasthenic/myopathic syndrome. *Neuromuscul. Disord. NMD* **24**, 353–359 (2014).

76. Katata, Y. *et al.* The longest reported sibling survivors of a severe form of congenital myasthenic syndrome with the ALG14 pathogenic variant. *Am. J. Med. Genet. A.* **188**, 1293–1298 (2022).

77. Dean, N. & Gao, X.-D. Heterodimeric Alg13/Alg14 UDP-GlcNAc Transferase (ALG13,14). in *Handbook of Glycosyltransferases and Related Genes* 1231–1238 (Springer, Tokyo, 2014). doi:10.1007/978-4-431-54240-7_37.

78. Jiang, K. *et al.* Diverse myopathological features in the congenital myasthenia syndrome with GFPT1 mutation. *Brain Behav.* **12**, e2469 (2022).

79. Senderek, J. *et al.* Hexosamine Biosynthetic Pathway Mutations Cause Neuromuscular Transmission Defect. *Am. J. Hum. Genet.* **88**, 162–172 (2011).

80. Szelinger, S. *et al.* Congenital myasthenic syndrome caused by a frameshift insertion mutation in GFPT1. *Neurol. Genet.* **6**, e468 (2020).

81. Selcen, D. *et al.* GFPT1-myasthenia: clinical, structural, and electrophysiologic heterogeneity. *Neurology* **81**, 370–378 (2013).

82. Zoltowska, K. *et al.* Mutations in GFPT1 that underlie limb-girdle congenital myasthenic syndrome result in reduced cell-surface expression of muscle AChR. *Hum. Mol. Genet.* **22**, 2905–2913 (2013).

83. Bauché, S. *et al.* Mutations in GFPT1-related congenital myasthenic syndromes are associated with synaptic morphological defects and underlie a tubular aggregate myopathy with synaptopathy. *J. Neurol.* **264**, 1791–1803 (2017).

84. Dusl, M. *et al.* A 3'-UTR mutation creates a microRNA target site in the GFPT1 gene of patients with congenital myasthenic syndrome. *Hum. Mol. Genet.* **24**, 3418–3426 (2015).

85. Guergueltcheva, V. *et al.* Congenital myasthenic syndrome with tubular aggregates caused by GFPT1 mutations. *J. Neurol.* **259**, 838–850 (2012).

86. Vallepu, S. B. *et al.* Phenotypic variability in congenital myasthenic syndrome with GFPT1 mutation. *Acta Neurol. Belg.* https://doi.org/10.1007/s13760-024-02694-8 (2024) doi:10.1007/s13760-024-02694-8.

87. Issop, Y. *et al.* GFPT1 deficiency in muscle leads to myasthenia and myopathy in mice. *Hum. Mol. Genet.* **27**, 3218–3232 (2018).

88. Chen, Q. *et al.* Global N-linked Glycosylation is Not Significantly Impaired in Myoblasts in Congenital Myasthenic Syndromes Caused by Defective Glutamine-Fructose-6-Phosphate Transaminase 1 (GFPT1). *Biomolecules* **5**, 2758–2781 (2015).

89. Camelo-Filho, A. E. *et al.* Expanding the phenotypic and imaging spectrum of GFPT1-related congenital myasthenic syndromes: a Brazilian case series. *Front. Neurol.* **16**, (2025).

90. Helman, G. *et al.* Leukoencephalopathy due to variants in GFPT1-associated congenital myasthenic syndrome. *Neurology* **92**, e587–e593 (2019).

91. Vasta, V. *et al.* The Utility of Next Generation Sequencing in Genetic Diagnosis of Early-Onset Neuromuscular Disorders. *J. Med. Genet.* **52**, (2015).

92. Marques, M. J. & Neto, H. S. Acetylcholine receptors and nerve terminal distribution at the neuromuscular junction of non-obese diabetic mice. *Anat. Rec.* **267**, 112–119 (2002).

93. Souayah, N. *et al.* Motor unit number estimate as a predictor of motor dysfunction in an animal model of type 1 diabetes. *Am. J. Physiol.-Endocrinol. Metab.* **297**, E602–E608 (2009).

94. Garcia, C. C. *et al.* Acetylcholinesterase deficiency contributes to neuromuscular junction dysfunction in type 1 diabetic neuropathy. *Am. J. Physiol.-Endocrinol. Metab.* **303**, E551–E561 (2012).

95. Reily, C., Stewart, T. J., Renfrow, M. B. & Novak, J. Glycosylation in health and disease. *Nat. Rev. Nephrol.* **15**, 346–366 (2019).

96. Dang, K., Jiang, S., Gao, Y. & Qian, A. The role of protein glycosylation in muscle diseases. *Mol. Biol. Rep.* **49**, 8037–8049 (2022).

97. He, M., Zhou, X. & Wang, X. Glycosylation: mechanisms, biological functions and clinical implications. *Signal Transduct. Target. Ther.* **9**, 194 (2024).

98. Hao, C., Zou, Q., Bai, X. & Shi, W. Effect of glycosylation on protein folding: From biological roles to chemical protein synthesis. *iScience* **28**, 112605 (2025).

99. Lambert, M. *et al.* O-GlcNAcylation is a key modulator of skeletal muscle sarcomeric morphometry associated to modulation of protein–protein interactions. *Biochim. Biophys. Acta BBA - Gen. Subj.* **1860**, 2017–2030 (2016).

100. Rush, J. S., Gao, N., Lehrman, M. A. & Waechter, C. J. Recycling of dolichyl monophosphate to the cytoplasmic leaflet of the endoplasmic reticulum after the cleavage of dolichyl pyrophosphate on the lumenal monolayer. *J. Biol. Chem.* **283**, 4087–4093 (2008).

101. O'Connor, S. E. Reduction hits the sweet spot: A revised biosynthesis of dolichol. *Cell* **187**, 3502–3503 (2024).

102. Hirata, E. *et al.* Molecular characterization of Rft1, an ER membrane protein associated with congenital disorder of glycosylation RFT1-CDG. *J. Biol. Chem.* **300**, (2024).

103. Bai, L., Wang, T., Zhao, G., Kovach, A. & Li, H. The atomic structure of a eukaryotic oligosaccharyltransferase complex. *Nature* **555**, 328–333 (2018).

104. Shrimal, S. & Gilmore, R. Oligosaccharyltransferase structures provide novel insight into the mechanism of asparagine-linked glycosylation in prokaryotic and eukaryotic cells. *Glycobiology* **29**, 288–297 (2018).

105. Cherepanova, N. A., Venev, S. V., Leszyk, J. D., Shaffer, S. A. & Gilmore, R. Quantitative glycoproteomics reveals new classes of STT3A- and STT3B-dependent N-glycosylation sites. *J. Cell Biol.* **218**, 2782–2796 (2019).

106. Peric, D. *et al.* The Compartmentalisation of Phosphorylated Free Oligosaccharides in Cells from a CDG Ig Patient Reveals a Novel ER-to-Cytosol Translocation Process. *PLoS ONE* **5**, e11675 (2010).

107. Wanamaker, C. P. & Green, W. N. N-Linked Glycosylation Is Required for Nicotinic Receptor Assembly but Not for Subunit Associations with Calnexin *. *J. Biol. Chem.* **280**, 33800–33810 (2005).

108. Hetz, C., Zhang, K. & Kaufman, R. J. Mechanisms, regulation and functions of the unfolded protein response. *Nat. Rev. Mol. Cell Biol.* **21**, 421–438 (2020).

109. Zhang, R. *et al.* Muscle-specific lack of GFPT1 in knock-in mice triggers ER stress to alleviate misfolded proteins. *Dis. Model. Mech.* dmm.050768 (2024) doi:10.1242/dmm.050768.

110. Cox, N. J. *et al.* Dynamic Glycosylation Governs the Vertebrate COPII Protein Trafficking Pathway. *Biochemistry* **57**, 91–107 (2018).

111. Bisnett, B. J., Condon, B. M., Lamb, C. H., Georgiou, G. R. & Boyce, M. Export Control: Post-transcriptional Regulation of the COPII Trafficking Pathway. *Front. Cell Dev. Biol.* **8**, (2021).

112. Lee, B. E., Suh, P.-G. & Kim, J.-I. O-GlcNAcylation in health and neurodegenerative diseases. *Exp. Mol. Med.* **53**, 1674–1682 (2021).

113. Zhang, J. & Wang, Y. Emerging roles of O-GlcNAcylation in protein trafficking and secretion. *J. Biol. Chem.* **300**, 105677 (2024).

114. Chokchaitaweesuk, C., Kobayashi, T., Izumikawa, T. & Itano, N. Enhanced hexosamine metabolism drives metabolic and signaling networks involving hyaluronan production and O-GlcNAcylation to exacerbate breast cancer. *Cell Death Dis.* **10**, 1–15 (2019).

115. Liu, Y. *et al.* O-GlcNAcylation: the “stress and nutrition receptor” in cell stress response. *Cell Stress Chaperones* **26**, 297–309 (2021).

116. Akella, N. M., Ciraku, L. & Reginato, M. J. Fueling the fire: emerging role of the hexosamine biosynthetic pathway in cancer. *BMC Biol.* **17**, 52 (2019).

117. Lambert, M. *et al.* O-GlcNAcylation is a key modulator of skeletal muscle sarcomeric morphometry associated to modulation of protein–protein interactions. *Biochim. Biophys. Acta BBA - Gen. Subj.* **1860**, 2017–2030 (2016).

118. Jaiswal, R. *et al.* A reference dataset of O-GlcNAc proteins in quadriceps skeletal muscle from mice. *Glycobiology* cwaf005 (2025) doi:10.1093/glycob/cwaf005.

119. Wulff-Fuentes, E. *et al.* The human O-GlcNAcome database and meta-analysis. *Sci. Data* **8**, 25 (2021).

120. Lambert, M., Bastide, B. & Cieniewski-Bernard, C. Involvement of O-GlcNAcylation in the Skeletal Muscle Physiology and Physiopathology: Focus on Muscle Metabolism. *Front. Endocrinol.* **9**, 578 (2018).

121. Sampson, C. *et al.* Exploring the metabolic signaling network of GFPT in cancer. *Cell Death Discov.* **11**, 388 (2025).

122. Ruegenberg, S. *et al.* Loss of GFAT-1 feedback regulation activates the hexosamine pathway that modulates protein homeostasis. *Nat. Commun.* **11**, 687 (2020).

123. Chang, Q. *et al.* Phosphorylation of human glutamine:fructose-6-phosphate amidotransferase by cAMP-dependent protein kinase at serine 205 blocks the enzyme activity. *J. Biol. Chem.* **275**, 21981–21987 (2000).

124. Zhou, J. *et al.* Regulation of glutamine:fructose-6-phosphate amidotransferase by cAMP-dependent protein kinase. *Diabetes* **47**, 1836–1840 (1998).

125. Zibrova, D. *et al.* GFAT1 phosphorylation by AMPK promotes VEGF-induced angiogenesis. *Biochem. J.* **474**, 983–1001 (2017).

126. Li, Y. *et al.* Identification of a novel serine phosphorylation site in human glutamine:fructose-6-phosphate amidotransferase isoform 1. *Biochemistry* **46**, 13163–13169 (2007).

127. Hamiel, C. R., Pinto, S., Hau, A. & Wischmeyer, P. E. Glutamine enhances heat shock protein 70 expression via increased hexosamine biosynthetic pathway activity. *Am. J. Physiol. Cell Physiol.* **297**, C1509-1519 (2009).

128. Yang, X. *et al.* O-linkage of N-acetylglucosamine to Sp1 activation domain inhibits its transcriptional capability. *Proc. Natl. Acad. Sci. U. S. A.* **98**, 6611–6616 (2001).

129. Kastreva, K. *et al.* Characterization of Clinical Phenotypes in Congenital Myasthenic Syndrome Associated with the c.1327delG Frameshift Mutation in CHRNE Encoding the Acetylcholine Receptor Epsilon Subunit. *J. Neuromuscul. Dis.* **11**, 1011–1020.

130. Abicht, A. *et al.* A common mutation (ε1267delG) in congenital myasthenic patients of Gypsy ethnic origin. *Neurology* **53**, 1564–1564 (1999).

131. Thompson, R., Bonne, G., Missier, P. & Lochmüller, H. Targeted therapies for congenital myasthenic syndromes: systematic review and steps towards a treatabolome. *Emerg. Top. Life Sci.* **3**, 19–37 (2019).

132. Iorio, R. Myasthenia gravis: the changing treatment landscape in the era of molecular therapies. *Nat. Rev. Neurol.* **20**, 84–98 (2024).

133. Engel, A. G., Shen, X.-M., Selcen, D. & Sine, S. M. Congenital myasthenic syndromes: pathogenesis, diagnosis, and treatment. *Lancet Neurol.* **14**, 420–434 (2015).

134. Lee, M., Beeson, D. & Palace, J. Therapeutic strategies for congenital myasthenic syndromes. *Ann. N. Y. Acad. Sci.* **1412**, 129–136 (2018).

135. Finlayson, S., Beeson, D. & Palace, J. Congenital myasthenic syndromes: an update. *Pract. Neurol.* **13**, 80–91 (2013).

136. Schara, U. & Lochmüller, H. Therapeutic Strategies in Congenital Myasthenic Syndromes. *Neurotherapeutics* **5**, 542–547 (2008).

137. Shao, S., Shi, G., Bi, F.-F. & Huang, K. Pharmacological Treatments for Congenital Myasthenic SyndromesCaused by *COLQ* Mutations. *Curr. Neuropharmacol.* **21**, 1594–1605 (2023).

138. McMacken, G. M. *et al.* Salbutamol modifies the neuromuscular junction in a mouse model of ColQ myasthenic syndrome. *Hum. Mol. Genet.* **28**, 2339–2351 (2019).

139. Takhman, M. *et al.* Salbutamol in Congenital Myasthenic Syndrome: A Systematic Review. *BMC Neurol.* https://doi.org/10.1186/s12883-025-04569-8 (2025) doi:10.1186/s12883-025-04569-8.

140. Ito, M. *et al.* Protein-anchoring Strategy for Delivering Acetylcholinesterase to the Neuromuscular Junction. *Mol. Ther.* **20**, 1384–1392 (2012).

141. Lin, C. V. *et al.* Adeno-Associated Virus Type 9-Mediated Gene Therapy of Choline Acetyltransferase-Deficient Mice. *Hum. Gene Ther.* **35**, 123–131 (2024).

142. Korpetinou, A. *et al.* Serglycin: At the Crossroad of Inflammation and Malignancy. *Front. Oncol.* **3**, (2014).

143. Spendiff, S. *et al.* Modulation of the Acetylcholine Receptor Clustering Pathway Improves Neuromuscular Junction Structure and Muscle Strength in a Mouse Model of Congenital Myasthenic Syndrome. *Front. Mol. Neurosci.* **13**, 594220 (2020).

144. Vanhauwaert, R. *et al.* ARGX-119 is an agonist antibody for human MuSK that reverses disease relapse in a mouse model of congenital myasthenic syndrome. *Sci. Transl. Med.* **16**, eado7189 (2024).

145. van Bragt, T. *et al.* First-in-Human Dose Selection and Pharmacokinetics, Safety, Tolerability, and Immunogenicity of ARGX-119, an Agonist Antibody for Human Muscle-Specific Kinase (P10-2.007). *Neurology* **104**, 5060 (2025).

146. Francisco, R. *et al.* Congenital disorders of glycosylation (CDG): state of the art in 2022. *Orphanet J. Rare Dis.* **18**, 329 (2023).

147. Cline, A. *et al.* A zebrafish model of PMM2-CDG reveals altered neurogenesis and a substrate-accumulation mechanism for N-linked glycosylation deficiency. *Mol. Biol. Cell* **23**, 4175–4187 (2012).

148. Francisco, R. *et al.* The challenge of CDG diagnosis. *Mol. Genet. Metab.* **126**, 1–5 (2019).

149. Boyer, S. W., Johnsen, C. & Morava, E. Nutrition Interventions in Congenital Disorders of Glycosylation. *Trends Mol. Med.* **28**, 463–481 (2022).

150. Altassan, R. *et al.* International consensus guidelines for phosphoglucomutase 1 deficiency (PGM1-CDG): Diagnosis, follow-up, and management. *J. Inherit. Metab. Dis.* **44**, 148–163 (2021).

151. Morelle, W. *et al.* Galactose Supplementation in Patients With TMEM165-CDG Rescues the Glycosylation Defects. *J. Clin. Endocrinol. Metab.* **102**, 1375–1386 (2017).

152. Potelle, S. *et al.* Glycosylation abnormalities in Gdt1p/TMEM165 deficient cells result from a defect in Golgi manganese homeostasis. *Hum. Mol. Genet.* **25**, 1489–1500 (2016).

153. Park, J. H. *et al.* SLC39A8 deficiency: biochemical correction and major clinical improvement by manganese therapy. *Genet. Med.* **20**, 259–268 (2018).

154. Quelhas, D. & Jaeken, J. Treatment of congenital disorders of glycosylation: An overview. *Mol. Genet. Metab.* **143**, 108567 (2024).

155. Vilas, A. *et al.* Proteostasis regulators as potential rescuers of PMM2 activity. *Biochim. Biophys. Acta BBA - Mol. Basis Dis.* **1866**, 165777 (2020).

156. Bortot, B. *et al.* In vitro treatment of congenital disorder of glycosylation type Ia using PLGA nanoparticles loaded with GDP-Man. *Int. J. Mol. Med.* **44**, 262–272 (2019).

157. Martínez-Monseny, A. F. *et al.* AZATAX: Acetazolamide safety and efficacy in cerebellar syndrome in PMM2 congenital disorder of glycosylation (PMM2-CDG). *Ann. Neurol.* **85**, 740–751 (2019).

158. Battisegola, C. *et al.* Galactose: A Versatile Vector Unveiling the Potentials in Drug Delivery, Diagnostics, and Theranostics. *Pharmaceuticals* **17**, 308 (2024).

159. Conte, F., van Buuringen, N., Voermans, N. C. & Lefeber, D. J. Galactose in human metabolism, glycosylation and congenital metabolic diseases: Time for a closer look. *Biochim. Biophys. Acta BBA - Gen. Subj.* **1865**, 129898 (2021).

160. Structure and Function of Enzymes of the Leloir Pathway for Galactose Metabolism* - Journal of Biological Chemistry. https://www.jbc.org/article/S0021-9258%2820%2982392-8/fulltext.

161. Succoio, M., Sacchettini, R., Rossi, A., Parenti, G. & Ruoppolo, M. Galactosemia: Biochemistry, Molecular Genetics, Newborn Screening, and Treatment. *Biomolecules* **12**, 968 (2022).

162. Wang, Y. *et al.* A case report of classic galactosemia with a GALT gene variant and a literature review. *BMC Pediatr.* **24**, 352 (2024).

163. Lin, L. Unconventional protein secretion: Exploring membrane proteins and beyond. *Curr. Opin. Cell Biol.* **93**, 102469 (2025).

164. Franco-Romero, A. & Sandri, M. Role of autophagy in muscle disease. *Mol. Aspects Med.* **82**, 101041 (2021).

165. Gómez-Virgilio, L. *et al.* Autophagy: A Key Regulator of Homeostasis and Disease: An Overview of Molecular Mechanisms and Modulators. *Cells* **11**, 2262 (2022).

166. Brandizzi, F. & Barlowe, C. Organization of the ER–Golgi interface for membrane traffic control. *Nat. Rev. Mol. Cell Biol.* **14**, 382–392 (2013).

167. Robinson, C. M., Duggan, A. & Forrester, A. ER exit in physiology and disease. *Front. Mol. Biosci.* **11**, (2024).

168. Downes, K. W. & Zanetti, G. Mechanisms of COPII coat assembly and cargo recognition in the secretory pathway. *Nat. Rev. Mol. Cell Biol.* **26**, 910–925 (2025).

169. Watson, E. T., Wegeng, W. R., Aravani, S., Ernst, A. M. & von Blume, J. Mechanistic insights into cargo sorting and export from the Golgi apparatus. *Nat. Rev. Mol. Cell Biol.* **26**, 940–956 (2025).

170. Luo, P. M. & Boyce, M. Directing Traffic: Regulation of COPI Transport by Post-translational Modifications. *Front. Cell Dev. Biol.* **7**, (2019).

171. Prichard, K. L., O'Brien, N. S., Murcia, S. R., Baker, J. R. & McCluskey, A. Role of Clathrin and Dynamin in Clathrin Mediated Endocytosis/Synaptic Vesicle Recycling and Implications in Neurological Diseases. *Front. Cell. Neurosci.* **15**, (2022).

172. Ke, P.-Y. Molecular Mechanism of Autophagosome–Lysosome Fusion in Mammalian Cells. *Cells* **13**, (2024).

173. Reggiori, F. *et al.* Glycans in autophagy, endocytosis and lysosomal functions. *Glycoconj. J.* **38**, 625–647 (2021).

174. O'Sullivan, M. J. & Lindsay, A. J. The Endosomal Recycling Pathway—At the Crossroads of the Cell. *Int. J. Mol. Sci.* **21**, (2020).

175. Wang, Z. V. *et al.* Spliced X-box Binding Protein 1 Couples the Unfolded Protein Response to Hexosamine Biosynthetic Pathway. *Cell* **156**, 1179–1192 (2014).

176. Chen, X., Shi, C., He, M., Xiong, S. & Xia, X. Endoplasmic reticulum stress: molecular mechanism and therapeutic targets. *Signal Transduct. Target. Ther.* **8**, 352 (2023).

177. Towler, M. C., Kaufman, S. J. & Brodsky, F. M. Membrane Traffic in Skeletal Muscle. *Traffic* **5**, 129–139 (2004).

178. Braulke, T., Carette, J. E. & Palm, W. Lysosomal enzyme trafficking: from molecular mechanisms to human diseases. *Trends Cell Biol.* **34**, 198–210 (2024).

179. Herzog, W. & Schappacher-Tilp, G. Molecular mechanisms of muscle contraction: A historical perspective. *J. Biomech.* **155**, 111659 (2023).

180. Brown, S. C. *et al.* Abnormalities in α-Dystroglycan Expression in MDC1C and LGMD2I Muscular Dystrophies. *Am. J. Pathol.* **164**, 727–737 (2004).

181. de Queiroz, R. M. *et al.* Hexosamine Biosynthetic Pathway and Glycosylation Regulate Cell Migration in Melanoma Cells. *Front. Oncol.* **9**, 116 (2019).

182. Carrillo, N., Malicdan, M. C. & Huizing, M. GNE Myopathy: Etiology, Diagnosis, and Therapeutic Challenges. *Neurotherapeutics* **15**, 900–914 (2018).

183. Hinderlich, S., Weidemann, W., Yardeni, T., Horstkorte, R. & Huizing, M. UDP-GlcNAc 2-Epimerase/ManNAc Kinase (GNE): A Master Regulator of Sialic Acid Synthesis. *Top Chem Curr* **366**, 97–138 (2015).

184. Vosseller, K. *et al.* O-linked N-acetylglucosamine proteomics of postsynaptic density preparations using lectin weak affinity chromatography and mass spectrometry. *Mol. Cell. Proteomics MCP* **5**, 923–934 (2006).

185. Gang, Q. *et al.* Genetic defects are common in myopathies with tubular aggregates. *Ann. Clin. Transl. Neurol.* **9**, 4–15 (2021).

186. Böhm, J. *et al.* Constitutive Activation of the Calcium Sensor STIM1 Causes Tubular-Aggregate Myopathy. *Am. J. Hum. Genet.* **92**, 271–278 (2013).

187. Ehrstedt, C., Liu, W.-W., Frykholm, C., Beeson, D. & Punga, A. R. Novel pathogenic ALG2 mutation causing congenital myasthenic syndrome: A case report. *Neuromuscul. Disord. NMD* **32**, 80–83 (2022).

188. Vainshtein, A., Grumati, P., Sandri, M. & Bonaldo, P. Skeletal muscle, autophagy, and physical activity: the ménage à trois of metabolic regulation in health and disease. *J. Mol. Med.* **92**, 127–137 (2014).

189. Franco-Romero, A., Sandri, M. & Schiaffino, S. Autophagy in Skeletal Muscle. *Cold Spring Harb. Perspect. Biol.* **17**, a041565 (2025).

190. Ganley, I. G. *et al.* ULK1·ATG13·FIP200 Complex Mediates mTOR Signaling and Is Essential for Autophagy *. *J. Biol. Chem.* **284**, 12297–12305 (2009).

191. Kim, J., Kundu, M., Viollet, B. & Guan, K.-L. AMPK and mTOR regulate autophagy through direct phosphorylation of Ulk1. *Nat. Cell Biol.* **13**, 132–141 (2011).

192. Shi, X. *et al.* ULK complex organization in autophagy by a C-shaped FIP200 N-terminal domain dimer. *J. Cell Biol.* **219**, e201911047 (2020).

193. Menon, M. B. & Dhamija, S. Beclin 1 Phosphorylation – at the Center of Autophagy Regulation. *Front. Cell Dev. Biol.* **6**, (2018).

194. Stjepanovic, G., Baskaran, S., Lin, M. G. & Hurley, J. H. Vps34 Kinase Domain Dynamics Regulate the Autophagic PI 3-Kinase Complex. *Mol. Cell* **67**, 528-534.e3 (2017).

195. Regulation of LC3 lipidation by the autophagy-specific class III phosphatidylinositol-3 kinase complex | Molecular Biology of the Cell. https://www.molbiolcell.org/doi/full/10.1091/mbc.E18-11-0743.

196. Bjørkøy, G. *et al.* Monitoring autophagic degradation of p62/SQSTM1. *Methods Enzymol.* **452**, 181–197 (2009).

197. Ye, Y. *et al.* Multifaceted membrane interactions of human Atg3 promote LC3-phosphatidylethanolamine conjugation during autophagy. *Nat. Commun.* **14**, 5503 (2023).

198. Franco-Juárez, B. *et al.* TFEB; Beyond Its Role as an Autophagy and Lysosomes Regulator. *Cells* **11**, 3153 (2022).

199. Settembre, C. *et al.* TFEB Links Autophagy to Lysosomal Biogenesis. *Science* **332**, 1429–1433 (2011).

200. Corona, A. K. & Jackson, W. T. Finding the Middle Ground for Autophagic Fusion Requirements. *Trends Cell Biol.* **28**, 869–881 (2018).

201. Leeman, D. S. *et al.* Lysosome activation clears aggregates and enhances quiescent neural stem cell activation during aging. *Science* **359**, 1277–1283 (2018).

202. Diao, J., Yip, C. K. & Zhong, Q. Molecular structures and function of the autophagosome-lysosome fusion machinery. *Autophagy Rep.* **3**, 2305594 (2024).

203. Zhu, S. *et al.* The Role and Regulatory Mechanism of Transcription Factor EB in Health and Diseases. *Front. Cell Dev. Biol.* **9**, (2021).

204. Fahie, K. & Zachara, N. E. Molecular Functions of Glycoconjugates in Autophagy. *J. Mol. Biol.* **428**, 3305–3324 (2016).

Chapter 2: A deficiency in Glutamine-Fructose-6-Phosphate Transaminase 1 (Gfpt1) in Skeletal Muscle Results in Reduced Glycosylation of the Delta Subunit of the Nicotinic Acetylcholine Receptor (AChRδ)

Holland, S.H.; Caromona-Martinez, R.; O'Connor, K.; O'Neil, D.; Roos, A.; Spendiff, S.; Lochmüller, H. *Biomolecules*. 2024, 14, 1252. https://doi.orf/10.3390/biom14101252.

2.1 Statement of author contributions

This manuscript details the first manuscript describing the role of Gfpt1 and the NMJ. We hypothesized that deficiency in Gfpt1 expression results in aberrant or reduced glycosylation, impairing the proper assembly and stability of key NMJ proteins. We identified for the first time, Gfpt1 is a glycosylation disorder impairing the proper glycosylation of the AChRδ subunit. We found that Gfpt1-deficient models have impaired protein O-GlcNAcylation and N-linked glycosylation. In our skeletal muscle specific conditional knockout of Gfpt1, termed, *Gfpt1*$^{tm1d/tm1d}$ we performed a long-term study to examine the impact of Gfpt1 loss on NMJ and muscle integrity. We identified that these mice exhibit fatigable muscle weakness with impaired NMJ morphology. Next, we identified that in *Gfpt1*-deficient models that exhibit a double molecular weight banding pattern for AChRδ which was not present in controls. We identified using glycanases, that both molecular weight species were N-linked glycosylated. Next, laser capture microdissection was performed to enrich NMJs, from skeletal muscle to examine protein expression. We identified that both molecular species of AChRδ were present at the NMJ in *Gfpt1*$^{tm1d/tm1d}$ mice. All together this paper described the first protein that is hypo-glycosylated in Gfpt1-deficent NMJs.

At the beginning of my PhD I re-established the *Gfpt1*$^{tm1d/tm1d}$ mouse model and maintained mouse cohorts. Eventually at the time of the long-term natural study for 40-weeks, mouse cohorts transitioned to the care of Daniel O'Neil. At the time of dissections, both Daniel O'Neil and Ricardo Carmona-Martinez assisted with tissue collection. Laser Capture Microdissection (LCM) was performed at the Ottawa Hospital Research Institute with Dr. Rashmi Kothary's lab. Ricardo Carmona-Martinez assisted with the cyrosectioning and α-BTX staining, while Stephen Holland optimized NMJ capture and protein detection via Western blot. Stephen Holland developed a doxycycline-inducible Gfpt1-deficient C2C12 myoblast model. Monoclonal colony development was performed with assistance from Kaela O'Connor, who had adequate training to use the University of Ottawa's Flow

Cytometry Core. Stephen Holland performed all confocal microscopy, qPCR and Western blots. Dr. Sally Spendiff and Dr. Hanns Lochmüller conceptualized the study with Stephen Holland and provided supervision. Dr. Andreas Roos aided with intellectual support and offered guidance during the editing process. All authors performed editing and accepted the final copy prior to publication. Stephen Holland wrote the original draft of the manuscript and contributed to all revisions.

Deficiency of glutamine-fructose-6-phosphate transaminase 1 (Gfpt1) in skeletal muscle results in reduced glycosylation of the delta subunit of the nicotinic acetylcholine receptor (AChRδ)

Stephen H. Holland[1,2,4], R. Carmona-Martinez[1], K. O'Connor[1,2], D. O'Neil[1], A. Roos[1,7,8], S. Spendiff[1], H. Lochmüller[1,2,3,4,5,6*]

[1] Children's Hospital of Eastern Ontario Research Institute, Ottawa, Ontario, Canada

[2] Department of Cellular and Molecular Medicine, Faculty of Medicine, University of Ottawa, Ottawa, Ontario, Canada

[3] Division of Neurology, Department of Medicine, The Ottawa Hospital, Ottawa, Ontario, Canada

[4] Dr. Eric Poulin Center for Neuromuscular Disorders, Brain and Mind Research Institute, University of Ottawa, Ottawa, Ontario, Canada

[5] Department of Neuropediatric and Muscle Disorders, Medical Center, University of Freiburg, Faculty of Medicine, Freiburg, Germany

[6] Centro Nacional de Analisis Genomico (CNAG-CRG), Center for Genomic Regulation, Barcelona Institute of Science and Technology (BIST), Barcelona, Catalonia, Spain

[7] Department of Neuropaediatrics, Neuromuscular Centre, Universitätsmedizin Essen, Essen, Germany

[8] Department of Neurology, Medical Faculty and University Hospital Düsseldorf, Heinrich Heine University, Düsseldorf, 40225, Germany

Abstract: The neuromuscular junction (NMJ) is the site where the motor neuron innervates skeletal muscle enabling muscular contraction. Congenital myasthenic syndromes (CMS) arise when mutations in any of the approximately 35 known causative genes cause impaired neuromuscular transmission at the NMJ resulting in fatigable muscle weakness. A subset of five of these CMS-causative genes are associated with protein glycosylation. Glutamine-fructose-6-phosphate transaminase 1 (Gfpt1) is the rate limiting enzyme within the hexosamine biosynthetic pathway (HBP), a metabolic pathway which produces the precursors for glycosylation. We hypothesized that deficiency in Gfpt1 expression results in aberrant or reduced glycosylation impairing the proper assembly and stability of key NMJ-associated proteins. Using both *in vitro* and *in vivo* Gfpt1-deficient models, we determined that the acetylcholine receptor delta subunit (AChRδ) has reduced expression and is hypo-glycosylated. Using laser capture microdissection, NMJs were harvested from Gfpt1 knockout mouse muscle. A lower molecular weight species of AChRδ was identified at the NMJ that was not detected in controls. Furthermore, Gfpt1-deficient muscle lysates showed an impairment in protein O-GlcNAcylation and sialylation, suggesting that multiple glycan chains are impacted. Other key NMJ-associated proteins in addition to the AChRδ may also be differentially glycosylated in Gfpt1 deficient muscle.

Keywords: Glutamine-fructose-6-phosphate transaminase 1 (Gfpt1), Congenital myasthenic syndrome (CMS), neuromuscular junction (NMJ), O-GlcNAcylation, Acetylcholine receptor delta subunit (AChRδ), glycosylation

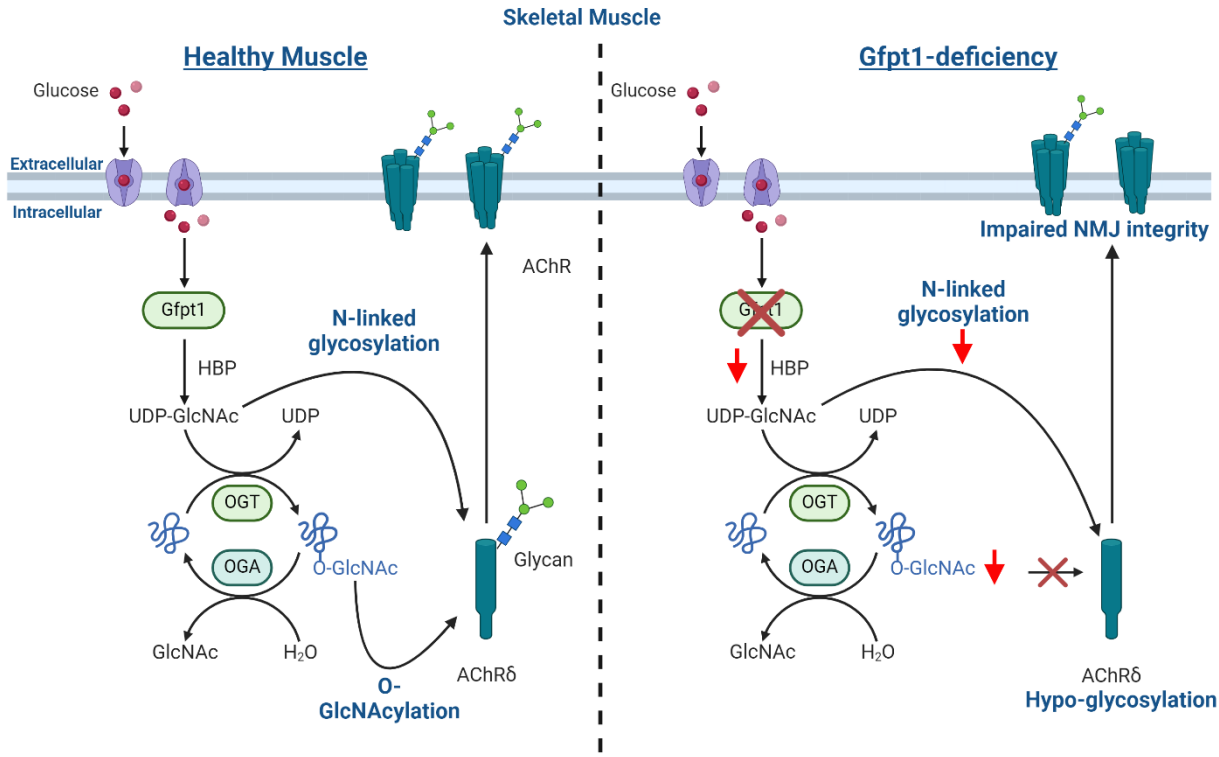

1. Introduction

Glycosylation, the attachment of sugar moieties to proteins, is the most common post-translational modification (PTM) that is associated with maintaining structure, function, stability, and localization of proteins within the cell. Initiated within the endoplasmic reticulum (ER), these modifications are diverse in nature ranging from the addition of a simple sugar to complex glycan chains with many branching points. Underscoring the vital role of glycans in protein homeostasis, many mutations to key genes associated with the glycosylation process are embryonically lethal **[1,2]**. However, some mutations within glycosylation enzymes correspond to a host of disorders called congenital disorders of glycosylation (CDGs), which typically have severe clinical manifestations impacting multiple organs and systems **[3,4]**. Numerous inherited muscle disorders have been associated with defects in glycosylation affecting primarily the alpha-dystroglycan protein including Fukuyama congenital muscular dystrophy (FCMD) **[5,6]**, Walker-Warburg syndrome **[7–10]**, congenital muscular dystrophy

type 1C and 1D (MDC1C/D) **[11–14]**, limb girdle muscular dystrophy type 2I **[15,16]** and muscle-eye-brain disease **[17]**.

The neuromuscular junction (NMJ) mediates the transmission of chemical signals from the pre-synaptic nerve terminal to the post-synaptic skeletal muscle, enabling muscular contraction. Congenital myasthenic syndromes (CMS) are early-onset inheritable neuromuscular disorders that result from mutation to proteins that are associated with NMJ development, function, maintenance and/or organization of the motor endplate **[20]**. Clinically, CMS are heterogeneous in nature but are typically characterized by fatigable muscle weakness to facial, bulbar, ocular, truncal, respiratory, limb and/or girdle muscles **[20]**. A subset of 5 of the CMS causative genes impair protein glycosylation, and results into CMS. These include glutamine-fructose-6-phosphate transaminase 1 (*GFPT1*) **[21–29]**, dolichol-phosphate N-acetylglucosaminephosphotransferase-1 (*DPAGT1*) **[30–33]**, GDP-mannose pyrophosphorylase B (*GMPPB*) **[34,35]**, α-1,3/1,6-mannosyltransferase (*ALG2*) **[36–38]**, and UDP-N-acetylglucosaminyltransferase subunit 14 (*ALG14*) **[36,38]**.

Gfpt1 is the rate-limiting enzyme of the hexosamine biosynthetic pathway (HBP), a metabolic signalling pathway that produces the precursor uridine diphosphate N-acetyl-glucosamine (UDP-GlcNAc) required for N- and O-linked protein glycosylation **[39,40]**. The HBP metabolizes key nutrients such as uridine triphosphate, glucose, glutamine, and acetyl-CoA, allowing for the regulation of integral processes such as cell growth **[41,42]**, differentiation **[43]**, stem cell differentiation **[44]**, metabolic reprogramming **[41,42]**, ER homeostasis **[45–47]**, transcriptional control **[48]**, and cancer pathogenesis **[42]**. UDP-GlcNAc is also involved in the creation of N-linked glycans through the conversion to the lipid carrier dolichol-phosphate (Dol-P) and in protein sialylation as a substrate of the UDP-GlcNAc epimerase 2 (*GNE)* enzyme **[49,50]**. As such, impairment to HBP activity could be associated with deficiency in the development of a variety of glycan side chains.

Biallelic mutations to *GFPT1* cause CMS characterized by fatigable limb-girdle muscle weakness, commonly presenting in the first years of life **[22–24,26,28]**. GFPT1-CMS muscle fibers contain tubular aggregates, which may originate from the sarcoplasmic reticulum, but their exact molecular origin remains unknown **[26]**. At the NMJ, GFPT1-CMS patients have reduced post-synaptic folding, reducing the efficiency of neuromuscular communication **[25]**. The biallelic mutations to *GFPT1* result in a decrease of GFPT1 protein levels, and/or impaired enzymatic activity, which may result in reduced or aberrant glycosylation **[22,24,27,51]**. However, glycomics of GFPT1-CMS patient myoblasts revealed no difference in global N-linked glycan chain development. while defective N-linked glycosylation has been shown in other GFPT1 CMS patient-derived myoblasts **[21,52]**. This suggests the need to molecularly study muscle cells to obtain insights into the underlying pathophysiology.

GFPT1 has been linked to protein O-GlcNAcylation, a reversible and highly dynamic modification that regulates the biological function **[53,54]**, stability, localization **[48]**, protein-protein interactions **[55]** and transcriptional control **[48,54]**. O-GlcNAcylation involves the binding of a single GlcNAc moiety, prepared by the HBP, to serine and threonine residues on a protein, via a β-configured O-glycosidic bond **[56,57]**. This is a reversible modification regulated by two enzymes: oligotransferase (OGT), and O-GlcNAcase (OGA) **[57]**. In skeletal muscle, O-GlcNAcylation remains an important regulator of immune response **[54]**, glucose metabolism, insulin sensitivity **[53]**, contractile properties **[55]**, and structural elements **[55]**. Impairment appears to be detrimental to various components of muscle health, and control of O-GlcNAcylation is important for various aspects of muscle function **[55,58]**. However, studies remain unclear whether GFPT1-deficiency impedes O-GlcNAcylation of NMJ-associated proteins. Elucidating the role of GFPT1 in protein glycosylation at the NMJ may not only reveal pathomechanisms of disease but also hint toward novel treatment strategies for CMS patients.

In this study, we hypothesize that deficient expression and enzymatic activity of GFPT1 impairs protein glycosylation resulting in dysfunction of NMJ-associated processes. We used a previously published

Gfpt1-CMS mouse with muscle specific removal of GFPT1 expression, termed *Gfpt1*$^{tm1d/tm1d}$, which recapitulates clinical features and muscle pathology of human GFPT1-CMS including exercise-induced skeletal muscle weakness, and tubular aggregates **[23,25,26]**. We identified a lower molecular weight species of the acetylcholine receptor delta subunit (AChRδ) in the *Gfpt1*-CMS mouse. Finally, we confirmed that *Gfpt1*-deficient mice show overall impaired O-GlcNAcylation levels, resulting in impairment to downstream glycan chain development.

2. Materials and Methods

2.1 Animal husbandry

Animals were housed at the University of Ottawa Animal Care and Veterinary Facility (Roger Guidon Hall, Ottawa, Canada) and all breeding and experimental protocols were approved by the internal Animal Care Committee (protocols: breeding - CHEO-3089 and experimental - CHEO-3120 approved on 16-11-2018 and 02-04-2019, respectively). Mice were maintained on a 12-hr light-dark cycle, with access to food and water *ad libitum.* Mice were generated and genotyped as previously reported **[25]**. For this study, Tm1C homozygous mice (containing the two LoxP sites flanking the 7th exon of *Gfpt1* but lack *Ckm-Cre* expression) were used as controls. *Gfpt1*$^{tm1d/tm1d}$ contains two LoxP sites flanking the 7th exon of *Gfpt1* but, also contains *Ckm-Cre* to create a skeletal muscle-specific knockout of *Gfpt1* **[25]**. Previously, *Gfpt1*$^{tmqd/tm1d}$ mice were characterized have knocked out Gfpt1 protein levels within cardiac and muscle tissues [25]. Also, Gfpt1 expression was found in brain and kidney demonstrating that this model is a Gfpt1 muscle specific knockout [25]. Mice were monitored and weighed three times per week and underwent a number of behavioural tests (see below) before tissue collection at 40-weeks.

2.2 Inverted screen test

Performed as described **[25]**. To briefly summarize, animals were suspended from an inverted wire grid, and the time to fall was recorded, with a cap of 10 minutes. Mice had a 30-minute rest, and the

test was repeated. The average time was recorded and normalized to body weight to calculate hanging impulse (g*sec). This behavioural test was performed weekly.

2.3 Grip strength and fatiguability measurements

Repetitive grip strength measurements were conducted weekly with 8 consecutive recordings on a grip strength meter (Chatillon DFE II Grip Meter, Columbus Instruments). Repetitive grip strength measurements were first conducted on the front paws. Animals then had a 30-minute rest period, followed by all four paws measurements. To calculate grip strength fatigability, all measurements were normalized to body weight (g) prior to calculation:

$$Muscle\ Fatigability\ \% = \left(\frac{Average\ of\ first\ four\ measurements - Average\ of\ last\ four\ measurements}{Average\ of\ measurements}\right)$$

2.4 EchoMRI and total activity measurements

EchoMRI body composition measurements of fat mass and lean mass were recorded weekly using the EchoMRI-700 Body Composition Analyzer. Animals also underwent 24-hour open activity monitoring using the Phenotyper™ system (Noldus Information Technology) at week 35. Total distance traveled was calculated using the Phenotyper™ analysis software.

2.5 Electrophysiology and repetitive nerve stimulation

Electromyography (EMG) was performed on a *Gfpt1*$^{tm1d/tm1d}$ and Tm1C homozygous mouse to examine compound muscle action potential (CMAP) and repetitive nerve stimulation (RNS) decrement with the Cadwell Sierra Summit EMG. Mice were anaesthetized with isoflurane (Baxter, #CA2L9108) prior to experimentation. To examine CMAP and RNS recording electrodes (Cadwell, #302353-000-100) were placed on the skin near the proximal portion of the gastrocnemius muscle of the hind limb, and the second electrode was placed in the *tibialis anterior*. For stimulation of the sciatic nerve two electrodes

(cathode and anode) were inserted in the proximal hind limb and subcutaneous tissue overlaying the sacrum respectively. Submaximal CMAP responses were performed by stimulation of the sciatic nerve with a square-wave pulse of 0.1 ms duration and an intensity range of 1 to 10 mA. CMAP response was increased in stimulus intensity until the amplitude of the response was seen on the monitor. To perform RNS, a stimulation series of 8 separate twitch contractions were elicited by 10 pulses ranging between 3 Hz and 20 Hz. The stimulation series was repeated after a rest of 30 seconds between measurements. Decrement was then calculated between the first and the fifth stimulus. CMAP and RNS calculations were performed with the Cadwell Sierra Summit software (Version 3.1.541) using a computer with Windows 10. Mice were euthanized after the recording without regaining consciousness.

2.6 Immunostaining for NMJs in whole muscle mounts

Soleus muscles were fixed in 2% paraformaldehyde (PFA) for 20 minutes. Skeletal muscle fibers were then separated into small bundles and placed in 2% PFA overnight. The fibers were washed with phosphate buffer saline (PBS) and then placed in ice cold Analar ethanol, then methanol for 10 minutes each. Fibers were then transferred to blocking/permeabilization solution (5% horse serum, 5% bovine serum albumin, 1% Triton X-100 in PBS) and incubated for 4 hours. The muscle fibers were then incubated with anti-SV2 (DSHB, 1:100) and neurofilament (DSHB (2H3), 1:100) in 5% horse serum, 5% BSA for 24 hours.

Fibers were then washed with PBS for 4 hours and incubated with secondary antibodies: alpha-bungarotoxin-488 (Invitrogen, #B13422, 1:200) and Alexa Fluor anti-mouse-568 (Life Technologies, #A11031, 1:250) overnight. Following this incubation, the muscle fibers were washed with PBS for 4 hours and mounted on glass microscope slides using Vectashield® Antifade Mounting Medium (Vector Laboratories, #H-1000-10). Prior to mounting the tissue, several layers of electrical tape were used to create a well to hold the tissue in place.

NMJ z-stacks were captured using a confocal microscope (Olympus Fluoview FV-1000) at 63x magnification and converted to maximum intensity projections. Image acquisition was performed sequentially with constant microscope settings.

2.7 Labelling of NMJs for laser capture microdissection

Gastrocnemius muscles were isolated from mice, embedded in O.C.T compound (Fisher Healthcare Tissue-Plus™, FisherScientific, #23-730-571) and stored at -80 ºC until sectioning. Gastrocnemius muscles were cryosectioned (Leica Biosystems, CM1860) longitudinally at 10 µm and placed on Superfrost™ Plus glass microscope slides (FisherScientific, #12-55015), and air-dried for 1 hour at room temperature. Sections were fixed with ice-cold acetone for 15 minutes at 4 °C and washed with PBS. Next, sections were incubated with permeabilization solution (PBS, 0.1% Triton X-100) for 15 minutes at room temperature, then washed with PBS. Then muscle sections were incubated with blocking buffer (1% BSA, 10% normal goat serum (NGS) in PBS) for 30 minutes at room temperature. Finally, the muscle sections were incubated with α-bungarotoxin-594 (Fisher Scientific, #B13423, 1:100) for 2 hours and washed with PBS. Muscle sections were stored at 4 ºC and allowed to air dry for 1 hour before laser capture microdissection.

2.8 Laser capture of NMJs

NMJs were identified using a PALM MicroBeam laser capture microdissection microscope at 20x magnification (Carl Zeiss Laser Microdissection, PALMRobo 48 FTSS355-Laser System). The laser speed during cutting was set at 5%, while the laser energy was set to 70 Hz, with a Delta of 60 Hz.

NMJs and neighbouring laser captured muscle was collected in separate Zeiss AdhesiveCap opaque 500 Eppendorf tubes (Zeiss, #415190-9201-000). Proteins were extracted by incubating the samples with RIPA buffer (containing phosphatase and protease inhibitors) for 1 hour on ice, followed by centrifugation (Sorvall Legend Micro 21 R, ThermoScientific™) at 15,000 x g for 20 minutes. The

supernatants were combined with Laemmli buffer and boiled at 100°C for 5 minutes, and proteins were resolved with SDS-PAGE.

2.9 Cell culture

C2C12 cells (ATCC, #CRL-1722) were cultured in Dulbecco's Modified Eagle Medium (DMEM) high glucose media supplemented with 10% fetal bovine serum (FBS), 1% glutamine, and 1% penicillin/streptomycin. When myoblasts reached 95% confluence, the cells were washed with PBS and the growth medium was replaced with differentiation medium (DMEM high glucose, 2% horse serum, and 1% penicillin/streptomycin) to promote myoblast fusion into myotubes. After five days, C2C12 myotubes were imaged with phase-contrast light microscopy (EVOS Cell Imaging Systems, Thermofisher) to confirm the presence of myotubes (elongated cells with more than one nuclei). All cell experiments were maintained in a humidified environment at 37 ºC with 5% CO_2.

The GFPT1/Gfpt1 inhibitor, 6-diazo-5-oxo-l-norleucine (DON) (500 μM, Sigma, #D2141), and the Oga inhibitor Thiamet-G (TG) (5 μM, Cayman, #13237) were administered for 48 hours.

2.10 Transducing C2C12 cells with lentiviruses expressing shGfpt1 transgenes

C2C12 cells were transduced with a lentivirus encoding a tetracycline repressor (TET-R) transgene (Vector Biolabs, pLV(EXP)-CMV>tTS/rtTA/Hygro, Vector ID: VB161122-1052kwm) at multiplicities of infection (MOIs) ranging from 1 to 500. Selective pressures were applied by adding 500 μg/mL of hygromycin B (Calbiochem, #400053) to generate a polyclonal stable cell line. *TET-R* expression was confirmed through RT-qPCR. C2C12 polyclonal TET-R positive cells were seeded to generate single-cell monoclonal colonies expressing TET-R.

Monoclonal TET-R positive C2C12 cells were then infected with lentiviruses containing the transgenes for either a scramble sequence (Vector ID: VB200625-1130ssr), shGfpt1 #1 (Vector ID: VB200624-1008wvj), or shGfpt1 #2 (Vector ID: VB200625-1131yeg), each containing a tetracycline promoter and

an eGFP reporter. C2C12 cells were infected with these viruses at varying Multiplicity of Infection (MOIs) and 5 μg/mL puromycin (Life Technologies, #A1113803) was applied as a selective pressure to establish a stable polyclonal expressing cell line.

To induce the expression of the transgenes, 2 μg/mL of doxycycline (Sigma, #D9891) was added. After 48 hours, eGFP expression in lentiviral infected C2C12 cells was documented using an EVOS cell imager. Polyclonal colonies were individually assessed to confirm a knockdown of Gfpt1 and subsequent activation of eGFP signal before monoclonal colony expansion.

2.11 Fluorescence-activated cell sorting (FACS) of Gfpt1-deficient C2C12 myoblasts

Doxycycline-inducible scramble, shGfpt1 #1, and shGfpt1 #2 C2C12 myoblasts were seeded onto 15 cm plates and treated with 2 μg/mL doxycycline for 72 hours. eGFP expression was assessed via an EVOS cell imager prior to FACS (Sony Biotechnologies SH800 Cell Sorter). C2C12 cells were trypsinized, centrifuged, and prepared to a concentration of 1.0 x 10^6 cells/mL. Dead cells were identified with 1 μg/mL propidium iodide (PI) (STEMCELL Technologies, #75002).

Cells were then sorted into the following groups: eGFP-/PI-, eGFP+/PI-, eGFP-/PI+, and eGFP+/PI+. Subsequently, eGFP+/PI- and eGFP-/PI+ populations were used to establish gates for removing any autofluorescence signal. Finally, a final population of eGFP+/PI+ cells was isolated and plated into a 6-well plate for expansion.

2.12 Gfpt1 enzymatic activity assay

The enzymatic activity of Gfpt1 was measured using the glutamate dehydrogenase method, as previously reported **[22,51]**. C2C12 cells were treated with a range of doses (between 0 μM and 500 μM) of Gfpt1 inhibitor DON for 48 hours. Additionally, scramble, shGfpt1 #1, and shGfpt1 #2 C2C12 myotubes were assessed for Gfpt1 enzymatic activity after 72 hours of induction with 2 μg/mL doxycycline. The change in absorbance is monitored at a wavelength of 370 nm (OD370) with a

spectrophotometer microplate reader (BioTek Synergy HTX Multimode Reader) using the Agilent Biotek Gen5 software v2.06. The enzymatic activity of each condition was normalized to the Gfpt1 protein levels determined by Western blot. All measurements were performed in triplicate.

2.13 Real time qPCR (RT-qPCR)

RNA collection for *in vitro* experiments was performed using the RNeasy™ Micro mini kit (Qiagen, #74134). Skeletal muscle RNA extraction was performed with the RNeasy™ Fibrous Micro mini kit (Qiagen, #74704) and quantified by nanodrop. RNA was converted to cDNA with the All-In-One 5x RT MasterMix (ABM, #G592). qPCR was performed using the PowerUp™ SYBR™ Green Master Mix (ThermoScientific, #A25741) with the QuantStudio™ Studio 6 Flex Real-Time PCR System (Thermofisher) (Supplementary Materials Table S1).

2.14 Tissue/cell lysis and Western blotting

Cell lysates and skeletal muscle homogenates were prepared with RIPA buffer supplemented with protease (Roche, #04693116001) and phosphatase (Roche, #PHOSS-RO) inhibitors, and Thiamet-G (Abcam, #ab146193) to prevent the loss of O-GlcNAc modification. Samples were centrifuged at 15,000 x g for 10 minutes at 4 °C, and the supernatant was collected. For muscle homogenates, tissue was combined with lysis buffer and a metal bead in 2 mL SafeLock™ Eppendorf tubes (Eppendorf, #022363352). Samples were then subjected to homogenization using a TissueLyser II (Qiagen) at 30Hz for 90 seconds, followed by an incubation on ice for 60 seconds. This process was repeated 3 times. After homogenization, samples were left at 4°C for 4 hours on a rotating platform and then centrifuged at 15,000 x g for 15 minutes at 4 °C. Total protein concentration was determined using a DC Protein Assay with BSA as a standard. Proteins were resolved by SDS-PAGE and transferred to PVDF membranes using a semi-dry BioRad™ Trans-Blot Turbo transfer system. For assessment of poly-sialyation measurements a wet-transfer was performed overnight at 40 V.

Membranes were blocked with Intercept TBS blocking buffer (Li-Cor, #927-6000) and incubated with primary antibodies in blocking solution overnight at 4 °C. After washing with TBS + 1% Tween-20, membranes were incubated with IR Dye®800CW Donkey anti-Mouse IgG (Li-Cor, #926-32212, 1:5000) and IR Dye®680RD Goat anti-Rabbit IgG (Li-Cor, #926-68071, 1:5000) for 1 hour at room temperature. Proteins were visualized using a Licor Odyssey, and densitometry was performed using Image Studio™.

2.15 PNGase F and α2-3, 6, 8 neuraminidase reactions

To examine the glycosylation status of the AChRδ subunit, 20 µg of tissue lysates were combined with either PNGaseF (New England Biolabs, #P0704S) or α2-3, 6, 8 Neuraminidase (New England Biolabs, #P0720S) according to manufacturer's instructions. AChRδ protein levels and molecular weight was assessed via Western blot.

2.16 Antibodies

The following antibodies were used for Western blot experiments: Gfpt1 (ProteinTech, #14132-1-AP, 1:500), Gapdh (14C10) (Cell Signalling, #2118, 1:2000), O-GlcNAc (RL2) (Novus, #NB300-524, 1:1000), Ogt (ProteinTech, #66823-1-Ig, 1:1000), Desmin (ProteinTech, #16520-1-AP, 1:1000), AChRα (ProteinTech, #10613-1-AP, 1:1000), AChRδ (C-4) (Santa Cruz, #sc-390896, 1:1000), MuSK (RD Systems, #AF562, 1:500), PolySia 735 (gift from Dr. Rita Gerardy-Schahn, Hannover, Germany, 1:1000), Vinculin (7F9) (Santa Cruz, #sc-73614, 1:2000), biotinylated- succinylated wheat germ agglutinin (sWGA) (Vector Laboratories, #B-1025S-5, 1:1000), IRDye® 800CW Streptavidin (Li-Cor, #926-32230, 1:5000). For NMJ staining from whole muscle mounts, SV2 antibody (DSHB, #, 1:250), and neurofilament M (DSHB, 2H3, 1:250).

2.17 Statistics

Data was analyzed with GraphPad Prism v 10.1.2. Data was checked for normality using the D'Agostino-Pearson test and the appropriate statistical test was applied as described in the figure legends. Any outlier was identified using the Robust regression and Outlier remover method (ROUT).

Statistical significance was determined by using unpaired two-tailed Student's t-tests or analysis of variance (ANOVA). If multiple comparisons were performed a Tukey's post-hoc test was performed. Results are given as mean ± S.D and $p < 0.05$ was considered significant.

3. Results

3.1. Skeletal muscle knockout of Gfpt1 (Gfpt1$^{tm1d/tm1d}$) in mice hasprogressive muscle fatigability with impaired NMJ morphology:

We used the previously published Gfpt1 skeletal muscle-specific knockout mouse model termed *Gfpt1$^{tm1d/tm1d}$* for these investigations [25]. These mice express two LoxP sites flanking the seventh exon of Gfpt1, which also contains Cre recombinase controlled by the creatine kinase (*Ckm*) promoter (Figure 1A). This causes a truncation to occur within Gfpt1, targeting it for degradation. These mice lack *Gfpt1* gene expression and thus the corresponding protein in muscle (Supplementary Figure 1A & B) The previous characterization of these mice revealed modest behavioural and phenotypic changes as well as NMJ abnormalities up to 26 weeks of age [25]**.** In this study we used 40-week-old mice to help identify the phenotypic and molecular changes, anticipating these would be progressive and more pronounced in older animals (Supplementary Figure 1C).

Over 40 weeks *Gfpt1$^{tm1d/tm1d}$* mice did not exhibit significant differences in body weight compared to Tm1C homozygous control animals (Figure 1B). However, they did have a significant increase in body fat percentage, reflecting a decrease in lean body mass (Figure 1C). *Gfpt1$^{tm1d/tm1d}$* mice also demonstrated a progressive impairment in the latency to fall (Figure 1D & Supplementary Figure 1D), no significant change in maximal grip strength, but an increase in grip strength fatigability was

observed (Figure 1E & Supplementary Figures 1E - 1G). Also a significant decrease in total mouse activity (Supplementary Figure 1H). Next, we performed EMG recordings in an older (54-week-old) *Gfpt1*$^{tm1d/tm1d}$ and Tm1C homozygous mouse. The *Gfpt1*$^{tm1d/tm1d}$ mouse had a shorter amlitude in sub-maximal CMAP measurments (14.8 mV to 36. 1mV) (Supplementary Figure 2A). The sub-maximal CMAP was used for RNS recordings at low-frequency (3 Hz) and high-frequency (20 Hz). We found that the *Gfpt1*$^{tm1d/tm1d}$ experienced a decrement at low-frequency (~12% at 3 Hz) and high-frequency (~25% at 20 Hz) RNS exceeding 10%, while minimal decrement was measured within the Tm1C homozygous control mouse (Supplementary Figure 2B – E). An CMAP decrement of 10% is commonly used as a threshold for to diagnose muscular fatigue in CMS patients [20,59]. Finally, examination of the NMJs revealed that *Gfpt1*$^{tm1d/tm1d}$ mouse skeletal muscle had smaller, and less complex NMJs when compared to Tm1C homozygous control animals (Figure 1F). These results confirm our previous study demonstrating that *Gfpt1*$^{tm1d/tm1d}$ mice exhibit increased muscle fatigability, reduced grip strength, and impaired NMJ morphology. The maintenance of body weight with an increasing body fat percentage suggests muscle loss may be occurring, explaining in part the changes in fatigue, strength and the failure of neuromuscular transmission.

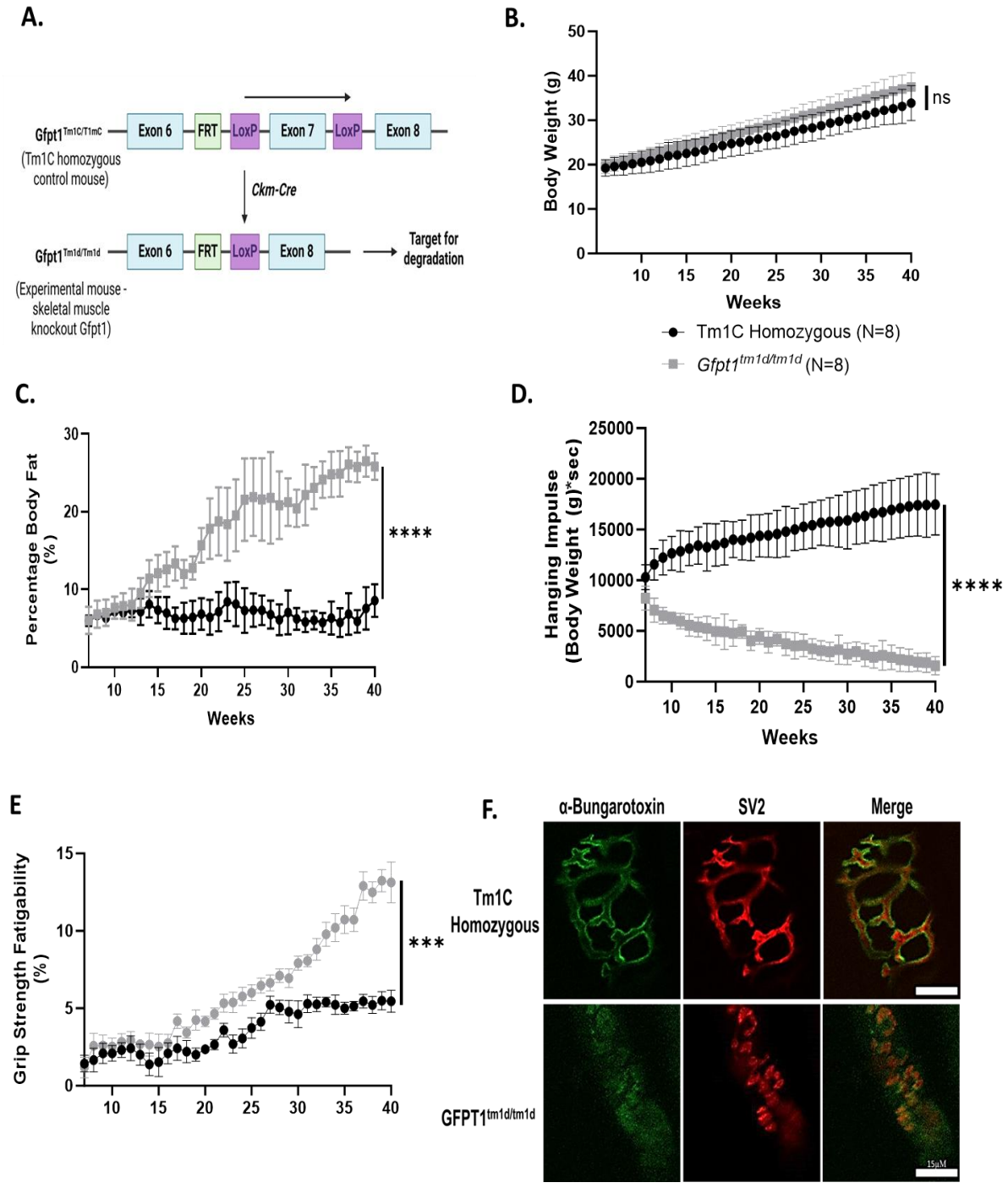

Figure 1: *Gfpt1*$^{tm1d/tm1d}$ mice exhibit progressive fatigable muscle weakness with disrupted NMJ morphology. (**A**) Our previously published, *Gftp1*$^{tm1d/tm1d}$ mouse model was developed with Cre/LoxP technology. This model contains two LoxP sites which flank the seventh exon of Gfpt1 (termed *Gftp1*$^{tm1c/tm1c}$). Gfpt1$^{tm1c/tm1c}$ mice are crossed with the Ckm-Cre expressing mouse to

produce a heterozygous mouse containing Ckm-Cre and the LoxP flanking Gfpt1, termed *Gfpt1*$^{Cre\text{-}Het}$. The *Gfpt1*$^{Cre\text{-}Het}$ mice were crossed with *Gfpt1*$^{tm1c/tm1c}$ mice to produce the *Gftp1*$^{tm1d/tm1d}$ mouse line. The *Gftp1*$^{tm1d/tm1d}$ mouse model expresses a skeletal muscle-specific truncation of Gfpt1 which is targeted for degradation. (**B**) Mice were weighed 3 times per week over 40 weeks; *Gfpt1*$^{tm1d/tm1d}$ mice showed no significant difference in body weight when compared to Tm1C homozygous control mice. (**C**) There was a significant increase in body fat percentage in *Gfpt1*$^{tm1d/tm1d}$ mice over the same period (EchoMRI). (**D**) *Gftp1*$^{tm1d/tm1d}$ mice have a progressive reduction in hanging impulse when compared to Tm1C homozygous control mice. (**E**) Repetitive grip strength measurements demonstrated *Gftp1*$^{tm1d/tm1d}$ mice have increased muscle fatigability compared to Tm1C homozygous control mice. (**F**) NMJs from soleus muscle were labelled with anti-synaptic vesicle 2, to label pre-synaptic nerve terminals (red) and α-bungarotoxin, to visualize AChR clusters (green). All graphs show mean ± SD, statistical significance was determined via a two-way ANOVA. N=8 for both Tm1C homozygous control mice and Gfpt1$^{tm1d/tm1d}$ mice. *** P – value < 0.001, **** < 0.0001.

3.2. *Gfpt1*$^{tm1d/t1md}$ mice exhibit hypo-glycosylated AChRδ subunits

A previous study indicated that a reduction in Gfpt1 protein levels resulted in a decrease in AChR subunit expression within TE671/DB40 cells [28]. Therefore, we investigated the expression of AChR subunits within skeletal muscle isolated from *Gfpt1*$^{tm1d/tm1d}$ mice. *Gfpt1*$^{tm1d/tm1d}$ skeletal muscle exhibited a significant reduction in *Chrnd* and *Chrna1* RNA (Figure 2A & B) and AChRδ protein levels in the quadriceps (Figure 2C & D). Furthermore, AChRδ appeared as two bands on the western blot of both Tm1C homozygous control and *Gfpt1*$^{tm1d/tm1d}$ skeletal muscle, an upper molecular weight species at ~65 kDa and a lower molecular weight species at ~60 kDa (Figure 2C). The lower molecular weight species of AChRδ was more prominent in *Gfpt1*$^{tm1d/tm1d}$ quadriceps muscle than control animals (Figure 2C and E). This effect was also observed in the gastrocnemius muscle (Supplementary Figure 3A - C).

No drop in protein levels or a 2nd molecular weight species of the AChRα subunit were visible in *Gfpt1*$^{tm1d/tm1d}$ quadriceps muscle (Figure 2F & G). Also, we assessed Lrp4 protein levels in whole muscle lysates. We established that there was also no drop in protein levels or a 2nd molecular weight species visible within *Gftp1*$^{tm1d/tm1d}$ quadriceps (Supplementary Figure 3D & E). The prominence of the lower molecular weight of AChRδ in *Gfpt1*$^{tm1d/tm1d}$ prompted us to determine its origin.

The AChRδ subunit is a tightly regulated glycoprotein with several previously reported sites for glycosylation *[60,61]*. We used the N-linked glycanase, PNGaseF, which cleaves the innermost GlcNAc modification of complex oligosaccharides bound to asparagine residues, to determine if the lower AChRδ molecular weight species is differentially glycosylated in *Gfpt1*$^{tm1d/tm1d}$ muscle. In both *Gfpt1*$^{tm1d/tm1d}$ muscle and Tm1C homozygous control muscle lysates, the upper molecular weight species disappeared after PNGase F treatment, to its unglycosylated core species (Figure 2H & I). Additionally, the lower molecular weight species of AChRδ found in *Gfpt1*$^{tm1d/tm1d}$ skeletal muscle also disappeared following treatment with PNGase F (Figure 2H & I). This indicates that both molecular weight species of AChRδ are glycoproteins, and that the lower molecular weight species shows an altered, potentially immature or aberrant, glycosylation profile.

UDP-GlcNAc, the product of the HBP, can be used for terminal N-linked glycan chain substrates such as sialyation. Sialyation is a terminal glycan chain PTM, which has been implicated in various disorders such as GNE Myopathy, and sarcopenia. We wanted to investigate whether protein sialylation is deficient in Gfpt1-depleted mouse muscle. While poly-sialylation was significantly reduced in *Gfpt1*$^{tm1d/tm1d}$ quadriceps (Supplementary Figure 3F & G) there were no changes in sialyation of the AChRδ subunit and Desmin (Supplementary Figure 3H). This indicated that AChRδ is siaylated, that modification did not account for a molecular weight shift. Taken together, these results suggest that AChRδ, has multiple glycoproteins present, which are differentially expressed in *Gfpt1*$^{tm1d/tm1d}$ skeletal muscle, and that this lower molecular weight species may be an immature glycoprotein.

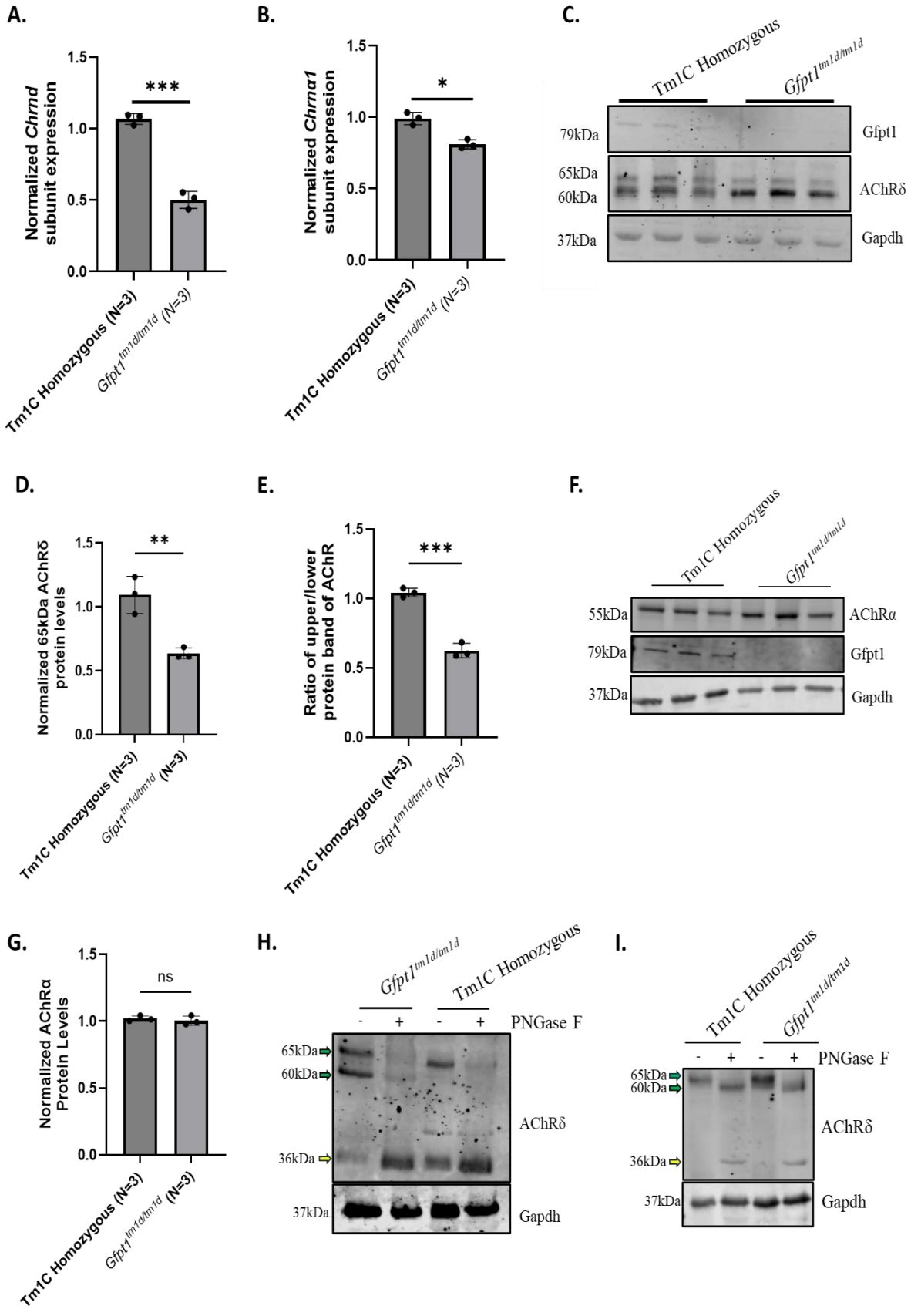
A.
Normalized Chrnd subunit expression
***
Tm1C Homozygous (N=3)
Gfpt1tm1d/tm1d (N=3)
B.
Normalized Chrna1 subunit expression
*
Tm1C Homozygous (N=3)
Gfpt1tm1d/tm1d (N=3)
C.
Tm1C Homozygous
Gfpt1tm1d/tm1d
79kDa
Gfpt1
65kDa
60kDa
AChRδ
37kDa
Gapdh
D.
Normalized 65kDa AChRδ protein levels
**
Tm1C Homozygous (N=3)
Gfpt1tm1d/tm1d (N=3)
E.
Ratio of upper/lower protein band of AChR
***
Tm1C Homozygous (N=3)
Gfpt1tm1d/tm1d (N=3)
F.
Tm1C Homozygous
Gfpt1tm1d/tm1d
55kDa
AChRα
79kDa
Gfpt1
37kDa
Gapdh
G.
Normalized AChRα Protein Levels
ns
Tm1C Homozygous (N=3)
Gfpt1tm1d/tm1d (N=3)
H.
Gfpt1tm1d/tm1d
Tm1C Homozygous
- + - +
PNGase F
65kDa
60kDa
AChRδ
36kDa
37kDa
Gapdh
I.
Tm1C Homozygous
Gfpt1tm1d/tm1d
- + - +
PNGase F
65kDa
60kDa
AChRδ
36kDa
37kDa
Gapdh

Figure 2: *Gfpt1*$^{tm1d/tm1d}$ mice exhibit impaired *Chrnd* gene and AChRδ protein expression with the presence of an altered molecular weight banding pattern. (**A**) *Chrnd* and (**B**) *Chrna1* gene expression are reduced in quadriceps isolated from 40-week-old *Gfpt1*$^{tm1d/tm1d}$ mice normalized to refernce gene expression. (**C**) A lower molecular weight species (60 kDa) can be detected in AChRδ in *Gftp1*$^{tm1d/tm1d}$ skeletal muscle lysates on western blot. (**D**) AChRδ protein levels are reduced in *Gfpt1*$^{tm1d/tm1d}$ skeletal muscle compared to Tm1C homozygous control mice, normalized to Gapdh loading control. (**E**) *Gfpt1*$^{tm1d/tm1d}$ mice exhibited a reduction in the ratio of the upper molecular weight species and the lower molecular weight species of AChRδ upon comparison to Tm1C homozygous control mice. (**F**) Provided the change in AChRδ, we examined additional AChR subunit protein levels. There was no discernable change in molecular wieght with AChRα. (**G)** There was no significnat change in AChRα protein levles within *Gfpt1*$^{tm1d/tm1d}$ quadricep. (**H**) A Western blot showing quadriceps and (**I**) gastrocnemius muscle lysates from *Gfpt1*$^{tm1d/tm1d}$ and Tm1C homozygous control following treatment with PNGase F. PNGaseF treatment resulted in the migtation of the 65kDa and 60kDa species of AChRδ species suggesting that the lower moelcular weight is hypo-glycosylated. The molecular weight species of AChRδ are labelled with a green and yellow arrows. For *invivo* experiments assessing protein levels and RNA expression three mice were assessed (n = 3). Graphs show mean ± SD, statistical significance was determined by student T-Test. * P-value < 0.05, *** P-value < 0.001.

3.3 Gfpt1-deficient C2C12 cells exhibit reduced AChRδ protein levels with a lower molecular weight species

To further investigate the impact of Gfpt1 deficiency on cellular processes, we established a Gfpt1-depleted C2C12 cell line (Figure 3A) using a lentiviral system to infect myoblasts with a tetracycline-inducible scramble, shGfpt1 #1 or shGfpt1 #2 transgene (Figure 3B, Supplementary Figures 4A – F).

These myoblasts had a ~70% and ~63% reduction in Gfpt1 protein levels with shGtpt1 #1 and 2 respectively, when compared to scramble (Figure 3C & D).

Next, we wanted to determine if our Gfpt1-deficient C2C12 myotubes had reduced AChR subunit expression. Following activation with doxycycline, both *Chrnd* and *Chrna1* expression levels were reduced by nearly ~50% in Gfpt1-depleted myotubes (Figure 3E & F). In addition, a decrease was also observed in the protein levels of AChRδ. (Figure 3G & H). Similarly to Gfpt1$^{tm1d/tm1d}$ skeletal muscle, AChRδ expressed two molecular weight species in Gfpt1-depleted myotubes (Figure 3G). The expression of the lower molecular weight species in Gfpt1-depleted C2C12 myotubes led to a reduced ratio in AChRδ protein levels of the upper to the lower molecular weight band (Figure 3I). In addition, as observed in *Gfpt1*$^{tm1d/tm1d}$ skeletal muscle there was no change in AChRα protein levels in Gfpt1-deficient C2C12 myotubes (Figure 3G & J). Taken together, these results support our findings in Gfpt1$^{tm1d/tm1d}$ mice indicating an impairment to Gfpt1 causes altered glycosylation of AChRδ resulting in the increased expression of a lower molecular weight species.

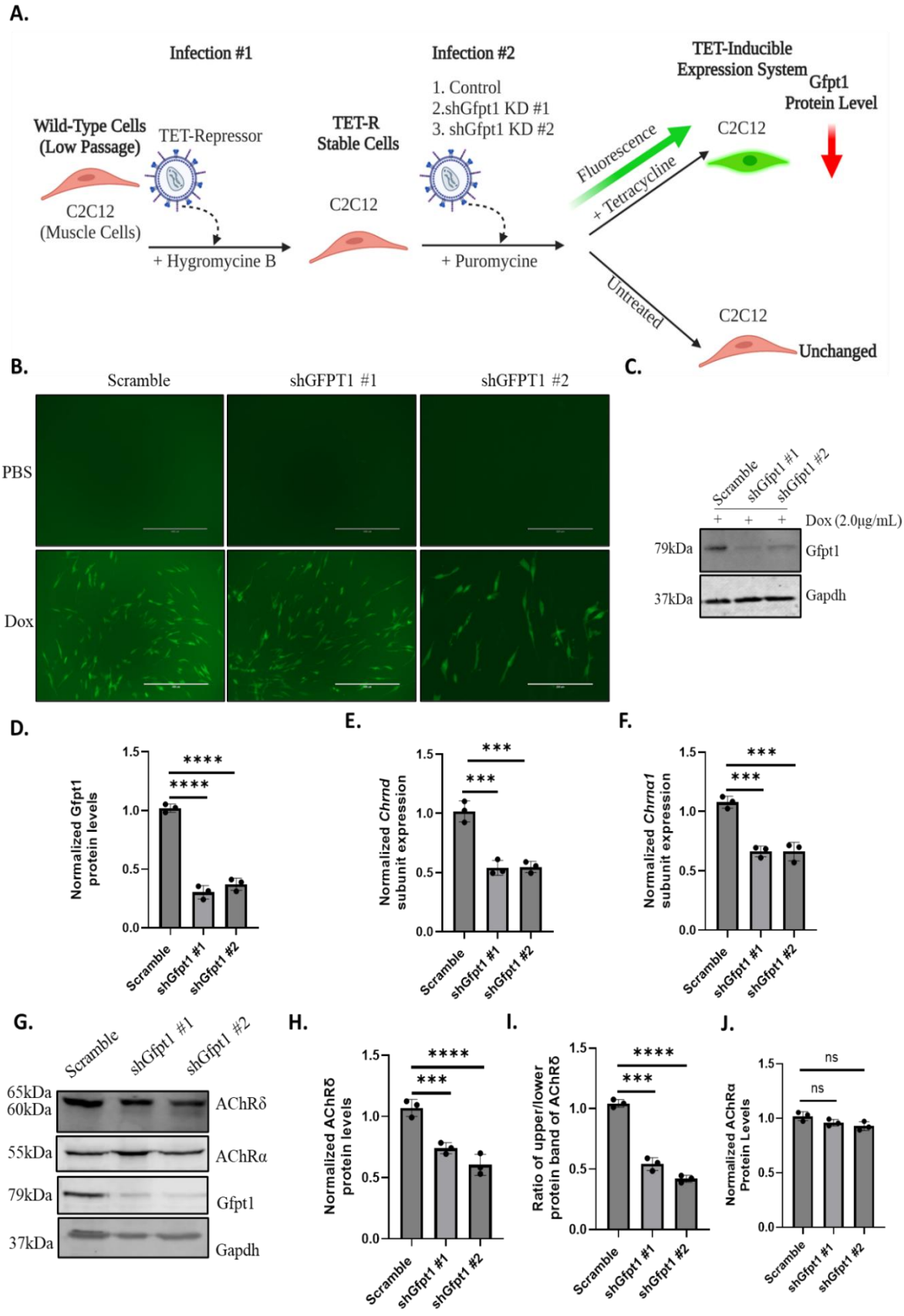
A.
Infection #1
Infection #2
TET-Inducible Expression System
Gfpt1 Protein Level
Wild-Type Cells (Low Passage)
TET-Repressor
C2C12 (Muscle Cells)
+ Hygromycine B
TET-R Stable Cells
C2C12
1. Control
2.shGfpt1 KD #1
3. shGfpt1 KD #2
+ Puromycine
Fluorescence
+ Tetracycline
C2C12
Untreated
C2C12
Unchanged
B.
Scramble
shGFPT1 #1
shGFPT1 #2
PBS
Dox
C.
Scramble
shGfpt1 #1
shGfpt1 #2
Dox (2.0μg/mL)
79kDa
Gfpt1
37kDa
Gapdh
D.
Normalized Gfpt1 protein levels
E.
Normalized Chrnd subunit expression
F.
Normalized Chrna1 subunit expression
G.
65kDa
60kDa
AChRδ
55kDa
AChRα
79kDa
Gfpt1
37kDa
Gapdh
H.
Normalized AChRδ protein levels
I.
Ratio of upper/lower protein band of AChRδ
J.
Normalized AChRα Protein Levels
ns

Figure 3: Gfpt1 deficient C2C12 myotubes exhibit impaired AChRδ protein levels, with the presence of a lower molecular weight species. (**A**) Gfpt1-deficient C2C12 myoblasts were created using a tetracycline-inducible lentiviral system. A lentivirus encoding a tetracycline repressor (TET-R) was used to infect C2C12 cells, under the selection of hygromycin. Next, a scramble, shGfpt1 #1 and shGfpt1 #2 expressing transgene was infected into Tet-R positive C2C12 cells. Cells infected with the scramble and Gfpt1-deficient transgenes were selected with puromycin. (**B)** Exposure to doxycycline activates an eGFP reporter in scramble, shGfpt1 #1 and shGfpt1 #2 stable C2C12 cells. Scale bar 200μm. Gfpt1 protein levels in Gfpt1-deficient C2C12 myoblasts upon activation with doxycycline. (**C** and **D**) A reduction in Gfpt1 protein levels after treatment with doxycycline in Gfpt1-deficient C2C12 myoblasts was observed. (**E**) Gfpt1-deficiency in C2C12 myotubes impairs the expression of *Chrnd* and (**F**) *Chrna1*. (**G**) Gfpt1-depleted myotubes express a lower molecular weight 60kDa species of AChRδ that was not present in scramble control conditions. (**H**) A reduction in AChRδ protein levels in Gfpt1-depleted C2C12 myotubes was observed. (**I**) Densitometry was used to show a reduction in the ratio of the upper molecular weight of AChRδ and the lower molecular weight species of AChRδ in C2C12 myotubes. (**J**) There was no significant change in AChRα protein levels between scramble and Gfpt1-deficient myotubes. For *in vitro* experiments protein levels and RNA expression were analyzed by three separate experiments (n = 3). Graphs are presented as mean ± SD, statistical significance was determined by one-way ANOVA. *** P-value< 0.001, **** P-value<0.0001.

3.4 NMJ-specific expression of the lower molecular weight AChRδ subunit

Whole muscle lysates have diluted levels of NMJ-associated proteins in large-scale proteomic analysis, and these analyses do not reveal whether the NMJ proteins are correctly localizedl[62,]. Therefore, we utilized laser capture microdissection (LCM) to isolate NMJs from cryo-sectioned skeletal muscle to assess NMJ-associated protein expression. We first validated this approach in gastrocnemius muscle

isolated from 25-week-old C57Bl/6N control mice (Supplementary Figure 5). NMJ-associated proteins AChRα, AChRδ, SV2, and MuSK were identified only in the NMJ isolate, but not in muscle tissue taken from bungarotoxin negative areas (Supplementary Figure 5D). The bungarotoxin negative areas served as our material with non-NMJs detected and were excised after each NMJ was collected. Additionally, both Desmin and Gapdh were detected in each isolate, suggesting that this enrichment technique successfully isolated NMJ-associated proteins.

To examine if both molecular weight species of AChRδ were found at the NMJs of *Gfpt1*$^{tm1d/tm1d}$ mice, muscle was sectioned longitudinally and stained for AChR clusters (Figure 4A). Approximately 1000 NMJs were isolated from *Gfpt1*$^{tm1d/tm1d}$ and Tm1C homozygous control mice (Figure 4B, Supplementary Figures 6A & B). Slightly more NMJs were collected from *Gfpt1*$^{tm1d/tm1d}$ mice, as previous studies had reported that *Gfpt1*$^{tm1d/tm1d}$ mice NMJs were smaller compared to Tm1C homozygous control (Supplementary Figure 6C). NMJ isolates expressed the AChRδ protein, which was absent in skeletal muscle (Figure 4C). The *Gfpt1*$^{tm1d/tm1d}$ NMJ isolate sample expressed both the upper and lower molecular weight species of AChRδ (Figure 4C). The lower molecular weight species was more abundant within the *Gfpt1*$^{tm1d/tm1d}$ NMJ isolate compared to the Tm1C homozygous control NMJs. Taken together, these results indicate that the lower molecular weight species localizes to the NMJ within all mice but is present in greater abundance in *Gfpt1*$^{tm1d/tm1d}$ NMJs, which may alter function of the AChR.

A.

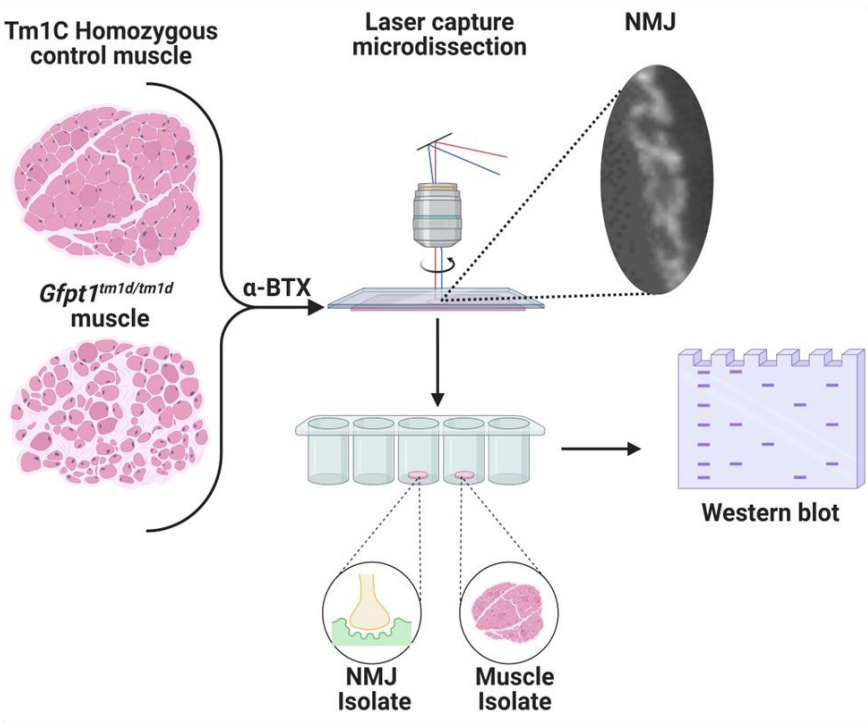
Tm1C Homozygous control muscle
Laser capture microdissection
NMJ
Gfpt1tm1d/tm1d muscle
α-BTX
Western blot
NMJ Isolate
Muscle Isolate

B.

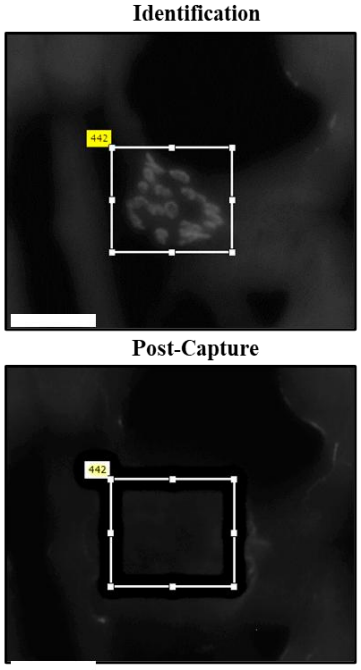
Identification
Post-Capture

C.

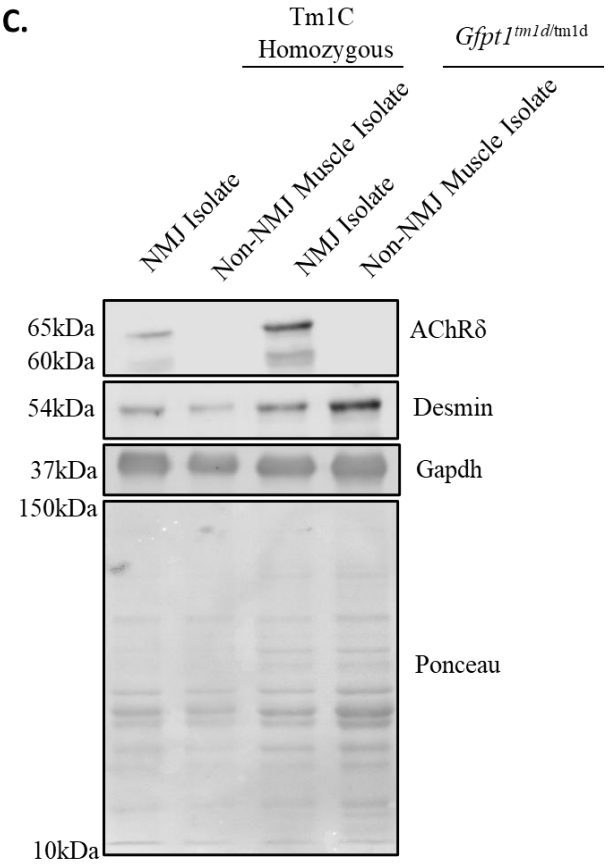
Tm1C Homozygous
Gfpt1tm1d/tm1d
NMJ Isolate
Non-NMJ Muscle Isolate
NMJ Isolate
Non-NMJ Muscle Isolate
65kDa
60kDa
AChRδ
54kDa
Desmin
37kDa
Gapdh
150kDa
Ponceau
10kDa

Figure 4: The lower molecular weight species is detected in the NMJs isolated from Gfpt$^{tm1d/tm1d}$ muscle. (**A**) Lasermicrodissection was used to enrich for NMJs in *Gfpt1*$^{tm1d/tm1d}$ and Tm1C homozygous control mice. Gastrocnemius muscles were longitudinally sectioned and stained for AChR clusters. (**B**) An image at 40x magnification of AChR clusters before and after isolation. Scale bar: 500 μm. (**C**) A Western blot of NMJ and muscle isolates from *Gfpt1*$^{tm1d/tm1d}$ and Tm1C homozygous control mice for the detection of AChRδ, Desmin and Gapdh. *Gfpt1*$^{tm1d/tm1d}$ NMJ isolate express an upper and lower molecular weight species for the AChRδ subunit, which was not observed in Tm1c homozygous control NMJ isolate. AChRδ was used to assess for NMJ-specific protein detection, while desmin and Gapdh were used to examine expression in both NMJ and muscle isolates to ensure sample purity.

3.5 Gfpt1-depleted models have impaired O-GlcNAcylation

UDP-GlcNAc, the downstream product of the HBP, is essential for the formation of N- and O-linked glycan structures, which are crucial for maintaining protein stability. In addition, UDP-GlcNAc can be used for protein O-GlcNAcylation, a small modification that is essential for cellular signalling (Figure 5A). OGT, an enzyme that transfers GlcNAc to protein moieties, regulates this reversible modification, along with the O-linked glycanase enzyme called OGA, which removes GlcNAc. We hypothesized that impairment to GFPT1/Gfpt1 expression and/or activity would result in reduced O-GlcNAcylation levels. Firstly, we used the Gfpt1 antagonist 6-diazo-5-oxo-l-norleucine (DON) to inhibit enzymatic activity *in vitro*. Through a dose-response analysis, we confirmed that Gfpt1 is inhibited without causing cellular toxicity in C2C12 cells at 500 μM DON for 48hrs (Figure 5B). Subsequently, we examined the levels of O-GlcNAcylation after DON treatment and showed a significant reduction in protein O-GlcNAcylation (Figure 5C & D). Additionally, treating cells with the Oga inhibitor, Thiamet-G, increased O-GlcNAcylation in wild-type C2C12 cells (Supplementary Figure 7A & B). These

results collectively indicate that Gfpt1 enzymatic activity is involved in O-GlcNAcylation of C2C12 cells *in vitro*.

Next, we wanted to determine if our Gfpt1-depleted cell models have reduced Gfpt1 enzymatic activity resulting in reduced protein O-GlcNAcylation levels. Gfpt1-depleted C2C12 myoblasts exhibited an altered Gfpt1 enzymatic activity (Supplementary Figure 7C). We found that Ogt levels were secondarily reduced in Gfpt1-depleted C2C12 myoblasts, indicating impaired output from O-GlcNAcylation as a result of reduced substrate availability (Figure 5E). To confirm these findings, we examined protein levels of Ogt and O-GlcNAcylation in Gfpt1-depleted C2C12 myoblasts and observed severe depletion in both (Figure 5F & G, Supplementary Figure 7D & E). We also used the lectin succinylated wheat germ agglutinin (sWGA), which has affinity for N-acetylglucosamine, but not sialic acid, and has been commonly used to observe alterations in O-GlcNAcylation levels with accompanying O-GlcNAc antibodies. Western blot was used on Gfpt1-deficient lysates which observed a significant decrease in the amount of sWGA bound to glycoproteins compared to controls, further suggesting glycosylation impairment is present (Supplementary Figure 7F & 7G).

Lastly, we examined if there was depleted O-GlcNAcylation in our *Gfpt1*$^{tm1d/tm1d}$ mouse model. We observed a reduction in protein O-GlcNAcylation levels in skeletal muscle derived of *Gfpt1*$^{tm1d/tm1d}$ mice. (Figure 5H & 5I). Additionally, using sWGA, we examined the amount of glycoprotein present within the *Gfpt1*$^{tm1d/tm1d}$ skeletal muscle and observed a significant decrease (Supplementary Figure 7H & 7I). These results collectively indicate that Gfpt1 depletion impairs protein glycosylation, which may be an important mechanism for Gfpt1-CMS by impacting on quality and abundance of NMJ-associated proteins. In addition, these results indicate that the impairment of O-GlcNAcylation likely affects many proteins at the NMJ and in skeletal muscle. However, further functional studies are needed to finally confirm if the AChRδ is O-GlcNAcylated.

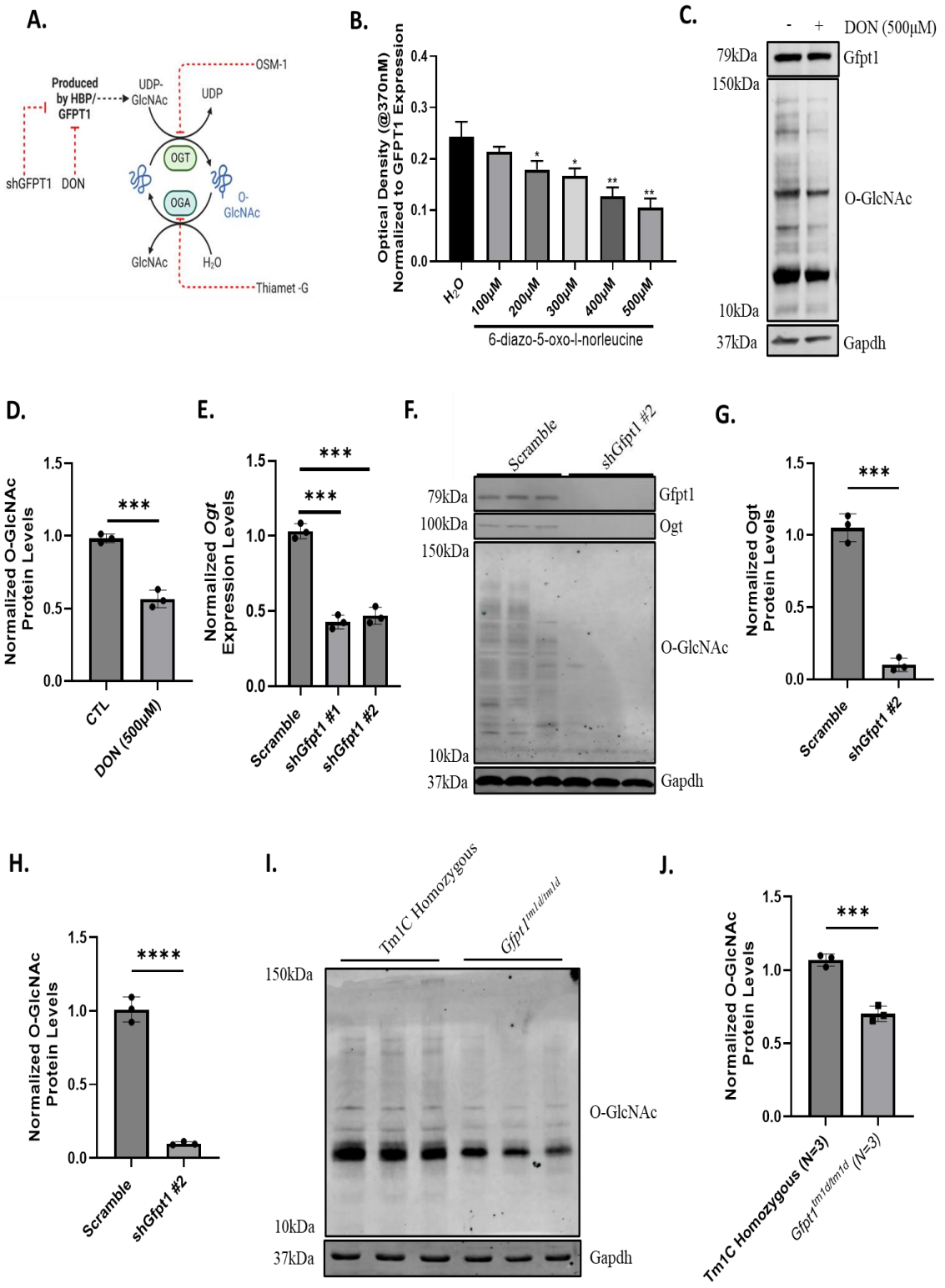
A.
Produced by HBP/-GFPT1
UDP-GlcNAc
UDP
OSM-1
OGT
OGA
O-GlcNAc
GlcNAc
H2O
shGFPT1
DON
Thiamet -G
B.
Optical Density (@370nM) Normalized to GFPT1 Expression
H2O
100μM
200μM
300μM
400μM
500μM
6-diazo-5-oxo-l-norleucine
C.
- + DON (500μM)
79kDa
Gfpt1
150kDa
O-GlcNAc
10kDa
37kDa
Gapdh
D.
Normalized O-GlcNAc Protein Levels
CTL
DON (500μM)
E.
Normalized Ogt Expression Levels
Scramble
shGfpt1 #1
shGfpt1 #2
F.
Scramble
shGfpt1 #2
79kDa
Gfpt1
100kDa
Ogt
150kDa
O-GlcNAc
10kDa
37kDa
Gapdh
G.
Normalized Ogt Protein Levels
Scramble
shGfpt1 #2
H.
Normalized O-GlcNAc Protein Levels
Scramble
shGfpt1 #2
I.
Tm1C Homozygous
Gfpt1tm1d/tm1d
150kDa
O-GlcNAc
10kDa
37kDa
Gapdh
J.
Normalized O-GlcNAc Protein Levels
Tm1C Homozygous (N=3)
Gfpt1tm1d/tm1d (N=3)

Figure 5: Impairment to GFPT1 activity or protein levels reduces protein O-GlcNAcylation *in vitro* and *in vivo*. (**A**) UDP-GlcNAc is a product of the HBP that, is required for O-GlcNAcylation. Ogt is used to transfer the GlcNAc moiety to the target protein, which can be reversed by Oga. These enzymes work in tandem to control the level of protein O-GlcNAcylation inside the cell. (**B**) The Gfpt1 antagonist, DON, gave a dose dependent decrease of Gfpt1 enzymatic activity in wild-type C2C12 cells. (**C**) Western blot of Gfpt1 protein and O-GlcNAc protein modification levels following treatment with DON in wild-type C2C12 cells. (**D**) DON treatment reduced O-GlcNAc modification levels in wild-type C2C12 cells. (**E**) Gfpt1-deficency reduces Ogt gene expression in C2C12 myotubes. (**F**) Gfpt1, Ogt, O-GlcNAc modification protein levels assessed via Western blot in Gfpt1-deficient C2C12 cells treated with doxycycline. (**G**) Gfpt1-deficient myotubes had reduced levels of Ogt and (**H**) protein O-GlcNAc modification after treatment with doxycycline. (**I**) A Western blot was used to examine O-GlcNAc levels in $Gfpt1^{tm1d/tm1d}$ and Tm1C homozygous control mice in quadricep muscle. (**J**) $Gfpt1^{tm1d/tm1d}$ mice exhibit a reduction in O-GlcNAc protein modification levels upon comparison Tm1C homozygous control mice isolated quadricep. Graphs are mean ± SD, N = 3 for all experiments, statistical significance was determined by student T-Test. A one-way ANOVA was perfromed for statistical significance. * P-value < 0.05, P-value ** < 0.01, P-value *** < 0.001 and **** P-value <0.0001.

4. Discussion

GFPT1 is the rate-limiting enzyme of the HBP, a metabolic pathway that produces UDP-GlcNAc, a key precursor for protein glycosylation **[39,40]**. Biallelic mutations to *GFPT1* cause CMS, a rare neuromuscular disease characterized by fatigable muscle weakness **[21,22,24–29]**. These mutations to *GFPT1* reduce enzymatic activity and protein expression within the skeletal muscle, decreasing the

production of UDP-GlcNAc, an essential precursor for protein glycosylation **[22,28,51]**. Glycosylation is a PTM which attaches sugar moieties to target proteins at various amino acids allowing for enhanced solubility and stability. At the NMJ, glycosylation is an essential modification that controls the stability of key receptor complexes both in the pre- and post-synaptic regions **[60,63]**. It remains unclear how an enzyme essential for protein glycosylation, which is ubiquitously expressed in the body, impairs neurotransmission and NMJ maintenance in GFPT1-related CMS. We hypothesized that a deficiency of Gfpt1 would result in the improper glycosylation of key NMJ-associated proteins impairing function and/or stability within the NMJ and thus analyzed murine *in vivo* and *in vitro* models depleted or even deficient for Gfpt1 in skeletal muscle cells.

We demonstrate that there is a glycosylation deficiency within Gftpt1-depleted models and that these models express an elevated amount of an immature glycoprotein of the AChRδ subunit. We show that both *in vitro* and *in vivo* models show a significant reduction in total AChRδ protein levels. We also identified a lower molecular weight species that was more prominent within *Gfpt1*$^{tm1d/tm1d}$ skeletal muscle. PNGase F treatment caused a molecular weight shift in both protein species indicating that the lower molecular weight species is an immature glycoprotein. We wanted to determine if this immature glycoprotein is localized to the NMJs of *Gfpt1*$^{tm1d/t1d}$ mice as part of the assembled AChR. LCM was used to excise NMJs from skeletal muscle in Tm1C homozygous control and *Gfpt1*$^{tm1d/tm1d}$ mice. We identified that both species were present within the NMJs of *Gfpt1*$^{tm1d/tm1d}$ mice suggesting that deficiently glycosylated AChRδ is localized within close proximity to the NMJ. Furthermore, we showed that in both *in vitro* and *in vivo* models, reduced Ogt protein levels were present which resulted in a decrease in total O-GlcNAcylation. Also, succinylated-WGA, a lectin with affinity for O-GlcNAc residues **[64]**, showed reduced expression in *Gfpt1*$^{tm1d/tm1d}$ skeletal muscle. Lastly, we also showed that terminal glycosylation through poly-sialylation was reduced in *Gfpt1*$^{tm1d/tm1d}$ skeletal muscle suggesting that in totality several glycan chain assembly pathways are impaired.

The AChRδ is a member of the pentameric muscle nicotinic AChR, a ligand gated ion channel with affinity for ACh. The AChR is regulated by glycosylation at the γ and δ subunits, allowing for enhanced stability and trafficking towards the post-synaptic membrane **[61]**. The AChRδ contains three glycosylation sites: Asn76, Asn143, and Asn169 **[60]**. Site directed mutagenesis has previously caused similar molecular weight shifts when expressed in COS cells, suggesting that our lower molecular weight species is an immature glycoprotein **[60]**. In addition, these glycosylation deficient mutants of the AChRδ subunit when co-expressed with AChRα, β, ε subunits had impaired AChR receptor assembly and reduced surface expression **[60]**. It has been previously shown that AChRδ and AChRβ contain novel motifs with lysine residues that enable Golgi retention, promote ubiquitination, and contributes to intracellular retention **[61]**. As such, this immature glycoprotein may be a target for protein degradation through the proteasomal degradation pathway, a pathway previously shown to regulate the expression of AChRδ through its interaction with the RING domain of Rapsyn **[65,66]**. Our data suggests that in Gfpt1-deficient samples, an immature glycoprotein of AChRδ is localized to the NMJ. In addition, impairment of glycosylation, may impair AChR stability through a similar mechanism as outlined above.

Young *Gfpt1*$^{tm1d/tm1d}$ mice were previously shown to have phenotypic changes as well as NMJ abnormalities consistent with Gfpt1-related CMS **[25]**. In this study we used 40-week-old mice to better identify the molecular changes, anticipating these would be amplified in older animals. We found that *Gfpt1*$^{tm1d/tm1d}$ mice have a progressive impairment of muscle endurance and increased fatigability of grip strength. An aged *Gfpt1*$^{tm1d/tm1d}$ mouse were also found to have reduced CMAP amplitudes, compared to control, likely a result of an impairment to the skeletal muscle, nerve and/or NMJ within the hindlimbs **[67]**. Importantly, *Gfpt1*$^{tm1d/tm1d}$ exhibited a fatigable decrement exceeding 15% after low-frequency (3Hz) and high-frequency (20Hz and 30Hz) RNS. In patients with CMS a decrement greater than 10% is typically observed **[59]**. Given this decrement seen with RNS in *Gfpt1*$^{tm1d/tm1d}$

mice, this technique could be used as a prognostic marker for therapeutic strategies in the future, however more samples would be required for full analysis. Similar to our previous paper, *Gfpt1*$^{tm1d/tm1d}$ NMJs were small, fragmented with less complexity compared to Tm1C homozygous control mice **[25]**. This has also been reported in other models with deficient Gfpt1 expression. One study, targeted the muscle-specific 18 amino acid insertion within human GFPT1, termed Gfpt1-L **[23,70]**. Loss of Gfpt1-L revealed impaired motor performance and NMJ integrity which progressively worsened over time **[23,70]**. In addition, both these models contain tubular aggregates within the skeletal muscle fiber, a hallmark of GFPT1-related CMS **[21,24,26,28]**. As a result, the *Gfpt1*$^{tm1d/tm1d}$ models progressive skeletal muscle weakness seen in GFPT1-related CMS patients and is consistent with other models.

Previous studies suggested that global N-linked glycosylation is not altered in Gfpt1-CMS myoblasts **[52]** However, our data indicate that Gfpt1-deficiency impairs protein glycosylation of specific proteins, through both N- and O-linked pathways. A potential difference between these studies is that *Gfpt1*$^{tm1d/tm1d}$ mice exhibit a complete Gfpt1 knockout within skeletal muscle, while patients observe a deficiency in expression **[22,24,28,29,51]**. This could exacerbate the issues with glycosylation within our tissue compared to patient controls. To that end, Gfpt1-depleted C2C12 cells were prepared which expressed a similar knockdown in expression compared to GFPT1-related-CMS patient-derived myoblasts. We identified that AChRδ subunit was hypo-glycosylated within both our models. The previous study examined global N-linked glycosylation levels, not glycosylation of an individual protein. Therefore, the occupancy of glycosylated glycan side chains was not examined in that previous study. Our study builds upon this research by highlighting for the first time an individual protein, AChRδ subunit, was hypo-glycosylated within both Gfpt1-deficient models, thus introducing the first target protein of perturbed glycosylation for this subtype of CMS. In addition, the impact of total N-linked glycosylation may not be a global reduction in one specific glycan chain, perhaps various glycoproteins are individually improperly glycosylated leading to neurotransmission impairment. This

explanation would be appropriate given that GFPT1-related CMS patients have limited total body clinical manifestations as seen with CDG patients **[4,26]**. Importantly, these results indicate that future studies should examine Gfpt1-related CMS and other glycosylation-based disorders within the context of glyco-proteomics to examine an individual protein change as opposed to global glycosylation impairment. This could reveal other target glycopeptides that could hypo-glycosylated similarly as we found with the AChRδ subunit in Gfpt1-depleted or even deficient models.

We identified that in Gfpt1-deficient models terminal sialyation was also reduced. Sialyation is a terminal modification towards proteins that can be highly unstable under mass spectrometric analyses. There have been several advancements over the recent years to enhance the detection glycan chains within different specimen, one of which has been the detection of terminal sialyation, an often unstable glycan modification that is produced from UDP-GlcNAc **[50,71,72]**. To date, the purpose of protein sialyation within skeletal muscle and the NMJ remains unknown. Dysfunction within protein sialyation has been associated with the neuromuscular condition called GNE myopathy, caused by a mutation to *GNE* **[19,71]**. The role of protein sialylation within the NMJ is not fully resolved however, sialic acids play an important role in nerve and skeletal muscle tissue **[73]**. Within skeletal muscle specifically proteins such as α-dystroglycan and neprilysin are complex glycoprotein within the sarcolemma. These proteins function by preserving sarcolemma integrity through the coupling of the actin cytoskeleton to extracellular matrix proteins laminin, neurexin and agrin **[74]**. Therefore, sialyation impairment could disrupt muscle morphology, which was present in *Gftp1*$^{tm1d/tm1d}$ mice. At the NMJ, Sialylation appears to have a role in laminin-induced AChR, suggesting another pathway which could impair NMJ integrity. **[75]**.

Glycosylation is a key PTM within the NMJ and skeletal muscle so investigation of other NMJ-associated proteins should be considered. Firstly, beyond the AChRδ subunit, the other AChR subunits (α, β, γ, and ε) have been reported to be glycosylated. Inhibiting these glycosylation sites completely by

site-directed mutagenesis, and/or tunicamycin treatment impaired AChR surface expression and receptor assembly, suggesting that other AChR subunits may be impaired within Gfpt1-deficient samples **[76]**. Although we found no molecular weight shifts within the AChRα in our models the other AChR subunits (β, γ, and ε) were not investigated, and could be hypo-glycosylated. In addition to the other AChR subunits, other NMJ associated peptides, such as components of the AChR clustering pathway: MuSK, LRP4, RAPSYN **[77,78]** and Agrin **[79]** are glycosylated. Recent studies suggest that mesoderm development candidate 2 (Mesdc2) binds to Lrp4 facilitating the glycosylation and cell surface expression of Lrp4, reducing the number of AChR receptor complexes and decreasing MuSK phosphorylation levels **[80]**. Also, MuSK glycosylation at amino acids sites N222, N338 and N459 have been attributed to a deficiency in phosphorylation of MuSk, and impairs downstream signalling **[63]**. As such, glycosylation may hinder MuSK dimerization in the absence of agrin, suggesting that glycosylation may be a control mechanism for MuSK by providing adequate steric hinderance/electrostatic repulsion of MuSK monomers **[63]**. These proteins should be investigated in future studies. Our data describes that a mis-glycosylation of AChRδ is present within Gfpt1-deficient samples. It remains unclear if solely hypo-glycosylation of AChRδ would result in the structural changes at the NMJ. We hypothesize that with advanced glycoproteomic studies and/or further individual protein glycosylation assessment, other key NMJ-associated proteins that factor into function and/or maintenance of the NMJ may be mis-glycosylated providing further consequences towards NMJ maintenance and neurotransmission in terms of a more complex molecular interplay. In addition, this also does not discount that beyond NMJ maintenance and neurotransmission, other proteins and pathways may be dysregulated in *GFPT1*-CMS pathology.

We identified that that in both Gfpt1 depleted cells and deficient skeletal muscle that there is deficient protein O-GlcNAcylation. O-GlcNAcylation, a small modification that primarily regulates nuclear, cytosolic, and cellular organelles such as the mitochondria, cytoskeletal and endoplasmic reticulum

[42,55,58]. O-GlcNAcylation attaches a GlcNAc moiety catalyzed by OGT to serine/threonine residues which can further undergo phosphorylation, suggesting that there may be extensive cellular pathways implicated in Gfpt1-deficient skeletal muscle **[43]**. In addition, knockout of the hexosamine biosynthetic enzymes OGT and/or OGA, impeded NMJ morphology and maintenance in *Drosophila* **[81]**. O-GlcNAcylation is enriched within the synapses playing an essential role in regulating synaptic and neuronal proteins essential for vesicular trafficking **[82]**. Thiamet-G, a compound which inhibits OGA, causes in enhanced O-GlcNAcylation and suppresses the synaptic transmission in hippocampal neurons **[83]**. To our knowledge, O-GlcNAcylation has not been studied in mammalian NMJs specifically. However, these structures do contain an enrichment in glycoproteins, mitochondria and sub-synaptic nuclei, suggesting that proteins are essential for NMJ maintenance and neurotransmission may be impacted.

Within skeletal muscle, O-GlcNAcylation has been associated with regulating transcriptional control through the beta-catenin/Wnt signalling pathway, which serves as a vital component for muscle and NMJ development **[48]**. Within neuromuscular disease increased O-GlcNAcylation was detected within regenerating muscle, atrophic, and vacuolated fibers from muscular dystrophy, myositis, rhabdomyolysis, sporadic inclusion body myositis (s-IBM) and distal myopathy with rimmed vacuoles (DMRV) **[84]**. Suggesting that the regulation of protein O-GlcNAcylation is important for muscle health **[55]**. Furthermore, O-GlcNAcylation is critical to maintain the structure of the sarcomere, through preserving protein-protein interactions of structural proteins in the cytoskeleton **[55]**. Preserving and/or restoring O-GlcNAcylation within the skeletal muscle may maintain muscle integrity. Lastly, O-GlcNAcylation a PTM that regulates protein phosphorylation and has been shown to regulate the activity of various pathways inside the cell [85]. It appears this crosstalk is essential to control cellular signalling pathways and transcription, thus impaired O-GlcNAcylation may have deleterious impacts to these target proteins [85].

Therefore, understanding the importance of the crosstalk between O-GlcNAcylation and phosphorylation may lead to additional pathways that are perturbed in *GFPT1*-CMS pathology.

In Gfpt1-CMS, muscle fibers have tubular aggregates, deemed a "hallmark" for disease identification **[21,24,26]**. The presence of these tubular aggregates has been speculated to be associated with hypo-glycosylation of ORAI1, an essential protein in regulating calcium ion flux within the sarcoplasmic reticulum. This has been hypothesized as ORAI1 hypo-glycosylation has been linked to the development of tubular aggregate myopathy and in limb-girdle CMS patients harbouring mutation to DPAGT1 **[85]**. Also disorders such as tubular aggregate myopathies arise from mutations within STIM1 and/or ORAI1 proteins resulting in defective sarcoplasmic reticulum calcium flux **[86]**. As such, defective glycosylation of key proteins responsible for calcium homeostasis may play a role in the presence of tubular aggregates within GFPT1-related CMS. Alternatively, a recent finding suggested endoplasmic reticulum associated stress due to hypo-glycosylation attributed to the formation of tubular aggregates within GFPT1-L knock-in mice **[70]**. In addition, this finding demonstrated that aged Gfpt-L knock-in progressive decrement on aged mice **[70]**. Accumulated ER stress attributed to a worsening phenotype, over time tubular aggregates were observed and eventual activation of autophagy degradation and apoptosis **[70]**. This study, demonstrated that impairment to Gfpt1 activity attributes to an ER stress environment due to hypo-glycosylation **[70]**. As such, more hypo-glycosylated proteins may be mis-localized and present within these tubular aggregates, that are beyond NMJ-associated peptides.

Importantly, beyond the skeletal muscle, the NMJ is comprised of three specific cell types: the skeletal muscle, the motor neuron and the Schwan cell. The motor neuron is essential for propagating the action potential and release of neurotransmitters into the synaptic cleft. The Schwann cell supports the motor neuron by creating the myelin sheath around peripheral neural axons. Our models within this study examine solely the skeletal muscle. As mentioned above, the *Gfpt1*$^{tm1d/tm1d}$ mouse model is a skeletal

muscle specific knockout of Gfpt1, while C2C12 cells are murine muscle myoblasts. Importantly, N- and O-linked glycosylation is essential for the function of critical proteins that are essential for motor neuron and Schwann cell development **[87,88]**. As such, further examination of the role of glycosylation within these cell types may elucidate more mechanisms within GFPT1-related CMS patients.

5. Conclusions

In conclusion, this study identified, a deficiently glycosylated protein within Gfpt1-deficient models, the AChRδ subunit, a key component that forms the AChR complex. We identified that the AChRδ contains an increase of an immature glycoprotein that is localized to the NMJs of *Gfpt1*$^{tm1d/tm1d}$ mice. In addition, we identified that Gfpt1-depleted cells and Gfpt1-deficient tissue have impaired protein O-GlcNAcylation, an abundant modification within the NMJ and skeletal muscle. This study further adds evidence of deficient glycosylation in GFPT1-related-CMS and maintains that other proteins essential for NMJ integrity may be differentially glycosylated, further impairing NMJ maintenance and neurotransmission.

Supplementary Materials: The following supporting information can be downloaded at: www.mdpi.com/xxx/s1, Figure S1: *In vivo* characterization of the long-term effects of Gfpt1-deficiency; Figure S2: Characterization of AChRδ protein levels in *Gfpt1*$^{tm1d/tm1d}$ mice; Figure S3: Production and validation of the doxycycline-inducible Gfpt1-deficent C2C12 cell model; Figure S4: Laser capture microdissection collection of NMJ enriched proteins in C57Bl/6N mice; Figure S5: Laser capture isolation of NMJs from *Gfpt1*$^{tm1d/tm1d}$ and Tm1C homozygous control mice; Figure S6: Modulation of hexosamine biosynthetic pathway with Thiamet-G or knockdown of Gfpt1 alters O-GlcNAcylation levels; Table S1: Primer sequences for Rt-qPCR.

Author Contributions: Conceptualization, H. L., S. S., and S. H. H.; methodology, S. H. H., R. C., K. O., and D. O.; validation, S. H. H., R. C., K. O., and D. O.; formal analysis, S. H. H., S. S., and K. O.; investigation, S. H. H., R. C., and K. O.; resources, H. L., S. S.; data curation, S. H. H., R. C., K. O., and D. O; writing—original draft preparation, S. H. H; review and editing, S. H. H, R.C., K. O., D. O., S. S., A. R., and H. L.; Final draft preparation and writing, S. H. H, S. S., A. R., H. L.; visualization, S. H. H., S. S, A. R., H. L; supervision, S. S and H. L.; project administration, S. S., and H. L.; funding acquisition, H. L., S. H. H. All authors have read and agreed to the published version of the manuscript.

Funding: HL receives support from the Canadian Institutes of Health Research (CIHR) for Foundation Grant FDN-167281 (Precision Health for Neuromuscular Diseases), Transnational Team Grant ERT-174211 (ProDGNE) and Network Grant OR2-189333 (NMD4C), from the Canada Foundation for Innovation (CFI-JELF 38412), the Canada Research Chairs program (Canada Research Chair in Neuromuscular Genomics and Health, 950-232279), the European Commission (Grant # 101080249) and the Canada Research Coordinating Committee New Frontiers in Research Fund (NFRFG-2022-00033) for SIMPATHIC, and from the Government of Canada, Canada First Research Excellence Fund (CFREF) for the Brain-Heart Interconnectome (CFREF-2022-00007). S.H.H received support from the Bob Korneluk CHEO Trainee Research Grant, Ontario Graduate Scholarship (OGS), Queen Elizabeth II Scholarship (QE2-GSST), and a STaR award by the University of Ottawa Dr. Eric Poulin Center for Neuromuscular Disease. AR receives funding from the Deutsche Gesellschaft für Muskelkranke (DGM) e. V.

Institutional Review Board Statement: The animal study protocol was approved by the Animal Care and Veterinary Board of the University of Ottawa (CHEOb-3089 and CHEOe-3120, approved on 16-11-2018 and 02-04-2019, respectively).

Data Availability Statement: Data are contained within the article and Supplementary Materials.

Acknowledgments: I would like to thank Dr. Rashmi Kothary and his research team for allowing me to have constant access to the laser capture microdissection microscope at the Ottawa Hospital Research Institute (OHRI). The SV2 antibody was deposited by Buckley, K. M and the neurofilament (2H3) antibody deposited by Jessell, T.M/Doss, J were obtained from the Developmental Studies Hybridoma Bank, created by the NICHD of the NIH and maintained at The University of Iowa, Department of Biology, 'Iowa City, IA 52242.

Conflicts of Interest: The authors declare no conflicts of interest.

References.

1. Stanley, P. What have we learned from glycosyltransferase knockouts in mice? *J. Mol. Biol.* **428**, 3166–3182 (2016).
2. Reily, C., Stewart, T. J., Renfrow, M. B. & Novak, J. Glycosylation in health and disease. *Nat. Rev. Nephrol.* **15**, 346–366 (2019).
3. Lipiński, P. & Tylki-Szymańska, A. Congenital Disorders of Glycosylation: What Clinicians Need to Know? *Front. Pediatr.* **9**, 715151 (2021).
4. Verheijen, J., Tahata, S., Kozicz, T., Witters, P. & Morava, E. Therapeutic approaches in Congenital Disorders of Glycosylation (CDG) involving N-linked glycosylation: an update. *Genet. Med.* **22**, 268–279 (2020).
5. Saito, F. & Matsumura, K. Fukuyama-type congenital muscular dystrophy and defective glycosylation of α-dystroglycan. *Skelet. Muscle* **1**, 22 (2011).
6. Hiroi, A., Yamamoto, T., Shibata, N., Osawa, M. & Kobayashi, M. Roles of fukutin, the gene responsible for fukuyama-type congenital muscular dystrophy, in neurons: possible involvement in synaptic function and neuronal migration. *Acta Histochem. Cytochem.* **44**, 91–101 (2011).
7. Willer, T. *et al.* ISPD loss-of-function mutations disrupt dystroglycan O-mannosylation and cause Walker-Warburg syndrome. *Nat. Genet.* **44**, 575–580 (2012).
8. van Reeuwijk, J. *et al.* Intragenic deletion in the LARGE gene causes Walker-Warburg syndrome. *Hum. Genet.* **121**, 685–690 (2007).
9. van Reeuwijk, J. *et al.* POMT2 mutations cause α-dystroglycan hypoglycosylation and Walker-Warburg syndrome. *J. Med. Genet.* **42**, 907–912 (2005).
10. d Beltran-Valero *et al.* A homozygous nonsense mutation in the Fukutin gene causes a Walker-Warburg syndrome phenotype. *J. Med. Genet.* **40**, 845–848 (2003).

11. Brown, S. C. *et al.* Abnormalities in α-Dystroglycan Expression in MDC1C and LGMD2I Muscular Dystrophies. *Am. J. Pathol.* **164**, 727–737 (2004).
12. Torelli, S. *et al.* Sub-cellular localisation of fukutin related protein in different cell lines and in the muscle of patients with MDC1C and LGMD2I. *Neuromuscul. Disord. NMD* **15**, 836–843 (2005).
13. Longman, C. *et al.* Mutations in the human LARGE gene cause MDC1D, a novel form of congenital muscular dystrophy with severe mental retardation and abnormal glycosylation of α-dystroglycan. *Hum. Mol. Genet.* **12**, 2853–2861 (2003).
14. Brockington, M. *et al.* Localization and functional analysis of the LARGE family of glycosyltransferases: significance for muscular dystrophy. *Hum. Mol. Genet.* **14**, 657–665 (2005).
15. Okazaki, T. *et al.* Duchenne muscular dystrophy–like phenotype in an LGMD2I patient with novel FKRP gene variants. *Hum. Genome Var.* **7**, 1–4 (2020).
16. Brockington, M. *et al.* Mutations in the fukutin-related protein gene (FKRP) identify limb girdle muscular dystrophy 2I as a milder allelic variant of congenital muscular dystrophy MDC1C. *Hum. Mol. Genet.* **10**, 2851–2859 (2001).
17. Bernabé, D. B.-V. de *et al.* Mutations in the FKRP gene can cause muscle-eye-brain disease and Walker–Warburg syndrome. *J. Med. Genet.* **41**, e61–e61 (2004).
18. Carmen, L. *et al.* Role of proteoglycans and glycosaminoglycans in Duchenne muscular dystrophy. *Glycobiology* **29**, 110–123 (2019).
19. Sela, I. *et al.* The glycomic sialylation profile of GNE Myopathy muscle cells does not point to consistent hyposialylation of individual glycoconjugates. *Neuromuscul. Disord.* **30**, 621–630 (2020).
20. Pugliese, A., Holland, S. H., Rodolico, C., Lochmüller, H. & Spendiff, S. Presynaptic Congenital Myasthenic Syndromes: Understanding Clinical Phenotypes through In vivo Models. *J. Neuromuscul. Dis.* 1–29 (2023) doi:10.3233/JND-221646.

21. Bauché, S. *et al.* Mutations in GFPT1-related congenital myasthenic syndromes are associated with synaptic morphological defects and underlie a tubular aggregate myopathy with synaptopathy. *J. Neurol.* **264**, 1791–1803 (2017).
22. Dusl, M. *et al.* A 3'-UTR mutation creates a microRNA target site in the GFPT1 gene of patients with congenital myasthenic syndrome. *Hum. Mol. Genet.* **24**, 3418–3426 (2015).
23. Farshadyeganeh, P. *et al.* Splicing regulation of GFPT1 muscle-specific isoform and its roles in glucose metabolisms and neuromuscular junction. *iScience* **26**, 107746 (2023).
24. Guergueltcheva, V. *et al.* Congenital myasthenic syndrome with tubular aggregates caused by GFPT1 mutations. *J. Neurol.* **259**, 838–850 (2012).
25. Issop, Y. *et al.* GFPT1 deficiency in muscle leads to myasthenia and myopathy in mice. *Hum. Mol. Genet.* **27**, 3218–3232 (2018).
26. Jiang, K. *et al.* Diverse myopathological features in the congenital myasthenia syndrome with GFPT1 mutation. *Brain Behav.* **12**, e2469 (2022).
27. Ma, Y. *et al.* Novel compound heterozygous variants in the GFPT1 gene leading to rare limb-girdle congenital myasthenic syndrome with rimmed vacuoles. *Neurol. Sci. Off. J. Ital. Neurol. Soc. Ital. Soc. Clin. Neurophysiol.* **42**, 3485–3490 (2021).
28. Zoltowska, K. *et al.* Mutations in GFPT1 that underlie limb-girdle congenital myasthenic syndrome result in reduced cell-surface expression of muscle AChR. *Hum. Mol. Genet.* **22**, 2905–2913 (2013).
29. Szelinger, S. *et al.* Congenital myasthenic syndrome caused by a frameshift insertion mutation in GFPT1. *Neurol. Genet.* **6**, e468 (2020).
30. Belaya, K. *et al.* Identification of DPAGT1 as a new gene in which mutations cause a congenital myasthenic syndrome. *Ann. N. Y. Acad. Sci.* **1275**, 29–35 (2012).

31. Finlayson, S. *et al.* Clinical features of congenital myasthenic syndrome due to mutations in DPAGT1. *J. Neurol. Neurosurg. Psychiatry* **84**, 1119–1125 (2013).
32. Ohno, K., Ohkawara, B., Shen, X.-M., Selcen, D. & Engel, A. G. Clinical and Pathologic Features of Congenital Myasthenic Syndromes Caused by 35 Genes—A Comprehensive Review. *Int. J. Mol. Sci.* **24**, 3730 (2023).
33. Basiri, K. *et al.* Clinical features in a large Iranian family with a limb-girdle congenital myasthenic syndrome due to a mutation in DPAGT1. *Neuromuscul. Disord.* **23**, 469–472 (2013).
34. Belaya, K. *et al.* Mutations in GMPPB cause congenital myasthenic syndrome and bridge myasthenic disorders with dystroglycanopathies. *Brain* **138**, 2493–2504 (2015).
35. Rodríguez Cruz, P. M. *et al.* Clinical features of the myasthenic syndrome arising from mutations in GMPPB. *J. Neurol. Neurosurg. Psychiatry* **87**, 802–809 (2016).
36. Cossins, J. *et al.* Congenital myasthenic syndromes due to mutations in ALG2 and ALG14. *Brain* **136**, 944–956 (2013).
37. Ehrstedt, C., Liu, W.-W., Frykholm, C., Beeson, D. & Punga, A. R. Novel pathogenic ALG2 mutation causing congenital myasthenic syndrome: A case report. *Neuromuscul. Disord.* **32**, 80–83 (2022).
38. Katata, Y. *et al.* The longest reported sibling survivors of a severe form of congenital myasthenic syndrome with the ALG14 pathogenic variant. *Am. J. Med. Genet. A.* **188**, 1293–1298 (2022).
39. Akella, N. M., Ciraku, L. & Reginato, M. J. Fueling the fire: emerging role of the hexosamine biosynthetic pathway in cancer. *BMC Biol.* **17**, 52 (2019).
40. Paneque, A., Fortus, H., Zheng, J., Werlen, G. & Jacinto, E. The Hexosamine Biosynthesis Pathway: Regulation and Function. *Genes* **14**, 933 (2023).
41. de Queiroz, R. M. *et al.* Hexosamine Biosynthetic Pathway and Glycosylation Regulate Cell Migration in Melanoma Cells. *Front. Oncol.* **9**, 116 (2019).

42. Chokchaitaweesuk, C., Kobayashi, T., Izumikawa, T. & Itano, N. Enhanced hexosamine metabolism drives metabolic and signaling networks involving hyaluronan production and O-GlcNAcylation to exacerbate breast cancer. *Cell Death Dis.* **10**, 1–15 (2019).
43. Claeyssen, C., Bastide, B. & Cieniewski-Bernard, C. Global O-GlcNAcylation changes impact desmin phosphorylation and its partition toward cytoskeleton in C2C12 skeletal muscle cells differentiated into myotubes. *Sci. Rep.* **12**, 9831 (2022).
44. Sheikh, M. A., Emerald, B. S. & Ansari, S. A. Stem cell fate determination through protein O-GlcNAcylation. *J. Biol. Chem.* **296**, 100035 (2020).
45. Wang, Z. V. *et al.* Spliced X-box Binding Protein 1 Couples the Unfolded Protein Response to Hexosamine Biosynthetic Pathway. *Cell* **156**, 1179–1192 (2014).
46. Watson, L. J. *et al.* Cardiomyocyte Ogt is essential for postnatal viability. *Am. J. Physiol. Heart Circ. Physiol.* **306**, H142-153 (2014).
47. Nagy, T., Champattanachai, V., Marchase, R. B. & Chatham, J. C. Glucosamine inhibits angiotensin II-induced cytoplasmic Ca2+ elevation in neonatal cardiomyocytes via protein-associated O-linked N-acetylglucosamine. *Am. J. Physiol. Cell Physiol.* **290**, C57-65 (2006).
48. Sayat, R., Leber, B., Grubac, V., Wiltshire, L. & Persad, S. O-GlcNAc-glycosylation of beta-catenin regulates its nuclear localization and transcriptional activity. *Exp. Cell Res.* **314**, 2774–2787 (2008).
49. Roth, J. *et al.* Protein *N*-Glycosylation, Protein Folding, and Protein Quality Control. *Mol. Cells* **30**, 497–506 (2010).
50. Hinderlich, S., Weidemann, W., Yardeni, T., Horstkorte, R. & Huizing, M. UDP-GlcNAc 2-Epimerase/ManNAc Kinase (GNE): A Master Regulator of Sialic Acid Synthesis. *Top Chem Curr* **366**, 97–138 (2015).

51. Senderek, J. *et al.* Hexosamine Biosynthetic Pathway Mutations Cause Neuromuscular Transmission Defect. *Am. J. Hum. Genet.* **88**, 162–172 (2011).
52. Chen, Q. *et al.* Global N-linked Glycosylation is Not Significantly Impaired in Myoblasts in Congenital Myasthenic Syndromes Caused by Defective Glutamine-Fructose-6-Phosphate Transaminase 1 (GFPT1). *Biomolecules* **5**, 2758–2781 (2015).
53. Whelan, S. A., Lane, M. D. & Hart, G. W. Regulation of the *O*-Linked β-*N*-Acetylglucosamine Transferase by Insulin Signaling*. *J. Biol. Chem.* **283**, 21411–21417 (2008).
54. Qiang, A., Slawson, C. & Fields, P. E. The Role of O-GlcNAcylation in Immune Cell Activation. *Front. Endocrinol.* **12**, (2021).
55. Lambert, M. *et al.* O-GlcNAcylation is a key modulator of skeletal muscle sarcomeric morphometry associated to modulation of protein–protein interactions. *Biochim. Biophys. Acta BBA - Gen. Subj.* **1860**, 2017–2030 (2016).
56. Haltiwanger, R. S., Holt, G. D. & Hart, G. W. Enzymatic addition of O-GlcNAc to nuclear and cytoplasmic proteins. Identification of a uridine diphospho-N-acetylglucosamine:peptide beta-N-acetylglucosaminyltransferase. *J. Biol. Chem.* **265**, 2563–2568 (1990).
57. Hart, G. W., Housley, M. P. & Slawson, C. Cycling of O-linked beta-N-acetylglucosamine on nucleocytoplasmic proteins. *Nature* **446**, 1017–1022 (2007).
58. Shi, H. *et al.* Skeletal muscle O-GlcNAc transferase is important for muscle energy homeostasis and whole-body insulin sensitivity. *Mol. Metab.* **11**, 160–177 (2018).
59. Finsterer, J. Congenital myasthenic syndromes. *Orphanet J. Rare Dis.* **14**, 57 (2019).
60. Ramanathan, V. K. & Hall, Z. W. Altered Glycosylation Sites of the δ Subunit of the Acetylcholine Receptor (AChR) Reduce αδ Association and Receptor Assembly *. *J. Biol. Chem.* **274**, 20513–20520 (1999).

61. Rudell, J. C., Borges, L. S., Yarov-Yarovoy, V. & Ferns, M. The MX-Helix of Muscle nAChR Subunits Regulates Receptor Assembly and Surface Trafficking. *Front. Mol. Neurosci.* **13**, 48 (2020).

62. Hui, T., Jing, H. & Lai, X. Neuromuscular junction-specific genes screening by deep RNA-seq analysis. *Cell Biosci.* **11**, 81 (2021).

63. Watty, A. & Burden, S. J. MuSK Glycosylation Restrains MuSK Activation and Acetylcholine Receptor Clustering*. *J. Biol. Chem.* **277**, 50457–50462 (2002).

64. Zachara, N. E., Vosseller, K. & Hart, G. W. Detection and Analysis of Proteins Modified by O-Linked N-Acetylglucosamine. *Curr. Protoc. Protein Sci.* **CHAPTER**, Unit12.8 (2011).

65. Li, L. *et al.* Enzymatic Activity of the Scaffold Protein Rapsyn for Synapse Formation. *Neuron* **92**, 1007–1019 (2016).

66. Xing, G., Xiong, W.-C. & Mei, L. Rapsyn as a signaling and scaffolding molecule in neuromuscular junction formation and maintenance. *Neurosci. Lett.* **731**, 135013 (2020).

67. Arnold, W. D. *et al.* Electrophysiological Motor Unit Number Estimation (MUNE) Measuring Compound Muscle Action Potential (CMAP) in Mouse Hindlimb Muscles. *J. Vis. Exp. JoVE* 52899 (2015) doi:10.3791/52899.

68. LoRusso, S. J. & Iyadurai, S. J. Decrement with high frequency repetitive nerve stimulation in a RAPSN congenital myasthenic syndrome. *Muscle Nerve* **57**, E106–E108 (2018).

69. An, R. *et al.* Abnormal decrement on high-frequency repetitive nerve stimulation in congenital myasthenic syndrome with GFPT1 mutations and review of literature. *Front. Neurol.* **13**, 926786 (2022).

70. Zhang, R. *et al.* Muscle-specific lack of GFPT1 in knock-in mice triggers ER stress to alleviate misfolded proteins. *Dis. Model. Mech.* dmm.050768 (2024) doi:10.1242/dmm.050768.

71. Awasthi, K., Srivastava, A., Bhattacharya, S. & Bhattacharya, A. Tissue specific expression of sialic acid metabolic pathway: role in GNE myopathy. *J. Muscle Res. Cell Motil.* **42**, 99–116 (2021).

72. NISHIKAZE, T. Sialic acid derivatization for glycan analysis by mass spectrometry. *Proc. Jpn. Acad. Ser. B Phys. Biol. Sci.* **95**, 523–537 (2019).

73. Marini, M., Tani, A., Manetti, M. & Sgambati, E. Overview of sialylation status in human nervous and skeletal muscle tissues during aging. *Acta Histochem.* **123**, 151813 (2021).

74. Nilsson, J., Nilsson, J., Larson, G. & Grahn, A. Characterization of site-specific O-glycan structures within the mucin-like domain of α-dystroglycan from human skeletal muscle. *Glycobiology* **20**, 1160–1169 (2010).

75. McDearmon, E. L., Combs, A. C. & Ervasti, J. M. Core 1 Glycans on α-Dystroglycan Mediate Laminin-induced Acetylcholine Receptor Clustering but Not Laminin Binding*. *J. Biol. Chem.* **278**, 44868–44873 (2003).

76. Wanamaker, C. P. & Green, W. N. N-Linked Glycosylation Is Required for Nicotinic Receptor Assembly but Not for Subunit Associations with Calnexin *. *J. Biol. Chem.* **280**, 33800–33810 (2005).

77. Apel, E. D., Glass, D. J., Moscoso, L. M., Yancopoulos, G. D. & Sanes, J. R. Rapsyn is required for MuSK signaling and recruits synaptic components to a MuSK-containing scaffold. *Neuron* **18**, 623–635 (1997).

78. Liao, X., Wang, Y., Lai, X. & Wang, S. The role of Rapsyn in neuromuscular junction and congenital myasthenic syndrome. *Biomol. Biomed.* **23**, 772–784 (2023).

79. Kim, M.-L. *et al.* O-fucosylation of muscle agrin determines its ability to cluster acetylcholine receptors. *Mol. Cell. Neurosci.* **39**, 452–464 (2008).

80. Hoshi, T. *et al.* Mesdc2 plays a key role in cell-surface expression of Lrp4 and postsynaptic specialization in myotubes. *FEBS Lett.* **587**, 3749–3754 (2013).

81. Fenckova, M. *et al.* Intellectual disability-associated disruption of O-GlcNAc cycling impairs habituation learning in Drosophila. *PLOS Genet.* **18**, e1010159 (2022).

82. Lee, B. E., Suh, P.-G. & Kim, J.-I. O-GlcNAcylation in health and neurodegenerative diseases. *Exp. Mol. Med.* **53**, 1674–1682 (2021).

83. Hwang, H. & Rhim, H. Acutely elevated O-GlcNAcylation suppresses hippocampal activity by modulating both intrinsic and synaptic excitability factors. *Sci. Rep.* **9**, 7287 (2019).

84. Nakamura, S., Nakano, S., Nishii, M., Kaneko, S. & Kusaka, H. Localization of O-GlcNAc-modified proteins in neuromuscular diseases. *Med. Mol. Morphol.* **45**, 86–90 (2012).

85. Hart, G. W., Slawson, C., Ramirez-Correa, G. & Lagerlof, O. Cross Talk Between O-GlcNAcylation and Phosphorylation: Roles in Signaling, Transcription, and Chronic Disease. *Annu. Rev. Biochem.* **80**, 825–858 (2011).

86. vanden Brande, L. *et al.* Pathogenic DPAGT1 variants in limb-girdle congenital myasthenic syndrome (LG-CMS) associated with tubular aggregates and ORAI1 hypoglycosylation. *Neuropathol. Appl. Neurobiol.* **50**, e12952 (2024).

87. Gang, Q. *et al.* Genetic defects are common in myopathies with tubular aggregates. *Ann. Clin. Transl. Neurol.* **9**, 4–15 (2021).

88. Kim, S. *et al.* Schwann Cell O-GlcNAc Glycosylation Is Required for Myelin Maintenance and Axon Integrity. *J. Neurosci. Off. J. Soc. Neurosci.* **36**, 9633–9646 (2016).

89. Kwon, S. E. & Chapman, E. R. Glycosylation is dispensable for sorting of synaptotagmin 1 but is critical for targeting of SV2 and synaptophysin to recycling synaptic vesicles. *J. Biol. Chem.* **287**, 35658–35668 (2012).

Supplementary Figures: Deficiency of glutamine-fructose-6-phosphate transaminase 1 (Gfpt1) in skeletal muscle results in reduced glycosylation of the delta subunit of the nicotinic acetylcholine receptor (AchRδ)

Stephen H. Holland[1,2,4], Ricardo Caromona-Martinez[1], Kaela O'Connor[1,2], Daniel O'Neil[1], Andreas Roos[1,7,8], Sally Spendiff[1], Hanns Lochmuller[1,2,3,4,5,6*]

[1] Children's Hospital of Eastern Ontario Research Institute, Ottawa, Ontario, Canada

[2] Department of Cellular Molecular Medicine, Faculty of Medicine, University of Ottawa, Ottawa, Ontario, Canada

[3] Division of Neurology, Department of Medicine, The Ottawa Hospital, Ottawa, Canada

[4] Dr. Eric Poulin Center for Neuromuscular Disease, Brain and Mind Research Institute, University of Ottawa, Ottawa, Canada

[5] Department of Neuropediatric and Muscle Disorders, Medical Center, University of Freiburg, Faculty of Medicine, Freiburg, Germany

[6] Centro Nacional de Analisis Genomico (CNAG-CRG), Center for Genomic Regulation, Barcelona Institute of Science and Technology (BIST), Barcelona, Catalonia, Spain

[7] Department of Neuropaediatrics, Neuromuscular Centre, Universitätsmedizin Essen, Essen, Germany

[8]Department of Neurology, Medical Faculty and University Hospital Düsseldorf, Heinrich Heine University, Düsseldorf, 40225, Germany

This file contains :

- Figures:
    - S1: *In vivo* characterization of the long-term effects of Gfpt1-deficiency.

- S2: *In vivo* repetitive nerve stimulation: decrement in *Gfpt1*$^{tm1d/tm1d}$ mice.
- S3: Characterization of AChRδ protein levels in *Gfpt1*$^{tm1d/tm1d}$ mice.
- S4: Production and validation of the doxycycline-inducible Gfpt1-deficient C2C12 cell model.
- S5: Laser capture microdissection collection of NMJ enriched proteins in C57bl/6 mice.
- S6: Laser capture isolation of NMJs from *Gfpt1*$^{tm1d/tm1d}$ and Tm1C homozygous control mice
- S7: Modulation of hexosamine biosynthetic pathway with thiamet-G or knockdown of Gfpt1 alters in O-GlcNAcylation levels.

- Table S1: Primer sequences for Rt-qPCR

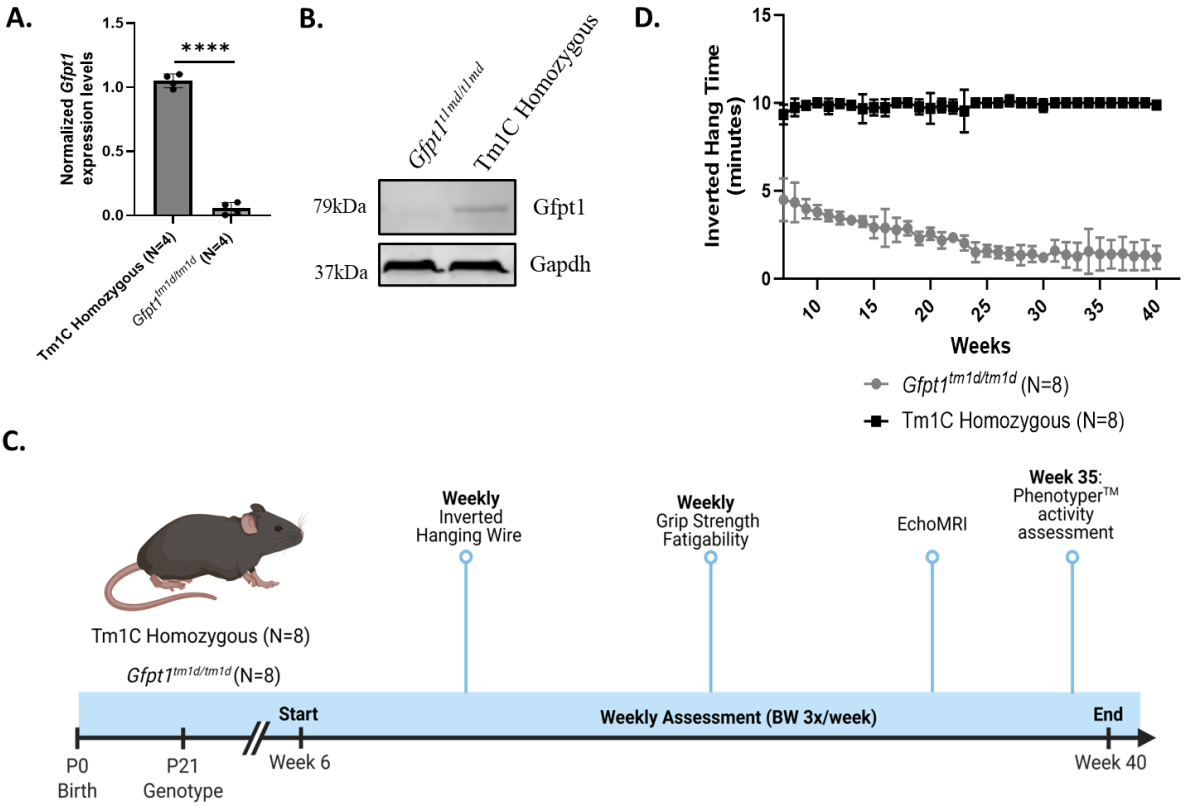
A.
Normalized Gfpt1 expression levels
****
Tm1C Homozygous (N=4)
Gfpt1tm1d/tm1d (N=4)
B.
Gfpt1tm1d/tm1d
Tm1C Homozygous
79kDa
Gfpt1
37kDa
Gapdh
D.
Inverted Hang Time (minutes)
Weeks
Gfpt1tm1d/tm1d (N=8)
Tm1C Homozygous (N=8)
C.
Tm1C Homozygous (N=8)
Gfpt1tm1d/tm1d (N=8)
Weekly Inverted Hanging Wire
Weekly Grip Strength Fatigability
EchoMRI
Week 35: Phenotyper™ activity assessment
Start
Weekly Assessment (BW 3x/week)
End
P0 Birth
P21 Genotype
Week 6
Week 40

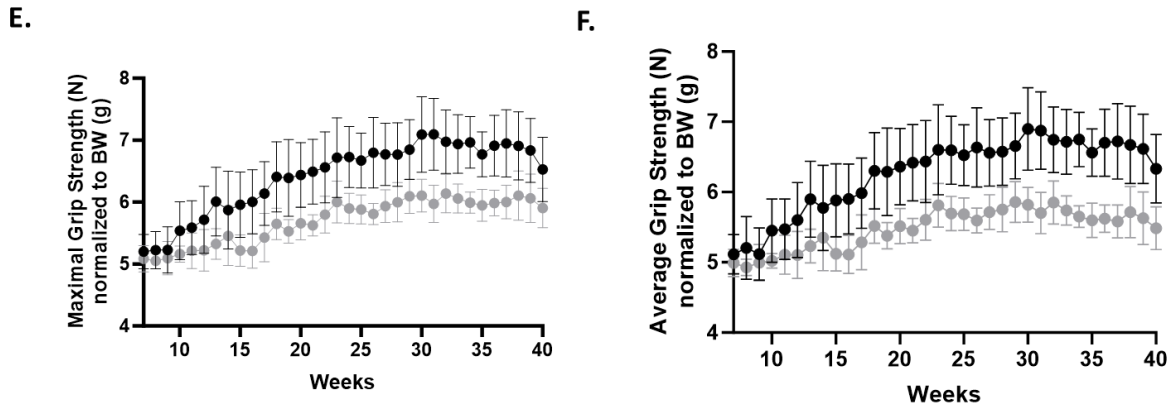
E.
Maximal Grip Strength (N) normalized to BW (g)
Weeks
F.
Average Grip Strength (N) normalized to BW (g)
Weeks

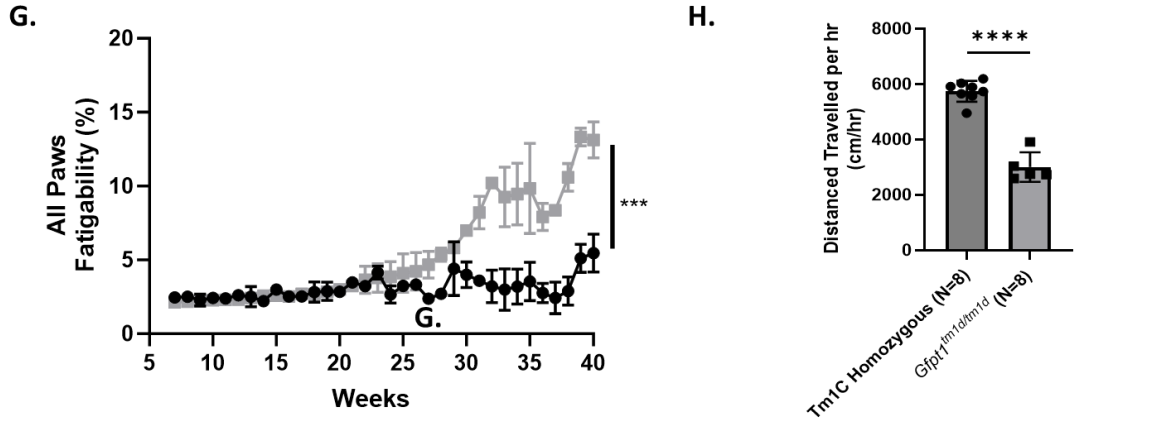
G.
All Paws Fatigability (%)
***
G.
Weeks
H.
Distanced Travelled per hr (cm/hr)
****
Tm1C Homozygous (N=8)
Gfpt1tm1d/tm1d (N=8)

Supplementary Figure 1: *In vivo* characterization of the long-term effects of Gfpt1-deficiency.

A) RT-qPCR assessment of *Gfpt1* expression showed a significant depletion in *Gfpt1*$^{tm1d/tm1d}$ skeletal muscle compared to Tm1C homozygous control mice. B) *Gftp1*$^{tm1d/tm1d}$ mice exhibit a knockout of Gfpt1 protein (79kDa) within the quadriceps. statistical significance was determined via a two-way ANOVA test where N=8 for both Tm1C homozygous control mice and *Gfpt1*$^{tm1d/tm1d}$ mice. C) Weekly behavioural assessments were conducted to assess for muscle endurance, strength, and fatigability. These included the inverted hanging wire and repetitive grip strength measurements. Body weight was measured three times per week, EchoMRI measurements were taken every week. A 24hr Phenotyper™ assessment was performed at week 35. statistical significance was determined via a two-way ANOVA test where N=8 for both Tm1C homozygous control mice and *Gfpt1*$^{tm1d/tm1d}$ mice. D) The raw inverted hanging wire latency to fall recordings before normalization to mouse body weight. *Gfpt1*$^{tm1d/tm1d}$ mice show a progressive impairment to the latency to fall throughout this study. E) Weekly maximal and F) average grip strength was calculated from *Gfpt1*$^{tm1d/tm1d}$ and Tm1C homozygous control mice. Maximal grip strength was calculated by taking the highest grip strength measurement normalized to body weight. statistical significance was determined via a two-way ANOVA test where N=8 for both Tm1C homozygous control mice and *Gfpt1*$^{tm1d/tm1d}$ mice. G) *Gfpt1*$^{tm1d/tm1d}$ mice exhibit an increase in muscle fatigability compared to Tm1C homozygous control mice using repetitive grip strength measurements from all-paw recordings. statistical significance was determined via a two-way ANOVA test where N=8 for both Tm1C homozygous control mice and *Gfpt1*$^{tm1d/tm1d}$ mice. H) A 24hr Phenotyper™ activity assessment was performed in *Gfpt1*$^{tm1d/tm1d}$ mice and Tm1C homozygous control mice. Measurements were calculated as total distance travelled (cm) per hour (hr). Statistical significance was determined via a Student T-Test. All graphs show mean ± SD. *** $P < 0.001$, **** < 0.0001.

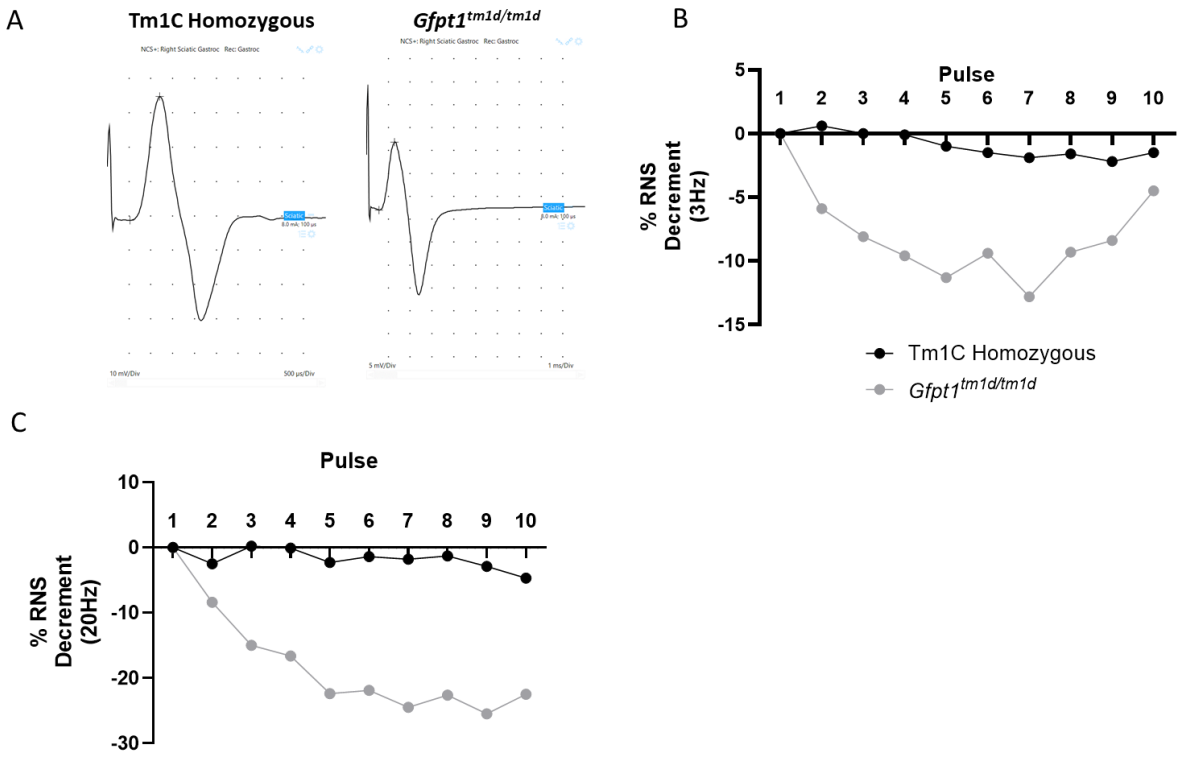

Supplementary Figure 2: *In vivo* characterization RNS decrement in *Gfpt1*$^{tm1d/tm1d}$ mice.

A) There was a decrease in CMAP amplitude (mV) recorded from the gastrocnemius medialis muscle following repetitive stimulation of the sciatic nerve for both the Tm1C homozygous and Gfpt1$^{tm1d/tm1d}$ mouse. Typically, clinicians look for a decrement between the first and the 7th stimulus and consider a decrement of more than 10% as indicative for neuromuscular transmission defects. In the control mice decrement did not exceed 5% at any of the RNS tests. B) There was a noticeable decrement in Gfpt1$^{tm1d/tm1d}$ skeletal muscle during low-frequency RNS at 3Hz. C) There was a noticeable decrement in Gfpt1$^{tm1d/tm1d}$ skeletal muscle during high-frequency RNS at 20Hz. For all calculations, one *Gfpt1*$^{tm1d/tm1d}$ and one Tm1C homozygous mouse was recorded at 54 weeks of age before they were sacrificed.

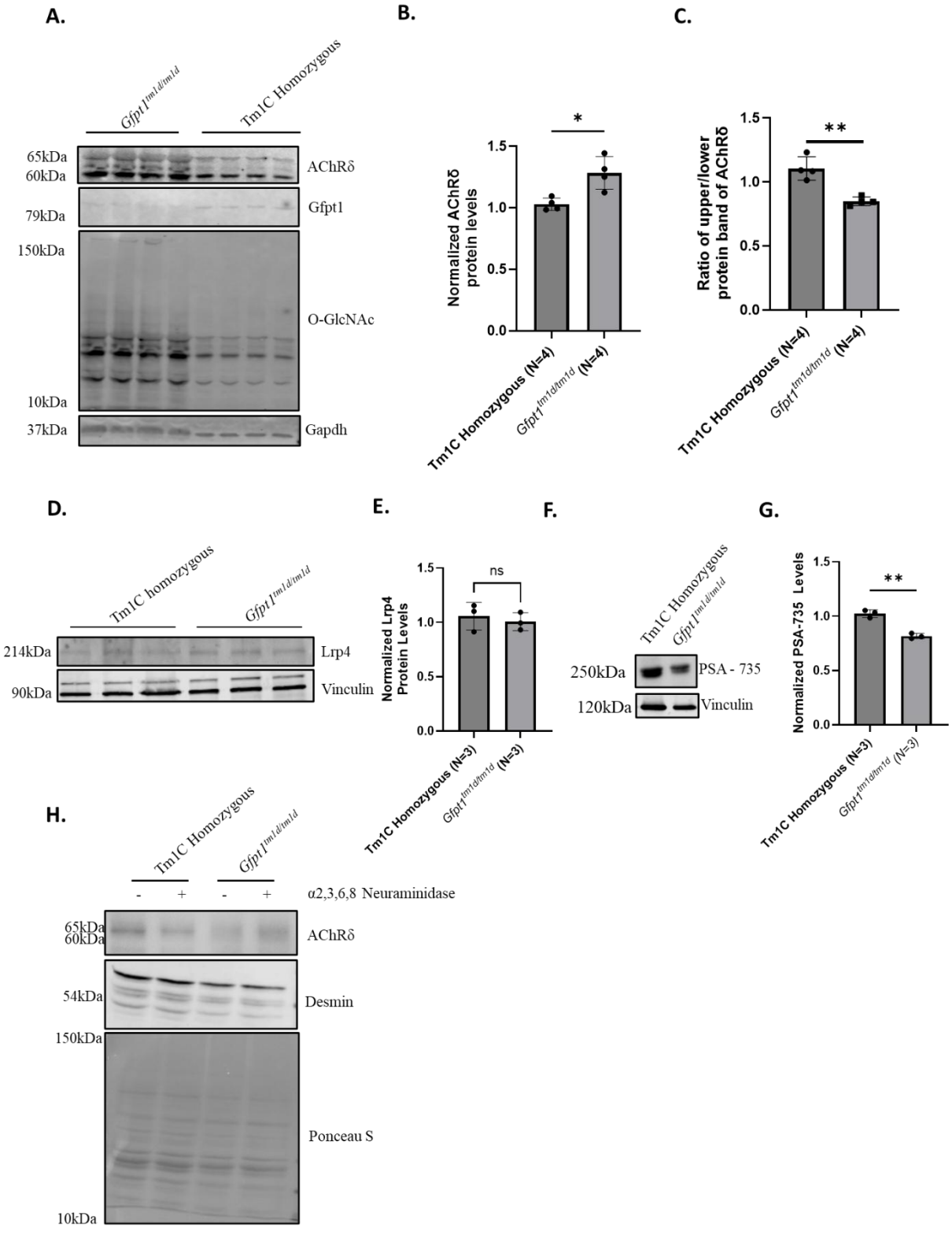
A.
Gfpt1tm1d/tm1d
Tm1C Homozygous
65kDa
60kDa
AChRδ
79kDa
Gfpt1
150kDa
O-GlcNAc
10kDa
37kDa
Gapdh
B.
Normalized AChRδ protein levels
*
Tm1C Homozygous (N=4)
Gfpt1tm1d/tm1d (N=4)
C.
Ratio of upper/lower protein band of AChRδ
**
Tm1C Homozygous (N=4)
Gfpt1tm1d/tm1d (N=4)
D.
Tm1C homozygous
Gfpt1tm1d/tm1d
214kDa
Lrp4
90kDa
Vinculin
E.
Normalized Lrp4 Protein Levels
ns
Tm1C Homozygous (N=3)
Gfpt1tm1d/tm1d (N=3)
F.
Tm1C Homozygous
Gfpt1tm1d/tm1d
250kDa
PSA - 735
120kDa
Vinculin
G.
Normalized PSA-735 Levels
**
Tm1C Homozygous (N=3)
Gfpt1tm1d/tm1d (N=3)
H.
Tm1C Homozygous
Gfpt1tm1d/tm1d
- + - +
α2,3,6,8 Neuraminidase
65kDa
60kDa
AChRδ
54kDa
Desmin
150kDa
Ponceau S
10kDa

Supplementary Figure 3: Characterization of AChRδ protein levels in *Gfpt1*$^{tm1d/tm1d}$ mice.

A) AChRδ protein levels (65kDa) were examined in *gastrocnemius* muscle isolated from 40-week-old *Gfpt1*$^{tm1f/tm1d}$ mice and Tm1C homozygous control mice. A 60kDa lower molecular weight species was detected in the *Gfpt1*$^{tm1d/tm1d}$ specimen. B) There was an increase in the 65kDa AChRδ protein levels in the *gastrocnemius* isolated from *Gfpt1*$^{tm1d/tm1d}$ mice. C) The ratio of the upper molecular weight species and the lower molecular weight species was reduced in *Gfpt1*$^{tm1d/tm1d}$ skeletal muscle. D) Lrp4 protein levels (214kDa) were examined in quadriceps muscle isolated from 40-week-old *Gfpt1*$^{tm1f/tm1d}$ mice and Tm1C homozygous control mice. E) There was no significant change in the 214kDa Lrp4 protein levels in the quadriceps isolated from *Gfpt1*$^{tm1d/tm1d}$ mice. F) Total protein poly-sialyation was examined in quadricep muscle isolated from 40-week-old *Gfpt1*$^{tm1d/tm1d}$ and Tm1C homozygous control mice. G) There was a significant reduction in total poly-sialyation level in *Gfpt1*$^{tm1d/tm1d}$ quadriceps. H) To examine sialyation levels of AChRδ quadricep muscle lysates were treated with α2-3,6, 8 Neuraminidase. I)

The molecular weight of AChRδ protein species did not change after treatment. All graphs show mean ± SD, statistical significance was determined via student T-Test. * $P < 0.05$, ** < 0.01.

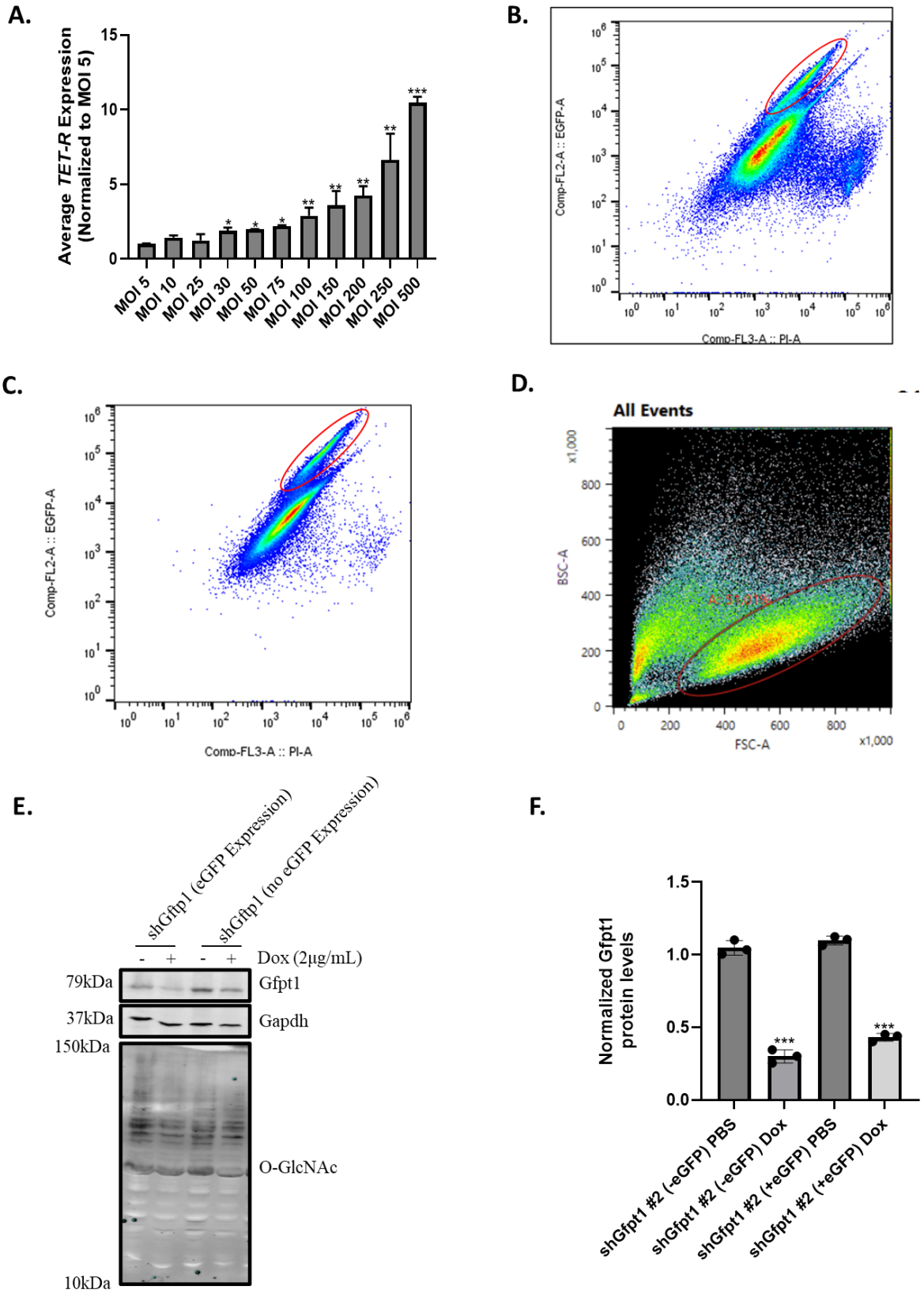
A.
Average TET-R Expression (Normalized to MOI 5)
MOI 5
MOI 10
MOI 25
MOI 30
MOI 50
MOI 75
MOI 100
MOI 150
MOI 200
MOI 250
MOI 500
B.
Comp-FL2-A :: EGFP-A
Comp-FL3-A :: PI-A
C.
Comp-FL2-A :: EGFP-A
Comp-FL3-A :: PI-A
D.
All Events
BSC-A
FSC-A
x1,000
E.
shGftp1 (eGFP Expression)
shGftp1 (no eGFP Expression)
Dox (2µg/mL)
79kDa
Gfpt1
37kDa
Gapdh
150kDa
O-GlcNAc
10kDa
F.
Normalized Gfpt1 protein levels
shGfpt1 #2 (-eGFP) PBS
shGfpt1 #2 (-eGFP) Dox
shGfpt1 #2 (+eGFP) PBS
shGfpt1 #2 (+eGFP) Dox

Supplementary Figure 4: Production and validation of the doxycycline-inducible Gfpt1-deficient C2C12 cell model.

A) TET-R positive colonies of C2C12 myoblasts were assessed for the expression of *TET-R* at different MOIs of lentivirus. This was used to establish whether wild-type C2C12 cells expressed *TET-R* after infection with a TET-R expressing lentivirus and create a polyclonal colony. Statistical test performed was a one-way ANOVA. B) After monoclonal colonies were established post-infection with scramble, shGfpt1 #1 and shGfpt1 #2 lentivirus transgene and treated with doxycycline to activate the expression of eGFP. Then FACS was performed to isolate eGFP positive expressing colonies: scramble, C) shGfpt1 #1, and D) shGfpt1 #2 C2C12 cells. E) We noticed that some C2C12 cells had low levels of eGFP expression, these were isolated after cell sorting to establish an eGFP-negative population. To examine Gfpt1 and O-GlcNAc protein modification levels in these cells, treatment with doxycycline was performed in both known populations of eGFP positive and negative C2C12 myoblasts. A Western blot was performed to examine protein levels from Gfpt1 and O-GlcNAc protein levels. F) Notably, regardless of the eGFP expression level, Gfpt1 protein levels were reduced upon activation with doxycycline. Graphs are mean ± SD, statistical significance was determined by Student T-Test. *Denotes a significant difference between scramble and Gfpt1-deficient C2C12 cells, * $P < 0.05$, ** $P < 0.01$. *** $P < 0.001$.

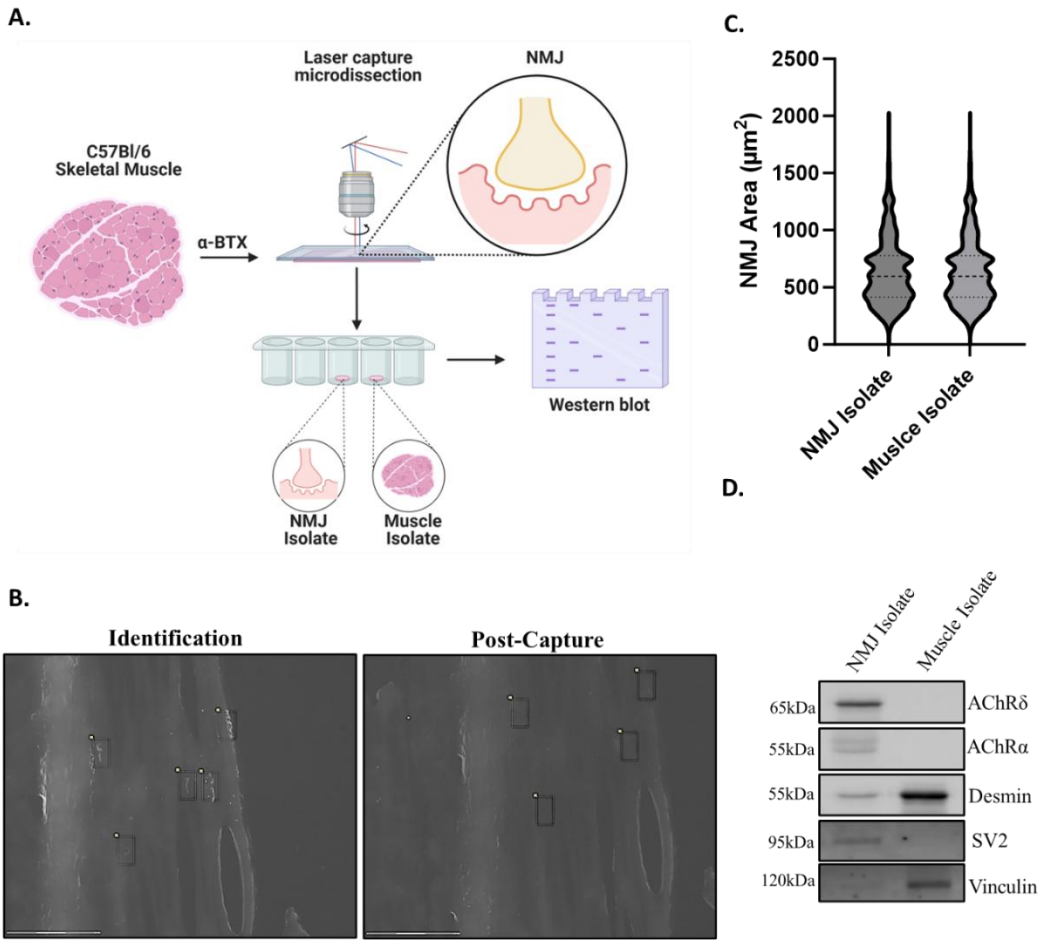

Supplementary Figure 5: Laser capture microdissection of NMJ enriched proteins in C57bl/6 mice.

A) 25-week-old C57bl/6 mice *gastrocnemius* muscles were longitudinally sectioned and stained for AChR clusters using α-BTX-594. NMJs were identified at 20x magnification and extracted with LCM. Samples were collected for Western blot to assess protein levels. B) A representative image of before and after laser capture microdissection of NMJs from *gastrocnemius* muscles stained with α-BTX-594. Scale bar: 200μm. C) The protein levels of NMJ and skeletal muscle markers after LCM enrichment. NMJ post-synaptic markers such as AChRδ, and AChRα, as well as pre-synaptic marker SV2 were enriched in the NMJ isolates and barely detectable in the muscle isolates. Skeletal muscle proteins such as Desmin and Gapdh were detected in both NMJ and skeletal muscle isolates.

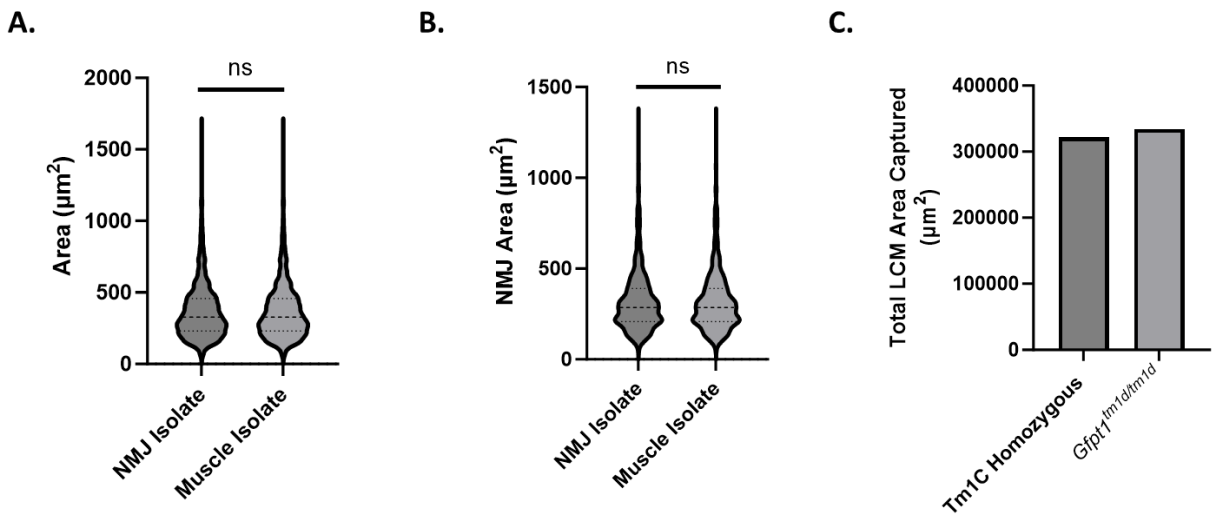

Supplementary Figure 6: Laser capture isolation of NMJs from *Gfpt1*$^{tm1d/tm1d}$ and Tm1C homozygous control mice

A) For Western blot analysis ~750 NMJs were isolated from Tm1C homozygous control and B) *Gfpt1*$^{tm1d/tm1d}$ muscle stained with α-BTX-594. The average area of the LCM sectioning to represent that there was no change between the NMJ and muscle isolates containing no NMJ material. The data is presented as a violin plot ± SD. C) There was a slight increase in the total LCM area in *Gfpt1*$^{tm1d/tm1d}$ muscle due a smaller AChR area size upon comparison to Tm1C homozygous control muscle.

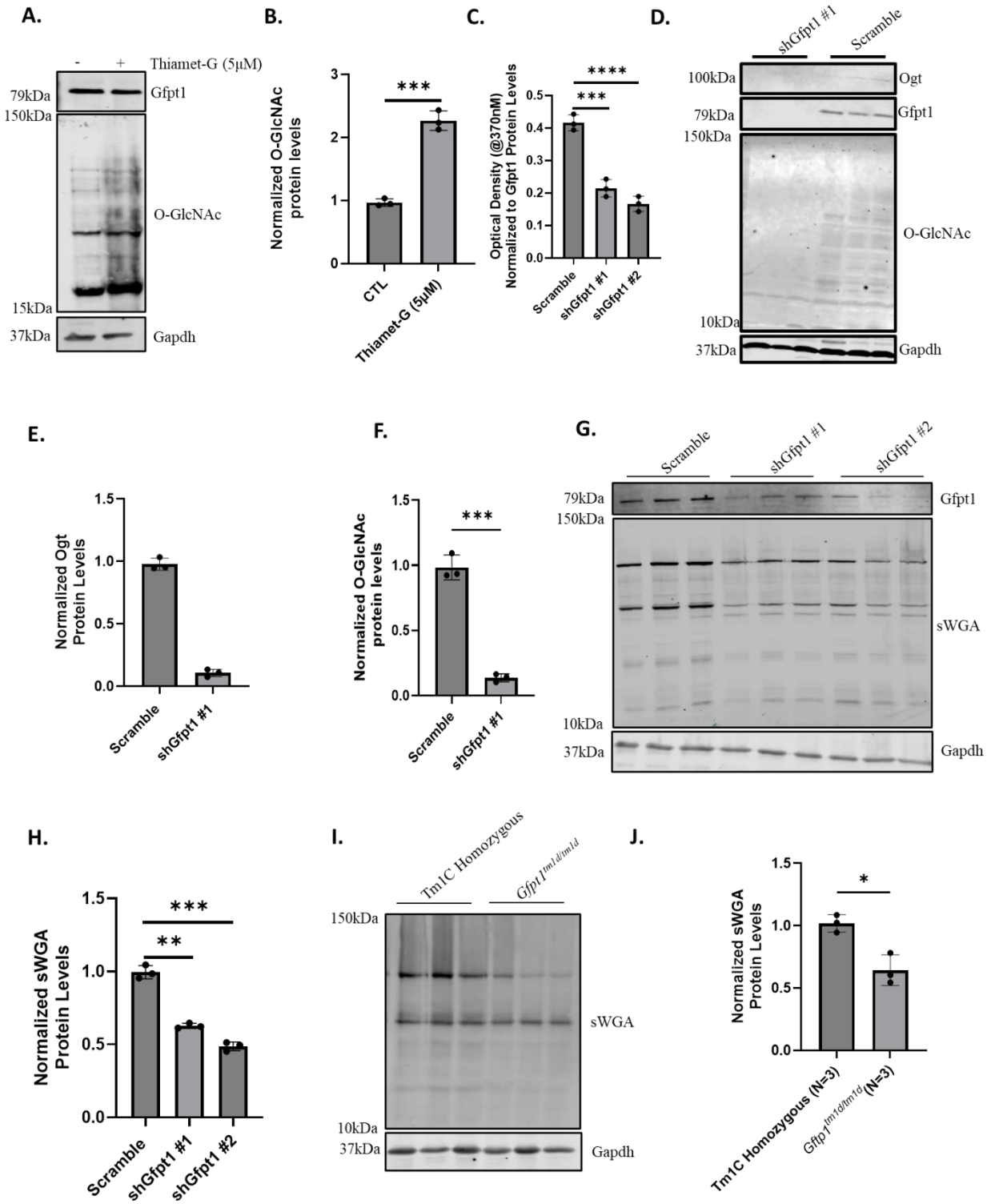
A.
- +
Thiamet-G (5μM)
79kDa
150kDa
Gfpt1
O-GlcNAc
15kDa
37kDa
Gapdh
B.
Normalized O-GlcNAc protein levels
***
CTL
Thiamet-G (5μM)
C.
Optical Density (@370nM) Normalized to Gfpt1 Protein Levels
****
***
Scramble
shGfpt1 #1
shGfpt1 #2
D.
shGfpt1 #1
Scramble
100kDa
Ogt
79kDa
Gfpt1
150kDa
O-GlcNAc
10kDa
37kDa
Gapdh
E.
Normalized Ogt Protein Levels
Scramble
shGfpt1 #1
F.
Normalized O-GlcNAc protein levels
***
Scramble
shGfpt1 #1
G.
Scramble
shGfpt1 #1
shGfpt1 #2
79kDa
150kDa
Gfpt1
sWGA
10kDa
37kDa
Gapdh
H.
Normalized sWGA Protein Levels
***
**
Scramble
shGfpt1 #1
shGfpt1 #2
I.
Tm1C Homozygous
Gfpt1tm1d/tm1d
150kDa
sWGA
10kDa
37kDa
Gapdh
J.
Normalized sWGA Protein Levels
*
Tm1C Homozygous (N=3)
Gfpt1tm1d/tm1d (N=3)

Supplementary Figure 7: Modulation of hexosamine biosynthetic pathway with thiamet-G or knockdown of Gfpt1 alters in O-GlcNAcylation levels.

A) Western blot assessing wild type C2C12 myotubes treated with 5μM thiamet-G for 72hrs to inhibit the enzymatic activity of Oga, an O-GlcNAcylation glycanase enzyme. B) Thiamet-G treatment increased the O-GlcNAcylation levels in wild-type C2C12 myotubes. C) Enzymatic activity of Gfpt1 was significantly reduced in Gfpt1-depleted C2C12 cells. D) A Western blot examining Gfpt1, Ogt, and O-GlcNAc modification protein levels assessed in scramble, shGfpt1 #1 and infected C2C12 cells treated with doxycycline. E) Ogt and F) O-GlcNAc modification protein levels was reduced in shGfpt1 #1 infected C2C12 myotubes treated with doxycycline upon comparison to scramble infected C2C12 cells. G) A Western blot examining the levels of sWGA lectin expression bound to glycan chains in scramble and Gfpt1-depleted C2C12 cells. H) sWGA lectin binding was significantly reduced in Gfpt1-depleted C2C12 myotubes treated with doxycycline upon comparison to scramble C2C12 myotubes. I) A Western blot examining the levels of sWGA lectin expression bound to glycan chains in the quad isolated from 40-week-old *Gfpt1*$^{tm1d/tm1d}$ and Tm1C homozygous control mice. J) sWGA lectin binding was significantly reduced the quad isolated from 40-week-old *Gfpt1*$^{tm1d/tm1d}$ mice. Graphical representations are represented as mean ± SD, statistical significance was determined by student T-Test. ** $P < 0.01$, *** $P < 0.001$.

Supplementary Table S1: Primer Sequences for qPCR.

Primer	Primer Sequence
Gfpt1-F	5’- CCA ACG CCT GCA AAA TCC AG-3’
Gfpt1-R	5’-TTC TCC ATG TGT CGC CCA AC-3’
Ogt-F	5’- -3’CTGTCACCCTTGACCCAAA
Ogt-R	5’- -3’ATGGGGTTGCAGTTCGATAG
Chrnd-F	5’- CGC TGC TTC TGC TTC TAG GG -3’
Chrnd-R	5’- ATC AGT TGG CCT TCG GCT T -3’
Chrna-F	5’- CCA CAG ACT CAG GGG AGA TAG
Chrna-R	5’- AAC GGT GGT CTG TGT TGA TGA TG -3’
Gapdh-F	5’- CTC CCA CTC TTC CAC CTT CG -3’
Gapdh-R	5’- GCC TCT CTT GCT CAG TGT CC – 3
Ppia-F	5’- GCC TTC CTC CTT TCA CAG AA -3’
Ppia-R	5’- GAT GCC AGG ACC TGT ATG CT-3’
Rpl27-F	5’- AAG CCG TCA TCG AGA ACA -3’
Rpl27-R	5’- CTT GAT CTT GGA TCG CTT GGC -3’
rtTA-F	5’- CTG GAG TTG AGC AGC CTA C -3’
rtTA-R	5’- AGA GCA CAG CGG AAT GAC TT -3’

Chapter 3: Galactose treatment rescues protein glycosylation and neuromuscular junction function in glutamine-fructose-6-phosphate transaminase 1 (Gfpt1) and Congenital Myasthenic Syndromes (CMS)

Holland, S.H.; Caromona-Martinez, O'Neil, D.; Ho, K.; O'Connor, K.; Azuma, Y.; Spendiff, S.; Lochmüller, H. *Human Molecular Genetics*. 2025

3.1 Statement of author contributions

This second research paper furthered the understanding of *GFPT1*-CMS pathogenesis and elucidated a novel treatment strategy for these patients. In our previous chapter we confirmed that *Gfpt1*-deficiency corresponds to a glycosylation disorder impacting both N- and O-linked glycan formation. In addition, we identified that NMJ-associated proteins such as the AChRδ was hypo-glycosylated in *Gfpt1*-deficeint samples. GFPT1 controls the HBP, a metabolic signalling pathway that produces UDP-GlcNAc the necessary precursor for both N- and O-linked glycan formation. The Leloir pathway, metabolizes galactose, a monosaccharide, into UDP-GalNAc. The final enzymatic step uses the enzyme *Gale* which can convert UDP-GalNAc into UDP-GlcNAc, potentially offering a mechanism to bypass the defective HBP in *GFPT1*-CMS. We then used our *Gfpt1*$^{tm1d/tm1d}$ mouse model to examine whether galactose supplementation could improve NMJ morphology and the neuromuscular deficit. We identified that indeed galactose supplementation in *Gfpt1*$^{tm1d/tm1d}$ improved behavioural assessments such as grip strength muscle fatigability and inverted hanging wire. We also identified that galactose supplementation in *Gfpt1*$^{tm1d/tm1d}$ improved the NMJ morphology. Lastly, we identified that indeed the Leloir pathway can rescue protein O-GlcNAcylation and N-linked glycosylation of AChRδ after galactose supplementation. All together these results indicate that galactose may be a suitable treatment strategy for *GFPT1*-CMS patients.

In addition, to this finding we identified that *Gfpt1*$^{tm1d/tm1d}$ NMJs exhibit substantial impairment to pre- and postsynaptic measurements. Our skeletal specific knockout of *Gfpt1* has substantial reduction to axonal thickness, and nerve terminal area suggesting that the motor neuron may also have a phenotype that has not been previously examined. This suggests the need to further investigate the role of Gfpt1 within the motor neuron, which has been addressed in the next chapter.

At the beginning of my PhD, I re-established the *Gfpt1*$^{tm1d/tm1d}$ mouse model and maintained mouse cohorts. Eventually, our laboratory technician, Daniel O'Neil took over for mouse breeding and

genotyping during this experiment protocol. Behavioural assessment of the mice was performed by Stephen Holland with assistance from the uOttawa BEH Core. At the time of dissections, both Daniel O'Neil, Ricardo Carmona-Martinez and Kelly Ho assisted with tissue collection. Stephen Holland developed a doxycycline-inducible Gfpt1-deficient C2C12 myoblast model. Monoclonal colony development was performed with assistance from Kaela O'Connor, who had adequate training to use the University of Ottawa's Flow Cytometry Core. Stephen Holland performed all additional experiments for this manuscript. Ricardo Carmona-Martinez assisted with tissue sectioning for muscle morphology; however, staining, image collection and analysis was performed by Stephen. Dr. Sally Spendiff and Dr. Hanns Lochmüller helped Stephen conceptualized the study and provided supervision for the entirety of the project. Originally, Dr. Azuma, a former student from Dr. Hanns Lochmüller lab back in Newcastle, conceptualized preliminary assessment of galactose treatment in *Gfpt1*-morpholino zebrafish. This work was not completed but served as the mechanism to support this work. Dr. Andreas Roos aided with intellectual support and offered guidance during the editing process. All authors performed editing and accepted the final copy prior to publication. Stephen Holland wrote the original draft of the manuscript and performed all revisions.

Galactose treatment rescues neuromuscular junction transmission in glutamine-fructose-6-phosphate transaminase 1 (Gfpt1) deficient mice

Stephen H. Holland[1, 2, 3], R. Carmona-Martinez[1], D. O'Neil[1], K. Ho[1, 2], K. O'Connor[1, 2], Y. Azuma[4, 5], A. Roos[3, 6, 7, 8], S. Spendiff[1], H. Lochmüller[1, 2, 3, 9, 10, 11*]

Affiliations

1. Children's Hospital of Eastern Ontario Research Institute, Ottawa, ON K1H 8L1, Canada

2. Department of Cellular and Molecular Medicine, Faculty of Medicine, University of Ottawa, ON K1H 8M5, Canada

3. Eric Poulin Center for Neuromuscular Disease, Brain and Mind Research Institute, University of Ottawa, Ottawa ON K1H 8M5, Canada

4. Department of Human Genetics, Graduate School of Medicine, Yokohama City University, Yokohama, Japan

5. Department of Pediatrics, Aichi Medical University, Nagakute, Japan

6. Department of Pediatric Neurology, Center for Neuromuscular Disorders, University Duisburg-Essen, 45147 Essen, Germany

7. Medical Faculty, University Hospital Düsseldorf, Heinrich Heine University, 40225 Düsseldorf, Germany

8. Department of Neurology with Heimer Institute for Muscle Research, University Hospital Bergmannsheil, Bochum, Germany.

9. Division of Neurology, Department of Medicine, The Ottawa Hospital Civic Campus, Ottawa, ON K1Y 4E9, Canada

10. Faculty of Medicine, Medical Center, University of Freiburg, 79085, Freiburg, Germany

11. Centro Nacional de Análisis Genómico (CNAG), 08028 Barcelona, Spain

Abstract:

Congenital myasthenic syndromes (CMS) arise from mutations to proteins involved in neuromuscular junction (NMJ) development, maintenance, and neurotransmission. To date, mutations in more than 35 genes have been linked to CMS development. Glutamine fructose-6-phosphate transaminase 1 (*GFPT1/Gfpt1)* serves as the rate-limiting enzyme of the hexosamine biosynthetic pathway (HBP), producing the byproduct (UDP-GlcNAc) necessary for protein glycosylation. Gfpt1-deficient models have impaired protein glycosylation, impacting key proteins at the NMJ. The Leloir pathway is a galactose metabolizing pathway which produces UDP-GalNAc as its final product. The enzyme UDP-GalNAc Epimerase (*GALE)* can also convert excess UDP-GalNAc into UDP-GlcNAc, the byproduct of the HBP. We hypothesized that treatment with galactose both *in vitro* and *in vivo* in Gfpt1-deficient models would rescue impaired protein O-GlcNAcylation and reverse the glycosylation status of key NMJ-associated proteins. We show that galactose treatment *in vitro* activated the Leloir pathway and rescued protein O-GlcNAcylation in Gfpt1-deficient C2C12 myoblasts. In addition, we demonstrated that galactose therapy rescued neuromuscular deficits, improved muscle fatigue and restored NMJ morphology in a skeletal muscle-specific Gfpt1 knockout mouse model. Lastly, we showed that galactose treatment rescued protein O-GlcNAcylation in skeletal muscle, preserving the glycosylation status of the delta (δ) subunit of the acetylcholine receptor (AChRδ). We hypothesize that supplementation can be further explored as a therapy for *GFPT1*-CMS patients.

1.0 Introduction

The neuromuscular junction (NMJ) is the site where the motor neuron innervates the skeletal muscle, enabling muscular contraction. Congenital myasthenic syndromes (CMS) are inheritable early-onset neuromuscular disorders that arise from mutations to proteins involved in NMJ development, maintenance, and function [1,2]. CMS is a heterogeneous disorder characterized by fatigable muscle weakness [1]. To date, over 35 genes have been associated with CMS [1,3]. These genes encode proteins that are localized to the presynaptic nerve terminal, postsynaptic skeletal muscle, and synaptic cleft. A subset of five CMS-causative genes impair glycosylation: glutamine-fructose-6-phosphate transaminase 1 (*GFPT1*), dolichol-phosphate N-acetylglucosaminephosphotransferase-1 (*DPAGT1*) [4–8], GDP-mannose pyrophosphorylase B (*GMPPB*) [9,10], α-1,3/1,6-mannosyltransferase (*ALG2*) [11,12], and UDP-N-acetylglucosaminyltransferase subunit 14 (*ALG14*) [11].

GFPT1 encodes the rate-limiting enzyme of the hexosamine biosynthetic pathway (HBP), a metabolic signaling pathway that produces the precursors for the formation of N- and O-linked glycans [13–16]. It has been speculated that hypoglycosylation of key NMJ proteins impairs neurotransmission and disrupts postsynaptic folding [15,17]. Biallelic mutations to *GFPT1* result in decreased protein levels, and impaired enzymatic activity [14,18–22]. Most recently, we identified that protein O-GlcNAcylation and N-linked glycosylation was impaired in Gfpt1-depleted models, confirming that *GFPT1*-CMS is a protein glycosylation disorder [15]. In addition, we discovered that the delta subunit of the acetylcholine receptor (AChRδ) in Gfpt1-depleted models was hypoglycosylated within the NMJ, resulting in a lower molecular weight species, thus defining the first NMJ-relevant glycosylation target of loss of Gfpt1-function [15].

Clinically, *GFPT1*-CMS patients present predominantly with limb/girdle muscle weakness [14,18,23]. Examination of muscle biopsies from patients reveals diverse myopathological features, including tubular aggregates and rimmed vacuoles [23,24]. In addition, these myopathological features were identified in our previously published skeletal-muscle specific mouse model, termed *Gfpt1*$^{tm1d/tm1d}$, demonstrating

that the mouse model accurately maps towards *GFPT1*-CMS in humans [15,17]. Electron microscopy analysis of NMJs show loss of postsynaptic folds and simplification [23,24]. Patients have frequently responded well to treatments that increase the availability of acetylcholine (ACh) in the synaptic cleft, such as pyridostigmine, an acetylcholine esterase (AChE) inhibitor, and potassium channel inhibitor 3,4-diaminopyridine [25,26]. However, long-term use of these compounds has been associated with adverse side effects in some patients [27]. Furthermore, the efficacy of these drugs may decrease over time, leading to worsening motor weakness [25,27]. Given these challenges, there is an urgent need for alternative therapies or co-therapeutic strategies to improve the long-term outcomes for CMS patients.

Congenital disorders of glycosylation (CDGs) arise from mutations to genes responsible for the synthesis or the attachment of glycans to glycoproteins [28]. Patients diagnosed with CDGs with variants in *PGM1*, *SLC34A2*, *SLC39A8,* and *TMEM165* show improved endocrine function, restored glycosylation, improved seizure control and improved blood coagulation with galactose supplementation [29–31]. We hypothesized that galactose supplementation could offer a beneficial treatment strategy for *GFPT1*-CMS patients, bypassing the defective HBP and restoring protein glycosylation.

In this study, we show galactose supplementation restores protein O-GlcNAcylation and rescues pathological features, including NMJ morphology and AChRδ glycosylation status in cell and animal models of Gfpt1-deficiency.

2.0 Methods

2.1 Cell culture

C2C12 cells (ATCC, CRL-1722, Burlington, Ontario) were cultured in high glucose Dulbecco's Modified Eagle Medium (DMEM) supplemented with 10% fetal bovine serum (FBS), 1% glutamine, and 1% penicillin/streptomycin. A Gfpt1-deficient C2C12 cell model was established using a TET-ON miR-30 tetracycline-inducible system (VectorBuilder, Chicago, IL) as previously described [15]. Gfpt1

silencing was achieved by doxycycline treatment at 2 μg/mL for 48 hours. (Sigma, D9891). Galactose treatment was performed with 10 mM of D-galactose (Caymen Chemicals, 20890) for 48 hours.

2.2 Real-Time qPCR (RT-qPCR)

RNA collection for *in vitro* experiments was performed using the RNeasy™ Micro mini kit (Qiagen, #74134, Toronto, Canada). Skeletal muscle RNA extraction was performed with the RNeasy™ Fibrous Micro mini kit (Qiagen, #74704) and quantified by NanoDrop (ND-1000, Spectrophotometer, NanoDrop®. RNA was converted to complementary DNA (cDNA) with the All-In-One 5x RT MasterMix (ABM, #G592, Richmond, BC, Canada) following kit guidelines. RT-qPCR was performed using the PowerUp™ SYBR™ Green Master Mix (FisherSci, #A25741, Ottawa, Canada) with the QuantStudio™ Studio 6 Flex Real-Time PCR System (Thermofisher, Ottawa, Canada) (see Supplementary Materials Table S1 for primer sequences). To analyze the expression of our target genes the geometric mean of three reference genes (*Gapdh, Rpl27, Ppia*) was used. Average CT values for these experiments can be found in the supplemental data.

2.3 Tissue/Cell lysis and Western blotting

Cell lysates and skeletal muscle homogenates were prepared with radioimmunoprecipitation assay (RIPA) buffer (150mM NaCl, 50mM Tris-HCl (pH 8), 1% Triton X-100, 0.5% NaDOC, 0.1% SDS) supplemented with protease (Roche, 04693116001, Mississauga, ON, Canada) and phosphatase (Roche, PHOSS-RO) inhibitors. Cell lysates were centrifuged at 15,000 × *g* for 10 minutes at 4 °C and the supernatants collected. Skeletal muscle samples were combined with lysis buffer and a metal bead in 2 mL SafeLock™ Eppendorf tubes (Eppendorf, 022363352, Mississauga, ON, Canada), then homogenized using a TissueLyser II (Qiagen, Toronto, ON, Canada). The protocol comprised of 3 rounds of homogenization at 30 Hz for 90 seconds followed by incubation on ice for 60 seconds. Afterwards, samples were kept at 4 °C for 4 hours on a rotating platform then centrifuged at 15,000 × *g* for 15 minutes

at 4 °C. Total protein concentration was determined using a DC Protein Assay (BioRad, 5000111) with BSA dilutions (Pierce, 23209) as standards. Proteins were resolved by SDS-PAGE and transferred to PVDF membranes using a BioRad™ Trans-Blot Turbo system (1704150EDU, Mississauga, ON, Canada).

Membranes were blocked with Intercept TBS blocking buffer (Li-Cor, 927-6000, Lincoln, NE, USA) for 1 hr and incubated with primary antibodies in blocking solution overnight at 4 °C. After washing with TBS + 1% Tween-20, membranes were incubated with IR Dye®800CW Donkey anti-Mouse IgG (Li-Cor, 926-32212, 1:5000) and IR Dye®680RD Goat anti-Rabbit IgG (Li-Cor, 926-68071, 1:5000) for 1 hour at room temperature. Blots were imaged using a Licor Odyssey DLX (Lincoln, NE, USA) and densitometry performed using Image Studio™ (Licor, version 6.0). Gapdh was used to normalize protein expression as it remained unchanged in experimental conditions.

2.4 Animal husbandry

Animals were housed at the University of Ottawa Animal Care and Veterinary Facility (Roger Guidon Hall, Ottawa, Canada) and all breeding and experimental protocols were approved by the internal Animal Care Committee (protocols: breeding – CHEO-3089 and experimental – CHEO-3120 approved on 16 November 2018 and 2 April 2019, respectively). Mice were maintained on a 12-hour light-dark cycle, with access to food and water *ad libitum* for the duration of this study. Mice were generated and genotyped as previously reported [15,17]. For this study, Tm1C homozygous mice (which contain two LoxP sites flanking the seventh exon of *Gfpt1* but lack *Ckm-Cre* expression) were used as controls. *Gfpt1*$^{tm1d/tm1d}$ mice contain two LoxP sites flanking the 7th exon of *Gfpt1* but also express a Cre recombinase tied to the *Ckm* reporter, which creates a skeletal muscle-specific knockout of *Gfpt1* [15,17]. For our study, we introduced a 10% (w/v) solution of D-galactose (Caymen Chemicals, 20890) in the drinking water starting at week 4, with water bottles weighed weekly to measure consumption. Mice

were weighed three times per week, and underwent several behavioural tests: inverted hanging wire, repetitive grip strength, EchoMRI, and Phenotyper™ activity test before tissue collection at 20 weeks.

2.5 Inverted screen test

Mice were suspended from an inverted wire grid and the time to fall was recorded, with the test being stopped after 10 mins if the mice had not yet fallen. The test was repeated 3 times, with 30 minutes between each trial. The average time was recorded and normalized to body weight to calculate hanging impulse (g x s).

2.6 Grip fatigability measurements

Repetitive grip strength measurements were conducted weekly on the fore and then all four paws. For this measurement, 8 consecutive recordings were performed on a grip strength meter (Chatillon DFE II Grip Meter, Columbus Instruments, Columbus, OH) to assess the fatigability of the forelimbs. Animals then were allowed to rest for 30 minutes and the test repeated with all four paws. The following equation was used to calculate grip strength fatigability:

$$Muscle\ Fatigability\ \%$$
$$= \left(\frac{Average\ of\ first\ four\ measurements - Average\ of\ last\ four\ measurements}{Average\ of\ total\ measurements}\right)$$

2.7 EchoMRI and total activity measurements

Body composition of fat and lean mass was measured weekly using the EchoMRI-700 Body Composition Analyzer (EchoMRI, Houston, TX). Animals also underwent 24-hour open activity monitoring using the Phenotyper™ system (Noldus Information Technology, Leesburg, VA) at week 15. Total distance travelled per hour was calculated using Phenotyper™ analysis software (EthoVision v15, Noldus Information Technology).

2.8 Immunostaining for NMJs in whole muscle mounts

Soleus muscles were fixed in 2% paraformaldehyde (PFA) for 20 minutes and then separated into small bundles and placed in 2% PFA overnight. The fibers were then washed with PBS (Sigma, P4417, Oakville, Canada), and placed in ice-cold analar ethanol followed by analar methanol for 10 minutes each. Fibers were transferred to blocking/permeabilization solution (5% horse serum, 5% bovine serum albumin, 1% triton X-100 in PBS) and incubated for 4 hours. The muscle fibers were then incubated with anti-SV2 (DSHB, 1:100, University of Iowa, Iowa City, IA) and neurofilament antibodies (DSHB (2H3), 1:100, University of Iowa, Iowa City, IA) in 5% horse serum/ 5% BSA for 24 hrs.

Fibers were washed with blocking buffer for 4 hours and incubated with alpha-bungarotoxin-488 (Invitrogen, B13422, 1:200, Burlington, Canada) and the secondary antibody Alexa Fluor anti-mouse-568 (Life Technologies, A11031, 1:250, Toronto, Canada) overnight. Following this incubation, the muscle fibers were washed with PBS for 4 hours and mounted on glass microscope slides using Vectashield® Antifade Mounting Medium (Vector Laboratories, H-1000-10, Newark, CA). To aid in mounting, several layers of electrical tape were used to create a reservoir to hold the muscle in place. A glass coverslip was applied and sealed with nail varnish. Imaging was performed on a confocal microscope (Olympus Fluoview FV-1000, Olympus, Richmond Hill, Canada). NMJ z-stacks were captured at 40× magnification with image acquisition being performed sequentially with consistent microscope settings. Efforts were made to capture all NMJs in each soleus muscle. Analysis was performed blinded on maximum intensity projection images according to the automated NMJ-Morph (aNMJ-Morph) protocol developed using FIJI [32,33].

2.9 Muscle histology

10 µm *Gastrocnemius* muscle sections were dried at room temperature for 1 hour and rinsed in tap water prior to staining with Harris's hematoxylin (Sigma, HHS32) for 2 minutes followed by rinsing in tap

water. Eosin Y (Sigma, HT110132) was then applied for 30 seconds, then the sections again washed in tap water. The slides were then dehydrated through a graded ethanol series ending with xylene, and mounted using DPX mounting media (Sigma, 6522). Images were acquired with a Zeiss Axio Imager M2 microscope at 10x magnification. For assessment of muscle morphology, randomized images of *gastrocnemius* muscle were used and approximately 500 muscle fibers were analyzed from each mouse. The polygonal function with ImageJ was used to trace muscle fibers and the "analyze particles" tool was then used to assess individual muscle fiber area and distribution. Centrally located nuclei were counted and presented as a percentage of total fibers measured.

2.10 Antibodies

The following antibodies were used for Western blot experiments: Gfpt1 (ProteinTech, #14132-1-AP, 1:500, Rosemont, IL), Gapdh (14C10) (Cell Signalling, 2118, 1:2000, Danvers, MA), O-GlcNAc (RL2) (Novus Biologicals, NB300-524, 1:1000, Toronto, Ontario), Ogt (ProteinTech, 66823-1-Ig, 1:1000, Rosemont, IL), AChRδ (C-4) (Santa Cruz, sc-390896, 1:1000, Dallas, TX). Antibodies for NMJ staining from whole muscle mounts were SV2 antibody (DSHB, 1:100, University of Iowa, Iowa City, IA) and neurofilament (DSHB (2H3), 1:100, University of Iowa, Iowa City, IA). Postsynaptic AChR clusters were detected with alpha-bungarotoxin-488 (Invitrogen, B13422, 1:200, Burlington, Canada).

2.11 Statistics

Data was analyzed with GraphPad Prism v 10.1.2. Data was checked for normality using the D'Agostino-Pearson test and outliers were identified using the robust regression and outlier remover (ROUT) method.

Statistical significance was determined by using unpaired two-tailed Student *t*-tests or analysis of variance (ANOVA) tests. If multiple comparisons were used, a Tukey's post-hoc test was performed. Results are presented as mean ± SD, where $p < 0.05$ was considered significant. For variables that were

not normally distributed, statistical significance was determined by a Kruskal-Wallis test followed by a Dunn's multiple comparisons test.

3.0 Results

3.1 Galactose treatment in C2C12 myoblasts activates Leloir pathway enzymes and increases protein O-GlcNAcylation

Monosaccharide supplementation has been shown to bypass defective glycosylation in different forms of CDGs [28–31,34]. *GFPT1*-CMS has been previously shown to have defects in HBP flux, which in turn impairs both protein O-GlcNAcylation and the production of complex N-linked glycan structures [15,17]. Galactose is a monosaccharide that is metabolized via the Leloir pathway to produce UDP-GalNAc (Figure 1A). The galactose-metabolizing enzyme *Gale* converts UDP-GalNAc into UDP-GlcNAc, the precursor for protein O-GlcNAcylation (Figure 1A). We investigated whether the inhibition of Gfpt1 with 6-diazo-5-oxo-L-norleucine (DON) activated the expression of galactose metabolizing enzymes *Galk, Galt,* and *Gale* in C2C12 myoblasts. We observed a slight, but significant increase in the expression of *Galk*, *Galt*, and *Gale* (Figure 1B to 1D). Treatment with galactose similarly enhanced the expression of *Galk, Galt,* and *Gale* (Figure 1E to 1G) along with *Slc35a2*, the UDP-galactose transporter (Figure 1H). Next, we studied whether there is a dose-dependent effect of galactose treatment on protein O-GlcNAcylation. By examining *Ogt* expression, the enzyme responsible for attaching the GlcNAc moiety to proteins, we showed that galactose treatment between 1 mM to 10 mM enhanced *Ogt* expression, with the effect plateauing at concentrations above 10 mM galactose (Figure 1I). This increase in *Ogt* expression is mirrored by an elevation in total protein O-GlcNAcylation after galactose treatment (Figure 1J and 1K). Similarly, at dosages exceeding 10 mM, protein O-GlcNAcylation levels plateau and all subsequent galactose experiments were therefore performed at 10 mM. Together, these data demonstrate that HBP flux in C2C12 myoblasts can be altered with galactose metabolism, leading to an overall increase in total protein O-GlcNAcylation.

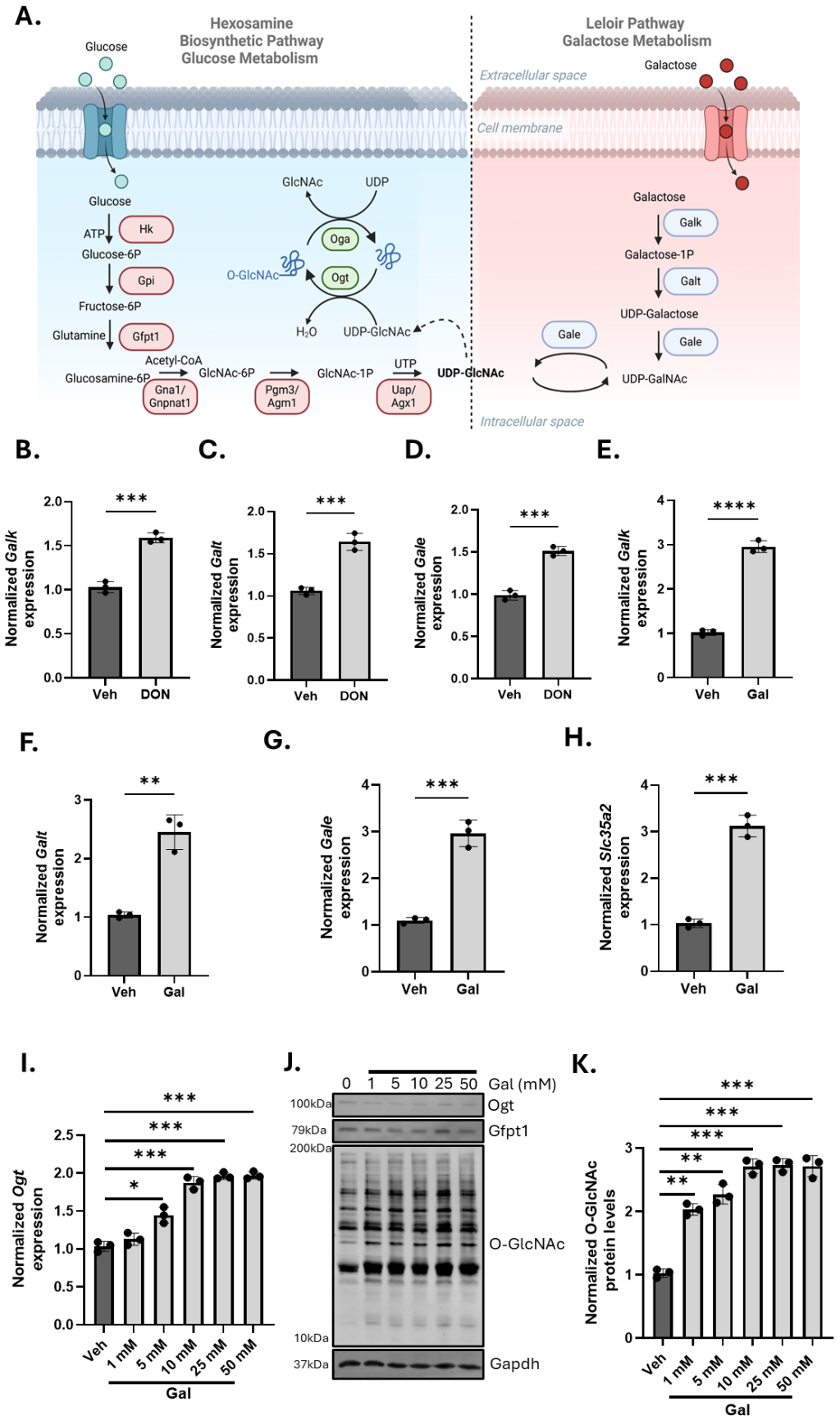
A.
Hexosamine
Biosynthetic Pathway
Glucose Metabolism
Leloir Pathway
Galactose Metabolism
Extracellular space
Cell membrane
Intracellular space
Glucose
Galactose
ATP
Hk
Glucose-6P
Gpi
Fructose-6P
Glutamine
Gfpt1
Acetyl-CoA
Glucosamine-6P
Gna1/
Gnpnat1
GlcNAc-6P
Pgm3/
Agm1
GlcNAc-1P
UTP
Uap/
Agx1
UDP-GlcNAc
GlcNAc
UDP
Oga
Ogt
O-GlcNAc
H2O
UDP-GlcNAc
Galk
Galactose-1P
Galt
UDP-Galactose
Gale
UDP-GalNAc
B.
C.
D.
E.
Normalized Galk expression
Normalized Galt expression
Normalized Gale expression
Normalized Galk expression
Veh
DON
Gal
F.
G.
H.
Normalized Galt expression
Normalized Gale expression
Normalized Slc35a2 expression
I.
J.
K.
Normalized Ogt expression
0 1 5 10 25 50 Gal (mM)
100kDa
Ogt
79kDa
Gfpt1
200kDa
O-GlcNAc
10kDa
37kDa
Gapdh
Normalized O-GlcNAc protein levels
1 mM
5 mM
10 mM
25 mM
50 mM

Figure 1: Galactose treatment elevates protein O-GlcNAcylation in C2C12 myoblasts. A. Gfpt1 serves as the rate-limiting enzyme of the hexosamine biosynthetic pathway (HBP), a metabolic signaling pathway which metabolizes glucose into UDP-GlcNAc, a precursor for N- and O-linked protein glycosylation. Galactose is a monosaccharide that feeds into the Leloir pathway within skeletal muscle. The Leloir pathway produces UDP-GalNAc, which can be converted by the Gale enzyme into UDP-GalNAc, effectively bypassing the defective HBP. **B**. In wild type C2C12 myoblasts, inhibition of Gfpt1 with DON for 48 hrs substantially increases the expression of Leloir pathway enzymes *Galk;* **C**. *Galt*; **D**. and *Gale*. **E**. C2C12 treatment with galactose significantly increases the expression of genes associated with the Leloir pathway: *Galk;* **F**. *Galt*; **G**. *Gale*; **H**. and the UDP-Galactose transporter, *Slc35a2*. **I.** Following galactose treatment, there is a dose-dependent increase in *Ogt* expression. **J.** A Western blot showing the protein levels of Ogt, Gfpt1 and O-GlcNAc within C2C12 myoblasts treated with varying concentrations of galactose. **K.** There is a significant increase in protein O-GlcNAcylation that plateaus beyond 10 mM of galactose. All graphs show mean ± SD. Statistical significance was determined via a Student t-test (Panels B through H) or a one-way ANOVA (Panels I and K). All experiments were performed with three biological replicates. * p-value < 0.05, ** p-value < 0.01, *** p-value < 0.001, and **** < 0.0001.

3.2 Galactose supplementation in Gfpt1-depleted C2C12 myoblasts improves protein O-GlcNAcylation.

Using an inducible *Gfpt1*-deficient C2C12 model with reduced Gfpt1, Ogt, and total protein O-GlcNAcylation levels [15], we examined if galactose treatment could improve the expression of *Scl35a2* and activate the Leloir pathway. We confirmed that Gfpt1 deficiency does not impact *Slc35a2* and *Gale* expression, though treatment with 10 mM galactose resulted in a notable increase in their expression when compared to the galactose-treated scramble C2C12 myoblasts (Figure 2A and 2B).

A 10 mM galactose treatment was administered with and without 2 μg/mL of doxycycline to induce the expression of shGfpt1 transgenes. While galactose treatment did not impact the expression of

Ogt in scramble control C2C12 myoblasts, Gfpt1-deficient myoblasts had a significant reduction in *Ogt* expression compared to scramble that was partially rescued with galactose treatment (Figure 2C). Gfpt1 depletion correlated with a decrease in overall protein O-GlcNAcylation levels after doxycycline activation (Figure 2D – 2F). While galactose treatment had no impact on Gfpt1 protein levels, it did improve total protein O-GlcNAcylation in both Gfpt1-depleted myoblasts (Figure 2D – 2F). All together, these results suggest that galactose supplementation *in vitro* can partially rescue protein O-GlcNAcylation.

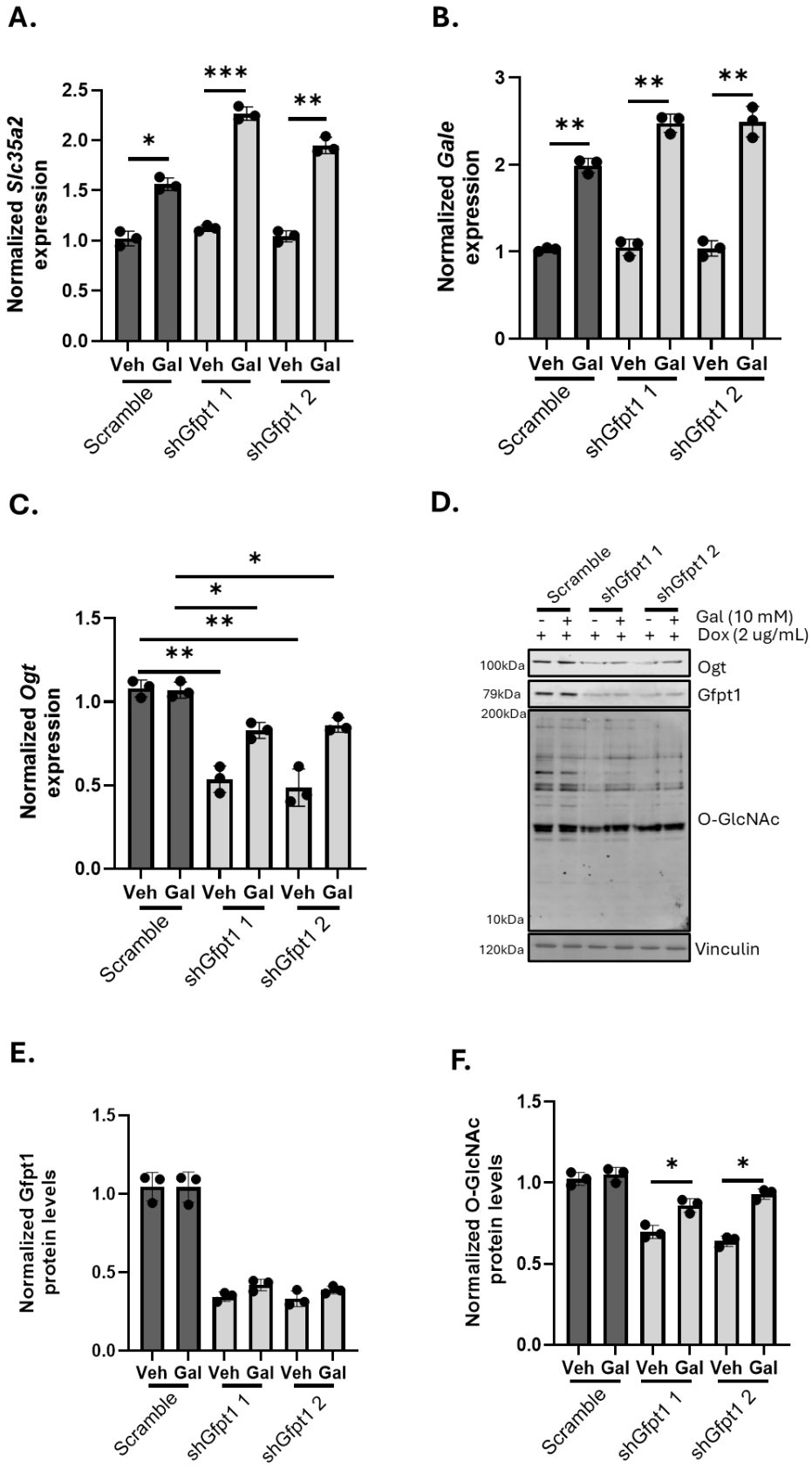
A.
Normalized Slc35a2 expression
2.5
2.0
1.5
1.0
0.5
0.0
*
***
**
Veh Gal Veh Gal Veh Gal
Scramble
shGfpt1 1
shGfpt1 2
B.
Normalized Gale expression
3
2
1
0
**
**
**
Veh Gal Veh Gal Veh Gal
Scramble
shGfpt1 1
shGfpt1 2
C.
Normalized Ogt expression
1.5
1.0
0.5
0.0
*
*
**
**
Veh Gal Veh Gal Veh Gal
Scramble
shGfpt1 1
shGfpt1 2
D.
Scramble
shGfpt1 1
shGfpt1 2
Gal (10 mM)
Dox (2 ug/mL)
100kDa
Ogt
79kDa
Gfpt1
200kDa
O-GlcNAc
10kDa
120kDa
Vinculin
E.
Normalized Gfpt1 protein levels
1.5
1.0
0.5
0.0
Veh Gal Veh Gal Veh Gal
Scramble
shGfpt1 1
shGfpt1 2
F.
Normalized O-GlcNAc protein levels
1.5
1.0
0.5
0.0
*
*
Veh Gal Veh Gal Veh Gal
Scramble
shGfpt1 1
shGfpt1 2

Figure 2: Galactose supplementation in Gfpt1-depleted C2C12 cells improves protein O-GlcNAcylation. A. Following galactose treatment, both control and Gfpt1-depleted C2C12 myoblasts [15] saw increased expression of *Slc35a2;* **B.** *Gale*; **C.** and *Ogt*. **D.** A Western blot showing protein levels of Ogt, Gfpt1, and O-GlcNAc after galactose treatment. **E.** Gfpt1 deficiency in shGfpt1 1 and 2 cells remains unchanged following galactose treatment. **F.** Gfpt1-depletion impairs protein O-GlcNAcylation, yet can be partially rescued with galactose treatment. All graphs show mean ± SD. Statistical significance was determined via a one-way ANOVA with a Tukey's multiple test correction. All experiments were performed with three biological replicates. Statistical comparison to untreated scramble, * p-value < 0.05, ** p-value < 0.01, *** p-value < 0.001, and **** < 0.0001.

3.3 10% (w/v) galactose treatment in Gfpt1$^{tm1d/tm1d}$ mice improves muscle strength and endurance

We previously showed Gfpt1 knockout results in progressive muscle fatigability with impaired NMJ morphology in mice [15,17]. We hypothesized that *ad libitum* access to a 10% (w/v) galactose solution would improve muscle fatigability and NMJ morphology in *Gfpt1$^{tm1d/tm1d}$* mice (Figure 3A). Over the course of 20 weeks, galactose treatment did not affect body weight in male or female mice (Figure 3B, Supplementary Figure 1A and B) and did not change body fat percentage [15] (Figure 3C, Supplementary Figure 1C and 1D). Water consumption remained consistent between the treatment groups regardless of galactose supplementation (data not shown).

Weekly behavioural studies were conducted to examine muscle endurance and grip strength fatigability. Untreated *Gfpt1$^{tm1d/tm1d}$* mice demonstrated a progressive impairment to hanging impulse (Figure 3D, Supplementary Figure 2A, B, and C) and increased grip strength fatigability (Figure 3E, Supplementary Data). Galactose treatment partially rescued the hanging impulse (Figure 3D, Supplementary Figure 2A) and both front paw and all-paw grip strength fatigability (Figure 3E and 3F, Supplementary Data – Excel Sheet). Comparisions between mouse body wieght and inverted hanging time at Week 10 and Week 20 showed differences between mice are driven by muscle fatigue, rather

than body wieght (Supplementary Figure 2B and 2C). In addition, while there was no substantive changes in maximal and average grip strength measurements between experiemental groups (Supplementary Figure 3). *Gfpt1*$^{tm1d/tm1d}$ mice also exhibited a decrease in total activity over 24 hours compared to control Tm1C homozygous mice (Figure 3G) which was partially rescued with galactose treatment (Figure 3E). All together, these results suggest that galactose treatment in *Gfpt1*$^{tm1d/tm1d}$ mice improved behavioural deficits.

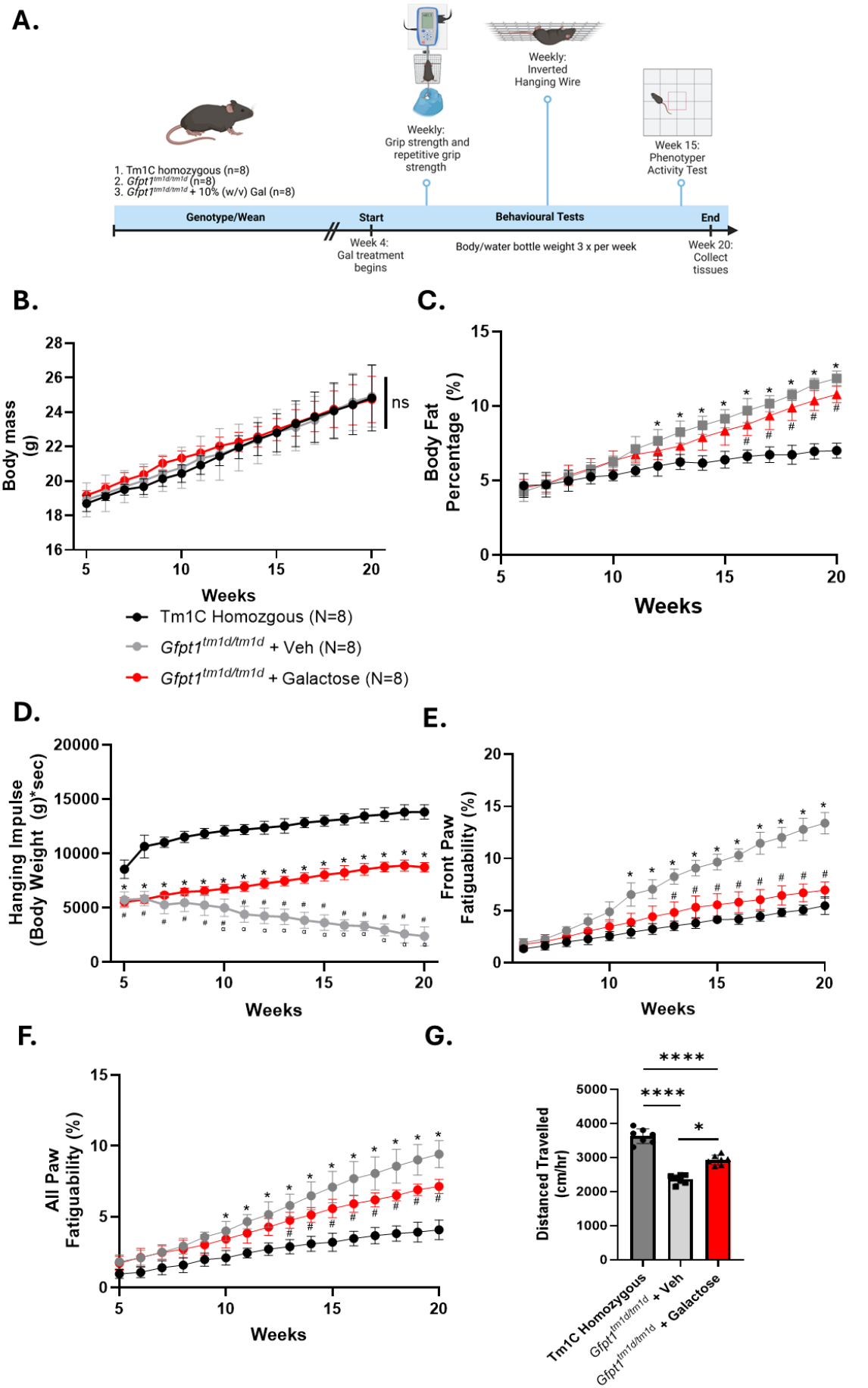
A.
1. Tm1C homozygous (n=8)
2. Gfpt1tm1d/tm1d (n=8)
3. Gfpt1tm1d/tm1d + 10% (w/v) Gal (n=8)
Weekly: Grip strength and repetitive grip strength
Weekly: Inverted Hanging Wire
Week 15: Phenotyper Activity Test
Genotype/Wean
Start
Week 4: Gal treatment begins
Behavioural Tests
Body/water bottle weight 3 x per week
End
Week 20: Collect tissues
B.
Body mass (g)
ns
Weeks
C.
Body Fat Percentage (%)
Weeks
Tm1C Homozgous (N=8)
Gfpt1tm1d/tm1d + Veh (N=8)
Gfpt1tm1d/tm1d + Galactose (N=8)
D.
Hanging Impulse (Body Weight (g)*sec)
Weeks
E.
Front Paw Fatigability (%)
Weeks
F.
All Paw Fatigability (%)
Weeks
G.
Distanced Travelled (cm/hr)
****
****
*
Tm1C Homozygous
Gfpt1tm1d/tm1d + Veh
Gfpt1tm1d/tm1d + Galactose

Figure 3: Galactose treatment of Gfpt1 mice (*Gfpt1*$^{tm1d/tm1d}$) partially rescues fatigable muscle weakness. A. A graphical overview of the galactose treatment timeline for 20 weeks. *Gfpt1*$^{tm1d/tm1d}$ mice received either drinking water or a 10% (w/v) solution of galactose. All mice underwent weekly behavioural testing, with the exception of a Phenotyper activity test at week 15. The study was completed at week 20. **B.** There was no significant difference in body weights between Tm1C homozygous control mice and *Gfpt1*$^{tm1d/tm1d}$ mice, regardless of treatment. **C.** Weekly EchoMRI measurements were performed to examine differences between fat mass. **D.** *Gfpt1*$^{tm1d/tm1d}$ mice displayed progressive impairment in inverted hanging wire impulse compared to Tm1C homozygous control mice, which was partially rescued with galactose treatment. **E.** *Gfpt1*$^{tm1d/tm1d}$ mice had a significant increase in grip strength fatigability compared to control mice, which saw moderate improvements with galactose treatment. **F.** A similar pattern was seen in four paw measurements, with galactose treatment rescuing the grip strength fatigability in *Gfpt1*$^{tm1d/tm1d}$ mice. **G.** At week 15, galactose treatment partially rescued *Gfpt1*$^{tm1d/tm1d}$ mouse activity after a 24 hr spontaneous activity assessment. All graphs show mean ± SD. Statistical significance was determined via a two-way ANOVA for Figures B through F, n=8 for all groups. Statistical comparison from Tm1C homozygous control to *Gfpt1*$^{tm1d/tm1d}$, * p-value < 0.05. Statistical comparison from Tm1C homozygous control to galactose-treated *Gfpt1*$^{tm1d/tm1d}$, # p-value < 0.05. Statistical significance for Figure G was determined via a one-way ANOVA, **** p-value < 0.0001.

3.4 Galactose treatment improves skeletal muscle morphology in Gfpt1$^{tm1d/tm1d}$ *mice*

Hematoxyline and eosin (H&E) staining was used to assess muscle fiber morphology. Muscle fibres from Tm1C homozygous mice appeared healthy and polygonal, with no signs of tubular aggregate formation or necrosis (Figure 4A). In contrast, vehicle-treated *Gfpt1*$^{tm1d/tm1d}$ mice showed classic *GFPT1*-CMS features, including rounded fibers (black asteriks), tubular aggregates (white arrows), centrally located nuceli (black arrow head), fibrotic (white astericks), necrotic (black arrows) and regenerative muscle fibers (blue arrows) (Figure 4A). Galactose-treated mice lacked fibrotic and necrotic fibers though

tubular aggreates were still present, albeit less abundant (Figure 4A). Galactose treatment in *Gfpt1*$^{tm1d/tm1d}$ mice restored mean muscle fiber area, which was reduced in vehicle-treated counterparts (Figure 4B). There were more centrally located nuclei in vehicle-treated *Gfpt1*$^{tm1d/tm1d}$ mice compared to Tm1C homozyogous control and galactose treated mice (Figure 4C). Muscle fiber size distribution showed smaller fibers in vehicle-treated *Gfpt1*$^{tm1d/tm1d}$ mice with an increase in the number of larger fibres being observed in galatose treated animals (Figure 4D). Collectively, these findings indicate that galactose treatment improves muscle fiber morphology, and pathology in *Gfpt1*$^{tm1d/tm1d}$ mice.

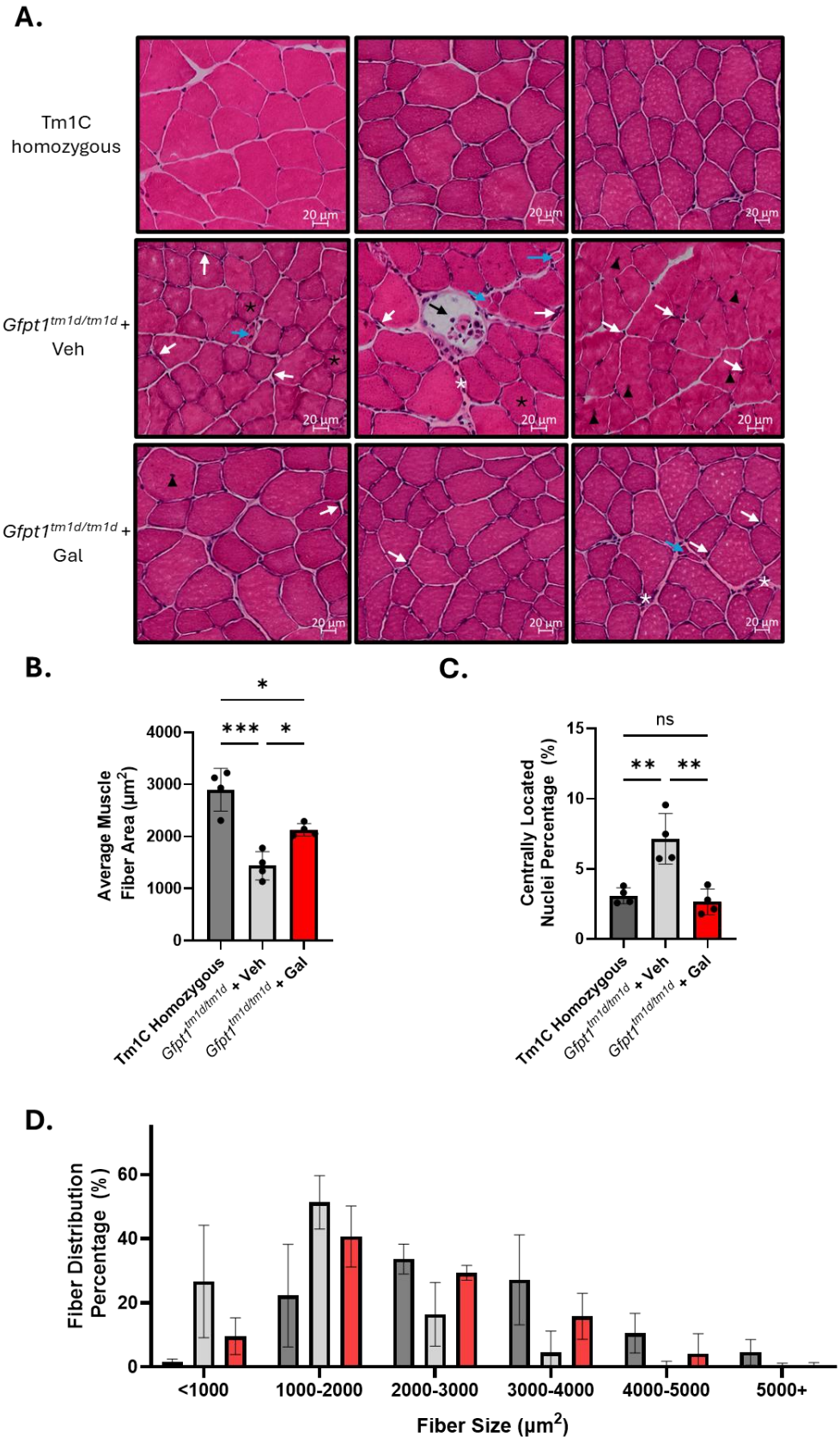
A.
Tm1C homozygous
Gfpt1tm1d/tm1d + Veh
Gfpt1tm1d/tm1d + Gal
20 µm
B.
Average Muscle Fiber Area (µm2)
4000
3000
2000
1000
0
*
***
*
Tm1C Homozygous
Gfpt1tm1d/tm1d + Veh
Gfpt1tm1d/tm1d + Gal
C.
Centrally Located Nuclei Percentage (%)
15
10
5
0
ns
**
**
Tm1C Homozygous
Gfpt1tm1d/tm1d + Veh
Gfpt1tm1d/tm1d + Gal
D.
Fiber Distribution Percentage (%)
60
40
20
0
<1000
1000-2000
2000-3000
3000-4000
4000-5000
5000+
Fiber Size (µm2)

Figure 4: Galactose treatment rescues histological and morphometric analysis of *gastrocnemius* muscle in *Gfpt1*$^{tm1d/tm1d}$ mice. A. Representative H&E stained sections (250 μm by 250 μm) showing healthy polygonal fibers in Tm1C homozygous controls, pathological features including rounded fibers (black asteriks), tubular aggregates (white arrow), fibrosis (white asteriks), necrosis (black arrow), regenerating fibers (blue arrow) and centrally located nuceli (black arrowhead), and a partial rescue in galactose treated *Gfpt1*$^{tm1d/tm1d}$ mice. Scale bar 20 μm. **B.** Quantification of mean muscle fiber area showed a decrease in vehicle-treated *Gfpt1*$^{tm1d/tm1d}$ mice compared to Tm1C homozygous control mice, while galactose treatment rescued mean fiber area. **C.** Quantification of centrally located nuclei per muslce fiber showed that vehicle-treated *Gfpt1*$^{tm1d/tm1d}$ mice had an increased percentage of centrally located nuclei, while galactose treatment signficantly reduced the percentage of centrally located nuclei. **D.** Muscle fiber distribution was then analyzed which shows vehicle-treated *Gfpt1*$^{tm1d/tm1d}$ mice tend to have smaller muslce fibers, while galactose treatment restores muscle fiber size towards healthy Tm1C homozygous control mice. All graphs show mean ± SD. Statistical significance was determined via a one-way ANOVA with an additional Tukey post-hoc test for Figures B through D, n=4 for all groups: * p-value < 0.05, ** p-value < 0.01, *** p-value < 0.001. For Figure 4D a two-way ANOVA was performed with a Dunnett's multiple comparision test, n=4 for all groups: *Gfpt1*$^{tm1d/tm1d}$ mice had smaller muscle fibers <1000 μm^2 compared to Tm1C homozygous control *** p-value < 0.001, while galactose treated mice tend to have a more normal fiber distribution.

3.5 Galactose treatment improves neuromuscular junction morphology and integrity

Abnormal NMJ morphology has been observed in both humans with *GFPT1*-CMS and *Gfpt1*$^{tm1d/tm1d}$ mice [14,15,17–19,21–24]. Untreated *Gfpt1*$^{tm1d/tm1d}$ mice have smaller, less complex NMJs compared to those of healthy control mice which appear as large, pretzel-like structures (Figure 5A).

To quantify these changes, we used NMJ-Morph to measure core and derived variables of synaptic morphology [32,33]. Within *Gfpt1*$^{tm1d/tm1d}$ NMJs, axonal diameter was significantly decreased

compared to controls (Figure 5B). Furthermore, we observed a significant decrease in presynaptic nerve terminal perimeter and area (Figure 5C and Supplementary Table S2). Galactose treatment in *Gfpt1*$^{tm1d/tm1d}$ mice partially rescued both axonal diameter and presynaptic nerve terminal area/perimeter (Figure 5B, 5C, Supplementary Table S2).

Next, we examined postsynaptic morphology in *Gfpt1*$^{tm1d/tm1d}$ NMJs and observed a significant decrease in the AChR area (Figure 5D). Beyond AChR area, we found substantive morphological alterations to endplate area, perimeter, and diameter (Supplementary Tables S2). Again, galactose treatment in *Gfpt1*$^{tm1d/tm1d}$ mice partially rescued AChR area (Figure 5D). In addition, galactose treated *Gfpt1*$^{tm1d/tm1d}$ mice had improved endplate area and diameter compared to untreated *Gfpt1*$^{tm1d/tm1d}$ mice (Supplementary Table S2).

Gfpt1$^{tm1d/tm1d}$ mice also had a reduction in area of synaptic contact (Figure 5E) and percent overlap of the pre- and postsynaptic apparatus (Supplementary Table S2) that was improved with galactose treatment (Figure 5E and Supplementary Table S2). No significant alterations in NMJ fragmentation was noted in any group. All together, these results demonstrate substantial pre- and postsynaptic defects in NMJ morphology of *Gfpt1*$^{tm1d/tm1d}$ mice that were partially rescued following galactose supplemention.

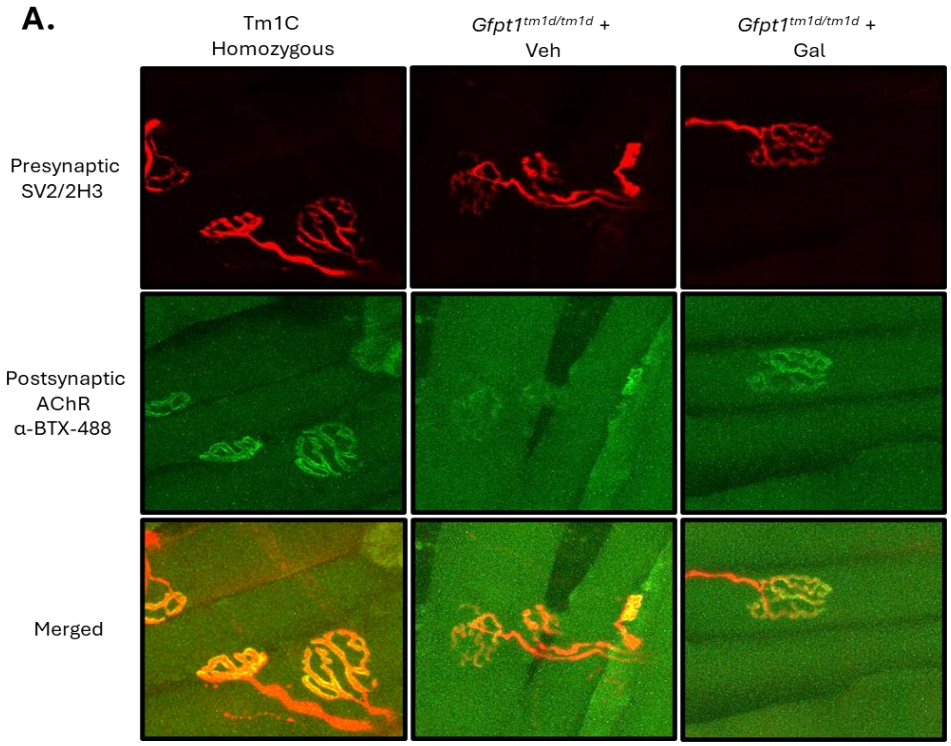
A.
Tm1C Homozygous
Gfpt1tm1d/tm1d + Veh
Gfpt1tm1d/tm1d + Gal
Presynaptic SV2/2H3
Postsynaptic AChR α-BTX-488
Merged

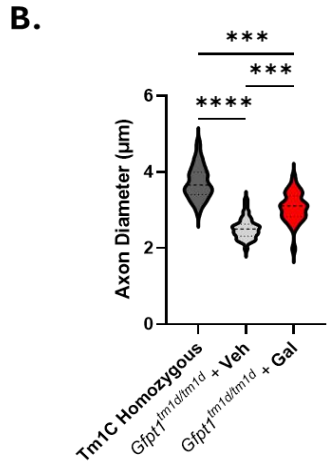
B.
Axon Diameter (µm)
***
***
****
Tm1C Homozygous
Gfpt1tm1d/tm1d + Veh
Gfpt1tm1d/tm1d + Gal

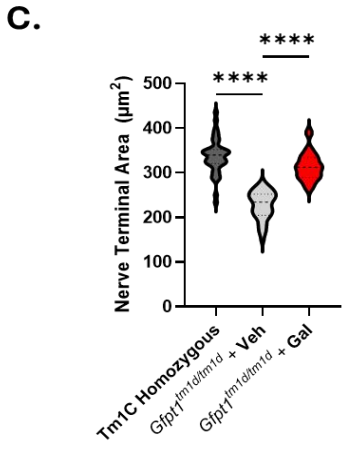
C.
Nerve Terminal Area (µm2)
****
****
Tm1C Homozygous
Gfpt1tm1d/tm1d + Veh
Gfpt1tm1d/tm1d + Gal

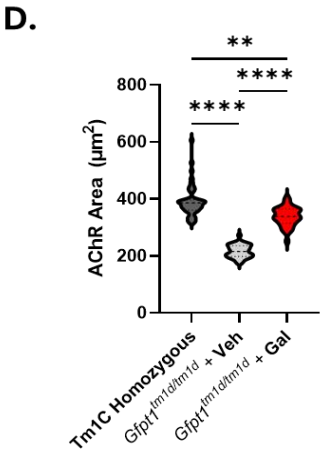
D.
AChR Area (µm2)
**
****
****
Tm1C Homozygous
Gfpt1tm1d/tm1d + Veh
Gfpt1tm1d/tm1d + Gal

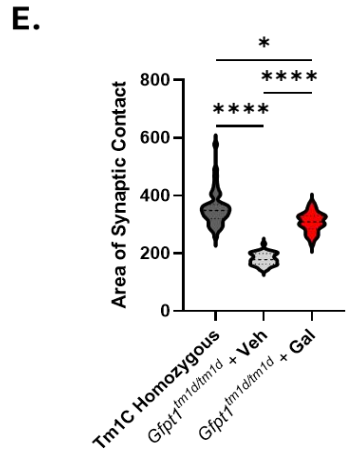
E.
Area of Synaptic Contact
*
****
****
Tm1C Homozygous
Gfpt1tm1d/tm1d + Veh
Gfpt1tm1d/tm1d + Gal

Figure 5: Galactose treatment in *Gfpt1*$^{tm1d/tm1d}$ mice improves NMJ morphology. A. A representative max intensity projection of whole mounted soleus muscle obtained from Tm1C homozygous control, untreated *Gfpt1*$^{tm1d/tm1d}$, and galactose treated *Gfpt1*$^{tm1d/tm1d}$ mice. Muscles were stained for NMJs using alpha-bungarotoxin-488 (green) to label postsynaptic AChR clusters and neurofilament/SV2 to label the presynaptic terminal. **B.** Pre- and postsynaptic morphological characteristics of NMJs were examined using aNMJ-morph. We identified that galactose therapy partially rescued deficits in axonal diameter (μm); **C.** nerve terminal area (μm^2); **D.** AChR area (μm^2); **E.** and area of synaptic contact (μm^2). These features were significantly impaired in untreated *Gfpt1*$^{tm1d/tm1d}$ mice compared to control mice. Normality of data was examined using a D'Agostino-Pearson test followed by a Kruskal-Wallis test, with a correction by Dunn's multiple comparisons test. Total NMJs analyzed were n = 162, n = 178, and n = 152 for Tm1C homozygous, untreated *Gfpt1*$^{tm1d/tm1d}$ and galactose treated *Gfpt1*$^{tm1d/tm1d}$ mice, respectively from 6 mice in each treatment group. Statistical comparison to untreated scramble, * p-value < 0.05, ** p-value < 0.01, *** p-value < 0.001, and **** < 0.0001.

3.6 Galactose treatment improves deficient O-GlcNAcylation within skeletal muscle and improves the glycosylation status of AChRδ.

We have demonstrated that galactose therapy rescues the neuromuscular deficits and improves NMJ morphology in *Gfpt1*$^{tm1d/tm1d}$ mice. We hypothesized that galactose would also restore deficient glycosylation of critical NMJ-associated proteins in *Gfpt1*$^{tm1d/tm1d}$ skeletal muscle.

First, we demonstrated that *Gfpt1*$^{tm1d/tm1d}$ quadriceps express Leloir pathway enzymes *Galt, Galk* and *Gale*. We identified that they were unchanged when compared to control quadriceps (Figure 6A to 6C). However, galactose treated *Gfpt1*$^{tm1d/tm1d}$ mice displayed a three-fold increase in the expression of *Galt, Galk* and *Gale* enzymes, suggesting that the excess galactose is being metabolized by the Leloir pathway (Figure 6A to 6C). Since the Leloir pathway had elevated enzyme expression, we hypothesized that excess UDP-GalNAc could be converted to UDP-GlcNAc through the enzyme *Gale*. This would

boost the expression of *Ogt*, the enzyme responsible for proper protein O-GlcNAcylation. Galactose treated *Gfpt1*$^{tm1d/tm1d}$ mice displayed elevated expression of *Ogt* compared to untreated *Gfpt1*$^{tm1d/tm1d}$ mice (Figure 6D). However, this was still significantly lower than that of Tm1C homozygous mice, suggesting a partial restoration of O-GlcNAcylation (Figure 6D). We then performed a Western blot and used antibodies targeting the O-GlcNAc moiety on proteins (Figure 6E). We found that galactose treatment in *Gfpt1*$^{tm1d/tm1d}$ mice restored deficient protein O-GlcNAcylation (Figure 6F), confirming that galactose treatment rescues skeletal muscle glycosylation in *Gfpt1*$^{tm1d/tm1d}$ mice.

Finally, we previously published that a hypoglycosylated AChRδ subunit is expressed as a result of defective protein glycosylation in *Gfpt1*$^{tm1d/tm1d}$ mice [15]. In healthy Tm1C homozygous skeletal muscle, a single 65 kDa protein is visible, whereas *Gfpt1*$^{tm1d/tm1d}$ samples also contained a lower 60 kDa protein species [15]. A Western blot was performed to examine whether galactose could restore the glycosylation status of AChRδ within *Gfpt1*$^{tm1d/tm1d}$ skeletal muscle (Figure 6G). Indeed, galactose treated *Gfpt1*$^{tm1d/tm1d}$ mice had restored expression of AChRδ in skeletal muscle and reversed the glycosylation status of AChRδ to a single molecular weight species at 65 kDa (Figure 6G to 6I). Taken together, these results indicate that galactose treatment restores defective N- and O-linked glycosylation in *Gfpt1*$^{tm1d/tm1d}$ skeletal muscle, suggesting that galactose supplementation may be an effective treatment strategy for *GFPT1*-CMS patients.

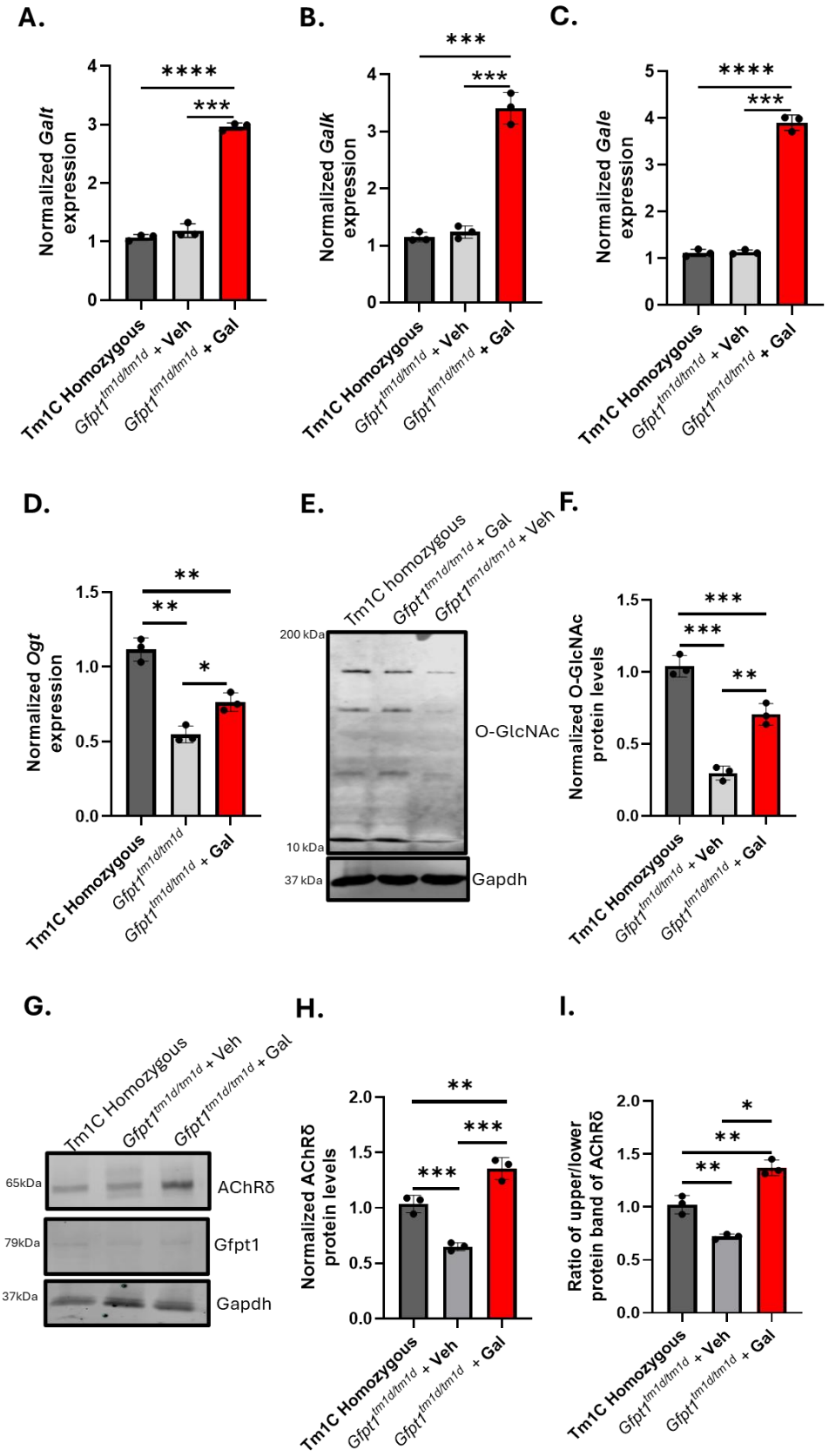
A.
B.
C.
Normalized Galt expression
Normalized Galk expression
Normalized Gale expression
****
***
Tm1C Homozygous
Gfpt1tm1d/tm1d + Veh
Gfpt1tm1d/tm1d + Gal
D.
E.
F.
Normalized Ogt expression
Tm1C homozygous
Gfpt1tm1d/tm1d + Gal
Gfpt1tm1d/tm1d + Veh
200 kDa
10 kDa
37 kDa
O-GlcNAc
Gapdh
Normalized O-GlcNAc protein levels
Gfpt1tm1d/tm1d
G.
H.
I.
65kDa
79kDa
37kDa
AChRδ
Gfpt1
Gapdh
Normalized AChRδ protein levels
Ratio of upper/lower protein band of AChRδ

Figure 6: Galactose treatment of *Gfpt1*$^{tm1d/tm1d}$ mice rescues protein O-GlcNAcylation and maintains glycosylation of NMJ-associated proteins. A. Gene expression of the Leloir pathway enzymes *Galt;* **B.** *Galk;* **C.** and *Gale* increased significantly within the quadriceps of galactose treated *Gfpt1*$^{tm1d/tm1d}$ mice. **D.** Untreated *Gfpt1*$^{tm1d/tm1d}$ mice exhibited reduced *Ogt* expression, which was partially rescued with galactose treatment **E.** A Western blot showing protein O-GlcNAcylation levels in Tm1C homozygous control, untreated *Gfpt1*$^{tm1d/tm1d}$, and galactose treated *Gfpt1*$^{tm1d/tm1d}$ mice. **F.** There was a significant decrease in protein O-GlcNAcylation in *Gfpt1*$^{tm1d/tm1d}$ mice, while galactose treated *Gfpt1*$^{tm1d/tm1d}$ mice had a significant increase in protein O-GlcNAcylation compared to untreated *Gfpt1*$^{tm1d/tm1d}$ mice. **G.** A Western blot showing protein levels of Gfpt1 and AChRδ obtained from the quadriceps of Tm1C homozygous control, untreated *Gfpt1*$^{tm1d/tm1d}$, and galactose treated *Gfpt1*$^{tm1d/tm1d}$ mice. **H.** There is a significant decrease in AChRδ protein levels in *Gfpt1*$^{tm1d/tm1d}$ which was rescued following galactose treatment. **I.** In *Gfpt1*$^{tm1d/tm1d}$ muscle, AChRδ contains two molecular weight species at 65 kDa and a hypoglycosylated protein at 60 kDa. Galactose treatment reduces the expression of the lower molecular weight species, improving the ratio of expression between the 65 kDa and 60 kDa molecular weight species. All graphs show mean ± SD. Statistical significance was determined via a one-way ANOVA. All experiments were performed with three mice in each group. Statistical comparision to from Tm1C homozygous control to untreated or galactose treated *Gfpt1*$^{tm1d/tm1d}$ mice, ** p-value < 0.01, *** p-value < 0.001, and **** < 0.0001. Statistical comparision between untreated *Gfpt1*$^{tm1d/tm1d}$ mice to galactose treated mice, # p-value < 0.05, ## p-value < 0.01, ### p-value < 0.001.

4.0 Discussion

In this study we tested the hypothesis that galactose supplementation could bypass the defective HBP in *Gfpt1*-deficient samples, rescuing protein glycosylation, NMJ morphology, and the neuromuscular phenotype in *Gfpt1*$^{tm1d/tm1d}$ mice. Earlier studies have shown that *GFPT1*-CMS patients display fatigable weakness of limb girdle muscles [18,19,23–25,35]. While there is no approved treatment

option for CMS patients, off-label drugs such as AChE inhibitors and salbutamol have provided some benefit. We previously identified that *Gfpt1*-deficient mice have impaired N-linked glycosylation and O-GlcNAcylation [15]. Gfpt1 has been shown to be the rate-limiting enzyme of the HBP, a metabolic pathway required to produce the precursors for protein glycosylation and O-GlcNAcylation [13–15,36]. Monosaccharide sugar supplementation has been an effective strategy for CDG patients as it can bypass defective pathways, repairing the glycosylation status of proteins [29,37,38]. The Leloir pathway breaks down galactose into UDP-GlcNAc, the precursor for glycosylation and O-GlcNAcylation [30,39]. Therefore, galactose may be a suitable treatment strategy for *GFPT1*-CMS patients. To our knowledge, this is the first study that examined nutritional monosaccharide supplementation in a CMS model.

As previously shown [40], Leloir pathway enzymes *Galt, Galk* and *Gale* were expressed within skeletal muscle and C2C12 myoblasts and treatment with galactose increased their expression Furthermore, galactose treatment increased expression of *Ogt* and total protein O-GlcNAcylation in *Gfpt1*-deficient C2C12 myoblasts. We showed that DON inhibition at 500 μM inhibits Gfpt1 enzymatic activity – whereas, *Gfpt1*-deficient C2C12 myoblasts still have residual enzymatic activity[14,15,18]. Therefore, the Leloir pathway shunt may not be requried within this condition, until galactose is present to stimulate the production of excess UDP-GlcNAc and O-GlcNAcylation. This could account for the discrepancy between chemical inhibition of Gfpt1 and knockdown models for the expression of *Gale* and *Slc35a2.* In addition, we identified that Ogt protein levels did not significantly increase in *Gfpt1*-deficient myoblasts, which may be explained through residual expression of Gfpt1, as UDP-GlcNAc production requires feedback loop inhibiton for Gfpt1 and Ogt activity [41].

Gfpt1$^{tm1d/tm1d}$ mice were previously shown to have exercise-induced muscle weakness, impaired NMJ morphology, and defective glycosylation of AChRδ [15,17]. In our study, galactose supplementation in *Gfpt1*$^{tm1d/tm1d}$ mice partially rescued muscle fatigue, improved NMJ morphology, and restored AChRδ

glycosylation status. These findings suggest that galactose supplementation improves *GFPT1*-CMS phenotype *in vitro* and *in vivo*.

We identified that galactose supplementation restored N-linked protein glycosylation of AChRδ. Previously, it has been demonstrated that within *GFPT1*-CMS patient-derived myoblasts that global N-linked glycosylation levels were unchanged [42]. However, we have recently shown that AChRδ, an extensive N-linked glycosylated protein, was hypoglycosylated within *Gfpt1*-deficient specimens [15]. This global glycomic approach may miss individual changes that might be diluted in larger samples. In addition, the occupancy of glycosylated proteins was not accounted for in global glycomic approaches [42]. As such, future work in *GFPT1*-CMS should be focused on targeted glycoproteomic assessment, to examine the glycan chain occupancy of individual proteins at the NMJ. We speculate that hypoglycosylated AChRδ may have impaired channel kinetics and stability at the postsynaptic membrane. Studies have shown that altering the glycosylation sites on AChRδ impairs the surface expression of AChR complexes [43–45]. One study identified that N-linked glycosylation is necessary for AChR complex assembly but is not required for trafficking towards the surface by the ER chaperone calnexin [45]. Furthermore, removal of key ubiquitination sites from lysine residues also perturbed Golgi-based AChR glycosylation, impacting surface expression [44]. We have identified that hypoglycosylated AChRδ is expressed at the NMJ after laser capture enrichment of NMJs from *Gfpt1*$^{tm1d/tm1d}$ mice, but had weaker α-BTX staining [15,17]. In addition, CMS patients with mutations to AChR subunits often show reduced AChR complexes at the NMJ, due to an impairment to the interaction of AChR subunits with RAPSN [46]. As such, we anticipate that *Gfpt1*$^{tm1d/tm1d}$ mice may have an AChR docking or anchoring impairment that is partially resolved after galactose treatment.

In addition to the rescued N-linked glycosylation of AChRδ, galactose supplementation restored total protein O-GlcNAcylation levels. O-GlcNAcylation has been shown to regulate protein activity, stability, and cellular localization, with turnover rates similar to that of protein phosphorylation [47–49]. To

date, over 8,000 proteins have been associated with protein O-GlcNAcylation [50]. In particular, O-GlcNAcylation has been shown to be essential for muscle health and contractile properties [41]. At the NMJ, sub-synaptic nuclei and associated mitochondria are in high abundance. Thus, modulation of O-GlcNAcylation may impair energetics and gene expression of NMJ-associated genes [51–53]. As such, identifying which proteins are not O-GlcNAcylated within *Gfpt1*-deficient NMJs may yield alternative therapeutic strategies and further understanding of the pathomechanisms of disease. Importantly, galactose supplementation restored protein O-GlcNAcylation through bypassing the defective HBP in *Gfpt1*-deficient specimens, suggesting that this impairment can be rescued.

We showed that galactose supplementation partially restored NMJ morphology, accounting for an improvement in the *Gfpt1*$^{tm1d/tm1d}$ phenotype. NMJ-Morph analysis revealed substantial impairment in *Gfpt1*$^{tm1d/tm1d}$ mouse nerve terminal area and perimeter, along with a significant decrease in axonal thickness – all novel findings within *Gfpt1*-deficient models [16,21]. It has been shown that skeletal muscle produces retrograde signals which preserve presynaptic motor neuron integrity [54]. Previous studies have demonstrated presynaptic nerve terminal morphological changes in skeletal muscle-specific transgenic mice [55,56]. Additional evidence for motor nerve terminal morphological changes is present in postsynaptic *Agrn-, Musk-, Rapsn-, Dok7, ColQ*-CMS mouse models [57–62].

Therefore, we speculate that hypoglycosylated retrograde signals from the skeletal muscle to the motor neuron may be impaired within *Gfpt1*$^{tm1d/tm1d}$ mice. Interestingly, we did not observe any significant changes in the degree of fragmentation across treatment groups, a common metric of NMJ dysfunction [63]. However, recent studies indicate no correlation between AChR fragmentation and neurotransmission efficiency [63,64]. In fact, it has been suggested that AChR fragmentation allows the NMJ to adapt to the changing conditions to preserve neuromuscular transmission [63]. We show a positive association between galactose supplementation and NMJ morphology of both core and derived variables using aNMJ-Morph in both pre- and postsynaptic measurements.

Previous studies with the *Gfpt1*$^{tm1d/tm1d}$ mouse model identified muscle morphological alterations with the presence of rounded myofibers, internalization of nuclei, necrotic fibers and the presence of atrophic and hypertrophic fibers [17]. In addition, a hallmark of *GFPT1*-CMS in humans, *Gfpt1*$^{tm1d/tm1d}$ mice contained tubular aggregates within the myofibers [6,17,25]. The exact origin of these accumulations are unknown, however, it is hypothesized that these formations are due to a mass catabolism of misglycosylated proteins [17,23,25]. The balance of the HBP is critical for muscle health [41,65] and other unknown proteins may be improperly glycosylated in *GFPT1*-CMS, beyond AChRδ [15]. In addition, O-GlcNAcylation, a product the HBP has been linked to the regulation of cellular stress response pathways which have been shown to negatively impair skeletal muscle health, leading to muscle fiber necrosis [41,65]. Therefore, understanding the glycosylation status of other proteins in *Gfpt1*$^{tm1d/tm1d}$ mice may reveal additional pathomechanism of *GFPT1*-CMS.

This study identified the therapeutic potential of monosaccharide supplementation for *GFPT1*-CMS patients. With the emergence of monosaccharide therapies in CDGs, our findings provide preliminary support for exploring similar approaches in other glycosylation-based CMS cases or for combining them with existing CMS therapies. Currently, *GFPT1*-CMS patients benefit from treatment with AChE inhibitor pyridostigmine and sympathomimetic compounds salbutamol and ephedrine [19,22–25]. These treatment strategies have poor long-term efficacy as the sympathomimetics can lead to cardiac complications which require alternative treatment strategies [23,25,26]. CDGs have shown benefit with nutritional supplementation of monosaccharides which rescued the phenotype and restored protein glycosylation [29]. For example, galactose supplementation in *TMEM165*-CDG improved the glycosylation of LAMP2, an extensively N-linked glycosylated lysosomal protein [29,38]. In glycosylation-based CMS disorders such as *GMPPB*-CMS, long-term pyridostigmine treatment has shown diminished efficacy over time [27]. Monosaccharide therapies such as GDP-mannose supplementation have shown promise in preclinical models, including zebrafish lacking *Gmppb* expression [66]. This approach has been effective

in *PMM2*-CDGs [67]. However, use of compounds upstream of *GMPPB* like glucose and mannose failed to rescue muscle deficits and abnormal development of motor neurons [66]. These findings underscore the potential for nutritional therapeutics in glycosylation-based CMS, given their success in preclinical models and established efficacy in CDGs.

During this short-term study, we identified that galactose supplementation may be a suitable treatment strategy for *GFPT1*-CMS patients. However, further studies should be conducted to examine the long-term effects of galactose in *Gfpt1*-deficient models. The Leloir pathway was initially characterized within the liver[39]. In classic galactosemia, patients with a mutation to GALT, display a well-documented hepatoxicity in early disease manifestation which later can present as liver failure, and jaundice [68]. Additionally, further investigation is warranted to elucidate why the *Gfpt1*$^{tm1d/tm1d}$ mouse model exhibits a higher body fat percentage compared to control animals. O-GlcNAcylation is important for mitochondrial health, as such, hypo-glycosylation of mitochondrial proteins, may impede overall metabolism, leading to a fat mass gain compared to controls [51,69]. While we primarily focused on quadriceps for muscle gene and protein levels, and on soleus muscle for NMJ morphological assessment it would be beneficial to sample more muscle types to fully characterize the impact of galactose supplementation on *Gfpt1*$^{tm1d/tm1d}$ mice. NMJ morphology can vary across different muscles, and therefore additional characterization could reveal additional phenotypes [70,71]. Lastly, electrophysiological recordings of repetitive nerve stimulation could provide further direct evidence of the restoration of NMJ function.

In conclusion, treatment with galactose in *Gfpt1*$^{tm1d/tm1d}$ mice restored defective protein glycosylation of key NMJ-associated proteins and partially rescued impairments in both pre- and postsynaptic NMJ morphology. This improvement in NMJ morphology was beneficial to *Gfpt1*$^{tm1d/tm1d}$ mice, rescuing their neuromuscular phenotype. This study contributes to the growing evidence that, similar to CDGs, monosaccharide supplementation can be an effective treatment strategy for

glycosylation-based CMS in improving the glycosylation status and restoring NMJ function. These findings strongly suggest that patients with CMS due to mutations in *GFPT1* could see benefit from galactose supplementation as part of their treatment regime.

Author Contributions

Conceptualization, H.L., S.S., Y.A., and S.H.H.; methodology, S.H.H., R.C.-M., K.O., K. H., and D.O.; validation, S.H.H., R.C.-M., K.O. and D.O.; formal analysis, S.H.H., S.S. and K.O.; investigation, S.H.H., R.C.-M. and K.O.; resources, H.L. and S.S.; data curation, S.H.H., R.C.-M., K.O. ; writing—original draft preparation, S.H.H.; review and editing, S.H.H., R.C.-M., K.O., D.O., S.S., Y. A., A.R. and H.L.; final draft preparation and writing, S.H.H., S.S., and H.L.; visualization, S.H.H., S.S, and H.L.; supervision, S.S. and H.L.; project administration, S.S. and H.L.; funding acquisition, H.L. and S.H.H. All authors have read and agreed to the published version of the manuscript.

Funding

H.L. received support from the Canadian Institutes of Health Research (CIHR) for Foundation Grant FDN-167281 (Precision Health for Neuromuscular Diseases), Transnational Team Grant ERT-174211 (ProDGNE), and Network Grant OR2-189333 (NMD4C) from the Canada Foundation for Innovation (CFI-JELF 38412); the Canada Research Chairs program (Canada Research Chair in Neuromuscular Genomics and Health, 950-232279); the European Commission (Grant # 101080249); and the Canada Research Coordinating Committee New Frontiers in Research Fund (NFRFG-2022-00033) for SIMPATHIC and from the Government of Canada, Canada First Research Excellence Fund (CFREF) for the Brain-Heart Interconnectome (CFREF-2022-00007). S.H.H. received support from the Bob Korneluk CHEO Trainee Research Grant, Ontario Graduate Scholarship (OGS), Queen Elizabeth II Scholarship (QE2-GSST), and a STaR award by the University of Ottawa Dr. Eric Poulin Center for Neuromuscular Disease. A.R. acknowledges the financial support of the Deutsche Gesellschaft für Muskelkranke (DGM) e.V. as well as by the European Regional Development Fund (ERDF) (project B2B-RARE).

Animal Ethics Statement

The animal study protocol was approved by the Animal Care and Veterinary Board of the University of Ottawa (CHEOb-3089 and CHEOe-3120, approved on 16 November 2018 and 2 April 2019, respectively).

Data Availability Statement

Data are contained within the article and Supplementary Materials.

Conflict of Interest Statement

The authors declare no conflict of interest.

Acknowledgements

The SV2 antibody was deposited by Buckley, K. M., and the neurofilament (2H3) antibody deposited by Jessell, T.M/Doss, J was obtained from the Developmental Studies Hybridoma Bank, created by the NICHD of the NIH and maintained at The University of Iowa, Department of Biology, Iowa City, IA 52242. Schematics were prepared with Biorender.com.

5.0 References

1. Finsterer, J. Congenital myasthenic syndromes. *Orphanet J. Rare Dis.* **14**, 57 (2019).
2. Pugliese, A., Holland, S. H., Rodolico, C., Lochmüller, H. & Spendiff, S. Presynaptic Congenital Myasthenic Syndromes: Understanding Clinical Phenotypes through In vivo Models. *J. Neuromuscul. Dis.* 1–29 (2023) doi:10.3233/JND-221646.
3. Beeson, D. Chapter 5 - Congenital myasthenic syndromes. in *Handbook of Clinical Neurology* (ed. Hanna, M. G.) vol. 203 69–88 (Elsevier, 2024).
4. Basiri, K. *et al.* Clinical features in a large Iranian family with a limb-girdle congenital myasthenic syndrome due to a mutation in DPAGT1. *Neuromuscul. Disord.* **23**, 469–472 (2013).
5. Belaya, K. *et al.* Identification of DPAGT1 as a new gene in which mutations cause a congenital myasthenic syndrome. *Ann. N. Y. Acad. Sci.* **1275**, 29–35 (2012).
6. Belaya, K. *et al.* Mutations in DPAGT1 Cause a Limb-Girdle Congenital Myasthenic Syndrome with Tubular Aggregates. *Am. J. Hum. Genet.* **91**, 193–201 (2012).
7. vanden Brande, L. *et al.* Pathogenic DPAGT1 variants in limb-girdle congenital myasthenic syndrome (LG-CMS) associated with tubular aggregates and ORAI1 hypoglycosylation. *Neuropathol. Appl. Neurobiol.* **50**, e12952 (2024).
8. Finlayson, S. *et al.* Clinical features of congenital myasthenic syndrome due to mutations in DPAGT1. *J. Neurol. Neurosurg. Psychiatry* **84**, 1119–1125 (2013).
9. Belaya, K. *et al.* Mutations in GMPPB cause congenital myasthenic syndrome and bridge myasthenic disorders with dystroglycanopathies. *Brain* **138**, 2493–2504 (2015).
10. Rodríguez Cruz, P. M. *et al.* Clinical features of the myasthenic syndrome arising from mutations in GMPPB. *J. Neurol. Neurosurg. Psychiatry* **87**, 802–809 (2016).
11. Cossins, J. *et al.* Congenital myasthenic syndromes due to mutations in ALG2 and ALG14. *Brain* **136**, 944–956 (2013).

12. Ehrstedt, C., Liu, W.-W., Frykholm, C., Beeson, D. & Punga, A. R. Novel pathogenic ALG2 mutation causing congenital myasthenic syndrome: A case report. *Neuromuscul. Disord.* **32**, 80–83 (2022).
13. Paneque, A., Fortus, H., Zheng, J., Werlen, G. & Jacinto, E. The Hexosamine Biosynthesis Pathway: Regulation and Function. *Genes* **14**, 933 (2023).
14. Senderek, J. *et al.* Hexosamine Biosynthetic Pathway Mutations Cause Neuromuscular Transmission Defect. *Am. J. Hum. Genet.* **88**, 162–172 (2011).
15. Holland, S. H. *et al.* A Deficiency in Glutamine-Fructose-6-Phosphate Transaminase 1 (Gfpt1) in Skeletal Muscle Results in Reduced Glycosylation of the Delta Subunit of the Nicotinic Acetylcholine Receptor (AChRδ). *Biomolecules* **14**, 1252 (2024).
16. Zhang, R. *et al.* Muscle-specific lack of GFPT1 in knock-in mice triggers ER stress to alleviate misfolded proteins. *Dis. Model. Mech.* dmm.050768 (2024) doi:10.1242/dmm.050768.
17. Issop, Y. *et al.* GFPT1 deficiency in muscle leads to myasthenia and myopathy in mice. *Hum. Mol. Genet.* **27**, 3218–3232 (2018).
18. Zoltowska, K. *et al.* Mutations in GFPT1 that underlie limb-girdle congenital myasthenic syndrome result in reduced cell-surface expression of muscle AChR. *Hum. Mol. Genet.* **22**, 2905–2913 (2013).
19. Dusl, M. *et al.* A 3'-UTR mutation creates a microRNA target site in the GFPT1 gene of patients with congenital myasthenic syndrome. *Hum. Mol. Genet.* **24**, 3418–3426 (2015).
20. An, R. *et al.* Abnormal decrement on high-frequency repetitive nerve stimulation in congenital myasthenic syndrome with GFPT1 mutations and review of literature. *Front. Neurol.* **13**, 926786 (2022).
21. Farshadyeganeh, P. *et al.* Splicing regulation of GFPT1 muscle-specific isoform and its roles in glucose metabolisms and neuromuscular junction. *iScience* **26**, 107746 (2023).

22. Ma, Y. *et al.* Novel compound heterozygous variants in the GFPT1 gene leading to rare limb-girdle congenital myasthenic syndrome with rimmed vacuoles. *Neurol. Sci. Off. J. Ital. Neurol. Soc. Ital. Soc. Clin. Neurophysiol.* **42**, 3485–3490 (2021).
23. Jiang, K. *et al.* Diverse myopathological features in the congenital myasthenia syndrome with GFPT1 mutation. *Brain Behav.* **12**, e2469 (2022).
24. Vallepu, S. B. *et al.* Phenotypic variability in congenital myasthenic syndrome with GFPT1 mutation. *Acta Neurol. Belg.* https://doi.org/10.1007/s13760-024-02694-8 (2024) doi:10.1007/s13760-024-02694-8.
25. Bauché, S. *et al.* Mutations in GFPT1-related congenital myasthenic syndromes are associated with synaptic morphological defects and underlie a tubular aggregate myopathy with synaptopathy. *J. Neurol.* **264**, 1791–1803 (2017).
26. Thompson, R., Bonne, G., Missier, P. & Lochmüller, H. Targeted therapies for congenital myasthenic syndromes: systematic review and steps towards a treatabolome. *Emerg. Top. Life Sci.* **3**, 19–37 (2019).
27. Remijn-Nelissen, L., Verschuuren, J. J. G. M. & Tannemaat, M. R. The effectiveness and side effects of pyridostigmine in the treatment of myasthenia gravis: a cross-sectional study. *Neuromuscul. Disord.* **32**, 790–799 (2022).
28. Verheijen, J., Tahata, S., Kozicz, T., Witters, P. & Morava, E. Therapeutic approaches in Congenital Disorders of Glycosylation (CDG) involving N-linked glycosylation: an update. *Genet. Med.* **22**, 268–279 (2020).
29. Morelle, W. *et al.* Galactose Supplementation in Patients With TMEM165-CDG Rescues the Glycosylation Defects. *J. Clin. Endocrinol. Metab.* **102**, 1375–1386 (2017).
30. Witters, P. *et al.* Clinical and biochemical improvement with galactose supplementation in SLC35A2-CDG. *Genet. Med. Off. J. Am. Coll. Med. Genet.* **22**, 1102–1107 (2020).

31. Altassan, R. *et al.* International consensus guidelines for phosphoglucomutase 1 deficiency (PGM1-CDG): Diagnosis, follow-up, and management. *J. Inherit. Metab. Dis.* **44**, 148–163 (2021).
32. Jones, R. A. *et al.* NMJ-morph reveals principal components of synaptic morphology influencing structure–function relationships at the neuromuscular junction. *Open Biol.* **6**, (2016).
33. Minty, G. *et al.* aNMJ-morph: a simple macro for rapid analysis of neuromuscular junction morphology. *R. Soc. Open Sci.* **7**, 200128 (2020).
34. Park, J. H. *et al.* SLC39A8 deficiency: biochemical correction and major clinical improvement by manganese therapy. *Genet. Med.* **20**, 259–268 (2018).
35. Szelinger, S. *et al.* Congenital myasthenic syndrome caused by a frameshift insertion mutation in GFPT1. *Neurol. Genet.* **6**, e468 (2020).
36. Akella, N. M., Ciraku, L. & Reginato, M. J. Fueling the fire: emerging role of the hexosamine biosynthetic pathway in cancer. *BMC Biol.* **17**, 52 (2019).
37. Boyer, S. W., Johnsen, C. & Morava, E. Nutrition Interventions in Congenital Disorders of Glycosylation. *Trends Mol. Med.* **28**, 463–481 (2022).
38. Potelle, S. *et al.* Glycosylation abnormalities in Gdt1p/TMEM165 deficient cells result from a defect in Golgi manganese homeostasis. *Hum. Mol. Genet.* **25**, 1489–1500 (2016).
39. Conte, F., van Buuringen, N., Voermans, N. C. & Lefeber, D. J. Galactose in human metabolism, glycosylation and congenital metabolic diseases: Time for a closer look. *Biochim. Biophys. Acta BBA - Gen. Subj.* **1865**, 129898 (2021).
40. Podlogar, T. *et al.* Postexercise muscle glycogen synthesis with glucose, galactose, and combined galactose-glucose ingestion. *Am. J. Physiol. - Endocrinol. Metab.* **325**, E672–E681 (2023).
41. Lambert, M. *et al.* O-GlcNAcylation is a key modulator of skeletal muscle sarcomeric morphometry associated to modulation of protein–protein interactions. *Biochim. Biophys. Acta BBA - Gen. Subj.* **1860**, 2017–2030 (2016).

42. Chen, Q. *et al.* Global N-linked Glycosylation is Not Significantly Impaired in Myoblasts in Congenital Myasthenic Syndromes Caused by Defective Glutamine-Fructose-6-Phosphate Transaminase 1 (GFPT1). *Biomolecules* **5**, 2758–2781 (2015).
43. Ramanathan, V. K. & Hall, Z. W. Altered Glycosylation Sites of the δ Subunit of the Acetylcholine Receptor (AChR) Reduce αδ Association and Receptor Assembly *. *J. Biol. Chem.* **274**, 20513–20520 (1999).
44. Rudell, J. C., Borges, L. S., Yarov-Yarovoy, V. & Ferns, M. The MX-Helix of Muscle nAChR Subunits Regulates Receptor Assembly and Surface Trafficking. *Front. Mol. Neurosci.* **13**, 48 (2020).
45. Wanamaker, C. P. & Green, W. N. N-Linked Glycosylation Is Required for Nicotinic Receptor Assembly but Not for Subunit Associations with Calnexin *. *J. Biol. Chem.* **280**, 33800–33810 (2005).
46. Müller, J. S. *et al.* CHRND mutation causes a congenital myasthenic syndrome by impairing co-clustering of the acetylcholine receptor with rapsyn. *Brain* **129**, 2784–2793 (2006).
47. Chokchaitaweesuk, C., Kobayashi, T., Izumikawa, T. & Itano, N. Enhanced hexosamine metabolism drives metabolic and signaling networks involving hyaluronan production and O-GlcNAcylation to exacerbate breast cancer. *Cell Death Dis.* **10**, 1–15 (2019).
48. Claeyssen, C., Bastide, B. & Cieniewski-Bernard, C. Global O-GlcNAcylation changes impact desmin phosphorylation and its partition toward cytoskeleton in C2C12 skeletal muscle cells differentiated into myotubes. *Sci. Rep.* **12**, 9831 (2022).
49. Hart, G. W., Slawson, C., Ramirez-Correa, G. & Lagerlof, O. Cross Talk Between O-GlcNAcylation and Phosphorylation: Roles in Signaling, Transcription, and Chronic Disease. *Annu. Rev. Biochem.* **80**, 825–858 (2011).

50. Jaiswal, R. *et al.* A reference dataset of O-GlcNAc proteins in quadriceps skeletal muscle from mice. *Glycobiology* cwaf005 (2025) doi:10.1093/glycob/cwaf005.

51. Xue, Q., Yan, R., Ji, S. & Yu, S. Regulation of mitochondrial network homeostasis by O-GlcNAcylation. *Mitochondrion* **65**, 45–55 (2022).

52. O'Connor, K., Spendiff, S., Lochmüller, H. & Horvath, R. Mitochondrial Mutations Can Alter Neuromuscular Transmission in Congenital Myasthenic Syndrome and Mitochondrial Disease. *Int. J. Mol. Sci.* **24**, 8505 (2023).

53. Belotti, E. & Schaeffer, L. Regulation of Gene expression at the neuromuscular Junction. *Neurosci. Lett.* **735**, 135163 (2020).

54. Yumoto, N., Kim, N. & Burden, S. J. Lrp4 is a retrograde signal for presynaptic differentiation at neuromuscular synapses. *Nature* **489**, 438–442 (2012).

55. Arnold, A.-S. *et al.* Morphological and functional remodelling of the neuromuscular junction by skeletal muscle PGC-1α. *Nat. Commun.* **5**, 3569 (2014).

56. Rossor, A. M. *et al.* Loss of BICD2 in muscle drives motor neuron loss in a developmental form of spinal muscular atrophy. *Acta Neuropathol. Commun.* **8**, 34 (2020).

57. McMacken, G. M. *et al.* Salbutamol modifies the neuromuscular junction in a mouse model of ColQ myasthenic syndrome. *Hum. Mol. Genet.* **28**, 2339–2351 (2019).

58. Oury, J. *et al.* Mechanism of disease and therapeutic rescue of Dok7 congenital myasthenia. *Nature* **595**, 404–408 (2021).

59. Xing, G. *et al.* A mechanism in agrin signaling revealed by a prevalent Rapsyn mutation in congenital myasthenic syndrome. *eLife* **8**, e49180.

60. Chevessier, F. *et al.* A mouse model for congenital myasthenic syndrome due to MuSK mutations reveals defects in structure and function of neuromuscular junctions. *Hum. Mol. Genet.* **17**, 3577–3595 (2008).

61. Spendiff, S. *et al.* Modulation of the Acetylcholine Receptor Clustering Pathway Improves Neuromuscular Junction Structure and Muscle Strength in a Mouse Model of Congenital Myasthenic Syndrome. *Front. Mol. Neurosci.* **13**, 594220 (2020).
62. Bogdanik, L. P. & Burgess, R. W. A valid mouse model of AGRIN-associated congenital myasthenic syndrome. *Hum. Mol. Genet.* **20**, 4617–4633 (2011).
63. Slater, C. R. 'Fragmentation' of NMJs: a sign of degeneration or regeneration? A long journey with many junctions. *Neuroscience* **439**, 28–40 (2020).
64. Willadt, S., Nash, M. & Slater, C. R. Age-related fragmentation of the motor endplate is not associated with impaired neuromuscular transmission in the mouse diaphragm. *Sci. Rep.* **6**, (2016).
65. Dang, K., Jiang, S., Gao, Y. & Qian, A. The role of protein glycosylation in muscle diseases. *Mol. Biol. Rep.* **49**, 8037–8049 (2022).
66. Liu, Z. *et al.* GMPPB-congenital disorders of glycosylation associate with decreased enzymatic activity of GMPPB. *Mol. Biomed.* **2**, 13 (2021).
67. Cline, A. *et al.* A zebrafish model of PMM2-CDG reveals altered neurogenesis and a substrate-accumulation mechanism for N-linked glycosylation deficiency. *Mol. Biol. Cell* **23**, 4175–4187 (2012).
68. Wang, Y. *et al.* A case report of classic galactosemia with a GALT gene variant and a literature review. *BMC Pediatr.* **24**, 352 (2024).
69. Akinbiyi, E. O. *et al.* Blocked O-GlcNAc cycling alters mitochondrial morphology, function, and mass. *Sci. Rep.* **11**, 22106 (2021).
70. Seene, T., Umnova, M. & Kaasik, P. Morphological peculiarities of neuromuscular junctions among different fiber types: Effect of exercise. *Eur. J. Transl. Myol.* **27**, 6708 (2017).
71. Mech, A. M., Brown, A., Schiavo, G. & Sleigh, J. N. Morphological variability is greater at developing than mature mouse neuromuscular junctions. *J. Anat.* **237**, 603–617 (2020).

Supplementary Figures: Galactose treatment rescues neuromuscular junction transmission in glutamine-fructose-6-phosphate transaminase 1 (Gfpt1) deficient mice

Stephen H. Holland[1, 2, 3], R. Carmona-Martinez[1], D. O'Neil[1], K. Ho[1, 2], K. O'Connor[1, 2], Y. Azuma[4, 5], A. Roos[3, 6, 7, 8], S. Spendiff[1], H. Lochmüller[1, 2, 3, 9, 10, 11*]

Affiliations

1. Children's Hospital of Eastern Ontario Research Institute, Ottawa, ON K1H 8L1, Canada

2. Department of Cellular and Molecular Medicine, Faculty of Medicine, University of Ottawa, ON K1H 8M5, Canada

3. Eric Poulin Center for Neuromuscular Disease, Brain and Mind Research Institute, University of Ottawa, Ottawa ON K1H 8M5, Canada

4. Department of Human Genetics, Graduate School of Medicine, Yokohama City University, Yokohama, Japan

5. Department of Pediatrics, Aichi Medical University, Nagakute, Japan

6. Department of Pediatric Neurology, Center for Neuromuscular Disorders, University Duisburg-Essen, 45147 Essen, Germany

7. Medical Faculty, University Hospital Düsseldorf, Heinrich Heine University, 40225 Düsseldorf, Germany

8. Department of Neurology with Heimer Institute for Muscle Research, University Hospital Bergmannsheil, Bochum, Germany.

9. Division of Neurology, Department of Medicine, The Ottawa Hospital Civic Campus, Ottawa, ON K1Y 4E9, Canada

10. Faculty of Medicine, Medical Center, University of Freiburg, 79085, Freiburg, Germany

11. Centro Nacional de Análisis Genómico (CNAG), 08028 Barcelona, Spain

Supplementary Table S1: Primers used for study

Primer	Primer Sequence
Gfpt1-F	5'–CCA ACG CCT GCA AAA TCC AG–3'
Gfpt1-R	5'–TTC TCC ATG TGT CGC CCA AC–3'
Ogt-F	5'–CTG TCA CCC TTG ACC CAA A–3'
Ogt-R	5'–ATG GGG TTG CAG TTC GAT AG–3'
Gapdh-F	5'–CTC CCA CTC TTC CAC CTT CG–3'
Gapdh-R	5'–GCC TCT CTT GCT CAG TGT CC–3
Ppia-F	5'–GCC TTC CTC CTT TCA CAG AA–3'
Ppia-R	5'–GAT GCC AGG ACC TGT ATG CT–3'
Rpl27-F	5'–AAG CCG TCA TCG AGA ACA–3'
Rpl27-R	5'–CTT GAT CTT GGA TCG CTT GGC–3'
rtTA-F	5'–CTG GAG TTG AGC AGC CTA C–3'
rtTA-R	5'–AGA GCA CAG CGG AAT GAC TT–3'
Galk-F	5'–AGA GTC ACT ACT CAC TCA GGG AT –3'
Galk-R	5'– GGG ACA CCT CAC AAG CTC AG–3'
Galt-F	5'–CGA GTG GGT GTT AGT GTC GG–3'
Galt-R	5'–ATA GTG GGG ATT CAC CTC CC–3'
Gale-F	5'–ACG CCA TTC GTG GAG AAG AC–3'
Gale-R	5'–CCC TCA TGA TCT CTA GAA GCT GG –3'
Slc35a2-F	5'–GCC TCT GAC TCC TTC CTC CTA T–3'
Slc35a2-R	5'–AGG TGA GAC CTT TGA GCA CTT C–3'
Gfpt1Geno-F	5'–CAT GCG TGA ACC TGT GTA CA–3'
Gfpt1Geno-R	5'–GGG TTT CGT AAT TGG AAG AG–3'
Cre-F	5'–TAA GTC TGA ACC CGG TCT GC–3'
Cre-R	5'–GTG AAA CAG CAT TGC TGT CAC TT–3'

Supplementary Table S2: Morphological variables of NMJs from study. Initial NMJ structure in the soleus muscle revealed differences in variables, including pre- and postsynaptic parameters. Data were tested for nomality with a D'Agostino Pearson test, followed by a Kruskal-Wallis test and a Dunn's multiple comparisions test. For significance, *p*-value $^{*/\#}$ < 0.05, $^{**/\#\#}$ <0.005, $^{***/\#\#\#}$ < 0.0005, $^{****/\#\#\#\#}$ < 0.0001 * indicates significant differences from Tm1C homozygous control, while # indicates significant differences from vehicle to galactose treated *Gfpt1*$^{tm1d/tm1d}$ mice. Values that did not pass Gaussian normality through D'Agostino Pearson test are presented as a median (25th percentile, 75th percentile) and the number of NMJs assessed. Values that did pass Gaussian normality through the D'Agostino Pearson test are presented as a mean (standard deviation) and the number of NMJs assessed.

Variable	Tm1C homozygous control	*Gfpt1*$^{tm1d/tm1d}$ mice + Veh	*Gfpt1*$^{tm1d/tm1d}$ mice + 10% Galactose
Presynaptic			
Nerve terminal perimeter (μm)	367.59 (276.22, 397.54) 162	222.67*** (198.32, 267.58) 178	336.12$^{\#\#\#}$ (301.33, 399.22) 152
Nerve terminal area (μm^2)	342.28 (310.74, 405.77) 162	222.85*** (187.83, 278.48) 178	310.58$^{\#\#\#}$ (271.65, 351.91) 152
Number of terminal branches	15.50 (12, 24) 162	14 (11, 21) 178	18 (14, 23.25) 152
Number of branch points	21.84 (13.51, 31.36) 162	12.32* (10.36, 15.12) 178	12.88 (10.92, 16.59) 152152
Total length of branches	124.48 (91.67, 182.57) 162	198.44*** (315.19, 139.93) 178	181.88$^{\#\#\#}$ (113.44, 198.17) 152
Average length of branches	5.12 (3.72, 6.73) 162	4.97 (3.89, 8.64) 178	8.06$^{\#}$ (5.99, 12.32) 152
Complexity	4.82	4.60*	4.56

	(4.44, 5.29) 162	(4.30, 4.82) 178	(4.36, 4.73) 152
Postsynaptic			
AChR perimeter (μm)	419.99 (323.15, 498.25) 162	243.25*** (210.45, 287.32) 178	381.88### (333.60, 414.91) 152
AChR Area (μm^2)	383.54 (294.61, 437.23) 162	212.32*** (187.32, 256.32) 178	339.44### (301.41, 383.32) 152
Endplate perimeter (μm)	151.54 (85.33, 202.42) 162	88.99*** (81.23, 99.23) 178	103.14 # (94.29, 110.97) 152
Endplate area (μm^2)	501.35 (406.71, 572.34) 162	271.23*** (236.42, 304.23) 178	339.44# (301.41, 383.32) 152
Endplate diameter (μm)	49.96 (41.32, 77.43) 162	24.11** (19.93, 27.38) 178	31.88# (26.38, 37.33) 152
Average area of AChR clusters (μm^2)	100.24 (77.66, 131.62) 162	70.80** (58.67, 89.12) 178	98.82## (79.38, 117.36) 152
Fragmentation	0.75 (0.125) 162	0.67 (0.1) 178	0.67 (0.125) 152
Compactness (%)	81.72 (65.94, 92.88) 162	80.84 (74.54, 87.86) 178	82.63 (77.09, 89.58) 152
Overlap (%)	92.08 (88.95, 94.26) 162	82.92** (79.90, 85.90) 178	91.28## (89.42, 92.91) 152
Area of synaptic contact	348.46 (259.96, 409.10) 162	173.08** (146.23, 215.85) 178	310.29## (274.12, 352.61) 152
Axon Variables			
Axon diameter (μm)	3.66 (3.10, 4.13) 162	2.34**** (2.12, 2.89) 178	3.03### (2.71, 3.51) 152
Number of axonal inputs	2.0 (1.0) 162	1.0 (1.0) 178	1.0 (0.5) 152

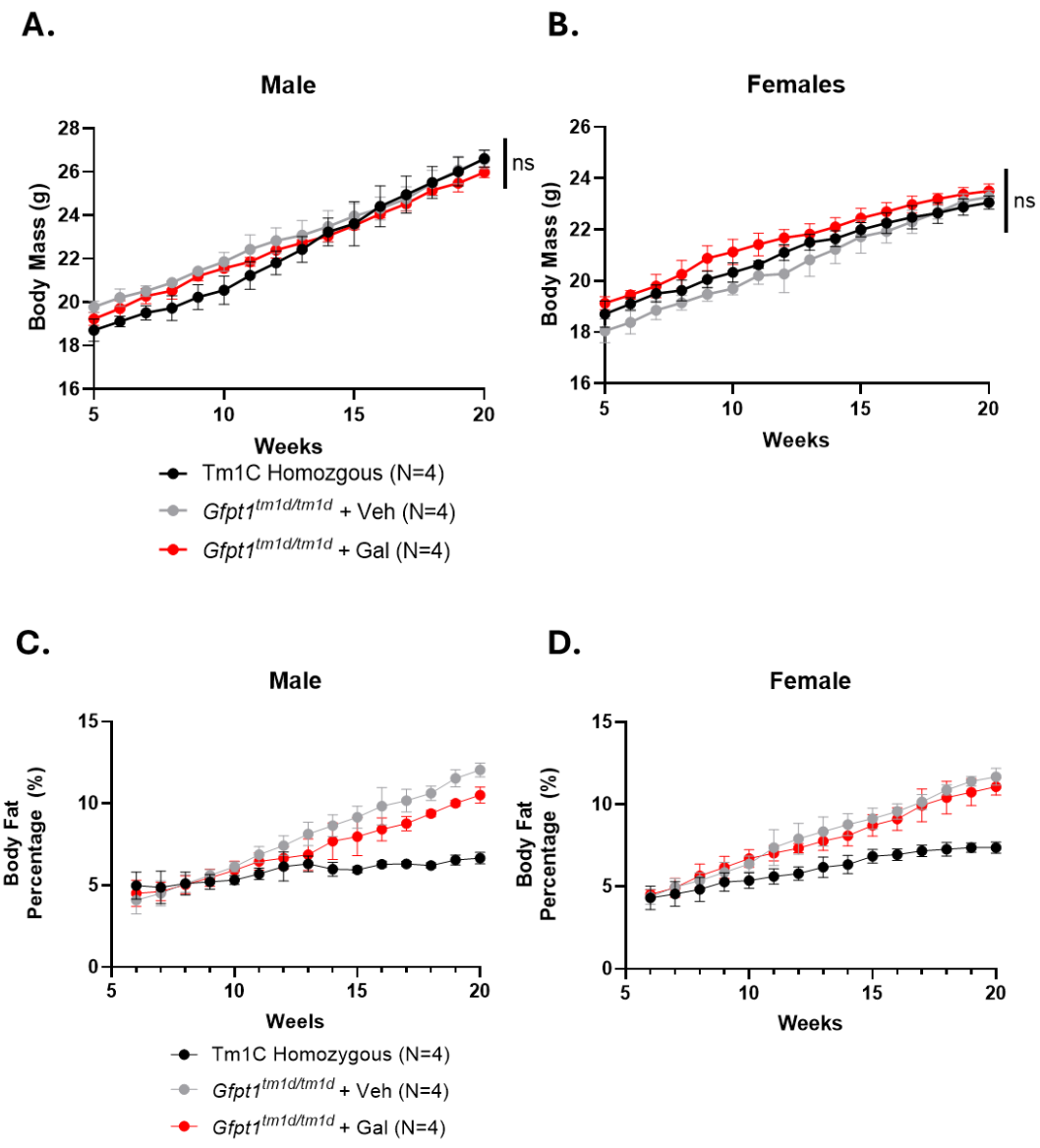

Supplementary Figure 1: There was no sex-related differences to the body mass of male and female mice **A.** Body weight recordings of male and **B.** female mice. showedthere was no sex-dependent significant differences between experiemental groups **C.** EchoMRI measurements for male and **D.** female mice in this study, highlights that there were no sex-dependent differnces in body fat perrcentage in relation to response to galactose treatment. *Gfpt1*$^{tm1d/tm1d}$ mice have a significant increase in body fat percentage, regardless of galactose or vehicle treatment.

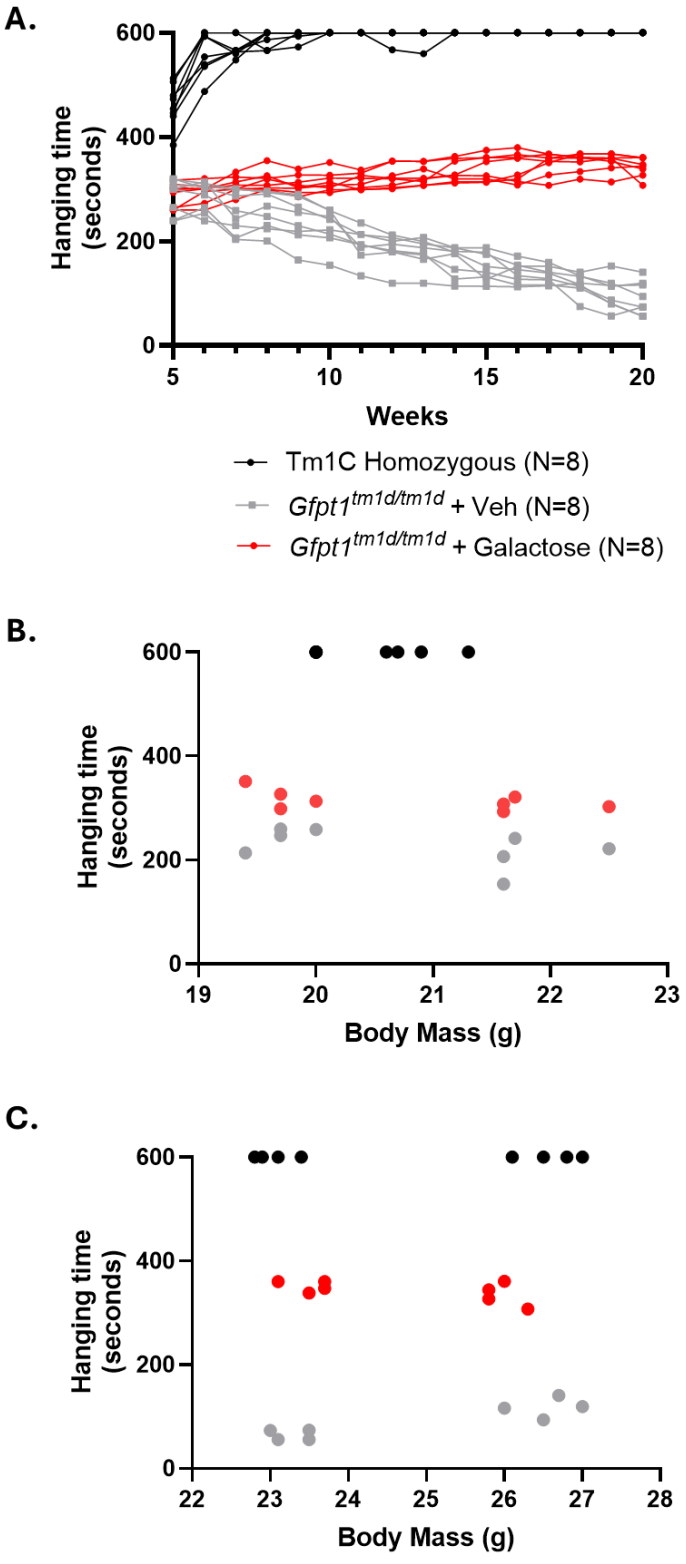
A.
600
400
200
0
Hanging time (seconds)
5
10
15
20
Weeks
Tm1C Homozygous (N=8)
Gfpt1tm1d/tm1d + Veh (N=8)
Gfpt1tm1d/tm1d + Galactose (N=8)
B.
600
400
200
0
Hanging time (seconds)
19
20
21
22
23
Body Mass (g)
C.
600
400
200
0
Hanging time (seconds)
22
23
24
25
26
27
28
Body Mass (g)

Supplementary Figure 2: Galactose treatment of Gfpt1 mice (*Gfpt1*$^{tm1d/tm1d}$) partially rescues muscle endurance. A. *Gfpt1*$^{tm1d/tm1d}$ mice displayed progressive impairment in inverted hanging wire impulse compared to Tm1C homozygous control mice, which was partially rescued with galactose treatment. This figure represents the raw hanging time data (seconds) prior to normalization to body weight. **B.** A body mass (g) to hanging time (seconds) comparision between males and female mice for each treatment group. Measurements were conducted at Week 10 and **C.** Week 20.

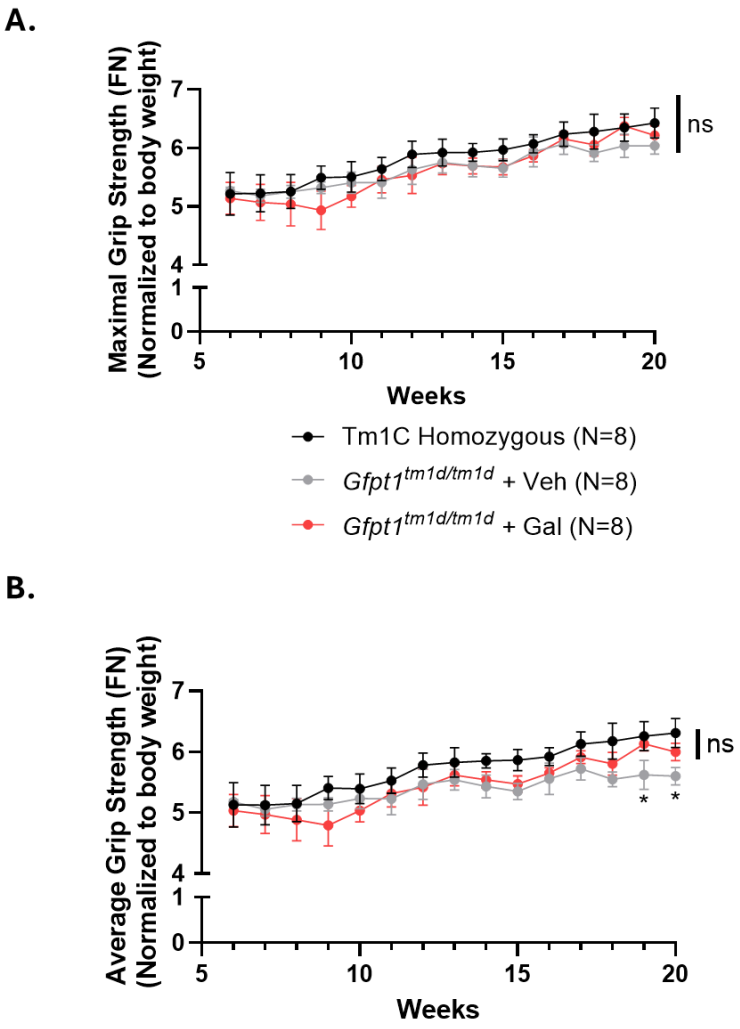

Supplementary Figure 3: Galactose treatment of Gfpt1 mice (*Gfpt1*$^{tm1d/tm1d}$) does not significantly improve grip strength. A. All experimental groups displayed no significant differences in maximal grip strength (force newtons) normalized to mouse body weight (g) **B.** *Gfpt1*$^{tm1d/tm1d}$ mice displayed a slight, but significance decrease in average grip strength measurements taken after 8 successive grip strength recordings via forelimbs. Galactose treatment appears to slightly improve the average grip strength in *Gfpt1*$^{tm1d/tm1d}$ although these changes were not significant. Statistical significance was performed via a two-way ANOVA followed by a Tukey's post-hoc test. * indicates p-value < 0.05, comparision to Tm1C homozygous control.

Chapter 4: Hexosamine biosynthetic pathway disruption by GFPT1 loss drives coordinated defects in glycosylation, autophagy, and trafficking.

Stephen H. Holland[1,2,4], R. Carmona-Martinez[1], Andreas Hentschel, K. O'Connor[1,2], D. O'Neil[1], S. Baird[1], A. Roos[1,7,8], S. Spendiff[l], H. Lochmüller[1,2,3,4,5,6]*

4.1 Statement of author contributions

This third paper concludes the published work included in my doctoral thesis. As lead author, I performed the majority of the experimental work, including Western blotting, immunostaining, RT-qPCR, and other essential cellular and biochemical assays. Proteomic analyses were carried out by Dr. Andreas Roos and Dr. Hentschel in Essen, Germany, whose group also performed the initial data processing and contributed extensively to data interpretation; I consulted closely with them throughout the study to guide downstream analyses and refine experimental direction. Additional contributors assisted in the generation of cellular models and the extraction of skeletal muscle from mouse models, which also supported complementary studies in related manuscripts. Daniel O'Neil contributed to muscle section preparation and provided critical feedback during manuscript editing prior to submission. Supervision of this work was provided by Dr. Hanns Lochmüller and Dr. Sally Spendiff, with additional guidance from Dr. Andreas Roos. Funding for this project was obtained through support from Dr. Hanns Lochmüller, Dr. Andreas Roos, and myself. Dr. Stephen Baird assisted with image acquisition using the Opera™ system and contributed to downstream image analysis using Columbus™ software. Alexa Derksen provided additional support in the analysis and validation of serglycin-related data as part of her doctoral work, offering critical input for troubleshooting and experimental interpretation throughout this component of the study.

4.2 Background and Rationale

Disruption of the HBP through loss of Gfpt1 represents a fundamental metabolic defect that propagates across multiple layers of cellular homeostasis. As a rate-limiting enzyme controlling the conversion of fructose-6-phosphate into glucosamine-6-phosphate, Gfpt1 governs the cellular availability of UDP-GlcNAc, the essential substrate for N-linked glycosylation, O-linked glycosylation, and O-GlcNAcylation. Consequently, Gfpt1 deficiency imposes a global limitation on glycosylation

capacity, directly impairing the folding, stability and maturation of a broad range of secretory and membrane proteins. In highly specialized and secretory tissues such as skeletal muscle, even modest reductions in glycosylation disrupt the assembly and trafficking of proteins required for structural integrity and neuromuscular transmission.

The immediate consequences of this hypoglycosylated state is collapse in the ER proteostasis. Nascent proteins that fail to acquire appropriate glycan structures exhibit reduced stability and prolonged engagement with the ER quality control machinery, leading to their retention or targeting for ERAD. As misfolded and immature proteins accumulate adaptive stress pathways such as the UPR are activated in an attempt to restore ER homeostasis. However, chronic or unresolved glycosylation defects overwhelm this compensatory response, resulting in sustained ER and altered chaperone capacity. In parallel, impaired glycan processing disrupts the acquisition of export competence, limiting the efficient loading of cargo into COPII vesicles and thereby attenuating ER-to-Golgi trafficking.

Defective trafficking represented a critical amplification point of this cascade. Since glycosylation is tightly coupled to vesicle transport, cargo sorting and Golgi maturation, loss of Gfpt1 function leads to intracellular retention of proteins that would normally be secreted or correctly localized. This results in a dual defect characterized by accumulation of immature cargo within the secretory pathway and reduced secretion of key extracellular proteins. Such defects are particularly detrimental in skeletal muscle, where continuous protein export is required to maintain extracellular matrix composition, membrane stability and NMJ integrity. As trafficking becomes progressively compromised, cells may attempt to compensate through stress-induced or unconventional secretion pathways, further reflecting a breakdown of canonical secretory processes.

Importantly, the consequences of impaired glycosylation and trafficking extend beyond the early secretory pathway to the autophagy-lysosome system. Autophagy, as stated in the introduction,

relies on coordinated membrane flux, vesicle fusion events, and proper lysosomal enzyme targeting. These processes are dependent on intact glycosylation and ER-Golgi function. In the context of Gfpt1 deficiency, disruption of these pathways impairs autophagosome maturation and lysosomal degradation, leading to accumulation of p62-aggergates, elevated LC3-II and defective autophagic flux. This failure of cellular clearance mechanism reinforces proteotoxic stress creating self-perpetuating cycle where impaired folding, defective trafficking and insufficient degradation converge to destabilize cellular homeostasis.

Together, these interconnected processes define a unified pathophysiological cascade in which loss of Gfpt1 ats as an upstream metabolic trigger that destabilizes glycosylation-dependent proteostasis. Rather than affecting a single pathway, Gfpt1 deficiency initiates a coordinated network failure encompassing ER stress signaling, vesicle trafficking, secretion, and autophagic turnover. Understanding how these pathways intersect is essential for explaining the molecular basis of skeletal muscle dysfunction in GFPT1-associated congenital myasthenic syndromes and for identifying therapeutic strategies aimed at restoring glycosylation capacity or reinforcing cellular proteostasis.

Hexosamine Pathway Disruption by GFPT1 Loss Drives Coordinated Defects in Glycosylation, Autophagy, and Trafficking

Stephen H. Holland[1,2,4], R. Carmona-Martinez[1], Andreas Hentschel, A. Derksen[1, 2], K. O'Connor[1,2], D. O'Neil[1], K. Ho[1, 2] S. Baird[1], A. Roos[1,7,8], S. Spendiff[1], H. Lochmüller[1,2,3,4,5,6*]

[1] Children's Hospital of Eastern Ontario Research Institute, Ottawa, Ontario, Canada

[2] Department of Cellular and Molecular Medicine, Faculty of Medicine, University of Ottawa, Ottawa, Ontario, Canada

[3] Division of Neurology, Department of Medicine, The Ottawa Hospital, Ottawa, Ontario, Canada

[4] Dr. Eric Poulin Center for Neuromuscular Disorders, Brain and Mind Research Institute, University of Ottawa, Ottawa, Ontario, Canada

[5] Department of Neuropediatric and Muscle Disorders, Medical Center, University of Freiburg, Faculty of Medicine, Freiburg, Germany

[6] Centro Nacional de Analisis Genomico (CNAG-CRG), Center for Genomic Regulation, Barcelona Institute of Science and Technology (BIST), Barcelona, Catalonia, Spain

[7] Department of Pediatric Neurology / Centre for Neuromuscular Disorders in Children, University Duisburg-Essen, Hufelandstrasse 55, 45122, Essen, Germany

[8] Department of Neurology with Heimer Institute for Muscle Research, University Hospital Bergmannsheil, Bochum, Germany

Abstract:

Glutamine-Fructose-6-Phosphate Transaminase 1 (Gfpt1), the rate limiting enzyme of the hexosamine biosynthetic pathway (HBP), provides the UDP-N-acetylglucosamine (UDP-GlcNAc) required for protein glycosylation. Biallelic mutations in *GFPT1* cause congenital myasthenic syndromes (*GFPT1*-CMS), yet the molecular mechanisms linking impaired glycosylation to skeletal muscle dysfunction remain incompletely understood. Here, we combine cellular models of inducible *Gfpt1* knockdown and a skeletal muscle-specific *Gfpt1* knockout mouse (*Gfpt1*$^{Tm1d/Tm1d}$) with whole-cell proteomics, immunoblot studies and secretomics to define glycosylation-dependent defects in intracellular trafficking, ER stress signaling and autophagy. Global proteomic profiling of *Gfpt1*-deficient myoblasts revealed marked downregulation of protein trafficking pathways and impaired secretion of key muscle cargo proteins, including serglycin (Srgn). Loss of GFPT1 reduced both high–molecular-weight glycosylated serglycin and its core protein, accompanied by intracellular retention and decreased secretion. These trafficking defects coincide with robust activation of the unfolded protein response (UPR), evidenced by increased *Xbp1* expression and accumulation of spliced Xbp1s across pharmacologic, cellular, and mouse models of *GFPT1* deficiency. Converging evidence from proteomics, immunoblotting, and immunofluorescence demonstrated impaired autophagy, including increased LC3-II accumulation, elevated p62/Sqstm1 levels, and enhanced p62-positive puncta in both Gfpt*1*-deficient C2C12 myoblasts and skeletal muscle. Soluble/insoluble fractionation further confirmed p62 accumulation, indicating defective autophagic flux and buildup of aggregated cargo. Together, these findings identify a glycosylation-dependent failure in protein trafficking that triggers ER stress, UPR activation, and autophagy impairment in -deficient skeletal muscle. This mechanistic cascade provides a unifying explanation for muscle pathology in *GFPT1*-CMS and suggests that restoring glycosylation or improving proteostasis may represent viable therapeutic approaches

1.0 Introduction:

Protein glycosylation is essential for proper folding, stability, secretion and intracellular trafficking of thousands of proteins across mammalian cell types [1–3]. Glycoproteins represent nearly half of the mammalian proteome, and defects in glycosylation disrupt critical processes - particularly in highly secretory or structurally demanding tissues such as skeletal muscle [3]. The hexosamine biosynthetic pathway (HBP) provides the essential nucleotide sugars that fuel these glycosylation reactions, with UDP-GlcNAc serving as a central substrate for N-, O-linked glycosylation and O-GlcNAcylation [4,5]. At the apex of this pathway sits glutamine-fructose-6-phosphate transaminase 1 (GFPT1), the rate-limiting enzyme that controls the metabolic flux into the HBP by converting fructose-6-phosphate into glucosamine-6-phosphate [4,5]. Since GFPT1 function determines the availability of UDP-GlcNAc, it acts as a critical metabolic gatekeeper linking nutrient status, cellular stress responses, and post-translational protein modifications [4–6]. Even modest reductions in HBP flux can compromise protein folding, vesicle export, and quality control systems that depend on glycan maturation, underscoring the central role of GFPT1 in maintaining cellular proteostasis.

Congenital myasthenic syndromes (CMS) are a group of inheritable, early-onset neuromuscular disorders caused by mutations in proteins critical for the development, maintenance and function of the neuromuscular junction (NMJ) [7,8]. Clinically, CMS is characterized by fatigable muscle weakness and exhibits considerable genetic and phenotypic heterogeneity [7–9]. To date, approximately 40 genes have been implicated in CMS, with a subset of five genes linked to defects in protein glycosylation [8,10–13]. Biallelic pathogenic variants to *GFPT1* lead to reduced protein abundance and impaired enzymatic activity [10,14–22]. Patients with *GFPT1*-CMS typically present with predominant limb-girdle muscle weakness [10,14,15]. Histopathological analysis of patient muscle biopsies reveals diverse myopathic features, including tubular aggregates and rimmed vacuoles [15,16]. Notably, these pathological hallmarks are recapitulated in our skeletal muscle-specific *Gfpt1* knock out mouse model (*Gfpt1*$^{tm1d/tm1d}$),

validating its relevance to human *GFPT1*-CMS [6,23,24]. Recent work from our group demonstrated that Gfpt1 depletion disrupts multiple glycosylation processes, including protein O-GlcNAcylation and N-linked glycosylation [6,24]. Although GFPT1-deficiency is known to impact protein glycosylation, the downstream mechanisms linking disrupted glycosylation to skeletal muscle pathology remain poorly understood.

Protein glycosylation is intimately coupled to intracellular trafficking and endoplasmic reticulum (ER) homeostasis. Hypoglycosylation disrupts protien folding in the ER, leading to protein misfolding, ER retention, and preferential targeting to ER-associated degradation (ERAD) due to failure to pass glycan-dependent quality control checkpoints [25,26]. When misfolded proteins accumulate, cells activate the unfolded protein response (UPR) to restore proteostasis by enhancing chaperone expression, attenuating translation and upregulating ERAD [27]. In parallel, disruptions in protein folding and trafficking can impair autophagy, a degradative pathway essential for the clearance of damaged proteins, aggregated cargo, and dysfunctional organelles [28–30]. A hallmark of impaired autophagic flux is the accumulation of p62 and LC3-II, reflecting defective cargo degradation and contributing to the formation of protein aggregates [31]. Intriguingly, prior studies with *Gfpt1*$^{tm1d/tm1d}$ mice demonstrated a ~2.5-fold increase in p62 suggesting that autophagy may be impaired within *Gfpt1*-deficient models [23].

Here, we combine whole-cell proteomics, secretomics, cellular models of *Gfpt1*-depletion and a *Gfpt1*$^{tm1d/tm1d}$ mouse model to define how Gfpt1 deficiency disrupts proteostasis within skeletal muscle. We identify downregulation of vesicle trafficking proteins, intracellular retention of secreted proteins such as serglycin (Srgn), activation of the UPR pathway and a profound impairment of autophagic flux characterized by p62 and LC3-II accumulation. Together, our findings reveal a glycosylation-dependent cascade in which defective trafficking and ER stress converge on impaired autophagy, providing a unified mechanistic framework for muscle pathology in *GFPT1*-CMS.

Methods

2.0 Cell Culture

C2C12 cells (ATCC, CRL-1722, Burlington, Ontario) were cultured in high glucose Dulbecco's Modified Eagle Medium (DMEM) supplemented with 10% fetal bovine serum (FBS), 1% glutamine, and 1% penicillin/streptomycin. A *Gfpt1*-deficient C2C12 cell model was established using a TET-ON miR-30 tetracycline-inducible system with two different short hairpin sequences targeting Gfpt1 (shGfpt1 #1, and shGfpt1 #2) (VectorBuilder, Chicago, IL) as previously described [6]. *Gfpt1* silencing was achieved by doxycycline treatment at 2 μg/mL for 72 hours (Sigma, D9891).

2.1 Animal Husbandry

Animals were housed at the University of Ottawa Animal Care and Veterinary Facility (Roger Guidon Hall, Ottawa, Canada) and all breeding and experimental protocols were approved by the internal Animal Care Committee (protocols: breeding – CHEO-3089 and experimental – CHEO-3120 approved on 16 November 2018 and 2 April 2019, respectively). Mice were maintained on a 12-hour light-dark cycle, with access to food and water *ad libitum* for the duration of this study. Mice were generated and genotyped as previously reported [6,23,24]. For this study, Tm1C homozygous mice (which contain two LoxP sites flanking the seventh exon of *Gfpt1* but lack *Ckm-Cre* expression) were used as controls. *Gfpt1*$^{tm1d/tm1d}$ mice contain two LoxP sites flanking the 7th exon of *Gfpt1* but also express a Cre recombinase tied to the *Ckm* reporter, which creates a skeletal muscle-specific knockout of *Gfpt1* [6,23].

2.2 Sample Preparation and Protein Digestion

Gfpt1-deficient and scramble cells were seeded into separate 15 cm plates. At 75% confluency *Gfpt1* silencing was achieved by doxycycline treatment at 2 μg/mL for 72 hours (Sigma, D9891). Prior to collection, cells were serum starved for three hours, followed by a replacement with growth media for

one hour, and finally serum starved for an additional 4 hours. Afterwards, conditioned media was collected, centrifuged at 1,000 x g for 15 minutes. The supernatant was collected and snap frozen. This sample represents the secretome.

Frozen cell pellets were treated with 200 µL of lysis buffer (50 mM TEAB, pH 7.8, 5% SDS, supplemented with cOmplete™ ULTRA protease inhibitor cocktail, Roche), followed by mechanical disruption using a Bioruptor® sonication system (Diagenode) for 10 min (30 s on/30 s off, 10 cycles) at 4 °C. To achieve complete homogenization, samples were additionally subjected to probe sonication (30 s, 1 s on/1 s off, amplitude 40%), and insoluble material was removed by centrifugation (20,000 × g, 15 min, 4 °C). Protein concentration in the cleared supernatant was quantified using DC Protein Assay (BioRad, 5000111) with BSA dilutions (Pierce, 23209) as standards according to the manufacturer's instructions.

Reduction of disulfide bonds was performed by incubation with 10 mM TCEP at 37 °C for 30 min, followed by alkylation with 15 mM IAA at room temperature for 30 min in the dark. For proteolytic digestion, 100 µg of total protein from each sample was processed using the S-Trap protocol (Protifi) with a protein-to-trypsin ratio of 20:1. Digestion was carried out for 2 h at 42 °C, and the reaction was terminated by acidification with formic acid to a final pH below 3.

The completeness of proteolytic cleavage was evaluated following desalting by monolithic column separation (PepSwift PS-DVB PL-CAP200-PM, Dionex) using an UltiMate 3000 HPLC system (Dionex, Germering, Germany). For each analysis, 1 µg of digest was injected directly. Chromatographic separation was achieved with a binary gradient (solvent A: 0.1% TFA; solvent B: 0.08% TFA in 84% acetonitrile), starting at 5–12% B over 5 min, followed by 12–50% B over 15 min, at a flow rate of 2.2 µL/min and 60 °C. UV detection was carried out at 214 nm [32].

2.3 DDA-LC-MS/MS analysis

A total of 1 µg of the prepared samples were analyzed using an UltiMate 3000 RSLC nano UHPLC system paired with a QExactive HF mass spectrometer. Initially, the samples were loaded onto a 75 µm x 2 cm, 100 Å, C18 pre-column at a flow rate of 20 µl/min for 20 minutes. Subsequently, separation was carried out on a 75 µm x 50 cm, 100 Å, C18 main column with a flow rate of 250 nl/min, utilizing a binary gradient (solvent A: 0.1% formic acid (Sigma-Aldrich, Hamburg, Germany; solvent B: 84% acetonitrile (Sigma-Aldrich, Hamburg, Germany)) with 0.1% formic acid; 5% B for 3 min, linear increase to 25% for 102 min, a further linear increase to 33% for 10 min, and a final linear increase to 95% for 2 min followed by a linear decrease to 5% for 5 min).For MS survey scans, the parameters included operating MS in data-dependent acquisition mode (DDA) with full MS scans from 300 to 1600 m/z (resolution 60,000) and the polysiloxane ion at 371.10124 m/z as a lock mass. The maximum injection time was set to 120 ms, and the automatic gain control (AGC) was set to 1E6. Fragmentation involved selecting the 15 most intense ions (above the threshold ion count of 5E3) at a normalized collision energy (nCE) of 27% in each cycle, following each survey scan. Fragment ions were acquired (resolution 15,000) with an AGC of 5E4 and a maximum injection time of 50 ms. Dynamic exclusion was set to 15 s.

2.4 **DDA data analysis of C2C12 cells**

All MS raw data underwent processing using Proteome Discoverer software version 2.5.0.400 (Thermo Scientific, Bremen, Germany) and were subjected to a target/decoy mode search against a mouse Uniprot database (www.uniprot.org, downloaded on 08 October 2019) utilizing the MASCOT and Sequest algorithm. The search parameters included precursor and fragment ion tolerances of 10 ppm and 0.02 Da for MS and MS/MS, respectively. Trypsin was designated as the enzyme with a maximum of 2 allowed missed cleavages. Carbamidomethylation of cysteine was set as a fixed modification, and oxidation of methionine was set as a dynamic modification. Percolator false discovery rate (strict) was established at 0.01 for both peptide and protein identification.

For reliable label-free quantification, only proteins identified with ≥ 2 unique peptides were considered for further analysis. Subsequently, the average normalized abundances (determined using Spectronaut) were calculated for each protein and used to determine the ratio between the different conditions. Finally, a Student's t-test with p-values was calculated in MS Excel. Only proteins with a p-value of ≤ 0.05 and an abundance ratio of ≥ 2 or ≤ 0.5 (up-regulated as well as down-regulated) were considered as regulated.

To further interpret the proteomic alterations, list of significantly upregulated proteins (expression ratio ≥ 2.0) and downregulated proteins (expression ratio ≤ 0.5) were analyzed using STRING database for functional enrichment. Gene Ontology (GO) Biological Process enrichment analysis was performed to identify overrepresented functional pathways. Protein-protein interactions networks were constructed using a minimum required interaction score of 0.7 (high confidence). Functional clustering was applied based on a similarity threshold greater than 0.7 to group proteins into related biological processes. This approach enabled the identification of key pathways and biological processes most affected by the observed proteomic changes.

2.5 Proteomic analysis from conditioned medium

Scramble and Gfpt1-deficient C2C12 myoblasts were seeded into 10 cm plates. At 75% confluency, growth medium was changed into serum free medium for four hours, then growth medium was applied for an hour, followed by another three hour incubation with starvation medium. Media was collected and centrifuged to remove cell debris and snap frozen in 10 mL aliquots for proteomic analysis.

Each sample was divided into two aliquots of 1 mL cultured medium. Protein precipitation was carried out by adding 3 mL of ice-cold acetone to each aliquot, followed by incubation overnight at -20 ^{o}C. Subsequently, the samples were centrifuged at 20,000 x g for 20 minutes at 4^{o}C to pellet the proteins. The acetone supernatant was carefully removed, and the pellets were air dried for 3 to 5 minutes. To

bring the protein pellets into solution, 100 µL lysis buffer (50 mM TEAB, pH 7.8; 5% SDS; and cOmplete ULTRA protease inhibitor, Roche) was added to each sample. Complete lysis was ensured using a Bioruptor® (Diagenode) for 10 minutes at 4 °C (30-second cycles of sonication and rest, 10 cycles total). Finally, the aliquots were combined to reconstitute the original sample. Reduction of disulfide bonds was performed by incubation with 10 mM TCEP at 37 °C for 30 min, followed by alkylation with 15 mM IAA at room temperature for 30 min in the dark. For proteolytic digestion, 100 µg of total protein from each sample was processed using the S-Trap protocol (Protifi) with a protein-to-trypsin ratio of 20:1. Digestion was carried out for 2 h at 42 °C, and the reaction was terminated by acidification with formic acid to a final pH below 3.

For the analysis of the samples acquired with nano-LC-MS/MS in DIA mode, the data was introduced to the Spectronaut software (Biognosys) and analyzed with a direct DIA-based search. As library the mouse proteome data was selected from UniProt (www.uniprot.org) containing 17,175 entries (downloaded on August 23rd 2023). Search and extraction settings were kept as standard (BGS Factory settings) Normalization was done by the software, using global normalization based on the median. For reliable label-free quantification, only proteins identified with ≥ 2 unique peptides were considered for further analysis. Subsequently, the average normalized abundances (determined using Spectronaut) were calculated for each protein and used to determine the ratio between the leukocytes from the patients and the corresponding controls. Finally, a Student's t-test with p-values was calculated in MS Excel. Only proteins with a p-value of ≤0.05 and an abundance ratio of ≥2 or ≤0.5 (up-regulated as well as down-regulated) were considered as finally regulated.

2.6 DIA LC-MS/MS analysis of conditioned medium samples

All samples were subjected to analysis using an UltiMate 3000 RSLC nano UHPLC system paired with a QExactive HF mass spectrometer, consistently applying 1 µg of peptide per sample.

Initially, the samples were loaded onto a 75 µm x 2 cm, 100 Å, C18 pre-column at a flow rate of 20 µl/min for 20 minutes. Subsequently, separation was carried out on a 75 µm x 50 cm, 100 Å, C18 main column with a flow rate of 250 nl/min, utilizing a linear gradient composed of solution A (99.9% water, 0.1% formic acid) and solution B (84% acetonitrile, 15.9% water, 0.1% formic acid). The gradient length was set to 120 minutes (3-45% solution B). The gradient protocol included: 3% solution B for 20 minutes, 3-35% over 120 minutes, followed by three wash steps each reaching 95% solution B for 3 minutes. Post-wash, the instrument was allowed to equilibrate for 20 minutes. MS data acquisition was performed in DIA (data-independent acquisition) mode, utilizing an in-house developed spectral library. Each sample was spiked with an appropriate quantity of iRT standard (Biognosys). Full MS scans were recorded from 300-1100 m/z at a resolution of 60,000 (Orbitrap), using the polysiloxane ion at 445.12002 m/z as a lock mass. The automatic gain control (AGC) was set at 3E6, with a maximum injection time of 20 milliseconds. Full MS scans were succeeded by 23 DIA windows, each covering 28 m/z with a 1 m/z overlap, starting at 400 m/z, acquired at a resolution of 30,000 (Orbitrap) with an AGC of 3E6 and a normalized collision energy (nCE) of 27 (CID).

For the analysis of the samples acquired with nano-LC-MS/MS in DIA mode, the data was introduced to the Spectronaut software (Biognosys) and analyzed with a direct DIA-based search. As library the mouse proteome data was selected from UniProt (www.uniprot.org) containing 17,175 entries (downloaded on August 23rd 2023). Search and extraction settings were kept as standard (BGS Factory settings) Normalization was done by the software, using global normalization based on the median. For reliable label-free quantification, only proteins identified with ≥ 2 unique peptides were considered for further analysis. Subsequently, the average normalized abundances (determined using Spectronaut) were calculated for each protein and used to determine the ratio between the leukocytes from the patients and the corresponding controls. Finally, a student's t-test with p-values was calculated in MS Excel.

2.7 Gfpt1-deficient myoblast immunofluorescence staining

1,000 Scramble and Gfpt1-deficient C2C12 myoblasts were seeded on 96-well µ-PLATE square ibiTreat plates (Ibidi). Gfpt1 silencing was achieved by doxycycline treatment at 2 µg/mL for 72 hours. (Sigma, D9891). Prior to staining cells were fixed with 2% paraformaldehyde for 15 minutes at room temperature. Blocking buffer (5% horse serum, 1% bovine serum albumin, 0.1% Trition X-100) was incubated for 1 hour. Cells were washed three times with PBS, prior to primary antibody incubation overnight. Primary antibodies included: Srgn (1:100, #C-11, Santa-Cruz Biotechnology), and p62 (1:100, Cedarlane, PM045). Cells were washed three times with PBS and incubated with goat-anti rabbi AlexaFluor 594 (1:500, #A-11012, FisherSci). Cells were then washed three times with PBS for 5 minutes and then incubated with DAPI (1:2000) for an additional five minutes. The 96-well µ-PLATE square ibiTreat plates were then imaged using the Opera high content imaging system and analyzed by Columbus™ software to measure Srgn and p62 puncta size and area.

2.7 Lysis of cells

Cell lysates and skeletal muscle homogenates were prepared with radioimmunoprecipitation assay (RIPA) buffer (150mM NaCl, 50mM Tris-HCl (pH 8), 1% Triton X-100, 0.5% NaDOC, 0.1% SDS) supplemented with protease (Roche, 04693116001, Mississauga, ON, Canada) and phosphatase (Roche, PHOSS-RO) inhibitors. Cell lysates were centrifuged at 15,000 × *g* for 10 minutes at 4 °C and the supernatants collected. Skeletal muscle samples were combined with lysis buffer and a metal bead in 2 mL SafeLock™ Eppendorf tubes (Eppendorf, 022363352, Mississauga, ON, Canada), then homogenized using a TissueLyser II (Qiagen, Toronto, ON, Canada). The protocol comprised of 3 rounds of homogenization at 30 Hz for 90 seconds followed by incubation on ice for 60 seconds. Afterwards, samples were kept at 4 °C for 4 hours on a rotating platform then centrifuged at 15,000 × *g* for 15 minutes at 4 °C. Total protein concentration was determined using a DC Protein Assay (BioRad, 5000111) with BSA dilutions (Pierce, 23209) as standards.

2.8 Conditioned medium collection for Srgn secretion

To examine Srgn protein levels within conditioned medium 2C12 cells were seeding in 10cm plates. Gfpt1 silencing was achieved by doxycycline treatment at 2 μg/mL for 72 hours. (Sigma, D9891). Cell media was replaced with serum starved growth medium for 1 hour. Afterwards, growth medium was reapplied and incubated for 1, 3, 5, 8, 12, 18, and 24 hours. At each timepoint cells media was collected and combined in a 1:5 ratio with ice-cold 100% methanol, and place in the -80ºC overnight. The next morning solution was centrifuged at 8,000 x g for 30 minutes. The supernatant was discarded, and pellets were dried for 1 hour in a fume hood. Cell pellet was homogenized with RIPA buffer, followed by a brief sonification.

2.9 Western Blotting

To examine protein levels within *Gfpt1*-deficient cell pellets and skeletal muscle lysates were resolved by SDS-PAGE and transferred to PVDF membranes using a BioRad™ Trans-Blot Turbo system (1704150EDU, Mississauga, ON, Canada). All samples were heated at 100^0C for 5 minutes in 4x Laemmli sample buffer, prior to resolution with Western blot.. When examining Srgn protein levels SDS-PAGE gels were transferred to PVDF membranes with wet transfer (40 V, overnight, 4ºC). All membranes were blocked for 1 hr and incubated with primary antibody overnight at 4 °C. Multiple secondary antibodies were used for this analysis including with IR Dye®800CW Donkey anti-Mouse IgG (Li-Cor, 926-32212, 1:5000) and IR Dye®680RD Goat anti-Rabbit IgG (Li-Cor, 926-68071, 1:5000) for 1 hour at room temperature.

Blots were imaged using a Licor Odyssey DLX (Lincoln, NE, USA) and densitometry performed using Image Studio™ (Licor, version 6.0) or with ChemiDoc (BioRad, Mississauga, ON, Canada) and analyzed with ImageJ. Gapdh or Ponceau S stain was used to normalize protein expression.

2.10 Real-Time qPCR (RT-qPCR)

RNA collection for *in vitro* experiments was performed using the RNeasy™ Micro mini kit (Qiagen, #74134, Toronto, Canada). Skeletal muscle RNA extraction was performed with the RNeasy™ Fibrous Micro mini kit (Qiagen, #74704) and quantified by NanoDrop (ND-1000, Spectrophotometer, NanoDrop®. RNA was converted to complementary DNA (cDNA) with the All-In-One 5x RT MasterMix (ABM, #G592, Richmond, BC, Canada) following kit guidelines. RT-qPCR was performed using the PowerUp™ SYBR™ Green Master Mix (FisherSci, #A25741, Ottawa, Canada) with the QuantStudio™ Studio 6 Flex Real-Time PCR System (Thermofisher, Ottawa, Canada) (see Supplementary Materials Table S1 for primer sequences). To analyze the expression of our target genes the geometric mean of three reference genes (*Gapdh, Rpl27, Ppia*) was used.

2.11 Soluble/Insoluble Fractionation

Gfpt1-deficient and scramble myoblasts were seeded in 10 cm plates. Following activation for gene silencing with 2 μg/mL doxycycline for 72 hours the cells were pelleted and resuspended in cell lysis buffer (20 mM HEPES pH 7.9, 0.2 M KCl, 1 mM $MgCl_2$, 1 mM EGTA, 1% Triton X-100, 10% glycerol and protease/phosphatase inhibitor) and incubated on ice for 30 minutes. The soluble fraction was taken from the supernatant which was collected after centrifugation at 13,000 x g for 20 minutes at 4 ^{0}C. The pellet (insoluble membrane) was solubilized in an SDS-detergent buffer (20 mM HEPES pH 7.9, 0.2 M KCl, 1 mM $MgCl_2$, 1 mM EGTA, 1% Triton X-100, 1% SDS 10% glycerol and protease/phosphatase inhibitor). Cell pellets were solubilized through a motor and pestle. All samples were headed at 100 ^{0}C for 5 minutes in 4x Laemmli Sample Buffer, prior to resolution with Western blot.

2.12 Antibodies

The following antibodies were used for immunoblot experiments: Gfpt1 (ProteinTech, #14132-1-AP, 1:500, Rosemont, IL), Gapdh (14C10) (Cell Signalling, 2118, 1:2000, Danvers, MA), O-GlcNAc (RL2) (Novus Biologicals, NB300-524, 1:1000, Toronto, Ontario), Ogt (ProteinTech, 66823-1-Ig,

1:1000, Rosemont, IL), Srgn (#C-11, Santa Cruz) , Srgn (H9, Santa Cruz), p62 (Cedarlane, #PM045), LC3 (Sigma, #L7543).

2.13 Statistics

Data was analyzed with GraphPad Prism v 10.1.2. Data was checked for normality using the D'Agostino-Pearson test and outliers were identified using the robust regression and outlier remover (ROUT) method. Statistical significance was determined by using unpaired two-tailed Student *t*-tests or analysis of variance (ANOVA) tests. If multiple comparisons were used, a Tukey's post-hoc test was performed. Results are presented as mean ± SD, where $p < 0.05$ was considered significant.

3.0 Results

3.1 Whole-cell proteomics in Gfpt1-deficient myoblasts reveals dysregulation of autophagy and intracellular trafficking pathways

To define the global proteomic consequences of reduced hexosamine biosynthetic pathway flux, we performed whole-cell mass spectroscopy on both the conditioned medium (secretome) and cell pellets (proteome) of doxycycline-inducible *Gfpt1*-deficient C2C12 myoblasts (Figure 1A). Prior to proteomic profiling we confirmed efficient knockdown of Gfpt1, oligotransferase (Ogt), and a decrease in global O-GlcNAcylation by Western blotting which is consistent with diminished HBP flux (Figure 1B).

Comparative proteomic analysis between *Gfpt1*-deficient and scramble myoblasts identified 74 significantly upregulated and 229 significantly downregulated proteins (Figure 1C). Our comparative analysis revealed that Stead3 (6.65-fold), Slc25a10 (6.45-fold), Rab34 (6.23-fold), Rhob (5.20-fold) and Supt16h (4.50-fold) had the highest magnitude of change (Table 1). The magnitude and directionality of these broad changes suggest widespread alterations in proteostasis and cellular responses. STRING pathway enrichment analysis of upregulated proteins demonstrated prominent

activation of pathways relevant to protein homeostasis, protein folding and stress-responsive chaperone systems (Figure 1D). These findings are consistent with adaptive response to impaired glycosylation and an increased burden of misfolded or immature proteins.

In contrast, our comparative analysis revealed that Ppp1r14b (0.02-fold), Lima1 (0.04-fold), Gmfb (0.05-fold), Cttn (0.07-fold), and Denr (0.08-fold) represent the most downregulated proteins (Table 1). Overall, downregulated proteins showed a strong enrichment for pathways associated with intracellular transport including vesicle-mediated trafficking, and protein processing in the secretory pathway (Figure 1E). Along this line, several components of COPII-mediated ER-to-Golgi transport machinery, Golgi organization, and vesicle cargo sorting systems were reduced suggesting compromised protein trafficking capacity (Table 1). Together, these proteomic changes indicate that *Gfpt1* deficiency disrupts the balance between protein synthesis, folding, and notably trafficking, resulting in the coordinated activation of stress-mitigating pathways and suppression of secretory transport machinery.

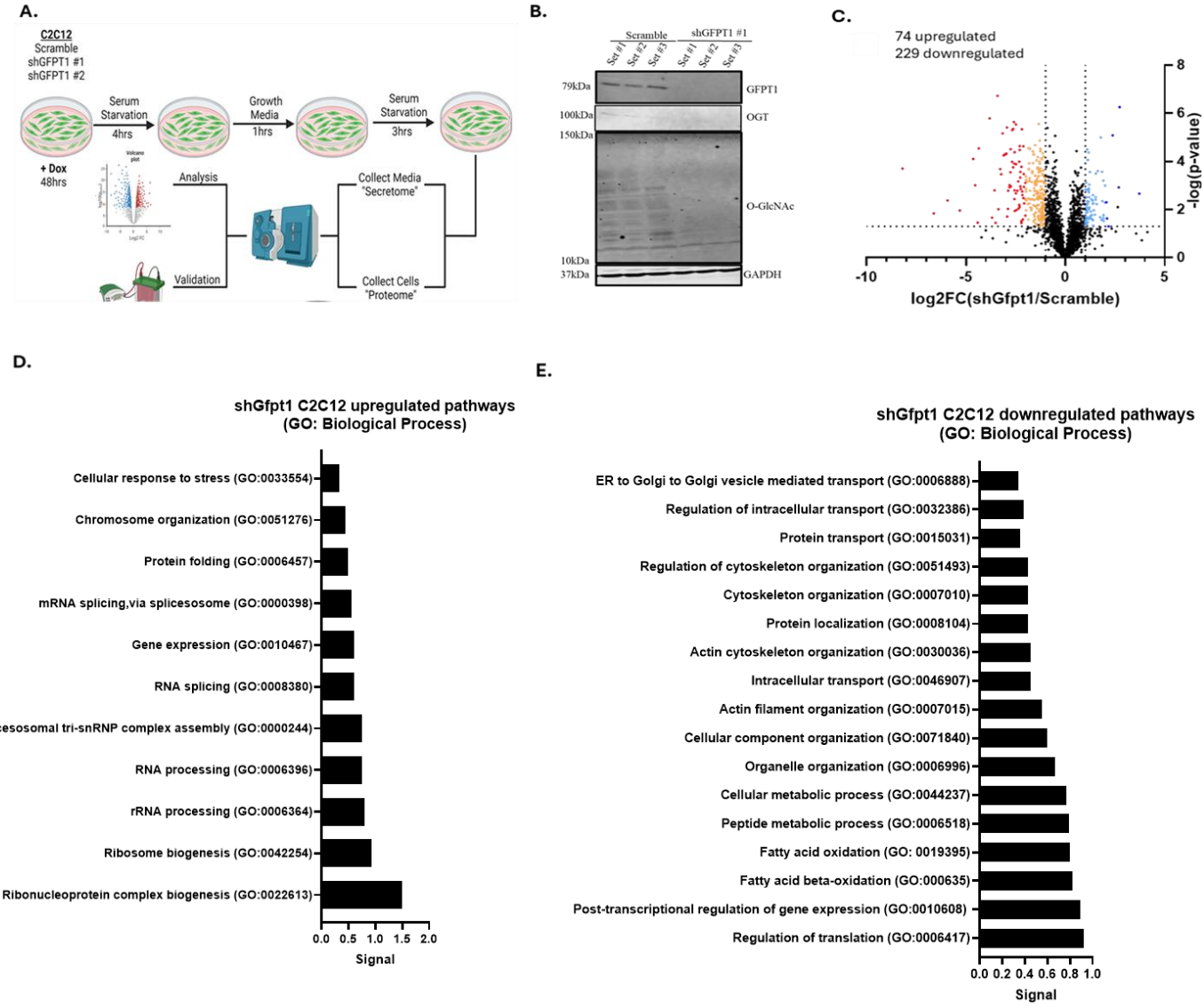
A.
C2C12
Scramble
shGFPT1 #1
shGFPT1 #2
Serum Starvation 4hrs
Growth Media 1hrs
Serum Starvation 3hrs
+ Dox 48hrs
Analysis
Validation
Collect Media "Secretome"
Collect Cells "Proteome"
B.
Scramble
shGFPT1 #1
Set #1
Set #2
Set #3
79kDa
100kDa
150kDa
10kDa
37kDa
GFPT1
OGT
O-GlcNAc
GAPDH
C.
74 upregulated
229 downregulated
-log(p-value)
log2FC(shGfpt1/Scramble)
D.
shGfpt1 C2C12 upregulated pathways
(GO: Biological Process)
Cellular response to stress (GO:0033554)
Chromosome organization (GO:0051276)
Protein folding (GO:0006457)
mRNA splicing,via splicesosome (GO:0000398)
Gene expression (GO:0010467)
RNA splicing (GO:0008380)
Splicesosomal tri-snRNP complex assembly (GO:0000244)
RNA processing (GO:0006396)
rRNA processing (GO:0006364)
Ribosome biogenesis (GO:0042254)
Ribonucleoprotein complex biogenesis (GO:0022613)
Signal
E.
shGfpt1 C2C12 downregulated pathways
(GO: Biological Process)
ER to Golgi to Golgi vesicle mediated transport (GO:0006888)
Regulation of intracellular transport (GO:0032386)
Protein transport (GO:0015031)
Regulation of cytoskeleton organization (GO:0051493)
Cytoskeleton organization (GO:0007010)
Protein localization (GO:0008104)
Actin cytoskeleton organization (GO:0030036)
Intracellular transport (GO:0046907)
Actin filament organization (GO:0007015)
Cellular component organization (GO:0071840)
Organelle organization (GO:0006996)
Cellular metabolic process (GO:0044237)
Peptide metabolic process (GO:0006518)
Fatty acid oxidation (GO: 0019395)
Fatty acid beta-oxidation (GO:000635)
Post-transcriptional regulation of gene expression (GO:0010608)
Regulation of translation (GO:0006417)
Signal

Figure 1: Whole cell proteomics in Gfpt1-deficient myoblasts reveals impaired autophagy and protein trafficking: A. A schematic of the proteomic (cell pellets) and secretomic (conditioned medium) isolated from *Gfpt1*-deficient myoblasts. The cell pellets (containing all possible membrane, cytosolic and nuclear proteins) were harvested and snap-frozen in liquid nitrogen for downstream proteomic analysis of both conditioned media and whole-cell lysates. **B.** Immunoblot analysis performed prior to proteomic assessment confirms reduced Gfpt1 protein levels and decreased global O-GlcNAcylation in doxycycline-treated myoblast lysates. Samples were isolated from three independent biological experiments. **C.** Volcano plot of whole-cell proteomics comparing Gfpt1-deficient and scramble control C2C12 myoblasts identifies 74 upregulated and 220 downregulated proteins. Differential expression was defined as a fold change ≥ 2.0 or ≤ 0.5 with statistical significance ($p < 0.05$). **D.** STRING pathway analysis was performed on upregulated proteins and **E.** downregulated proteins. For both conditions, the top 15 pathways implicated with Gfpt1-deficient myoblasts. The size of the circle for each pathway indicates the number of proteins implicated in each respective pathway.

Table 1: Key proteins up-or downregulated in Gfpt1-deficeint C2C12 myoblasts compared with scramble. Proteins with a p-value of <0.05 and an abundance ratio of either ≥ 2-fold (upregulated) or ≤0.5-fold (downregulated) are included below

Protein	Description	Autophagy-relevant pathway role	KO / Ctrl
Map1lc3b	LC3B, autophagosome membrane protein	Core macroautophagy machinery; autophagosome formation, mitophagy, pexophagy	2.25
Rheb	mTORC1 activator GTPase	Master negative regulator of autophagy via mTORC1	4.17
Rab34	Rab GTPase	Lysosome positioning; autophagosome–lysosome fusion	6.23
Rhob	Rho GTPase	Endosomal/lysosomal trafficking; autophagosome maturation	5.20
Emc6	ER membrane complex subunit	ER-derived phagophore membrane source	2.36
Calr	ER Ca^{2+} chaperone	ER stress, ER-phagy, autophagy induction	2.19
Erp29	ER folding protein	UPR/ER stress–induced autophagy	2.18
Erlin2	ERAD/ER stress protein	ER stress signaling to autophagy	2.17
Psmb3	Proteasome subunit	Proteasome–autophagy compensatory axis	2.35
Hspbp1	Hsp70 co-chaperone	Chaperone-assisted autophagy/proteostasis	2.11
Ppib	ER peptidyl-prolyl isomerase	ER proteostasis → autophagy induction	2.40
Clcn5	Endolysosomal Cl^- channel	Lysosome acidification; autophagic degradation	2.63
Arsb	Lysosomal enzyme	Lysosomal throughput during autophagy	2.31
Ndufs1	ETC Complex I subunit	Mitophagy cargo indicator	3.80
Ndufa6	ETC Complex I subunit	Mitophagy cargo indicator	2.27
Mtco2	ETC Complex IV subunit	Mitophagy cargo indicator	2.27
Cox6c	ETC Complex IV subunit	Mitophagy cargo indicator	2.15
Bcat1	BCAA metabolism enzyme	Nutrient sensing → mTOR regulation	2.52
Slc25a10	Mitochondrial carrier	Redox/TCA control → AMPK/mTOR/autophagy	6.45
Ampd2	AMP metabolism enzyme	AMP/ATP ratio → AMPK → autophagy	2.61
Copg1	Coatomer subunit gamma-1	COPI vesicle trafficking (Golgi ↔ ER retrograde transport)	0.50
Sec23a	COPII vesicle component	ER → Golgi export (cargo sorting)	0.49
Sec22b	SNARE protein	ER–Golgi vesicle fusion, ER-phagosome pathway	0.31
Uso1	Vesicle tethering factor (p115)	Golgi vesicle docking and fusion	0.42

Rab5b	Small GTPase	Early endosome formation, endocytosis	0.44
Snx9	Sorting nexin-9	Clathrin-mediated endocytosis	0.46
Gapvd1	Rab5 GEF	Endosome maturation and trafficking	0.43
Clta	Clathrin light chain A	Vesicle coat formation (endocytosis)	0.25
Prkaa1 (AMPKα1)	Energy sensor kinase	Autophagy induction, mTOR regulation	0.42
Hspb8	Small heat shock protein	BAG3-mediated selective autophagy (aggrephagy)	0.42
Bag3	Co-chaperone	Protein quality control, autophagy targeting	0.12
Stub1 (CHIP)	E3 ubiquitin ligase	Proteasome targeting + autophagy crosstalk	0.43
Psmb7	Proteasome subunit β7	Proteasomal protein degradation	0.36
Psme1	Proteasome activator	Proteasome function enhancement	0.35
Ufm1	Ubiquitin-like modifier	Protein turnover and ER stress responses	0.47
Nedd8	Ubiquitin-like protein	Cullin activation, ubiquitin ligase regulation	0.30
Atp6v1b2	V-ATPase subunit B2	Lysosomal acidification, autophagic degradation	0.45
Atp6v1g1	V-ATPase subunit G1	Lysosomal acidification	0.43
Lonp1	Mitochondrial protease	Mitochondrial protein quality control	0.40
Atad3	Mitochondrial AAA protein	Mitochondrial dynamics, mitophagy regulation	0.44
Park7 (DJ-1)	Stress response protein	Oxidative stress, aggrephagy support	0.36
Dync1i2	Dynein intermediate chain	Microtubule-based vesicle transport	0.35
Tubb4b	β-tubulin	Cytoskeletal trafficking, autophagosome movement	0.48
Ckap4	ER-associated protein	ER structure and protein trafficking	0.48

3.2 Gfpt1 deficiency activates UPR through increased Xbp1 splicing and Atf4

Our proteomic results revealed many proteins associated with trafficking and ER homeostasis. As a result, in elevated hypoglycosylation stress, we hypothesized that the unfolded protein response (UPR) pathway would also be impaired. The UPR consists of three coordinated signaling branches – IRE1, PERK and ATF6 – that collectively restore ER proteostasis by enhancing chaperone expression, attenuating protein synthesis, and promoting ER-associated degradation (ERAD) (Figure 2A). Under ER stress, the IRE1 arm generates the active transcription factor Xbp1s via unconventional mRNA splicing, thereby increasing the transcription of ERAD components and ER chaperones. XBP1 exists in two forms: an unspliced, relatively unstable transcript (Xbp1u) and a spliced form (Xbp1s) produced during ER stress (Figure 2A). Consistent with activation of this pathway, we observed increased levels of Xbp1s accompanied by a relative reduction in Xbp1u, indicating enhanced IRE1 signaling and unfolded protein response induction.

To determine whether hypoglycosylation is sufficient to activate Xbp1, we treated C2C12 cells with increasing doses of tunicamycin, an inhibitor of N-linked glycosylation. We found a significant dose-dependent increase in total *Xbp1*, *Xbp1s*, and a decrease in *Xbp1u* expression (Supplementary Figures 1A to 1C). We next aimed to examine whether pharmacological inhibition of Gfpt1 with 6-diazo-l-norleuncine (DON) could activate *Xbp1* expression. Indeed, DON inhibition of Gfpt1 significantly increased total *Xbp1* transcript levels, robustly elevated *Xbp1s* and decreased *Xbp1u* expression levels (Figure 2A to 2B, Supplementary Figure 1D). As such, both inhibition of N-linked glycosylation and Gfpt1 directly engages of the IRE1 pathway in response to hypoglycosylation stress.

We next examined whether *Gfpt1* knockdown directly activates the UPR. Doxycycline-inducible *Gfpt1*-deficient myoblasts (shGfpt1 #1, and shGfpt1 #2) displayed significantly elevated expression of both total *Xbp1* and *Xbp1s* relative to scramble controls (Figure 2D and 2E). There was a

significant decrease in *Xbp1u* expression levels (Supplementary Figure 1E). As such, this demonstrates that reduced HBP flux through *Gfpt1* deficiency activates the IRE1–*Xbp1* axis.

To evaluate whether this response also occurs *in vivo*, we assessed ER stress markers in whole skeletal muscle isolates from 20-week *Gfpt1*$^{tm1d/tm1d}$ mice. *Gfpt1*$^{tm1d/tm1d}$ mice harbour a conditional skeletal muscle-specific knockout of *Gfpt1*, which contains a pathological resemblance to *GFPT1*-CMS patients, and has been used to test the efficacy of new therapeutic strategies . Quadriceps muscle from *Gfpt1*$^{tm1d/tm1d}$ mice exhibited significantly increased total *Xbp1*, and *Xbp1s* expression compared to Tm1C homozygous control mice (Figure 2F and 2G). We also highlighted a significant decreased in *Xbp1u* confirming activation of the UPR in *Gfpt1*$^{tm1d/tm1d}$ mice (Supplementary Figure 1F).

Together these findings demonstrate that *Gfpt1* deficiency consistently activates the IRE1-*Xbp1* branch of the UPR across Gfpt1-deficient myoblast and skeletal muscle. This indicates that impaired glycosylation creates sufficient proteotoxic stress to engage ER-adaptive pathways.

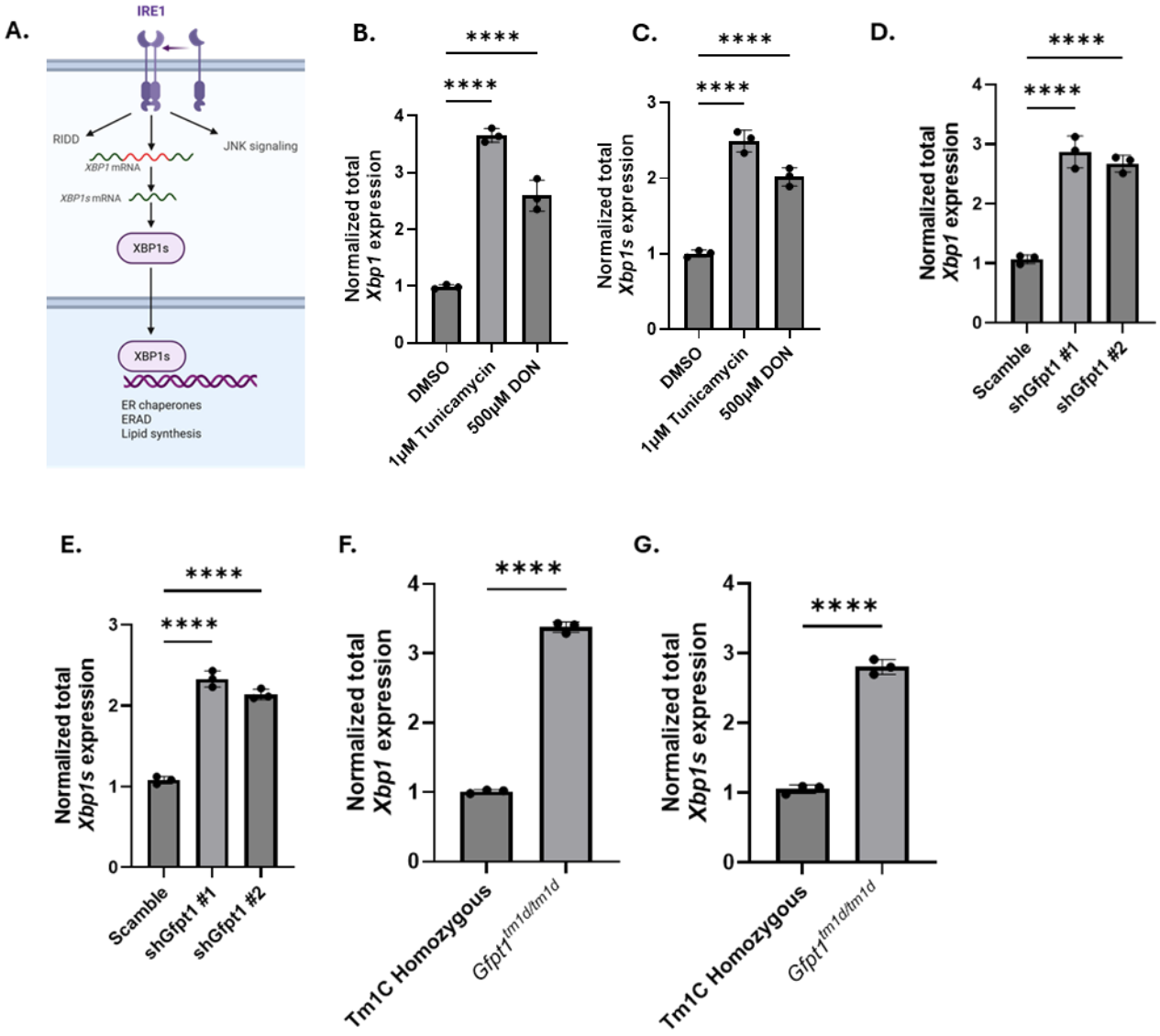

Figure 2: Gfpt1-deficient models show elevated levels of *Xbp1s* expression, indicating activation of the unfolded protein response. A. Schematic illustration of IRE1-XBP1 arm of the unfolded protein response (UPR). Gfpt1 deficiency reduces protein glycosylation, resulting in a hypoglycosylated cellular environment. To prevent accumulation of misfolded proteins, cells activate UPR pathways that regulate protein folding and degradation. Under ER stress, X-box binding protein 1 (XBP1) undergoes IRE1-dependent alternative splicing to generate XBP1s, a transcription factor that induces expression of ERAD components and ER chaperones. **B.** C2C2 myoblasts were treated with tunicamycin or 6-diazo-5-oxo-L-norleucine (DON) to induce hypoglycosylation. RT-qPCR analysis shows increased expression of total Xbp1 and **C.** spliced Xbp1 (Xbp1s). **D.** Doxycycline-treated Gfpt1-deficient C2C12 myoblasts (shGfpt1 #1 and shGfpt1 #2) exhibit increased expression of total Xbp1 and **E.** Xbp1s relative to scramble controls. **F.** RT-qPCR analysis of quadriceps muscle from *Gfpt1*$^{tm1d/tm1d}$ mice and Tm1C homozygous control mice shows increased total Xbp1 expression and, **G.** elevated Xbp1s expression in Gfpt1-deficient samples. Gene expression values were normalized to the geometric mean of Rpl27, Gapdh, and Actb. Three

biological replicates were analyzed for all experiments. Statistical significance was determined by one-way ANOVA (B through E) or Student's *t*-test (F through G). * $p < 0.05$; *** $p < 0.001$; **** $p < 0.000$.

3.3 Gfpt1-deficiency impairs autophagy and leads to p62 accumulation in myoblasts and skeletal muscle

Since our proteomics and secretion analyses suggested broad disruption in proteostasis, we next examined whether Gfpt1-deficiency alters autophagy, a major pathway responsible for clearing misfolded and aggregated proteins. Notably, whole-cell proteomics identified multiple autophagy-related proteins as dysregulated in Gfpt1-deficient myoblasts, including components involved in cargo recognition, autophagosome formation, and lysosomal turnover (summarized in, Table 1).

To validate these findings, we performed biochemical analyses in doxycycline-induced Gfpt1-deficient C2C12 myoblasts. Immunoblotting showed a robust accumulation of p62 and increased LC3-II levels compared with scramble controls (Figure 3A), and densitometric quantification confirmed significant elevations in both proteins (Figure 3B and 3C, respecively). To further dissect p62 behaviour, we performed soluble/insoluble fractionation. In control cells, p62 was primarily detected in the soluble fraction; however, Gfpt1-deficient myoblasts displayed marked accumulation of p62 in both soluble and insoluble fractions (Supplementary Figure 2A). Insoluble p62 is a biochemical hallmark of defective autophagic flux and protein aggregation, further supporting a block in cargo clearance (REF).

To determine whether Gfpt1 deficiency affects autophagic degradation rather than initiation, we inhibited lysosomal acidification with chloroquine. In C2C12 cells, chloroquine treatment increased p62 staining intensity (Supplementary Figure 2B to 2D). Notably, Gfpt1-deficient myoblasts displayed elevated p62 levels following choloroquine treatment (Supplementary Figure 2E and 2F). We next assessed whether Gfpt1 deficiency exacerbates inhibition of autophagic flux. Consistent with the biochemcial data, immunofluorescence analysis revealed increased p62 signal intensity in *Gfpt1*-deficiet myoblasts (Figure 3D). Quantitative image analysis revaled significantly increased number of

p62 positive puncta (Figure 3E) and area (Figure 3F), respectively. These results suggest that there may be an accumulation of autophagic cargo.

Next, we explored whether p62 puncta accumulation within *Gfpt1*$^{tm1d/tm1d}$ mice skeletal muscle. Previous whole cell proteomics from *Gfpt1*$^{tm1d/tm1d}$ revelaed an ~2.5 fold increase in p62 protein levels in intercostal muscles (REF). To confirm this proteomic result, we performed p62 staining within the gastrocnemus muscle isolated from *Gfpt1*$^{tm1d/tm1d}$ and Tm1C homozygous muscle. We demonstrate that indeed overall p62 postive puncta accumulate within the gastrocnemius muscle, further demonstrating that dysfunctional autophagy extends ot the skeletal muslce (Figure 3G).

Together, these findings demonstrate that Gfpt1-deficiency leads to persistent accumulation of p62, elevated LC3-II, increased puncta formation. This autophagy defect is consistent with the pronounced proteostasis and trafficking abnormalities observed in Gfpt1-deficient myoblasts and *Gfpt1*$^{tm1d/tm1d}$ skeletal muscle.

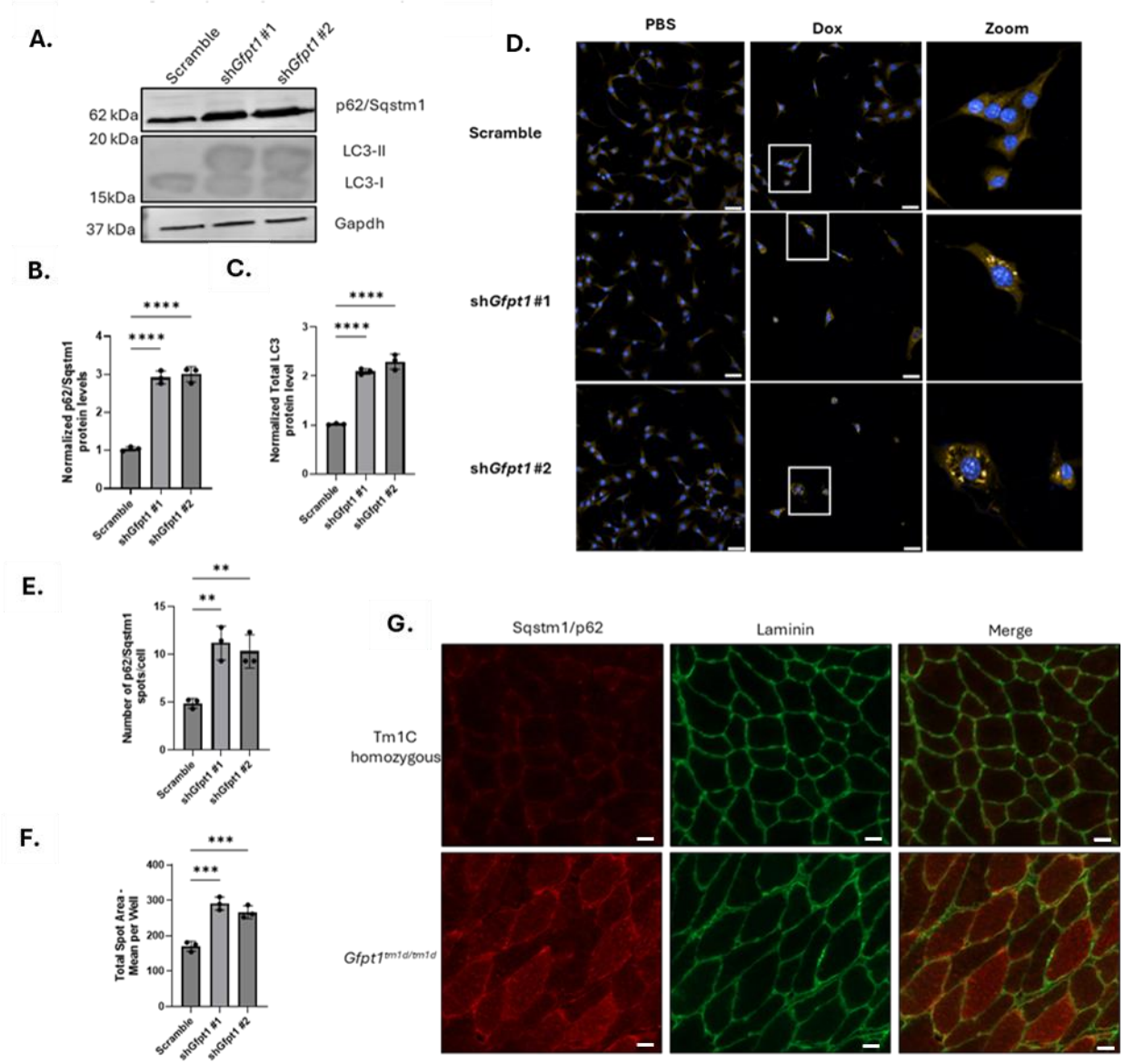

Figure 3: Whole cell proteomics in Gfpt1-deficient myoblasts reveals impaired autophagy A. Western blot analysis shows increased p62 and LC3-II protein levels in Gfpt1-deficient myoblasts compared with scramble controls. **B.** Quantification of immunoblot data reveals a significant increase in p62 and **C.** LC3-II protien levels in Gfpt1-deficient myoblasts.. **D.** Immunofluorescence analysis demonstrates increased p62 staining intensity in Gfpt1-deficient myoblasts. **E.** Quantification of autophagic markers shows a signficantly higher percentage of cells containing p62-positive puncta and **F.** an increase in p62 puncta area in Gfpt1-deficient myoblasts, indicative of impaired autophagic flux. **G.** Immunofluorescence staning of p62 in gastrocnemius muscle from *Gfpt1*$^{tm1d/tm1d}$ mice reveal increased signal intesnity and punctate accumulation within muscle fibers. Muscle fibers were marked with α1 laminin (Lama1). Scale bar: 20 µm. All graphs represent mean ± SD. Statistical significance was assessed using one-way ANOVA. All experiemnts were performed with three biological replicates per group. Comparisions were made between scramble control and Gfpt1-deficient samples. *** $p < 0.001$, **** $p < 0.0001$.

3.4 Gfpt1 deficiency impairs protein trafficking and reduces secretion of skeletal muscle proteoglycan serglycin

Our whole-cell proteomic analysis indicated suppression of intracellular trafficking pathways in *Gfpt1*-deficient myoblasts. This led us to examine whether defects in protein transport affect the secretion of muscle-derived cargo proteins. Secretomic profiling detected 140 proteins in conditioned medium, with 13 proteins significantly altered in *Gfpt1*-deficient C2C12 myoblasts. (Table 2). Among stress-associated proteins, we observed a pronounced reduction in extracellular abundance of Binding immunoglobulin Protein (BiP) in Gfpt1-deficient C2C12 cells (Table 2). Reduced BiP secretion likely reflects increased ER rentation due to elevated chaperone engagement with misfolded proteins, together with impaired ER-to-Golgi trafficking obtained from the proteomics from *Gfpt1*-deficient myoblasts.

Serglycin (Srgn) is a secreted proteoglycan with roles in skeletal muscle biology {Citation}. Given our proteomic and secretomic analyses suggested impaired protein trafficking, we next investigated whether Srgn secretion is affected by Gfpt1 deficiency. In this context, impaired glycosylation may disrupt proper Srgn processing and export, thereby impacting muscle homeostasis. Immunoblot analysis of doxycycline-induced Gfpt1-deficient C2C12 cells demonstrated a marked reduction in Srgn protein levels in both shGfpt1 #1 and shGfpt1 #2 lines, normalized to Ponceau S staining (Figure 4A and 4B).

To determine whether Srgn dysregulation occurs *in vivo*, we analyzed quadriceps from muscle from 20-week-old *Gfpt1*$^{tm1d/tm1d}$ mice. Consistent with the *in vitro* results , Gfpt1-deficient quadriceps exhibited reduced levels of both the core Srgn protein (~32 kDa) and the high molecular weight glycosylated Srgn species (~120 kDa) (Figure 4C to 4E). Together these results indicate that Gfpt1-deficiency alters the abundance of Srgn.

Immunofluorescence microscopy revealed an abnormal intracellular distribution of Srgn in Gfpt1-deficient C2C12 myoblasts. Compared with scramble controls, where Srgn was predominantly localized in subsarcolemmal regions, Gfpt1-deficient cells exhibited increased cytoplasmic Srgn-positive puncta and enhanced intracellular staining intensity (Figure 4F). Quantitative image analysis using Columbus™ software showed significant increases in both the total Srgn-positive spot area (Figure 4G) and the number of Srgn-positive puncta per cell (Figure 4I), indicating intracellular accumulation. Taken together these data indicate that overall Srgn levels are reduced in Gfpt1-deficient myoblasts. However, the remaining Srgn is predominantly retained intracellularly, as opposed to being membrane bound and secreted.

Finally, analysis of conditioned medium collected over a 24-hour time course revealed a reduction in secreted Srgn from Gfpt1-deficient myoblasts relative to scramble controls (Figure 4J, and Supplementary Figure 3B and C). Consistently, reduced total Srgn levels were observed at 24 hours (Supplementary Figure 3C and 3D). Together, these findings indicate that Gfpt1-deficiency disrupts intracellular protein trafficking, leading to retention and decreased secretion of Srgn in murine myoblasts.

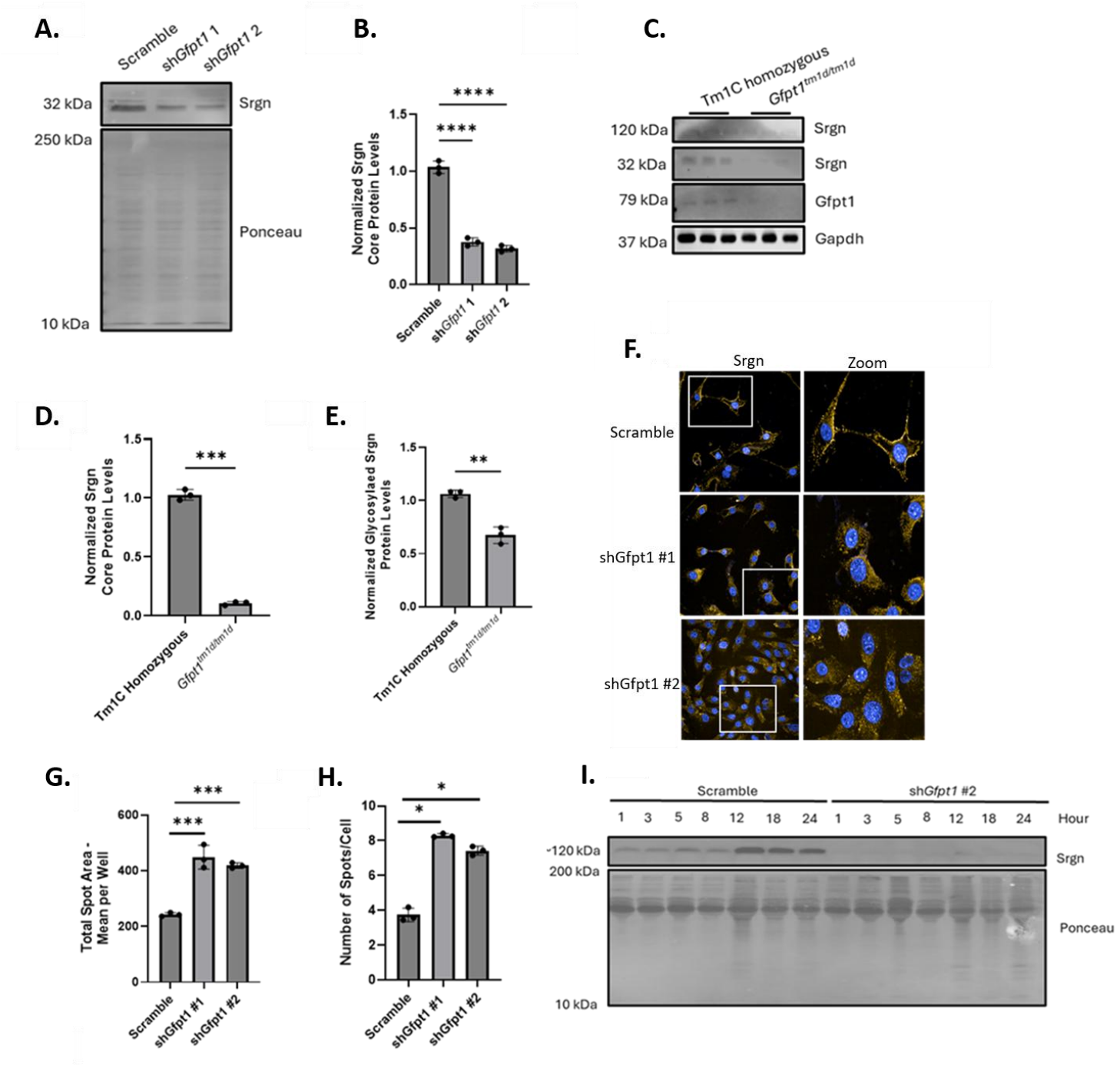

Figure 4: Proteomics reveals downregulation in protein trafficking pathways and altered secretion of skeletal muscle proteins : A. Western blot analysis of serglycin (Srgn) protein levels in Gfpt1-deficient C2C12 myoblasts. Protein levels was normalized to total protein loading using Ponceau S staining. **B.** Quantification shows a significant reduction in Srgn protein levels in Gfpt1-deficient myoblasts using two independent shRNA constructs. **C.** Western blot analysis of quadriceps muscle lysates from 20-week-old *Gfpt1*$^{tm1d/tm1d}$ mice and Tm1C homozygous controls, showing high-molecular weight (~120 kDa) glycosylated Srgn species, core (~32 kDa) Srgn, and Gfpt1. **D.** Quantification of

core Srgn and **E.** high-molecular weight glycosylated Srgn species, normalized to Gapdh protein levels. **F.** Immunofluorescence staining of scramble control and Gfpt1-deficient C2C12 myoblasts labeled for SRGN. Images were acquired at 40× magnification using the OPERA™ high-content imaging system. Scale bar = 10 µm. **G.** Quantitative image analysis using Columbus™ software shows increased total Srgn-positive spot area (μm^2) and **H.** an increased average number of Srgn-positive puncta per cell in deficient Gfpt1-deficient myoblasts. **I.** Immunoblot analysis of conditioned medium collected over a 24-hour time course from scramble control and shGfpt1 #2 C2C12 myoblasts. All graphs represent mean ± SD. Statistical significance was assessed using one-way ANOVA. All experiments were performed with three biological replicates per group. ** $p < 0.01$, *** $p < 0.001$.

Table 2: Key proteins up-or downregulated in Gfpt1-deficeint C2C12 myoblasts secretome compared with scramble. Proteins detected with an adjusted *p*-value of < 0.05 were deemed significantly altered from scrambled control.

Proteins with an adjusted *p*-value of < 0.05 were deemed significantly altered from the

Protein	Description	Relevant role	Fold Change
Eno1 (α-enolase)	Glycolytic enzyme; also moonlights as plasminogen receptor when extracellular	Promotes ECM remodeling and cell migration via plasmin activation; supports myoblast differentiation and tissue remodeling	1.7
A2m (Alpha-2-macroglobulin)	Broad-spectrum protease inhibitor	Regulates extracellular proteolysis, cytokine binding, and growth factor availability → impacts myogenesis and muscle repair environment	1.49
ApoA1	Major HDL apolipoprotein	Lipid transport and anti-inflammatory signaling; supports metabolic homeostasis in muscle and may influence differentiation under stress	1.45
Actb / Actg1 (β- and γ-actin)	Cytoskeletal proteins	Released during stress/damage; function as DAMPs (damage-associated signals); linked to cell motility and myoblast fusion dynamics	1.44
Fbln1 (Fibulin-1)	ECM glycoprotein	Regulates ECM organization, cell adhesion, and migration; important for myoblast alignment and differentiation niche	1.22
Anxa2 (Annexin A2)	Calcium-dependent phospholipid-binding protein	Membrane repair, vesicle trafficking, exosome release, and plasmin generation → key for myoblast membrane remodeling and fusion	0.67
Hspa5 (BiP / GRP78)	ER chaperone protein	ER stress marker; when secreted acts as stress signal; indicates UPR activation and	0.63

		secretory pathway dysfunction in myoblasts	
Histones (H2B variants)	Core nucleosome proteins	Extracellular histones act as alarmins → trigger inflammation, immune signaling, and cell stress responses; may reflect cell damage/death or vesicular release	0.35
Histones (H4)	Core nucleosome protein	Same as above; linked to inflammatory signaling, cytotoxicity, and stress-induced secretion	0.30
Histones (H2A variants)	Core chromatin proteins	Extracellular roles include immune modulation and DAMP signaling, indicating nuclear stress or impaired degradation	0.27
Histones (H3 variants)	Core chromatin proteins	Released under stress; may influence inflammatory and regenerative signaling in muscle environment	0.27
Hspa9 (Mortalin / GRP75)	Mitochondrial chaperone	Indicates mitochondrial stress/damage; involved in mitochondrial protein folding and quality control, relevant to mitophagy defects	0.09
Hspd1 (HSP60)	Mitochondrial chaperonin	Mitochondrial stress marker; extracellularly promotes immune signaling and stress adaptation; linked to metabolic dysfunction in myoblasts	0.01

4.0 Discussion

Gfpt1 is the rate-limiting enzyme of the HBP, generating UDP-GlcNAc, the obligate donor substrate for multiple forms of protein glycosylation. Since the HBP sits at the interface of nutrient sensing, protein quality control and membrane trafficking, disruptions in Gfpt1 activity, as evident in *GFPT1*-CMS, are expected to impose broad metabolic and proteostatic consequences on muscle cells [4,5]. In this study, we demonstrate that loss of Gfpt1 leads to coordinated disturbances of glycosylation-dependent proteostasic mechanisms, spanning ER stress, vesicle trafficking, secretion and autophagy. This provides mechanistic insights into the skeletal muscle pathology observed in *GFPT1*-CMS patients.

GFPT1-CMS is characterized by fatigable muscle weakness caused by biallelic mutations that reduce GFPT1 protein abundance and enzymatic levels [10,14,18–21]. We previously showed that impaired Gfpt1 function disrupts protein glycosylation, leading to hypoglycosylation of AChRδ, a defect that can

be rescued by galactose supplementation [6,24]. This hypoglycosylated environment may also contribute to the formation of tubular aggregates, a shared feature of other glycosylation-related CMS subtypes (GMPPB, ALG2, ALG14, and DPAGT1), highlighting the need to define upstream drivers of pathology [11–13,33–36].

Consistent with this, we observed robust activation of IRE1-XBP1 arms of the UPR in both pharmacologic and genetic models of Gfpt1-deficiency [27,37]. Given the sensitivity of IRE1 signaling to defects in glycan maturation, these findings indicate that ER stress arises as a primary consequence of impaired HBP flux rather than secondary degeneration [38,39]. This finding is consistent with other myopathies driven by glycosylation defects such as GNE myopathy and congenital disorders of glycosylation (CDGs) where early pathological features depict UPR activation and ER stress [40–47].

A significant finding of this study is the global downregulation of vesicle trafficking pathways. Proteomic analysis revealed abundance of COP-I/COP-II components, ER-Golgi transport factors, and proteins involved in vesicle formation and cargo sorting. As these processes depend on proper glycosylation for protein stability, folding, and export, these data suggest a multi-level disruption of secretory pathway function [1,3,48]. This is functionally supported by impaired secretion of Srgn, a highly glycosylated proteoglycan requiring intact ER-Golgi processing for maturation and export. Its intracellular punctate accumulation alongside reduced secretion indicates a failure of secretory machinery and highlights a broader defect in extracellular matrix (ECM) protein handling [49].

These changes could have negative consequences for skeletal muscle health [3]. Secretory defects may affect skeletal muscle health because myofibers rely heavily on efficient export of ECM proteins, proteoglycans, and signaling factors to maintain structural stability and intercellular communication [50,51]. Importantly, Srgn knockout mice develop normally and do not display an overt skeletal muscle phenotype, suggesting that Srgn itself is not essential for muscle development under basal conditions [52]. Therefore, the reduction and intracellular accumulation of Srgn observed in our models likely reflect

impaired glycosylation-dependent trafficking rather than a primary pathogenic driver. In this context, Srgn may serve as a sensitive marker for secretory pathway dysfunction, highlighting broader defects in protein export that could ultimately compromise muscle homeostasis. A potential mechanism of impact could be through immunological responses, which has been shown in Srgn deficient mouse models [53]. Importantly, similar defects in proteoglycan secretion has been identified in other muscle disorders, and CDGs, all of which exhibit impaired extracellular matrix assembly, disrupted sarcolemmal stability and progressive myofiber degeneration [54–56]. As such, examination of additional proteoglycan synthesis, packaging and trafficking should be extensively studied within Gfpt1-deficient models.

It is important to note, that while Srgn was not detected within the secretomic profiling of conditioned medium from Gfpt1-deficient myoblasts, this likely reflects inherent limitation in mass spectroscopy-based detection of heavily glycosylated proteoglycans rather than true absence [57,58]. Consistent with this, immunoblot analysis confirmed reduced secretion, and intracellular accumulation of Srgn, supporting a defect in glycosylation-dependent trafficking. Together, these findings suggest that Srgn may represent a sensitive marker of impaired secretory pathway function in the context of Gfpt1 deficiency.

However, secretomic profiling of Gfpt1-deficient myoblasts did reveal a secreted-BiP deficiency. . BiP is a central regulator of ER proteostasis and secretory capacity as it supports folding of nascent luminal proteins, enforces ER quality control, and maintains export-competent cargo; thus, reduced BiP is expected to constrain secretion by promoting ER retention, ERAD and stress-induced translational attenuation [59,60]. This defect is exacerbated by impaired glycosylation in Gfpt1-deficient cells, as glycan medication is critical for protein stability, chaperone engagement, and trafficking [1,6,61]. Consistently, we observed reduced secretion of Srgn, a highly glycosylated proteoglycan that serves as a sensitive readout of ER quality control.

Although BiP is primarily ER-resident, it can also be secreted where it participates in stress signaling. BiP secretion has been reported to decrease under ER stress, including tunicamycin treatment, suggesting a role in adaptive intercellular communication [62–64]. The reduction observed here therefore indicates not only impaired folding capacity but also defective stress-responsive secretion. Given BiP's central role in regulating the UPR, reduced intracellular and secreted BiP may limit the ability to buffer ER stress, in Gfpt1-deficient myoblasts [59,62]. Moreover, extracellular BiP has been linked to cytoskeletal regulation and neurite outgrowth, raising the possibility that its loss affects stress resilience and cellular remodeling [65]. Together impaired glycosylation, reduced BiP and defective secretion of Srgn support a model in which ER proteostasis failure manifests as both intracellular folding insufficiency and loss of adaptive secretory signaling.

In parallel, Gfpt1-depleted myoblasts show increased release of cytosolic proteins consistent with stress-induced unconventional secretion during proteotoxic states [66,67]. This shift from classical ER-Golgi trafficking to noncanonical export may reflect membrane instability, impaired vesicle maturation or increased extracellular vesicle release [68,69]. Similar secretory remodeling has been observed in myopathies associated with ER stress or impaired autophagy reinforcing the idea that proteostasis disruption fundamentally reshapes the muscle secretome [70,71].

Given that the NMJ is highly dependent on efficient secretion, defects in intracellular trafficking provide a direct mechanistic link to CMS pathology. NMJ maintenance requires continuous export of synaptic organizers including agrin, laminin α2/β2, perlecan, and collagens, as well as trafficking of AChR complexes and associated signaling factors [72–74]. These processes rely on an intact ER-Golgi transport and glycosylation-dependent cargo maturation. Consistent with this, reduced AChR surface has been detected *in vitro*, along with decreased α-BTX staining at the NMJs in *Gfpt1*$^{tm1d/tm1d}$ muscle. Previously, AChR subunits were found to have reduced surface expression in transfected HEK293T cells [14]. In addition, previous data shows reduced α-BTX staining at the NMJ of *Gfpt1*$^{tm1d/tm1d}$ suggesting

impairment to the surface expression and/or stability of the AChR complex [6,24]. Thus, trafficking defects observed in our models, including Srgn retention, likely impairs delivery of essential synaptic proteins and chaperones such as BiP. In this context, impaired secretion may represent a central pathogenic mechanism, weakening synaptic integrity and increasing NMJ susceptibility to stress [7,75–77].

We also demonstrate defects in autophagic clearance, likely downstream of ER stress and trafficking disruption. Autophagy requires coordinated membrane trafficking, ER-Golgi dynamics, and lipidation, processes dependent on intact glycosylation pathways [28,30]. In Gfpt1-deficient myoblasts, elevated p62 and LC3-II levels indicated impaired autophagic flux rather than increased initiation, a finding recapitulated in *Gfpt1*$^{tm1d/tm1d}$ muscle [78–80]. This aligns with prior reports showing enhanced protein aggregation and reduced autophagy following Gfpt1 silencing attenuated [81]. Thus, protein aggregation and impaired autophagy may contribute to muscle fiber pathology in *GFPT1*-CMS.

In addition, future studies should aim to further define the mechanistic links between impaired HBP flux and defects in protein trafficking, secretion and autophagy. Previous work demonstrated metabolic supplementation with galactose has been shown to improve skeletal muscle health, NMJ morphology, and neurotransmission in *Gfpt1*$^{tm1d/tm1d}$ models, making it of particular interest to determine whether the proteostasis and secretory defects observed in this study could be rescued through similar approaches [24]. In addition, building on the identification of hypoglycosylated AChRδ, further investigation of NMJ integrity in the context of disrupted trafficking may help clarify the contribution of these pathways to disease pathology. Finally, targeted analysis of extracellular matrix components and secreted proteoglycans may help establish whether molecules such as Srgn could serve as a biomarker or therapeutic targets in *GFPT1*-CMS.

5.0 Conclusion

In summary, this study demonstrates that Gfpt1 deficiency disrupts glycosylation-dependent proteostasis in skeletal muscle, leading to broad alterations in ER homeostasis, intracellular trafficking, secretion and autophagic flux. Reduced HBP flux triggers activation of IRE1-XBP1 branch of the UPR, while impairing vesicular transport and secretory capacity. These defects result in intracellular retention and reduced secretion of key glycoproteins including proteoglycan Srgn, highlighting disruption of protein secretion. Importantly, these interconnected defects provide a unifying mechanistic framework linking impaired glycosylation to NMJ dysfunction, reduced stress resilience, and skeletal muscle pathology in *GFPT1*-CMS. Overall, this work identifies glycosylation-dependent proteostasis as a central determinant of muscle integrity and highlights intracellular trafficking and secretory dysfunction as key contributors to disease pathogenesis.

Author Contributions

Conceptualization, H.L., S.S., A.R and S.H.H.; methodology, S.H.H., R.C.-M., K.O., K. H., and D.O., S.B; validation, S.H.H., R.C.-M., K.O. and D.O.; formal analysis, S.H.H., S.S. and K.O.; investigation, S.H.H., R.C.-M. and K.O.; resources, H.L. and S.S.; data curation, S.H.H., R.C.-M., K.O. ; writing—original draft preparation, S.H.H.; review and editing, S.H.H., R.C.-M., K.O., D.O., S.S., Y. A., A.R. and H.L.; final draft preparation and writing, S.H.H., S.S., and H.L.; visualization, S.H.H., S.S, and H.L.; supervision, S.S. and H.L.; project administration, S.S. and H.L.; funding acquisition, H.L. and S.H.H. All authors have read and agreed to the published version of the manuscript.

Funding

H.L. received support from the Canadian Institutes of Health Research (CIHR) for Foundation Grant FDN-167281 (Precision Health for Neuromuscular Diseases), Transnational Team Grant ERT-174211 (ProDGNE), and Network Grant OR2-189333 (NMD4C) from the Canada Foundation for Innovation (CFI-JELF 38412); the Canada Research Chairs program (Canada Research Chair in Neuromuscular

Genomics and Health, 950-232279); the European Commission (Grant # 101080249); and the Canada Research Coordinating Committee New Frontiers in Research Fund (NFRFG-2022-00033) for SIMPATHIC and from the Government of Canada, Canada First Research Excellence Fund (CFREF) for the Brain-Heart Interconnectome (CFREF-2022-00007). S.H.H. received support from the Bob Korneluk CHEO Trainee Research Grant, Ontario Graduate Scholarship (OGS), Queen Elizabeth II Scholarship (QE2-GSST), and a STaR award by the University of Ottawa Dr. Eric Poulin Center for Neuromuscular Disease. A.R. acknowledges the financial support of the Deutsche Gesellschaft für Muskelkranke (DGM) e.V. as well as by the European Regional Development Fund (ERDF) (project B2B-RARE). AH acknowledges the support by the "Ministerium für Kultur und Wissenschaft des Landes Nordrhein-Westfalen" and "Der Regierende Bürgermeister von Berlin, Senatskanzlei Wissenschaft und Forschung" and the Bundesministerium für Forschung, Technologie und Raumfahrt (BMFTR).

Animal Ethics Statement

The animal study protocol was approved by the Animal Care and Veterinary Board of the University of Ottawa (CHEOb-3089 and CHEOe-3120, approved on 16 November 2018 and 2 April 2019, respectively).

Data Availability Statement

Data are contained within the article and Supplementary Materials. The mass spectrometry proteomics data have been deposited to the ProteomeXchange Consortium via the PRIDE partner repository with the dataset identifier PXD079191.

Conflict of Interest Statement

The authors declare no conflict of interest.

Acknowledgements

References

1. Reily, C.; Stewart, T.J.; Renfrow, M.B.; Novak, J. Glycosylation in Health and Disease. *Nat. Rev. Nephrol.* **2019**, *15*, 346–366, doi:10.1038/s41581-019-0129-4.
2. He, M.; Zhou, X.; Wang, X. Glycosylation: Mechanisms, Biological Functions and Clinical Implications. *Signal Transduct. Target. Ther.* **2024**, *9*, 194, doi:10.1038/s41392-024-01886-1.
3. Dang, K.; Jiang, S.; Gao, Y.; Qian, A. The Role of Protein Glycosylation in Muscle Diseases. *Mol. Biol. Rep.* **2022**, *49*, 8037–8049, doi:10.1007/s11033-022-07334-z.
4. Akella, N.M.; Ciraku, L.; Reginato, M.J. Fueling the Fire: Emerging Role of the Hexosamine Biosynthetic Pathway in Cancer. *BMC Biol.* **2019**, *17*, 52, doi:10.1186/s12915-019-0671-3.
5. Paneque, A.; Fortus, H.; Zheng, J.; Werlen, G.; Jacinto, E. The Hexosamine Biosynthesis Pathway: Regulation and Function. *Genes* **2023**, *14*, 933, doi:10.3390/genes14040933.
6. Holland, S.H.; Carmona-Martinez, R.; O'Connor, K.; O'Neil, D.; Roos, A.; Spendiff, S.; Lochmüller, H. A Deficiency in Glutamine-Fructose-6-Phosphate Transaminase 1 (Gfpt1) in Skeletal Muscle Results in Reduced Glycosylation of the Delta Subunit of the Nicotinic Acetylcholine Receptor (AChRδ). *Biomolecules* **2024**, *14*, 1252, doi:10.3390/biom14101252.
7. Finsterer, J. Congenital Myasthenic Syndromes. *Orphanet J. Rare Dis.* **2019**, *14*, 57, doi:10.1186/s13023-019-1025-5.
8. Review of 40 Genes Causing Congenital Myasthenic Syndromes | Journal of Human Genetics Available online: https://www.nature.com/articles/s10038-025-01355-9 (accessed on 7 January 2026).
9. Beeson, D. Chapter 5 - Congenital Myasthenic Syndromes. In *Handbook of Clinical Neurology*; Hanna, M.G., Ed.; Neurologic Channelopathies; Elsevier, 2024; Vol. 203, pp. 69–88.

10. Senderek, J.; Müller, J.S.; Dusl, M.; Strom, T.M.; Guergueltcheva, V.; Diepolder, I.; Laval, S.H.; Maxwell, S.; Cossins, J.; Krause, S.; et al. Hexosamine Biosynthetic Pathway Mutations Cause Neuromuscular Transmission Defect. *Am. J. Hum. Genet.* **2011**, *88*, 162–172, doi:10.1016/j.ajhg.2011.01.008.
11. Cossins, J.; Belaya, K.; Hicks, D.; Salih, M.A.; Finlayson, S.; Carboni, N.; Liu, W.W.; Maxwell, S.; Zoltowska, K.; Farsani, G.T.; et al. Congenital Myasthenic Syndromes Due to Mutations in ALG2 and ALG14. *Brain* **2013**, *136*, 944–956, doi:10.1093/brain/awt010.
12. Belaya, K.; Finlayson, S.; Slater, C.R.; Cossins, J.; Liu, W.W.; Maxwell, S.; McGowan, S.J.; Maslau, S.; Twigg, S.R.F.; Walls, T.J.; et al. Mutations in DPAGT1 Cause a Limb-Girdle Congenital Myasthenic Syndrome with Tubular Aggregates. *Am. J. Hum. Genet.* **2012**, *91*, 193–201, doi:10.1016/j.ajhg.2012.05.022.
13. Belaya, K.; Rodríguez Cruz, P.M.; Liu, W.W.; Maxwell, S.; McGowan, S.; Farrugia, M.E.; Petty, R.; Walls, T.J.; Sedghi, M.; Basiri, K.; et al. Mutations in GMPPB Cause Congenital Myasthenic Syndrome and Bridge Myasthenic Disorders with Dystroglycanopathies. *Brain* **2015**, *138*, 2493–2504, doi:10.1093/brain/awv185.
14. Zoltowska, K.; Webster, R.; Finlayson, S.; Maxwell, S.; Cossins, J.; Müller, J.; Lochmüller, H.; Beeson, D. Mutations in GFPT1 That Underlie Limb-Girdle Congenital Myasthenic Syndrome Result in Reduced Cell-Surface Expression of Muscle AChR. *Hum. Mol. Genet.* **2013**, *22*, 2905–2913, doi:10.1093/hmg/ddt145.
15. Jiang, K.; Zheng, Y.; Lin, J.; Wu, X.; Yu, Y.; Zhu, M.; Fang, X.; Zhou, M.; Li, X.; Hong, D. Diverse Myopathological Features in the Congenital Myasthenia Syndrome with GFPT1 Mutation. *Brain Behav.* **2022**, *12*, e2469, doi:10.1002/brb3.2469.

16. Vallepu, S.B.; Dhamija, K.; Rajan, G.K.; Panchal, T.; Saran, R.K.; Roshan, S. Phenotypic Variability in Congenital Myasthenic Syndrome with GFPT1 Mutation. *Acta Neurol. Belg.* **2024**, doi:10.1007/s13760-024-02694-8.
17. An, R.; Chen, H.; Lei, S.; Li, Y.; Xu, Y.; He, C. Abnormal Decrement on High-Frequency Repetitive Nerve Stimulation in Congenital Myasthenic Syndrome with GFPT1 Mutations and Review of Literature. *Front. Neurol.* **2022**, *13*, 926786, doi:10.3389/fneur.2022.926786.
18. Bauché, S.; Vellieux, G.; Sternberg, D.; Fontenille, M.-J.; De Bruyckere, E.; Davoine, C.-S.; Brochier, G.; Messéant, J.; Wolf, L.; Fardeau, M.; et al. Mutations in GFPT1-Related Congenital Myasthenic Syndromes Are Associated with Synaptic Morphological Defects and Underlie a Tubular Aggregate Myopathy with Synaptopathy. *J. Neurol.* **2017**, *264*, 1791–1803, doi:10.1007/s00415-017-8569-x.
19. Dusl, M.; Senderek, J.; Müller, J.S.; Vogel, J.G.; Pertl, A.; Stucka, R.; Lochmüller, H.; David, R.; Abicht, A. A 3'-UTR Mutation Creates a microRNA Target Site in the GFPT1 Gene of Patients with Congenital Myasthenic Syndrome. *Hum. Mol. Genet.* **2015**, *24*, 3418–3426, doi:10.1093/hmg/ddv090.
20. Ma, Y.; Xiong, T.; Lei, G.; Ding, J.; Yang, R.; Li, Z.; Guo, J.; Shen, D. Novel Compound Heterozygous Variants in the GFPT1 Gene Leading to Rare Limb-Girdle Congenital Myasthenic Syndrome with Rimmed Vacuoles. *Neurol. Sci. Off. J. Ital. Neurol. Soc. Ital. Soc. Clin. Neurophysiol.* **2021**, *42*, 3485–3490, doi:10.1007/s10072-020-05021-0.
21. Selcen, D.; Shen, X.-M.; Milone, M.; Brengman, J.; Ohno, K.; Deymeer, F.; Finkel, R.; Rowin, J.; Engel, A.G. GFPT1-Myasthenia: Clinical, Structural, and Electrophysiologic Heterogeneity. *Neurology* **2013**, *81*, 370–378, doi:10.1212/WNL.0b013e31829c5e9c.

22. Vallepu, S.B.; Dhamija, K.; Rajan, G.K.; Panchal, T.; Saran, R.K.; Roshan, S. Phenotypic Variability in Congenital Myasthenic Syndrome with GFPT1 Mutation. *Acta Neurol. Belg.* **2025**, *125*, 209–213, doi:10.1007/s13760-024-02694-8.
23. Issop, Y.; Hathazi, D.; Khan, M.M.; Rudolf, R.; Weis, J.; Spendiff, S.; Slater, C.R.; Roos, A.; Lochmüller, H. GFPT1 Deficiency in Muscle Leads to Myasthenia and Myopathy in Mice. *Hum. Mol. Genet.* **2018**, *27*, 3218–3232, doi:10.1093/hmg/ddy225.
24. Holland, S.H.; Carmona-Martinez, R.; O'Neil, D.; Ho, K.; O'Connor, K.; Azuma, Y.; Roos, A.; Spendiff, S.; Lochmüller, H. Galactose Treatment Rescues Neuromuscular Junction Transmission in Glutamine-Fructose-6-Phosphate Transaminase 1 (Gfpt1) Deficient Mice. *Hum. Mol. Genet.* **2025**, ddaf140, doi:10.1093/hmg/ddaf140.
25. Bisnett, B.J.; Condon, B.M.; Lamb, C.H.; Georgiou, G.R.; Boyce, M. Export Control: Post-Transcriptional Regulation of the COPII Trafficking Pathway. *Front. Cell Dev. Biol.* **2021**, *8*, doi:10.3389/fcell.2020.618652.
26. Zhang, J.; Wang, Y. Emerging Roles of O-GlcNAcylation in Protein Trafficking and Secretion. *J. Biol. Chem.* **2024**, *300*, 105677, doi:10.1016/j.jbc.2024.105677.
27. Hetz, C.; Zhang, K.; Kaufman, R.J. Mechanisms, Regulation and Functions of the Unfolded Protein Response. *Nat. Rev. Mol. Cell Biol.* **2020**, *21*, 421–438, doi:10.1038/s41580-020-0250-z.
28. Diao, J.; Yip, C.K.; Zhong, Q. Molecular Structures and Function of the Autophagosome-Lysosome Fusion Machinery. *Autophagy Rep.* **2024**, *3*, 2305594, doi:10.1080/27694127.2024.2305594.
29. Franco-Romero, A.; Sandri, M.; Schiaffino, S. Autophagy in Skeletal Muscle. *Cold Spring Harb. Perspect. Biol.* **2025**, *17*, a041565, doi:10.1101/cshperspect.a041565.
30. Franco-Romero, A.; Sandri, M. Role of Autophagy in Muscle Disease. *Mol. Aspects Med.* **2021**, *82*, 101041, doi:10.1016/j.mam.2021.101041.

31. Bjørkøy, G.; Lamark, T.; Pankiv, S.; Øvervatn, A.; Brech, A.; Johansen, T. Monitoring Autophagic Degradation of P62/SQSTM1. *Methods Enzymol.* **2009**, *452*, 181–197, doi:10.1016/S0076-6879(08)03612-4.
32. Hirano, H.; Kimura, Y.; Kimura, A. Biological Significance of Co- and Post-Translational Modifications of the Yeast 26S Proteasome. *J. Proteomics* **2016**, *134*, 37–46, doi:10.1016/j.jprot.2015.11.016.
33. Dean, N.; Gao, X.-D. Heterodimeric Alg13/Alg14 UDP-GlcNAc Transferase (ALG13,14). In *Handbook of Glycosyltransferases and Related Genes*; Springer, Tokyo, 2014; pp. 1231–1238 ISBN 978-4-431-54240-7.
34. Dean, N. Alg1, Alg2, and Alg11 Mannosyltransferases of the Endoplasmic Reticulum. In *Handbook of Glycosyltransferases and Related Genes*; Springer, Tokyo, 2014; pp. 1239–1247 ISBN 978-4-431-54240-7.
35. Belaya, K.; Finlayson, S.; Cossins, J.; Liu, W.W.; Maxwell, S.; Palace, J.; Beeson, D. Identification of DPAGT1 as a New Gene in Which Mutations Cause a Congenital Myasthenic Syndrome. *Ann. N. Y. Acad. Sci.* **2012**, *1275*, 29–35, doi:10.1111/j.1749-6632.2012.06790.x.
36. Cheli, M.; Brugnoni, R.; Gibertini, S.; Mantegazza, R.; Maggi, L. Novel DPAGT1 Gene Mutation in Two Twins with Congenital Myasthenic Syndrome and a Review of the Literature. *J. Neuromuscul. Dis.* **2023**, *10*, 449–458, doi:10.3233/JND-221675.
37. Wang, Z.V.; Deng, Y.; Gao, N.; Pedrozo, Z.; Li, D.L.; Morales, C.R.; Criollo, A.; Luo, X.; Tan, W.; Jiang, N.; et al. Spliced X-Box Binding Protein 1 Couples the Unfolded Protein Response to Hexosamine Biosynthetic Pathway. *Cell* **2014**, *156*, 1179–1192, doi:10.1016/j.cell.2014.01.014.
38. Siwecka, N.; Rozpędek-Kamińska, W.; Wawrzynkiewicz, A.; Pytel, D.; Diehl, J.A.; Majsterek, I. The Structure, Activation and Signaling of IRE1 and Its Role in Determining Cell Fate. *Biomedicines* **2021**, *9*, 156, doi:10.3390/biomedicines9020156.

39. Exploring the IRE1 Interactome: From Canonical Signaling Functions to Unexpected Roles - Journal of Biological Chemistry Available online: https://www.jbc.org/article/S0021-9258(24)01664-8/fulltext (accessed on 22 March 2026).
40. Awasthi, K.; Srivastava, A.; Bhattacharya, S.; Bhattacharya, A. Tissue Specific Expression of Sialic Acid Metabolic Pathway: Role in GNE Myopathy. *J. Muscle Res. Cell Motil.* **2021**, *42*, 99–116, doi:10.1007/s10974-020-09590-7.
41. Carrillo, N.; Malicdan, M.C.; Huizing, M. GNE Myopathy: Etiology, Diagnosis, and Therapeutic Challenges. *Neurotherapeutics* **2018**, *15*, 900–914, doi:10.1007/s13311-018-0671-y.
42. Hinderlich, S.; Weidemann, W.; Yardeni, T.; Horstkorte, R.; Huizing, M. UDP-GlcNAc 2-Epimerase/ManNAc Kinase (GNE): A Master Regulator of Sialic Acid Synthesis. *Top Chem Curr* **2015**, *366*, 97–138, doi:10.1007/128_2013_464.
43. Pogoryelova, O.; González Coraspe, J.A.; Nikolenko, N.; Lochmüller, H.; Roos, A. GNE Myopathy: From Clinics and Genetics to Pathology and Research Strategies. *Orphanet J. Rare Dis.* **2018**, *13*, 70, doi:10.1186/s13023-018-0802-x.
44. Clinical, Pathological and Genetic Characteristics of GNE Myopathy: A Single-Center Observational Study | BMC Musculoskeletal Disorders | Springer Nature Link Available online: https://link.springer.com/article/10.1186/s12891-025-09282-8 (accessed on 22 March 2026).
45. Molecular Genetics and Therapeutic Development for GNE Myopathy | Journal of Human Genetics Available online: https://www.nature.com/articles/s10038-025-01398-y (accessed on 22 March 2026).
46. GNE Myopathy: Current Update and Future Therapy | Journal of Neurology, Neurosurgery & Psychiatry Available online: https://jnnp.bmj.com/content/86/4/385 (accessed on 16 February 2026).

47. Cannata Serio, M.; Graham, L.A.; Ashikov, A.; Larsen, L.E.; Raymond, K.; Timal, S.; Le Meur, G.; Ryan, M.; Czarnowska, E.; Jansen, J.C.; et al. Mutations in the V-ATPase Assembly Factor VMA21 Cause a Congenital Disorder of Glycosylation With Autophagic Liver Disease. *Hepatology* **2020**, *72*, 1968–1986, doi:10.1002/hep.31218.
48. Hao, C.; Zou, Q.; Bai, X.; Shi, W. Effect of Glycosylation on Protein Folding: From Biological Roles to Chemical Protein Synthesis. *iScience* **2025**, *28*, 112605, doi:10.1016/j.isci.2025.112605.
49. Athanasopoulos, E.N.; Labropoulou, V.T.; Theocharis, A.D. Serglycin Across the Disease Spectrum: A Multifunctional Proteoglycan in Inflammation and Cancer. *Curr. Issues Mol. Biol.* **2026**, *48*, 454, doi:10.3390/cimb48050454.
50. Florin, A.; Lambert, C.; Sanchez, C.; Zappia, J.; Durieux, N.; Tieppo, A.M.; Mobasheri, A.; Henrotin, Y. The Secretome of Skeletal Muscle Cells: A Systematic Review. *Osteoarthr. Cartil. Open* **2020**, *2*, 100019, doi:10.1016/j.ocarto.2019.100019.
51. Denervation Alters the Secretome of Myofibers and Thereby Affects Muscle Stem Cell Lineage Progression and Functionality | Npj Regenerative Medicine Available online: https://www.nature.com/articles/s41536-024-00353-3 (accessed on 22 March 2026).
52. Abrink, M.; Grujic, M.; Pejler, G. Serglycin Is Essential for Maturation of Mast Cell Secretory Granule. *J. Biol. Chem.* **2004**, *279*, 40897–40905, doi:10.1074/jbc.M405856200.
53. Meen, A.J.; Drevon, C.A.; Pejler, G.; Jenssen, T.G.; Olstad, O.K.; Åbrink, M.; Kolset, S.O. Serglycin Protects against High Fat Diet-Induced Increase in Serum LDL in Mice. *Glycoconj. J.* **2015**, *32*, 703–714, doi:10.1007/s10719-015-9621-7.
54. Brockington, M.; Yuva, Y.; Prandini, P.; Brown, S.C.; Torelli, S.; Benson, M.A.; Herrmann, R.; Anderson, L.V.B.; Bashir, R.; Burgunder, J.-M.; et al. Mutations in the Fukutin-Related Protein Gene (FKRP) Identify Limb Girdle Muscular Dystrophy 2I as a Milder Allelic Variant of

Congenital Muscular Dystrophy MDC1C. *Hum. Mol. Genet.* **2001**, *10*, 2851–2859, doi:10.1093/hmg/10.25.2851.

55. Okazaki, T.; Matsuura, K.; Kasagi, N.; Adachi, K.; Kai, M.; Okubo, M.; Nishino, I.; Nanba, E.; Maegaki, Y. Duchenne Muscular Dystrophy–like Phenotype in an LGMD2I Patient with Novel FKRP Gene Variants. *Hum. Genome Var.* **2020**, *7*, 1–4, doi:10.1038/s41439-020-0099-x.
56. Carmen, L.; Maria, V.; Morales-Medina, J.C.; Vallelunga, A.; Palmieri, B.; Iannitti, T. Role of Proteoglycans and Glycosaminoglycans in Duchenne Muscular Dystrophy. *Glycobiology* **2019**, *29*, 110–123, doi:10.1093/glycob/cwy058.
57. Noborn, F.; Nilsson, J.; Larson, G. Site-Specific Glycosylation of Proteoglycans: A Revisited Frontier in Proteoglycan Research. *Matrix Biol. J. Int. Soc. Matrix Biol.* **2022**, *111*, 289–306, doi:10.1016/j.matbio.2022.07.002.
58. Iozzo, R.V.; Schaefer, L. Proteoglycan Form and Function: A Comprehensive Nomenclature of Proteoglycans. *Matrix Biol.* **2015**, *42*, 11–55, doi:10.1016/j.matbio.2015.02.003.
59. Pobre, K.F.R.; Poet, G.J.; Hendershot, L.M. The Endoplasmic Reticulum (ER) Chaperone BiP Is a Master Regulator of ER Functions: Getting by with a Little Help from ERdj Friends. *J. Biol. Chem.* **2019**, *294*, 2098–2108, doi:10.1074/jbc.REV118.002804.
60. Adams, B.M.; Canniff, N.P.; Guay, K.P.; Hebert, D.N. The Role of ER Chaperones in Protein Folding and Quality Control. *Prog. Mol. Subcell. Biol.* **2021**, *59*, 27–50, doi:10.1007/978-3-030-67696-4_3.
61. Ma, M.; Dubey, R.; Jen, A.; Pusapati, G.V.; Singal, B.; Shishkova, E.; Overmyer, K.A.; Cormier-Daire, V.; Fedry, J.; Aravind, L.; et al. Regulated N-Glycosylation Controls Chaperone Function and Receptor Trafficking. *Science* **2024**, *386*, 667–672, doi:10.1126/science.adp7201.
62. Li, M.; Duan, M.; Yang, Y.; Li, X.; Li, D.; Gao, W.; Ji, X.; Bai, J. Combination of Brefeldin A and Tunicamycin Induces Apoptosis in HepG2 Cells through the Endoplasmic Reticulum Stress-

Activated PERK-eIF2α-ATF4-CHOP Signaling Pathway. *Liver Res.* **2025**, *9*, 49–56, doi:10.1016/j.livres.2025.01.004.

63. The Structural and Functional Dynamics of BiP and Grp94: Opportunities for Therapeutic Discovery: Trends in Pharmacological Sciences Available online: https://www.cell.com/trends/pharmacological-sciences/abstract/S0165-6147(25)00044-6 (accessed on 10 April 2026).
64. BIP Orchestrates Bidirectional ER Protein Trafficking via Co-Chaperone Complexes | Cellular & Molecular Biology Letters | Springer Nature Link Available online: https://link.springer.com/article/10.1186/s11658-026-00875-2 (accessed on 10 April 2026).
65. Favero, C.B.; Henshaw, R.N.; Grimsley-Myers, C.M.; Shrestha, A.; Beier, D.R.; Dwyer, N.D. Mutation of the BiP/GRP78 Gene Causes Axon Outgrowth and Fasciculation Defects in the Thalamocortical Connections of the Mammalian Forebrain. *J. Comp. Neurol.* **2013**, *521*, 677–696, doi:10.1002/cne.23199.
66. Sheetz, J.B.; Chandrasekhar, S.; Rapé, M. Function and Regulation of the Mitochondrial Stress Response. *Nat. Struct. Mol. Biol.* **2026**, *33*, 382–393, doi:10.1038/s41594-026-01769-9.
67. Suh, J.; Lee, Y.-S. Mitochondria as Secretory Organelles and Therapeutic Cargos. *Exp. Mol. Med.* **2024**, *56*, 66–85, doi:10.1038/s12276-023-01141-7.
68. Disease-Associated Factors at the Endoplasmic Reticulum–Golgi Interface - Maeda - 2025 - Traffic - Wiley Online Library Available online: https://onlinelibrary.wiley.com/doi/full/10.1111/tra.70001?msockid=2a3f1685a95b6044003e0652a8f1612e (accessed on 23 March 2026).
69. McCaughey, J.; Stephens, D.J. ER-to-Golgi Transport: A Sizeable Problem. *Trends Cell Biol.* **2019**, *29*, 940–953, doi:10.1016/j.tcb.2019.08.007.

70. Iannibelli, E.; Gibertini, S.; Cheli, M.; Blasevich, F.; Cavaliere, A.; Riolo, G.; Ruggieri, A.; Maggi, L. VCP-Related Myopathy: A Case Series and a Review of Literature. *Acta Myol.* **2023**, *42*, 2–13, doi:10.36185/2532-1900-244.

71. Chen, X.; Shi, C.; He, M.; Xiong, S.; Xia, X. Endoplasmic Reticulum Stress: Molecular Mechanism and Therapeutic Targets. *Signal Transduct. Target. Ther.* **2023**, *8*, 352, doi:10.1038/s41392-023-01570-w.

72. Molecular Mechanisms Underlying Assembly and Maintenance of the Neuromuscular Junction | Frontiers Research Topic Available online: https://www.frontiersin.org/research-topics/9335/molecular-mechanisms-underlying-assembly-and-maintenance-of-the-neuromuscular-junction/magazine (accessed on 24 March 2026).

73. Samuel, M.A.; Valdez, G.; Tapia, J.C.; Lichtman, J.W.; Sanes, J.R. Agrin and Synaptic Laminin Are Required to Maintain Adult Neuromuscular Junctions. *PLoS ONE* **2012**, *7*, e46663, doi:10.1371/journal.pone.0046663.

74. Ham, A.S.; Lin, S.; Tse, A.; Thürkauf, M.; McGowan, T.J.; Jörin, L.; Oliveri, F.; Rüegg, M.A. Single-Nuclei Sequencing of Skeletal Muscle Reveals Subsynaptic-Specific Transcripts Involved in Neuromuscular Junction Maintenance. *Nat. Commun.* **2025**, *16*, 2220, doi:10.1038/s41467-025-57487-1.

75. Ohno, K.; Ohkawara, B.; Shen, X.-M.; Selcen, D.; Engel, A.G. Clinical and Pathologic Features of Congenital Myasthenic Syndromes Caused by 35 Genes—A Comprehensive Review. *Int. J. Mol. Sci.* **2023**, *24*, 3730, doi:10.3390/ijms24043730.

76. O'Connor, E.; Phan, V.; Cordts, I.; Cairns, G.; Hettwer, S.; Cox, D.; Lochmüller, H.; Roos, A. MYO9A Deficiency in Motor Neurons Is Associated with Reduced Neuromuscular Agrin Secretion. *Hum. Mol. Genet.* **2018**, *27*, 1434–1446, doi:10.1093/hmg/ddy054.

77. Xie, T.; Xu, G.; Liu, Y.; Quade, B.; Lin, W.; Bai, X. Structural Insights into the Assembly of the Agrin/LRP4/MuSK Signaling Complex. *Proc. Natl. Acad. Sci.* **2023**, *120*, e2300453120, doi:10.1073/pnas.2300453120.

78. Fahie, K.; Zachara, N.E. Molecular Functions of Glycoconjugates in Autophagy. *J. Mol. Biol.* **2016**, *428*, 3305–3324, doi:10.1016/j.jmb.2016.06.011.

79. Franco-Juárez, B.; Coronel-Cruz, C.; Hernández-Ochoa, B.; Gómez-Manzo, S.; Cárdenas-Rodríguez, N.; Arreguin-Espinosa, R.; Bandala, C.; Canseco-Ávila, L.M.; Ortega-Cuellar, D. TFEB; Beyond Its Role as an Autophagy and Lysosomes Regulator. *Cells* **2022**, *11*, 3153, doi:10.3390/cells11193153.

80. Gómez-Virgilio, L.; Silva-Lucero, M.-C.; Flores-Morelos, D.-S.; Gallardo-Nieto, J.; Lopez-Toledo, G.; Abarca-Fernandez, A.-M.; Zacapala-Gómez, A.-E.; Luna-Muñoz, J.; Montiel-Sosa, F.; Soto-Rojas, L.O.; et al. Autophagy: A Key Regulator of Homeostasis and Disease: An Overview of Molecular Mechanisms and Modulators. *Cells* **2022**, *11*, 2262, doi:10.3390/cells11152262.

81. Zhang, R.; Farshadyeganeh, P.; Ohkawara, B.; Nakajima, K.; Takeda, J.-I.; Ito, M.; Zhang, S.; Miyasaka, Y.; Ohno, T.; Mori-Yoshimura, M.; et al. Muscle-Specific Lack of GFPT1 in Knock-in Mice Triggers ER Stress to Alleviate Misfolded Proteins. *Dis. Model. Mech.* **2024**, dmm.050768, doi:10.1242/dmm.050768.

Hexosamine Pathway Disruption by GFPT1 Loss Drives Coordinated Defects in Glycosylation, Autophagy, and Trafficking

Stephen H. Holland [1,2,3], Ricardo Carmona-Martinez [1], Andreas Hentschel [4], Alexa Derksen [1,2], Kaela O'Connor [1,2], Daniel O'Neil [1], Kelly Ho [1,2], Stephen D. Baird [1], Andreas Roos [1,5,6], Sally Spendiff [1] and Hanns Lochmüller [1,2,3,7,8,9]*

[1] Children's Hospital of Eastern Ontario Research Institute, Ottawa, ON, Canada. K1H8L1

[2] Department of Cellular and Molecular Medicine, Faculty of Medicine, University of Ottawa, Ottawa, ON, Canada, K1H 8M5.

[3] Dr. Eric Poulin Center for Neuromuscular Disorders, Brain and Mind Research Institute, University of Ottawa, Ottawa, ON, Canada, K1H 8M5.

[4] Leibniz-Institute for Analytical Sciences – ISAS- e.V, Dortmund, Germany, 44139.

[5] Department of Pediatric Neurology, Centre for Neuromuscular Disorders in Children, University Duisburg-Essen, Hufelandstrasse 55, 45122 Essen, Germany

[6] Department of Neurology with Heimer Institute for Muscle Research, University Hospital Bergmannsheil, Bochum, Germany, 44789.

[7] Division of Neurology, Department of Medicine, The Ottawa Hospital, Ottawa, ON, Canada, K1H8L6.

[8] Department of Neuropediatric and Muscle Disorders, Medical Center, University of Freiburg, Faculty of Medicine, Freiburg, Germany, 79106.

[9] Centro Nacional de Analisis Genomico (CNAG-CRG), Center for Genomic Regulation, Barcelona Institute of Science and Technology (BIST), Barcelona, Spain, 08028.

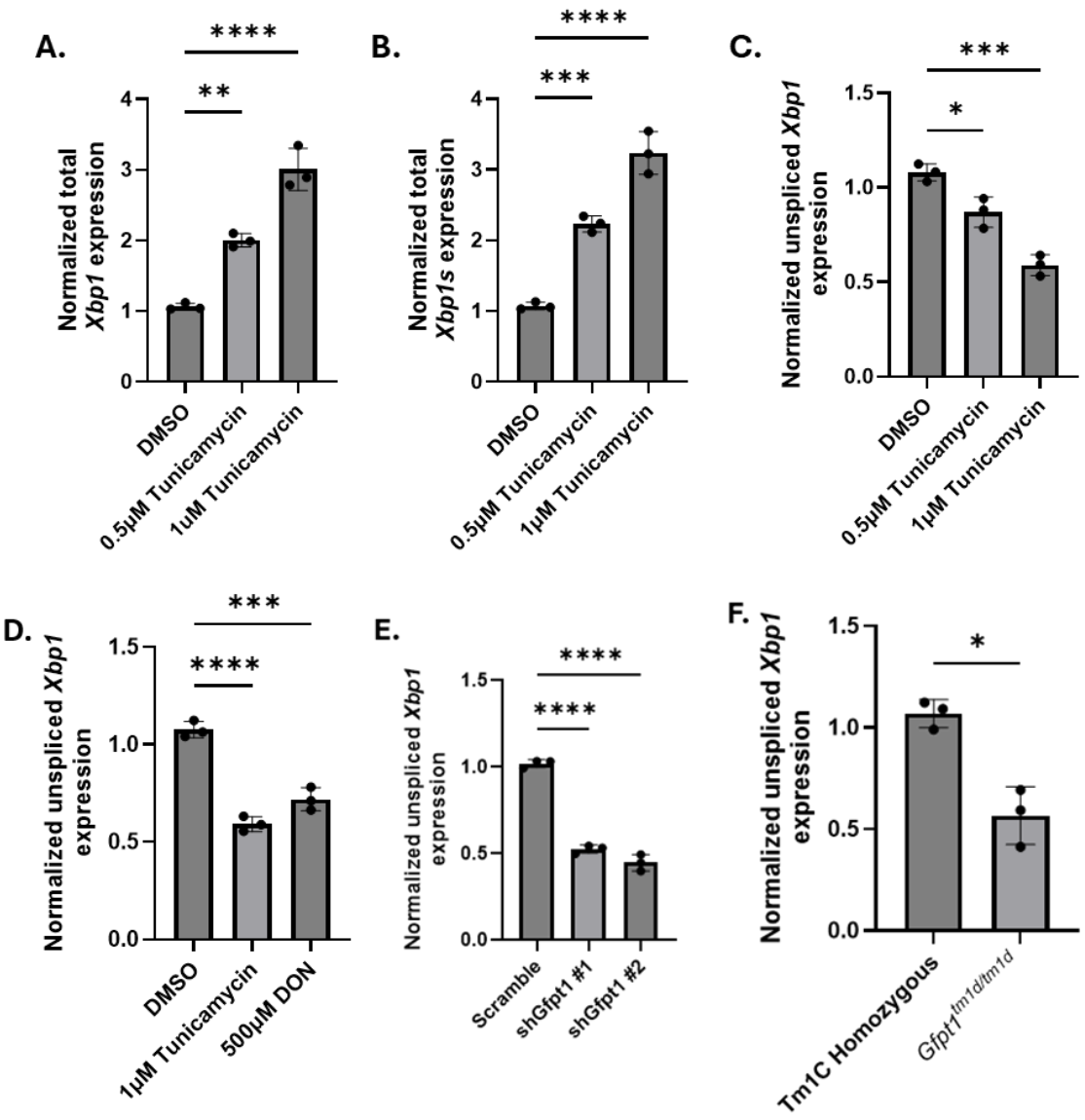

Supplementary Figure 1: Supplementary experiments for *Xbp1* expression determination: A. Dose–response analysis of tunicamycin, an N-linked glycosylation inhibitor that induces glycosylation stress. RT-qPCR revealed a dose-dependent increase in total Xbp1 expression**. B.** Increasing doses of tunicamycin led to elevated expression of spliced *Xbp1s*, and **C.** a corresponding decrease in unspliced *Xbp1u***. D.** Treatment with tunicamycin or DON significantly reduced unspliced *Xbp1u* expression compared to untreated controls. **E.** Gfpt1-deficient C2C12 myoblasts treated with doxycycline (shGfpt1 #1 and shGfpt1 #2) exhibited a significant decrease in unspliced *Xbp1u* expression by RT-qPCR. **F.** RT-qPCR performed on quadriceps muscle from *Gfpt1*$^{tm1d/tm1d}$ mice and *Tm1c* control mice showed reduced unspliced *Xbp1u* expression in *Gfpt1*$^{tm1d/tm1d}$ tissue. Three biological replicates were analyzed for each experiment. Statistical significance was determined by one-way ANOVA for panels B–E, and by Student's *t*-test for F–G. Gene expression was normalized to the geometric mean of Rpl27, Gapdh, and Actb. * $p < 0.05$; ** $p < 0.01$; *** $p < 0.001$; **** $p < 0.0001$.

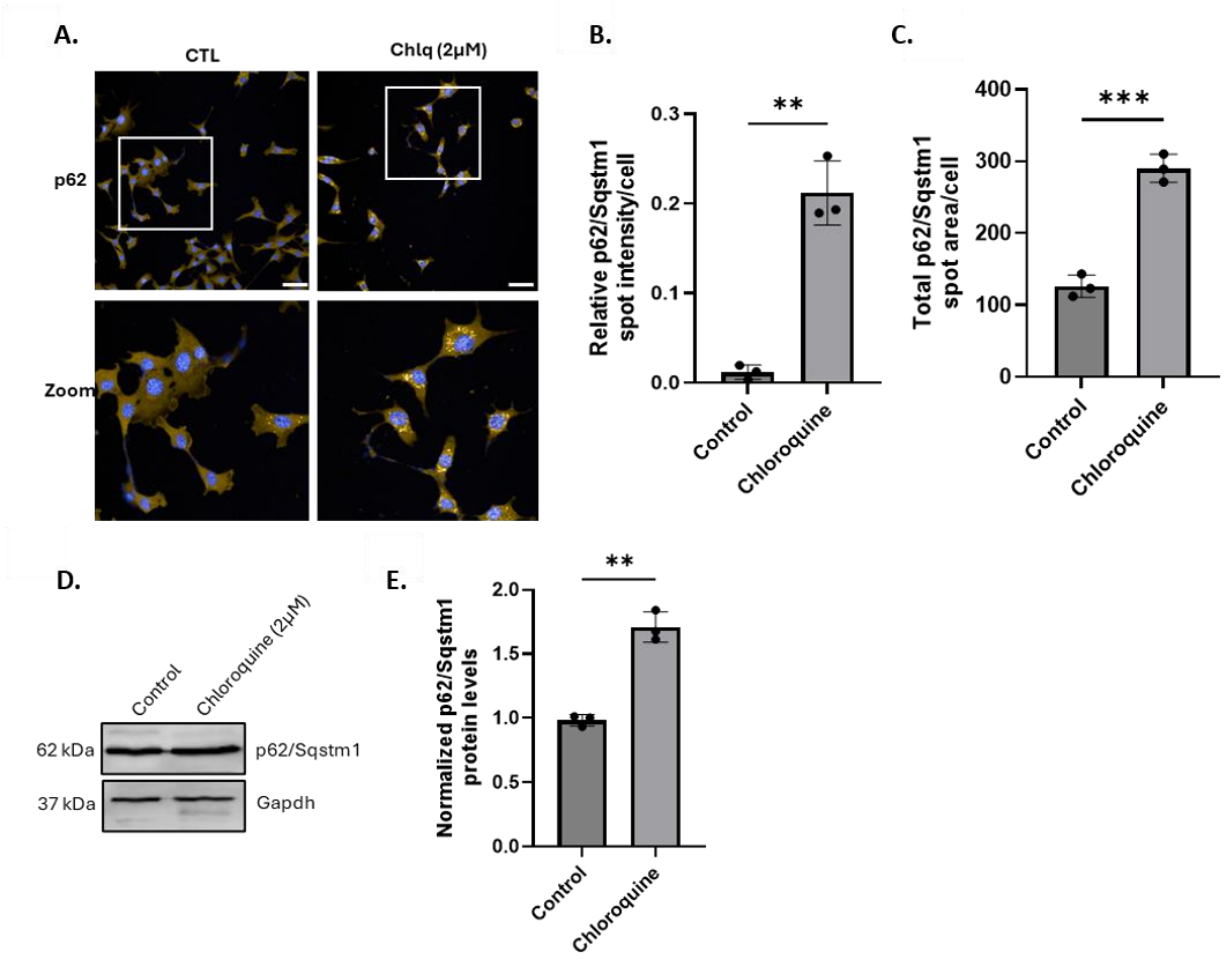

Supplementary Figure 2: p62 protein levels express a punctate pattern within Gfpt1-deficient myoblasts. A. Immunofluorescence staining of C2C12 myoblasts treated with 25 μM chloroquine and labeled for p62/SQSTM1. Images were acquired at 40× magnification using the OPERA™ high-content imaging system. Scale bar = 10 μm. **B.** Image analysis using Columbus™ software shows that chloroquine treatment increases p62/SQSTM1 staining intensity, **C.** increases the average number of p62-positive puncta per cell compared with untreated controls. **D.** Western blot analysis of soluble and insoluble fractions from control and Gfpt1-deficient C2C12 myoblasts demonstrates accumulation of p62/SQSTM1 in both fractions, with or without chloroquine treatment. **E.** Quantification shows elevated levels of soluble p62/SQSTM1 in Gfpt1-deficient myoblasts. All graphs show mean ± SD. Statistical significance was determined using one-way ANOVA. All experiments were performed with three biological replicates per group. Comparisons between control and Gfpt1-deficient samples: ** $p < 0.01$, *** $p < 0.001$.

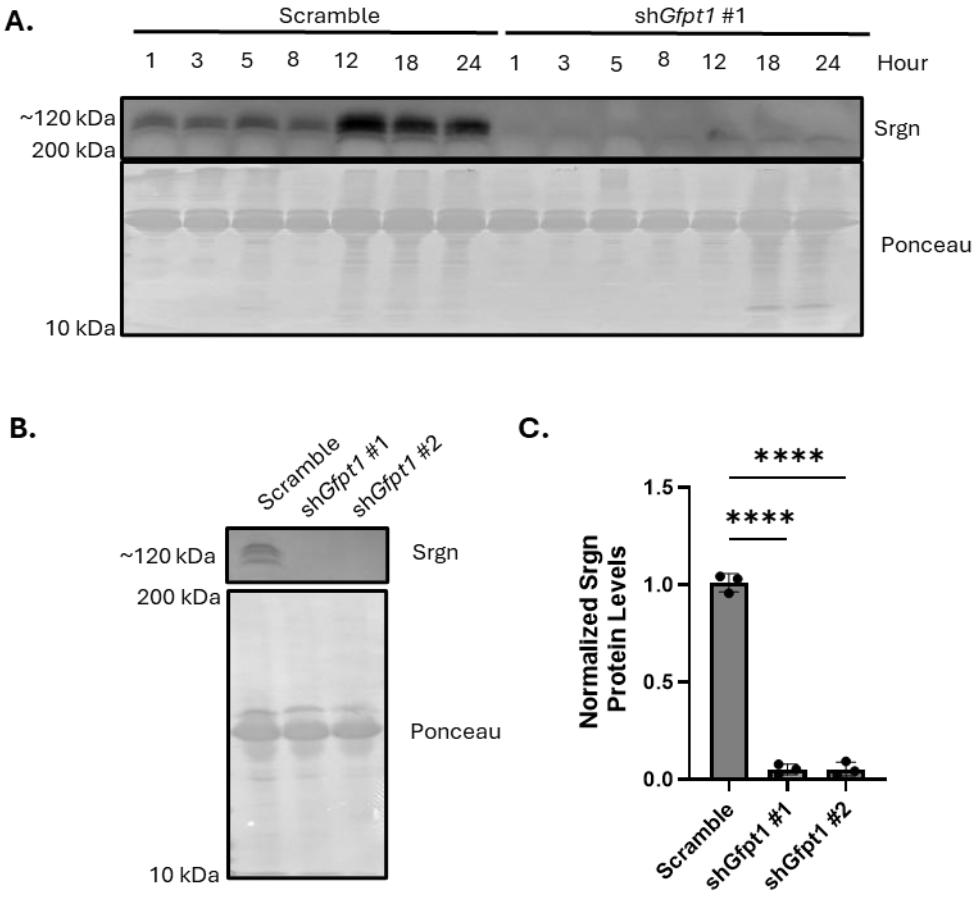

Supplementary Figure 3: Srgn is retained by Gfpt1-deficient myoblasts, and has reduced protein secretion. A. Western blot analysis of conditioned medium collected over a 24-hour time course from control and shGfpt1 #2 C2C12 myoblasts, alongside SRGN protein levels in the insoluble fraction of Gfpt1-deficient myoblasts. **B.** Western blot of conditioned medium collected at 24 hours from control and Gfpt1-deficient C2C12 myoblasts showing reduced secretion of SRGN. **C.** Quantification demonstrates a significant reduction in high–molecular-weight SRGN species in Gfpt1-deficient myoblasts. All graphs show mean ± SD. Statistical significance was determined using one-way ANOVA. All experiments were performed with three biological replicates per group. Comparisons between control and Gfpt1-deficient samples: **** $p < 0.0001$.

Supplementary Table S1: RT-qPCR Primer Design.

Target Gene	Forward Primer	Reverse Primer
Unspliced Xbp1	5’-cagactacgtgcacctctgc-3’	5’-cagggtccaacttgaccagaat-3’
Spliced Xbp1	5’-gctgagtccgcagcaggt-3’	5’-cagggtccaacttgaccagaat-3’
Total Xbp1	5’-tgaaaaacagagtagcagcctaga-3’	5’cccaagcgctttcttcactc-3’
Gapdh	5’- ctcccactcttccaccttcg-3’	5’- gcctctcttgctcagtgtcc-3’
Ppia	5’- gccttcctcctttcacagaa-3’	5’- gatgccaggacctgtatgct-3’
Rpl27	5’- aagccgtcatcgagaaca-3’	5’- cttgatcttggatcgcttggc-3’
Gfpt1	5’- ccaacgcctgcaaaatccag-3’	5’-ttctccatgtgtcgcccaac-3’

5.0 General Discussion

5.1 General Summary of Research

Glycosylation is increasingly recognized as a critical post-translational modification regulating NMJ integrity and skeletal muscle function [1–5]. Across the studies presented in this thesis, we demonstrate for the first time that Gfpt1 impairment reduces protein O-GlcNAcylation, N-linked glycosylation and sialyation in Gfpt1 deficient models (Chapter 2) [6]. Notably, our findings show that reduced Gfpt1 protein levels compromises glycosylation of key NMJ-associated proteins, most prominently AChRδ (Chapter 2) [6]. Although hypoglycosylated AChRδ remains localized to the NMJ, its altered molecular weight indicates reduced receptor stability and/or an impairment in function of the AChR complex (Chapter 2) [6]. Collectively, these findings identify hypoglycosylation of critical NMJ proteins as a central pathogenic mechanism of *GFPT1*-CMS.

To determine whether restoring glycosylation could rescue NMJ deficits, we tested galactose supplementation, which bypasses the defective HBP and supports UDP-GlcNAc production via the Leloir pathway. Galactose treatment restored protein glycosylation in Gfpt1-deficient models and recued AChRδ hypoglycosylation (Chapter 3) [7]. In addition, *in vivo* galactose supplementation improved NMJ morphology and reduced muscle pathology in *Gfpt1*$^{trm1d/tm1d}$ mice (Chapter 3) [7]. These findings provide a promising therapeutic strategy for patients with *GFPT1*-CMS.

Next, we aimed to further understand the role of Gfpt1 within muscle myoblasts. As the rate-limiting enzyme of the hexosamine biosynthetic pathway, we discovered that cellular proteostasis is impacted via loss of protein glycosylation, which in turn impairs protein folding, trafficking and degradation. Using our inducible Gfpt1-deficient myoblasts and a muscle-specific Gfpt1-knockout mouse, we demonstrated that hypoglycosylation leads to broad downregulation of vesicle trafficking machinery, intracellular retention and reduced secretion of key glycoproteins such as Srgn, and activation

of ER stress through the IRE1-XBP1 unfolded protein response pathway. Concurrently, autophagic flux was found to be impaired, evidenced by the accumulation of LC3-II, p62/Sqstm1, and insoluble protein aggregates, indicating defective clearance rather than increased autophagy initiation. these findings define a coordinated pathological cascade in which impaired glycosylation disrupts trafficking and ER homeostasis, triggering stress response and autophagy failure, providing a unified mechanistic explanation for muscle dysfunction in *GFPT1*-CMS.

5.2 Glycosylation as a Central Regulator for NMJ Integrity

GFPT1 is the rate limiting enzyme of the HBP, a necessary metabolic pathway that produces the glycoconjugates for N- and O-linked glycosylation [4,8–11]. As such, GFPT1 functions as a central regulator linking cellular metabolism to protein maturation, stability and trafficking. Biallelic mutations in GFPT1 reduce protein abundance and impair enzymatic activity, thereby limiting HBP flux and compromising glycosylation capacity [8,12–15,15–21]. Although earlier work in patient-derived myoblasts suggested that global N-linked glycan may be preserved, our Gfpt1-deficient models revealed clear reductions in both protein O-GlcNAcylation and N-linked glycosylation [16]. These findings indicate that even modest reductions in UDP-GlcNAc availability can selectively disrupt glycosylation of key substrates, rather than globally abolishing the process.

We hypothesized that specific glycoproteins critical for neuromuscular transmission would be particularly sensitive to reduced HBP flux. Indeed, we identified hypoglycosylation of the AChRδ, representing the first mis-glycosylated protein directly linked towards *GFPT1*-CMS pathology. Importantly, laser capture microdissection demonstrated that AChRδ remains present at the motor endplate in *Gfpt1*$^{tm1d/tm1d}$ muscle, suggesting that impaired glycosylation does not fully prevent receptor trafficking to the NMJ. Rather, these findings support a model in which partial glycosylation permits receptor export towards the motor endplate but compromises downstream maturation and function.

The nicotinic AChR is a pentameric ligand-gated ion channel composed of $\alpha_2\beta\gamma/\varepsilon\delta$ subunits that mediates neuromuscular transmission [22–24]. Multiple conserved N-linked glycosylation sites within AChR subunits are required for proper folding, ligand binding, and channel activity. Mutagenesis studies have demonstrated that removal of glycosylation sites of the α-subunit reduces α-BTX binding and ACh-evoked currents, while disruption of δ-subunit glycosylation further impairs channel assembly and function [23] . Thus, N-linked glycosylation is indispensable for AChR assembly and stability [25]. Consistent with these findings, we observed that Gfpt1 deficiency produces a lower molecular weight AChRδ species, indicative of hypoglycosylation. This species was sensitive to glycanase treatment with PNGase F [6]. Notably, prior work has shown that mutation of AChRδ glycosylation sites (N76, N143, and N169) disrupts αδ heterodimer formation, thereby reducing surface expression [23]. Although we did not directly measure αδ heterodimers in our models, reduced α-BTX binding in *Gfpt1*$^{tm1d/tm1d}$ muscle suggests impaired heterodimerization and receptor stability. This observation is supported by αδ heterodimers being a site for α-BTX binding [22,26,27].

These results indicate that glycosylation plays a critical role not only in receptor folding but also in assembly efficiency and quality control. AChR assembly is inherently inefficient, with only 10 – 30% of synthesized subunits successfully incorporated into pentameric complexes [28,29]. Assembly proceeds through a formation of an αβγ/ε trimer followed by incorporation of the α-δ heterodimer [28]. Therefore, disruption of AChRδ glycosylation would be expected to impair this rate-limiting step, reducing overall receptor yield. In addition, glycosylation contributes to ER and Golgi quality control mechanisms, where retention motifs prevent export of misassembled receptors and target them for ERAD [25]. Our data suggest that partial glycosylation allows some AChRδ to escape quality control and reach the NMJ, but the proportion of fully functional receptors is reduced. This results in a population of receptors that are structurally present but functionally compromised, sufficient to permit partial transmission but insufficient to maintain a normal safety factor.

Functionally, these molecular defects translate directly into impaired neuromuscular transmission. *Gfpt1*$^{tm1d/tm1d}$ mice exhibit reduced CMAP amplitudes and a frequency-dependent RNS decrement at 3 Hz, 10 Hz and 20 Hz. These electrophysiological features are characteristic of impaired synaptic transmission and mirror clinical findings in *GFPT1*-CMS patients [8,12–15,15–21]. Reduced glycosylation likely decreases density and stability at the motor endplate, lowering the safety factor and increasing susceptibility to transmission failure, particularly during repetitive stimulation, such as exercise [12,30].

In addition to receptor-level defects, structural remodeling of the NMJ further amplifies functional impairment. *Gfpt1*$^{tm1d/tm1d}$ muscle exhibits simplification of the postsynaptic apparatus, consistent with ultrastructural observations in patient biopsies showing loss of junctional folds [18]. These junctional folds normally enhance synaptic efficiency by concentrating voltage-gated sodium channels (Nav1.4) and amplifying their endplate potentials [31]. Their disruption reduces the local depolarization required to trigger action potentials, rendering neuromuscular transmission more vulnerable [31]. This effect is particularly pronounced during high-frequency stimulation, where sodium channels undergo cumulative inactivation and require robust depolarization for recovery [32–34]. Supporting this, our proteomic analysis identified a downregulation of multiple cytoskeletal and scaffolding proteins involved in maintaining NMJ architecture, suggesting that structural integrity and receptor stability are coordinately compromised [32,35–39]. These proteomic makers include Des, Vim, Tpm2/3, Tmod3, Mapre1, Arpc3, and Vasp/Lasp1.

An additional, non-mutually exclusive mechanism may involve altered AChR stoichiometry. Recent cyro-EM studies have identified alternative subunit assemblies under stress conditions, including configuration lacking the AChRδ, which exhibit impaired channel function [40]. One particular configuration identified was the $\alpha_3\varepsilon_2$ subunit which lacks a δ-subunit, was found to be nonfunctional due to a collapsed pore, highlighting δ-subunit's critical structural role [40]. By analogy to neuronal AChRs, where subunit composition influences channel kinetics, AChRδ deficiency may produce receptors with

reduced conductance, shorter open times, and enhanced desensitization, resembling a "fast-channel" phenotype [41–43]. Such changes would be expected to produced lower CMAPs and a RNS decrement, which is seen in *GFPT1*-CMS patients. While speculative, this model provides a plausible explanation for reduced synaptic efficacy despite preserved localization. However, since hypoglycosylated AChRδ was still detectable within the NMJ, further work is needed to trace its localization, stability and incorporation into the pentameric complex within skeletal muscle.

Our findings also highlight subunit-specific vulnerabilities to impaired glycosylation. Notably, AChRα and AChRβ did not exhibit detectable molecular weight shifts or significant changes in abundance, suggesting that the δ-subunit is particularly sensitive to glycosylation defects. This selective vulnerability may reflect structural or trafficking dependences unique to AChRδ [44]. Importantly, our proteomic data revealed reduced expression of key ER chaperones, including calnexin and calreticulin, which are essential for glycoprotein folding and AChR assembly [45,46]. Thus, impaired chaperone availability may further exacerbate defects in receptor maturation in Gfpt1-deficient cells.

Beyond AChRδ, other glycoproteins critical for NMJ formation and maintenance, including the other AChR subunits, Lrp4, Agrn, MuSK, ColQ and Rapyn, may also be vulnerable to hypoglycosylation [1,5,47]. While we did not detect overt molecular weight shifts in Lrp4 and AChRα, subtle or partial glycosylation defects cannot be excluded [48–52]. Comprehensive glycoproteomic analyses will be required to determine the broader impact of GFPT1 deficiency on NMJ-associated proteins. Particular focus should be on NMJs extracted with laser capture microdissection, in order to yield key NMJ associated proteins which are diluted within whole muscle protein lysates.

Finally, our observations suggest that NMJ vulnerability may be muscle- and fiber type-dependent. Differences between the intercostal and quadricep muscles, along with early and progressive exercised-induced phenotypes observed in *Gfpt1*$^{tm1d/tm1d}$ mice, indicate that intrinsic NMJ architecture influences

susceptibility [21]. Furthermore, immunofluorescence staining of p62/Sqstm1 revealed a pattern of impacting fast-twitch fibers with impaired autophagic flux. As such, impaired glycosylation in fast-twitch fibers, which possess more elaborate junctional folds and higher synaptic demands, may be preferentially affected, consistent with their known vulnerability to synaptic fatigue and degeneration. Prior studies have revealed that fast-twitch fibers posses NMJs with deeper folds, higher neurotransmitter turnover, and greater vulnerability for synaptic fatigue and degeneration, while slow-twitch fiber NMJs exhibit simpler structures and are deemed more stable [53].

Taken together, these findings establish glycosylation as a central determinant of NMJ integrity. GFPT1 deficiency initiates a cascade of subunit-specific receptor defects, impaired assembly, and quality control, structural remodeling of the synapse and ultimately reduced neuromuscular transmission. This positions glycosylation not as a secondary modifier, but as an upstream regulator of synaptic structure and function in skeletal muscle.

5.3 Metabolic Bypass Strategies for CMS

Metabolic bypass strategies provide a rational and mechanism-based approach to treat *GFPT1*-CMS by restoring HBP output and rescuing glycosylation of NMJ proteins. In Gfpt1-deficient models, reduced enzymatic limits HBP flux, depletes UDP-GlcNAc, and results in hypoglycosylation of key substrates such as the AChRδ, thereby compromising receptor assembly, stability, and NMJ integrity. Targeting this upstream metabolic deficiency offers a means to correct the fundamental biochemical defect rather than its downstream consequences.

To this end, we investigated galactose supplementation as a metabolic bypass strategy. Galactose enters cellular metabolism via the Leloir pathway, increasing UDP-hexose pools, particularly UDP-galactose and UDP-GalNAc which can be interconverted by GALE into UDP-GlcNAc, thereby indirectly replenishing HBP-derived substrates [54]. In both Gfpt1-deficient cells and mice, galactose

supplementation restored global protein glycosylation, corrected supplementation, restored global protein glycosylation, corrected AChRδ hypoglycosylation, and improved NMJ architecture and skeletal muscle morphology. These findings demonstrate that substrate supplementation can partially compensate for impaired GFPT1 function and restore glycosylation-dependent processes essential for neuromuscular function.

In parallel, we preliminarily explored a complementary strategy aimed at enhancing endogenous HBP flux by targeting a negative regulator of the HBP, Amdhd2. Amdhd2 catalyses the breakdown of GlcNAc-6-phsophate, thereby limiting flux through the HBP [55]. Knockdown of Amdhd2 reduces this catabolic loss, resulting in increased substrate availability for UDP-GlcNAc synthesis. In our models, Amdhd2 suppression led to increased OGT abundance and elevated global O-GlcNAcylation, consistent with enhanced pathway throughput. Together, these approaches demonstrate that both increasing supply and reducing loss of HBP intermediates can effectively restore glycosylation capacity in Gfpt1-deficiency.

From a translational standpoint, metabolic rerouting strategies such as galactose supplementation offer a potentially accessible and rapidly deployable therapeutic avenue. However, global elevation of UDP-GlcNAc and related metabolites necessitates careful evaluation of systemic effects. Increased O-GlcNAcylation regulates a wide range of cellular processes, including transcription, insulin signaling and stress responses, raising the possibility that chronic activation could lead to insulin resistance or broader signaling dysregulation [56–58]. Similarly, high-dose galactose exposure may impose osmotic, or hepatorenal stress [59–61]. Accordingly, dose-finding and safety monitoring (ex. liver enzymes, eGFR, fasting insulin) will be required to ensure toxic effects are detected early.

Notably, our findings also demonstrate Amdhd2 upregulation (~2.45 fold) in the sciatic nerve after galactose treatment, consistent with feedback compensation to restrain HBP flux [55]; whether this

occurs in other tissues and whether it signals UDP-GlcNAc over accumulation requires an additional systemic study. Additional regulatory layers, including transcriptional control of HBP enzymes by factors such as Sp1 and Xbp1, may further dampen pathway activation [10,62]. Over time, cells may also undergo metabolic adaptation, reducing the expression or activity of sugar transporters, Leloir pathway enzymes, or HBP components. These feedback mechanisms highlight the importance of defining a therapeutic window that maximizes glycosylation rescue while minimizing compensatory downregulation and systemic toxicity.

Interestingly, developmental context appears to influence disease progression and therapeutic responsiveness. Early characterization of *Gfpt1*$^{tm1d/tm1d}$ revealed poor viability *in utero*, suggesting that glycosylation is essential for viability. Offspring which survive are generally healthy and experience exercise fatigue as of week 6 [21]. During the suckling period, pups receive lactose-rich maternal milk, which provides both glucose and galactose substrates that may partially support glycosylation. While maternal lactose levels were not examined in pregnant dams, other mouse models such as *Duk6* mice have ~1.5-2.5% lactose in milk, suggesting a protective galactose effect until weaning [63]. Following weaning, dietary galactose intake declines, coinciding with onset of neuromuscular symptoms. This observation is consistent with the requirement that glycosylation stabilizes the NMJ, and the rapid rescue of NMJ architecture and neuromuscular transmission in *Gfpt1*$^{tm1d/tm1d}$ mice. These findings emphasize the importance of early intervention and raise the possibility that timing of therapy may influence clinical outcomes.

The concept of metabolic bypass is well established in inherited metabolic disorders, providing a strong precedent for its application in *GFPT1*-CMS. Substrate supplementation strategies have demonstrated efficacy across multiple CDGs, including mannose in *MPI*-CDG and galactose in *PGM1*-, *SLC35A2*-, *SLC39A8*-, and *TMEM165*-CDGs [64–68]. Similar principles apply in other neurometabolic diseases, where targeted dietary or cofactor supplementation such as L-serine, riboflavin, or ketogenic

diets can meaningfully improve clinical outcomes [69–71]. These parallels place *GFPT1*-CMS within a broader class of metabolically responsive disorders and support the translational potential of glycosylation-directed therapies.

Importantly, therapeutic responses are likely to vary depending on the underlying genetic and metabolic context. Patients with missense mutations that retain partial GFPT1 activity may respond more favorably to substrate-driven flux enhancement, whereas those with splicing defects or alterations in isoform regulation may exhibit more limited response [12,13,15,17–20,30,44,62]. For example, presence of the *GFPT1-L* variants or splicing defects at the 3'UTR, should be examined specifically for therapeutic efficacy, as O-GlcNAcylation expression may be altered. Additionally, systemic metabolic factors such as insulin sensitivity, glucose homeostasis, and expression of HBP regulators may further influence treatment outcomes. These considerations underscore the need for precision medicine approaches that integrate genotype, metabolic state, and functional NMJ assessment to optimize therapeutic strategies.

Among emerging approaches, targeting Amdhd2 represents a particularly promising avenue for more selective modulation of HBP flux. While prior studies have primarily examined Amdhd2 function in the context of Gfpt2-dominant systems, our findings suggest that its modulation may also be relevant in Gfpt1-deficient muscles [55]. Notably, cell-type-specific differences were observed, with neuronal cells exhibiting greater sensitivity to changes in HBP flux than skeletal muscle cells [55]. While this work emphasized the Gfpt2-Amdhd2 relationship, Gfpt1 should be investigated specifically in a Gfpt1-deficient model. In our hands, Gfpt1 knockdown lead to a decrease in Amdhd2 in NSC-34 cells, whereas C2C12 cells maintained Amdhd2 expression, suggesting that Amdhd2 may be targetable in Gfpt1-depleted myotubes. Furthermore, these results suggest that neuronal cells are more sensitive to changes in HBP flux than skeletal muscle cells, another relationship that will require further exploration. In systems that lean on salvage and/or Gfpt2 for HBP entry, Amdhd2 functions as a principal brake on GlcNAc-6-P backflow, removing this brake raises UDP-GlcNAc more strongly [55]. Neuronal cells, can

also amplify smaller pool changes due to their higher O-GlcNAc sensitivity of synaptic/trafficking regulators [72]. In contrast, myogenic cells rely on Gfpt1 *de novo* capacity for buffering these swings, and does not utilize Gfpt2 for buffering [10,62]. Therefore, this may help explain why NSC-34 cells were more sensitive to Amdhd2 changes in Gfpt1-depleted cells.

Further preclinical validation will require *in vivo* modeling. While the *Gfpt1*$^{tm1d/tm1d}$ mouse recapitulates key aspects of disease pathology, complete muscle-specific knockout may not fully reflect the spectrum of human patients [18,21]. Other models harbouring patient-specific variants or expressing human GFPT1-L isoforms will be important for therapeutic evaluation [62,73]. In parallel, zebrafish models offer a rapid and scalable platform for screening metabolic and genetic interventions, which has been validated for *GFPT1*-CMS [8]. Preclinical assessment of an anti-sense oligonucleotide morpholino targeting Amdhd2 may serve as a therapeutic target for future *GFPT1*-CMS.

Taken together, our findings establish metabolic bypass as a viable therapeutic paradigm for *GFPT1*-CMS. By restoring glycosylation through substrate supplementation or modulation of pathway flux, these strategies directly address the underlying biochemical defects and provide a foundation for translational development. Integrating these approaches with emerging insights into proteostasis, trafficking, and NMJ biology may ultimately enable combination therapies that more effectively restore NMJ function.

5.4 Biomarker Development and Translational Relevance

Current diagnostic strategies for CMS rely primarily on genetic testing and clinical evaluation [74,75]. While electrophysiological assessments such as RNS decrement and CMAP recordings confirm impaired neuromuscular transmission, they lack molecular specificity and cannot distinguish among mechanistically distinct NMDs [34]. As a result, misdiagnosis remains common, particularly when genetic testing is delayed or inaccessible [74,75]. Given the central role of glycosylation in the NMJ organization

and stability, there is a clear clinical need for a molecular biomarker that reflects glycosylation status, NMJ integrity, and therapeutic responsiveness. Such biomarkers would not only improve diagnostic precision but also enable early detection, real-time monitoring of disease progression and allow for the assessment of different therapies.

Carbohydrate-deficient transferrin (CDT) is a well-established biomarker for N-linked glycosylation defects in CDGs, typically detected with isoelectric focusing, capillary electrophoresis or mass spectrometry [76,77]. CDT has proven valuable for both diagnosis and therapeutic monitoring in multiple N-linked glycosylation CDG subtypes, but was less impactful for O-linked glycosylation and GPI-anchoring CDG phenotypes [76]. However, CDT or related transferrin-based assays have not been systematically investigated in CMS, despite shared biochemical features between CDGs and glycosylation-related CMS. This gap underscores the opportunity to identify CMS specific biomarkers, particularly for *GFPT1*-CMS, where the underlying metabolic defect disrupts early glycan precursor synthesis.

Our results highlight Srgn as a potential candidate biomarker for *GFPT1*-CMS. Srgn is a secreted proteoglycan requiring GAG chain assembly, a process dependent on nucleotide-sugar donors produced by the HBP and related metabolic pathways [78]. We observed reduced Srgn expression and impaired secretion in Gfpt1-deficient models, suggesting that HBP dysfunction affects proteoglycan synthesis in addition to N-linked and O-GlcNAc modification. This reduction in Srgn abundance implies broader impairments in secretory granule formation and vesicular trafficking [78]. Since Srgn is synthesized as a 32 kDa core protein but can exceed 200 kDa once fully glycan-modified, its molecular weight profile may serve as a sensitive readout of disrupted GAG biosynthesis.

Notably, cross-species comparisons revealed an apparent discrepancy: Srgn was reduced in Gfpt1-deficient muscle and cell models, whereas circulating SRGN was elevated in human serum derived

from *GFPT1*-CMS patients. These findings are not contradictory but instead highlight the context-dependent nature of SRGN biology. SRGN is a secreted proteoglycan whose abundance in circulation reflects a balance of (i) tissue-specific production and secretion (muscle, immune cells, endothelium), (ii) post-translational processing (GAG chain initiation/elongation, sulfation), (iii) extracellular retention and (iv) clearance kinetics (liver/kidney uptake, complex half-life) [79,80]. While many of these components remain incompletely defined in SRGN biology, in mouse models, muscle-intrinsic hypoglycosylation likely limits SRGN secretion due to impaired packaging and trafficking. In contrast, in human diseases, systemic factors such as inflammation, muscle stress, or compensatory secretion from hematopoietic and endothelial sources may elevate circulating SRGN levels [79]. In addition, glycoform-specific changes, not captured in total SRGN measurements, may further contribute to these differences [79,80]. Together, these observations position SRGN as a context-dependent biomarker that reports on both muscle-intrinsic secretory dysfunction and systemic compensatory responses.

A key species difference likely relevant to our findings is the presence of the muscle-restricted *GFPT1-L* isoform in humans and its absence in mice [10,21,73]. GFPT1-L carries the 18aa insertion in exon 9 that alters enzymatic kinetics, increasing sensitivity to UDP-GlcNAc feedback and reducing affinity for fructose-6-phosphate, and is regulated by muscle splicing factors [10,21,73]. In human skeletal muscle, this configuration may confer a tighter, more dynamic coupling between nutrient status and HBP output, thereby shaping substrate partitioning among N-linked glycosylation, O-GlcNAcylation and GAG biosynthesis [10,21,73]. In human CMS, human muscle could engage distinct feedback loops that simply do not exist in mice, producing divergent systemic readouts such as elevated serum SRGN from immune/endothelial sources in patients despite muscle-intrinsic secretion defects in the mouse model. More broadly, the lack of GFPT1-L in mice may blunt or shift flux-control behaviour at the NMJ and influence AChRδ glycan occupancy, stoichiometric assembly stress, and the temporal course of NMJ

remodeling. These factors that could partially account for species-specific differences in Srgn/SRGN secretion levels.

This thesis provides evidence for future biomarker research in glycosylation-related neuromuscular disorders. We identified the hypoglycosylation of the AChRδ potential diagnostic and therapeutic biomarker candidate. In *Gfpt1*-deficient samples, AChRδ hypo-glycosylation was consistently observed and is likely to contribute to impaired neurotransmission. We identified that this hypo-glycosylated AChRδ was present at the NMJ, but AChR clustering was impaired with *Gfpt1*$^{tm1d/tm1d}$ muscle. Given that *GFPT1*-CMS muscle biopsies contain tubular aggregates, these archival specimens could be repurposed for AChRδ glycosylation analysis, providing a robust diagnostic adjunct prior to genetic confirmation [18].

AChRδ hypoglycosylation also serves as a therapeutic biomarker. We identified that AChRδ hypoglycosylation was rescued after treatment with galactose, paralleling improvements in NMJ transmission and morphology. This response to treatment, suggests that when targeting glycosylation pathway rescue within *Gfpt1*-deficient models AChRδ glycosylation status may be an amenable readout for therapeutic efficacy. Monosaccharide supplementation has served as a key therapy for different subtypes of CDGs [65,67,68]. Therapies such as dietary supplementation with mannose, galactose, complex carbohydrate feeding and manganese all represent improvement in the glycosylation status of various proteins [67,81]. In terms of galactose supplementation in *PMM1-, SLC35A2-, SLC39A8-* and *TMEM165*-CDG shows improvement in the glycosylation biological patterns with patient blood and serum [68]. These precedents reinforce the feasibility of using AChRδ glycosylation as translational biomarkers for *GFPT1*-CMS.

Finally, recognizing that in our Gfpt1-deficient models impaired trafficking and secretion is present other glycoproteins may be impacted. Future directions would be to engage with this cellular secretory pathway examining protein secretion through glyco-proteomics [82]. This will help decipher improperly glycosylated proteins that are differentially secreted in Gfpt1-deficiency. In addition, accompanying these tests with other glycosylation-based CMS cases, and glycosylation related muscle disorder may determine a shared biomarker for future testing.

Altogether, this thesis recognizes the foundational evidence supporting two potential biomarkers for *GFPT1*-CMS: SRGN and AChRδ hypoglycosylation. Both capture distinct aspects of HBP dysfunction and offer complementary diagnostic and therapeutic value.

5.5 Implications for Muscle Pathophysiology

This thesis defines an explicit role for Gfpt1 in skeletal muscle, showing that reduced HBP flux impairs glycosylation-dependent signaling across multiple cellular systems. Using whole cell proteomics and secretomics on Gfpt1-deficient C2C12 myoblasts, we observed 74 upregulated proteins, and 229 downregulated proteins, indicating broad remodeling. Prominent among the altered pathways were autophagy/proteostasis, ER-GA trafficking, and energy metabolism, with convergent effects on NMJ stability and muscle fiber resilience.

One major consequence of reduced HBP flux is impaired proteostasis. Accumulation of p62/Sqstm1 and LC3 indicated autophagic disruption, corroborated by p62 accumulation in the insoluble fraction and elevated LC3-II, consistent with impaired autophagic flux, rather than increased autophagy initiation [83]. This suggests an inability to clear damaged proteins and aggregates, a process critical for maintaining muscle integrity and stress adaptation [84]. Notably, although ER stress and UPR activation were consistently observed, particularly via XBP1 and ATF4 signalling, canonical ER-phagy pathways were not activated, distinguishing GFPT1 deficiency from other glycosylation disorders such as GNE

myopathy [85–88]. Consistent with this, a recent muscle-specific GFPT1-L model reported robust UPR activation, ER stress, protein aggregation and apoptosis without compensatory autophagic signalling [73].These findings suggest that GFPT1 loss disrupts autophagy through glycosylation-dependent regulatory mechanisms rather than classical ER stress pathways alone. Impaired clearance of misfolded proteins likely contributes to mitochondrial dysfunction, NMJ stability, and the accumulation of pathological structures such as tubular aggregates [89,90].

In parallel, we identify a broad impairment of intracellular trafficking as a key pathogenic mechanism. Proteomic analysis revealed down regulation of components of COPI/COPII transport, clatherin-mediated endocytosis, and vesicle trafficking systems, alongside upregulation of ER protein folding and ERAD pathways, consistent with compensatory responses to misfolded proteins [91–93]. Functionally, this defect is reflected in impaired secretion of Srgn, which accumulates intracellularly in Gfpt1-deficient cells. Mechanistically, reduced O-GlcNAcylation of trafficking regulators likely disrupts vesicle formation, cargo sorting, and ER-to-Golgi transport, thereby compromising delivery of glycoproteins to the sarcolemma and NMJ [57,93,94].

To support this, several trafficking regulators were identified in our proteomic dataset including depletion of Rab34, Copg1, Sec23a, and Rab5b. Reduced Rab34 function may impair lysosome positioning and autophagosome clearance, consistent with accumulated LC3-II and p62 [95]. Disruption of Copg1-dependent COPI trafficking likely compromises retrograde transport and ER homeostasis, exacerbating ER stress [92,96]. Sec23a loss may impair ER export of secretory cargo, while Rab5b dysfunction may weaken endocytic recycling and receptor turnover [97]. Together, these convergent defects result in inefficient protein trafficking, impaired receptor maintenance, and defective autophagic clearance, ultimately destabilizing muscle fiber structure and function.

Beyond proteostasis and trafficking, Gfpt1 deficiency also drives metabolic reprogramming [89,98–101]. Proteomic analysis revealed downregulation of key mitochondrial enzymes involved in the TCA cycle (ex. Oddh, Aco2, Suclg2) and fatty acid β-oxidation, suggesting impaired oxidative metabolism [102]. Given the role of O-GlcNAcylation in regulating mitochondrial function, reduced UDP-GlcNAc availability likely disrupts mitochondrial dynamics, oxidative phosphorylation, and stress responses [89,98,100,101,103]. This metabolic bottleneck may lead to diminished ATP production, lipid accumulation, and increased susceptibility to metabolic stress, consistent with increased fat mass observed in *Gfpt1*$^{tm1d/tm1d}$ mice [104,105].

Importantly, we also observed downregulation of Prkaa1, encoding the catalytic α1 subunit of AMP-activated protein kinase (AMPK), a master regulator of cellular homeostasis [106]. Reduced AMPK signaling would further impair mitochondrial biogenesis and fatty acid oxidation, compounding the metabolic defect [107]. Given the well established cross-regulation between O-GlcNAcylation and AMPK signaling, these findings suggest that Gfpt1 deficiency disrupts two major nutrient sensing axes, the HBP/O-GlcNAc pathway and AMPK resulting in impaired metabolic flexibility and reduced stress resilience in skeletal muscle [106,108].

At the structural level, these molecular defects manifest in the formation of tubular aggregates , a hallmark of *GFPT1*-CMS [13,17,18,30]. Tubular aggregates, are derived from sarcoplasmic reticulum membranes and are associated with ER stress, calcium dysregulation, and proteostatic imbalance [109]. Glycosylation defects likely contribute to tubular aggregate formation through multiple mechanisms, including impaired folding of ER-resident proteins, disrupted ER-to-Golgi trafficking, and altered regulation of calcium-handling proteins. Defective O-GlcNAcylation of sarcoplasmic reticulum components such as SERCA and STIM1 may further destabilize calcium homeostasis, promoting SR remodeling and aggregate formation [109–111]. Consistent with this model, we observed UPR activation and

impaired autophagic clearance, indicating that tubular aggergates arise in the context of unresolved proteotoxic stress.

Importantly, tubular aggregates were markedly reduced following galactose supplementation, demonstrating that these structures are dynamic and responsive to metabolic intervention. Restoration of UDP-GlcNAc availability likely improves glycosylation of ER chaperones and trafficking machinery, stabilizes calcium handling, and alleviates ER stress, collectively reducing aggregate formation. This finding reinforces the concept that glycosylation defects are upstream drivers of structural pathology and highlights the therapeutic potential of metabolic bypass strategies.

In summary, Gfpt1-deficiency initiates a multi-system collapse of skeletal muscle homeostasis driven by reduced HBP flux and impaired glycosylation. This manifests as coordinated defects in NMJ integrity, intracellular trafficking, proteostasis, and energy metabolism. Together, these disruptions lead to reduced muscle fiber stability, contractile performance, and stress resilience. These findings position glycosylation as a central regulator for muscle physiology and highlight the HBP as a critical node linking metabolism to neuromuscular function and disease.

5.6 Nerve Alterations in a Muscle-specific model

A key limitation of this work is that Gfpt1 deficiency was investigated predominantly from a skeletal muscle-centric perspective. However, the NMJ is a tripartite structure composed of the motor neuron, skeletal muscle fiber and terminal Schwan cell. While the Schwann cell contributions were not examined here due to the lack of an appropriate model system, our findings nonetheless suggest that Gfpt1 deficiency exerts effects beyond muscle, particularly within the presynaptic compartment.

Morphological analysis of *Gfpt1*$^{tm1d/tm1d}$ NMJ revealed alterations in motor nerve terminal structure that paralleled changes in the post-synaptic membrane, including reduced NMJ area and perimeter. These coordinated changes suggest the presence of bidirectional synaptic plasticity, whereby

defects in the postsynaptic muscle fiber elicit adaptive or maladaptive responses in the presynaptic motor neuron. While novel in the context CMS, this finding has been demonstrated previously, where skeletal muscle calcium channels ($Ca_V1.1$) controls presynaptic differentiation [112]. Our work may suggest that postsynaptic signalling may impair important signaling pathways in the presynaptic motor neuron. This highlights the interdependence of NMJ compartments and suggests that muscle-intrinsic glycosylation may indirectly drive presynaptic remodeling.

Proteomic profiling of sciatic nerve derived from *Gfpt1*$^{tm1d/tm1d}$ mice revealed reductions in Fxf1 and Caprin1, proteins associated with stress granules and neuronal injury responses, may suggest that overt neurodegeneration is limited in this model, consistent with relatively preserved nerve morphology [113]. Indeed, ultrastructural analysis revealed only subtle changes in myelin sheath thickness and G-ratio, with no overt alterations in axonal diameter. While differences were modest, even small deviations in G-ratio can influence conduction velocity, suggesting that functional deficits in nerve signaling may still occur [114–116]. Together, these findings indicate that while neuronal integrity is largely preserved, subtle alterations in myelination and trafficking may contribute to impaired neurotransmission.

Notably, several trafficking proteins implicated in vesicle fusion and secretion were reduced in *Gfpt1*$^{tm1d/tm1d}$ sciatic nerve, including Snap23 and Vps26b. These proteins are critical for membrane trafficking and exocytosis, particularly in glial cells where they regulate the release of neurotrophic factors such as nerve growth factors [117–119]. Disruption of these pathways may impair communication between Schwann cells and motor neurons, further destabilizing the NMJ. Additionally, reduced Snap23 may compromise Ca^{+2}-dependent vesicle fusion, potentially limiting neurotransmitter release under conditions of high demand [117,120].

Consistent with these observations, Gfpt1-depleted neuronal cells (NSC-34) exhibited pronounced metabolic and stress-related reprogramming. Proteomic analysis revealed coordinated

suppression of mitochondrial oxidative phosphorylation, with downregulation of electron transport chain components, mitochondrial ribosomal proteins, and cofactor synthesis pathways. This was accompanied by upregulation of antioxidant defenses, indicating increased oxidative stress and a shift toward a stress-adaptive state. Concurrent activation of the UPR is present, including elevated ATF6, BiP and Selenos, further supporting the presence of glycosylation-induced ER stress in neuronal cells [121–124].

Although autophagy-related proteins were upregulated, reductions in key components of autophagic machinery suggest incomplete flux, mirroring findings in skeletal muscle. In parallel, suppression of synaptic proteins including Syn1, Syn2, Syt1, and Rab3 suggest a potential impairment of synaptic vesicle dynamics and neurotransmission that remains to be investigated and confirmed [125,126]. These changes point to a broader neuronal vulnerability linked to disrupted glycosylation, proteostasis imbalance, and metabolic stress.

Collectively, these findings support a model in which Gfpt1 depletion initiates ER stress and integrated stress response signaling, driving a global metabolic slowdown, mitochondrial dysfunction, and autophagic remodeling. The combination of impaired glycosylation, disrupting energy metabolism, and synaptic protein loss may underlie neuronal vulnerability in Gfpt1-related disorders. Future work should validate these pathways functionally, focusing on ER stress markers, mitochondrial respiration, autophagic flux, glycosylation-dependent adhesion and signaling.

5.7 Broader Implications for CDGs and Rare Myopathies

The findings presented in this thesis extend beyond *GFPT1*-CMS and position glycosylation as a central regulator of neuromuscular health, intersecting with mechanisms implicated in other CDGs and rare myopathies. CDGs comprise a heterogenous group of disorders arising from defects in glycan synthesis, processing, or trafficking, and typically manifest as multisystem diseases [127,128]. Although the predominant phenotype in our Gfpt1-deficient models localizes to the NMJ, multiple lines of this work

indicate that impaired HBP flux engages systemic responses that are not restricted to muscle. These observations suggest that glycosylation-dependent processes governed by Gfpt1 are fundamental to cellular homeostasis across multiple tissues.

Supporting this view, Gfpt1-deficient neuronal models and sciatic nerve tissues exhibited mitochondrial dysfunction, suppressed lipid metabolism, impaired vesicular and synaptic signaling, paralleling observations in skeletal muscle. These shared alterations indicate that glycosylation defects compromise organelle integrity and stress resilience across cell types. Given the role of O-GlcNAcylation as a nutrient-sensing modification regulating endocrine, immune, and metabolic pathways, disruption of HBP flux likely impacts multiple physiological systems [72,93,98,101,129,130]. Indeed, *GFPT1*-CMS has been associated in select patients with central nervous system manifestations, including seizures, leukoencephalopathy, and cognitive impairment, suggesting that the clinical spectrum may be expanded beyond classical neuromuscular fatigue [14,30,131].

Despite these systemic signals, *GFPT1*-CMS remains primarily a neuromuscular disorder characterized by fatigable weakness and prominent involvement of skeletal muscle and the NMJ. This tissue specificity likely reflects the unique structural and metabolic demands of the motor unit, which amplify the consequences of impaired glycosylation [5]. The NMJ is a highly specialized, glycoprotein-rich synapse that depends on tightly regulated assembly, trafficking, and maintenance of receptor and adhesion complexes. As demonstrated in this thesis, even subtle glycosylation defects such as AChRδ hypoglycosylation can destabilize receptor clustering and impair synaptic transmission. In parallel, skeletal muscle requires precise coordination of proteostasis and metabolism to sustain contractile activity [132]. Reduced HBP flux compromises this adaptive system, promoting ER stress, impaired autophagic clearance, and UPR activation. Together, these features explain why the NMJ and skeletal muscle are disproportionately vulnerable to Gfpt1- loss: they operate at the limits of secretory capacity,

proteostasis, and metabolic flux, such that even modest reductions in glycosylation disrupt function and homeostasis.

From a therapeutic perspective, the success of galactose supplementation in Gfpt1-deficient models aligns with established treatment paradigms in CDGs, where monosaccharide supplementation can restore glycosylation and improve clinical outcomes [68]. This supports the concept of metabolic bypass therapy as a broadly applicable strategy across glycosylation disorders.

These findings underscore the need for expanded systemic characterization of Gfpt1-deficient models. Integration of multi-omic approaches including glycoproteomics, metabolomics and transcriptomics will be essential to identify shared disease signatures and refine biomarker development across disorders. From a clinical perspective, basket trial designs targeting common glycosylation pathways across multiple CDGs and related myopathies may accelerate therapeutic development and enable more efficient evaluation of metabolic interventions. The idea of umbrella and basket clinical trials has been well adapted for cancer research, and could be an ideal method to increase sample sizes for screening therapeutics within rare disease [133].

Finally, emergence of galactose as an alternative treatment strategy for *GFPT1*-CMS opens the door for nutritional therapy for other glycosylation-related disorders. Key metabolomic studies need to be performed in *GMPPB, ALG2, ALG14* and *DPAGT1*-CMS specimen to decipher if any metabolic pathways can be rescued by alternative substrates. Translation of galactose therapy to other glycosylation enzymes implicated in CMS work solely in N-linked glycosylation (ALG2, ALG14 and DPAGT1), and O-mannosylation (GMPPB), as such galactose would have limited effect on subtypes. Thus, these glycosylation-CMS subtypes may benefit from targeted nutritional support through different pathways. External mannose supplementation appears to ameliorate GMPPB-related muscle disease suggesting these nutritional therapies are emergent for CDGs and glycosylation-based CMS [81].

5.8 Emerging Model for *GFPT1*-CMS

The findings in this thesis support a unified model in which GFPT1-deficiency disrupts NMJ neurotransmission through convergent defects in glycosylation, proteostasis, and trafficking (summarized in Figure). Reduced HBP flux lowers UDP-GlcNAc availability, leading to substrate specific hypoglycosylation, exemplified by the identification of AChRδ as the first misglycosylated protein in *GFPT1*-CMS. This defect compromises AChR assembly, stability reducing the NMJ safety factor and weakening neurotransmission. Restricted glycan donor availability simultaneously perturbs O-GlcNAcylation-dependent signalling, engaging the UPR while impairing autophagic flux, resulting in accumulation of misfolded proteins and the formation of tubular aggregates, a hallmark of *GFPT1*-CMS muscle pathology.

Beyond the synapse, impaired glycosylation disrupts ER–Golgi trafficking by reducing O-GlcNAcylation of COPI/COPII, Rab GTPases, and SNARE components, limiting delivery and recycling of key NMJ proteins and impairing secretion of factors such as Srgn. Concurrent suppression of mitochondrial enzymes and AMPK signaling reshapes metabolic capacity, producing an ATP deficit that further weakens NMJ resilience, particularly under high-frequency stimulation. Although GFPT1-CMS has traditionally been conceptualized as a postsynaptic disorder, nerve-side analyses here indicate additional vulnerabilities in vesicle cycling, exocytosis, and conduction fidelity, suggesting that impaired retrograde signaling and mild axonal stress may amplify the postsynaptic deficit.

Together, these findings describe GFPT1-CMS as a glycosylation-driven, multi-axis disorder in which reduced HBP flux destabilizes synaptic glycoprotein maturation, proteostasis networks, intracellular trafficking, and metabolic support. This model explains both low-frequency transmission weakness and the disproportionate high-frequency RNS decrement characteristic of the disease. It also provides a mechanistic rationale for therapeutic rescue by galactose supplementation, which restore

glycosylation capacity and synaptic integrity. This emerging model offers a framework for future mechanistic studies, biomarker development, and targeted therapeutic strategies in GFPT1-CMS and related glycosylation disorders.

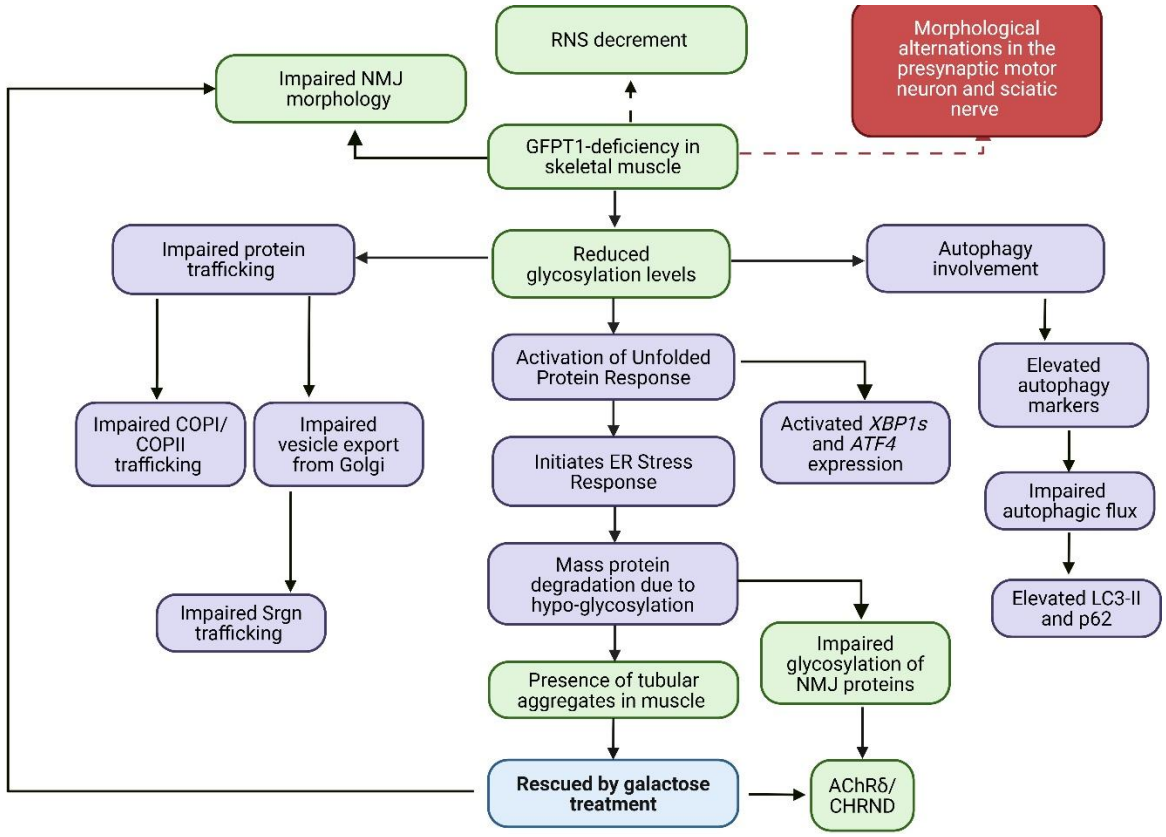

Figure 1: Integrated mechanistic model of GFPT1 deficiency across skeletal muscle, proteostasis, and therapeutic rescue pathways: Green boxes represent findings from Chapter 2, defining the role of GFPT1 deficiency in skeletal muscle leading to reduced glycosylation, impaired neuromuscular junction (NMJ) integrity, abnormal morphology, and functional deficits such as repetitive nerve stimulation (RNS) decrement. Blue boxes represent Chapter 3, demonstrating metabolic rescue through galactose supplementation, which restores glycosylation and improves NMJ structure and function. Purple boxes represents Chapter 4, highlighting downstream consequences of hypoglycosylation, including activation of the unfolded protein response (UPR), impaired ER–Golgi trafficking, and defective autophagic flux characterized by LC3-II and p62 accumulation. Red boxes depict unpublished findings, including morphological changes in the presynaptic motor neuron and sciatic nerve, suggesting broader neuromuscular system involvement. Together, this model illustrates how impaired HBP flux drives glycosylation-dependent defects in trafficking, stress responses, and autophagy, ultimately compromising muscle function, and how metabolic bypass strategies can partially restore these processes.

6.0 Conclusions

To conclude this doctoral thesis, I determined that the HBP governed by Gftp1 is a central regulator for neuromuscular health. By integrating biochemical assays, proteomics, secretomics, laser capture microdissection, electrophysiology and *in vivo* interventions, I (i) identified the first misglycosylated substrate in *GFPT1*-CMS (AChRδ), directly linking reduced HBP flux to impaired synaptic protein maturation and NMJ transmission inefficiencies; (ii) demonstrated that metabolic bypass via galactose supplementation and Amdhd2 knockdown can restore glycosylation capacity. With respect to galactose supplementation, we furthermore confirmed that there was a restoration in NMJ architecture, tubular aggregate formation, muscle morphology and behavioural measurements; and (iii) nominated serglycin (Srgn) and AChRδ glycan occupancy as biomarkers and pharmaceutical readouts, while explaining their matrix- and species-dependent behaviours. Mechanistically, Gfpt1 deficiency lowers the UDP-GlcNAc pools, driving substrate-specific hypoglycosylation, UPR activation with impaired autophagic flux, ER-GA trafficking defects, and potential bioenergetic shortfall by suppression of mitochondrial OXPHOS, a convergent network that erodes the neuromuscular safety factor. Our model for *GFPT1*-CMS pathogenesis helps explain the vulnerabilities in both low-frequency and high-frequencies while accommodating motor neuron vulnerabilities.

Beyond *GFPT1*-CMS, these data frame a broader view of glycosylation-centric neuromuscular pathophysiology. The same axes that destabilize the NMJ (selective misglycosylation, proteostasis collapse, secretory/trafficking bottlenecks, and metabolic reprogramming) are recurrent across CDGs and rare myopathies. Clinically, this supports mechanism-based therapeutics that increase substrate supply, preserve flux, and motivates basket-trial design across glycosylation disorders. It also motivates precision medicine in *GFPT1*-CMS, accounting for variant class, tissue-specific feedback and a baseline metabolic state required for dosing optimization.

In summary, this thesis defines a unified, testable model in which GFPT1 deficiency reduces HBP output to trigger substrate-specific hypoglycosylation (anchored by AChRδ), proteostasis and trafficking failure, culminating clinical physiology of fatigable muscle weakness with RNS decrement. It delivers actionable therapies, quantitative biomarkers, and analytical tools to track structure-function and rescue. The work advances our understanding of glycosylation-dependent neuromuscular disease and sets a translational path toward mechanism guided-clinical trails for *GFPT1*-CMS and related glycosylation disorders.

References

1. Dang, K., Jiang, S., Gao, Y. & Qian, A. The role of protein glycosylation in muscle diseases. *Mol. Biol. Rep.* **49**, 8037–8049 (2022).
2. Ferraro, E., Molinari, F. & Berghella, L. Molecular control of neuromuscular junction development. *J. Cachexia Sarcopenia Muscle* **3**, 13–23 (2012).
3. Reily, C., Stewart, T. J., Renfrow, M. B. & Novak, J. Glycosylation in health and disease. *Nat. Rev. Nephrol.* **15**, 346–366 (2019).
4. Akella, N. M., Ciraku, L. & Reginato, M. J. Fueling the fire: emerging role of the hexosamine biosynthetic pathway in cancer. *BMC Biol.* **17**, 52 (2019).
5. Lambert, M. *et al.* O-GlcNAcylation is a key modulator of skeletal muscle sarcomeric morphometry associated to modulation of protein–protein interactions. *Biochim. Biophys. Acta BBA - Gen. Subj.* **1860**, 2017–2030 (2016).
6. Holland, S. H. *et al.* A Deficiency in Glutamine-Fructose-6-Phosphate Transaminase 1 (Gfpt1) in Skeletal Muscle Results in Reduced Glycosylation of the Delta Subunit of the Nicotinic Acetylcholine Receptor (AChRδ). *Biomolecules* **14**, 1252 (2024).
7. Holland, S. H. *et al.* Galactose treatment rescues neuromuscular junction transmission in glutamine-fructose-6-phosphate transaminase 1 (Gfpt1) deficient mice. *Hum. Mol. Genet.* ddaf140 (2025) doi:10.1093/hmg/ddaf140.
8. Senderek, J. *et al.* Hexosamine Biosynthetic Pathway Mutations Cause Neuromuscular Transmission Defect. *Am. J. Hum. Genet.* **88**, 162–172 (2011).
9. Coomer, M. & Essop, M. F. Differential hexosamine biosynthetic pathway gene expression with type 2 diabetes. *Mol. Genet. Metab. Rep.* **1**, 158–169 (2014).

10. Paneque, A., Fortus, H., Zheng, J., Werlen, G. & Jacinto, E. The Hexosamine Biosynthesis Pathway: Regulation and Function. *Genes* **14**, 933 (2023).
11. Ruegenberg, S. *et al.* Loss of GFAT-1 feedback regulation activates the hexosamine pathway that modulates protein homeostasis. *Nat. Commun.* **11**, 687 (2020).
12. An, R. *et al.* Abnormal decrement on high-frequency repetitive nerve stimulation in congenital myasthenic syndrome with GFPT1 mutations and review of literature. *Front. Neurol.* **13**, 926786 (2022).
13. Bauché, S. *et al.* Mutations in GFPT1-related congenital myasthenic syndromes are associated with synaptic morphological defects and underlie a tubular aggregate myopathy with synaptopathy. *J. Neurol.* **264**, 1791–1803 (2017).
14. Camelo-Filho, A. E. *et al.* Expanding the phenotypic and imaging spectrum of GFPT1-related congenital myasthenic syndromes: a Brazilian case series. *Front. Neurol.* **16**, (2025).
15. Dusl, M. *et al.* A 3'-UTR mutation creates a microRNA target site in the GFPT1 gene of patients with congenital myasthenic syndrome. *Hum. Mol. Genet.* **24**, 3418–3426 (2015).
16. Chen, Q. *et al.* Global N-linked Glycosylation is Not Significantly Impaired in Myoblasts in Congenital Myasthenic Syndromes Caused by Defective Glutamine-Fructose-6-Phosphate Transaminase 1 (GFPT1). *Biomolecules* **5**, 2758–2781 (2015).
17. Guergueltcheva, V. *et al.* Congenital myasthenic syndrome with tubular aggregates caused by GFPT1 mutations. *J. Neurol.* **259**, 838–850 (2012).
18. Jiang, K. *et al.* Diverse myopathological features in the congenital myasthenia syndrome with GFPT1 mutation. *Brain Behav.* **12**, e2469 (2022).
19. Szelinger, S. *et al.* Congenital myasthenic syndrome caused by a frameshift insertion mutation in GFPT1. *Neurol. Genet.* **6**, e468 (2020).

20. Selcen, D. *et al*. GFPT1-myasthenia: clinical, structural, and electrophysiologic heterogeneity. *Neurology* **81**, 370–378 (2013).

21. Issop, Y. *et al*. GFPT1 deficiency in muscle leads to myasthenia and myopathy in mice. *Hum. Mol. Genet.* **27**, 3218–3232 (2018).

22. Missias, A. C., Chu, G. C., Klocke, B. J., Sanes, J. R. & Merlie, J. P. Maturation of the acetylcholine receptor in skeletal muscle: regulation of the AChR gamma-to-epsilon switch. *Dev. Biol.* **179**, 223–238 (1996).

23. Ramanathan, V. K. & Hall, Z. W. Altered Glycosylation Sites of the δ Subunit of the Acetylcholine Receptor (AChR) Reduce αδ Association and Receptor Assembly *. *J. Biol. Chem.* **274**, 20513–20520 (1999).

24. Chen, P.-J., Valenzuela, I. M.-P. y, Aittaleb, M. & Akaaboune, M. AChRs Are Essential for the Targeting of Rapsyn to the Postsynaptic Membrane of NMJs in Living Mice. *J. Neurosci.* **36**, 5680–5685 (2016).

25. Rudell, J. C., Borges, L. S., Yarov-Yarovoy, V. & Ferns, M. The MX-Helix of Muscle nAChR Subunits Regulates Receptor Assembly and Surface Trafficking. *Front. Mol. Neurosci.* **13**, 48 (2020).

26. Vincent, A., Jacobson, L. & Curran, L. *α*-Bungarotoxin binding to human muscle acetylcholine receptor: measurement of affinity, delineation of AChR subunit residues crucial to binding, and protection of AChR function by synthetic peptides. *Neurochem. Int.* **32**, 427–433 (1998).

27. Cetin, H., Beeson, D., Vincent, A. & Webster, R. The Structure, Function, and Physiology of the Fetal and Adult Acetylcholine Receptor in Muscle. *Front. Mol. Neurosci.* **13**, (2020).

28. Eertmoed, A. L. & Green, W. N. Nicotinic Receptor Assembly Requires Multiple Regions throughout the γ Subunit. *J. Neurosci.* **19**, 6298–6308 (1999).
29. Richard, M., Boulin, T., Robert, V. J. P., Richmond, J. E. & Bessereau, J.-L. Biosynthesis of ionotropic acetylcholine receptors requires the evolutionarily conserved ER membrane complex. *Proc. Natl. Acad. Sci.* **110**, (2013).
30. Zhang, J. *et al.* A cohort of GFPT1 related congenital myasthenic syndrome in China: high frequency of c.331 c > t variant. *Orphanet J. Rare Dis.* **20**, 259 (2025).
31. Zou, S. & Pan, B.-X. Post-synaptic specialization of the neuromuscular junction: junctional folds formation, function, and disorders. *Cell Biosci.* **12**, 93 (2022).
32. Zhang, C. *et al.* Ankyrin-dependent Na+ channel clustering prevents neuromuscular synapse fatigue. *Curr. Biol.* **31**, 3810-3819.e4 (2021).
33. Fish, L. A. *et al.* MuSK Regulates Neuromuscular Junction Nav1.4 Localization and Excitability. *J. Neurosci.* **45**, (2025).
34. Katzberg, H. D. & Abraham, A. Electrodiagnostic Assessment of Neuromuscular Junction Disorders. *Neurol. Clin.* **39**, 1051–1070 (2021).
35. Lambert, M. R. & Gussoni, E. Tropomyosin 3 (TPM3) function in skeletal muscle and in myopathy. *Skelet. Muscle* **13**, 18 (2023).
36. Cox-Paulson, E. A. *et al.* Tropomodulin Protects α-Catenin-Dependent Junctional-Actin Networks under Stress during Epithelial Morphogenesis. *Curr. Biol.* **22**, 1500–1505 (2012).
37. Basu, S. *et al.* Acetylcholine Receptor (AChR) Clustering Is Regulated Both by Glycogen Synthase Kinase 3β (GSK3β)-dependent Phosphorylation and the Level of CLIP-associated Protein 2 (CLASP2) Mediating the Capture of Microtubule Plus-ends *. *J. Biol. Chem.* **289**, 30857–30867 (2014).

38. Beckmann, D. *et al.* Focal adhesion protein Lasp1 links the Arp2/3 complex to adherens junctions and promotes motility of arthritic fibroblast-like synoviocytes. *Ann. Rheum. Dis.* **83**, 816–819 (2024).

39. Butt, E. & Raman, D. New Frontiers for the Cytoskeletal Protein LASP1. *Front. Oncol.* **8**, (2018).

40. Li, A. *et al.* Structures of the human adult muscle-type nicotinic receptor in resting and desensitized states. *Cell Rep.* **44**, (2025).

41. Kaaki, S., Cartereau, A., Boussaine, K., Taillebois, E. & Thany, S. H. The stoichiometry of the α4β2 neuronal nicotinic acetylcholine receptors determines the pharmacological properties of the neonicotinoids, and recently introduced butenolide and sulfoximine. *NeuroToxicology* **107**, 1–10 (2025).

42. Mazzaferro, S., Bermudez, I. & Sine, S. M. α4β2 Nicotinic Acetylcholine Receptors: RELATIONSHIPS BETWEEN SUBUNIT STOICHIOMETRY AND FUNCTION AT THE SINGLE CHANNEL LEVEL *. *J. Biol. Chem.* **292**, 2729–2740 (2017).

43. Mazzaferro, S., Kang, G., Natarajan, K., Hibbs, R. E. & Sine, S. M. Structural bases for stoichiometry-selective calcium potentiation of a neuronal nicotinic receptor. *Br. J. Pharmacol.* **181**, 1973–1992 (2024).

44. Zoltowska, K. *et al.* Mutations in GFPT1 that underlie limb-girdle congenital myasthenic syndrome result in reduced cell-surface expression of muscle AChR. *Hum. Mol. Genet.* **22**, 2905–2913 (2013).

45. Kweon, H.-J. *et al.* NACHO Engages N-Glycosylation ER Chaperone Pathways for α7 Nicotinic Receptor Assembly. *Cell Rep.* **32**, 108025 (2020).

46. Gelman, M. S., Chang, W., Thomas, D. Y., Bergeron, J. J. M. & Prives, J. M. Role of the Endoplasmic Reticulum Chaperone Calnexin in Subunit Folding and Assembly of Nicotinic Acetylcholine Receptors (∗). *J. Biol. Chem.* **270**, 15085–15092 (1995).

47. Pratt, S. J. P., Valencia, A. P., Le, G. K., Shah, S. B. & Lovering, R. M. Pre- and postsynaptic changes in the neuromuscular junction in dystrophic mice. *Front. Physiol.* **6**, (2015).

48. Kim, M.-L. *et al.* O-fucosylation of muscle agrin determines its ability to cluster acetylcholine receptors. *Mol. Cell. Neurosci.* **39**, 452–464 (2008).

49. Zong, Y. & Jin, R. Structural mechanisms of the agrin-LRP4-MuSK signaling pathway in neuromuscular junction differentiation. *Cell. Mol. Life Sci. CMLS* **70**, 3077–3088 (2013).

50. Shapira, Y. A. *et al.* Three novel *COLQ* mutations and variation of phenotypic expressivity due to G240X. *Neurology* **58**, 603–609 (2002).

51. Apel, E. D., Glass, D. J., Moscoso, L. M., Yancopoulos, G. D. & Sanes, J. R. Rapsyn is required for MuSK signaling and recruits synaptic components to a MuSK-containing scaffold. *Neuron* **18**, 623–635 (1997).

52. Habes, M., Hénault, C. M. & Baenziger, J. E. Rapsyn-acetylcholine receptor interactions: structural models inform mechanisms of clustering at the neuromuscular junction. *Biophys. Rev.* https://doi.org/10.1007/s12551-025-01386-8 (2025) doi:10.1007/s12551-025-01386-8.

53. Qaisar, R. Fiber-type-specific architecture and pathophysiology of the neuromuscular junction. *Neuroscience* **597**, 13–26 (2026).

54. Structure and Function of Enzymes of the Leloir Pathway for Galactose Metabolism* - Journal of Biological Chemistry. https://www.jbc.org/article/S0021-9258%2820%2982392-8/fulltext.

55. Kroef, V. *et al.* GFPT2/GFAT2 and AMDHD2 act in tandem to control the hexosamine pathway. *eLife* **11**, e69223 (2022).

56. Shi, H. *et al.* Skeletal muscle O-GlcNAc transferase is important for muscle energy homeostasis and whole-body insulin sensitivity. *Mol. Metab.* **11**, 160–177 (2018).

57. Liu, Y. *et al.* O-GlcNAcylation: the “stress and nutrition receptor” in cell stress response. *Cell Stress Chaperones* **26**, 297–309 (2021).

58. Xue, Q., Ji, S., Xu, H. & Yu, S. O-GlcNAcylation: a pro-survival response to acute stress in the cardiovascular and central nervous systems. *Eur. J. Med. Res.* **29**, 174 (2024).

59. Succoio, M., Sacchettini, R., Rossi, A., Parenti, G. & Ruoppolo, M. Galactosemia: Biochemistry, Molecular Genetics, Newborn Screening, and Treatment. *Biomolecules* **12**, 968 (2022).

60. Cardoso, A., Magano, S., Marrana, F. & Andrade, J. P. d-Galactose High-Dose Administration Failed to Induce Accelerated Aging Changes in Neurogenesis, Anxiety, and Spatial Memory on Young Male Wistar Rats. *Rejuvenation Res.* **18**, 497–507 (2015).

61. Fridovich-Keil, J. L. & Berry, G. T. Pathophysiology of long-term complications in classic galactosemia: What we do and do not know. *Mol. Genet. Metab.* **137**, 33–39 (2022).

62. Farshadyeganeh, P. *et al.* Splicing regulation of GFPT1 muscle-specific isoform and its roles in glucose metabolisms and neuromuscular junction. *iScience* **26**, 107746 (2023).

63. Görs, S., Kucia, M., Langhammer, M., Junghans, P. & Metges, C. C. Technical note: Milk composition in mice—Methodological aspects and effects of mouse strain and lactation day. *J. Dairy Sci.* **92**, 632–637 (2009).

64. Altassan, R. *et al.* International consensus guidelines for phosphoglucomutase 1 deficiency (PGM1-CDG): Diagnosis, follow-up, and management. *J. Inherit. Metab. Dis.* **44**, 148–163 (2021).

65. Witters, P. *et al.* Clinical and biochemical improvement with galactose supplementation in SLC35A2-CDG. *Genet. Med. Off. J. Am. Coll. Med. Genet.* **22**, 1102–1107 (2020).

66. Park, J. H. *et al.* SLC39A8 deficiency: biochemical correction and major clinical improvement by manganese therapy. *Genet. Med.* **20**, 259–268 (2018).

67. Morelle, W. *et al.* Galactose Supplementation in Patients With TMEM165-CDG Rescues the Glycosylation Defects. *J. Clin. Endocrinol. Metab.* **102**, 1375–1386 (2017).

68. Boyer, S. W., Johnsen, C. & Morava, E. Nutrition Interventions in Congenital Disorders of Glycosylation. *Trends Mol. Med.* **28**, 463–481 (2022).

69. Ye, L., Sun, Y., Jiang, Z. & Wang, G. L-Serine, an Endogenous Amino Acid, Is a Potential Neuroprotective Agent for Neurological Disease and Injury. *Front. Mol. Neurosci.* **14**, 726665 (2021).

70. Manole, A. *et al.* Clinical, pathological and functional characterization of riboflavin-responsive neuropathy. *Brain* **140**, 2820–2837 (2017).

71. Distelmaier, F., Haack, T. B., Wortmann, S. B., Mayr, J. A. & Prokisch, H. Treatable mitochondrial diseases: cofactor metabolism and beyond. *Brain* **140**, e11 (2017).

72. Lee, B. E., Suh, P.-G. & Kim, J.-I. O-GlcNAcylation in health and neurodegenerative diseases. *Exp. Mol. Med.* **53**, 1674–1682 (2021).

73. Zhang, R. *et al.* Muscle-specific lack of GFPT1 in knock-in mice triggers ER stress to alleviate misfolded proteins. *Dis. Model. Mech.* dmm.050768 (2024) doi:10.1242/dmm.050768.

74. Finsterer, J. Congenital myasthenic syndromes. *Orphanet J. Rare Dis.* **14**, 57 (2019).

75. Beeson, D. Chapter 5 - Congenital myasthenic syndromes. in *Handbook of Clinical Neurology* (ed. Hanna, M. G.) vol. 203 69–88 (Elsevier, 2024).

76. Chang, I. J., He, M. & Lam, C. T. Congenital disorders of glycosylation. *Ann. Transl. Med.* **6**, 477 (2018).

77. Sturiale, L., Barone, R. & Garozzo, D. The impact of mass spectrometry in the diagnosis of congenital disorders of glycosylation. *J. Inherit. Metab. Dis.* **34**, 891–899 (2011).

78. Kolset, S. O. & Tveit, H. Serglycin – Structure and biology. *Cell. Mol. Life Sci. CMLS* **65**, 1073–1085 (2007).

79. Korpetinou, A. *et al.* Serglycin: At the Crossroad of Inflammation and Malignancy. *Front. Oncol.* **3**, (2014).

80. Scully, O. J., Chua, P.-J., Harve, K. S., Bay, B.-H. & Yip, G. W. Serglycin in Health and Diseases. *Anat. Rec.* **295**, 1415–1420 (2012).

81. Chompoopong, P. & Milone, M. GDP-Mannose Pyrophosphorylase B (GMPPB)-Related Disorders. *Genes* **14**, 372 (2023).

82. He, K. *et al.* Decoding the glycoproteome: a new frontier for biomarker discovery in cancer. *J. Hematol. Oncol.J Hematol Oncol* **17**, 12 (2024).

83. Franco-Romero, A., Sandri, M. & Schiaffino, S. Autophagy in Skeletal Muscle. *Cold Spring Harb. Perspect. Biol.* **17**, a041565 (2025).

84. Gómez-Virgilio, L. *et al.* Autophagy: A Key Regulator of Homeostasis and Disease: An Overview of Molecular Mechanisms and Modulators. *Cells* **11**, 2262 (2022).

85. Mo, J., Chen, J. & Zhang, B. Critical roles of FAM134B in ER-phagy and diseases. *Cell Death Dis.* **11**, 983 (2020).

86. Lyu, P. & Jiang, H. RNA-Sequencing Reveals Upregulation and a Beneficial Role of Autophagy in Myoblast Differentiation and Fusion. *Cells* **11**, 3549 (2022).

87. Hetz, C., Zhang, K. & Kaufman, R. J. Mechanisms, regulation and functions of the unfolded protein response. *Nat. Rev. Mol. Cell Biol.* **21**, 421–438 (2020).

88. Wang, Z. V. *et al.* Spliced X-box Binding Protein 1 Couples the Unfolded Protein Response to Hexosamine Biosynthetic Pathway. *Cell* **156**, 1179–1192 (2014).

89. Zhao, L., Feng, Z., Yang, X. & Liu, J. The regulatory Roles of O-GlcNAcylation in mitochondrial Homeostasis and metabolic Syndrome. *Free Radic. Res.* **50**, 1080–1088 (2016).

90. Gang, Q. *et al.* Genetic defects are common in myopathies with tubular aggregates. *Ann. Clin. Transl. Neurol.* **9**, 4–15 (2021).

91. Bisnett, B. J., Condon, B. M., Lamb, C. H., Georgiou, G. R. & Boyce, M. Export Control: Post-transcriptional Regulation of the COPII Trafficking Pathway. *Front. Cell Dev. Biol.* **8**, (2021).

92. Cox, N. J. *et al.* Dynamic Glycosylation Governs the Vertebrate COPII Protein Trafficking Pathway. *Biochemistry* **57**, 91–107 (2018).

93. Zhang, J. & Wang, Y. Emerging roles of O-GlcNAcylation in protein trafficking and secretion. *J. Biol. Chem.* **300**, 105677 (2024).

94. Han, S. *et al.* Modulation of synaptic transmission through O-GlcNAcylation. *Mol. Brain* **17**, 1 (2024).

95. Interorganellar Regulation of Lysosome Positioning by the Golgi Apparatus through Rab34 Interaction with Rab-interacting Lysosomal Protein | Molecular Biology of the Cell. https://www.molbiolcell.org/doi/10.1091/mbc.E02-05-0280.

96. Jain Goyal, M. *et al.* A paralog-specific role of COPI vesicles in the neuronal differentiation of mouse pluripotent cells. *Life Sci. Alliance* **3**, e202000714 (2020).

97. Jing, J., Wang, B. & Liu, P. The Functional Role of SEC23 in Vesicle Transportation, Autophagy and Cancer. *Int. J. Biol. Sci.* **15**, 2419–2426 (2019).

98. Xue, Q., Yan, R., Ji, S. & Yu, S. Regulation of mitochondrial network homeostasis by O-GlcNAcylation. *Mitochondrion* **65**, 45–55 (2022).

99. Sacoman, J. L., Dagda, R. Y., Burnham-Marusich, A. R., Dagda, R. K. & Berninsone, P. M. Mitochondrial O-GlcNAc Transferase (mOGT) Regulates Mitochondrial Structure, Function, and Survival in HeLa Cells. *J. Biol. Chem.* **292**, 4499–4518 (2017).

100. Jóźwiak, P. *et al.* Mitochondrial O-GlcNAc Transferase Interacts with and Modifies Many Proteins and Its Up-Regulation Affects Mitochondrial Function and Cellular Energy Homeostasis. *Cancers* **13**, 2956 (2021).

101. Akinbiyi, E. O. *et al.* Blocked O-GlcNAc cycling alters mitochondrial morphology, function, and mass. *Sci. Rep.* **11**, 22106 (2021).

102. Substantial downregulation of mitochondrial and peroxisomal proteins during acute kidney injury revealed by data-independent acquisition proteomics - Burton - 2024 - PROTEOMICS - Wiley Online Library. https://analyticalsciencejournals.onlinelibrary.wiley.com/doi/10.1002/pmic.202300162.

103. Suh, J. & Lee, Y.-S. Mitochondria as secretory organelles and therapeutic cargos. *Exp. Mol. Med.* **56**, 66–85 (2024).

104. Amorim, J. A. *et al.* Mitochondrial and metabolic dysfunction in ageing and age-related diseases. *Nat. Rev. Endocrinol.* **18**, 243–258 (2022).

105. Bhatti, J. S., Bhatti, G. K. & Reddy, P. H. Mitochondrial dysfunction and oxidative stress in metabolic disorders — A step towards mitochondria based therapeutic strategies. *Biochim. Biophys. Acta BBA - Mol. Basis Dis.* **1863**, 1066–1077 (2017).

106. Cork, G. K., Thompson, J. & Slawson, C. Real Talk: The Inter-play Between the mTOR, AMPK, and Hexosamine Biosynthetic Pathways in Cell Signaling. *Front. Endocrinol.* **9**, (2018).

107. Kim, J., Kundu, M., Viollet, B. & Guan, K.-L. AMPK and mTOR regulate autophagy through direct phosphorylation of Ulk1. *Nat. Cell Biol.* **13**, 132–141 (2011).

108. Gélinas, R. *et al.* AMP-Activated Protein Kinase and O-GlcNAcylation, Two Partners Tightly Connected to Regulate Key Cellular Processes. *Front. Endocrinol.* **9**, 519 (2018).

109. Gang, Q. *et al.* Genetic defects are common in myopathies with tubular aggregates. *Ann. Clin. Transl. Neurol.* **9**, 4–15 (2021).

110. Böhm, J. *et al.* Constitutive Activation of the Calcium Sensor STIM1 Causes Tubular-Aggregate Myopathy. *Am. J. Hum. Genet.* **92**, 271–278 (2013).

111. Sallinger, M. *et al.* Luminal STIM1 Mutants that Cause Tubular Aggregate Myopathy Promote Autophagic Processes. *Int. J. Mol. Sci.* **21**, 4410 (2020).

112. Kaplan, M. M. & Flucher, B. E. Postsynaptic CaV1.1-driven calcium signaling coordinates presynaptic differentiation at the developing neuromuscular junction. *Sci. Rep.* **9**, 18450 (2019).

113. Valina, A. A. *et al.* Functional amyloid protein FXR1 is recruited into neuronal stress granules. *Prion* **19**, 1–16.

114. Skoven, C. S. *et al.* Axonal structure-function relationships across experimental modalities. *Imaging Neurosci.* **3**, IMAG.a.1058 (2025).

115. Newman, B. T. *et al.* Conduction velocity, G-ratio, and extracellular water as microstructural characteristics of autism spectrum disorder. *PLOS ONE* **19**, e0301964 (2024).

116. Gow, A. Demystifying The Myelin *g* Ratio: Its Origin, Derivation and Interpretation. *ASN Neuro* **17**, 2542166 (2025).

117. Suh, Y. H. *et al.* A neuronal role for SNAP-23 in postsynaptic glutamate receptor trafficking. *Nat. Neurosci.* **13**, 338–343 (2010).

118. Kaul, S., Mittal, S. K., Feigenbaum, L., Kruhlak, M. J. & Roche, P. A. Expression of the SNARE Protein SNAP-23 Is Essential for Cell Survival. *PLoS ONE* **10**, e0118311 (2015).

119. Bugarcic, A. *et al.* Vps26A and Vps26B subunits define distinct retromer complexes. *Traffic* **12**, 1759–1773 (2011).

120. Sugiura, Y. & Lin, W. Neuron–glia interactions: the roles of Schwann cells in neuromuscular synapse formation and function. *Biosci. Rep.* **31**, 295–302 (2011).

121. Selenoprotein S: Deciphering the function in endoplasmic reticulum stress resolution: Biophysical Journal. https://www.cell.com/biophysj/fulltext/S0006-3495(23)03607-X.

122. Oka, O. B. V. *et al.* Activation of the UPR sensor ATF6α is regulated by its redox-dependent dimerization and ER retention by ERp18. *Proc. Natl. Acad. Sci. U. S. A.* **119**, e2122657119 (2022).

123. Pobre, K. F. R., Poet, G. J. & Hendershot, L. M. The endoplasmic reticulum (ER) chaperone BiP is a master regulator of ER functions: Getting by with a little help from ERdj friends. *J. Biol. Chem.* **294**, 2098–2108 (2019).

124. Favero, C. B. *et al.* Mutation of the BiP/GRP78 gene causes axon outgrowth and fasciculation defects in the thalamocortical connections of the mammalian forebrain. *J. Comp. Neurol.* **521**, 677–696 (2013).

125. Correlation between evoked neurotransmitter release and adaptive functions in SYT1-associated neurodevelopmental disorder - eBioMedicine. https://www.thelancet.com/journals/ebiom/article/PIIS2352-3964(24)00452-3/fulltext.

126. The Rab3 family proteins in age-related neurodegeneration: unraveling molecular pathways and potential therapeutic targets | npj Aging. https://www.nature.com/articles/s41514-025-00257-6.

127. Francisco, R. *et al.* Congenital disorders of glycosylation (CDG): state of the art in 2022. *Orphanet J. Rare Dis.* **18**, 329 (2023).

128. Verheijen, J., Tahata, S., Kozicz, T., Witters, P. & Morava, E. Therapeutic approaches in Congenital Disorders of Glycosylation (CDG) involving N-linked glycosylation: an update. *Genet. Med.* **22**, 268–279 (2020).

129. Parker, M. P., Peterson, K. R. & Slawson, C. O-GlcNAcylation and O-GlcNAc Cycling Regulate Gene Transcription: Emerging Roles in Cancer. *Cancers* **13**, 1666 (2021).

130. Nakamura, S., Nakano, S., Nishii, M., Kaneko, S. & Kusaka, H. Localization of O-GlcNAc-modified proteins in neuromuscular diseases. *Med. Mol. Morphol.* **45**, 86–90 (2012).

131. Helman, G. *et al.* Leukoencephalopathy due to variants in GFPT1-associated congenital myasthenic syndrome. *Neurology* **92**, e587–e593 (2019).

132. Höhfeld, J. *et al.* Maintaining proteostasis under mechanical stress. *EMBO Rep.* **22**, e52507 (2021).

133. Klas, K. *et al.* Risk and Benefit for Basket Trials in Oncology: A Systematic Review and Meta-Analysis. *Target. Oncol.* **20**, 89–101 (2025).

7.0 Additional Resources

The following sections contains printed copies of the following manuscripts referenced in my doctoral thesis. Please note, only the second paper required a copy license to include within the manuscript as MDPI does not require this under the open access publishing agreement.

1. Holland SH, Carmona-Martinez R, O'Connor K, O'Neil D, Roos A, Spendiff S, Lochmüller H. A Deficiency in Glutamine-Fructose-6-Phosphate Transaminase 1 (Gfpt1) in Skeletal Muscle Results in Reduced Glycosylation of the Delta Subunit of the Nicotinic Acetylcholine Receptor (AChRδ). Biomolecules. 2024 Oct 3;14(10):1252. doi: 10.3390/biom14101252. PMID: 39456185; PMCID: PMC11506803.
2. Holland SH, Carmona-Martinez R, O'Neil D, Ho K, O'Connor K, Azuma Y, Roos A, Spendiff S, Lochmüller H. Galactose treatment rescues neuromuscular junction transmission in glutamine-fructose-6-phosphate transaminase 1 (Gfpt1) deficient mice. Hum Mol Genet. 2025 Oct 14;34(21):1765-1779. doi: 10.1093/hmg/ddaf140. PMID: 40879313; PMCID: PMC12529661.
3. Holland SH, Carmona-Martinez R, Hentschel A, Derksen A, O'Connor K, O'Neil D, Ho K, Baird SD, Roos A, Spendiff S, Lochmüller H. Hexosamine Pathway Disruption by GFPT1 Loss Drives Coordinated Defects in Glycosylation, Autophagy, and Trafficking. Biomolecules. 2026 Jun 30;16(7):966. doi: 10.3390/biom16070966. PMID: 42509760; PMCID: PMC13406536.
4. Pugliese A, Holland SH, Rodolico C, Lochmüller H, Spendiff S. Presynaptic Congenital Myasthenic Syndromes: Understanding Clinical Phenotypes through In vivo Models. J Neuromuscul Dis. 2023;10(5):731-759. doi: 10.3233/JND-221646. PMID: 37212067; PMCID: PMC10578258.

biomolecules

MDPI

Article

A Deficiency in Glutamine-Fructose-6-Phosphate Transaminase 1 (Gfpt1) in Skeletal Muscle Results in Reduced Glycosylation of the Delta Subunit of the Nicotinic Acetylcholine Receptor (AChRδ)

Stephen Henry Holland [1,2,3], Ricardo Carmona-Martinez [1], Kaela O'Connor [1,2], Daniel O'Neil [1], Andreas Spendiff [1] and Hanns Lochmüller [1,2,3,6,7,*]

[2] Department of Cellular and Molecular Medicine, Faculty of Medicine, University of Ottawa, Ottawa, ON K1N 6N5, Canada

[3] Dr. Eric Poulin Center for Neuromuscular Disorders, Brain and Mind Research Institute, University of Ottawa, Ottawa, ON K1N 6N5, Canada

[4] Department of Pediatric Neurology, Center for Neuromuscular Disorders, Centre for Translational Neuro- and Behavioral Sciences, University Duisburg-Essen, 45147 Essen, Germany

[5] Medical Faculty, University Hospital Düsseldorf, Heinrich Heine University, 40225 Düsseldorf, Germany

[6] Faculty of Medicine, Medical Center, University of Freiburg, 79085 Freiburg, Germany

[7] Centro Nacional de Analisis Genomico (CNAG), 08028 Barcelona, Spain

check for updates

Citation: Holland, S.H.; CarmonaMartinez, R.; O'Connor, K.; O'Neil, D.; Roos, A.; Spendiff, S.; Lochmüller, H. A Deficiency in Glutamine-Fructose-6-Phosphate Transaminase 1 (Gfpt1) in Skeletal Muscle Results in Reduced Glycosylation of the Delta Subunit of the Nicotinic Acetylcholine Receptor (AChRδ). *Biomolecules* **2024**, *14*, 1252. https://doi.org/10.3390/ biom14101252

Academic Editor: Rosario Francesco Donato

Received: 12 August 2024
Revised: 25 September 2024
Accepted: 28 September 2024 Published: 3 October 2024

[1] Children's Hospital of Eastern Ontario Research Institute, Ottawa, ON K1H 8L1, Canada

Abstract: The neuromuscular junction (NMJ) is the site where the motor neuron innervates skeletal muscle, enabling muscular contraction. Congenital myasthenic syndromes (CMS) arise when mutations in any of the approximately 35 known causative genes cause impaired neuromuscular transmission at the NMJ, resulting in fatigable muscle weakness. A subset of five of these CMS-causative genes are associated with protein glycosylation. Glutamine-fructose-6-phosphate transaminase 1 (Gfpt1) is the rate-limiting enzyme within the hexosamine biosynthetic pathway (HBP), a metabolic pathway that produces the precursors for glycosylation. We hypothesized that deficiency in Gfpt1 expression results in aberrant or reduced glycosylation, impairing the proper assembly and stability of key NMJ-associated proteins. Using both in vitro and in vivo Gfpt1deficient models, we determined that the acetylcholine receptor delta subunit (AChRδ) has reduced expression and is hypo-glycosylated. Using laser capture microdissection, NMJs were harvested from Gfpt1 knockout mouse muscle. A lower-molecular-weight species of AChRδ was identified at the NMJ that was not detected in controls. Furthermore, Gfpt1-deficient muscle lysates showed impairment in protein OGlcNAcylation and sialylation, suggesting that multiple glycan chains are impacted. Other key NMJ-associated proteins, in addition to AChRδ, may also be differentially glycosylated in Gfpt1-deficient muscle.

Keywords: glutamine-fructose-6-phosphate transaminase 1 (Gfpt1); congenital myasthenic syndrome (CMS); neuromuscular junction (NMJ); O-GlcNAcylation; acetylcholine receptor delta subunit (AChRδ); glycosylation

1. Introduction

Glycosylation, the attachment of sugar moieties to proteins, is the most common post-translational modification (PTM) associated with maintaining the structure, function, stability, and localization of proteins within the cell. Initiated within the endoplasmic reticulum (ER), these modifications are diverse in nature, ranging from the addition of a simple sugar to complex glycan chains with many branching points. Underscoring the vital role of glycans in protein homeostasis, many mutations to key genes associated with the glycosylation process are embryonically lethal [1,2]. However, some mutations within glycosylation enzymes correspond to a host of disorders called congenital disorders of glycosylation (CDGs), which typically have severe clinical manifestations impacting multiple organs and systems [3,4].

Numerous inherited muscle disorders have been associated with defects in glycosylation affecting primarily, the alpha-dystroglycan protein, including Fukuyama congenital muscular dystrophy (FCMD) [5,6], Walker–Warburg syndrome [7–10], congenital muscular dystrophy type 1C and 1D (MDC1C/D) [11–14], limb–girdle muscular dystrophy type 2I [15,16], muscle–eye–brain disease [17], Duchene's Muscular Dystrophy [18] and GNE Myopathy [19].

The neuromuscular junction (NMJ) mediates the transmission of chemical signals from the pre-synaptic nerve terminal to the post-synaptic skeletal muscle, enabling muscular contraction. Congenital myasthenic syndromes (CMS) are early onset inheritable neuromuscular disorders that result from mutation to proteins that are associated with NMJ development, function, maintenance, and/or organization of the motor endplate [20]. Clinically, CMS are heterogeneous in nature but are typically characterized by fatigable muscle weakness to facial, bulbar, ocular, truncal, respiratory, limb, and/or girdle muscles [20]. A subset of five of the CMS causative genes impair protein glycosylation and results in CMS. These include glutamine-fructose-6-phosphate transaminase 1 (*GFPT1*) [21–29], dolicholphosphate N-acetylglucosaminephosphotransferase-1 (*DPAGT1*) [30–33], GDP-mannose pyrophosphorylase B (*GMPPB*) [34,35], α-1,3/1,6mannosyltransferase (*ALG2*) [36–38], and UDP-N-acetylglucosaminyltransferase subunit 14 (*ALG14*) [36,38].

Gfpt1 is the rate-limiting enzyme of the hexosamine biosynthetic pathway (HBP), a metabolic signaling pathway that produces the precursor uridine diphosphate N-acetylglucosamine (UDPGlcNAc) required for N- and O-linked protein glycosylation [39,40]. The HBP metabolizes key nutrients, such as uridine triphosphate, glucose, glutamine, and acetyl-CoA, allowing for the regulation of integral processes such as cell growth [41,42], differentiation [43], stem cell differentiation [44], metabolic reprogramming [41,42], ER homeostasis [45–47], transcriptional control [48], and cancer pathogenesis [42]. UDPGlcNAc is also involved in the creation of N-linked glycans through the conversion to the lipid carrier dolichol-phosphate (Dol-P) and in protein sialylation as a substrate of the UDP-GlcNAc epimerase 2 (*GNE*) enzyme [49,50]. As such, impairment in HBP activity could be associated with a deficiency in the development of a variety of glycan side chains.

Biallelic mutations to *GFPT1* cause CMS characterized by fatigable limb–girdle muscle weakness, commonly presenting in the first years of life [22–24,26,28]. GFPT1-CMS muscle fibers contain tubular aggregates, which may originate from the sarcoplasmic reticulum, but their exact molecular origin remains unknown [26]. At the NMJ, GFPT1-CMS patients have reduced postsynaptic folding, reducing the efficiency of neuromuscular communication [25]. The biallelic mutations to *GFPT1* result in a decrease in GFPT1 protein levels and/or impaired enzymatic activity, which may result in reduced or aberrant glycosylation [22,24,27,51]. However, glycomics of GFPT1CMS patient myoblasts revealed no difference in global N-linked glycan chain development, while defective N-linked glycosylation has been shown in other GFPT1 CMS patient-derived myoblasts [21,52]. This suggests the need to study muscle cells molecularly to obtain insights into the underlying pathophysiology.

GFPT1 has been linked to protein O-GlcNAcylation, a reversible and highly dynamic modification that regulates biological function [53,54], stability, localization [48], protein– protein interactions [55], and transcriptional control [48,54]. O-GlcNAcylation involves the binding of a single GlcNAc moiety, prepared by the HBP, to serine and threonine residues on a protein via a βconfigured O-glycosidic bond [56,57]. This is a reversible modification regulated by two enzymes: oligotransferase (OGT) and O-GlcNAcase (OGA) [57]. In skeletal muscle, O-GlcNAcylation remains an important regulator of the immune response [54], glucose metabolism, insulin sensitivity [53], contractile properties [55], and structural elements [55]. Impairment appears to be detrimental to various components of muscle health, and control of O-GlcNAcylation is important for various aspects of muscle function [55,58]. However, studies remain unclear whether GFPT1-deficiency impedes O-GlcNAcylation of NMJ-associated proteins. Elucidating the role of GFPT1 in protein glycosylation at the NMJ may not only reveal pathomechanisms of disease but also hint toward novel treatment strategies for CMS patients.

In this study, we hypothesize that deficient expression and enzymatic activity of GFPT1 impair protein glycosylation, resulting in the dysfunction of NMJ-associated processes. We used a previously published *Gfpt1*-CMS mouse with muscle-specific removal of GFPT1 expression, termed *Gfpt1*$^{tm1d/tm1d}$, which recapitulates clinical features and muscle pathology of human GFPT1-CMS, including exercise-induced skeletal muscle weakness, and tubular aggregates [23,25,26]. We identified a lower-molecular-weight species of the acetylcholine receptor delta subunit (AChRδ) in the *Gfpt1*-CMS mouse. Finally, we confirmed that *Gfpt1*deficient mice show overall impaired OGlcNAcylation levels, resulting in impairment to downstream glycan chain development.

2. Materials and Methods

2.1. Animal Husbandry

Animals were housed at the University of Ottawa Animal Care and Veterinary Facility (Roger Guidon Hall, Ottawa, ON, Canada), and all breeding and experimental protocols were approved by the internal Animal Care Committee (protocols: breeding—CHEO3089 and experimental—CHEO3120 approved on 16 November 2018 and 2 April 2019, respectively). Mice were maintained on a 12 hr light–dark cycle, with access to food and water ad libitum. Mice were generated and genotyped as previously reported [25]. For this study, Tm1C homozygous mice (containing the two LoxP sites flanking the 7th exon of *Gfpt1* but lacking *Ckm-Cre* expression) were used as controls. *Gfpt1*$^{tm1d/tm1d}$ contains two LoxP sites flanking the 7th exon of *Gfpt1* but also contains *Ckm-Cre* to create a skeletal muscle-specific knockout of *Gfpt1* [25]. Previously, *Gfpt1*$^{tmqd/tm1d}$ mice were characterized as having knocked out Gfpt1 protein levels within cardiac and muscle tissues [25]. Also, Gfpt1 expression was found in brain and kidney, demonstrating that this model is a Gfpt1 muscle-specific knockout [25]. Mice were monitored and weighed three times per week and underwent a number of behavioral tests (see below) before tissue collection at 40 weeks.

2.2. Inverted Screen Test

This was performed as described [25]. To briefly summarize, animals were suspended from an inverted wire grid, and the time to fall was recorded, with a cap of 10 min. Mice had a 30 min rest, and the test was repeated. The average time was recorded and normalized to body weight to calculate hanging impulse (g × s). This behavioral test was performed weekly.

2.3. Grip Strength and Fatiguability Measurements

Repetitive grip strength measurements were conducted weekly with 8 consecutive recordings on a grip strength meter (Chatillon DFE II Grip Meter, Columbus Instruments, Columbus, OH, USA). Repetitive grip strength measurements were first conducted on the front paws. Animals then had a 30 min rest period, followed by all four paws measurements. To calculate grip strength fatigability, all measurements were normalized to body weight (g) prior to calculation:

$$= \left(\frac{\textit{Average of first four measurements} - \textit{Average of last four measurements}}{\textit{Average of measurements}} \quad \textit{Muscle Fatigability \%} \right.$$

2.4. EchoMRI and Total Activity Measurements

EchoMRI body composition measurements of fat mass and lean mass were recorded weekly using the EchoMRI-700 Body Composition Analyzer (EchoMRI, Houston, TX, USA). Animals also underwent 24 h open activity monitoring using the Phenotyper™ system (Noldus Information Technology, Leesburg, VA, USA) at week 35. Total distance traveled was calculated using Phenotyper™ analysis software (EthoVision v15, Noldus Information Technology).

2.5. Electrophysiology and Repetitive Nerve Stimulation

Electromyography (EMG) was performed on a *Gfpt1*$^{tm1d/tm1d}$ and Tm1C homozygous mouse to examine compound muscle action potential (CMAP) and repetitive nerve stimulation (RNS) decrement with the Cadwell Sierra Summit EMG. Mice were anesthetized with isoflurane (Baxter,

#CA2L9108, Toronto, ON, Canada) prior to experimentation. To examine CMAP and RNS, recording electrodes (Cadwell US, #302353-000-100, Kennewick, WA, USA) were placed on the skin near the proximal portion of the *gastrocnemius* muscle of the hind limb, and the second electrode was placed in the *tibialis anterior*. For stimulation of the sciatic nerve, two electrodes (cathode and anode) were inserted into the proximal hind limb and subcutaneous tissue overlaying the sacrum, respectively. Submaximal CMAP responses were performed by stimulation of the sciatic nerve with a square-wave pulse of 0.1 ms duration and an intensity range of 1 to 10 mA. CMAP response was increased in stimulus intensity until the amplitude of the response was seen on the monitor. To perform RNS, a stimulation series of 8 separate twitch contractions were elicited by 10 pulses ranging between 3 Hz and 20 Hz. The stimulation series was repeated after a rest of 30 s between measurements. Decrement was then calculated between the first and the fifth stimulus. CMAP and RNS calculations were performed with the Cadwell Sierra Summit software (Version 3.1.541) using a computer with Windows 10. Mice were euthanized after the recording without regaining consciousness.

2.6. Immunostaining for NMJs in Whole Muscle Mounts

Soleus muscles were fixed in 2% paraformaldehyde (PFA) for 20 min. Skeletal muscle fibers were then separated into small bundles and placed in 2% PFA overnight. The fibers were washed with phosphate-buffered saline (PBS) (Sigma, #P4417, Oakville, ON, Canada) and then placed in ice-cold Analar ethanol, then methanol for 10 min each. Fibers were then transferred to blocking/permeabilization solution (5% horse serum, 5% bovine serum albumin, 1% Triton X-100 (Sigma, #X100, Oakville, ON, Canada) in PBS) and incubated for 4 h. The muscle fibers were then incubated with anti-SV2 (DSHB, 1:100, University of Iowa, Iowa City, IA, USA) and neurofilament (DSHB (2H3), 1:100, University of Iowa, Iowa City, IA, USA) in 5% horse serum, 5% BSA, for 24 h.

Fibers were then washed with PBS for 4 h and incubated with secondary antibodies: alphabungarotoxin-488 (Invitrogen, #B13422, 1:200, Burlington, ON, Canada) and Alexa Fluor antimouse-568 (Life Technologies, #A11031, 1:250, Toronto, ON, Canada) overnight. Following this incubation, the muscle fibers were washed with PBS for 4 h and mounted on glass microscope slides using Vectashield® Antifade Mounting Medium (Vector Laboratories, #H-1000-10, Newark, CA, USA). Prior to mounting the tissue, several layers of electrical tape were used to create a well to hold the tissue in place.

NMJ z-stacks were captured using a confocal microscope (Olympus Fluoview FV1000, Olympus, Richmond Hill, ON, Canada) at 63× magnification and converted to maximum-intensity projections. Image acquisition was performed sequentially with constant microscope settings.

2.7. Labeling of NMJs for Laser Capture Microdissection

Gastrocnemius muscles were isolated from mice, embedded in O.C.T compound (Fisher Healthcare Tissue-Plus™, FisherScientific, #23-730-571, Ottawa, ON, Canada), and stored at −80 °C until sectioning. Gastrocnemius muscles were cryosectioned (Leica Biosystems, CM1860, Concord, ON, Canada) longitudinally at 10 µm, placed on Superfrost™ Plus glass microscope slides (FisherScientific, #12-55015), and air-dried for 1 h at room temperature. Sections were fixed with ice-cold acetone for 15 min at 4 °C and washed with PBS. Next, sections were incubated with permeabilization solution (PBS, 0.1% Triton X-100) for 15 min at room temperature, then washed with PBS. Then, muscle sections were incubated with blocking buffer (1% BSA, 10% normal goat serum (NGS) in PBS) for 30 min at room temperature. Finally, the muscle sections were incubated with α-bungarotoxin-594 (Fisher Scientific, #B13423, 1:100, Ottawa, ON, Canada) for 2 h and washed with PBS. Muscle sections were stored at 4 °C and allowed to air dry for 1 h before laser capture microdissection.

2.8. Laser Capture of NMJs

NMJs were identified using a PALM MicroBeam laser capture microdissection microscope at 20× magnification (Carl Zeiss Laser Microdissection, PALMRobo 48 FTSS355-Laser System, Dorval,

QC, Canada). The laser speed during cutting was set at 5%, while the laser energy was set to 70 Hz, with a Delta of 60 Hz.

NMJs and neighboring laser-captured muscle were collected in separate Zeiss AdhesiveCap opaque 500 Eppendorf tubes (Zeiss, #415190-9201-000, Dorval, QC, Canada). Proteins were extracted by incubating the samples with RIPA buffer (containing phosphatase and protease inhibitors) for 1 h on ice, followed by centrifugation (Sorvall Legend Micro 21 R, ThermoScientific™, Ottawa, ON, Canada) at 15,000× *g* for 20 min. The supernatants were combined with Laemmli buffer and boiled at 100 °C for 5 min, and proteins were resolved with SDS-PAGE.

2.9. Cell Culture

C2C12 cells (ATCC, #CRL-1722, Burlington, ON, Canada) were cultured in Dulbecco's Modified Eagle Medium (DMEM) high-glucose media supplemented with 10% fetal bovine serum (FBS), 1% glutamine, and 1% penicillin/streptomycin. When myoblasts reached 95% confluence, the cells were washed with PBS, and the growth medium was replaced with differentiation medium (DMEM high glucose, 2% horse serum, and 1% penicillin/streptomycin) to promote myoblast fusion into myotubes. After five days, C2C12 myotubes were imaged with phase-contrast light microscopy (EVOS Cell Imaging Systems, Thermofisher, Ottawa, ON, Canada) confirm the presence of myotubes (elongated cells with more than one nuclei). All cell experiments were maintained in a humidified environment at 37 °C with 5% CO_2.

The GFPT1/Gfpt1 inhibitor, 6-diazo-5-oxo-l-norleucine (DON) (500 µM, Sigma, #D2141, Oakville, ON, Canada), and the Oga inhibitor Thiamet-G (TG) (5 µM, Cayman, #13237, Ann Arbor, MI, USA) were administered for 48 h.

2.10. Transducing C2C12 Cells with Lentiviruses Expressing shGfpt1 Transgenes

C2C12 cells were transduced with a lentivirus encoding a tetracycline repressor (TET-R) transgene (VectorBuilder, pLV(EXP)-CMV>tTS/rtTA/Hygro, Vector ID: VB1611221052kwm, Chicago, IL, USA) at multiplicities of infection (MOIs) ranging from 1 to 500.
Selective pressures were applied by adding 500 µg/mL of hygromycin B (Sigma, #400053, Oakville, ON, Canada) to generate a polyclonal stable cell line. *TET-R* expression was confirmed through RT-qPCR. C2C12 polyclonal TET-R positive cells were seeded to generate single-cell monoclonal colonies expressing TET-R.

Monoclonal TET-R positive C2C12 cells were then infected with lentiviruses containing the transgenes for either a scramble sequence (Vector ID: VB200625-1130ssr), shGfpt1 #1 (Vector ID: VB200624-1008wvj), or shGfpt1 #2 (Vector ID: VB200625-1131yeg), each containing a tetracycline promoter and an eGFP reporter. C2C12 cells were infected with these viruses at varying Multiplicity of Infections (MOIs), and 5 µg/mL of puromycin (Life Technologies, #A1113803, Toronto, ON, Canada) was applied as a selective pressure to establish a stable polyclonal expressing cell line.

To induce the expression of the transgenes, 2 µg/mL of doxycycline (Sigma, #D9891) was added. After 48 h, eGFP expression in lentiviral-infected C2C12 cells was documented using an EVOS cell imager. Polyclonal colonies were individually assessed to confirm the knockdown of Gfpt1 and subsequent activation of eGFP signal before monoclonal colony expansion.

2.11. Fluorescence-Activated Cell Sorting (FACS) of Gfpt1-Deficient C2C12 Myoblasts

Doxycycline-inducible scramble, shGfpt1 #1, and shGfpt1 #2 C2C12 myoblasts were seeded onto 15 cm plates and treated with 2 µg/mL of doxycycline for 72 h. eGFP expression was assessed via an EVOS cell imager prior to FACS (Sony Biotechnologies SH800 Cell Sorter, San Jose, CA, USA). C2C12 cells were trypsinized, centrifuged, and prepared to a concentration of 1.0×10^6 cells/mL. Dead cells were identified with 1 µg/mL of propidium iodide (PI) (STEMCELL Technologies, #75002, Vancouver, BC, Canada).

Cells were then sorted into the following groups: eGFP−/PI−, eGFP+/PI−, eGFP−/PI+, and eGFP+/PI+. Subsequently, eGFP+/PI− and eGFP−/PI+ populations were used to establish gates for removing any autofluorescence signal. Finally, a final population of eGFP+/PI+ cells was isolated and plated into a 6-well plate for expansion.

2.12. Gfpt1 Enzymatic Activity Assay

The enzymatic activity of Gfpt1 was measured using the glutamate dehydrogenase method, as previously reported [22,51]. C2C12 cells were treated with a range of doses (between 0 µM and 500 µM) of Gfpt1 inhibitor DON for 48 h. Additionally, scramble, shGfpt1 #1, and shGfpt1 #2 C2C12 myotubes were assessed for Gfpt1 enzymatic activity after 72 h of induction with 2 µg/mL of doxycycline. The change in absorbance is monitored at a wavelength of 370 nm (OD370) with a spectrophotometer microplate reader
(BioTek Synergy HTX Multimode Reader, Santa Clara, CA, USA) using Agilent Biotek Gen5 software v2.06. The enzymatic activity of each condition was normalized to the Gfpt1 protein levels determined by Western blot. All measurements were performed in triplicate.

2.13. Real-Time qPCR (RT-qPCR)

RNA collection for in vitro experiments was performed using the RNeasy™ Micro mini kit (Qiagen, #74134, Toronto, ON, Canada). Skeletal muscle RNA extraction was performed with the RNeasy™ Fibrous Micro mini kit (Qiagen, #74704) and quantified by nanodrop. RNA was converted to cDNA with the All-In-One 5x RT MasterMix (ABM, #G592, Richmond, BC, Canada). qPCR was performed using the PowerUp™ SYBR™
Green Master Mix (FisherSci, #A25741, Ottawa, ON, Canada) with the QuantStudio™ Studio 6 Flex Real-Time PCR System (Thermofisher, Ottawa, ON, Canada) (Supplementary Materials Table S1).

2.14. Tissue/Cell Lysis and Western Blotting

Cell lysates and skeletal muscle homogenates were prepared with RIPA buffer supplemented with protease (Roche, #04693116001, Mississauga, ON, Canada) and phosphatase (Roche, #PHOSS-RO) inhibitors, as well as Thiamet-G (Cayman, #13237) to prevent the loss of O-GlcNAc modification. Samples were centrifuged at 15,000× *g* for 10 min at 4 °C, and the supernatant was collected. For muscle homogenates, tissue was combined with lysis buffer and a metal bead in 2 mL SafeLock™ Eppendorf tubes (Eppendorf, #022363352, Mississauga, ON, Canada). Samples were then subjected to homogenization using a TissueLyser II (Qiagen, Toronto, ON, Canada) at 30 Hz for 90 s, followed by an incubation on ice for 60 s. This process was repeated 3 times. After homogenization, samples were left at 4 °C for 4 h on a rotating platform and then centrifuged at 15,000× *g* for 15 min at 4 °C. Total protein concentration was determined using a DC Protein Assay with BSA as a standard. Proteins were resolved by SDS-PAGE and transferred to PVDF membranes using a semi-dry BioRad™ Trans-Blot Turbo (#1704150EDU, Mississauga, ON, Canada transfer system. For assessment of poly-sialyation measurements, a wet-transfer was performed overnight at 40 V.

Membranes were blocked with Intercept TBS blocking buffer (Li-Cor, #927-6000, Lincoln, NE, USA) and incubated with primary antibodies in blocking solution overnight at 4 °C. After washing with TBS + 1% Tween-20, membranes were incubated with IR Dye®800CW Donkey anti-Mouse IgG (Li-Cor, #926-32212, 1:5000) and IR Dye®680RD Goat anti-Rabbit IgG (Li-Cor, #926-68071, 1:5000) for 1 h at room temperature. Proteins were visualized using a Licor Odyssey, and densitometry was performed using Image Studio™ (Licor, version 6.0).

2.15. PNGase F and α2-3, 6, 8 Neuraminidase Reactions

To examine the glycosylation status of the AChRδ subunit, 20 µg of tissue lysates were combined with either PNGaseF (New England Biolabs, #P0704S, Whitby, ON, Canada) or α2-3, 6, 8 Neuraminidase (New England Biolabs, #P0720S) according to manufacturer's instructions. AChRδ protein levels and molecular weight were assessed via Western blot.

2.16. Antibodies

The following antibodies were used for Western blot experiments: Gfpt1 (ProteinTech, #14132-1-AP, 1:500, Rosemont, IL, USA), Gapdh (14C10) (Cell Signalling, #2118, 1:2000,

Danvers, MA, USA), O-GlcNAc (RL2) (Novus Biologicals, #NB300-524, 1:1000, Toronto, ON, Canada), Ogt (ProteinTech, #66823-1-Ig, 1:1000, Rosemont, IL, USA), Desmin (ProteinTech, #16520-1-AP, 1:1000, Rosemont, IL, USA), AChRα (ProteinTech, #10613-1-AP, 1:1000, Rosemont, IL, USA), AChRδ (C-4) (Santa Cruz, #sc-390896, 1:1000, Dallas, TX, USA), PolySia 735 (gift from Dr. Rita Gerardy-Schahn, Hannover, Germany, 1:1000), Vinculin (7F9) (Santa Cruz, #sc-73614, 1:2000, Dallas, TX, USA), Lrp4 (extracellular) (NeuroMab N207/27, #75221, UC Davis/NIH NeuroMab Facility, Davis, CA, USA), biotinylated-succinylated wheat germ agglutinin (sWGA) (Vector Laboratories, #B-1025S-5, 1:1000, Newark, CA, USA), and IRDye® 800CW Streptavidin (Li-Cor, #926-32230, 1:5000). For NMJ staining from whole muscle mounts, SV2 antibody (DSHB, #, 1:250, The University of Iowa, Department of Biology, Iowa City, IA, USA), and neurofilament M were used (DSHB, 2H3, 1:250).

2.17. Statistics

Data were analyzed with GraphPad Prism v 10.1.2. Data were checked for normality using the D'Agostino-Pearson test, and the appropriate statistical test was applied as described in the figure legends. Any outlier was identified using the robust regression and outlier remover method (ROUT).

Statistical significance was determined by using unpaired two-tailed Student's *t*-tests or analysis of variance (ANOVA). If multiple comparisons were performed, a Tukey's post hoc test was performed. Results are given as mean ± S.D, and $p < 0.05$ was considered significant.

3. Results

3.1. Skeletal Muscle Knockout of Gfpt1 (Gfpt1$^{tm1d/tm1d}$) in Mice Hasprogressive Muscle Fatigability with Impaired NMJ Morphology

We used the previously published Gfpt1 skeletal muscle-specific knockout mouse model termed *Gfpt1$^{tm1d/tm1d}$* for these investigations [25]. These mice express two LoxP sites flanking the seventh exon of Gfpt1, which also contains Cre recombinase controlled by the creatine kinase (Ckm) promoter (Figure 1A). This causes truncation to occur within Gfpt1, targeting it for degradation. These mice lack *Gfpt1* gene expression and thus the corresponding protein in muscle (Supplementary Figure S1A,B). The previous characterization of these mice revealed modest behavioral and phenotypic changes as well as NMJ abnormalities up to 26 weeks of age [25]. In this study, we used 40-week-old mice to help identify the phenotypic and molecular changes, anticipating these would be progressive and more pronounced in older animals (Supplementary Figure S1C).

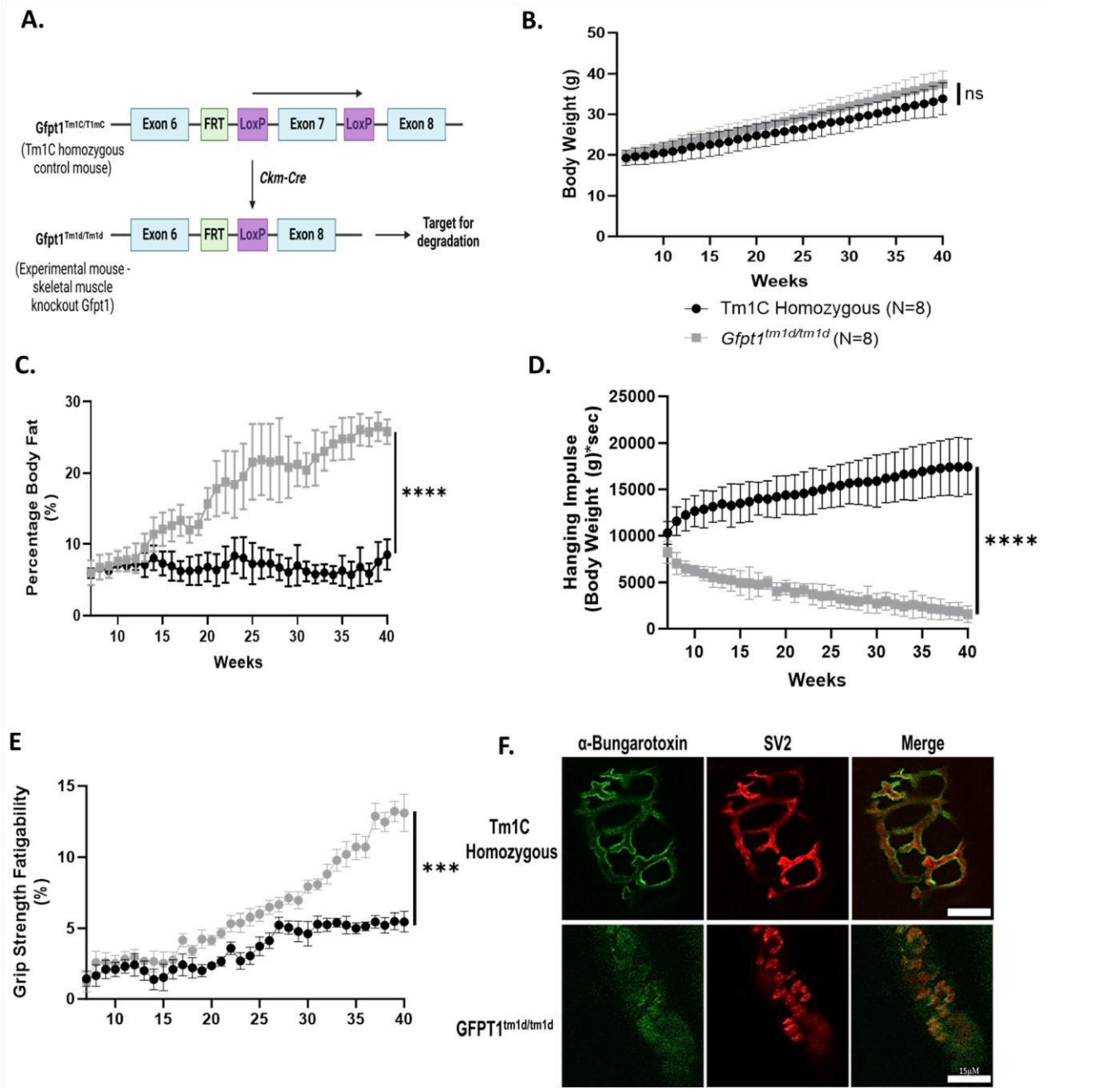

Figure 1. *Gfpt1*$^{tm1d/tm1d}$ mice exhibit progressive fatigable muscle weakness with disrupted NMJ morphology. (**A**) Our previously published *Gftp1*$^{tm1d/tm1d}$ mouse model was developed with Cre/LoxP technology. This model contains two LoxP sites, which flank the seventh exon of Gfpt1 (termed *Gftp1*$^{tm1c/tm1c}$). Gfpt1$^{tm1c/tm1c}$ mice are crossed with the Ckm-Cre expressing mouse to produce a heterozygous mouse containing Ckm-Cre and the LoxP flanking Gfpt1, termed *Gfpt1*$^{Cre\text{-}Het}$. The *Gfpt1*$^{Cre\text{-}Het}$ mice were crossed with *Gfpt1*$^{tm1c/tm1c}$ mice to produce the *Gfpt1*$^{tm1d/tm1d}$ mouse line. The

Gfpt1$^{tm1d/tm1d}$ mouse model expresses a skeletal muscle-specific truncation of Gfpt1, which is targeted for degradation. (**B**) Mice were weighed 3 times per week over 40 weeks; *Gfpt1*$^{tm1d/tm1d}$ mice (grey line) showed no significant difference in body weight when compared to Tm1C homozygous control mice (black line). (**C**) There was a significant increase in body fat percentage in *Gfpt1*$^{tm1d/tm1d}$ mice over the same period (EchoMRI). (**D**) *Gfpt1*$^{tm1d/tm1d}$ mice have a progressive reduction in hanging impulse when compared to Tm1C homozygous control mice. (**E**) Repetitive grip strength measurements demonstrated that *Gfpt1*$^{tm1d/tm1d}$ mice have increased

muscle fatigability compared to Tm1C homozygous control mice. (**F**) NMJs from soleus muscle were labeled with anti-synaptic vesicle 2 to label presynaptic nerve terminals (red) and α-bungarotoxin to visualize AChR clusters (green). All graphs show mean ± SD, and statistical significance was determined via a two-way ANOVA. *n* = 8 for both Tm1C homozygous control mice and Gfpt1$^{tm1d/tm1d}$ mice. *** *p*-value < 0.001, **** *p*-value < 0.0001, ns: not significant.

Over 40 weeks, *Gfpt1*$^{tm1d/tm1d}$ mice did not exhibit significant differences in body weight compared to Tm1C homozygous control animals (Figure 1B). However, they did have a significant increase in body fat percentage, reflecting a decrease in lean body mass (Figure 1C). *Gfpt1*$^{tm1d/tm1d}$ mice also demonstrated a progressive impairment in the latency to fall (Figure 1D and Supplementary Figure S1D) and no significant change in maximal grip strength, but an increase in grip strength fatigability was observed (Figure 1E and Supplementary Figure S1E–G). Also, a significant decrease in total mouse activity was noted (Supplementary Figure S1H). Next, we performed EMG recordings in an older (54-weekold) *Gfpt1*$^{tm1d/tm1d}$ and Tm1C homozygous mouse. The *Gfpt1*$^{tm1d/tm1d}$ mouse had a shorter amplitude in sub-maximal CMAP measurements (14.8 mV to 36.1 mV) (Supplementary Figure S2A). The sub-maximal CMAP was used for RNS recordings at low frequency (3 Hz) and high frequency (20 Hz). We found that the *Gfpt1*$^{tm1d/tm1d}$ experienced a decrement at low-frequency (~12% at 3 Hz) and high-frequency (~25% at 20 Hz) RNS exceeding 10%, while minimal decrement was measured within the Tm1C homozygous control mouse (Supplementary Figure S2B,C). A CMAP decrement of 10% is commonly used as a threshold for diagnosing muscular fatigue in CMS patients [20,59]. Finally, examination of the NMJs revealed that *Gfpt1*$^{tm1d/tm1d}$ mouse skeletal muscle had smaller and less complex NMJs when compared to Tm1C homozygous control animals (Figure 1F). These results confirm our previous study demonstrating that *Gfpt1*$^{tm1d/tm1d}$ mice exhibit increased muscle fatigability, reduced grip strength, and impaired NMJ morphology. The maintenance of body weight with an increasing body fat percentage suggests muscle loss may be occurring, explaining in part the changes in fatigue, strength, and failure of neuromuscular transmission.

3.2. Gfpt1$^{tm1d/t1md}$ *Mice Exhibit Hypo-Glycosylated AChRδ Subunits*

A previous study indicated that a reduction in Gfpt1 protein levels resulted in a decrease in AChR subunit expression within TE671/DB40 cells [28]. Therefore, we investigated the expression of AChR subunits within skeletal muscle isolated from *Gfpt1*$^{tm1d/tm1d}$ mice. *Gfpt1*$^{tm1d/tm1d}$ skeletal muscle exhibited a significant reduction in Chrnd and Chrna1 RNA (Figure 2A,B) and AChRδ protein levels in the quadriceps (Figure 2C,D). Furthermore, AChRδ appeared as two bands on the Western blot of both Tm1C homozygous control and *Gfpt1*$^{tm1d/tm1d}$ skeletal muscle, a high-molecular-weight species at ~65 kDa and a lowmolecular-weight species at ~60 kDa (Figure 2C). The low-molecularweight species of AChRδ was more prominent in Gfpt1$^{tm1d/tm1d}$ quadriceps muscle than control animals
(Figure 2C,E). This effect was also observed in the gastrocnemius muscle (Supplementary Figure S3A–C). No drop in protein levels or a second molecular weight species of the
AChRα subunit was visible in Gfpt1$^{tm1d/tm1d}$ quadriceps muscle (Figure 2F,G). Also, we assessed Lrp4 protein levels in whole muscle lysates. We established that there was also no drop in protein levels or a second molecular weight species visible within *Gfpt1*$^{tm1d/tm1d}$ quadriceps (Supplementary Figure S3D,E). The prominence of the lower molecular weight of AChRδ in *Gfpt1*$^{tm1d/tm1d}$ prompted us to determine its origin.

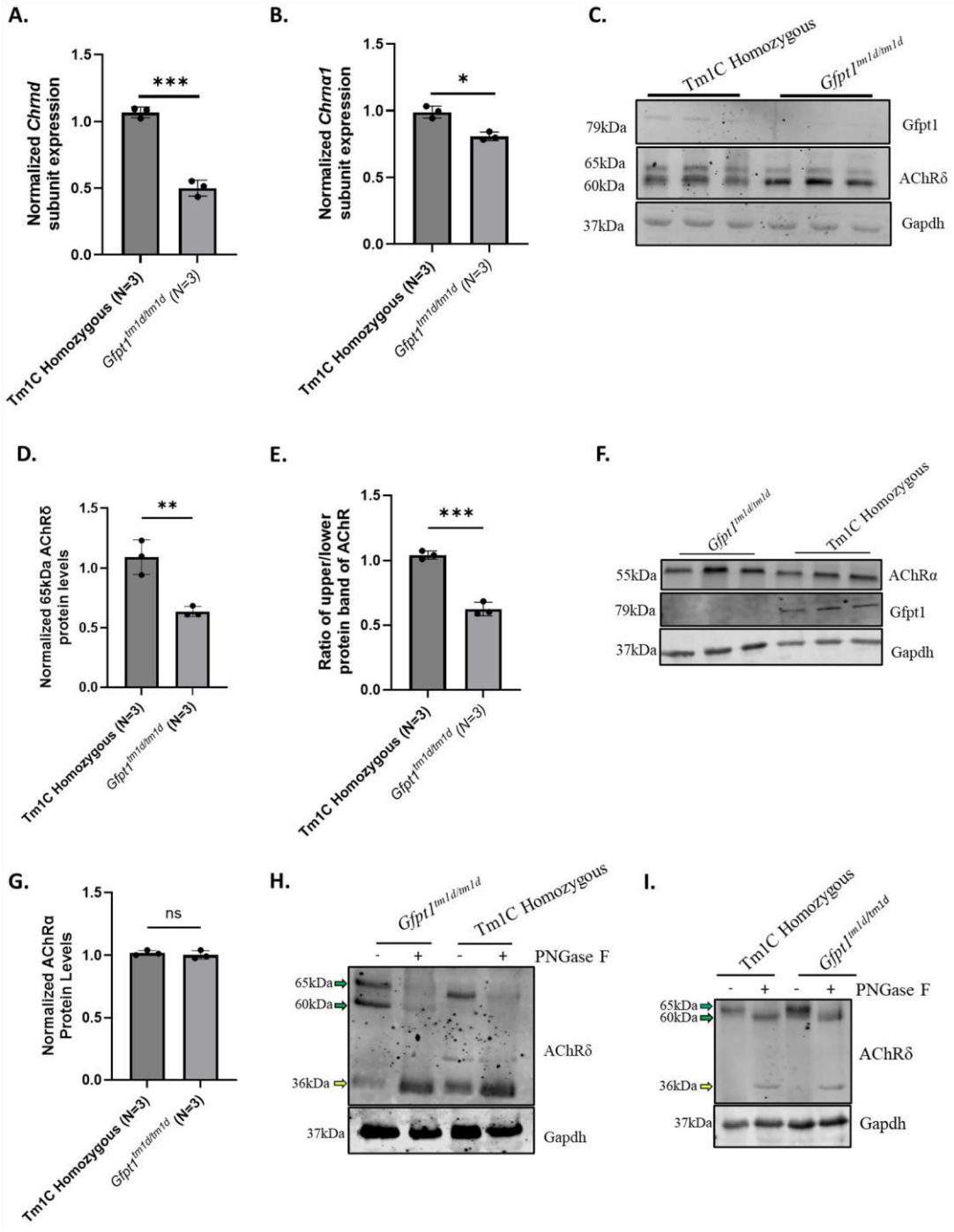

Figure 2. *Gfpt1*$^{tm1d/tm1d}$ mice exhibit impaired *Chrnd* gene and AChRδ protein expression with the presence of an altered molecular weight banding pattern. (**A**) *Chrnd* and (**B**) *Chrna1* gene expression are reduced in quadriceps isolated from 40-week-old *Gfpt1*$^{tm1d/tm1d}$ mice normalized to reference gene expression. (**C**) A lowmolecular-weight species (60 kDa) can be detected in AChRδ in *Gfpt1*$^{tm1d/tm1d}$ skeletal muscle lysates on Western blot. (**D**) AChRδ protein levels are reduced in *Gfpt1*$^{tm1d/tm1d}$ skeletal muscle compared to Tm1C homozygous control mice, normalized to Gapdh loading control. (**E**) *Gfpt1*$^{tm1d/tm1d}$ mice exhibited a reduction in the ratio of the high-molecular-weight species and the low-molecular-weight species of AChRδ upon comparison to Tm1C homozygous control mice. (**F**) Provided the change in AChRδ, we examined additional AChR subunit protein levels. There was no discernable change in molecular weight with AChRα. (**G**) There was no significant change in AChRα protein levels within *Gfpt1*$^{tm1d/tm1d}$ quadricep. (**H**) A Western blot showing

quadriceps and (**I**) gastrocnemius muscle lysates from *Gfpt1*$^{tm1d/tm1d}$ and Tm1C homozygous control following treatment with PNGase F. PNGase F treatment resulted in the migration of the 65 kDa and 60 kDa species of AChRδ species, suggesting that the lower molecular weight is hypo-glycosylated. The molecular weight species of AChRδ are labeled with 65kDa and 60kDa in green. A lower 36kDa species is labelled with yellow arrows. For in vivo experiments assessing protein levels and RNA expression, three mice were assessed (n = 3). Original images can be found in Supplementary File S1. Graphs show mean ± SD; statistical significance was determined by Student's t-Test. * p-value < 0.05, ** p-value < 0.01, *** p-value < 0.001, ns: not significant.

The AChRδ subunit is a tightly regulated glycoprotein with several previously reported sites for glycosylation [60,61]. We used the N-linked glycanase, PNGaseF, which cleaves the innermost GlcNAc modification of complex oligosaccharides bound to asparagine residues, to determine if the lower AChRδ molecular weight species is differentially glycosylated in *Gfpt1*$^{tm1d/tm1d}$ muscle. In both *Gfpt1*$^{tm1d/tm1d}$ muscle and Tm1C homozygous control muscle lysates, the high-molecularweight species disappeared after PNGase F treatment, to its unglycosylated core species (Figure 2H,I). Additionally, the low-molecular-weight species of AChRδ found in *Gfpt1*$^{tm1d/tm1d}$ skeletal muscle also disappeared following treatment with PNGase F (Figure 2H,I). This indicates that both the molecular weight species of AChRδ are glycoproteins and that the low-molecular-weight species shows an altered, potentially immature, or aberrant glycosylation profile.

UDP-GlcNAc, the product of the HBP, can be used for terminal N-linked glycan chain substrates such as sialyation. Sialyation is a terminal glycan chain PTM, which has been implicated in various disorders such as GNE Myopathy and sarcopenia. We wanted to investigate whether protein sialylation is deficient in Gfpt1-depleted mouse muscle. While poly-sialylation was significantly reduced in *Gfpt1*$^{tm1d/tm1d}$ quadriceps (Supplementary Figure S3F,G), there were no changes in sialyation of the AChRδ subunit and Desmin (Supplementary Figure S3H). This indicated that AChRδ is siaylated and that modification did not account for a molecular weight shift. Taken together, these results suggest that AChRδ has multiple glycoproteins present, which are differentially expressed in *Gfpt1*$^{tm1d/tm1d}$ skeletal muscle, and that this low-molecular-weight species may be an immature glycoprotein.

3.3. Gfpt1-Deficient C2C12 Cells Exhibit Reduced AChRδ Protein Levels with a Low-Molecular-Weight Species

To further investigate the impact of Gfpt1 deficiency on cellular processes, we established a Gfpt1-depleted C2C12 cell line (Figure 3A) using a lentiviral system to infect myoblasts with a tetracycline-inducible scramble, shGfpt1 #1 or shGfpt1 #2 transgene (Figure 3B, Supplementary Figures S4A–F). These myoblasts had a ~70% and ~63% reduction in Gfpt1 protein levels with shGtpt1 #1 and 2, respectively, when compared to scramble (Figure 3C,D).

Next, we wanted to determine if our Gfpt1-deficient C2C12 myotubes had reduced AChR subunit expression. Following activation with doxycycline, both *Chrnd* and *Chrnα1* expression levels were reduced by nearly ~50% in Gfpt1-depleted myotubes (Figure 3E,F). In addition, a decrease was also observed in the protein levels of AChRδ. (Figure 3G,H). Similarly to *Gfpt1*$^{tm1d/tm1d}$ skeletal muscle, AChRδ expressed two molecular weight species in Gfpt1-depleted myotubes (Figure 3G). The expression of the low-molecular-weight species in Gfpt1-depleted C2C12 myotubes led to a reduced ratio in AChRδ protein levels of the upper- to lower-molecular-weight band (Figure 3I). In addition, as observed in *Gfpt1*$^{tm1d/tm1d}$ skeletal muscle, there was no change in AChRα protein levels in Gfpt1deficient C2C12 myotubes (Figure 3G,J). Taken together, these results support our findings in *Gfpt1*$^{tm1d/tm1d}$ mice, indicating that impairment to Gfpt1 causes altered glycosylation of AChRδ, resulting in the increased expression of a low-molecular-weight species.

3.4. NMJ-Specific Expression of the Lower-Molecular-Weight AChRδ Subunit

Whole-muscle lysates have diluted levels of NMJ-associated proteins in large-scale proteomic analysis, and these analyses do not reveal whether the NMJ proteins are correctly localized [62]. Therefore, we utilized laser capture microdissection (LCM) to isolate NMJs from cryo-sectioned

skeletal muscle to assess NMJ-associated protein expression. We first validated this approach in gastrocnemius muscle isolated from 25-week-old C57Bl/6N control mice (Supplementary Figure S5). NMJ-associated proteins AChRα, AChRδ, SV2, and MuSK were only identified in the NMJ isolate but not in muscle tissue taken from bungarotoxin-negative areas (Supplementary Figure S5D). The bungarotoxin-negative areas served as our material with non-NMJs detected and were excised after each NMJ was collected. Additionally, both Desmin and Gapdh were detected in each isolate, suggesting that this enrichment technique successfully isolated NMJ-associated proteins.

To examine if both molecular weight species of AChRδ were found at the NMJs of Gfpt1$^{tm1d/tm1d}$ mice, the muscle was sectioned longitudinally and stained for AChR clusters (Figure 4A). Approximately 1000 NMJs were isolated from *Gfpt1*$^{tm1d/tm1d}$ and Tm1C homozygous control mice (Figure 4B, Supplementary Figure S6A,B). Slightly more NMJs were collected from *Gfpt1*$^{tm1d/tm1d}$ mice, as previous studies had reported that *Gfpt1*$^{tm1d/tm1d}$ mice NMJs were smaller compared to the Tm1C homozygous control (Supplementary Figure S6C). NMJ isolates expressed the AChRδ protein, which was absent in skeletal muscle (Figure 4C). The *Gfpt1*$^{tm1d/tm1d}$ NMJ isolate sample expressed both the upper- and low-molecular-weight species of AChRδ (Figure 4C). The low-molecular-weight species were more abundant within the *Gfpt1*$^{tm1d/tm1d}$ NMJ isolate compared to the Tm1C homozygous control NMJs. Taken together, these results indicate that the lowmolecular-weight species localizes to the NMJ within all mice but is present in greater abundance in *Gfpt1*$^{tm1d/tm1d}$ NMJs, which may alter the function of the AChR.

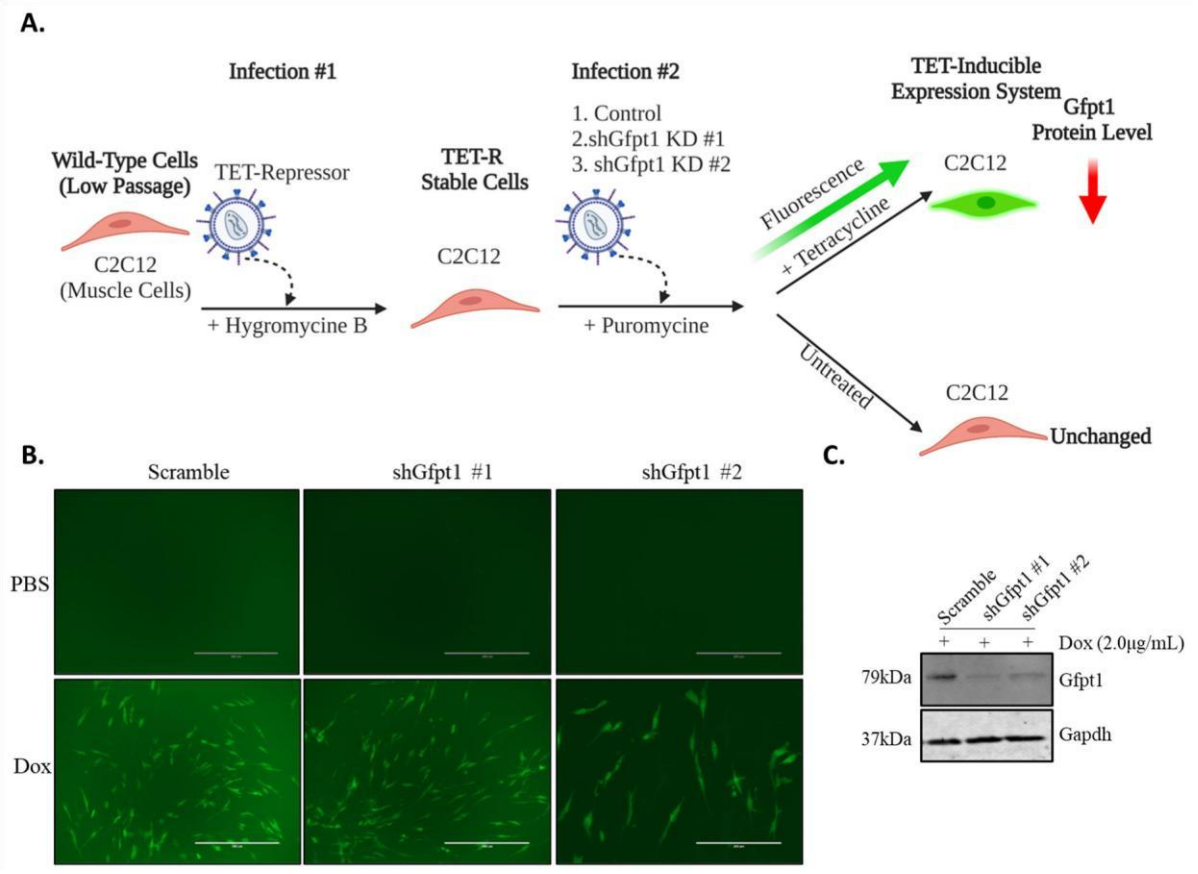

Figure 3. *Cont*.

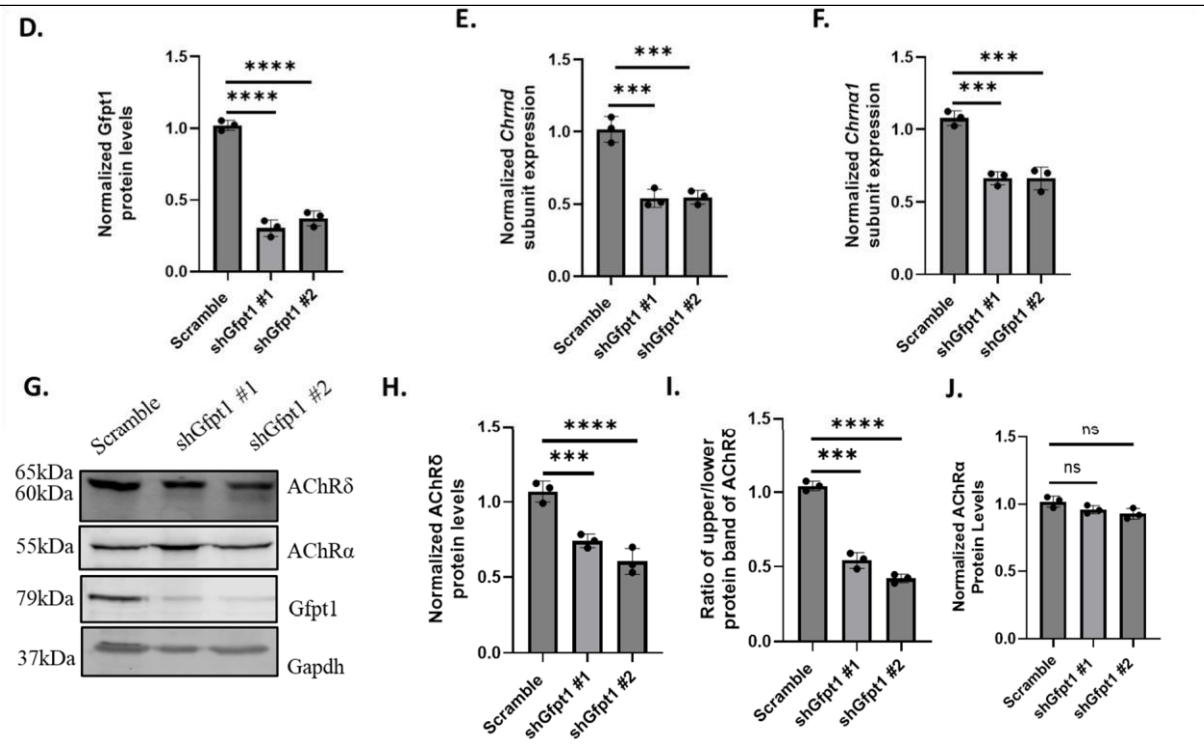

Figure 3. Gfpt1 deficient C2C12 myotubes exhibit impaired AChRδ protein levels, with the presence of a lowmolecular-weight species. (**A**) Gfpt1-deficient C2C12 myoblasts were created using a tetracycline-inducible lentiviral system. A lentivirus encoding a tetracycline repressor (TET-R) was used to infect C2C12 cells under the selection of hygromycin. Next, a scramble, shGfpt1 #1 and shGfpt1 #2 expressing transgene, was infected into Tet-R positive C2C12 cells. Cells infected with the scramble and Gfpt1-deficient transgenes were selected with puromycin. (**B**) Exposure to doxycycline activates an eGFP reporter in scramble, shGfpt1 #1 and shGfpt1 #2 stable C2C12 cells. Scale bar is 200 µm. Gfpt1 protein levels were found in Gfpt1-deficient C2C12 myoblasts upon activation with doxycycline. (**C**,**D**) A reduction in Gfpt1 protein levels after treatment with doxycycline in Gfpt1-deficient C2C12 myoblasts was observed. (**E**) Gfpt1-deficiency in C2C12 myotubes impairs the expression of Chrnd and (**F**) Chrna1. (**G**) Gfpt1-depleted myotubes express a lower-molecular-weight 60 kDa species of AChRδ that was not present in scramble control conditions. (**H**) A reduction in AChRδ protein levels in Gfpt1-depleted C2C12 myotubes was observed. (**I**) Densitometry was used to show a reduction in the ratio of the upper molecular weight of AChRδ and the low-molecularweight species of AChRδ in C2C12 myotubes. (**J**) There was no significant change in AChRα protein levels between scramble and Gfpt1-deficient myotubes. For in vitro experiments, protein levels and RNA expression were analyzed by three separate experiments (n = 3). Original images can be found in Supplementary File S1. Graphs are presented as mean ± SD, and statistical significance was determined by one-way ANOVA. ns p-value > 0.05, *** p-value< 0.001, **** $p$value < 0.0001, ns: not significant.

3.5. Gfpt1-Depleted Models Have Impaired O-GlcNAcylation

UDP-GlcNAc, the downstream product of the HBP, is essential for the formation of N- and Olinked glycan structures, which are crucial for maintaining protein stability. In addition, UDP-GlcNAc can be used for protein O-GlcNAcylation, a small modification that is essential for cellular signaling (Figure 5A). OGT, an enzyme that transfers GlcNAc to protein moieties, regulates this reversible modification, along with the O-linked glycanase enzyme called OGA, which removes GlcNAc. We hypothesized that impairment to GFPT1/Gfpt1 expression and/or activity would result in reduced O-GlcNAcylation levels. Firstly, we used the Gfpt1 antagonist 6-diazo-5-oxo-l-norleucine (DON) to inhibit enzymatic activity in vitro. Through a dose–response analysis, we confirmed that Gfpt1 is inhibited without causing cellular toxicity in C2C12 cells at 500 µM of DON for 48 h (Figure 5B). Subsequently, we examined the levels of O-GlcNAcylation after DON treatment and showed a significant reduction in protein O-GlcNAcylation (Figure 5C,D). Additionally, treating cells with the Oga inhibitor, Thiamet-G, increased O-GlcNAcylation in wild-type C2C12 cells (Supplementary

Figure S7A,B). These results collectively indicate that Gfpt1 enzymatic activity is involved in OGlcNAcylation of C2C12 cells in vitro.

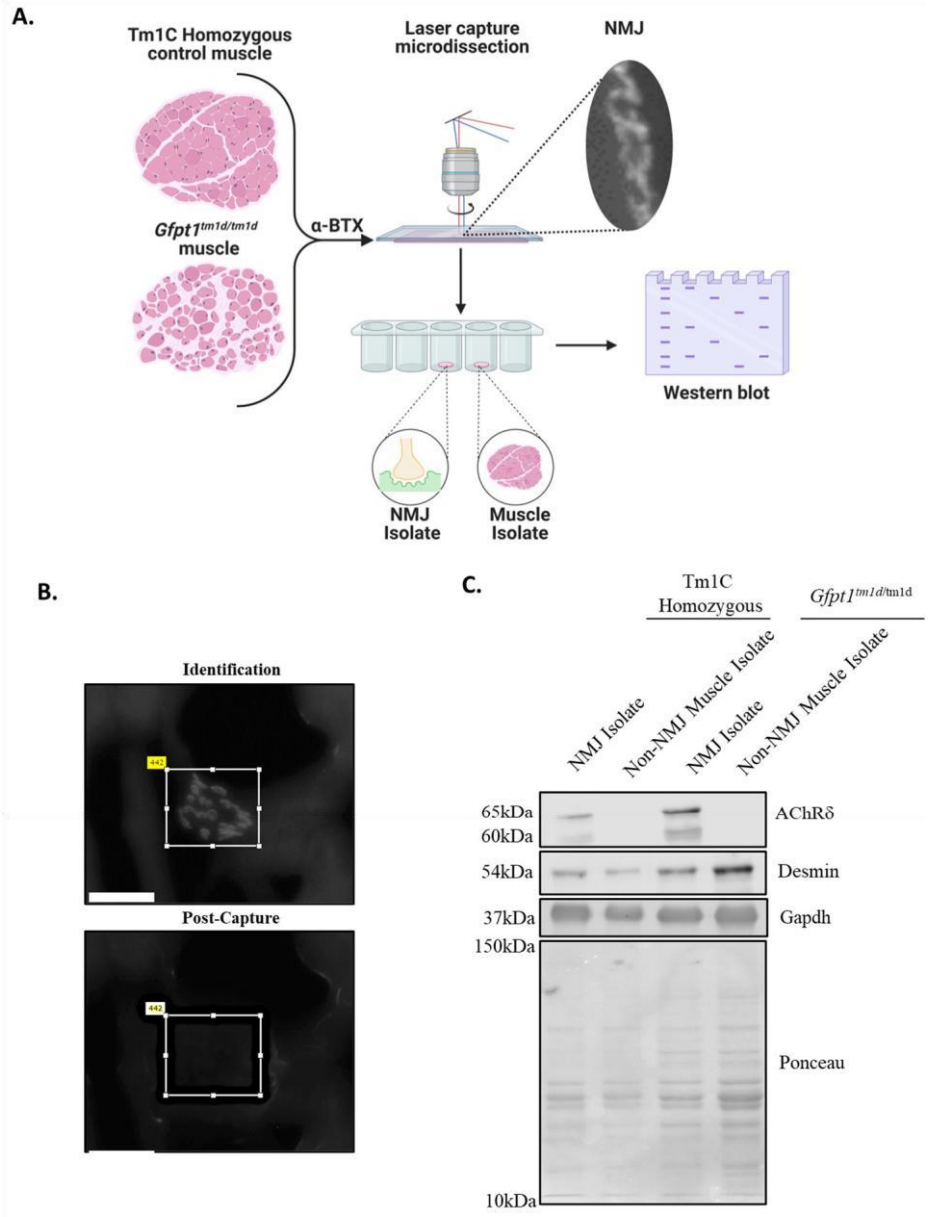

Figure 4. The low-molecular-weight species is detected in the NMJs isolated from *Gfpt1*$^{tm1d/tm1d}$ muscle. (**A**) Laser microdissection was used to enrich NMJs in *Gfpt1*$^{tm1d/tm1d}$ and Tm1C homozygous control mice. Gastrocnemius muscles were longitudinally sectioned and stained for AChR clusters. (**B**) An image at 40× magnification of AChR clusters before and after isolation. Scale bar: 500 µm. (**C**) A Western blot of NMJ and muscle isolates from *Gfpt1*$^{tm1d/tm1d}$ and Tm1C homozygous control mice for the detection of AChRδ, Desmin, and Gapdh. *Gfpt1*$^{tm1d/tm1d}$ NMJ isolates express an upper- and low-molecular-weight species for the AChRδ subunit, which was not observed in Tm1c homozygous control NMJ isolate. AChRδ was used to assess for NMJ-specific protein detection, while desmin and Gapdh were used to examine expression in both NMJ and muscle isolates to ensure sample purity. Original image can be found in Supplementary File S1.

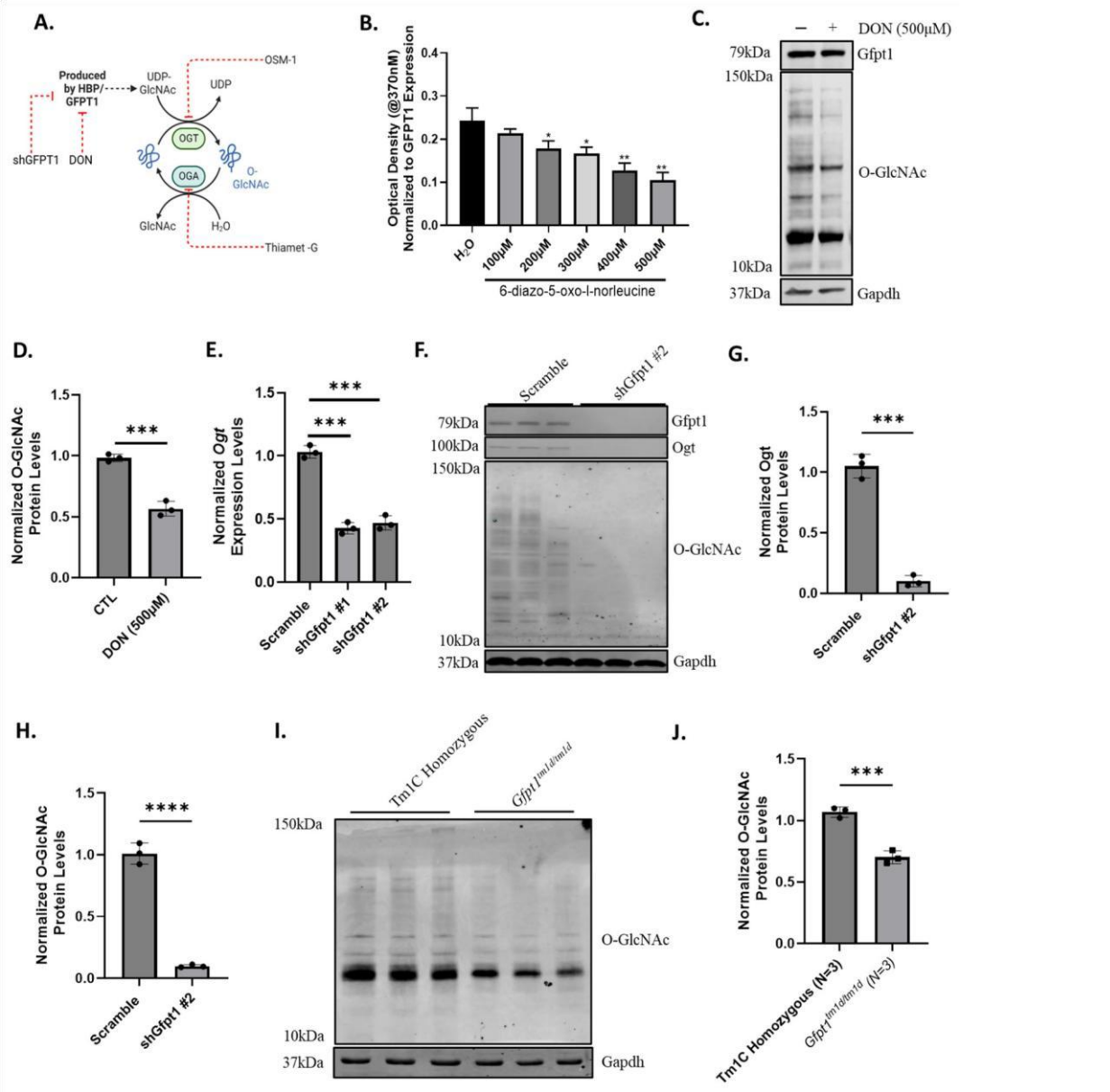

Figure 5. Impairment to GFPT1 activity or protein levels reduces protein O-GlcNAcylation in vitro and in vivo. (**A**) UDP-GlcNAc is a product of the HBP that is required for O-GlcNAcylation. Ogt is used to transfer the GlcNAc moiety to the target protein, which can be reversed by Oga. These enzymes work in tandem to control the level of protein O-GlcNAcylation inside the cell. (**B**) The Gfpt1 antagonist, DON, provided a dose-dependent decrease in Gfpt1 enzymatic activity in wild-type C2C12 cells. (**C**) Western blot of Gfpt1 protein and O-GlcNAc protein modification levels following treatment with DON in wild-type C2C12 cells. (**D**) DON treatment reduced O-GlcNAc modification levels in wild-type C2C12 cells. (**E**) Gfpt1 deficiency reduces Ogt gene expression in C2C12 myotubes. (**F**) Gfpt1, Ogt, and O-GlcNAc modification protein levels assessed via Western blot in Gfpt1-deficient C2C12 cells treated with doxycycline. (**G**) Gfpt1-deficient myotubes had reduced levels of Ogt and

(**H**) protein O-GlcNAc modification after treatment with doxycycline. (**I**) A Western blot was used to examine O-GlcNAc levels in *Gfpt1*$^{tm1d/tm1d}$ and Tm1C homozygous control mice in quadriceps muscle. (**J**) *Gfpt1*$^{tm1d/tm1d}$ mice exhibit a reduction in O-GlcNAc protein modification levels upon comparison with Tm1C homozygous control mice isolated quadriceps. Original images can be found in Supplementary File S1. Graphs are mean ± SD, $n = 3$ for all experiments, and statistical significance was determined by Student's *t*-Test. A one-way ANOVA was performed for statistical significance. * p-value < 0.05, p-value ** < 0.01, p-value *** < 0.001 and **** $p$value < 0.0001.

Next, we wanted to determine if our Gfpt1-depleted cell models have reduced Gfpt1 enzymatic activity, resulting in reduced protein O-GlcNAcylation levels. Gfpt1-depleted C2C12 myoblasts exhibited altered Gfpt1 enzymatic activity (Supplementary Figure S7C). We found that Ogt levels were secondarily reduced in Gfpt1-depleted C2C12 myoblasts, indicating impaired output from O-GlcNAcylation as a result of reduced substrate availability (Figure 5E). To confirm these findings, we examined protein levels of Ogt and O-GlcNAcylation in Gfpt1-depleted C2C12 myoblasts and observed severe depletion in both (Figure 5F,G, Supplementary Figure S7D,E). We also used the lectin succinylated wheat germ agglutinin (sWGA), which has an affinity for Nacetylglucosamine but not sialic acid and has been commonly used to observe alterations in OGlcNAcylation levels with accompanying O-GlcNAc antibodies. Western blot was used on Gfpt1deficient lysates, which observed a significant decrease in the amount of sWGA bound to glycoproteins compared to controls, further suggesting that glycosylation impairment is present (Supplementary Figure S7F,G).

Lastly, we examined if there was depleted O-GlcNAcylation in our *Gfpt1*$^{tm1d/tm1d}$ mouse model. We observed a reduction in protein O-GlcNAcylation levels in skeletal muscle derived in Gfpt1$^{tm1d/tm1d}$ mice (Figure 5H,I). Additionally, using sWGA, we examined the amount of glycoprotein present within the *Gfpt1*$^{tm1d/tm1d}$ skeletal muscle and observed a significant decrease (Supplementary Figure S7H,I). These results collectively indicate that Gfpt1 depletion impairs protein glycosylation, which may be an important mechanism for Gfpt1-CMS by impacting the quality and abundance of NMJ-associated proteins. In addition, these results indicate that the impairment of O-GlcNAcylation likely affects many proteins at the NMJ and in skeletal muscle. However, further functional studies are needed to finally confirm if the AChRδ is O-GlcNAcylated.

4. Discussion

GFPT1 is the rate-limiting enzyme of the HBP, a metabolic pathway that produces UDP-GlcNAc, a key precursor for protein glycosylation [39,40]. Biallelic mutations to *GFPT1* cause CMS, a rare neuromuscular disease characterized by fatigable muscle weakness [21,22,24–29]. These mutations to *GFPT1* reduce enzymatic activity and protein expression within the skeletal muscle, decreasing the production of UDP-GlcNAc, an essential precursor for protein glycosylation [22,28,51]. Glycosylation is a PTM that attaches sugar moieties to target proteins at various amino acids, allowing for enhanced solubility and stability. At the NMJ, glycosylation is an essential modification that controls the stability of key receptor complexes both in the pre- and post-synaptic regions [60,63]. It remains unclear how an enzyme essential for protein glycosylation, which is ubiquitously expressed in the body, impairs neurotransmission and NMJ maintenance in GFPT1-related CMS. We hypothesized that a deficiency of Gfpt1 would result in the improper glycosylation of key NMJ-associated proteins impairing function and/or stability within the NMJ and thus analyzed murine in vivo and in vitro models depleted or even deficient for Gfpt1 in skeletal muscle cells.

We demonstrate that there is a glycosylation deficiency within Gftpt1-depleted models and that these models express an elevated amount of an immature glycoprotein of the AChRδ subunit. We show that both in vitro and in vivo models show a significant reduction in total AChRδ protein levels. We also identified a low-molecular-weight species that was more prominent within *Gfpt1*$^{tm1d/tm1d}$ skeletal muscle. PNGase F treatment caused a molecular weight shift in both protein species, indicating that the low-molecular-weight species is an immature glycoprotein. We wanted to determine if this immature glycoprotein is localized to the NMJs of *Gfpt1*$^{tm1d/t1d}$ mice as part of the assembled AChR. LCM was used to excise NMJs from skeletal muscle in the Tm1C homozygous control and *Gfpt1*$^{tm1d/tm1d}$ mice. We identified that both species were present within the NMJs of *Gfpt1*$^{tm1d/tm1d}$ mice, suggesting that deficiently glycosylated AChRδ is localized within proximity to the NMJ. Furthermore, we showed that in both in vitro and in vivo models, reduced Ogt protein levels were present, which resulted in a decrease in total O-GlcNAcylation. Also, succinylated-WGA, a lectin with an affinity for O-GlcNAc residues [64], showed reduced expression in *Gfpt1*$^{tm1d/tm1d}$ skeletal muscle. Lastly, we also showed that terminal glycosylation through poly-sialylation was

reduced in *Gfpt1*$^{tm1d/tm1d}$ skeletal muscle, suggesting that, in totality, several glycan chain assembly pathways are impaired.

The AChRδ is a member of the pentameric muscle nicotinic AChR, a ligand-gated ion channel with affinity for ACh. The AChR is regulated by glycosylation at the γ and δ subunits, allowing for enhanced stability and trafficking toward the post-synaptic membrane [61]. The AChRδ contains three glycosylation sites: Asn76, Asn143, and Asn169 [60]. Site-directed mutagenesis has previously caused similar molecular weight shifts when expressed in COS cells, suggesting that our low-molecular-weight species is an immature glycoprotein [60]. In addition, these glycosylationdeficient mutants of the AChRδ subunit, when co-expressed with AChRα, β, ε subunits, had impaired AChR receptor assembly and reduced surface expression [60]. It was previously shown that AChRδ and AChRβ contain novel motifs with lysine residues that enable Golgi retention, promote ubiquitination, and contribute to intracellular retention [61]. As such, this immature glycoprotein may be a target for protein degradation through the proteasomal degradation pathway, a pathway previously shown to regulate the expression of AChRδ through its interaction with the RING domain of Rapsyn [65,66]. Our data suggest that in Gfpt1-deficient samples, an immature glycoprotein of AChRδ is localized to the NMJ. In addition, impairment of glycosylation may impair AChR stability through a similar mechanism, as outlined above.

Young *Gfpt1*$^{tm1d/tm1d}$ mice were previously shown to have phenotypic changes as well as NMJ abnormalities consistent with Gfpt1-related CMS [25]. In this study, we used 40-week-old mice to better identify the molecular changes, anticipating these would be amplified in older animals. We found that *Gfpt1*$^{tm1d/tm1d}$ mice have a progressive impairment of muscle endurance and increased fatigability of grip strength. An aged *Gfpt1*$^{tm1d/tm1d}$ mouse was also found to have reduced CMAP amplitudes, compared to the control, likely a result of impairment to the skeletal muscle, nerve, and/or NMJ within the hindlimbs [67]. Importantly, *Gfpt1*$^{tm1d/tm1d}$ exhibited a fatigable decrement exceeding 15% after low-frequency (3Hz) and high-frequency (20Hz and 30Hz) RNS. In patients with CMS, a decrement greater than 10% is typically observed [59,68,69]. Given this decrement seen with RNS in *Gfpt1*$^{tm1d/tm1d}$ mice, this technique could be used as a prognostic marker for therapeutic strategies in the future. However, more samples would be required for full analysis. Similar to our previous paper, *Gfpt1*$^{tm1d/tm1d}$ NMJs were small and fragmented, with less complexity compared to Tm1C homozygous control mice [25]. This has also been reported in other models with deficient Gfpt1 expression. One study targeted the muscle-specific 18 amino acid insertion within human GFPT1, termed Gfpt1-L [23,70]. Loss of Gfpt1-L revealed impaired motor performance and NMJ integrity, which progressively worsened over time [23,70]. In addition, both these models contain tubular aggregates within the skeletal muscle fiber, a hallmark of GFPT1related CMS [21,24,26,28]. As a result, the *Gfpt1*$^{tm1d/tm1d}$ models had progressive skeletal muscle weakness seen in GFPT1-related CMS patients and is consistent with other models.

Previous studies suggested that global N-linked glycosylation is not altered in Gfpt1CMS myoblasts [52]. However, our data indicate that Gfpt1 deficiency impairs protein glycosylation of specific proteins through both N- and O-linked pathways. A potential difference between these studies is that *Gfpt1*$^{tm1d/tm1d}$ mice exhibit a complete Gfpt1 knockout within skeletal muscle, while patients observe a deficiency in expression [22,24,28,29,51]. This could exacerbate the issues with glycosylation within our tissue compared to patient controls. To this end, Gfpt1-depleted C2C12 cells were prepared, which expressed a similar knockdown in expression compared to GFPT1-related-CMS patient-derived myoblasts. We identified that the AChRδ subunit was hypo-glycosylated within both our models. The previous study examined global N-linked glycosylation levels, not glycosylation of an individual protein. Therefore, the occupancy of glycosylated glycan side chains was not examined in that previous study. Our study builds upon this research by highlighting, for the first time, that an individual protein, the AChRδ subunit, was hypo-glycosylated within both Gfpt1-deficient models, thus introducing the first target protein of perturbed glycosylation for this subtype of CMS. In addition, the impact of total N-linked glycosylation may not be a global reduction in one specific glycan chain; perhaps various glycoproteins are individually improperly glycosylated, leading to neurotransmission impairment.

This explanation would be appropriate given that GFPT1-related CMS patients have limited total body clinical manifestations, as seen with CDG patients [4,26]. Importantly, these results indicate that future studies should examine Gfpt1-related CMS and other glycosylationbased disorders within the context of glyco-proteomics to examine an individual protein change as opposed to global glycosylation impairment. This could reveal other target glycopeptides that could be hypoglycosylated similarly, as we found with the AChRδ subunit in Gfpt1-depleted or even deficient models.

We identified that in Gfpt1-deficient models, terminal sialyation was also reduced. Sialyation is a terminal modification of proteins that can be highly unstable under mass spectrometric analyses. There have been several advancements in recent years to enhance the detection of glycan chains within different specimens, one of which has been the detection of terminal sialyation, an often unstable glycan modification that is produced from UDP-GlcNAc [50,71,72]. To date, the purpose of protein sialyation within skeletal muscle and the NMJ remains unknown. Dysfunction within protein sialyation has been associated with the neuromuscular condition called GNE myopathy, caused by a mutation to *GNE* [19,50,71]. The role of protein sialylation within the NMJ is not fully resolved. However, sialic acids play an important role in nerve and skeletal muscle tissue [73]. Within skeletal muscle specifically, proteins such as α-dystroglycan and neprilysin are complex glycoproteins within the sarcolemma. These proteins function by preserving sarcolemma integrity through the coupling of the actin cytoskeleton to extracellular matrix proteins laminin, neurexin, and agrin [74]. Therefore, sialyation impairment could disrupt muscle morphology, which was present in *Gftp1*$^{tm1d/tm1d}$ mice. At the NMJ, sialylation appears to have a role in laminin-induced AChR, suggesting another pathway that could impair NMJ integrity [75].

Glycosylation is a key PTM within the NMJ and skeletal muscle, so investigation of other NMJassociated proteins should be considered. Firstly, beyond the AChRδ subunit, the other AChR subunits (α, β, γ, and ε) have been reported to be glycosylated. Inhibiting these glycosylation sites completely by site-directed mutagenesis and/or tunicamycin treatment impaired AChR surface expression and receptor assembly, suggesting that other AChR subunits may be impaired within Gfpt1-deficient samples [76]. Although we found no molecular weight shifts within the AChRα in our models, the other AChR subunits (β, γ, and ε) were not investigated and could be hypoglycosylated. In addition to the other AChR subunits, other NMJ-associated peptides, such as components of the AChR clustering pathway MuSK, LRP4, RAPSYN [77,78], and Agrin [79], are glycosylated. Recent studies suggest that mesoderm development candidate 2 (Mesdc2) binds to Lrp4, facilitating the glycosylation and cell surface expression of Lrp4, reducing the number of AChR receptor complexes, and decreasing MuSK phosphorylation levels [80]. Also, MuSK glycosylation at amino acid sites N222, N338, and N459 has been attributed to a deficiency in the phosphorylation of MuSk and impairs downstream signaling [63]. As such, glycosylation may hinder MuSK dimerization in the absence of agrin, suggesting that glycosylation may be a control mechanism for MuSK by providing adequate steric hindrance/electrostatic repulsion of MuSK monomers [63]. These proteins should be investigated in future studies. Our data describe that mis-glycosylation of AChRδ is present within Gfpt1-deficient samples. It remains unclear if solely hypo-glycosylation of AChRδ would result in the structural changes at the NMJ. We hypothesize that with advanced glycoproteomic studies and/or further individual protein glycosylation assessment, other key NMJ-associated proteins that factor into function and/or maintenance of the NMJ may be mis-glycosylated, providing further consequences for NMJ maintenance and neurotransmission in terms of a more complex molecular interplay. In addition, this also does not discount that beyond NMJ maintenance and neurotransmission, other proteins and pathways may be dysregulated in *GFPT1*-CMS pathology.

We identified that in both Gfpt1-depleted cells and deficient skeletal muscle, there is deficient protein O-GlcNAcylation. O-GlcNAcylation is a small modification that primarily regulates nuclear, cytosolic, and cellular organelles such as the mitochondria, cytoskeletal, and endoplasmic reticulum [42,55,58]. O-GlcNAcylation attaches a GlcNAc moiety catalyzed by OGT to serine/threonine residues, which can further undergo phosphorylation, suggesting that there may

be extensive cellular pathways implicated in Gfpt1-deficient skeletal muscle [43]. In addition, the knockout of the hexosamine biosynthetic enzymes OGT and/or OGA impeded NMJ morphology and maintenance in *Drosophila* [81]. OGlcNAcylation is enriched within the synapses, playing an essential role in regulating synaptic and neuronal proteins essential for vesicular trafficking [82]. Thiamet-G, a compound that inhibits OGA, causes enhanced O-GlcNAcylation and suppresses synaptic transmission in hippocampal neurons [83]. To our knowledge, O-GlcNAcylation has not been studied in mammalian NMJs specifically. However, these structures contain an enrichment in glycoproteins, mitochondria, and sub-synaptic nuclei, suggesting that proteins are essential for NMJ maintenance and neurotransmission may be impacted.

Within skeletal muscle, O-GlcNAcylation has been associated with regulating transcriptional control through the beta-catenin/Wnt signaling pathway, which serves as a vital component for muscle and NMJ development [48]. Within neuromuscular disease, increased O-GlcNAcylation was detected within regenerating muscle, atrophic, and vacuolated fibers from muscular dystrophy, myositis, rhabdomyolysis, sporadic inclusion body myositis (s-IBM), and distal myopathy with rimmed vacuoles (DMRV) [84]. This suggests that the regulation of protein O-GlcNAcylation is important for muscle health [55]. Furthermore, O-GlcNAcylation is critical to maintaining the structure of the sarcomere through preserving protein–protein interactions of structural proteins in the cytoskeleton [55]. Preserving and/or restoring O-GlcNAcylation within the skeletal muscle may maintain muscle integrity. Lastly, O-GlcNAcylation is a PTM that regulates protein phosphorylation and has been shown to regulate the activity of various pathways inside the cell [85]. It appears that this crosstalk is essential to control cellular signaling pathways and transcription; thus, impaired O-GlcNAcylation may have deleterious impacts on these target proteins [85]. Therefore, understanding the importance of the crosstalk between O-GlcNAcylation and phosphorylation may lead to additional pathways that are perturbed in *GFPT1*-CMS pathology.

In Gfpt1-CMS, muscle fibers have tubular aggregates, deemed a “hallmark” for disease identification [21,24,26]. The presence of these tubular aggregates has been speculated to be associated with hypo-glycosylation of ORAI1, an essential protein in regulating calcium ion flux within the sarcoplasmic reticulum. This has been hypothesized as ORAI1 hypo-glycosylation has been linked to the development of tubular aggregate myopathy and in limb–girdle CMS patients harboring mutation to DPAGT1 [85]. Also, disorders such as tubular aggregate myopathies arise from mutations within STIM1 and/or ORAI1 proteins, resulting in defective sarcoplasmic reticulum calcium flux [86]. As such, defective glycosylation of key proteins responsible for calcium homeostasis may play a role in the presence of tubular aggregates within GFPT1-related CMS. Alternatively, a recent finding suggested endoplasmic reticulum-associated stress due to hypoglycosylation attributed to the formation of tubular aggregates within GFPT1-L knock-in mice [70]. In addition, this finding demonstrated aged Gfpt-L knock-in progressive decrement in aged mice [70]. Accumulated ER stress attributed to a worsening phenotype; over time, tubular aggregates were observed, as well as eventual activation of autophagy degradation and apoptosis [70]. This study demonstrated that impairment to Gfpt1 activity is attributed to an ER stress environment due to hypo-glycosylation [70]. As such, more hypo-glycosylated proteins may be mis-localized and present within these tubular aggregates that are beyond NMJassociated peptides.

Importantly, beyond the skeletal muscle, the NMJ comprises three specific cell types: the skeletal muscle, the motor neuron, and the Schwan cell. The motor neuron is essential for propagating the action potential and release of neurotransmitters into the synaptic cleft. The Schwann cell supports the motor neuron by creating a myelin sheath around peripheral neural axons. Our models within this study solely examine the skeletal muscle. As mentioned above, the *Gfpt1*$^{tm1d/tm1d}$ mouse model is a skeletal muscle-specific knockout of Gfpt1, while C2C12 cells are murine muscle myoblasts. Importantly, N- and O-linked glycosylation is essential for the function of critical proteins that are essential for motor neuron and Schwann cell development [87–89]. As such, further examination of the role of glycosylation within these cell types may elucidate more mechanisms within GFPT1-related CMS patients.

5. Conclusions

In conclusion, this study identified a deficiently glycosylated protein within Gfpt1deficient models, the AChRδ subunit, a key component that forms the AChR complex. We identified that the AChRδ contains an increase in an immature glycoprotein that is localized to the NMJs of *Gfpt1*$^{tm1d/tm1d}$ mice. In addition, we identified that Gfpt1-depleted cells and Gfpt1-deficient tissue have impaired protein O-GlcNAcylation, an abundant modification within the NMJ and skeletal muscle. This study further adds evidence of deficient glycosylation in GFPT1-related-CMS and maintains that other proteins essential for NMJ integrity may be differentially glycosylated, further impairing NMJ maintenance and neurotransmission.

Supplementary Materials: The following supporting information can be downloaded at: https://www.mdpi.com/article/10.3390/biom14101252/s1, Figure S1: In vivo characterization of the longterm effects of Gfpt1-deficiency; Figure S2: In vivo characterization RNS decrement in *Gfpt1*$^{tm1d/tm1d}$ mice; Figure S3: Characterization of AChRδ protein levels in *Gfpt1*$^{tm1d/tm1d}$ mice; Figure S4: Production and validation of the doxycycline-inducible Gfpt1-deficient C2C12 cell model; Figure S5: Laser capture microdissection collection of NMJ enriched proteins in C57Bl/6N mice; Figure S6: Laser capture isolation of NMJs from *Gfpt1*$^{tm1d/tm1d}$ and Tm1C homozygous control mice;
Figure S7: Modulation of hexosamine biosynthetic pathway with Thiamet-G or knockdown of Gfpt1 alters O-GlcNAcylation levels; Table S1: Primer sequences for Rt-qPCR; File S1: All original Western blot images.

Author Contributions: Conceptualization, H.L., S.S. and S.H.H.; methodology, S.H.H., R.C.-M., K.O. and D.O.; validation, S.H.H., R.C.-M., K.O. and D.O.; formal analysis, S.H.H., S.S. and K.O.; investigation, S.H.H., R.C.-M. and K.O.; resources, H.L. and S.S.; data curation, S.H.H., R.C.-M., K.O. and D.O.; writing—original draft preparation, S.H.H.; review and editing, S.H.H., R.C.-M.,
K.O., D.O., S.S., A.R. and H.L.; final draft preparation and writing, S.H.H., S.S., A.R. and H.L.; visualization, S.H.H., S.S, A.R. and H.L.; supervision, S.S. and H.L.; project administration, S.S. and H.L.; funding acquisition, H.L. and S.H.H. All authors have read and agreed to the published version of the manuscript.

Funding: H.L. received support from the Canadian Institutes of Health Research (CIHR) for Foundation Grant FDN-167281 (Precision Health for Neuromuscular Diseases), Transnational Team Grant ERT-174211 (ProDGNE), and Network Grant OR2-189333 (NMD4C) from the Canada Foundation for Innovation (CFI-JELF 38412); the Canada Research Chairs program (Canada Research Chair in Neuromuscular Genomics and Health, 950-232279); the European Commission (Grant # 101080249); and the Canada Research Coordinating Committee New Frontiers in Research Fund (NFRFG-2022-00033) for SIMPATHIC and from the Government of Canada, Canada First Research Excellence Fund (CFREF) for the Brain-Heart Interconnectome (CFREF-2022-00007). S.H.H. received support from the Bob Korneluk CHEO Trainee Research Grant, Ontario Graduate Scholarship (OGS), Queen Elizabeth II Scholarship (QE2-GSST), and a STaR award by the University of Ottawa Dr. Eric Poulin Center for Neuromuscular Disease. A.R. received funding from the Deutsche Gesellschaft für Muskelkranke (DGM) e. V.
Institutional Review Board Statement: The animal study protocol was approved by the Animal Care and Veterinary Board of the University of Ottawa (CHEOb-3089 and CHEOe-3120, approved on 16 November 2018 and 2 April 2019, respectively).

Data Availability Statement: Data are contained within the article and Supplementary Materials.

Acknowledgments: We would like to thank Rashmi Kothary and his research team for allowing us to have constant access to the laser capture microdissection microscope at the Ottawa Hospital Research Institute (OHRI). The SV2 antibody was deposited by Buckley, K. M., and the neurofilament (2H3) antibody deposited by Jessell, T.M/Doss, J was obtained from the Developmental Studies Hybridoma Bank, created by the NICHD of the NIH and maintained at The University of Iowa, Department of Biology, Iowa City, IA 52242. Graphical abstracts and schematics were prepared with Biorender.com.

Conflicts of Interest: The authors declare no conflicts of interest.

References

1. Stanley, P. What Have We Learned from Glycosyltransferase Knockouts in Mice? *J. Mol. Biol.* **2016**, *428*, 3166–3182. [CrossRef] [PubMed]
2. Reily, C.; Stewart, T.J.; Renfrow, M.B.; Novak, J. Glycosylation in Health and Disease. *Nat. Rev. Nephrol.* **2019**, *15*, 346–366. [CrossRef] [PubMed]
3. Lipin´ski, P.; Tylki-Szyman´ska, A. Congenital Disorders of Glycosylation: What Clinicians Need to Know? *Front. Pediatr.* **2021**, *9*, 715151. [CrossRef] [PubMed]
4. Verheijen, J.; Tahata, S.; Kozicz, T.; Witters, P.; Morava, E. Therapeutic Approaches in Congenital Disorders of Glycosylation (CDG) Involving N-Linked Glycosylation: An Update. *Genet. Med.* **2020**, *22*, 268–279. [CrossRef]
5. Saito, F.; Matsumura, K. Fukuyama-Type Congenital Muscular Dystrophy and Defective Glycosylation of α-Dystroglycan. *Skelet. Muscle* **2011**, *1*, 22. [CrossRef]
6. Hiroi, A.; Yamamoto, T.; Shibata, N.; Osawa, M.; Kobayashi, M. Roles of Fukutin, the Gene Responsible for Fukuyama-Type Congenital Muscular Dystrophy, in Neurons: Possible Involvement in Synaptic Function and Neuronal Migration. *Acta Histochem. Cytochem.* **2011**, *44*, 91–101. [CrossRef]
7. Willer, T.; Lee, H.; Lommel, M.; Yoshida-Moriguchi, T.; de Bernabe, D.B.V.; Venzke, D.; Cirak, S.; Schachter, H.; Vajsar, J.; Voit, T.; et al. ISPD Loss-of-Function Mutations Disrupt Dystroglycan O-Mannosylation and Cause Walker-Warburg Syndrome. *Nat. Genet.* **2012**, *44*, 575–580. [CrossRef]
8. van Reeuwijk, J.; Grewal, P.K.; Salih, M.A.M.; Beltrán-Valero de Bernabé, D.; McLaughlan, J.M.; Michielse, C.B.; Herrmann, R.; Hewitt, J.E.; Steinbrecher, A.; Seidahmed, M.Z.; et al. Intragenic Deletion in the LARGE Gene Causes Walker-Warburg Syndrome. *Hum. Genet.* **2007**, *121*, 685–690. [CrossRef]
9. van Reeuwijk, J.; Janssen, M.; van den Elzen, C.; de Bernabé, D.B.-V.; Sabatelli, P.; Merlini, L.; Boon, M.; Scheffer, H.; Brockington, M.; Muntoni, F.; et al. POMT2 Mutations Cause α-Dystroglycan Hypoglycosylation and Walker-Warburg Syndrome. *J. Med. Genet.* **2005**, *42*, 907–912. [CrossRef]
10. de Bernabé, D.B.-V.; van Bokhoven, H.; van Beusekom, E.; Van den Akker, W.; Kant, S.; Dobyns, W.; Cormand, B.; Currier, S.; Hamel, B.; Talim, B.; et al. A Homozygous Nonsense Mutation in the Fukutin Gene Causes a Walker-Warburg Syndrome Phenotype. *J. Med. Genet.* **2003**, *40*, 845–848. [CrossRef]
11. Brown, S.C.; Torelli, S.; Brockington, M.; Yuva, Y.; Jimenez, C.; Feng, L.; Anderson, L.; Ugo, I.; Kroger, S.; Bushby, K.; et al. Abnormalities in αDystroglycan Expression in MDC1C and LGMD2I Muscular Dystrophies. *Am. J. Pathol.* **2004**, *164*, 727–737. [CrossRef] [PubMed]
12. Torelli, S.; Brown, S.C.; Brockington, M.; Dolatshad, N.F.; Jimenez, C.; Skordis, L.; Feng, L.H.; Merlini, L.; Jones, D.H.; Romero, N.; et al. SubCellular Localisation of Fukutin Related Protein in Different Cell Lines and in the Muscle of Patients with MDC1C and LGMD2I. *Neuromuscul. Disord. NMD* **2005**, *15*, 836–843. [CrossRef] [PubMed]
13. Longman, C.; Brockington, M.; Torelli, S.; Jimenez-Mallebrera, C.; Kennedy, C.; Khalil, N.; Feng, L.; Saran, R.K.; Voit, T.; Merlini, L.; et al. Mutations in the Human LARGE Gene Cause MDC1D, a Novel Form of Congenital Muscular Dystrophy with Severe Mental Retardation and Abnormal Glycosylation of α-Dystroglycan. *Hum. Mol. Genet.* **2003**, *12*, 2853–2861. [CrossRef] [PubMed]
14. Brockington, M.; Torelli, S.; Prandini, P.; Boito, C.; Dolatshad, N.F.; Longman, C.; Brown, S.C.; Muntoni, F. Localization and Functional Analysis of the LARGE Family of Glycosyltransferases: Significance for Muscular Dystrophy. *Hum. Mol. Genet.* **2005**, *14*, 657–665. [CrossRef]
15. Okazaki, T.; Matsuura, K.; Kasagi, N.; Adachi, K.; Kai, M.; Okubo, M.; Nishino, I.; Nanba, E.; Maegaki, Y. Duchenne Muscular Dystrophy–like Phenotype in an LGMD2I Patient with Novel FKRP Gene Variants. *Hum. Genome Var.* **2020**, *7*, 12. [CrossRef]
16. Brockington, M.; Yuva, Y.; Prandini, P.; Brown, S.C.; Torelli, S.; Benson, M.A.; Herrmann, R.; Anderson, L.V.B.; Bashir, R.; Burgunder, J.-M.; et al. Mutations in the Fukutin-Related Protein Gene (FKRP) Identify Limb Girdle Muscular Dystrophy 2I as a Milder Allelic Variant of Congenital Muscular Dystrophy MDC1C. *Hum. Mol. Genet.* **2001**, *10*, 2851–2859. [CrossRef]
17. de Bernabé, D.B.-V.; Voit, T.; Longman, C.; Steinbrecher, A.; Straub, V.; Yuva, Y.; Herrmann, R.; Sperner, J.; Korenke, C.; Diesen, C.; et al. Mutations in the FKRP Gene Can Cause Muscle-Eye-Brain Disease and Walker–Warburg Syndrome. *J. Med. Genet.* **2004**, *41*, e61. [CrossRef]
18. Carmen, L.; Maria, V.; Morales-Medina, J.C.; Vallelunga, A.; Palmieri, B.; Iannitti, T. Role of Proteoglycans and Glycosaminoglycans in Duchenne Muscular Dystrophy. *Glycobiology* **2019**, *29*, 110–123. [CrossRef]
19. Pogoryelova, O.; Coraspe, J.A.G.; Nikolenko, N.; Lochmüller, H.; Roos, A. GNE myopathy: From clinics and genetics to pathology and research strategies. *Orphanet J. Rare Dis.* **2018**, *13*, 70. [CrossRef]
20. Pugliese, A.; Holland, S.H.; Rodolico, C.; Lochmüller, H.; Spendiff, S. Presynaptic Congenital Myasthenic Syndromes: Understanding Clinical Phenotypes through In Vivo Models. *J. Neuromuscul. Dis.* **2023**, *10*, 731–759. [CrossRef]
21. Bauché, S.; Vellieux, G.; Sternberg, D.; Fontenille, M.-J.; De Bruyckere, E.; Davoine, C.-S.; Brochier, G.; Messéant, J.; Wolf, L.; Fardeau, M.; et al. Mutations in GFPT1-Related Congenital Myasthenic Syndromes Are Associated with Synaptic Morphological Defects and Underlie a Tubular Aggregate Myopathy with Synaptopathy. *J. Neurol.* **2017**, *264*, 1791–1803. [CrossRef] [PubMed]
22. Dusl, M.; Senderek, J.; Müller, J.S.; Vogel, J.G.; Pertl, A.; Stucka, R.; Lochmüller, H.; David, R.; Abicht, A. A 3'-UTR Mutation Creates a microRNA Target Site in the GFPT1 Gene of Patients with Congenital Myasthenic Syndrome. *Hum. Mol. Genet.* **2015**, *24*, 3418–3426. [CrossRef] [PubMed]

23. Farshadyeganeh, P.; Nazim, M.; Zhang, R.; Ohkawara, B.; Nakajima, K.; Rahman, M.A.; Nasrin, F.; Ito, M.; Takeda, J.; Ohe, K.; et al. Splicing Regulation of GFPT1 Muscle-Specific Isoform and Its Roles in Glucose Metabolisms and Neuromuscular Junction. *iScience* **2023**, *26*, 107746. [CrossRef] [PubMed]
24. Guergueltcheva, V.; Müller, J.S.; Dusl, M.; Senderek, J.; Oldfors, A.; Lindbergh, C.; Maxwell, S.; Colomer, J.; Mallebrera, C.J.; Nascimento, A.; et al. Congenital Myasthenic Syndrome with Tubular Aggregates Caused by GFPT1 Mutations. *J. Neurol.* **2012**, *259*, 838–850. [CrossRef]

25. Issop, Y.; Hathazi, D.; Khan, M.M.; Rudolf, R.; Weis, J.; Spendiff, S.; Slater, C.R.; Roos, A.; Lochmüller, H. GFPT1 Deficiency in Muscle Leads to Myasthenia and Myopathy in Mice. *Hum. Mol. Genet.* **2018**, *27*, 3218–3232. [CrossRef]
26. Jiang, K.; Zheng, Y.; Lin, J.; Wu, X.; Yu, Y.; Zhu, M.; Fang, X.; Zhou, M.; Li, X.; Hong, D. Diverse Myopathological Features in the Congenital Myasthenia Syndrome with GFPT1 Mutation. *Brain Behav.* **2022**, *12*, e2469. [CrossRef]
27. Ma, Y.; Xiong, T.; Lei, G.; Ding, J.; Yang, R.; Li, Z.; Guo, J.; Shen, D. Novel Compound Heterozygous Variants in the GFPT1 Gene Leading to Rare Limb-Girdle Congenital Myasthenic Syndrome with Rimmed Vacuoles. *Neurol. Sci.* **2021**, *42*, 3485–3490. [CrossRef]
28. Zoltowska, K.; Webster, R.; Finlayson, S.; Maxwell, S.; Cossins, J.; Müller, J.; Lochmüller, H.; Beeson, D. Mutations in GFPT1 That Underlie Limb-Girdle Congenital Myasthenic Syndrome Result in Reduced Cell-Surface Expression of Muscle AChR. *Hum. Mol. Genet.* **2013**, *22*, 2905–2913. [CrossRef]
29. Szelinger, S.; Krate, J.; Ramsey, K.; Strom, S.P.; Shieh, P.B.; Lee, H.; Belnap, N.; Balak, C.; Siniard, A.L.; Russell, M.; et al. Congenital Myasthenic Syndrome Caused by a Frameshift Insertion Mutation in GFPT1. *Neurol. Genet.* **2020**, *6*, e468. [CrossRef]
30. Belaya, K.; Finlayson, S.; Cossins, J.; Liu, W.W.; Maxwell, S.; Palace, J.; Beeson, D. Identification of DPAGT1 as a New Gene in Which Mutations Cause a Congenital Myasthenic Syndrome. *Ann. N. Y. Acad. Sci.* **2012**, *1275*, 29–35. [CrossRef]
31. Finlayson, S.; Palace, J.; Belaya, K.; Walls, T.J.; Norwood, F.; Burke, G.; Holton, J.L.; Pascual-Pascual, S.I.; Cossins, J.; Beeson, D. Clinical Features of Congenital Myasthenic Syndrome Due to Mutations in DPAGT1. *J. Neurol. Neurosurg. Psychiatry* **2013**, *84*, 1119–1125. [CrossRef] [PubMed]
32. Ohno, K.; Ohkawara, B.; Shen, X.-M.; Selcen, D.; Engel, A.G. Clinical and Pathologic Features of Congenital Myasthenic Syndromes Caused by 35 Genes—A Comprehensive Review. *Int. J. Mol. Sci.* **2023**, *24*, 3730. [CrossRef] [PubMed]
33. Basiri, K.; Belaya, K.; Liu, W.W.; Maxwell, S.; Sedghi, M.; Beeson, D. Clinical Features in a Large Iranian Family with a Limb-Girdle Congenital Myasthenic Syndrome Due to a Mutation in DPAGT1. *Neuromuscul. Disord.* **2013**, *23*, 469–472. [CrossRef] [PubMed]
34. Belaya, K.; Rodríguez Cruz, P.M.; Liu, W.W.; Maxwell, S.; McGowan, S.; Farrugia, M.E.; Petty, R.; Walls, T.J.; Sedghi, M.; Basiri, K.; et al. Mutations in GMPPB Cause Congenital Myasthenic Syndrome and Bridge Myasthenic Disorders with Dystroglycanopathies. *Brain* **2015**, *138*, 2493–2504. [CrossRef]
35. Rodríguez Cruz, P.M.; Belaya, K.; Basiri, K.; Sedghi, M.; Farrugia, M.E.; Holton, J.L.; Liu, W.W.; Maxwell, S.; Petty, R.; Walls, T.J.; et al. Clinical Features of the Myasthenic Syndrome Arising from Mutations in GMPPB. *J. Neurol. Neurosurg. Psychiatry* **2016**, *87*, 802–809. [CrossRef]
36. Cossins, J.; Belaya, K.; Hicks, D.; Salih, M.A.; Finlayson, S.; Carboni, N.; Liu, W.W.; Maxwell, S.; Zoltowska, K.; Farsani, G.T.; et al. Congenital Myasthenic Syndromes Due to Mutations in ALG2 and ALG14. *Brain* **2013**, *136*, 944–956. [CrossRef]
37. Ehrstedt, C.; Liu, W.-W.; Frykholm, C.; Beeson, D.; Punga, A.R. Novel Pathogenic ALG2 Mutation Causing Congenital Myasthenic Syndrome: A Case Report. *Neuromuscul. Disord.* **2022**, *32*, 80–83. [CrossRef]
38. Katata, Y.; Uneoka, S.; Saijyo, N.; Aihara, Y.; Miyazoe, T.; Koyamaishi, S.; Oikawa, Y.; Ito, Y.; Abe, Y.; Numata-Uematsu, Y.; et al. The Longest Reported Sibling Survivors of a Severe Form of Congenital Myasthenic Syndrome with the ALG14 Pathogenic Variant. *Am. J. Med. Genet. A.* **2022**, *188*, 1293–1298. [CrossRef]
39. Akella, N.M.; Ciraku, L.; Reginato, M.J. Fueling the Fire: Emerging Role of the Hexosamine Biosynthetic Pathway in Cancer. *BMC Biol.* **2019**, *17*, 52. [CrossRef]
40. Paneque, A.; Fortus, H.; Zheng, J.; Werlen, G.; Jacinto, E. The Hexosamine Biosynthesis Pathway: Regulation and Function. *Genes* **2023**, *14*, 933. [CrossRef]
41. de Queiroz, R.M.; Oliveira, I.A.; Piva, B.; Bouchuid Catão, F.; da Costa Rodrigues, B.; da Costa Pascoal, A.; Diaz, B.L.; Todeschini, A.R.; Caarls, M.B.; Dias, W.B. Hexosamine Biosynthetic Pathway and Glycosylation Regulate Cell Migration in Melanoma Cells. *Front. Oncol.* **2019**, *9*, 116. [CrossRef] [PubMed]
42. Chokchaitaweesuk, C.; Kobayashi, T.; Izumikawa, T.; Itano, N. Enhanced Hexosamine Metabolism Drives Metabolic and Signaling Networks Involving Hyaluronan Production and O-GlcNAcylation to Exacerbate Breast Cancer. *Cell Death Dis.* **2019**, *10*, 803. [CrossRef] [PubMed]
43. Claeyssen, C.; Bastide, B.; Cieniewski-Bernard, C. Global O-GlcNAcylation Changes Impact Desmin Phosphorylation and Its Partition toward Cytoskeleton in C2C12 Skeletal Muscle Cells Differentiated into Myotubes. *Sci. Rep.* **2022**, *12*, 9831. [CrossRef] [PubMed]
44. Sheikh, M.A.; Emerald, B.S.; Ansari, S.A. Stem Cell Fate Determination through Protein O-GlcNAcylation. *J. Biol. Chem.* **2020**, *296*, 100035. [CrossRef] [PubMed]
45. Wang, Z.V.; Deng, Y.; Gao, N.; Pedrozo, Z.; Li, D.L.; Morales, C.R.; Criollo, A.; Luo, X.; Tan, W.; Jiang, N.; et al. Spliced X-Box Binding Protein 1 Couples the Unfolded Protein Response to Hexosamine Biosynthetic Pathway. *Cell* **2014**, *156*, 1179–1192. [CrossRef]
46. Watson, L.J.; Long, B.W.; DeMartino, A.M.; Brittian, K.R.; Readnower, R.D.; Brainard, R.E.; Cummins, T.D.; Annamalai, L.; Hill, B.G.; Jones, S.P. Cardiomyocyte Ogt Is Essential for Postnatal Viability. *Am. J. Physiol. Heart Circ. Physiol.* **2014**, *306*, H142–H153. [CrossRef]

47. Nagy, T.; Champattanachai, V.; Marchase, R.B.; Chatham, J.C. Glucosamine Inhibits Angiotensin II-Induced Cytoplasmic Ca^{2+} Elevation in Neonatal Cardiomyocytes via Protein-Associated O-Linked N-Acetylglucosamine. *Am. J. Physiol. Cell Physiol.* **2006**, *290*, C57–C65. [CrossRef]
48. Sayat, R.; Leber, B.; Grubac, V.; Wiltshire, L.; Persad, S. O-GlcNAc-Glycosylation of Beta-Catenin Regulates Its Nuclear Localization and Transcriptional Activity. *Exp. Cell Res.* **2008**, *314*, 2774–2787. [CrossRef]
49. Roth, J.; Zuber, C.; Park, S.; Jang, I.; Lee, Y.; Kysela, K.G.; Fourn, V.L.; Santimaria, R.; Guhl, B.; Cho, J.W. Protein *N*-Glycosylation, Protein Folding, and Protein Quality Control. *Mol. Cells* **2010**, *30*, 497–506. [CrossRef]
50. Hinderlich, S.; Weidemann, W.; Yardeni, T.; Horstkorte, R.; Huizing, M. UDP-GlcNAc 2-Epimerase/ManNAc Kinase (GNE): A Master Regulator of Sialic Acid Synthesis. *Top. Chem. Curr.* **2015**, *366*, 97–138. [CrossRef]

51. Senderek, J.; Müller, J.S.; Dusl, M.; Strom, T.M.; Guergueltcheva, V.; Diepolder, I.; Laval, S.H.; Maxwell, S.; Cossins, J.; Krause, S.; et al. Hexosamine Biosynthetic Pathway Mutations Cause Neuromuscular Transmission Defect. *Am. J. Hum. Genet.* **2011**, *88*, 162–172. [CrossRef] [PubMed]
52. Chen, Q.; Müller, J.S.; Pang, P.-C.; Laval, S.H.; Haslam, S.M.; Lochmüller, H.; Dell, A. Global N-Linked Glycosylation Is Not Significantly Impaired in Myoblasts in Congenital Myasthenic Syndromes Caused by Defective Glutamine-Fructose-6-Phosphate Transaminase 1 (GFPT1). *Biomolecules* **2015**, *5*, 2758–2781. [CrossRef] [PubMed]
53. Whelan, S.A.; Lane, M.D.; Hart, G.W. Regulation of the *O*-Linked β-*N*-Acetylglucosamine Transferase by Insulin Signaling. *J. Biol. Chem.* **2008**, *283*, 21411–21417. [CrossRef]
54. Qiang, A.; Slawson, C.; Fields, P.E. The Role of O-GlcNAcylation in Immune Cell Activation. *Front. Endocrinol.* **2021**, *12*, 596617. [CrossRef] [PubMed]
55. Lambert, M.; Richard, E.; Duban-Deweer, S.; Krzewinski, F.; Deracinois, B.; Dupont, E.; Bastide, B.; Cieniewski-Bernard, C. O-GlcNAcylation Is a Key Modulator of Skeletal Muscle Sarcomeric Morphometry Associated to Modulation of Protein–Protein Interactions. *Biochim. Biophys. Acta BBA Gen. Subj.* **2016**, *1860*, 2017–2030. [CrossRef]
56. Haltiwanger, R.S.; Holt, G.D.; Hart, G.W. Enzymatic Addition of O-GlcNAc to Nuclear and Cytoplasmic Proteins. Identification of a Uridine Diphospho-N-Acetylglucosamine:Peptide Beta-N-Acetylglucosaminyltransferase. *J. Biol. Chem.* **1990**, *265*, 2563–2568. [CrossRef]
57. Hart, G.W.; Housley, M.P.; Slawson, C. Cycling of O-Linked Beta-N-Acetylglucosamine on Nucleocytoplasmic Proteins. *Nature* **2007**, *446*, 1017–1022. [CrossRef]
58. Shi, H.; Munk, A.; Nielsen, T.S.; Daughtry, M.R.; Larsson, L.; Li, S.; Høyer, K.F.; Geisler, H.W.; Sulek, K.; Kjøbsted, R.; et al. Skeletal Muscle OGlcNAc Transferase Is Important for Muscle Energy Homeostasis and Whole-Body Insulin Sensitivity. *Mol. Metab.* **2018**, *11*, 160–177. [CrossRef]
59. Finsterer, J. Congenital Myasthenic Syndromes. *Orphanet J. Rare Dis.* **2019**, *14*, 57. [CrossRef]
60. Ramanathan, V.K.; Hall, Z.W. Altered Glycosylation Sites of the δ Subunit of the Acetylcholine Receptor (AChR) Reduce Aδ Association and Receptor Assembly. *J. Biol. Chem.* **1999**, *274*, 20513–20520. [CrossRef]
61. Rudell, J.C.; Borges, L.S.; Yarov-Yarovoy, V.; Ferns, M. The MX-Helix of Muscle nAChR Subunits Regulates Receptor Assembly and Surface Trafficking. *Front. Mol. Neurosci.* **2020**, *13*, 48. [CrossRef] [PubMed]
62. Hui, T.; Jing, H.; Lai, X. Neuromuscular Junction-Specific Genes Screening by Deep RNA-Seq Analysis. *Cell Biosci.* **2021**, *11*, 81. [CrossRef] [PubMed]
63. Watty, A.; Burden, S.J. MuSK Glycosylation Restrains MuSK Activation and Acetylcholine Receptor Clustering. *J. Biol. Chem.* **2002**, *277*, 50457–50462. [CrossRef] [PubMed]
64. Zachara, N.E.; Vosseller, K.; Hart, G.W. Detection and Analysis of Proteins Modified by O-Linked N-Acetylglucosamine. *Curr. Protoc. Protein Sci.* **2011**, *12*, 8.1–8.33. [CrossRef]
65. Li, L.; Cao, Y.; Wu, H.; Ye, X.; Zhu, Z.; Xing, G.; Shen, C.; Barik, A.; Zhang, B.; Xie, X.; et al. Enzymatic Activity of the Scaffold Protein Rapsyn for Synapse Formation. *Neuron* **2016**, *92*, 1007–1019. [CrossRef]
66. Xing, G.; Xiong, W.-C.; Mei, L. Rapsyn as a Signaling and Scaffolding Molecule in Neuromuscular Junction Formation and Maintenance. *Neurosci. Lett.* **2020**, *731*, 135013. [CrossRef]
67. Arnold, W.D.; Sheth, K.A.; Wier, C.G.; Kissel, J.T.; Burghes, A.H.; Kolb, S.J. Electrophysiological Motor Unit Number Estimation (MUNE) Measuring Compound Muscle Action Potential (CMAP) in Mouse Hindlimb Muscles. *J. Vis. Exp. JoVE* **2015**, *103*, 52899. [CrossRef]
68. LoRusso, S.J.; Iyadurai, S.J. Decrement with High Frequency Repetitive Nerve Stimulation in a RAPSN Congenital Myasthenic Syndrome. *Muscle Nerve* **2018**, *57*, E106–E108. [CrossRef]
69. An, R.; Chen, H.; Lei, S.; Li, Y.; Xu, Y.; He, C. Abnormal Decrement on High-Frequency Repetitive Nerve Stimulation in Congenital Myasthenic Syndrome with GFPT1 Mutations and Review of Literature. *Front. Neurol.* **2022**, *13*, 926786. [CrossRef]
70. Zhang, R.; Farshadyeganeh, P.; Ohkawara, B.; Nakajima, K.; Takeda, J.-I.; Ito, M.; Zhang, S.; Miyasaka, Y.; Ohno, T.; MoriYoshimura, M.; et al. Muscle-specific lack of Gfpt1 triggers ER stress to alleviate misfolded protein accumulation. *Dis. Model. Mech.* **2024**, *17*, dmm050768. [CrossRef]
71. Awasthi, K.; Srivastava, A.; Bhattacharya, S.; Bhattacharya, A. Tissue Specific Expression of Sialic Acid Metabolic Pathway: Role in GNE Myopathy. *J. Muscle Res. Cell Motil.* **2021**, *42*, 99–116. [CrossRef] [PubMed]

72. Nishikaze, T. Sialic Acid Derivatization for Glycan Analysis by Mass Spectrometry. *Proc. Jpn. Acad. Ser. B Phys. Biol. Sci.* **2019**, *95*, 523–537. [CrossRef] [PubMed]
73. Marini, M.; Tani, A.; Manetti, M.; Sgambati, E. Overview of Sialylation Status in Human Nervous and Skeletal Muscle Tissues during Aging. *Acta Histochem.* **2021**, *123*, 151813. [CrossRef] [PubMed]
74. Nilsson, J.; Nilsson, J.; Larson, G.; Grahn, A. Characterization of Site-Specific O-Glycan Structures within the Mucin-like Domain of αDystroglycan from Human Skeletal Muscle. *Glycobiology* **2010**, *20*, 1160–1169. [CrossRef] [PubMed]
75. McDearmon, E.L.; Combs, A.C.; Ervasti, J.M. Core 1 Glycans on α-Dystroglycan Mediate Laminin-Induced Acetylcholine Receptor Clustering but Not Laminin Binding. *J. Biol. Chem.* **2003**, *278*, 44868–44873. [CrossRef] [PubMed]
76. Wanamaker, C.P.; Green, W.N. N-Linked Glycosylation Is Required for Nicotinic Receptor Assembly but Not for Subunit Associations with Calnexin. *J. Biol. Chem.* **2005**, *280*, 33800–33810. [CrossRef] [PubMed]

77. Apel, E.D.; Glass, D.J.; Moscoso, L.M.; Yancopoulos, G.D.; Sanes, J.R. Rapsyn Is Required for MuSK Signaling and Recruits Synaptic Components to a MuSK-Containing Scaffold. *Neuron* **1997**, *18*, 623–635. [CrossRef]
78. Liao, X.; Wang, Y.; Lai, X.; Wang, S. The Role of Rapsyn in Neuromuscular Junction and Congenital Myasthenic Syndrome. *Biomol. Biomed.* **2023**, *23*, 772–784. [CrossRef]
79. Kim, M.-L.; Chandrasekharan, K.; Glass, M.; Shi, S.; Stahl, M.C.; Kaspar, B.; Stanley, P.; Martin, P.T. O-Fucosylation of Muscle Agrin Determines Its Ability to Cluster Acetylcholine Receptors. *Mol. Cell. Neurosci.* **2008**, *39*, 452–464. [CrossRef]
80. Hoshi, T.; Tezuka, T.; Yokoyama, K.; Iemura, S.; Natsume, T.; Yamanashi, Y. Mesdc2 Plays a Key Role in Cell-Surface Expression of Lrp4 and Postsynaptic Specialization in Myotubes. *FEBS Lett.* **2013**, *587*, 3749–3754. [CrossRef]
81. Fenckova, M.; Muha, V.; Mariappa, D.; Catinozzi, M.; Czajewski, I.; Blok, L.E.R.; Ferenbach, A.T.; Storkebaum, E.; Schenck, A.; van Aalten, D.M.F. Intellectual Disability-Associated Disruption of O-GlcNAc Cycling Impairs Habituation Learning in Drosophila. *PLoS Genet.* **2022**, *18*, e1010159. [CrossRef] [PubMed]
82. Lee, B.E.; Suh, P.-G.; Kim, J.-I. O-GlcNAcylation in Health and Neurodegenerative Diseases. *Exp. Mol. Med.* **2021**, *53*, 1674–1682. [CrossRef] [PubMed]
83. Hwang, H.; Rhim, H. Acutely Elevated O-GlcNAcylation Suppresses Hippocampal Activity by Modulating Both Intrinsic and Synaptic Excitability Factors. *Sci. Rep.* **2019**, *9*, 7287. [CrossRef] [PubMed]
84. Nakamura, S.; Nakano, S.; Nishii, M.; Kaneko, S.; Kusaka, H. Localization of O-GlcNAc-Modified Proteins in Neuromuscular Diseases. *Med. Mol. Morphol.* **2012**, *45*, 86–90. [CrossRef] [PubMed]
85. Hart, G.W.; Slawson, C.; Ramirez-Correa, G.; Lagerlof, O. Cross Talk Between O-GlcNAcylation and Phosphorylation: Roles in Signaling, Transcription, and Chronic Disease. *Annu. Rev. Biochem.* **2011**, *80*, 825–858. [CrossRef]
86. vanden Brande, L.; Bauché, S.; Pérez-Guàrdia, L.; Sternberg, D.; Seferian, A.M.; Malfatti, E.; Silva-Rojas, R.; Labasse, C.; Chevessier, F.; Carlier, P.; et al. Pathogenic DPAGT1 Variants in Limb-Girdle Congenital Myasthenic Syndrome (LG-CMS) Associated with Tubular Aggregates and ORAI1 Hypoglycosylation. *Neuropathol. Appl. Neurobiol.* **2024**, *50*, e12952. [CrossRef]
87. Gang, Q.; Bettencourt, C.; Brady, S.; Holton, J.L.; Healy, E.G.; McConville, J.; Morrison, P.J.; Ripolone, M.; Violano, R.; Sciacco, M.; et al. Genetic Defects Are Common in Myopathies with Tubular Aggregates. *Ann. Clin. Transl. Neurol.* **2021**, *9*, 4–15. [CrossRef]
88. Kim, S.; Maynard, J.C.; Sasaki, Y.; Strickland, A.; Sherman, D.L.; Brophy, P.J.; Burlingame, A.L.; Milbrandt, J. Schwann Cell O-GlcNAc Glycosylation Is Required for Myelin Maintenance and Axon Integrity. *J. Neurosci.* **2016**, *36*, 9633–9646. [CrossRef]
89. Kwon, S.E.; Chapman, E.R. Glycosylation Is Dispensable for Sorting of Synaptotagmin 1 but Is Critical for Targeting of SV2 and Synaptophysin to Recycling Synaptic Vesicles. *J. Biol. Chem.* **2012**, *287*, 35658–35668. [CrossRef]

OXFORD UNIVERSITY PRESS LICENSE
TERMS AND CONDITIONS

May 08, 2026

This Agreement between Stephen Holland ("You") and Oxford University Press ("Oxford University Press") consists of your license details and the terms and conditions provided by Oxford University Press and Copyright Clearance Center.

License Number	6264210763102
License date	May 08, 2026
Licensed content publisher	Oxford University Press
Licensed content publication	Human Molecular Genetics
Licensed content title	Galactose treatment rescues neuromuscular junction transmission in glutamine-fructose-6-phosphate transaminase 1 (Gfpt1) deficient mice
Licensed content author	Holland, Stephen Henry; Carmona-Martinez, Ricardo
Licensed content date	Aug 29, 2025
Type of Use	Thesis/Dissertation
Institution name	
Title of your work	Galactose treatment rescues neuromuscular junction transmission in glutamine-fructose-6-phosphate transaminase 1 (Gfpt1) deficient mice
Publisher of your work	University of Ottawa

Expected publication date	**Jun 2026**
Permissions cost	**0.00 USD**
Value added tax	**0.00 USD**
Total	**0.00 USD**
Title of new work	Galactose treatment rescues neuromuscular junction transmission in glutamine-fructose-6-phosphate transaminase 1 (Gfpt1) deficient mice
Institution name	University of Ottawa
Expected presentation date	Jun 2026
The Requesting Person / Organization to Appear on the License	Stephen Holland

Human Molecular Genetics, 2025, Vol. 34, 21, 1765–1779

OXFORD

https://doi.org/10.1093/hmg/ddaf140 Advance access publication date 29 August 2025

Original Article

Galactose treatment rescues neuromuscular junction transmission in glutamine-fructose-6-phosphate transaminase 1 (Gfpt1) deficient mice

Stephen Henry Holland [1,2,3], Ricardo Carmona-Martinez[1], Daniel O'Neil[1], Kelly Ho[1,2], Kaela O'Connor[1,2], Yoshiteru Azuma [4,5], Andreas Roos [3,6,7], Sally Spendiff[1], Hanns Lochmüller [1,2,3,8,9,10,*]

[1]Children's Hospital of Eastern Ontario Research Institute, 401 Smyth Road, Ottawa, ON K1H 8L1, Canada
[2]Department of Cellular and Molecular Medicine, Faculty of Medicine, University of Ottawa, 451 Smyth Road, Ottawa, ON K1H 8M5, Canada
[3]Eric Poulin Center for Neuromuscular Disease, Brain and Mind Research Institute, University of Ottawa, 451 Smyth Road, Ottawa, ON K1H 8M5, Canada
[4]Department of Human Genetics, Graduate School of Medicine, Yokohama City University, Kanazawa-ku, Yokohama 236-0027, Japan
[5]Department of Pediatrics, Aichi Medical University, Nagakute, Aichi, 480-1195, Japan
[6]Department of Pediatric Neurology, Center for Neuromuscular Disorders, University Duisburg-Essen, 45147 Essen, Germany
[7]Department of Neurology, Medical Faculty and University Hospital Düsseldorf, Heinrich Heine University Dusseldorf, 40225 Düsseldorf, Germany
[8]Division of Neurology, Department of Medicine, The Ottawa Hospital Civic Campus, 1053 Carling Avenue, Ottawa, ON K1Y 4E9, Canada
[9]Department of Neuropediatrics and Muscle Disorders, Medical Center – University of Freiburg, Faculty of Medicine, Mathildenstr, 179160, Freiburg, Germany [10]Centro Nacional de Análisis Genómico (CNAG), 4, Barcelona Science Park - Tower I, Barcelona 08028, Spain

Abstract

Congenital myasthenic syndromes (CMS) arise from mutations to proteins involved in neuromuscular junction (NMJ) development, maintenance, and neurotransmission. To date, mutations in more than 35 genes have been linked to CMS development. Glutamine fructose-6-phosphate transaminase 1 (*GFPT1/Gfpt1)* serves as the ratelimiting enzyme of the hexosamine biosynthetic pathway (HBP), producing the byproduct (UDP-GlcNAc) necessary for protein glycosylation.Gfpt1-deficient models have impaired protein glycosylation, impacting key proteins at the NMJ. The Leloir pathway is a galactose metabolizing pathway which produces UDP-GalNAc as its final product. The enzyme UDP-GalNAc Epimerase (*GALE)* can also convert excess UDP-GalNAc into UDP-GlcNAc, the byproduct of the HBP. We hypothesized that treatment with galactose both *in vitro* and *in vivo* in Gfpt1-deficient models would rescue impaired protein O-GlcNAcylation and reverse the glycosylation status of key NMJ-associated proteins. We show that galactose treatment *in vitro* activated the Leloir pathway and rescued protein O-GlcNAcylation in Gfpt1-deficient C2C12 myoblasts. In addition, we demonstrated that galactose therapy rescued neuromuscular deficits, improved muscle fatigue and restored NMJ morphology in a skeletal musclespecific Gfpt1 knockout mouse model. Lastly, we showed that galactose treatment rescued protein O-GlcNAcylation in skeletal muscle, preserving the glycosylation status of the delta (δ) subunit of the acetylcholine receptor (AChRδ). Taken together, we suggest that galactose supplementation can be further explored as a therapy for *GFPT1*-CMS patients.

Keywords: Glycosylation; Galactose; Glutamine-Fructose-6-Phosphate Transaminase 1; Congenital Myasthenic Syndrome; Neuromuscular Junction

Introduction

The neuromuscular junction (NMJ) is the site where the motor neuron

mannosyltransferase (*ALG2*) [11, 12], and UDP-Nacetylglucosaminyltransferase subunit 14 (*ALG14*) [11].

innervates the skeletal muscle, enabling muscular contraction. Congenital *GFPT1* encodes the rate-limiting enzyme of the hexosamine biosynthetic myasthenic syndromes (CMS) are inheritable early-onset neuromuscular pathway (HBP), a metabolic signaling pathway that produces the precursors disorders that arise from mutations to proteins involved in NMJ for the formation of N- and O-linked glycans [13–16]. It has been speculated development, maintenance, and function [1, 2]. CMS is a heterogeneous that hypoglycosylation of key NMJ proteins impairs neurotransmission and disorder characterized by fatigable muscle

weakness [1]. To date, over 35 disrupts postsynap- genes have been associated with CMS [1, 3]. These genes encode proteins tic folding [15,17].Biallelic mutations to *GFPT1* result in decreased protein

Received: April 8, 2025. **Revised:** July 9, 2025. **Accepted:** August 10, 2025

297

that are localized to the presynaptic nerve terminal, postsynaptic skeletal muscle, and synaptic cleft. A subset of five CMS-causative genes impair glycosylation: glutamine-fructose-6-phosphate transaminase 1 (*GFPT1*), dolichol-phosphate N-acetylglucosaminephosphotransferase-1 (*DPAGT1*) [4–8], GDP-mannose pyrophosphorylase B (*GMPPB*) [9, 10], α-

1,3/1,6levels, and impaired enzymatic activity [14, 18–22]. Most recently, we identified that protein O-GlcNAcylation and N-linked glycosylation was impaired in Gfpt1-depleted models, confirming that *GFPT1*-CMS is a protein glycosylation disorder [15]. In addition, we discovered that the delta subunit of the acetylcholine receptor (AChRδ) in Gfpt1-depleted models was hypoglycosylated within the NMJ, resulting in a lower molecular weight species, thus defining the first NMJ-relevant glycosylation target of loss of Gfpt1-function [15].

Clinically, *GFPT1*-CMS patients present predominantly with limb/girdle muscle weakness [14, 18, 23]. Examination of muscle biopsies from patients reveals diverse myopathological features, including tubular aggregates and rimmed vacuoles [23, 24]. In addition, these myopathological features were identified in our previously published skeletal-muscle specific mouse model, termed *Gfpt1*$^{tm1d/tm1d}$, declaring that the mouse model accurately maps towards *GFPT1*-CMS in humans [15, 17]. Electron microscopy analysis of NMJs show loss of postsynaptic folds and simplification [23, 24]. Patients have frequently responded well to treatments that increase the availability of acetylcholine (ACh) in the synaptic cleft, such as pyridostigmine, an acetylcholine esterase (AChE) inhibitor, and potassium channel inhibitor 3,4diaminopyridine [25, 26]. However, long-term use of these compounds has been associated with adverse side effects in some patients [27]. Furthermore, the efficacy of these drugs may decrease over time, leading to worsening motor weakness [25, 27]. Given these challenges, there is an urgent need for alternative therapies or co-therapeutic strategies to improve the long-term outcomes for CMS patients.

Congenital disorders of glycosylation (CDGs) arise from mutations to genes responsible for the synthesis or the attachment of glycans to glycoproteins [28]. Patients diagnosed with CDGs with variants in *PGM1*, *SLC34A2*, *SLC39A8,* and *TMEM165* show improved endocrine function, restored glycosylation, improved seizure control and improved blood coagulation with galactose supplementation [29–31].We hypothesized that galactose supplementation could offer a beneficial treatment strategy for *GFPT1*CMS patients, bypassing the defective HBP and restoring protein glycosylation.

In this study, we show galactose supplementation restores protein OGlcNAcylation and rescues pathological features,including NMJ morphology and AChRδ glycosylation status in cell and animal models of Gfpt1deficiency.

Results

Galactose treatment in C2C12 myoblasts activates Leloir pathway enzymes and increases protein OGlcNAcylation

Monosaccharide supplementation has been shown to bypass defective glycosylation in different forms of CDGs [28–32]. *GFPT1*CMS has been previously shown to have defects in HBP flux, which in turn impairs both protein O-GlcNAcylation and the production of complex N-linked glycan structures [15, 17]. Galactose is a monosaccharide that is metabolized via the Leloir pathway to produce UDP-GalNAc (Fig. 1A). The galactosemetabolizing enzyme *Gale* converts UDP-GalNAc into UDPGlcNAc, the precursor for protein O-GlcNAcylation (Fig. 1A). We investigated whether the inhibition of Gfpt1 with 6-diazo-5oxo-L-norleucine (DON) activated the expression of galactose metabolizing enzymes *Galk,*

278

Galt, and *Gale* in C2C12 myoblasts. We observed a slight, but significant increase in the expression of *Galk*, *Galt*, and *Gale* (Fig. 1B–D). Treatment with galactose similarly enhanced the expression of *Galk, Galt,* and *Gale* (Fig. 1E–G) along with *Slc35a2*, the UDP-galactose transporter (Fig. 1H). Next, we studied whether there is a dose-dependent effect of galactose treatment on protein O-GlcNAcylation. By examining *Ogt* expression, the enzyme responsible for attaching the GlcNAc moiety to proteins, we showed that galactose treatment between 1 mM to 10 mM enhanced *Ogt* expression, with the effect plateauing at concentrations above 10 mM galactose (Fig. 1I).This increase in *Ogt* expression is mirrored by an elevation in total protein OGlcNAcylation after galactose treatment (Fig. 1J and K). Similarly, at dosages exceeding 10 mM, protein O-GlcNAcylation levels plateau and all subsequent galactose experiments were therefore performed at 10 mM. Together, these data demonstrate that HBP flux in C2C12 myoblasts can be altered with galactose metabolism, leading to an overall increase in total protein OGlcNAcylation.

Galactose supplementation in Gfpt1-depleted C2C12 myoblasts improves protein O-GlcNAcylation

Using an inducible *Gfpt1*-deficient C2C12 model with reduced Gfpt1, Ogt, and total protein O-GlcNAcylation levels [15], we examined if galactose treatment could improve the expression of *Scl35a2* and activate the Leloir pathway. We confirmed that Gfpt1 deficiency does not impact *Slc35a2* and *Gale* expression, though treatment with 10 mM galactose resulted in a notable increase in their expression when compared to the galactosetreated scramble C2C12 myoblasts (Fig. 2A and B).

A 10 mM galactose treatment was administered with and without 2 μg/mL of doxycycline to induce the expression of shGfpt1 transgenes.While galactose treatment did not impact the expression of *Ogt* in scramble control C2C12 myoblasts, Gfpt1deficient myoblasts had a significant reduction in *Ogt* expression compared to scramble that was partially rescued with galactose treatment (Fig. 2C). Gfpt1 depletion correlated with a decrease in

302

overall protein O-GlcNAcylation levels after doxycycline activation (Fig. 2D–F). While galactose treatment had no impact on Gfpt1 protein levels, it did improve total protein O-GlcNAcylation in both Gfpt1-depleted myoblasts (Fig. 2D–F). All together, these results suggest that galactose supplementation *in vitro* can partially rescue protein O-GlcNAcylation.

10% (w/v) galactose treatment in *Gfpt1*$^{tm1d/tm1d}$ mice improves muscle strength and endurance

We previously showed Gfpt1 knockout results in progressive muscle fatigability with impaired NMJ morphology in mice [15, 17]. We hypothesized that *ad libitum* access to a 10% (w/v) galactose solution would improve muscle fatigability and NMJ morphology in *Gfpt1*$^{tm1d/tm1d}$ mice (Fig. 3A). Over the course of 20 weeks, galactose treatment did not affect body weight in male or female mice (Fig. 3B, Supplementary Fig. S1A and B) and normalized an increase in body fat [15] (Fig. 3C, Supplementary Fig. S1C and D). Water consumption remained consistent between the treatment groups regardless of galactose supplementation (data not shown).

Weekly behavioural studies were conducted to examine muscle endurance and grip strength fatigability. Untreated *Gfpt1*$^{tm1d/tm1d}$ mice demonstrated a progressive impairment to hanging impulse (Fig. 3D, Supplementary Fig. S2A) and increased grip strength fatigability (Fig. 3E, Supplementary Data). Galactose treatment partially rescued the hanging impulse (Fig. 3D, Supplementary Fig. S2A) and both front paw and allpaw grip strength fatigability (Fig. 3E and F, Supplementary 3A).

299
279

299

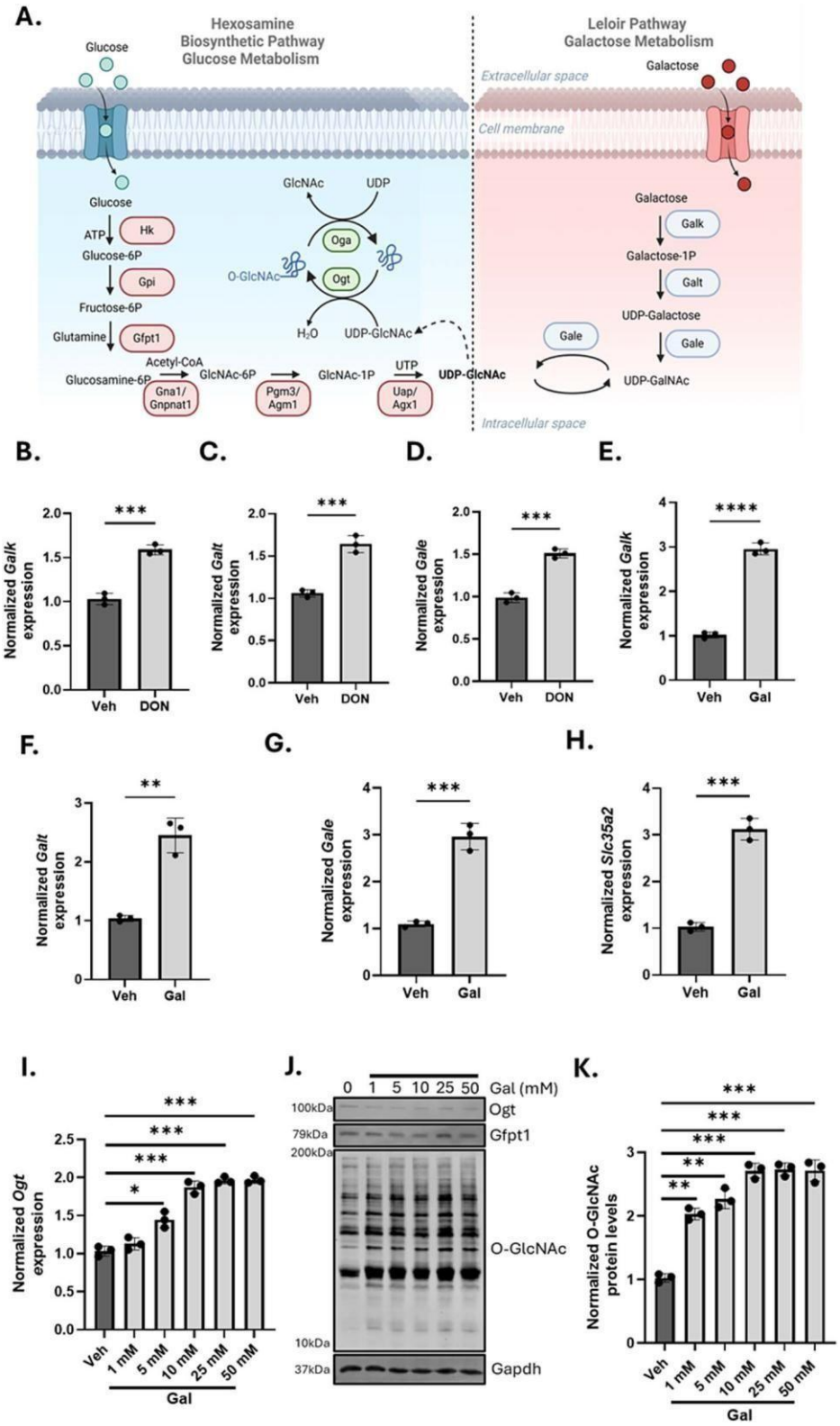

Figure 1. Galactose treatment elevates protein O-GlcNAcylation in C2C12 myoblasts. A. Gfpt1 serves as the rate-limiting enzyme of the hexosamine biosynthetic pathway (HBP), a metabolic signaling pathway which metabolizes glucose into UDP-GlcNAc, a precursor for N- and O-linked protein glycosylation. Galactose is a monosaccharide that feeds into the Leloir pathway within skeletal muscle. The Leloir pathway produces UDP-GalNAc, which can be converted by the Gale enzyme into UDP-GalNAc, effectively bypassing the defective HBP. B. In wild type C2C12 myoblasts, inhibition of Gfpt1 with DON for 48 hrs substantially increases the expression of Leloir pathway enzymes *Galk;* C. *Galt*; D. And *Gale*. E. C2C12 treatment with galactose significantly increases the expression of genes associated with the Leloir pathway: *Galk;* F. *Galt*; G. *Gale*; H. And the UDP-galactose transporter, *Slc35a2*. I. Following galactose treatment, there is a dose-dependent increase in *Ogt* expression. J. A western blot showing the protein levels of Ogt, Gfpt1 and O-GlcNAc within C2C12 myoblasts treated with varying concentrations of galactose. K. There is a significant increase in protein O-GlcNAcylation that plateaus beyond 10 mM of galactose.

All graphs show mean±SD. Statistical significance was determined via a student t-test (panels B through H) or a one-way ANOVA (panels I and K). All experiments were performed with three biological replicates. *P*-value <0.05, ** *P*-value <0.01, *** *P*-value <0.001, and **** <0.0001.

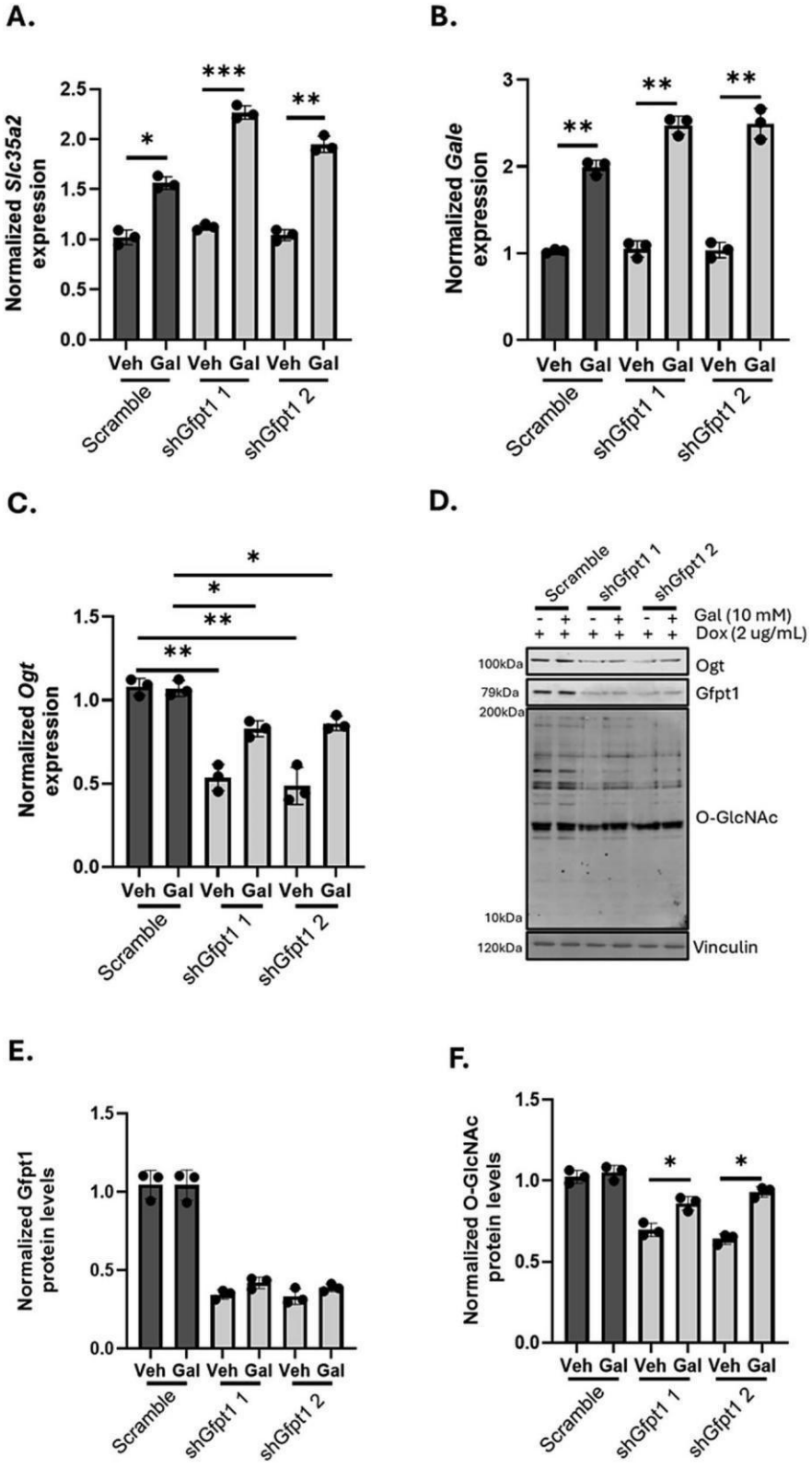

281

301

302

Figure 2. Galactose supplementation in Gfpt1-depleted C2C12 cells improves protein O-GlcNAcylation. A. Following galactose treatment, both control and Gfpt1-depleted C2C12 myoblasts [15] saw increased expression of *Slc35a2;* B. *Gale*; C. And *Ogt*. D. A western blot showing protein levels of Ogt, Gfpt1, and O-GlcNAc after galactose treatment. E. Gfpt1 deficiency in shGfpt1 1 and 2 cells remains unchanged following galactose treatment. F. Gfpt1depletionimpairsproteinO-GlcNAcylation,yetcanbepartiallyrescuedwithgalactosetreatment.Allgraphsshowmean±SD.Statisticalsignificancewas determined via a one-way ANOVA with a Tukey's multiple test correction. All experiments were performed with three biological replicates. Statistical comparison to untreated scramble, *P*-value <0.05, *P*-value <0.01, *P*-value <0.001, and ****<0.0001. Graphs and data describing how galactose supplementation restored protein O-GlcNAcylation deficiency in Gfpt1-deficient C2C12 myoblasts,with subfigures A to F,illustrating statistical analyses and gene/protein expression profiles.

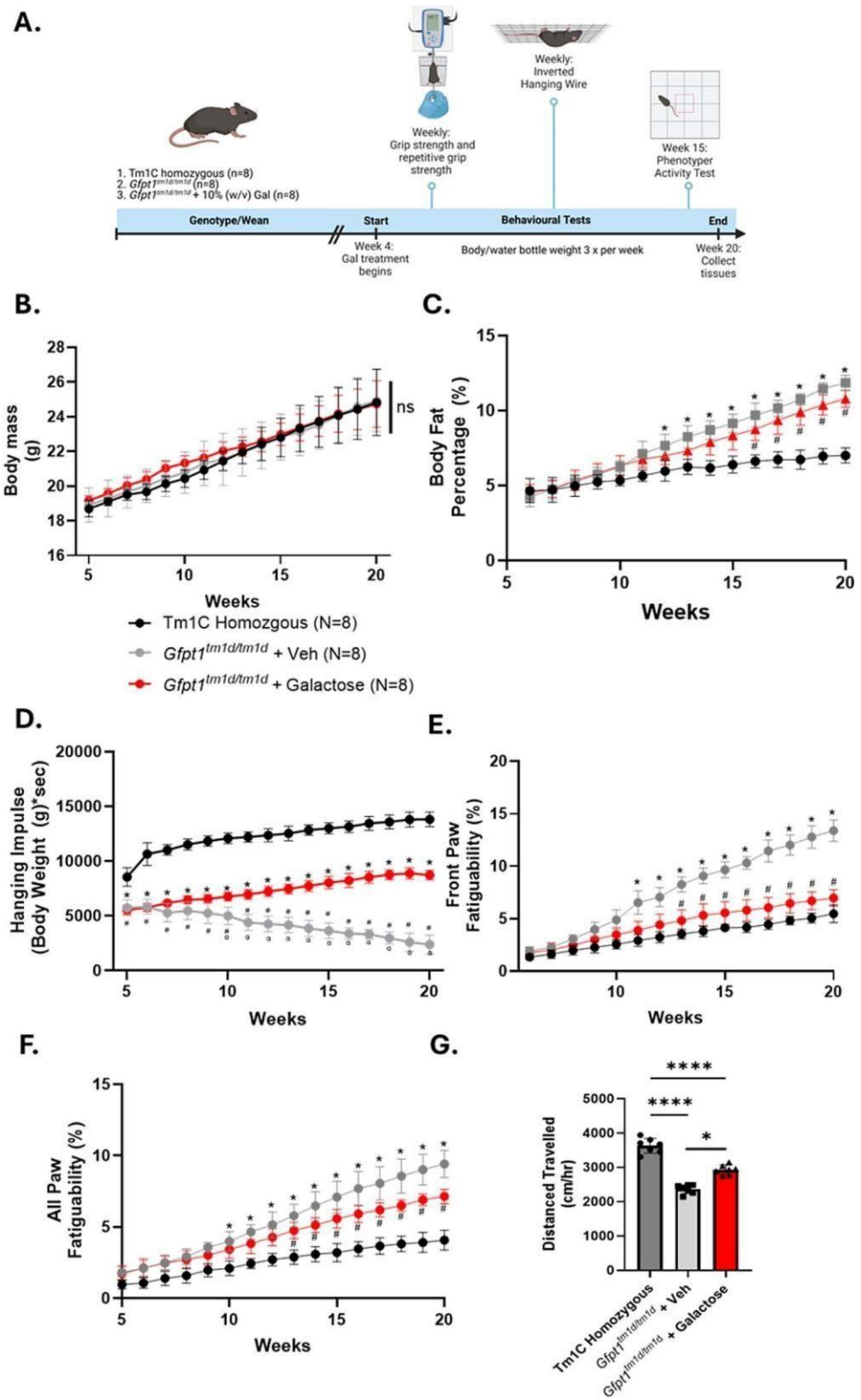

Figure 3. Galactose treatment of Gfpt1 mice (*Gfpt1*$^{tm1d/tm1d}$) partially rescues fatigable muscle weakness. A. A graphical overview of the galactose treatment timeline for 20 weeks. *Gfpt1*$^{tm1d/tm1d}$ mice received either drinking water or a 10% (w/v) solution of galactose. All mice underwent weekly behavioural testing, with the exception of a Phenotyper activity test at week 15. The study was completed at week 20. B. There was no significant difference in body weights between Tm1C homozygous control mice and *Gfpt1*$^{tm1d/tm1d}$ mice,regardless of treatment.C.Weekly EchoMRI measurements were performed to examine differences between fat mass. D. *Gfpt1*$^{tm1d/tm1d}$ mice displayed progressive impairment in inverted hanging wire impulse compared to Tm1C homozygous control mice, which was partially rescued with galactose treatment. E. *Gfpt1*$^{tm1d/tm1d}$ mice had a significant increase

in grip strength fatigability compared to control mice, which saw moderate improvements with galactose treatment. F. A similar pattern was seen in four paw measurements, with galactose treatment rescuing the grip strength fatigability in *Gfpt1*$^{tm1d/tm1d}$ mice. G. At week 15, galactose treatment partially rescued *Gfpt1*$^{tm1d/tm1d}$ mouse activity after a 24 hr spontaneous activity assessment. All graphs show mean±SD. Statistical significance was determined via a two-way ANOVA for figs. B through F, n=8 for all groups. Statistical comparison from Tm1C homozygous control to *Gfpt1*$^{tm1d/tm1d}$, *P*-value <0.05. Statistical comparison from Tm1C homozygous control to galactose-treated *Gfpt1*$^{tm1d/tm1d}$, # *P*-value <0.05. Statistical significance for fig. G was determined via a one-way ANOVA, ****P-value <0.0001.

Comparisions between mouse body wieght and inverted hanging time at Week 10 and Week 20 showed differences between mice are driven by muscle fatigue, rather than body wieght (Supplementary Fig. S2B and C). In addition, while there was no change in maximal grip strength measurements between experiemental groups, *Gfpt1*$^{tm1d/tm1d}$ mice did present with a small weakness in average grip strength which was improved by galactose treatment (Supplementary Fig. S3). *Gfpt1*$^{tm1d/tm1d}$ mice also exhibited a decrease in total activity over 24 hours compared to control Tm1C homozygous mice (Fig. 3G) which was partially rescued with galactose treatment (Fig. 3E). All together, these results suggest that galactose treatment in *Gfpt1*$^{tm1d/tm1d}$ mice improved behavioural deficits.

Galactose treatment improves skeletal muscle morphology in *Gfpt1*$^{tm1d/tm1d}$ mice

Hematoxyline and eosin (H&E) staining was used to assess muscle fiber morphology. Muscle fibres from Tm1C homozygous mice appeared healthy and polygonal, with no signs of tubular aggregate formation or necrosis (Fig. 4A). In contrast, vehicle-treated *Gfpt1*$^{tm1d/tm1d}$ mice showed classic *GFPT1*CMS features, including rounded fibers (black asterisk), tubular aggregates (white arrows), centrally located nuclei (black arrow head), fibrotic (white astericks), necrotic (black arrows) and regenerative muscle fibers (white hashtag) (Fig. 4A). Galactose-treated mice lacked fibrotic and necrotic fibers though tubular aggreates were still present, albeit less abundant (Fig. 4A).Galactose treatment in *Gfpt1*$^{tm1d/tm1d}$ mice restored mean muscle fiber area, which was reduced in vehicle-treated counterparts (Fig. 4B). There were more centrally located nuclei in vehicle-treated *Gfpt1*$^{tm1d/tm1d}$ mice compared to Tm1C homozyogous control and galactose treated mice (Fig. 4C). Muscle fiber size distribution showed smaller fibers in vehicletreated *Gfpt1*$^{tm1d/tm1d}$ mice with an increase in fibre size being observed in galatose treated animals (Fig. 4D). Collectively, these findings indicate that galactose treatment improves muscle fiber morphology, and pathology in *Gfpt1*$^{tm1d/tm1d}$ mice.

Galactose treatment improves neuromuscular junction morphology and integrity

Abnormal NMJ morphology has been observed in both humans with *GFPT1*CMS and *Gfpt1*$^{tm1d/tm1d}$ mice [14, 15, 17–19, 21–24]. Untreated *Gfpt1*$^{tm1d/tm1d}$ mice have smaller, less complex NMJs compared to those of healthy control mice which appear as large, pretzel-like structures (Fig. 5A).

To quantify these changes at the NMJ, we used NMJ-Morph to measure core and derived variables of synaptic morphology [33, 34]. Within *Gfpt1*$^{tm1d/tm1d}$ NMJs, axonal diameter was significantly decreased compared to controls (Fig. 5B). Furthermore, we observed a significant decrease in presynaptic motor neuron perimeter and area (Fig. 5C and Supplementary Table S1). Galactose treatment in *Gfpt1*$^{tm1d/tm1d}$ mice partially rescued both axonal diameter and presynaptic nerve terminal area/perimeter (Fig. 5B and C, Supplementary Table S1).

Next, we examined postsynaptic morphology in *Gfpt1*$^{tm1d/tm1d}$ NMJs and observed a significant decrease in the postsynaptic AChRarea (Fig. 5D).BeyondAChRarea,we foundsubstantivemorphological alterations to postsynaptic endplate area, perimeter, and diameter (Supplementary Tables S1). Again, galactose treatment in *Gfpt1*$^{tm1d/tm1d}$ mice partially rescued AChR area (Fig. 5D). In addition, galactose treated *Gfpt1*$^{tm1d/tm1d}$ mice had improved endplate area and diameter compared to untreated *Gfpt1*$^{tm1d/tm1d}$ mice (Supplementary Table S1).

Gfpt1$^{tm1d/tm1d}$ mice also had a reduction in area of synaptic contact (Fig. 5E) and percent overlap of the pre- and postsynaptic apparatus (Supplementary Table S1) that was improved with galactose treatment (Fig. 5E and Supplementary Table S1). No significant alterations in NMJ fragmentation was noted in any group.Alltogether,theseresultsdemonstratesubstantialpre-and postsynaptic defects in NMJ morphology of *Gfpt1*$^{tm1d/tm1d}$ mice that were partially rescued following galactose supplemention.

Galactose treatment improves deficient OGlcNAcylation within skeletal muscle and improves the glycosylation status of AChRδ

We have demonstrated that galactose therapy rescues the neuromuscular deficits and improves NMJ morphology in *Gfpt1*$^{tm1d/tm1d}$ mice.We hypothesized that galactose would also restore deficient glycosylation of critical NMJ-associated proteins in *Gfpt1*$^{tm1d/tm1d}$ skeletal muscle.

First, we demonstrated that *Gfpt1*$^{tm1d/tm1d}$ quadriceps express Leloir pathway enzymes *Galt, Galk* and *Gale*. We identified that they were unchanged when compared to control quadriceps (Fig. 6A–C). However, galactose treated *Gfpt1*$^{tm1d/tm1d}$ mice displayed a three-fold increase in the expression of *Galt,Galk* and *Gale* enzymes, suggesting that the excess galactose is being metabolized by the Leloir pathway (Fig. 6A–C). Since the Leloir pathway had elevated enzyme expression, we hypothesized that excess UDP-GalNAc could be converted to UDP-GlcNAc through the enzyme *Gale*. This would boost the expression of *Ogt*, the enzyme responsible for proper protein O-GlcNAcylation.Galactose treated *Gfpt1*$^{tm1d/tm1d}$ mice displayed elevated expression of *Ogt* compared to untreated *Gfpt1*$^{tm1d/tm1d}$ mice (Fig. 6D). However, this was still significantly lower than that of Tm1C homozygous mice, suggesting a partial restoration of O-GlcNAcylation (Fig. 6D). We then performed a Western blot and used antibodies targeting the OGlcNAc moiety on proteins (Fig. 6E). We found that galactose treatment in *Gfpt1*$^{tm1d/tm1d}$ mice restored deficient protein OGlcNAcylation (Fig. 6F), confirming that galactose treatment rescues skeletal muscle glycosylation in *Gfpt1*$^{tm1d/tm1d}$ mice.

Finally,we previously published that a hypoglycosylated AChRδ subunit is expressed as a result of defective protein glycosylation in *Gfpt1*$^{tm1d/tm1d}$ mice [15]. In healthy Tm1C homozygous skeletal muscle, a single 65 kDa protein is visible, whereas *Gfpt1*$^{tm1d/tm1d}$ samples also contained a lower 60 kDa protein species [15]. A Western blot was performed to examine whether

galactose could restore the glycosylation status of AChRδ within *Gfpt1*$^{tm1d/tm1d}$ skeletal muscle (Fig. 6G). Indeed, galactose treated *Gfpt1*$^{tm1d/tm1d}$ mice had restored expression of AChRδ in skeletal muscle and reversed the glycosylation status of AChRδ to a single molecular weight species at 65 kDa (Fig. 6G–I). Taken together, these results indicate that galactose treatment restores defective N- and Olinked glycosylation in *Gfpt1*$^{tm1d/tm1d}$

305

skeletal muscle, suggesting that galactose supplementation may be an effective treatment strategy for *GFPT1*-CMS patients. 285

Discussion

In this study we tested the hypothesis that galactose supplementation could bypass the defective HBP in *Gfpt1*-deficient samples, rescuing protein glycosylation, NMJ morphology, and the neuromuscular phenotype in *Gfpt1*$^{tm1d/tm1d}$ mice. Earlier studies have shown that *GFPT1*-CMS patients display fatigable weakness of limb girdle muscles [18, 19, 23–25, 35]. While there is no approved treatment option for CMS patients, off-label drugs such as AChE

305

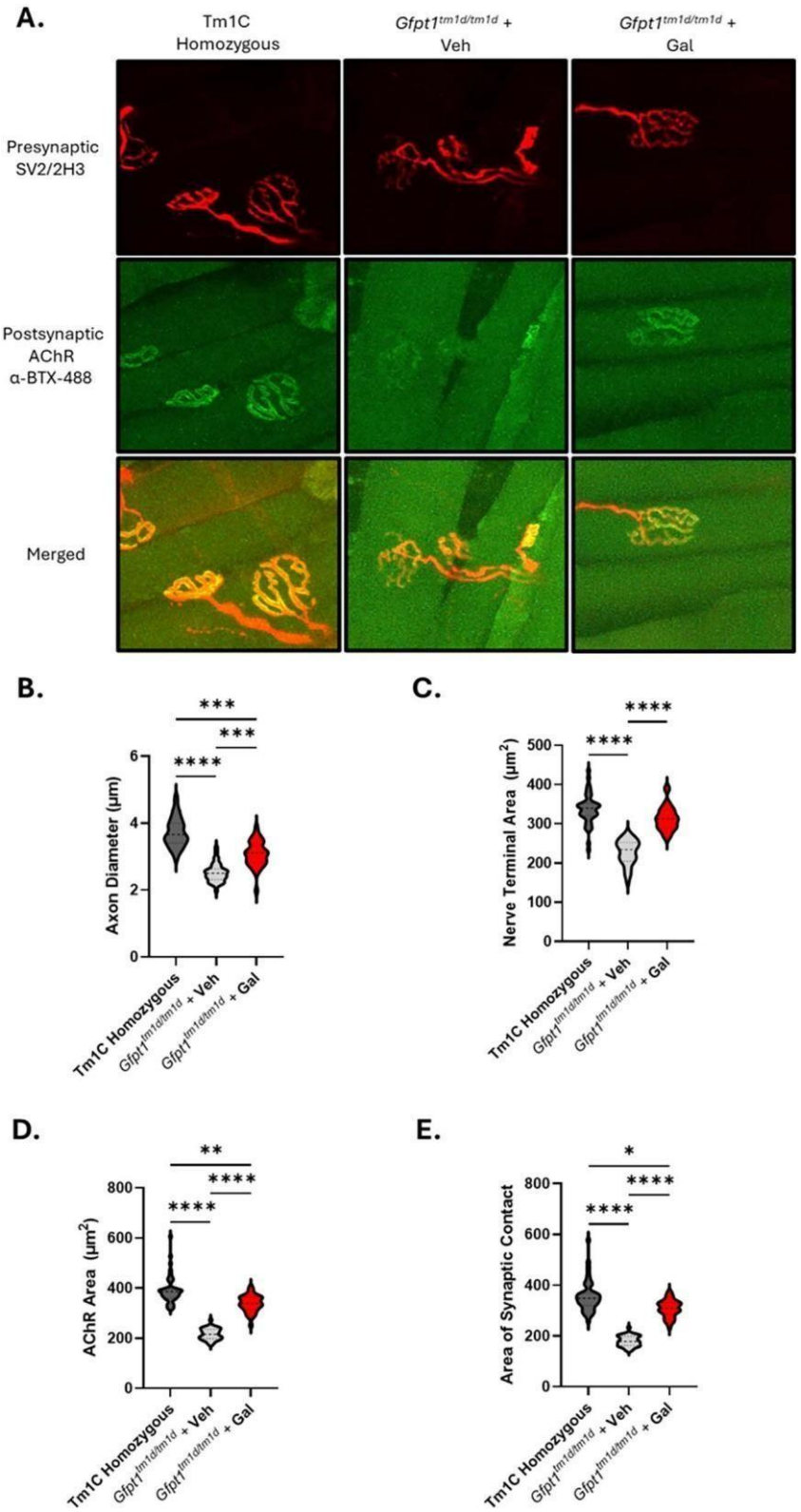

Figure 4. Galactose treatment rescues histological and morphometric analysis of *gastrocnemius* muscle in *Gfpt1*$^{tm1d/tm1d}$ mice. A. Representative H&E stained sections (250 µm by 250 µm) showing healthy polygonal fibers in Tm1C homozygous controls, pathological features including rounded fibers (black asterisks), tubular aggregates (white arrow), fibrosis (white asterisks), necrosis (black arrow), regenergative fibers (white hastag) and centrally located nuclei (black arrowhead), and a partial rescue in galactose treated *Gfpt1*$^{tm1d/tm1d}$ mice. Scale bar 20 µm. B. Quantification of mean muscle fiber area showed a decrease in vehicle-treated *Gfpt1*$^{tm1d/tm1d}$ mice compared to Tm1C homozygous control mice, while galactose treatment rescued mean fiber area. C. Quantification of centrally located nuclei per muslce fiber showed that vehicle-treated *Gfpt1*$^{tm1d/tm1d}$ mice had an increased percentage of centrally

located nuclei, while galactose treatment signficantly reduced the percentage of centrally located nuclei. D. Muscle fiber distribution was then analyzed which shows vehicle-treated *Gfpt1*$^{tm1d/tm1d}$ mice tend to have smaller muslce fibers, while galactose treatment restores muscle fiber size towards healthy Tm1C homozygous control mice. All graphs show mean±SD.

Statistical significance was determined via a one-way ANOVA with an additional Tukey post-hoc test for figs. B and C, n=4 for all groups: *, *P*-value <0.05, **, *P*value <0.01, *, *P*-value <0.001. For fig. D a two-way ANOVA was performed with a Dunnett's multiple comparision test, n=4 for all groups: *, *P*-value <0.05, **, *P*-value <0.01, ***, *P*value <0.001, ****, *P*-value <0.0001.**

308

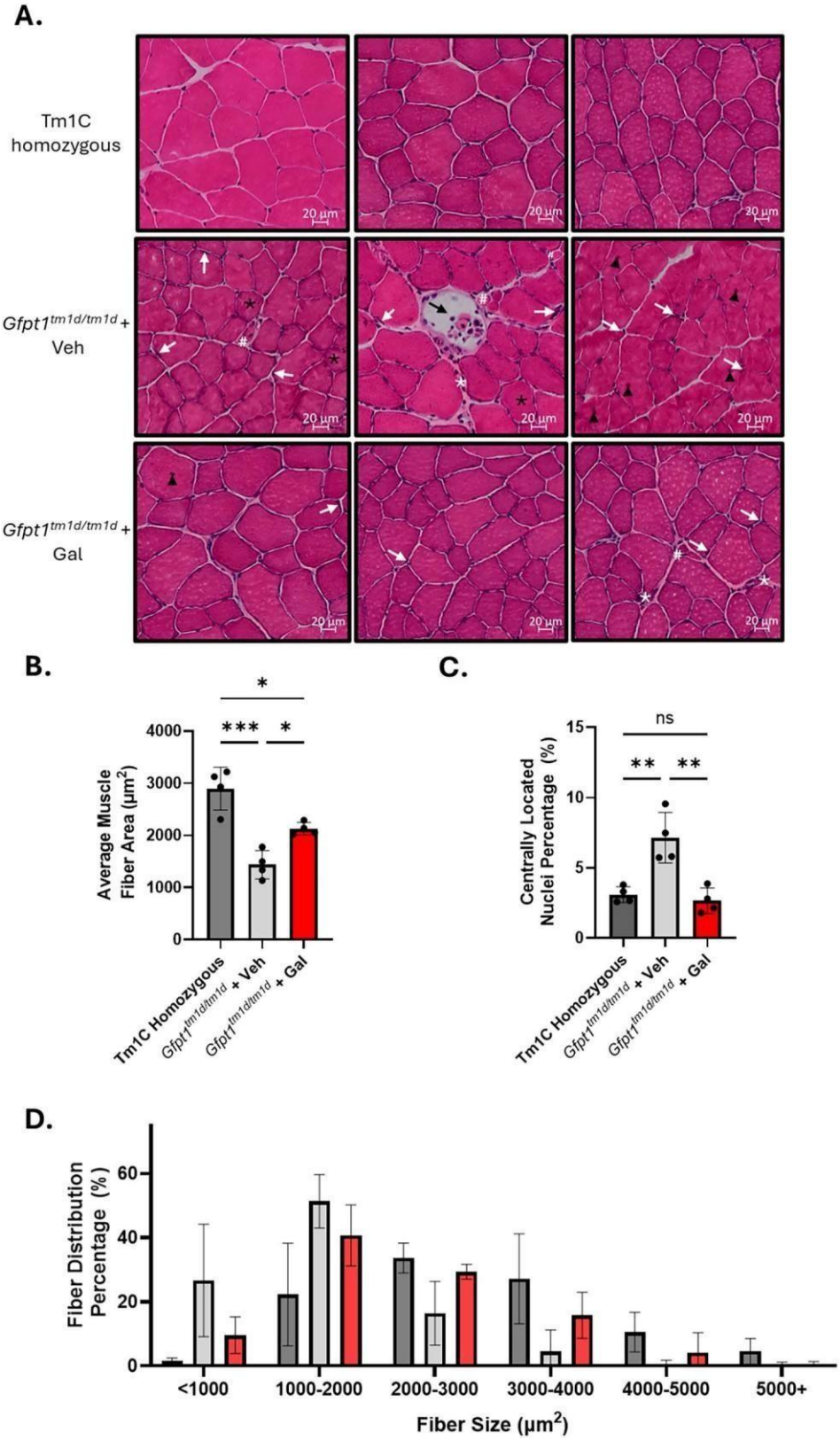

Figure 5. Galactose treatment in *Gfpt1*$^{tm1d/tm1d}$ mice improves NMJ morphology. A. A representative max intensity projection of whole mounted soleus muscle obtained from Tm1C homozygous control,untreated *Gfpt1*$^{tm1d/tm1d}$,and galactose treated *Gfpt1*$^{tm1d/tm1d}$ mice.Muscles were stained for NMJs with alpha-bungarotoxin-488 (middle row) to label postsynaptic AChR clusters and neurofilament/SV2 (top row) to label presynaptic nerve terminals.Images were merged (bottom row) observe overlap between the presynaptic and postsynaptic

compartments which represents a NMJ. B. Pre- and postsynaptic morphological characteristics of NMJs were examined using aNMJ-morph. We identified that galactose therapy partially rescued deficits in axonal diameter (μm); C. Nerve terminal area (μm^2); D. AChR area (μm^2); E. And area of synaptic contact (μm^2). These features were significantly impaired in untreated *Gfpt1*$^{tm1d/tm1d}$ mice compared to control mice. Normality of data was examined using a D'Agostino-Pearson test followed by a Kruskal-Wallis test, with a

correction by Dunn's multiple comparisons test. Total NMJs analyzed were n=162, n=178, and n=152 for Tm1C homozygous, untreated *Gfpt1*$^{tm1d/tm1d}$ and galactose treated *Gfpt1*$^{tm1d/tm1d}$ mice, respectively from 6 mice in each treatment group. Statistical comparison to untreated scramble, *P*-value <0.05, *P*-value <0.01, *P*-value <0.001, and **** <0.0001.

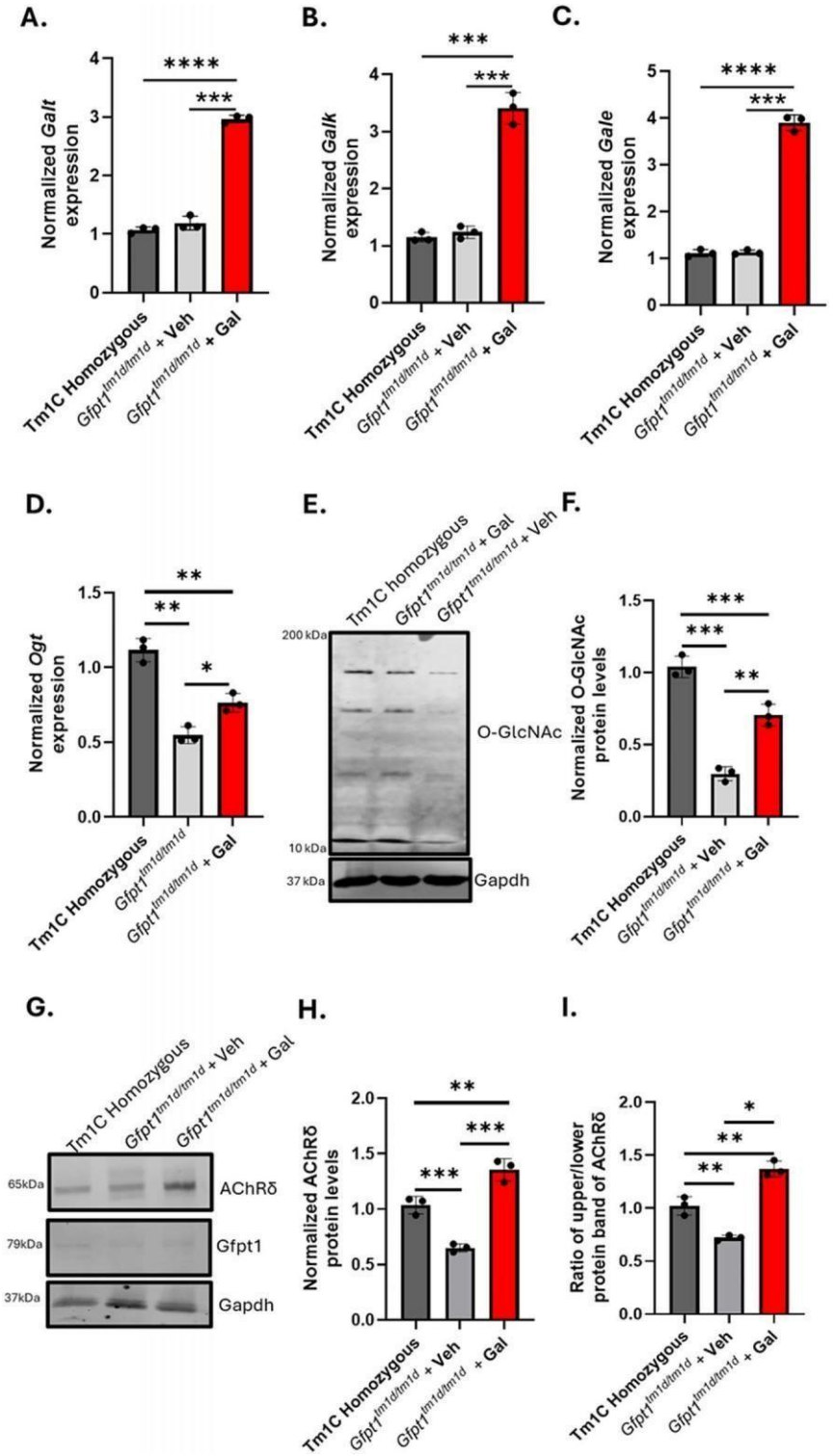

Figure 6. Galactose treatment of *Gfpt1*$^{tm1d/tm1d}$ mice rescues protein O-GlcNAcylation and maintains glycosylation of NMJ-associated proteins. A. Gene expression of the Leloir pathway enzymes *Galt;* B. *Galk;* C. And *Gale* increased significantly within the quadriceps of galactose treated *Gfpt1*$^{tm1d/tm1d}$ mice. D. Untreated *Gfpt1*$^{tm1d/tm1d}$ mice exhibited reduced

310

Ogt expression, which was partially rescued with galactose treatment E. A western blot showing protein O-GlcNAcylation levels in Tm1C homozygous control, untreated *Gfpt1*$^{tm1d/tm1d}$, and galactose treated *Gfpt1*$^{tm1d/tm1d}$ mice. F. There was a significant decrease in protein O-GlcNAcylation in *Gfpt1*$^{tm1d/tm1d}$ mice, while galactose treated *Gfpt1*$^{tm1d/tm1d}$ mice had a significant increase in protein O-GlcNAcylation compared to untreated *Gfpt1*$^{tm1d/tm1d}$ mice. G. A western blot showing protein levels of Gfpt1 and AChRδ obtained from the quadriceps of Tm1C homozygous control, untreated *Gfpt1*$^{tm1d/tm1d}$, and galactose treated *Gfpt1*$^{tm1d/tm1d}$ mice. H. There is a significant decrease in AChRδ protein levels in *Gfpt1*$^{tm1d/tm1d}$ which was rescued following galactose treatment. I. In *Gfpt1*$^{tm1d/tm1d}$ muscle, AChRδ contains two molecular weight species at 65 kDa and a hypoglycosylated protein at 60 kDa.Galactose treatment reduces the expression of the lower molecular weight species,improving the ratio of expression between the 65 kDa and 60 kDa molecular weight species. All graphs show mean±SD. Statistical significance was determined via a oneway ANOVA. All experiments were performed with three mice in each group. Statistical comparision to from Tm1C homozygous control to untreated or galactose treated *Gfpt1*$^{tm1d/tm1d}$ mice, *P*-value <0.01, *P*-value <0.001, and ****<0.0001. Statistical comparision between untreated *Gfpt1*$^{tm1d/tm1d}$ mice to galactose treated mice, # *P*-value <0.05, ## *P*-value <0.01, ### *P*-value <0.001.

inhibitors and salbutamol have provided some benefit. We previously identified that *Gfpt1*-deficient mice have impaired Nlinked glycosylation and O-GlcNAcylation [15]. Gfpt1 has been shown to be the rate-limiting enzyme of the HBP, a metabolic pathway required to produce the precursors for protein glycosylation and O-GlcNAcylation [13–15, 36]. Monosaccharide sugar supplementation has been an effective strategy for CDG patients as it can bypass defective pathways, repairing the glycosylation status of proteins [29, 37, 38]. The Leloir pathway breaks down galactose into UDP-GlcNAc, the precursor for glycosylation and OGlcNAcylation [30, 39]. Therefore, galactose may be a suitable treatment strategy for *GFPT1*-CMS patients. To our knowledge, this is the first study that examined nutritional monosaccharide supplementation in a CMS model.

As previously shown [40], Leloir pathway enzymes *Galt, Galk* and *Gale* were expressed within skeletal muscle and C2C12 myoblasts and treatment with galactose increased their expression Furthermore, galactose treatment increased expression of *Ogt* and total protein O-GlcNAcylation in *Gfpt1*deficient C2C12 myoblasts. We showed that DON inhibition at 500 μM inhibits Gfpt1 enzymatic activity—whereas, *Gfpt1*-deficient C2C12 myoblasts still have residual enzymatic activity [14, 15, 18]. Therefore, the Leloir pathway shunt may not be requried within this condition, until galactose is present to stimulate the production of excess UDP-GlcNAc and OGlcNAcylation. This could account for the discrepancy between chemical inhibition of Gfpt1 and knockdown models for the expression of *Gale* and *Slc35a2*. In addition, we identified that Ogt protein levels did not significantly increase in *Gfpt1*-deficient myoblasts, which may be explained through residual expression of Gfpt1, as UDP-GlcNAc production requires feedback loop inhibiton for Gfpt1 and Ogt activity [41]. *Gfpt1*$^{tm1d/tm1d}$ mice were previously shown to have exercise-induced muscle weakness, impaired NMJ morphology, and defective glycosylation of AChRδ [15, 17]. In our study, galactose supplementation in *Gfpt1*$^{tm1d/tm1d}$ mice partially rescued muscle fatigue, improved NMJ morphology, and restored AChRδ glycosylation status. These findings suggest that galactose supplementation improves *GFPT1*-CMS phenotype *in vitro* and *in vivo*.

We identified that galactose supplementation restored Nlinked protein glycosylation of AChRδ. Previously, it has been demonstrated that within *GFPT1*-CMS patient-derived myoblasts that global N-linked glycosylation levels were unchanged [42]. However, we have recently shown that AChRδ, an extensive Nlinked glycosylated protein, was hypoglycosylated within *Gfpt1*deficient specimens [15]. This global glycomic approach may miss individual changes that might be diluted due to poor sensitivity and/or resolution. In addition, the occupancy of glycosylated proteins was not accounted for in global glycomic approaches [42]. As such, future work in *GFPT1*-CMS should be focused on targeted glycoproteomic assessment, to examine the glycan chain occupancy of individual proteins at the NMJ. We speculate that hypoglycosylated AChRδ may have impaired channel kinetics and stability at the postsynaptic membrane. Studies have shown that altering the glycosylation sites on AChRδ impairs the surface expression of AChR complexes [43–45]. One study identified that N-linked glycosylation is necessary for AChR complex assembly but is not required for trafficking towards the surface by the ER chaperone calnexin [45]. Furthermore, removal of key ubiquitination sites from lysine residues also perturbed Golgi-based AChR glycosylation, impacting surface expression [44]. We have identified that hypoglycosylated AChRδ is expressed at the NMJ after laser capture enrichment of NMJs from *Gfpt1*$^{tm1d/tm1d}$ mice, but had weaker αBTX staining [15, 17]. In addition, CMS patients with mutations to AChR subunits often show reduced AChR complexes at the NMJ, due to an impairment to the interaction of AChR subunits with RAPSN [46]. As such, we anticipate that *Gfpt1*$^{tm1d/tm1d}$ mice may have an AChR docking or anchoring impairment that is partially resolved after galactose treatment.

In addition to the rescued N-linked glycosylation of AChRδ, galactosesupplementationrestoredtotalproteinO-GlcNAcylation levels. OGlcNAcylation has been shown to regulate protein activity, stability, and cellular localization, with turnover rates similar to that of protein phosphorylation [47–49]. To date, over 8000 proteins have been associated with protein O-GlcNAcylation [50].Inparticular,O-GlcNAcylationhasbeenshowntobeessential for muscle health and contractile properties [41]. At the NMJ, sub-synaptic nuclei and associated mitochondria are in high abundance. Thus, modulation of O-GlcNAcylation may impair energetics and gene expression of NMJ-associated genes [51– 53]. As such, identifying which proteins are not O-GlcNAcylated within *Gfpt1*-deficient NMJs may yield alternative therapeutic strategies and further understanding of the pathomechanisms of disease. Importantly, galactose supplementation restored protein O-GlcNAcylation through bypassing the defective HBP in *Gfpt1*deficient specimens, suggesting that this impairment can be rescued.

We showed that galactose supplementation partially restored NMJ morphology, accounting for an improvement in the *Gfpt1*$^{tm1d/tm1d}$ phenotype. NMJ-Morph analysis revealed substantial impairment in *Gfpt1*$^{tm1d/tm1d}$ mouse nerve terminal area and perimeter, along with a significant decrease in axonal thickness—all novel findings within *Gfpt1*-deficient models [16, 21]. It has been shown that skeletal muscle produces retrograde signals which preserve presynaptic motor neuron integrity [54]. Previous studies have demonstrated presynaptic nerve terminal morphological changes in skeletal muscle-specific transgenic mice [55, 56]. Additional evidence for motor nerve terminal morphological changes is present in postsynaptic *Agrn-, Musk-, Rapsn-, Dok7, ColQ*-CMS mouse models [57–62].

Therefore, we speculate that hypoglycosylated retrograde signals from the skeletal muscle to the motor neuron may be impaired within *Gfpt1*$^{tm1d/tm1d}$ mice. Interestingly, we did not observe any significant changes in the degree of

fragmentation across treatment groups, a common metric of NMJ dysfunction [63]. However, recent studies indicate no correlation between AChR fragmentation and neurotransmission efficiency [63, 64]. In fact, it has been suggested that AChR fragmentation allows the NMJ to adapt to the changing conditions to preserve neuromuscular transmission [63]. We show a positive association between galactose supplementation and NMJ morphology of both core and derived variables using aNMJ-Morph in both pre- and postsynaptic measurements.

Previous studies with the *Gfpt1*$^{tm1d/tm1d}$ mouse model identified muscle morphological alterations with the presence of rounded myofibers, internalization of nuclei, necrotic fibers and the presence of atrophic and hypertrophic fibers [17]. In addition, a hallmark of *GFPT1*-CMS in humans, *Gfpt1*$^{tm1d/tm1d}$ mice contained tubular aggregates within the myofibers [6, 17, 25]. The exact origin of these accumulations are unknown,however,it is hypothesized that these formations are due to a mass catabolism of misglycosylated proteins [17,23,25].Galactose treatment appears to reduce the accumulation of tubular aggregates within the skeletal muscle fibers. Future studies should focus on the origin of these tubular aggregates within muscle. The balance of the HBP is critical for muscle health [41, 65]. Other unknown proteins maybeimproperlyglycosylatedin *GFPT1*CMS,beyondAChRδ [15]. In addition, O-GlcNAcylation, a product the HBP has been linked to the regulation of cellular stress response pathways which have shown to negatively impair skeletal muscle health, leading to muscle fiber necrosis [41, 65]. Therefore, understanding the glycosylation status of other proteins in *Gfpt1*$^{tm1d/tm1d}$ mice may reveal additional pathomechanism of *GFPT1*-CMS.

This study identified the therapeutic potential of monosaccharide supplementation for *GFPT1*-CMS patients. With the emergence of monosaccharide therapies in CDGs, our findings provide preliminary support for exploring similar approaches in other glycosylation-based CMS cases or for combining them with existing CMS therapies. Currently, *GFPT1*-CMS patients benefit from treatment with AChE inhibitor pyridostigmine and sympathomimetic compounds salbutamol and ephedrine [19, 22–25]. These treatment strategies have poor long-term efficacy as the sympathomimetics can lead to cardiac complications which require alternative treatment strategies [23, 25, 26]. CDGs have shown benefit with nutritional supplementation of monosaccharides which rescued the phenotype and restored protein glycosylation [29]. For example, galactose supplementation in *TMEM165*-CDG improved the glycosylation of LAMP2, an extensively N-linked glycosylated lysosomal protein [29, 38]. In glycosylation-based CMS disorders such as *GMPPB*-CMS, longterm pyridostigmine treatment has shown diminished efficacy over time [27]. Monosaccharide therapies such as GDP-mannose supplementation have shown promise in preclinical models, including zebrafish lacking *Gmppb* expression [66]. This approach hasbeeneffectivein *PMM2*CDGs[67].However,useofcompounds upstream of *GMPPB* like glucose and mannose failed to rescue muscle deficits and abnormal development of motor neurons [66]. These findings underscore the potential for nutritional therapeutics in glycosylation-based CMS, given their success in preclinical models and established efficacy in CDGs.

During this short-term study, we identified that galactose supplementation may be a suitable treatment strategy for *GFPT1*CMS patients. However, further studies should be conducted to examine the longterm effects of galactose in *Gfpt1*-deficient models. The Leloir pathway was initially characterized within the liver. In classic galactosemia, patients with a mutation to GALT, display a well-documented hepatoxicity in early disease manifestation which later can present as liver failure, and jaundice [68]. Understanding the long-term effects of galactose supplementation in hepatic cells is essential, as the accumulation of galactose metabolites may lead to long-term complications [68]. Additionally, further investigation is warranted to elucidate why the *Gfpt1*$^{tm1d/tm1d}$ mouse model exhibits a higher body fat percentage compared to control animals. O-GlcNAcylation is important for mitochondrial health, as such, hypo-glycosylation of mitochondrial proteins, may impede overall metabolism, leading to a fat mass gain compared to controls [51, 69]. In this study galactose was administered over a period of 20 weeks but it will be important to assess supplementation over a longer duration as galactose has been shown to cause oxidative stress and accelerate aging in rodent models [70–72]. While we **311** primarily focused on quadriceps for muscle gene and protein levels, and on soleus muscle for NMJ morphological assessment it would be beneficial to sample more muscle types to fully characterize the impact of galactose supplementation on *Gfpt1*$^{tm1d/tm1d}$ mice.

NMJ morphology can vary across different muscles, and therefore additional characterization could reveal additional phenotypes [73, 74]. Lastly, electrophysiological recordings of repetitive nerve stimulation could provide further direct evidence of the restoration of NMJ function.

In conclusion, treatment with galactose in *Gfpt1*$^{tm1d/tm1d}$ mice restored defective protein glycosylation of key NMJ-associated proteins and partially rescued impairments in both pre- and postsynaptic NMJ morphology. This improvement in NMJ morphology was beneficial to *Gfpt1*$^{tm1d/tm1d}$ mice, rescuing their neuromuscular phenotype. This study contributes to the growing evidence that, similar to CDGs, monosaccharide supplementation can be an effective treatment strategy for glycosylation-based CMS in improving the glycosylation status and restoring NMJ function. These findings strongly suggest that patients with CMS due to mutations in *GFPT1* could see benefit from galactose supplementation as part of their treatment regime.

Materials and methods

Cell culture

C2C12 cells (ATCC, CRL-1722, Burlington, Ontario) were cultured in high glucose Dulbecco's Modified Eagle Medium (DMEM) supplemented with 10% fetal bovine serum (FBS), 1% glutamine, and 1% penicillin/streptomycin. A Gfpt1-deficient C2C12 cell model was established using a TET-ON miR-30 tetracyclineinducible system (VectorBuilder, Chicago, IL) as previously described [15]. Gfpt1 silencing was achieved by doxycycline treatment at 2 μg/mL for 48 hours. (Sigma, D9891). Galactose treatment was performed with 10 mM of D-galactose (Caymen Chemicals, 20890) for 48 hours.

Real-time qPCR (RT-qPCR)

RNA collection for *in vitro* experiments was performed using the RNeasy™ Micro mini kit (Qiagen, #74134, Toronto, Canada). Skeletal muscle RNA extraction was performed with the RNeasy™ Fibrous Micro mini kit (Qiagen, #74704) and quantified by NanoDrop (ND-1000, Spectrophotometer, NanoDrop®. RNA was converted to complementary DNA (cDNA) with the All-In-One 5x RT MasterMix (ABM, #G592, Richmond, bc, Canada) following kit guidelines. RT-qPCR was performed using the PowerUp™ SYBR™ Green Master Mix (FisherSci, #A25741, Ottawa, Canada) with the QuantStudio™ Studio 6 Flex Real-Time PCR System (Thermofisher, Ottawa, Canada) (see Supplementary Materials Table S2 for primer sequences). To analyze the expression of our target genes the geometric mean of three reference genes

(*Gapdh, Rpl27, Ppia*) were used. Average CT values for these experiments can be found in the supplemental data.

Tissue/cell lysis and western blotting

Cell lysates and skeletal muscle homogenates were prepared with radioimmunoprecipitation assay (RIPA) buffer (150 mM NaCl, 50 mM Tris–HCl (pH 8), 1% Triton X-100, 0.5% NaDOC, 0.1% SDS) supplemented with protease (Roche, #04693116001, Mississauga, ON,Canada) and phosphatase (Roche,#PHOSS-RO) inhibitors.Cell lysates were centrifuged at 15000×*g* for 10 minutes at 4°C and the supernatants collected. Skeletal muscle samples were combined with lysis buffer and a metal bead in 2 mL SafeLock™ Eppendorf tubes (Eppendorf, #022363352, Mississauga, ON, Canada), then homogenized using a TissueLyser II (Qiagen,Toronto,ON,Canada). The protocol comprised of 3 rounds of homogenization at 30 Hz for 90 seconds followed by incubation on ice for 60 seconds.

Afterwards, samples were kept at 4°C for 4 hours on a rotating platform then centrifuged at 15000×*g* for 15 minutes at 4°C. Total protein concentration was determined using a DC Protein Assay (BioRad, 5000111) with BSA dilutions (Pierce, #23209) as standards. Proteins were resolved by SDS-PAGE and transferred to PVDF membranes using a BioRad™ Trans-Blot Turbo system (#1704150EDU, Mississauga, ON, Canada).

Membranes were blocked with Intercept TBS blocking buffer (Li-Cor, 927– 6000, Lincoln, NE, USA) for 1 hr and incubated with primary antibodies in blocking solution overnight at 4°C. After washing with TBS+1% Tween-20, membranes were incubated with IR Dye®800CW Donkey anti-Mouse IgG (LiCor, #926–32212, 1:5000) and IR Dye®680RD Goat anti-Rabbit IgG (LiCor, #926– 68071, 1:5000) for 1 hour at room temperature. Blots were imaged using a Licor Odyssey DLX (Lincoln, NE, USA) and densitometry performed using Image Studio™ (Licor, version 6.0). Gapdh was used to normalize protein expression as it remained unchanged in experimental conditions.

Animal husbandry

Animals were housed at the University of Ottawa Animal Care and Veterinary Facility (Roger Guidon Hall, Ottawa, Canada) and all breeding and experimental protocols were approved by the internal Animal Care Committee (protocols: breeding—CHEO3089 and experimental—CHEO3120 approved on 16 November 2018 and 2 April 2019, respectively). Mice were maintained on a 12 hour light–dark cycle, with access to food and water *ad libitum* for the duration of this study. Mice were generated and genotyped as previously reported [15, 17]. For this study, Tm1C homozygous mice (which contain two LoxP sites flanking the seventh exon of *Gfpt1* but lack *Ckm-Cre* expression) were used as controls. *Gfpt1*$^{tm1d/tm1d}$ mice contain two LoxP sites flanking the 7th exon of *Gfpt1* but also express a Cre recombinase tied to the *Ckm* reporter, whichcreates askeletal muscle-specificknockout of *Gfpt1* [15,17]. For our study, we introduced a 10% (w/v) solution of Dgalactose (Caymen Chemicals,20890) in the drinking water starting at week 4, with water bottles weighed weekly to measure consumption. Mice were weighed three times per week, and underwent several behavioural tests: inverted hanging wire, repetitive grip strength, EchoMRI, and Phenotyper™ activity test before tissue collection at 20 weeks. These behavioural tests were conducted previously and are summarized in brief below [15, 17].

Inverted screen test

Mice were suspended from an inverted wire grid and the time to fall was recorded, with the test being stopped after 10 mins if the mice had not yet fallen. The test was repeated 3 times, with 30minutesbetweeneachtrial.Theaveragetimewasrecordedand normalized to body weight to calculate hanging impulse (g x s).

Grip fatigability measurements

Repetitive grip strength measurements were conducted weekly on the fore and then all four paws. For this measurement, 8 consecutive recordings were performed on a grip strength meter (Chatillon DFE II Grip Meter, Columbus Instruments, Columbus, OH) to assess the fatigability of the forelimbs. Animals then were allowed to rest for 30 minutes and the test repeated with all four paws. The following equation was used to calculate grip strength fatigability:

$$\textit{Muscle Fatigability\%} = \frac{\textit{Average of first four measurements}}{\textit{Average of total measurements}} - \textit{Average of last four measurements}$$

EchoMRI and Total activity measurements

Body composition of fat and lean mass was measured weekly using the EchoMRI-700 Body Composition Analyzer (EchoMRI, Houston, TX). Animals also underwent 24 hour open activity monitoring using the Phenotyper™ system (Noldus Information Technology, Leesburg, VA) at week 15. Total distance travelled per hour was calculated using Phenotyper™ analysis software (EthoVision v15, Noldus Information Technology).

Muscle histology

10 µm *Gastrocnemius* muscle sections were dried at room temperature for 1 hr and rinsed in tap water prior to staining with Harris's hematoxylin (Sigma, HHS32) for 2 minutes followed by a wash in tap water. Eosin Y (Sigma, HT110132) was then applied for 30 seconds, then washed with tap water. After this wash slides were dehydrated with ethanol and xylene,and mounted with DPX mounting media (Sigma,#6522),and images acquired with a Zeiss Axio Imager M2 microscope at 10x magnification. For assessment of muscle morphology, randomized images of *gastrocnemius* muscle were used and approximately 500 muscle fibers were analyzed from each mouse. The polygonal function with ImageJ was used to trace muscle fibers and the 'analyze particles' tool was then used to assess individual muscle fiber area,distribution.Centrally located nuclei were counted and presented as a percentage of total fibers measured.

Immunostaining for NMJs in whole muscle mounts

Soleus muscles were fixed in 2% paraformaldehyde (PFA) for 20 minutes and then separated into small bundles and placed in 2% PFA overnight. The fibers were then washed with PBS (Sigma, #P4417, Oakville, Canada), and placed in ice-cold analar ethanol followed by analar methanol for 10 minutes each. Fibers were transferred to blocking/permeabilization solution (5% horse serum, 5% bovine serum albumin, 1% triton X-100 in PBS) and incubated for 4 hours. The muscle fibers were then incubated with anti-SV2 (DSHB, 1:100, University of Iowa, Iowa City, IA) and neurofilament antibodies (DSHB (2H3), 1:100, University of Iowa, Iowa City, IA) in 5% horse serum/5% BSA for 24 hrs.

Fibers were washed with blocking buffer for 4 hours and incubated with alpha-bungarotoxin-488 (Invitrogen, #B13422, 1:200, Burlington, Canada) and the secondary antibody Alexa Fluor anti-mouse-568 (Life Technologies, #A11031, 1:250, Toronto, Canada) overnight. Following this incubation, the muscle fibers were washed with PBS for 4 hours and mounted on glass

microscope slides using Vectashield® Antifade Mounting Medium (VectorLaboratories,#H-1000-10,Newark,CA).Toaidinmounting, several layers of electrical tape were used to create a reservoir to hold the muscle in place. A glass coverslip was applied and sealed with nail varnish. Imaging was performed on a confocal microscope (Olympus Fluoview FV1000,Olympus,Richmond Hill, Canada). NMJ z-stacks were captured at 40× magnification with image acquisition being performed sequentially with consistent microscope settings.Efforts were made to captureall NMJs in each soleus muscle. Analysis was performed blinded on maximum intensity projection images according to the automated NMJMorph (aNMJ-Morph) protocol developed using FIJI [33, 34].

Antibodies

The following antibodies were used for Western blot experiments: Gfpt1 (ProteinTech, #14132–1-AP, 1:500, Rosemont, IL), Gapdh (14C10) (Cell Signalling, 2118, 1:2000, Danvers, MA), O-GlcNAc (RL2) (Novus Biologicals, NB300–524, 1:1000, Toronto, Ontario), Ogt (ProteinTech, 66823–1-Ig, 1:1000, Rosemont, IL), AChRδ (C-4) (Santa Cruz, sc-390896, 1:1000, Dallas, TX). Antibodies for NMJ staining from whole muscle mounts were SV2 antibody (DSHB, 1:100, University of Iowa, Iowa City, IA) and neurofilament (DSHB (2H3), 1:100, University of Iowa, Iowa City, IA). Postsynaptic AChR clusters were detected with alpha-bungarotoxin488 (Invitrogen, B13422, 1:200, Burlington, Canada).

Statistics

Data was analyzed with GraphPad Prism v 10.1.2. Data was checked for normality using the D'Agostino-Pearson test and outliers were identified using the robust regression and outlier remover (ROUT) method.

Statistical significance was determined by using unpaired twotailed Student *t*-tests or analysis of variance (ANOVA) tests. If multiple comparisons were used, a Tukey's post-hoc test was performed. Results are presented as mean±SD, where $p<0.05$ was considered significant. For NMJ morphological analysis, results were tested for normality using the D'Agostino-Pearson test. For variables that were not normally distributed, statistical significance was determined by a Kruskal-Wallis test followed by a Dunn's multiple comparisons test.

Animal ethics statement

The animal study protocol was approved by the Animal Care and Veterinary Board of the University of Ottawa (CHEOb-3089 and CHEOe-3120, approved on 16 November 2018 and 2 April 2019, respectively).

Acknowledgements

The SV2 antibody was deposited by Buckley, K. M., and the neurofilament (2H3) antibody deposited by Jessell, T.M/Doss, J was obtained from the Developmental Studies Hybridoma Bank, created by the NICHD of the NIH and maintained at The University of Iowa, Department of Biology, Iowa City, IA 52242. Schematics were prepared with Biorender.com.

Author contributions

Conceptualization,H.L.,S.S.,Y.A.,and S.H.H.; methodology,S.H.H., R.C.-M., K.O., K. H., and D.O.; validation, S.H.H., R.C.-M., K.O. and D.O.; formal analysis, S.H.H., S.S. and K.O.; investigation, S.H.H., R.C.M. and K.O.; resources, H.L. and S.S.; data curation, S.H.H., R.C.-M., K.O.; writing—original draft preparation, S.H.H.; review and editing,S.H.H.,R.C.M.,K.O.,D.O.,S.S.,Y.A.,A.R.and H.L.; final draft preparation and writing,

S.H.H., S.S., and H.L.; visualization, S.H.H., S.S, and H.L.; supervision, S.S. and H.L.; project administration, S.S. and H.L.; funding acquisition, H.L. and S.H.H. All authors have read and agreed to the published version of the manuscript.

Supplementary data

Supplementary data is available at *Human Molecular Genetics* online.

Conflict of interest statement: The authors declare no conflict of interest.

Funding

H.L. received support from the Canadian Institutes of Health Research (CIHR) for Foundation Grant FDN-167281 (Precision Health for Neuromuscular Diseases), Transnational Team Grant ERT-174211 (ProDGNE), and Network **313**

Grant OR2–189333 (NMD4C) from the Canada Foundation for Innovation (CFI-JELF 38412); the Canada Research Chairs program (Canada Research Chair in Neuromuscular Genomics and Health,950–232279); the European Commission (Grant # 101080249); and the Canada Research Coordinating Committee New Frontiers in Research Fund (NFRFG-2022-00033) for SIMPATHIC and from the Government of Canada, Canada First Research Excellence Fund (CFREF) for the Brain-Heart Interconnectome (CFREF2022-00007). S.H.H. received support from the Bob Korneluk CHEO Trainee Research Grant, Ontario Graduate Scholarship (OGS), Queen Elizabeth II Scholarship (QE2-GSST), and a STaR award by the University of Ottawa Dr Eric Poulin Center for Neuromuscular Disease. A.R. acknowledges the financial support of the Deutsche Gesellschaft für Muskelkranke (DGM) e.V. as well as by the European Regional Development Fund (ERDF) (project B2BRARE).

Data availability

Data are contained within the article and Supplementary Materials.

References

1. Finsterer J. Congenital myasthenic syndromes. *Orphanet J Rare Dis* 2019;**14**:57.
2. Pugliese A, Holland SH, Rodolico C. *et al.* Presynaptic congenital myasthenic syndromes: understanding clinical phenotypes through In vivo models. *J Neuromuscul Dis* 2023;**10**:731–759.
3. Beeson D. Chapter 5 - congenital myasthenic syndromes. In: Hanna M.G. (ed.), *Handbook of Clinical Neurology, Neurologic Channelopathies*, Vol. **203**. Oxford, United Kingdom: Elsevier, 2024, 69–88.
4. Basiri K, Belaya K, Liu WW. *et al.* Clinical features in a large Iranian family with a limb-girdle congenital myasthenic syndrome due to a mutation in DPAGT1.*Neuromuscul Disord* 2013;**23**: 469–472.
5. Belaya K,Finlayson S,Cossins J. *et al.* Identification of DPAGT1 as a new gene in which mutations cause a congenital myasthenic syndrome. *Ann N Y Acad Sci* 2012;**1275**:29–35.

6. Belaya K,Finlayson S,Slater CR.*et al.*Mutations in DPAGT1 cause a limbgirdle congenital myasthenic syndrome with tubular aggregates. *Am J Hum Genet* 2012;**91**:193–201.
7. vanden Brande L, Bauché S, Pérez-Guàrdia L. *et al.* Pathogenic DPAGT1 variants in limb-girdle congenital myasthenic syndrome (LG-CMS) associated with tubular aggregates and ORAI1 hypoglycosylation. *Neuropathol Appl Neurobiol* 2024;**50**:e12952.
8. Finlayson S, Palace J, Belaya K. *et al.* Clinical features of congenital myasthenic syndrome due to mutations in DPAGT1. *J Neurol Neurosurg Psychiatry* 2013;**84**:1119–1125.
9. Belaya K, Rodríguez Cruz PM, Liu WW. *et al.* Mutations in GMPPB cause congenital myasthenic syndrome and bridge myasthenic disorders with dystroglycanopathies. *Brain* 2015;**138**:2493–2504.
10. Rodríguez Cruz PM, Belaya K, Basiri K. *et al.* Clinical features of the myasthenic syndrome arising from mutations in GMPPB. *J Neurol Neurosurg Psychiatry* 2016;**87**:802–809.
11. Cossins J, Belaya K, Hicks D. *et al.* Congenital myasthenic syndromes due to mutations in ALG2 and ALG14. *Brain* 2013;**136**: 944–956.
12. Ehrstedt C, Liu W-W, Frykholm C. *et al.* Novel pathogenic ALG2 mutation causing congenital myasthenic syndrome: a case report. *Neuromuscul Disord* 2022;**32**:80–83.
13. Paneque A,Fortus H,Zheng J. *et al.*The hexosamine biosynthesis pathway: regulation and function. *Genes* 2023;**14**:933.

314

14. Senderek J, Müller JS, Dusl M. *et al.* Hexosamine biosynthetic pathway mutations cause neuromuscular transmission defect. *Am J Hum Genet* 2011;**88**:162–172.

293

15. Holland SH,Carmona-Martinez R,O'Connor K.*et al.*A deficiency in glutamineFructose-6-phosphate transaminase 1 (Gfpt1) in skeletal muscle results in reduced glycosylation of the Delta subunit of the nicotinic acetylcholine receptor (AChRδ). *Biomolecules* 2024;**14**:1252.
16. Zhang R, Farshadyeganeh P, Ohkawara B. *et al.* Muscle-specific lack of GFPT1 in knock-in mice triggers ER stress to alleviate misfolded proteins. *Dis Model Mech* 2024;**17**:dmm.050768.
17. Issop Y, Hathazi D, Khan MM. *et al.* GFPT1 deficiency in muscle leads to myasthenia and myopathy in mice. *Hum Mol Genet* 2018;**27**:3218–3232.
18. Zoltowska K, Webster R, Finlayson S. *et al.* Mutations in GFPT1 that underlie limb-girdle congenital myasthenic syndrome result in reduced cell-surface expression of muscle AChR. *Hum Mol Genet* 2013;**22**:2905–2913.
19. Dusl M, Senderek J, Müller JS. *et al.* A 3'-UTR mutation creates a microRNA target site in the GFPT1 gene of patients with congenital myasthenic syndrome. *Hum Mol Genet* 2015;**24**: 3418–3426.
20. An R, Chen H, Lei S. *et al.* Abnormal decrement on highfrequencyrepetitivenervestimulationincongenitalmyasthenic syndrome with GFPT1 mutations and review of literature. *Front Neurol* 2022;**13**:926786.
21. Farshadyeganeh P, Nazim M, Zhang R. *et al.* Splicing regulation of GFPT1 muscle-specific isoform and its roles in glucose metabolisms and neuromuscular junction. *iScience* 2023;**26**:107746.
22. Ma Y, Xiong T, Lei G. *et al.* Novel compound heterozygous variants in the GFPT1 gene leading to rare limb-girdle congenital myasthenic syndrome with rimmed vacuoles. *Neurol Sci Off J Ital Neurol Soc Ital Soc Clin Neurophysiol* 2021;**42**:3485–3490.
23. Jiang K, Zheng Y, Lin J. *et al.* Diverse myopathological features in the congenital myasthenia syndrome with GFPT1 mutation. *Brain Behav* 2022;**12**:e2469.
24. Vallepu SB, Dhamija K, Rajan GK. *et al.* Phenotypic variability in congenital myasthenic syndrome with GFPT1 mutation. *Acta Neurol Belg* 2024;**125**:209– 213.
25. Bauché S, Vellieux G, Sternberg D. *et al.* Mutations in GFPT1related congenital myasthenic syndromes are associated with synaptic morphological defects and underlie a tubular aggregate myopathy with synaptopathy. *J Neurol* 2017;**264**:1791–1803.
26. Thompson R, Bonne G, Missier P. *et al.* Targeted therapies for congenital myasthenic syndromes: systematic review and steps towards a treatabolome. *Emerg Top Life Sci* 2019;**3**:19–37.
27. Remijn-Nelissen L, Verschuuren JJGM, Tannemaat MR. The effectiveness and side effects of pyridostigmine in the treatment of myasthenia gravis: a crosssectional study.*Neuromuscul Disord* 2022;**32**:790–799.
28. Verheijen J, Tahata S, Kozicz T. *et al.* Therapeutic approaches in congenital disorders of glycosylation (CDG) involving N-linked glycosylation: an update. *Genet Med* 2020;**22**:268–279.
29. Morelle W, Potelle S, Witters P. *et al.* Galactose supplementation in patients with TMEM165-CDG rescues the glycosylation defects. *J Clin Endocrinol Metab* 2017;**102**:1375–1386.
30. Witters P, Tahata S, Barone R. *et al.* Clinical and biochemical improvement with galactose supplementation in SLC35A2-CDG. *Genet Med Off J Am Coll Med Genet* 2020;**22**:1102–1107.
31. Altassan R, Radenkovic S, Edmondson AC. *et al.* International consensus guidelines for phosphoglucomutase 1 deficiency (PGM1-CDG): diagnosis, follow-up, and management. *J Inherit Metab Dis* 2021;**44**:148–163.
32. Park JH, Hogrebe M, Fobker M. *et al.* SLC39A8 deficiency: biochemical correction and major clinical improvement by manganese therapy. *Genet Med* 2018;**20**:259–268.
33. Jones RA, Reich CD, Dissanayake KN. *et al.* NMJ-morph reveals principal components of synaptic morphology influencing structure–function relationships at the neuromuscular junction. *Open Biol* 2016;**6**:160240.
34. Minty G, Hoppen A, Boehm I. *et al.* aNMJ-morph: a simple macro for rapid analysis of neuromuscular junction morphology. *R Soc Open Sci* 2020;**7**:200128.
35. Szelinger S, Krate J, Ramsey K. *et al.* Congenital myasthenic syndrome caused by a frameshift insertion mutation in GFPT1. *Neurol Genet* 2020;**6**:e468.
36. Akella NM, Ciraku L, Reginato MJ. Fueling the fire: emerging role of the hexosamine biosynthetic pathway in cancer. *BMC Biol* 2019;**17**:52.
37. Boyer SW, Johnsen C, Morava E. Nutrition interventions in congenital disorders of glycosylation. *Trends Mol Med* 2022;**28**: 463–481.
38. Potelle S, Morelle W, Dulary E. *et al.* Glycosylation abnormalities in Gdt1p/TMEM165 deficient cells result from a defect in Golgi manganese homeostasis. *Hum Mol Genet* 2016;**25**:1489–1500.
39. Conte F, van Buuringen N, Voermans NC. *et al.* Galactose in humanmetabolism,glycosylation andcongenital metabolic diseases: time for a closer look. *Biochim Biophys Acta BBA - Gen Subj* 2021;**1865**:129898.
40. Podlogar T, Shad BJ, Seabright AP. *et al.* Postexercise muscle glycogen synthesis with glucose, galactose, and combined galactose-glucose ingestion. *Am J Physiol - Endocrinol Metab* 2023;**325**:E672–E681.
41. Lambert M, Richard E, Duban-Deweer S. *et al.* O-GlcNAcylation is a key modulator of skeletal muscle sarcomeric morphometry associated to modulation of protein–protein interactions. *Biochim Biophys Acta BBA - Gen Subj* 2016;**1860**:2017–2030.
42. Chen Q, Müller JS, Pang P-C. *et al.* Global N-linked glycosylation is not significantly impaired in myoblasts in congenital myasthenic syndromes caused by defective glutamineFructose-6-phosphate transaminase 1 (GFPT1). *Biomolecules* 2015;**5**:2758–2781.
43. Ramanathan VK, Hall ZW. Altered glycosylation sites of the δ subunit of the acetylcholine receptor (AChR) reduce αδ association and receptor assembly . *J Biol Chem* 1999;**274**:20513–20520.
44. Rudell JC,Borges LS,Yarov-Yarovoy V.*et al.*The MX-helix of muscle nAChR subunits regulates receptor assembly and surface trafficking. *Front Mol Neurosci* 2020;**13**:48.
45. Wanamaker CP, Green WN. N-linked glycosylation is required for nicotinic receptor assembly but not for subunit associations with calnexin . *J Biol Chem* 2005;**280**:33800–33810.

46. Müller JS, Baumeister SK, Schara U. *et al.* CHRND mutation causes a congenital myasthenic syndrome by impairing coclustering of the acetylcholine receptor with rapsyn. *Brain* 2006;**129**:2784–2793.
47. Chokchaitaweesuk C,Kobayashi T,Izumikawa T. *et al.* Enhanced hexosamine metabolism drives metabolic and signaling networks involving hyaluronan production and O-GlcNAcylation to exacerbate breast cancer. *Cell Death Dis* 2019;**10**:1–15.
48. Claeyssen C, Bastide B, Cieniewski-Bernard C. Global OGlcNAcylation changes impact desmin phosphorylation and its partition toward cytoskeleton in C2C12 skeletal muscle cells differentiated into myotubes. *Sci Rep* 2022;**12**:9831.
49. Hart GW, Slawson C, Ramirez-Correa G. *et al.* Cross talk between OGlcNAcylation and phosphorylation: roles in Signaling, transcription, and chronic disease. *Annu Rev Biochem* 2011;**80**:825–858.
50. Jaiswal R,Liu Y,Petriello M.*et al.*A reference dataset of O-GlcNAc proteins in quadriceps skeletal muscle from mice. *Glycobiology* 2025;**35**:cwaf005.
51. Xue Q, Yan R, Ji S. *et al.* Regulation of mitochondrial network homeostasis by O-GlcNAcylation. *Mitochondrion* 2022;**65**:45–55.
52. O'Connor K, Spendiff S, Lochmüller H. *et al.* Mitochondrial mutations can Alter neuromuscular transmission in congenital myasthenic syndrome and mitochondrial disease. *Int J Mol Sci* 2023;**24**:8505.
53. Belotti E, Schaeffer L. Regulation of gene expression at the neuromuscular junction. *Neurosci Lett* 2020;**735**:135163.
54. Yumoto N, Kim N, Burden SJ. Lrp4 is a retrograde signal for presynaptic differentiation at neuromuscular synapses. *Nature* 2012;**489**:438–442.
55. Arnold A-S, Gill J, Christe M. *et al.* Morphological and functional remodelling of the neuromuscular junction by skeletal muscle PGC-1α. *Nat Commun* 2014;**5**:3569.
56. Rossor AM, Sleigh JN, Groves M. *et al.* Loss of BICD2 in muscle drives motor neuron loss in a developmental form of spinal muscular atrophy. *Acta Neuropathol Commun* 2020; **8**:34.
57. McMacken GM, Spendiff S, Whittaker RG. *et al.* Salbutamol modifies the neuromuscular junction in a mouse model of ColQ myasthenic syndrome. *Hum Mol Genet* 2019;**28**:2339–2351.
58. Oury J, Zhang W, Leloup N. *et al.* Mechanism of disease and therapeutic rescue of Dok7 congenital myasthenia. *Nature* 2021;**595**: 404–408.
59. Xing G, Jing H, Zhang L. *et al.* A mechanism in agrin signaling revealed by a prevalent rapsyn mutation in congenital myasthenic syndrome. *eLife* **8**:e49180.
60. Chevessier F, Girard E, Molgó J. *et al.* A mouse model for congenital myasthenic syndrome due to MuSK mutations reveals defects in structure and function of neuromuscular junctions. *Hum Mol Genet* 2008;**17**:3577–3595.
61. Spendiff S, Howarth R, McMacken G. *et al.* Modulation of the acetylcholine receptor clustering pathway improves neuromuscular junction structure and muscle strength in a mouse model of congenital myasthenic syndrome. *Front Mol Neurosci* 2020;**13**:594220.
62. Bogdanik LP, Burgess RW. A valid mouse model of AGRINassociated congenital myasthenic syndrome. *Hum Mol Genet* 2011;**20**:4617–4633.
63. Slater CR. "Fragmentation" of NMJs: a sign of degeneration or regeneration? A long journey with many junctions. *Neuroscience* 2020;**439**:28–40.
64. Willadt S, Nash M, Slater CR. Age-related fragmentation of the motor endplate is not associated with impaired neuromuscular transmission in the mouse diaphragm. *Sci Rep* 2016;**6**:24849.

65. Dang K, Jiang S, Gao Y. *et al.* The role of protein glycosylation in muscle diseases. *Mol Biol Rep* 2022;**49**:8037–8049.
66. Liu Z, Wang Y, Yang F. *et al.* GMPPB-congenital disorders of glycosylation associate with decreased enzymatic activity of GMPPB. *Mol Biomed* 2021;**2**:13.
67. Cline A, Gao N, Flanagan-Steet H. *et al.* A zebrafish model of PMM2-CDG reveals altered neurogenesis and a substrateaccumulation mechanism for Nlinked glycosylation deficiency. *Mol Biol Cell* 2012;**23**:4175–4187.
68. Wang Y,Lan L,Yang X.*et al*.A case report of classic galactosemia with a GALT gene variant and a literature review. *BMC Pediatr* 2024;**24**:352.
69. Akinbiyi EO, Abramowitz LK, Bauer BL. *et al.* Blocked O-GlcNAc cycling alters mitochondrial morphology,function,and mass.*Sci Rep* 2021;**11**:22106.
70. Delwing-de Lima D, Hennrich SB, Delwing-Dal Magro D. *et al.* The effect of d-galactose induced oxidative stress on *in vitro* redox homeostasis in rat plasma and erythrocytes. *Biomed Pharmacother* 2017;**86**:686–693.
71. Martinovic J, Gusevac Stojanovic I, Nesic S. *et al.* Chronic oral Dgalactose induces oxidative stress but not overt organ dysfunction in male Wistar rats. *Curr Issues Mol Biol* 2025;**47**:161.
72. El-Far AH, Elghaity MM, Mohamed SA. *et al.* Diosgenin alleviates Dgalactose-induced oxidative stress in rats' brain and liver targeting aging and apoptotic marker genes. *Front Mol Biosci* 2024;**11**:1303379.
73. Seene T, Umnova M, Kaasik P. Morphological peculiarities of neuromuscular junctions among different fiber types: effect of exercise. *Eur J Transl Myol* 2017;**27**:6708.
74. Mech AM, Brown A, Schiavo G. *et al.* Morphological variability is greater at developing than mature mouse neuromuscular junctions. *J Anat* 2020;**237**:603–617.

biomolecules

MDPI

Article

Hexosamine Pathway Disruption by GFPT1 Loss Drives Coordinated Defects in Glycosylation, Autophagy, and Trafficking

Stephen H. Holland [1,2,3], Ricardo Carmona-Martinez [1], Andreas Hentschel [4], Alexa Derksen [1,2], Kaela O'Connor [1,2], Daniel O'Neil [1], Kelly Ho [1,2], Stephen D. Baird [1], Andreas Roos [1,5,6], Sally Spendiff [1] and Hanns Lochmüller [1,2,3,7,8,9*]

1 Children's Hospital of Eastern Ontario Research Institute, Ottawa, ON, Canada. K1H8L1
2 Department of Cellular and Molecular Medicine, Faculty of Medicine, University of Ottawa, Ottawa, ON, Canada, K1H 8M5.
3 Dr. Eric Poulin Center for Neuromuscular Disorders, Brain and Mind Research Institute, University of Ottawa, Ottawa, ON, Canada, K1H 8M5.
4 Leibniz-Institute for Analytical Sciences – ISAS- e.V, Dortmund, Germany, 44139.
5 Department of Pediatric Neurology, Centre for Neuromuscular Disorders in Children, University Duisburg-Essen, Hufelandstrasse 55, 45122 Essen, Germany
6 Department of Neurology with Heimer Institute for Muscle Research, University Hospital Bergmannsheil, Bochum, Germany, 44789.
7 Division of Neurology, Department of Medicine, The Ottawa Hospital, Ottawa, ON, Canada, K1H8L6.
8 Department of Neuropediatric and Muscle Disorders, Medical Center, University of Freiburg, Faculty of Medicine, Freiburg, Germany, 79106.
9 Centro Nacional de Analisis Genomico (CNAG-CRG), Center for Genomic Regulation, Barcelona Institute of Science and Technology (BIST), Barcelona, Spain, 08028.

Abstract

Glutamine-Fructose-6-Phosphate Transaminase 1 (GFPT1), the rate-limiting enzyme of the hexosamine biosynthetic pathway (HBP), provides the UDP-N-acetylglucosamine (UDP-GlcNAc) required for protein glycosylation. Biallelic mutations in *GFPT1* cause congenital myasthenic syndromes (*GFPT1*-CMS), yet the molecular mechanisms linking impaired glycosylation to skeletal muscle dysfunction remain incompletely understood. Here, we combine cellular models of inducible *Gfpt1* knockdown and a skeletal muscle-specific *Gfpt1* knockout mouse (*Gfpt1*$^{Tm1d/Tm1d}$) with whole-cell proteomics, immunoblot studies and secretomics to define glycosylation-dependent defects in intracellular trafficking, ER stress signaling and autophagy. Global proteomic profiling of *Gfpt1*-deficient myoblasts revealed marked downregulation of protein trafficking pathways and impaired secretion of key muscle cargo proteins, including serglycin (Srgn). Loss of GFPT1 reduced both high-molecular-weight glycosylated serglycin and its core protein, accompanied by intracellular retention and decreased secretion. These trafficking defects coincide with robust activation of the unfolded protein response (UPR), evidenced by increased *Xbp1* expression and accumulation of spliced Xbp1s across pharmacologic, cellular, and mouse models of *GFPT1* deficiency. Converging evidence from proteomics, immunoblotting, and immunofluorescence demonstrated impaired autophagy, including increased LC3-II accumulation, elevated p62/Sqstm1 levels, and enhanced p62-positive puncta in both *Gfpt1*-deficient C2C12 myoblasts and skeletal muscle. Soluble/insoluble fractionation further confirmed p62 accumulation, indicating defective autophagic flux and buildup of aggregated cargo. Together, these findings identify a glycosylation-dependent failure in protein trafficking that triggers ER stress, UPR activation, and autophagy impairment in *Gfpt1*-deficient skeletal muscle. This mechanistic cascade provides a unifying explanation for muscle pathology in *GFPT1*-CMS and suggests that restoring glycosylation or improving proteostasis may represent viable therapeutic approaches.

Keywords: Congenital Myasthenic Syndrome; GFPT1; trafficking; autophagy; glycosylation

Academic Editor(s): Rosario Francesco Donato

Received: 1 May 2026
Revised: 19 June 2026
Accepted: 22 June 2026
Published: date

1. Introduction

Protein glycosylation is essential for proper folding, stability, secretion and intracellular trafficking of thousands of proteins across mammalian cell types [1–3]. Glycoproteins represent nearly half of the mammalian proteome, and defects in glycosylation disrupt critical processes—particularly in highly secretory or structurally demanding tissues such as skeletal muscle [3]. The hexosamine biosynthetic pathway (HBP) provides the essential nucleotide sugars that fuel these glycosylation reactions, with UDP-GlcNAc serving as a central substrate for N-, O-linked glycosylation and O-GlcNAcylation [4,5]. At the apex of this pathway sits glutamine-fructose-6-phosphate transaminase 1 (GFPT1), the rate-limiting enzyme that controls the metabolic flux into the hexosamine biosynthetic pathway (HBP) by converting fructose-6-phosphate into glucosamine-6-phosphate [4,5]. Since GFPT1 function determines the availability of UDP-GlcNAc, it acts as a critical metabolic gatekeeper linking nutrient status, cellular stress responses, and post-translational protein modifications [4–6]. Even modest reductions in HBP flux can compromise protein folding, vesicle export, and quality control systems that depend on glycan maturation, underscoring the central role of GFPT1 in maintaining cellular proteostasis.

Congenital myasthenic syndromes (CMSs) are a group of inheritable, early-onset neuromuscular disorders caused by mutations in proteins critical for the development, maintenance and function of the neuromuscular junction (NMJ) [7,8]. Clinically, CMS is characterized by fatigable muscle weakness and exhibits considerable genetic and phenotypic heterogeneity [7–9]. To date, approximately 40 genes have been implicated in CMS, with a subset of five genes linked to defects in protein glycosylation [8,10–13]. Biallelic pathogenic variants to *GFPT1* lead to reduced protein abundance and impaired enzymatic activity [10,14–22]. Patients with *GFPT1*-CMS typically present with predominant limb-girdle muscle weakness [10,14,15]. Histopathological analysis of patient muscle biopsies reveals diverse myopathic features, including tubular aggregates and rimmed vacuoles [15,16]. Notably, these pathological hallmarks are recapitulated in our skeletal muscle-specific *Gfpt1* knockout mouse model (*Gfpt1*$^{tm1d/tm1d}$), validating its relevance to human *GFPT1*-CMS [6,22,23]. Recent work from our group demonstrated that *Gfpt1* depletion disrupts multiple glycosylation processes, including protein O-GlcNAcylation and N-linked glycosylation [6,23]. Although *GFPT1*-deficiency is known to impact protein glycosylation, the downstream mechanisms linking disrupted glycosylation to skeletal muscle pathology remain poorly understood.

Protein glycosylation is intimately coupled to intracellular trafficking and endoplasmic reticulum (ER) homeostasis. Hypoglycosylation disrupts protein folding in the ER, leading to protein misfolding, ER retention, and preferential targeting to ER-associated degradation (ERAD) due to failure to pass glycan-dependent quality control checkpoints [24,25]. When misfolded proteins accumulate, cells activate the unfolded protein response (UPR) to restore proteostasis by enhancing chaperone expression, attenuating translation, and upregulating ERAD [26]. In parallel, disruptions in protein folding and trafficking can impair autophagy, a degradative pathway essential for the clearance of damaged proteins, aggregated cargo, and dysfunctional organelles [27–29]. A hallmark of impaired autophagic flux is the accumulation of p62 and LC3-II, reflecting defective cargo degradation and contributing to the formation of protein aggregates [30]. Intriguingly, prior studies with *Gfpt1*$^{tm1d/tm1d}$ mice demonstrated a ~2.5-fold increase in p62, suggesting that autophagy may be impaired within *Gfpt1*-deficient models [22].

Here, we combine whole-cell proteomics, secretomics, cellular models of *Gfpt1*-depletion and a *Gfpt1*$^{tm1d/tm1d}$ mouse model to define how Gfpt1 deficiency disrupts proteostasis within skeletal muscle. We identify downregulation of vesicle trafficking proteins, intracellular retention of secreted proteins such as serglycin (Srgn), activation of the UPR pathway and a profound impairment of autophagic flux characterized by p62 and LC3-II accumulation. Together, our findings reveal a glycosylation-dependent cascade in which defective trafficking and ER stress converge on impaired autophagy, providing a unified mechanistic framework for muscle pathology in *GFPT1*-CMS.

2. Methods

2.1. Cell Culture

C2C12 cells (ATCC, CRL-1722, Burlington, ON, Canada) were cultured in high-glucose Dulbecco's Modified Eagle Medium (DMEM) supplemented with 10% fetal bovine serum (FBS), 1% glutamine, and 1% penicillin/streptomycin. A *Gfpt1*-deficient C2C12 cell model was established using a TET-ON miR-30 tetracycline-inducible system with two different short hairpin sequences targeting *Gfpt1* (shGfpt1 #1 and shGfpt1 #2) (VectorBuilder, Chicago, IL, USA) as previously described [6]. *Gfpt1* silencing was achieved by doxycycline treatment at 2 μg/mL for 72 h (Sigma, D9891, Toronto, ON, Canada).

2.2. Animal Husbandry

Animals were housed at the University of Ottawa Animal Care and Veterinary Facility (Roger Guidon Hall, Ottawa, ON, Canada), and all breeding and experimental protocols were approved by the internal Animal Care Committee (protocols: breeding—CHEO-3089 and experimental—CHEO-3120 approved on 16 November 2018 and 2 April 2019, respectively). Mice were maintained on a 12 h light–dark cycle, with access to food and water ad libitum for the duration of this study. Mice were generated and genotyped as previously reported [6,22,23]. For this study, Tm1C homozygous mice (which contain two LoxP sites flanking the seventh exon of *Gfpt1* but lack *Ckm-Cre* expression) were used as controls. *Gfpt1*$^{tm1d/tm1d}$ mice contain two LoxP sites flanking the 7th exon of *Gfpt1* but also express a Cre recombinase tied to the *Ckm* reporter, which creates a skeletal muscle-specific knockout of *Gfpt1* [6,22].

2.3. Sample Preparation and Protein Digestion

Gfpt1-deficient and scramble control cells were seeded into separate 15 cm plates. At 75% confluency, *Gfpt1* silencing was achieved by doxycycline treatment at 2 μg/mL for 72 h (Sigma, D9891). Prior to collection, cells were serum starved for three hours, followed by a replacement with growth media for one hour, and finally serum starved for an additional 4 h. Afterwards, conditioned media were collected, centrifuged at 1000× *g* for 15 min. The supernatant was collected and snap frozen. This sample represents the secretome.

Frozen cell pellets were treated with 200 μL of lysis buffer (50 mM TEAB, pH 7.8, 5% SDS, supplemented with cOmplete™ ULTRA protease inhibitor cocktail (Roche, #0589297001, Penzberg, Germany) followed by mechanical disruption using a Bioruptor® sonication system (Diagenode, Seraing, Belgium) for 10 min (30 s on/30 s off, 10 cycles) at 4 °C. To achieve complete homogenization, samples were additionally subjected to probe sonication (30 s, 1 s on/1 s off, amplitude 40%), and insoluble material was removed by centrifugation (20,000× *g*, 15 min, 4 °C). Protein concentration in the cleared supernatant was quantified using DC Protein Assay (BioRad, 5000111, Dreieich, Germnay) with BSA dilutions (Pierce, 23209, Dreieich, Germnay) as standards according to the manufacturer's instructions.

Reduction of disulfide bonds was performed by incubation with 10 mM TCEP at 37 °C for 30 min, followed by alkylation with 15 mM IAA at room temperature for 30 min in the dark. For proteolytic digestion, 100 μg of total protein from each sample was processed using the S-Trap protocol (Protifi, New York, USA) with a protein-to-trypsin ratio of 20:1. Digestion was carried out for 2 h at 42 °C, and the reaction was terminated by acidification with formic acid to a final pH below 3.

The completeness of proteolytic cleavage was evaluated following desalting by monolithic column separation (PepSwift PS-DVB PL-CAP200-PM, Dionex) using an UltiMate 3000 HPLC system (Dionex, Germering, Germany). For each analysis, 1 μg of digest was injected directly. Chromatographic separation was achieved with a binary gradient (solvent A: 0.1% TFA; solvent B: 0.08% TFA in 84% acetonitrile), starting at 5–12% B over 5

min, followed by 12–50% B over 15 min, at a flow rate of 2.2 µL/min and 60 °C. UV detection was carried out at 214 nm [31].

2.4. DDA-LC-MS/MS Analysis

A total of 1 µg of the prepared samples was analyzed using an UltiMate 3000 RSLC nano UHPLC system paired with a QExactive HF mass spectrometer (Both ThermoFisher Scientific, Breman, Germnay). Initially, the samples were loaded onto a 75 µm x 2 cm, 100 Å, C18 pre-column at a flow rate of 20 µL/min for 20 min. Subsequently, separation was carried out on a 75 µm × 50 cm, 100 Å, C18 main column with a flow rate of 250 nl/min, utilizing a binary gradient (solvent A: 0.1% formic acid (Sigma-Aldrich, Hamburg, Germany; solvent B: 84% acetonitrile (Sigma-Aldrich, Hamburg, Germany)) with 0.1% formic acid; 5% B for 3 min, linear increase to 25% for 102 min, a further linear increase to 33% for 10 min, and a final linear increase to 95% for 2 min followed by a linear decrease to 5% for 5 min). For MS survey scans, the parameters included operating MS in data-dependent acquisition mode (DDA) with full MS scans from 300 to 1600 *m*/*z* (resolution 60,000) and the polysiloxane ion at 371.10124 *m*/*z* as a lock mass. The maximum injection time was set to 120 ms, and the automatic gain control (AGC) was set to 1E6. Fragmentation involved selecting the 15 most intense ions (above the threshold ion count of 5E3) at a normalized collision energy (nCE) of 27% in each cycle, following each survey scan. Fragment ions were acquired (resolution 15,000) with an AGC of 5E4 and a maximum injection time of 50 ms. Dynamic exclusion was set to 15 s.

2.5. DDA Data Analysis of C2C12 Cells

All MS raw data underwent processing using Proteome Discoverer software version 2.5.0.400 (Thermo Scientific, Bremen, Germany) and were subjected to a target/decoy mode search against a mouse Uniprot database (www.uniprot.org, downloaded on 8 October 2019) utilizing the MASCOT and Sequest algorithm. The search parameters included precursor and fragment ion tolerances of 10 ppm and 0.02 Da for MS and MS/MS, respectively. Trypsin was designated as the enzyme with a maximum of 2 allowed missed cleavages. Carbamidomethylation of cysteine was set as a fixed modification, and oxidation of methionine was set as a dynamic modification. Percolator false discovery rate (strict) was established at 0.01 for both peptide and protein identification.

For reliable label-free quantification, only proteins identified with ≥2 unique peptides were considered for further analysis. Subsequently, the average normalized abundances (determined using Proteome Discoverer) were calculated for each protein and used to determine the ratio between the different conditions. Finally, a Student's *t*-test with *p*-values was calculated in MS Excel. Only proteins with a *p*-value of ≤0.05 and an abundance ratio of ≥2 or ≤0.5 (upregulated as well as downregulated) were considered as regulated.

To further interpret the proteomic alterations, a list of significantly upregulated proteins (expression ratio ≥ 2.0) and downregulated proteins (expression ratio ≤ 0.5) was analyzed using the STRING database for functional enrichment. Gene Ontology (GO) Biological Process enrichment analysis was performed to identify overrepresented functional pathways. Protein–protein interaction networks were constructed using a minimum required interaction score of 0.7 (high confidence). Functional clustering was applied based on a similarity threshold greater than 0.7 to group proteins into related biological processes. This approach enabled the identification of key pathways and biological processes most affected by the observed proteomic changes.

2.6. Proteomic Analysis from Conditioned Medium

Scramble and *Gfpt1*-deficient C2C12 myoblasts were seeded into 10 cm plates. At 75% confluency, the growth medium was changed into serum-free medium for four hours, then the growth medium was applied for an hour, followed by another three-hour

incubation with starvation medium. Media was collected and centrifuged to remove cell debris and snap frozen in 10 mL aliquots for proteomic analysis.

Each sample was divided into two aliquots of 1 mL cultured medium. Protein precipitation was carried out by adding 3 mL of ice-cold acetone to each aliquot, followed by incubation overnight at −20°C. Subsequently, the samples were centrifuged at 20,000× *g* for 20 min at 4 °C to pellet the proteins. The acetone supernatant was carefully removed, and the pellets were air-dried for 3 to 5 min. To bring the protein pellets into solution, 100 µL lysis buffer (50 mM TEAB (Merck, Taufkirchen, Germany), pH 7.8; 5% SDS (ThermoFisher Scientific, Dreieich, Germnay) ; and cOmplete ULTRA protease inhibitor, Roche, 05892970001, Penzberg, Germany) was added to each sample. Complete lysis was ensured using a Bioruptor® (Diagenode, Seraing, Belgium) for 10 min at 4 °C (30 s cycles of sonication and rest, 10 cycles total). Finally, the aliquots were combined to reconstitute the original sample. Reduction of disulfide bonds was performed by incubation with 10 mM TCEP at 37 °C for 30 min, followed by alkylation with 15 mM IAA at room temperature for 30 min in the dark. For proteolytic digestion, 100 µg of total protein from each sample was processed using the S-Trap protocol (Protifi) with a protein-to-trypsin ratio of 20:1. Digestion was carried out for 2 h at 42 °C, and the reaction was terminated by acidification with formic acid to a final pH below 3.

For the analysis of the samples acquired with nano-LC-MS/MS in DIA mode, the data were introduced to the Spectronaut software (Biognosys, Version 18.7.240506.55695) and analyzed with a direct DIA-based search. As a library, the mouse proteome data were selected from UniProt (www.uniprot.org), containing 17,175 entries (downloaded on 23 August 2023). Search and extraction settings were kept as standard (BGS Factory settings). Normalization was done by the software, using global normalization based on the median. For reliable label-free quantification, only proteins identified with ≥2 unique peptides were considered for further analysis. Subsequently, the average normalized abundances (determined using Spectronaut) were calculated for each protein and used to determine the ratio between the leukocytes from the patients and the corresponding controls. Finally, a Student's *t*-test with *p*-values was calculated in MS Excel. Only proteins with a *p*-value of ≤0.05 and an abundance ratio of ≥2 or ≤0.5 (upregulated as well as downregulated) were considered as finally regulated.

2.7. DIA LC-MS/MS Analysis of Conditioned Medium Samples

All samples were subjected to analysis using an UltiMate 3000 RSLC nano UHPLC system paired with a QExactive HF mass spectrometer (Both Thermo Fisher Scientific, Bremen, Germany), consistently applying 1 µg of peptide per sample. Initially, the samples were loaded onto a 75 µm x 2 cm, 100 Å, C18 pre-column at a flow rate of 20 µL/min for 20 min. Subsequently, separation was carried out on a 75 µm × 50 cm, 100 Å, C18 main column with a flow rate of 250 nl/min, utilizing a linear gradient composed of solution A (99.9% water, 0.1% formic acid) and solution B (84% acetonitrile, 15.9% water, 0.1% formic acid). The gradient length was set to 120 min (3–45% solution B). The gradient protocol included: 3% solution B for 20 min, 3–35% over 120 min, followed by three wash steps each reaching 95% solution B for 3 min. Post-wash, the instrument was allowed to equilibrate for 20 min. MS data acquisition was performed in DIA (data-independent acquisition) mode, utilizing an in-house developed spectral library. Each sample was spiked with an appropriate quantity of iRT standard (Biognosys). Full MS scans were recorded from 300 to 1100 *m*/*z* at a resolution of 60,000 (Orbitrap), using the polysiloxane ion at 445.12002 *m*/*z* as a lock mass. The automatic gain control (AGC) was set at 3×10^6, with a maximum injection time of 20 milliseconds. Full MS scans were succeeded by 23 DIA windows, each covering 28 *m*/*z* with a 1 *m*/*z* overlap, starting at 400 *m*/*z*, acquired at a resolution of 30,000 (Orbitrap) with an AGC of 3E6 and a normalized collision energy (nCE) of 27 (CID).

2.8. Gfpt1-Deficient Myoblast Immunofluorescence Staining

1000 Scramble and *Gfpt1*-deficient C2C12 myoblasts were seeded on 96-well µ-PLATE square ibiTreat plates (Ibidi, FisherSci, 50-305-829, Toronto, ON, Canada). *Gfpt1* silencing was achieved by doxycycline treatment at 2 µg/mL for 72 h. (Sigma, D9891, Toronto, ON, Canada). Prior to staining, cells were fixed with 2% paraformaldehyde for 15 min at room temperature. Blocking buffer (5% horse serum, 1% bovine serum albumin, 0.1% Triton X-100) was incubated for 1 h. Cells were washed three times with PBS prior to primary antibody incubation overnight. Primary antibodies included: Srgn (1:100, #C-11, Santa-Cruz Biotechnology, Dallas, TX, USA) and p62 (1:100, Cedarlane, PM045, Dallas, TX, USA). Cells were washed three times with PBS and incubated with goat anti-rabbit AlexaFluor 594 (1:500, #A-11012, FisherSci, Ottawa, ON, Canada) or goat-anti mouse AlexaFlour 594 (1:500, #A-11011, FischerSci, Ottawa, ON, Canada). Cells were then washed three times with PBS for 5 min and then incubated with DAPI (1:2000) for an additional five minutes. The 96-well µ-PLATE square ibiTreat plates were then imaged using the Opera high content imaging system and analyzed by Columbus™ software (Version 2.5) to measure Srgn and p62 puncta size and area.

2.9. Lysis of Cells

Cell lysates and skeletal muscle homogenates were prepared with radioimmunoprecipitation assay (RIPA) buffer (150 mM NaCl, 50 mM Tris-HCl (pH 8), 1% Triton X-100, 0.5% NaDOC, 0.1% SDS) supplemented with protease (Roche, 04693116001, Mississauga, ON, Canada) and phosphatase (Roche, PHOSS-RO) inhibitors. Cell lysates were centrifuged at 15,000× *g* for 10 min at 4 °C, and the supernatants were collected. Skeletal muscle samples were combined with lysis buffer and a metal bead in 2 mL SafeLock™ Eppendorf tubes (Eppendorf, 022363352, Mississauga, ON, Canada), then homogenized using a TissueLyser II (Qiagen, Toronto, ON, Canada). The protocol comprises 3 rounds of homogenization at 30 Hz for 90 s, followed by incubation on ice for 60 s. Afterwards, samples were kept at 4 °C for 4 h on a rotating platform, then centrifuged at 15,000× *g* for 15 min at 4 °C. Total protein concentration was determined using a DC Protein Assay (BioRad, 5000111, Toronto, ON, Canada) with BSA dilutions (Pierce, 23209, Toronto, ON, Canada) as standards.

2.10. Conditioned Medium Collection for Srgn Secretion

To examine Srgn protein levels within conditioned medium, C2C12 cells were seeded in 10 cm plates. *Gfpt1* silencing was achieved by doxycycline treatment at 2 µg/mL for 72 h. (Sigma, D9891, Toronto, ON, Canada). Cell media was replaced with serum-starved growth medium for 1 h. Afterwards, the growth medium was reapplied and incubated for 1, 3, 5, 8, 12, 18, and 24 h. At each timepoint, cell media was collected and combined in a 1:5 ratio with ice-cold 100% methanol and placed in the −80 °C overnight. The next morning, the solution was centrifuged at 8000× *g* for 30 min. The supernatant was discarded, and pellets were dried for 1 h in a fume hood. The cell pellet was homogenized with RIPA buffer, followed by a brief sonification.

2.11. Western Blotting

To examine protein levels within *Gfpt1*-deficient cells and skeletal muscle, lysates were resolved by SDS-PAGE and transferred to PVDF membranes using a BioRad™ Trans-Blot Turbo system (1704150EDU, Mississauga, ON, Canada). All samples were heated at 100 °C for 5 min in 4× Laemmli sample buffer, prior to resolution with Western blot. When examining Srgn protein levels, SDS-PAGE gels were transferred to PVDF membranes with wet transfer (40 V, overnight, 4 °C). All membranes were blocked for 1 h and incubated with primary antibody overnight at 4 °C. Multiple secondary antibodies were used for this analysis, including IR Dye®800CW Donkey anti-Mouse IgG (Li-Cor, 926-32212, 1:5000, Lincoln, NB, USA) and IR Dye®680RD Goat anti-Rabbit IgG (Li-Cor, 926-68071, 1:5000) for 1 h at room temperature.

Blots were imaged using a Licor Odyssey DLX (Lincoln, NE, USA) and densitometry performed using Image Studio™ (Licor, version 6.0) or with ChemiDoc (BioRad, Mississauga, ON, Canada) and analyzed with ImageJ (Version 1.54). Gapdh or Ponceau S stain was used to normalize protein expression.

2.12. Real-Time qPCR (RT-qPCR)

RNA collection for in vitro experiments was performed using the RNeasy™ Micro mini kit (Qiagen, #74134, Toronto, ON, Canada). Skeletal muscle RNA extraction was performed with the RNeasy™ Fibrous Micro mini kit (Qiagen, #74704) and quantified by NanoDrop (ND-1000, Spectrophotometer, NanoDrop®. RNA was converted to complementary DNA (cDNA) with the All-In-One 5x RT MasterMix (ABM, #G592, Richmond, BC, Canada) following kit guidelines. RT-qPCR was performed using the PowerUp™ SYBR™ Green Master Mix (FisherSci, #A25741, Ottawa, ON, Canada) with the QuantStudio™ Studio 6 Flex Real-Time PCR System (Thermofisher, Ottawa, ON, Canada) (see Supplementary Materials Table S1 for primer sequences). To analyze the expression of our target genes, the geometric mean of three reference genes (*Gapdh*, *Rpl27*, and *Ppia*) was used.

2.13. Soluble/Insoluble Fractionation

Gfpt1-deficient and scramble myoblasts were seeded in 10 cm plates. Following activation for gene silencing with 2 μg/mL doxycycline for 72 h, the cells were pelleted and resuspended in cell lysis buffer (20 mM HEPES, pH 7.9, 0.2 M KCl, 1 mM $MgCl_2$, 1 mM EGTA, 1% Triton X-100, 10% glycerol, and protease/phosphatase inhibitor) and incubated on ice for 30 min. The soluble fraction was taken from the supernatant, which was collected after centrifugation at 13,000× *g* for 20 min at 4°C. The pellet (insoluble membrane) was solubilized in an SDS-detergent buffer (20 mM HEPES, pH 7.9, 0.2 M KCl, 1 mM $MgCl_2$, 1 mM EGTA, 1% Triton X-100, 1% SDS, 10% glycerol and protease/phosphatase inhibitor). Cell pellets were solubilized using a mortar and pestle. All samples were heated at 100°C for 5 min in 4× Laemmli Sample Buffer, prior to resolution with Western blot.

2.14. Antibodies

The following antibodies were used for immunoblot or immunofluorescent experiments: Gfpt1 (ProteinTech, #14132-1-AP, 1:500, Rosemont, IL, USA), Gapdh (14C10) (Cell Signalling, 2118, 1:2000, Danvers, MA, USA), O-GlcNAc (RL2) (Novus Biologicals, NB300-524, 1:1000, Toronto, ON, Canada), Ogt (ProteinTech, 66823-1-Ig, 1:1000, Rosemont, IL, USA), Srgn (#C-11, Santa Cruz Technology, Dallas, TX, USA), Srgn (#H9, Santa Cruz), p62 (Cedarlane, #PM045), LC3 (Sigma, #L7543).

2.15. Statistics

Data was analyzed with GraphPad Prism v 10.1.2. Data was checked for normality using the D'Agostino-Pearson test and outliers were identified using the robust regression and outlier remover (ROUT) method. Statistical significance was determined by using unpaired two-tailed Student *t*-tests or analysis of variance (ANOVA) tests. If multiple comparisons were used, Tukey's post hoc test was performed. Results are presented as mean ± SD, where $p < 0.05$ was considered significant.

3. Results

3.1. Whole-Cell Proteomics in Gfpt1-Deficient Myoblasts Reveals Dysregulation of Autophagy and Intracellular Trafficking Pathways

To define the global proteomic consequences of reduced hexosamine biosynthetic pathway flux, we performed whole-cell mass spectroscopy on both the conditioned medium (secretome) and cell pellets (proteome) of doxycycline-inducible *Gfpt1*-deficient C2C12 myoblasts (Figure 1A). Prior to proteomic profiling, we confirmed efficient

knockdown of Gfpt1, oligotransferase (Ogt), and a decrease in global O-GlcNAcylation by Western blotting, which is consistent with diminished HBP flux (Figure 1B).

Comparative proteomic analysis between *Gfpt1*-deficient and scramble myoblasts identified 74 significantly upregulated and 229 significantly downregulated proteins (Figure 1C). Our comparative analysis revealed that Stead3 (6.65-fold), Slc25a10 (6.45-fold), Rab34 (6.23-fold), Rhob (5.20-fold), and Supt16h (4.50-fold) had the highest magnitude of change (Table 1). The magnitude and directionality of these broad changes suggest widespread alterations in proteostasis and cellular responses. STRING pathway enrichment analysis of upregulated proteins demonstrated prominent activation of pathways relevant to protein homeostasis, protein folding, and stress-responsive chaperone systems (Figure 1D). These findings are consistent with an adaptive response to impaired glycosylation and an increased burden of misfolded or immature proteins.

In contrast, our comparative analysis revealed that Ppp1r14b (0.02-fold), Lima1 (0.04-fold), Gmfb (0.05-fold), Cttn (0.07-fold), and Denr (0.08-fold) represent the most downregulated proteins (Table 1). Overall, downregulated proteins showed a strong enrichment for pathways associated with intracellular transport, including vesicle-mediated trafficking, and protein processing in the secretory pathway (Figure 1E). Along this line, several components of COPII-mediated ER-to-Golgi transport machinery, Golgi organization, and vesicle cargo sorting systems were reduced, suggesting compromised protein trafficking capacity (Table 1). Together, these proteomic changes indicate that *Gfpt1* deficiency disrupts the balance between protein synthesis, folding, and notably trafficking, resulting in the coordinated activation of stress-mitigating pathways and suppression of secretory transport machinery.

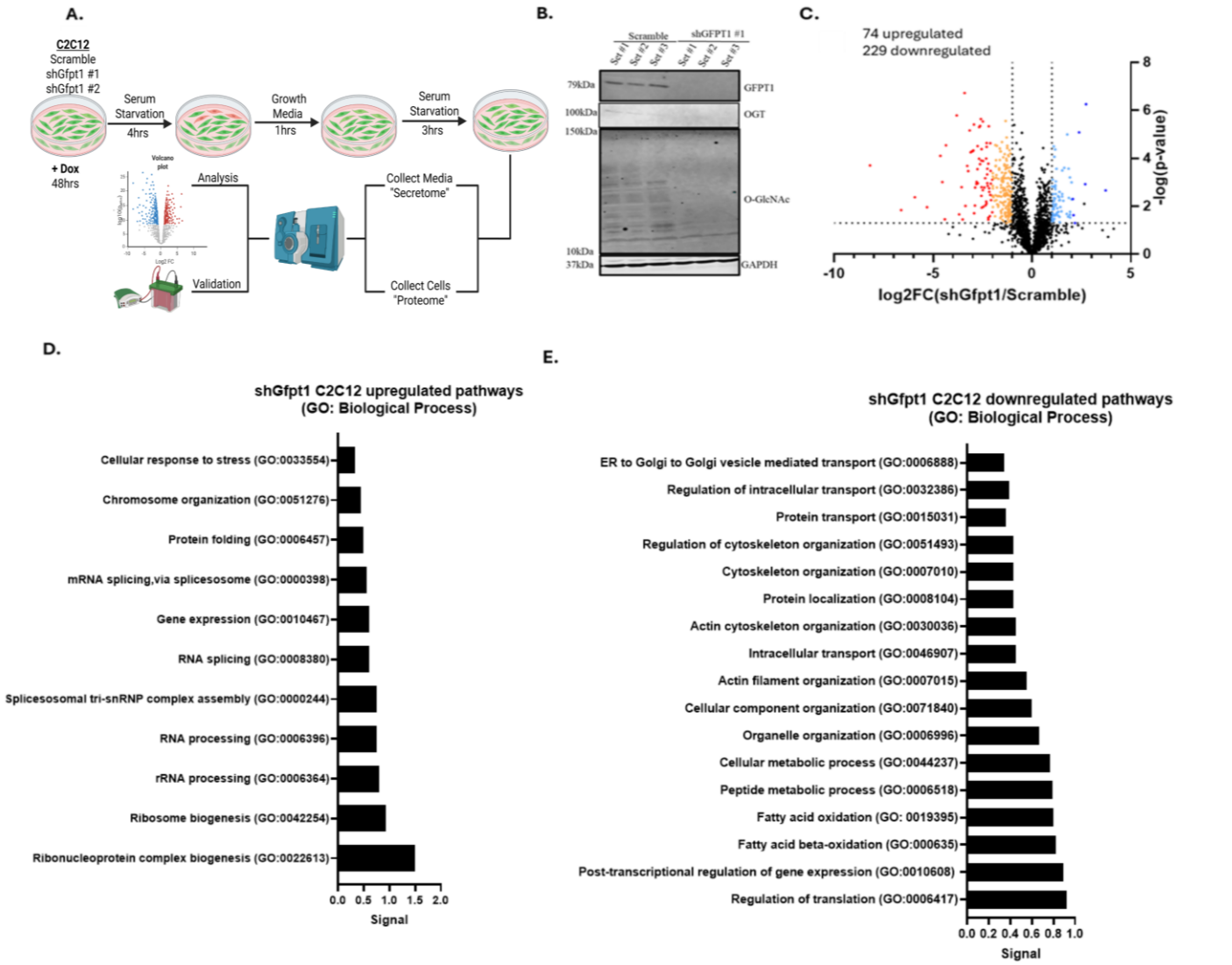

Figure 1. Whole-cell proteomics in *Gfpt1*-deficient myoblasts reveals impaired autophagy and protein trafficking: (**A**). A schematic of the proteomic (cell pellets) and secretomic (conditioned medium) isolated from *Gfpt1*-deficient myoblasts. The cell pellets (containing all possible membrane, cytosolic, and nuclear proteins) were harvested and snap-frozen in liquid nitrogen for downstream proteomic analysis of both conditioned media and whole-cell lysates. (**B**). Immunoblot analysis performed prior to proteomic assessment confirms reduced Gfpt1 protein levels and decreased global O-GlcNAcylation in doxycycline-treated myoblast lysates. Samples were isolated from three independent biological experiments. (**C**). Volcano plot of whole-cell proteomics comparing *Gfpt1*-deficient and scramble control C2C12 myoblasts identifies 74 upregulated and 220 downregulated proteins. Differential expression was defined as a fold change ≥ 2.0 or ≤0.5 with statistical significance ($p < 0.05$). (**D**). STRING pathway analysis was performed on upregulated proteins and (**E**). downregulated proteins. For both conditions, the top 15 pathways implicated with *Gfpt1*-deficient myoblasts. The size of the circle for each pathway indicates the number of proteins implicated in each respective pathway.

Table 1. Key proteins up- or downregulated in *Gfpt1*-deficient C2C12 myoblasts compared with scramble. Proteins with a *p*-value of <0.05 and an abundance ratio of either ≥2-fold (upregulated) or ≤0.5-fold (downregulated) are included below.

Protein	Description	Autophagy-Relevant Pathway Role	KD/Ctrl

Map1lc3b	LC3B, autophagosome membrane protein	Core macroautophagy machinery; autophagosome formation, mitophagy, pexophagy	2.25
Rheb	mTORC1 activator GTPase	Master negative regulator of autophagy via mTORC1	4.17
Rab34	Rab GTPase	Lysosome positioning; autophagosome–lysosome fusion	6.23
Rhob	Rho GTPase	Endosomal/lysosomal trafficking; autophagosome maturation	5.20
Emc6	ER membrane complex subunit	ER-derived phagophore membrane source	2.36
Calr	ER Ca^{2+} chaperone	ER stress, ER-phagy, autophagy induction	2.19
Erp29	ER folding protein	UPR/ER stress-induced autophagy	2.18
Erlin2	ERAD/ER stress protein	ER stress signaling to autophagy	2.17
Psmb3	Proteasome subunit	Proteasome–autophagy compensatory axis	2.35
Hspbp1	Hsp70 co-chaperone	Chaperone-assisted autophagy/proteostasis	2.11
Ppib	ER peptidyl-prolyl isomerase	ER proteostasis → autophagy induction	2.40
Clcn5	Endolysosomal Cl^- channel	Lysosome acidification; autophagic degradation	2.63
Arsb	Lysosomal enzyme	Lysosomal throughput during autophagy	2.31
Ndufs1	ETC Complex I subunit	Mitophagy cargo indicator	3.80
Ndufa6	ETC Complex I subunit	Mitophagy cargo indicator	2.27
Mtco2	ETC Complex IV subunit	Mitophagy cargo indicator	2.27
Cox6c	ETC Complex IV subunit	Mitophagy cargo indicator	2.15
Bcat1	BCAA metabolism enzyme	Nutrient sensing → mTOR regulation	2.52
Slc25a10	Mitochondrial carrier	Redox/TCA control → AMPK/mTOR/autophagy	6.45
Ampd2	AMP metabolism enzyme	AMP/ATP ratio → AMPK → autophagy	2.61
Copg1	Coatomer subunit gamma-1	COPI vesicle trafficking (Golgi ↔ ER retrograde transport)	0.50
Sec23a	COPII vesicle component	ER → Golgi export (cargo sorting)	0.49
Sec22b	SNARE protein	ER–Golgi vesicle fusion, ER-phagosome pathway	0.31
Uso1	Vesicle tethering factor (p115)	Golgi vesicle docking and fusion	0.42
Rab5b	Small GTPase	Early endosome formation, endocytosis	0.44
Snx9	Sorting nexin-9	Clathrin-mediated endocytosis	0.46
Gapvd1	Rab5 GEF	Endosome maturation and trafficking	0.43
Clta	Clathrin light chain A	Vesicle coat formation (endocytosis)	0.25
Prkaa1 (AMPKα1)	Energy sensor kinase	Autophagy induction, mTOR regulation	0.42
Hspb8	Small heat shock protein	BAG3-mediated selective autophagy (aggrephagy)	0.42
Bag3	Co-chaperone	Protein quality control, autophagy targeting	0.12
Stub1 (CHIP)	E3 ubiquitin ligase	Proteasome targeting + autophagy crosstalk	0.43
Psmb7	Proteasome subunit β7	Proteasomal protein degradation	0.36
Psme1	Proteasome activator	Proteasome function enhancement	0.35
Ufm1	Ubiquitin-like modifier	Protein turnover and ER stress responses	0.47
Nedd8	Ubiquitin-like protein	Cullin activation, ubiquitin ligase regulation	0.30

Atp6v1b2	V-ATPase subunit B2	Lysosomal acidification, autophagic degradation	0.45
Atp6v1g1	V-ATPase subunit G1	Lysosomal acidification	0.43
Lonp1	Mitochondrial protease	Mitochondrial protein quality control	0.40
Atad3	Mitochondrial AAA protein	Mitochondrial dynamics, mitophagy regulation	0.44
Park7 (DJ-1)	Stress response protein	Oxidative stress, aggrephagy support	0.36
Dync1i2	Dynein intermediate chain	Microtubule-based vesicle transport	0.35
Tubb4b	β-tubulin	Cytoskeletal trafficking, autophagosome movement	0.48
Ckap4	ER-associated protein	ER structure and protein trafficking	0.48

3.2. Gfpt1 Deficiency Activates UPR Through Increased Xbp1 Splicing and Atf4

Our proteomic results revealed many proteins associated with trafficking and ER homeostasis. As a result, in elevated hypoglycosylation stress, we hypothesized that the unfolded protein response (UPR) pathway would also be impaired. The UPR consists of three coordinated signaling branches—IRE1, PERK and ATF6—that collectively restore ER proteostasis by enhancing chaperone expression, attenuating protein synthesis, and promoting ER-associated degradation (ERAD) (Figure 2A). Under ER stress, the IRE1 arm generates the active transcription factor Xbp1s via unconventional mRNA splicing, thereby increasing the transcription of ERAD components and ER chaperones. XBP1 exists in two forms: an unspliced, relatively unstable transcript (*Xbp1u*) and a spliced form (*Xbp1s*) produced during ER stress (Figure 2A). Consistent with activation of this pathway, we observed increased levels of *Xbp1s* accompanied by a relative reduction in *Xbp1u*, indicating enhanced IRE1 signaling and unfolded protein response induction.

To determine whether hypoglycosylation is sufficient to activate Xbp1, we treated C2C12 cells with increasing doses of tunicamycin, an inhibitor of N-linked glycosylation. We found a significant dose-dependent increase in total *Xbp1*, *Xbp1s*, and a decrease in *Xbp1u* expression (Supplementary Figure S1A–C). We next aimed to examine whether pharmacological inhibition of Gfpt1 with 6-diazo-l-norleuncine (DON) could activate *Xbp1* expression. Indeed, DON inhibition of Gfpt1 significantly increased total *Xbp1* transcript levels, robustly elevated *Xbp1s* and decreased *Xbp1u* expression levels (Figure 2A,B, Supplementary Figure S1D). As such, both inhibition of N-linked glycosylation and Gfpt1 directly engage the IRE1 pathway in response to hypoglycosylation stress.

We next examined whether *Gfpt1* knockdown directly activates the UPR. Doxycycline-inducible *Gfpt1*-deficient myoblasts (shGfpt1 #1 and shGfpt1 #2) displayed significantly elevated expression of both total *Xbp1* and *Xbp1s* relative to scramble controls (Figure 2D,E). There was a significant decrease in *Xbp1u* expression levels (Supplementary Figure S1E). As such, this demonstrates that reduced HBP flux through *Gfpt1* deficiency activates the IRE1–*Xbp1* axis.

To evaluate whether this response also occurs in vivo, we assessed ER stress markers in whole skeletal muscle isolates from 20-week *Gfpt1*$^{tm1d/tm1d}$ mice. *Gfpt1*$^{tm1d/tm1d}$ mice harbor a conditional skeletal muscle-specific knockout of *Gfpt1*, which contains a pathological resemblance to *GFPT1*-CMS patients, and has been used to test the efficacy of new therapeutic strategies. Quadriceps muscle from *Gfpt1*$^{tm1d/tm1d}$ mice exhibited significantly increased total *Xbp1* and *Xbp1s* expression compared to Tm1C homozygous control mice (Figure 2F,G). We also highlighted a significant decrease in *Xbp1u*, confirming activation of the UPR in *Gfpt1*$^{tm1d/tm1d}$ mice (Supplementary Figure S1F).

Together, these findings demonstrate that *Gfpt1* deficiency consistently activates the IRE1-*Xbp1* branch of the UPR across *Gfpt1*-deficient myoblasts and skeletal muscle. This indicates that impaired glycosylation creates sufficient proteotoxic stress to engage ER-adaptive pathways.

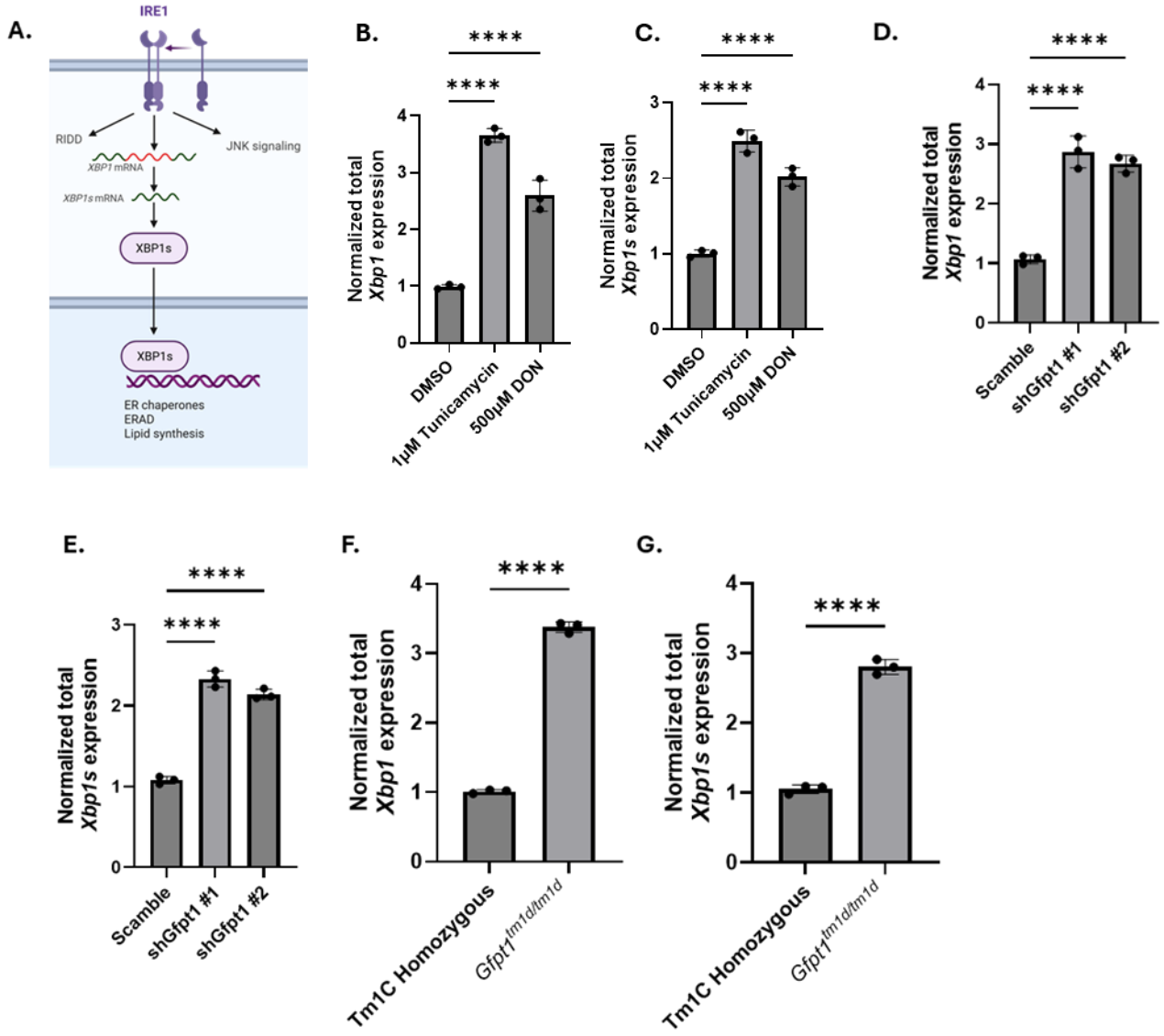

Figure 2. *Gfpt1*-deficient models show elevated levels of *Xbp1s* expression, indicating activation of the unfolded protein response. (**A**). Schematic illustration of the IRE1-XBP1 arm of the unfolded protein response (UPR). *Gfpt1* deficiency reduces protein glycosylation, resulting in a hypoglycosylated cellular environment. To prevent the accumulation of misfolded proteins, cells activate UPR pathways that regulate protein folding and degradation. Under ER stress, X-box binding protein 1 (XBP1) undergoes IRE1-dependent alternative splicing to generate *XBP1s*, a transcription factor that induces expression of ERAD components and ER chaperones. (**B**). C2C12 myoblasts were treated with tunicamycin or 6-diazo-5-oxo-L-norleucine (DON) to induce hypoglycosylation. RT-qPCR analysis shows increased expression of total *Xbp1* and (**C**). spliced *Xbp1* (*Xbp1s*). (**D**). Doxycycline-treated *Gfpt1*-deficient C2C12 myoblasts (shGfpt1 #1 and shGfpt1 #2) exhibit increased expression of total *Xbp1* and (**E**). *Xbp1s* relative to scramble controls. (**F**). RT-qPCR analysis of quadriceps muscle from *Gfpt1*$^{tm1d/tm1d}$ mice and Tm1C homozygous control mice shows increased total *Xbp1* expression and (**G**). elevated *Xbp1s* expression in *Gfpt1*-deficient samples. Gene expression values were normalized to the geometric mean of *Rpl27*, *Gapdh*, and *Actb*. Three biological replicates were analyzed for all experiments. Statistical significance was determined by one-way ANOVA (**B** through **E**) or Student's *t*-test (**F** through **G**). ; **** $p < 0.000$.

3.3. Gfpt1-Deficiency Impairs Autophagy and Leads to p62 Accumulation in Myoblasts and Skeletal Muscle

Since our proteomics and secretion analyses suggested broad disruption in proteostasis, we next examined whether *Gfpt1*-deficiency alters autophagy, a major pathway responsible for clearing misfolded and aggregated proteins. Notably, whole-cell proteomics identified multiple autophagy-related proteins as dysregulated in *Gfpt1*-deficient myoblasts, including components involved in cargo recognition, autophagosome formation, and lysosomal turnover (summarized in Table 1).

To validate these findings, we performed biochemical analyses in doxycycline-induced *Gfpt1*-deficient C2C12 myoblasts. Immunoblotting showed a robust accumulation of p62 and increased LC3-II levels compared with scramble controls (Figure 3A), and densitometric quantification confirmed significant elevations in both proteins (Figure 3B and 3C, respectively). To further dissect p62 behavior, we performed soluble/insoluble fractionation. In control cells, p62 was primarily detected in the soluble fraction; however, *Gfpt1*-deficient myoblasts displayed marked accumulation of p62 in both soluble and insoluble fractions (Supplementary Figure S2A). Insoluble p62 is a biochemical hallmark of defective autophagic flux and protein aggregation, further supporting a block in cargo clearance [30].

To determine whether *Gfpt1* deficiency affects autophagic degradation rather than initiation, we inhibited lysosomal acidification with chloroquine. In C2C12 cells, chloroquine treatment increased p62 staining intensity (Supplementary Figure S2B,C). Notably, *Gfpt1*-deficient myoblasts displayed elevated p62 levels following chloroquine treatment (Supplementary Figure S2D,E). We next assessed whether *Gfpt1* deficiency exacerbates inhibition of autophagic flux. Consistent with the biochemical data, immunofluorescence analysis revealed increased p62 signal intensity in *Gfpt1*-deficient myoblasts (Figure 3D). Quantitative image analysis revealed a significantly increased number of p62-positive puncta (Figure 3E) and area (Figure 3F), respectively. These results suggest that there may be an accumulation of autophagic cargo.

Next, we explored whether p62 puncta accumulated within *Gfpt1*$^{tm1d/tm1d}$ mice's skeletal muscle. Previous whole-cell proteomics from *Gfpt1*$^{tm1d/tm1d}$ revealed a ~2.5-fold increase in p62 protein levels in intercostal muscles [22]. To confirm this proteomic result, we performed p62 staining within the gastrocnemius muscle isolated from *Gfpt1*$^{tm1d/tm1d}$ and Tm1C homozygous muscle. We demonstrate that indeed p62-positive puncta accumulated within the gastrocnemius muscle, further demonstrating that dysfunctional autophagy extends to the skeletal muscle (Figure 3G).

Together, these findings demonstrate that *Gfpt1*-deficiency leads to persistent accumulation of p62, elevated LC3-II, and increased puncta formation. This autophagy defect is consistent with the pronounced proteostasis and trafficking abnormalities observed in *Gfpt1*-deficient myoblasts and *Gfpt1*$^{tm1d/tm1d}$ skeletal muscle.

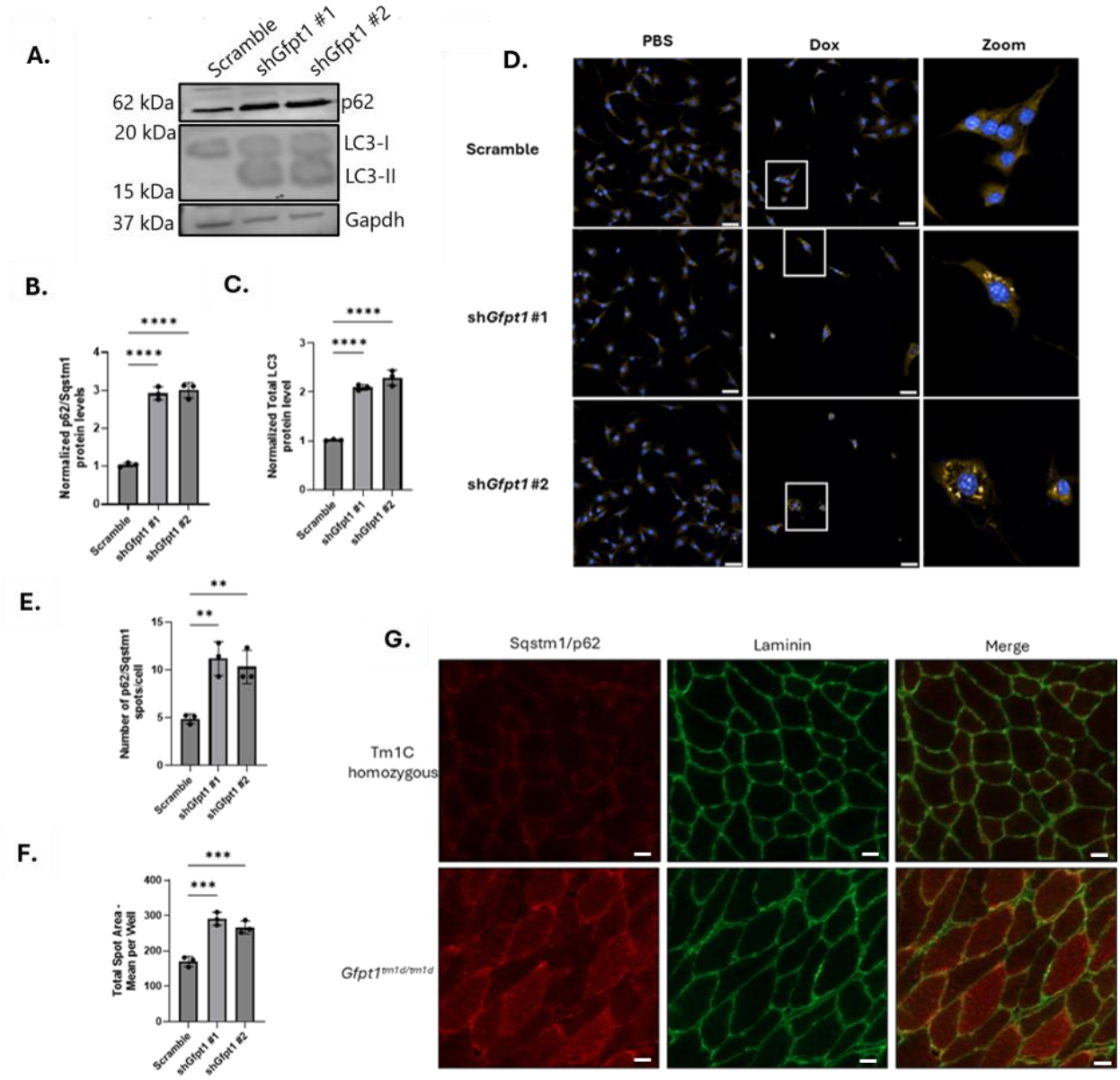

Figure 3. Whole-cell proteomics in *Gfpt1*-deficient myoblasts reveals impaired autophagy (**A**). Western blot analysis shows increased p62 and LC3-II protein levels in *Gfpt1*-deficient myoblasts compared with scramble controls. (**B**). Quantification of immunoblot data reveals a significant increase in p62 and (**C**). LC3-II protein levels in *Gfpt1*-deficient myoblasts. (**D**). Immunofluorescence analysis demonstrates increased p62 staining intensity in *Gfpt1*-deficient myoblasts. (**E**). Quantification of autophagic markers shows a significantly higher percentage of cells containing p62-positive puncta and (**F**). an increase in p62 puncta area in *Gfpt1*-deficient myoblasts, indicative of impaired autophagic flux. (**G**). Immunofluorescence staining of p62 in gastrocnemius muscle from *Gfpt1*$^{tm1d/tm1d}$ mice reveals increased signal intensity and punctate accumulation within muscle fibers. Muscle fibers were marked with α1 laminin (Lama1). Scale bar: 20 μm. All graphs represent mean ± SD. Statistical significance was assessed using one-way ANOVA. All experiments were performed with three biological replicates per group. Comparisons were made between scramble control and *Gfpt1*-deficient samples. ** $p < 0.01$, *** $p < 0.001$ and **** $p < 0.0001$.

3.4. Gfpt1 Deficiency Impairs Protein Trafficking and Reduces Secretion of Skeletal Muscle Proteoglycan Serglycin

Our whole-cell proteomic analysis indicated suppression of intracellular trafficking pathways in *Gfpt1*-deficient myoblasts. This led us to examine whether defects in protein transport affect the secretion of muscle-derived cargo proteins. Secretomic profiling detected 140 proteins in conditioned medium, with 13 proteins significantly altered in *Gfpt1*-deficient C2C12 myoblasts. (Table 2). Among stress-associated proteins, we observed a pronounced reduction in the extracellular abundance of Binding Immunoglobulin Protein (BiP) in *Gfpt1*-deficient C2C12 cells (Table 2). Reduced BiP secretion likely reflects increased ER retention due to elevated chaperone engagement with misfolded proteins, together with impaired ER-to-Golgi trafficking obtained from the proteomics of *Gfpt1*-deficient myoblasts.

Serglycin (Srgn) is a secreted proteoglycan with roles in skeletal muscle biology. Given that our proteomic and secretomic analyses suggested impaired protein trafficking, we next investigated whether Srgn secretion is affected by *Gfpt1* deficiency. In this context, impaired glycosylation may disrupt proper Srgn processing and export, thereby impacting muscle homeostasis. Immunoblot analysis of doxycycline-induced *Gfpt1*-deficient C2C12 cells demonstrated a marked reduction in Srgn protein levels in both shGfpt1 #1 and shGfpt1 #2 lines, normalized to Ponceau S staining (Figure 4A,B).

To determine whether Srgn dysregulation occurs in vivo, we analyzed quadriceps from muscle from 20-week-old *Gfpt1*$^{tm1d/tm1d}$ mice. Consistent with the in vitro results, *Gfpt1*-deficient quadriceps exhibited reduced levels of both the core Srgn protein (~32 kDa) and the high molecular weight glycosylated Srgn species (~120 kDa) (Figure 4C,E). Together, these results indicate that *Gfpt1*-deficiency alters the abundance of Srgn.

Immunofluorescence microscopy revealed an abnormal intracellular distribution of Srgn in *Gfpt1*-deficient C2C12 myoblasts. Compared with scramble controls, where Srgn was predominantly localized in subsarcolemmal regions, *Gfpt1*-deficient cells exhibited increased cytoplasmic Srgn-positive puncta and enhanced intracellular staining intensity (Figure 4F). Quantitative image analysis using Columbus™ software showed significant increases in both the total Srgn-positive spot area (Figure 4G) and the number of Srgn-positive puncta per cell (Figure 4H), indicating intracellular accumulation. Taken together, these data indicate that overall Srgn levels are reduced in *Gfpt1*-deficient myoblasts. However, the remaining Srgn is predominantly retained intracellularly, as opposed to being membrane-bound and secreted.

Finally, analysis of conditioned medium collected over a 24 h time course revealed a reduction in secreted Srgn from *Gfpt1*-deficient myoblasts relative to scramble controls (Figure 4I and Supplementary Figure S3A). Consistently, reduced total Srgn levels were observed at 24 h (Supplementary Figure S3B,C). Together, these findings indicate that *Gfpt1*-deficiency disrupts intracellular protein trafficking, leading to retention and decreased secretion of Srgn in murine myoblasts.

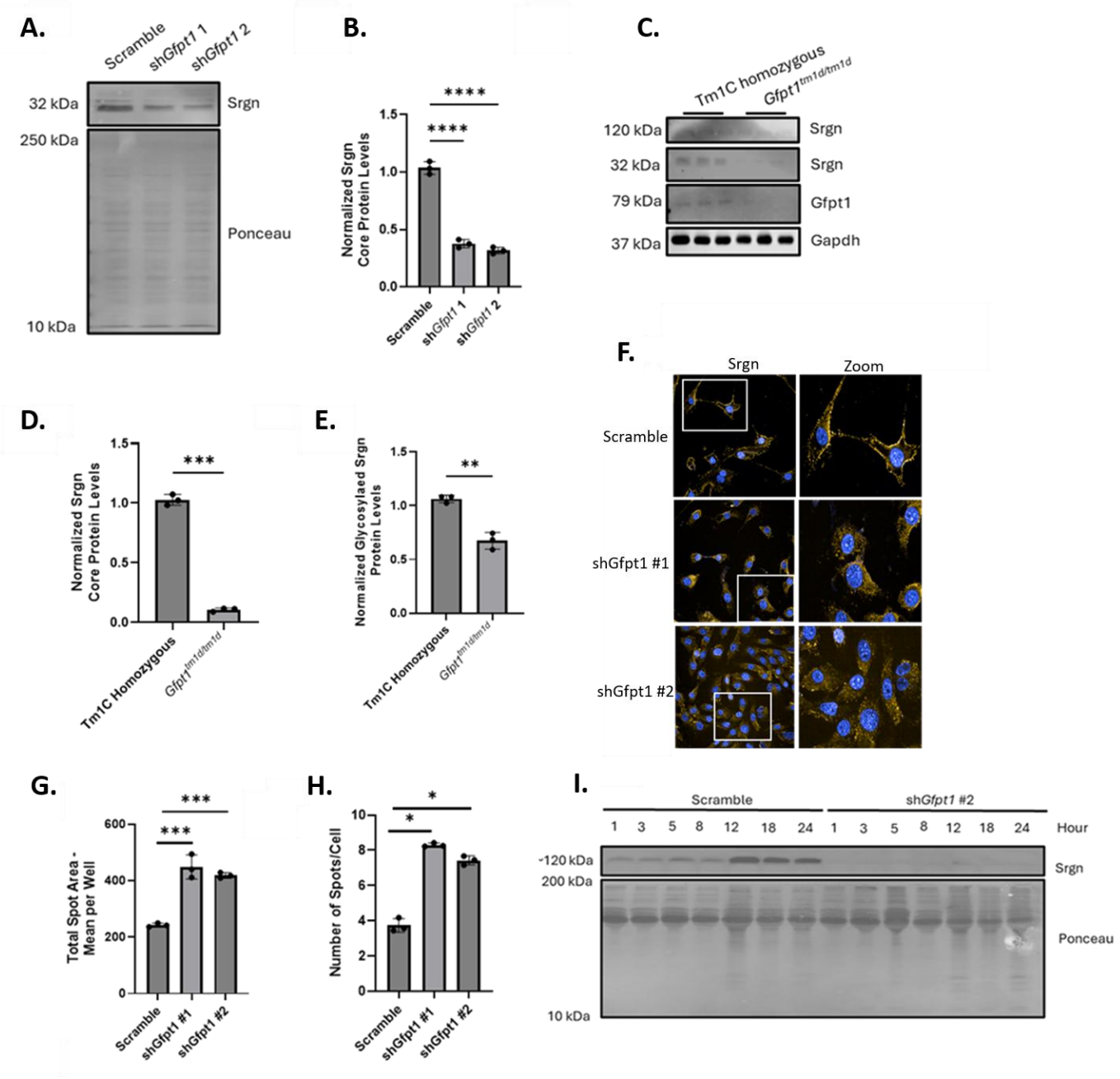

Figure 4. Proteomics reveals downregulation in protein trafficking pathways and altered secretion of skeletal muscle proteins. (**A**). Western blot analysis of serglycin (Srgn) protein levels in *Gfpt1*-deficient C2C12 myoblasts. Protein levels were normalized to total protein loading using Ponceau S staining. (**B**). Quantification shows a significant reduction in Srgn protein levels in *Gfpt1*-deficient myoblasts using two independent shRNA constructs. (**C**). Western blot analysis of quadriceps muscle lysates from 20-week-old *Gfpt1*$^{tm1d/tm1d}$ mice and Tm1C homozygous controls, showing high-molecular-weight (~120 kDa) glycosylated Srgn species, core (~32 kDa) Srgn, and Gfpt1. (**D**). Quantification of core Srgn and (**E**). high-molecular-weight glycosylated Srgn species, normalized to Gapdh protein levels. (**F**). Immunofluorescence staining of scramble control and *Gfpt1*-deficient C2C12 myoblasts labeled for Srgn. Images were acquired at 40× magnification using the OPERA™ high-content imaging system. Scale bar = 10 μm. (**G**). Quantitative image analysis using Columbus™ software shows increased total Srgn-positive spot area (μm²) and (**H**). an increased average number of Srgn-positive puncta per cell in *Gfpt1*-deficient myoblasts. (**I**). Immunoblot analysis of conditioned medium collected over a 24 h time course from scramble control and shGfpt1 #2 C2C12 myoblasts. All graphs represent mean ± SD. Statistical significance was assessed using one-way ANOVA. All

experiments were performed with three biological replicates per group. * $p < 0.05$, ** $p < 0.01$, *** $p < 0.001$, **** $p < 0.0001$.

Table 2. Key proteins up- or downregulated in the *Gfpt1*-deficient C2C12 myoblast secretome compared with scramble. Proteins detected with an adjusted *p*-value of <0.05 were deemed significantly altered from scrambled control. Proteins with an adjusted *p*-value of <0.05 were deemed significantly altered from the control.

Protein	Description	Relevant Role	Fold Change
Eno1 (α-enolase)	Glycolytic enzyme; also moonlights as plasminogen receptor when extracellular	Promotes ECM remodeling and cell migration via plasmin activation; supports myoblast differentiation and tissue remodeling	1.7
A2m (Alpha-2-macroglobulin)	Broad-spectrum protease inhibitor	Regulates extracellular proteolysis, cytokine binding, and growth factor availability → impacts myogenesis and muscle repair environment	1.49
ApoA1	Major HDL apolipoprotein	Lipid transport and anti-inflammatory signaling support metabolic homeostasis in muscle and may influence differentiation under stress	1.45
Actb/Actg1 (β- and γ-actin)	Cytoskeletal proteins	Released during stress/damage; function as DAMPs (damage-associated signals); linked to cell motility and myoblast fusion dynamics	1.44
Fbln1 (Fibulin-1)	ECM glycoprotein	Regulates ECM organization, cell adhesion, and migration; important for myoblast alignment and differentiation niche	1.22
Anxa2 (Annexin A2)	Calcium-dependent phospholipid-binding protein	Membrane repair, vesicle trafficking, exosome release, and plasmin generation → key for myoblast membrane remodeling and fusion	0.67
Hspa5 (BiP/GRP78)	ER chaperone protein	ER stress marker; when secreted, acts as stress signal; indicates UPR activation and secretory pathway dysfunction in myoblasts	0.63
Histones (H2B variants)	Core nucleosome proteins	Extracellular histones act as alarmins → trigger inflammation, immune signaling, and cell stress responses; may reflect cell damage/death or vesicular release	0.35
Histones (H4)	Core nucleosome protein	Same as above; linked to inflammatory signaling, cytotoxicity, and stress-induced secretion	0.30
Histones (H2A variants)	Core chromatin proteins	Extracellular roles include immune modulation and DAMP signaling, indicating nuclear stress or impaired degradation	0.27
Histones (H3 variants)	Core chromatin proteins	Released under stress; may influence inflammatory and regenerative signaling in muscle environment	0.27
Hspa9 (Mortalin/GRP75)	Mitochondrial chaperone	Indicates mitochondrial stress/damage; involved in mitochondrial protein folding and quality control, relevant to mitophagy defects	0.09
Hspd1 (HSP60)	Mitochondrial chaperonin	Mitochondrial stress marker; extracellularly promotes immune signaling and stress adaptation; linked to metabolic dysfunction in myoblasts	0.01

4. Discussion

GFPT1 is the rate-limiting enzyme of the HBP, generating UDP-GlcNAc, the obligate donor substrate for multiple forms of protein glycosylation. Since the HBP sits at the

interface of nutrient sensing, protein quality control and membrane trafficking, disruptions in GFPT1 activity, as evident in *GFPT1*-CMS, are expected to impose broad metabolic and proteostatic consequences on muscle cells [4,5]. In this study, we demonstrate that loss of Gfpt1 leads to coordinated disturbances of glycosylation-dependent proteostasic mechanisms, spanning ER stress, vesicle trafficking, secretion and autophagy. This provides mechanistic insights into the skeletal muscle pathology observed in *GFPT1*-CMS patients.

GFPT1-CMS is characterized by fatigable muscle weakness caused by biallelic mutations that reduce GFPT1 protein abundance and enzymatic levels [10,14,18–21]. We previously showed that impaired Gfpt1 function disrupts protein glycosylation, leading to hypoglycosylation of AChRδ, a defect that can be rescued by galactose supplementation [6,23]. This hypoglycosylated environment may also contribute to the formation of tubular aggregates, a shared feature of other glycosylation-related CMS subtypes (GMPPB, ALG2, ALG14, and DPAGT1), highlighting the need to define upstream drivers of pathology [11–13,32–35].

Consistent with this, we observed robust activation of IRE1-XBP1 arms of the UPR in both pharmacologic and genetic models of *Gfpt1*-deficiency [26,36]. Given the sensitivity of IRE1 signaling to defects in glycan maturation, these findings indicate that ER stress arises as a primary consequence of impaired HBP flux rather than secondary degeneration [37,38]. This finding is consistent with other myopathies driven by glycosylation defects, such as GNE myopathy and congenital disorders of glycosylation (CDGs), where early pathological features depict UPR activation and ER stress [39–46].

A significant finding of this study is the global downregulation of vesicle trafficking pathways. Proteomic analysis revealed an abundance of COP-I/COP-II components, ER–Golgi transport factors, and proteins involved in vesicle formation and cargo sorting. As these processes depend on proper glycosylation for protein stability, folding, and export, these data suggest a multi-level disruption of secretory pathway function [1,3,47]. This is functionally supported by impaired secretion of Srgn, a highly glycosylated proteoglycan requiring intact ER–Golgi processing for maturation and export. Its intracellular punctate accumulation alongside reduced secretion indicates a failure of secretory machinery and highlights a broader defect in extracellular matrix (ECM) protein handling [48].

These changes could have negative consequences for skeletal muscle health [3]. Secretory defects may affect skeletal muscle health because myofibers rely heavily on efficient export of ECM proteins, proteoglycans, and signaling factors to maintain structural stability and intercellular communication [49,50]. Importantly, Srgn knockout mice develop normally and do not display an overt skeletal muscle phenotype, suggesting that Srgn itself is not essential for muscle development under basal conditions [51]. Therefore, the reduction and intracellular accumulation of Srgn observed in our models likely reflect impaired glycosylation-dependent trafficking rather than a primary pathogenic driver. In this context, Srgn may serve as a sensitive marker for secretory pathway dysfunction, highlighting broader defects in protein export that could ultimately compromise muscle homeostasis. A potential mechanism of impact could be through immunological responses, which have been shown in Srgn-deficient mouse models [52]. Importantly, similar defects in proteoglycan secretion have been identified in other muscle disorders, and CDGs, all of which exhibit impaired extracellular matrix assembly, disrupted sarcolemmal stability, and progressive myofiber degeneration [53–55]. As such, examination of additional proteoglycan synthesis, packaging, and trafficking should be extensively studied within *Gfpt1*-deficient models.

It is important to note that while Srgn was not detected within the secretomic profiling of conditioned medium from *Gfpt1*-deficient myoblasts, this likely reflects inherent limitations in mass spectroscopy-based detection of heavily glycosylated proteoglycans rather than true absence [56,57]. Consistent with this, immunoblot analysis confirmed reduced secretion and intracellular accumulation of Srgn, supporting a defect in

glycosylation-dependent trafficking. Together, these findings suggest that Srgn may represent a sensitive marker of impaired secretory pathway function in the context of *Gfpt1* deficiency.

However, secretomic profiling of *Gfpt1*-deficient myoblasts did reveal a secreted-BiP deficiency. BiP is a central regulator of ER proteostasis and secretory capacity as it supports folding of nascent luminal proteins, enforces ER quality control, and maintains export-competent cargo; thus, reduced BiP is expected to constrain secretion by promoting ER retention, ERAD, and stress-induced translational attenuation [58,59]. This defect is exacerbated by impaired glycosylation in *Gfpt1*-deficient cells, as glycan modification is critical for protein stability, chaperone engagement, and trafficking [1,6,60]. Consistently, we observed reduced secretion of Srgn, a highly glycosylated proteoglycan that serves as a sensitive readout of ER quality control.

Although BiP is primarily an ER-resident protein, it can also be secreted when it participates in stress signaling. BiP secretion has been reported to decrease under ER stress, including tunicamycin treatment, suggesting a role in adaptive intercellular communication [61–63]. The reduction observed here therefore indicates not only impaired folding capacity but also defective stress-responsive secretion. Given BiP's central role in regulating the UPR, reduced intracellular and secreted BiP may limit the ability to buffer ER stress in *Gfpt1*-deficient myoblasts [58,61]. Moreover, extracellular BiP has been linked to cytoskeletal regulation and neurite outgrowth, raising the possibility that its loss affects stress resilience and cellular remodeling [64]. Together, impaired glycosylation, reduced BiP, and defective secretion of Srgn support a model in which ER proteostasis failure manifests as both intracellular folding insufficiency and loss of adaptive secretory signaling.

In parallel, *Gfpt1*-depleted myoblasts show increased release of cytosolic proteins consistent with stress-induced unconventional secretion during proteotoxic states [65,66]. This shift from classical ER–Golgi trafficking to noncanonical export may reflect membrane instability, impaired vesicle maturation or increased extracellular vesicle release [67,68]. Similar secretory remodeling has been observed in myopathies associated with ER stress or impaired autophagy, reinforcing the idea that proteostasis disruption fundamentally reshapes the muscle secretome [69,70].

Given that the NMJ is highly dependent on efficient secretion, defects in intracellular trafficking provide a direct mechanistic link to CMS pathology. NMJ maintenance requires continuous export of synaptic organizers, including agrin, laminin α2/β2, perlecan, and collagens, as well as trafficking of AChR complexes and associated signaling factors [71–73]. These processes rely on an intact ER–Golgi transport and glycosylation-dependent cargo maturation. Consistent with this, reduced AChR surface has been detected in vitro, along with decreased α-BTX staining at the NMJs in *Gfpt1*$^{tm1d/tm1d}$ muscle. Previously, AChR subunits were found to have reduced surface expression in transfected HEK293T cells [14]. In addition, previous data show reduced α-BTX staining at the NMJ of *Gfpt1*$^{tm1d/tm1d}$, suggesting impairment to the surface expression and/or stability of the AChR complex [6,23]. Thus, trafficking defects observed in our models, including Srgn retention, likely impair the delivery of essential synaptic proteins and chaperones such as BiP. In this context, impaired secretion may represent a central pathogenic mechanism, weakening synaptic integrity and increasing NMJ susceptibility to stress [7,74–77].

We also demonstrate defects in autophagic clearance, likely downstream of ER stress and trafficking disruption. Autophagy requires coordinated membrane trafficking, ER–Golgi dynamics, and lipidation, processes dependent on intact glycosylation pathways [27,29]. In *Gfpt1*-deficient myoblasts, elevated p62 and LC3-II levels indicate impaired autophagic flux rather than increased initiation, a finding recapitulated in *Gfpt1*$^{tm1d/tm1d}$ muscle [78–80].

This aligns with prior reports showing enhanced protein aggregation and reduced autophagy following *Gfpt1* silencing [81]. Thus, protein aggregation and impaired autophagy may contribute to muscle fiber pathology in *GFPT1*-CMS.

In addition, future studies should aim to further define the mechanistic links between impaired HBP flux and defects in protein trafficking, secretion and autophagy. Previous work demonstrated that metabolic supplementation with galactose has been shown to improve skeletal muscle health, NMJ morphology, and neurotransmission in *Gfpt1*$^{tm1d/tm1d}$ models, making it of particular interest to determine whether the proteostasis and secretory defects observed in this study could be rescued through similar approaches [23]. In addition, building on the identification of hypoglycosylated AChRδ, further investigation of NMJ integrity in the context of disrupted trafficking may help clarify the contribution of these pathways to disease pathology. Finally, targeted analysis of extracellular matrix components and secreted proteoglycans may help establish whether molecules such as Srgn could serve as a biomarker or therapeutic targets in *GFPT1*-CMS.

5. Conclusions

In summary, this study demonstrates that *Gfpt1* deficiency disrupts glycosylation-dependent proteostasis in skeletal muscle, leading to broad alterations in ER homeostasis, intracellular trafficking, secretion and autophagic flux. Reduced HBP flux triggers activation of the IRE1-XBP1 branch of the UPR, while impairing vesicular transport and secretory capacity. These defects result in intracellular retention and reduced secretion of key glycoproteins, including proteoglycan Srgn, highlighting disruption of protein secretion. Importantly, these interconnected defects provide a unifying mechanistic framework linking impaired glycosylation to NMJ dysfunction, reduced stress resilience, and skeletal muscle pathology in *GFPT1*-CMS. Overall, this work identifies glycosylation-dependent proteostasis as a central determinant of muscle integrity and highlights intracellular trafficking and secretory dysfunction as key contributors to disease pathogenesis.

Supplementary Materials: The supporting information can be downloaded at: https://www.mdpi.com/article/doi/s1. Supplementary Figure 1: Supplementary experiments for Xbp1 expression determination; Supplementary Figure 2: p62 protein levels express a punctate pattern within Gfpt1-deficient myoblasts; Supplementary Figure 3: Srgn is retained by Gfpt1-deficient myoblasts, and has reduced protein secretion; Supplementary Table S1: RT-qPCR Primer Design.

Author Contributions: Conceptualization, H.L., S.S., A.R. and S.H.H.; methodology, S.H.H., R.C.-M., A.H., A.D., S.B., K.O., K.H. and D.O.; validation, S.H.H., R.C.-M., K.O. and D.O.; formal analysis, S.H.H., S.S. and K.O.; investigation, S.H.H., R.C.-M. and K.O.; resources, H.L. and S.S.; data curation, S.H.H., R.C.-M. and K.O.; writing—original draft preparation, S.H.H.; review and editing, S.H.H., R.C.-M., K.O., D.O., S.S., A.R. and H.L.; final draft preparation and writing, S.H.H., S.S. and H.L.; visualization, S.H.H., S.S. and H.L.; supervision, S.S. and H.L.; project administration, S.S. and H.L.; funding acquisition, H.L. and S.H.H. All authors have read and agreed to the published version of the manuscript.

Funding: H.L. received support from the Canadian Institutes of Health Research (CIHR) for Foundation Grant FDN-167281 (Precision Health for Neuromuscular Diseases), Transnational Team Grant ERT-174211 (ProDGNE), and Network Grant OR2-189333 (NMD4C) from the Canada Foundation for Innovation (CFI-JELF 38412); the Canada Research Chairs program (Canada Research Chair in Neuromuscular Genomics and Health, 950-232279); the European Commission (Grant # 101080249); and the Canada Research Coordinating Committee New Frontiers in Research Fund (NFRFG-2022-00033) for SIMPATHIC and from the Government of Canada, Canada First Research Excellence Fund (CFREF) for the Brain–Heart Interconnectome (CFREF-2022-00007). S.H.H. received support from the Bob Korneluk CHEO Trainee Research Grant, Ontario Graduate Scholarship (OGS), Queen Elizabeth II Scholarship (QE2-GSST), and a STaR award by the University of Ottawa Dr. Eric Poulin Center for Neuromuscular Disease. A.R. acknowledges the financial support of the Deutsche Gesellschaft für Muskelkranke (DGM) e.V., as well as the European Regional Development Fund (ERDF) (project B2B-RARE). A.H. acknowledges the support by the "Ministerium

für Kultur und Wissenschaft des Landes Nordrhein-Westfalen" and "Der Regierende Bürgermeister von Berlin, Senatskanzlei Wissenschaft und Forschung" and the "Bundesministerium für Forschung, Technologie und Raumfahrt" (BMFTR).

Institutional Review Board Statement: The animal study protocol was approved by the Animal Care and Veterinary Board of the University of Ottawa (CHEOb-3089 and CHEOe-3120, approved on 16 November 2018 and 2 April 2019, respectively).

Informed Consent Statement: Not applicable.

Data Availability Statement: Data are contained within the article and Supplementary Materials. The nass spectrometry proteomics data have been deposited to the ProteomeXChange Consortium (ProteomeCentral Data and Tools)via the PRIDE partner repository with the data set identifier PXD079191.

Conflicts of Interest: The authors declare no conflicts of interest.

References

1. Reily, C.; Stewart, T.J.; Renfrow, M.B.; Novak, J. Glycosylation in Health and Disease. *Nat. Rev. Nephrol.* **2019**, *15*, 346–366. https://doi.org/10.1038/s41581-019-0129-4.
2. He, M.; Zhou, X.; Wang, X. Glycosylation: Mechanisms, Biological Functions and Clinical Implications. *Signal Transduct. Target. Ther.* **2024**, *9*, 194. https://doi.org/10.1038/s41392-024-01886-1.
3. Dang, K.; Jiang, S.; Gao, Y.; Qian, A. The Role of Protein Glycosylation in Muscle Diseases. *Mol. Biol. Rep.* **2022**, *49*, 8037–8049. https://doi.org/10.1007/s11033-022-07334-z.
4. Akella, N.M.; Ciraku, L.; Reginato, M.J. Fueling the Fire: Emerging Role of the Hexosamine Biosynthetic Pathway in Cancer. *BMC Biol.* **2019**, *17*, 52. https://doi.org/10.1186/s12915-019-0671-3.
5. Paneque, A.; Fortus, H.; Zheng, J.; Werlen, G.; Jacinto, E. The Hexosamine Biosynthesis Pathway: Regulation and Function. *Genes* **2023**, *14*, 933. https://doi.org/10.3390/genes14040933.
6. Holland, S.H.; Carmona-Martinez, R.; O'Connor, K.; O'Neil, D.; Roos, A.; Spendiff, S.; Lochmüller, H. A Deficiency in Glutamine-Fructose-6-Phosphate Transaminase 1 (Gfpt1) in Skeletal Muscle Results in Reduced Glycosylation of the Delta Subunit of the Nicotinic Acetylcholine Receptor (AChRδ). *Biomolecules* **2024**, *14*, 1252. https://doi.org/10.3390/biom14101252.
7. Finsterer, J. Congenital Myasthenic Syndromes. *Orphanet J. Rare Dis.* **2019**, *14*, 57. https://doi.org/10.1186/s13023-019-1025-5.
8. Ohno, K.; Ito, M.; Ohkawara, B. Review of 40 Genes Causing Congenital Myasthenic Syndromes. *J. Hum. Genet.* **2025**. https://doi.org/10.1038/s10038-025-01355-9.
9. Beeson, D. Chapter 5—Congenital Myasthenic Syndromes. In *Handbook of Clinical Neurology*; Hanna, M.G., Ed.; Neurologic Channelopathies; Elsevier: Amsterdam, The Netherlands, 2024; Volume 203, pp. 69–88.
10. Senderek, J.; Müller, J.S.; Dusl, M.; Strom, T.M.; Guergueltcheva, V.; Diepolder, I.; Laval, S.H.; Maxwell, S.; Cossins, J.; Krause, S.; et al. Hexosamine Biosynthetic Pathway Mutations Cause Neuromuscular Transmission Defect. *Am. J. Hum. Genet.* **2011**, *88*, 162–172. https://doi.org/10.1016/j.ajhg.2011.01.008.
11. Cossins, J.; Belaya, K.; Hicks, D.; Salih, M.A.; Finlayson, S.; Carboni, N.; Liu, W.W.; Maxwell, S.; Zoltowska, K.; Farsani, G.T.; et al. Congenital Myasthenic Syndromes Due to Mutations in ALG2 and ALG14. *Brain* **2013**, *136*, 944–956. https://doi.org/10.1093/brain/awt010.
12. Belaya, K.; Finlayson, S.; Slater, C.R.; Cossins, J.; Liu, W.W.; Maxwell, S.; McGowan, S.J.; Maslau, S.; Twigg, S.R.F.; Walls, T.J.; et al. Mutations in DPAGT1 Cause a Limb-Girdle Congenital Myasthenic Syndrome with Tubular Aggregates. *Am. J. Hum. Genet.* **2012**, *91*, 193–201. https://doi.org/10.1016/j.ajhg.2012.05.022.
13. Belaya, K.; Rodríguez Cruz, P.M.; Liu, W.W.; Maxwell, S.; McGowan, S.; Farrugia, M.E.; Petty, R.; Walls, T.J.; Sedghi, M.; Basiri, K.; et al. Mutations in GMPPB Cause Congenital Myasthenic Syndrome and Bridge Myasthenic Disorders with Dystroglycanopathies. *Brain* **2015**, *138*, 2493–2504. https://doi.org/10.1093/brain/awv185.
14. Zoltowska, K.; Webster, R.; Finlayson, S.; Maxwell, S.; Cossins, J.; Müller, J.; Lochmüller, H.; Beeson, D. Mutations in GFPT1 That Underlie Limb-Girdle Congenital Myasthenic Syndrome Result in Reduced Cell-Surface Expression of Muscle AChR. *Hum. Mol. Genet.* **2013**, *22*, 2905–2913. https://doi.org/10.1093/hmg/ddt145.

15. Jiang, K.; Zheng, Y.; Lin, J.; Wu, X.; Yu, Y.; Zhu, M.; Fang, X.; Zhou, M.; Li, X.; Hong, D. Diverse Myopathological Features in the Congenital Myasthenia Syndrome with GFPT1 Mutation. *Brain Behav.* **2022**, *12*, e2469. https://doi.org/10.1002/brb3.2469.
16. Vallepu, S.B.; Dhamija, K.; Rajan, G.K.; Panchal, T.; Saran, R.K.; Roshan, S. Phenotypic Variability in Congenital Myasthenic Syndrome with GFPT1 Mutation. *Acta Neurol. Belg.* **2024**, *125*, 209–213. https://doi.org/10.1007/s13760-024-02694-8.
17. An, R.; Chen, H.; Lei, S.; Li, Y.; Xu, Y.; He, C. Abnormal Decrement on High-Frequency Repetitive Nerve Stimulation in Congenital Myasthenic Syndrome with GFPT1 Mutations and Review of Literature. *Front. Neurol.* **2022**, *13*, 926786. https://doi.org/10.3389/fneur.2022.926786.
18. Bauché, S.; Vellieux, G.; Sternberg, D.; Fontenille, M.-J.; De Bruyckere, E.; Davoine, C.-S.; Brochier, G.; Messéant, J.; Wolf, L.; Fardeau, M.; et al. Mutations in GFPT1-Related Congenital Myasthenic Syndromes Are Associated with Synaptic Morphological Defects and Underlie a Tubular Aggregate Myopathy with Synaptopathy. *J. Neurol.* **2017**, *264*, 1791–1803. https://doi.org/10.1007/s00415-017-8569-x.
19. Dusl, M.; Senderek, J.; Müller, J.S.; Vogel, J.G.; Pertl, A.; Stucka, R.; Lochmüller, H.; David, R.; Abicht, A. A 3′-UTR Mutation Creates a microRNA Target Site in the GFPT1 Gene of Patients with Congenital Myasthenic Syndrome. *Hum. Mol. Genet.* **2015**, *24*, 3418–3426. https://doi.org/10.1093/hmg/ddv090.
20. Ma, Y.; Xiong, T.; Lei, G.; Ding, J.; Yang, R.; Li, Z.; Guo, J.; Shen, D. Novel Compound Heterozygous Variants in the GFPT1 Gene Leading to Rare Limb-Girdle Congenital Myasthenic Syndrome with Rimmed Vacuoles. *Neurol. Sci. Off. J. Ital. Neurol. Soc. Ital. Soc. Clin. Neurophysiol.* **2021**, *42*, 3485–3490. https://doi.org/10.1007/s10072-020-05021-0.
21. Selcen, D.; Shen, X.-M.; Milone, M.; Brengman, J.; Ohno, K.; Deymeer, F.; Finkel, R.; Rowin, J.; Engel, A.G. GFPT1-Myasthenia: Clinical, Structural, and Electrophysiologic Heterogeneity. *Neurology* **2013**, *81*, 370–378. https://doi.org/10.1212/WNL.0b013e31829c5e9c.
22. Issop, Y.; Hathazi, D.; Khan, M.M.; Rudolf, R.; Weis, J.; Spendiff, S.; Slater, C.R.; Roos, A.; Lochmüller, H. GFPT1 Deficiency in Muscle Leads to Myasthenia and Myopathy in Mice. *Hum. Mol. Genet.* **2018**, *27*, 3218–3232. https://doi.org/10.1093/hmg/ddy225.
23. Holland, S.H.; Carmona-Martinez, R.; O'Neil, D.; Ho, K.; O'Connor, K.; Azuma, Y.; Roos, A.; Spendiff, S.; Lochmüller, H. Galactose Treatment Rescues Neuromuscular Junction Transmission in Glutamine-Fructose-6-Phosphate Transaminase 1 (Gfpt1) Deficient Mice. *Hum. Mol. Genet.* **2025**, *34*, 1765–1779. https://doi.org/10.1093/hmg/ddaf140.
24. Bisnett, B.J.; Condon, B.M.; Lamb, C.H.; Georgiou, G.R.; Boyce, M. Export Control: Post-Transcriptional Regulation of the COPII Trafficking Pathway. *Front. Cell Dev. Biol.* **2021**, *8*, 618652. https://doi.org/10.3389/fcell.2020.618652.
25. Zhang, J.; Wang, Y. Emerging Roles of O-GlcNAcylation in Protein Trafficking and Secretion. *J. Biol. Chem.* **2024**, *300*, 105677. https://doi.org/10.1016/j.jbc.2024.105677.
26. Hetz, C.; Zhang, K.; Kaufman, R.J. Mechanisms, Regulation and Functions of the Unfolded Protein Response. *Nat. Rev. Mol. Cell Biol.* **2020**, *21*, 421–438. https://doi.org/10.1038/s41580-020-0250-z.
27. Diao, J.; Yip, C.K.; Zhong, Q. Molecular Structures and Function of the Autophagosome-Lysosome Fusion Machinery. *Autophagy Rep.* **2024**, *3*, 2305594. https://doi.org/10.1080/27694127.2024.2305594.
28. Franco-Romero, A.; Sandri, M.; Schiaffino, S. Autophagy in Skeletal Muscle. *Cold Spring Harb. Perspect. Biol.* **2025**, *17*, a041565. https://doi.org/10.1101/cshperspect.a041565.
29. Franco-Romero, A.; Sandri, M. Role of Autophagy in Muscle Disease. *Mol. Aspects Med.* **2021**, *82*, 101041. https://doi.org/10.1016/j.mam.2021.101041.
30. Bjørkøy, G.; Lamark, T.; Pankiv, S.; Øvervatn, A.; Brech, A.; Johansen, T. Monitoring Autophagic Degradation of P62/SQSTM1. *Methods Enzymol.* **2009**, *452*, 181–197. https://doi.org/10.1016/S0076-6879(08)03612-4.
31. Hirano, H.; Kimura, Y.; Kimura, A. Biological Significance of Co- and Post-Translational Modifications of the Yeast 26S Proteasome. *J. Proteom.* **2016**, *134*, 37–46. https://doi.org/10.1016/j.jprot.2015.11.016.
32. Athanasopoulos, E.N.; Labropoulou, V.T.; Theocharis, A.D. Serglycin Across the Disease Spectrum: A Multifunctional Proteoglycan in Inflammation and Cancer. *Curr. Issues Mol. Biol.* **2026**, *48*, 454. https://doi.org/10.3390/cimb48050454.
33. Hjorth, M.; Norheim, F.; Meen, A.J.; Pourteymour, S.; Lee, S.; Holen, T.; Jensen, J.; Birkeland, K.I.; Martinov, V.N.; Langleite, T.M.; et al. The Effect of Acute and Long-Term Physical Activity on Extracellular Matrix and Serglycin in Human Skeletal Muscle. *Physiol. Rep.* **2015**, *3*, e12473. https://doi.org/10.14814/phy2.12473.

34. Scully, O.J.; Chua, P.-J.; Harve, K.S.; Bay, B.-H.; Yip, G.W. Serglycin in Health and Diseases. *Anat. Rec.* **2012**, *295*, 1415–1420. https://doi.org/10.1002/ar.22536.
35. Dean, N.; Gao, X.-D. Heterodimeric Alg13/Alg14 UDP-GlcNAc Transferase (ALG13,14). In *Handbook of Glycosyltransferases and Related Genes*; Springer: Tokyo, Japan, 2014; pp. 1231–1238, ISBN 978-4-431-54240-7.
36. Dean, N. Alg1, Alg2, and Alg11 Mannosyltransferases of the Endoplasmic Reticulum. In *Handbook of Glycosyltransferases and Related Genes*; Springer: Tokyo, Japan, 2014; pp. 1239–1247, ISBN 978-4-431-54240-7.
37. Belaya, K.; Finlayson, S.; Cossins, J.; Liu, W.W.; Maxwell, S.; Palace, J.; Beeson, D. Identification of DPAGT1 as a New Gene in Which Mutations Cause a Congenital Myasthenic Syndrome. *Ann. N. Y. Acad. Sci.* **2012**, *1275*, 29–35. https://doi.org/10.1111/j.1749-6632.2012.06790.x.
38. Cheli, M.; Brugnoni, R.; Gibertini, S.; Mantegazza, R.; Maggi, L. Novel DPAGT1 Gene Mutation in Two Twins with Congenital Myasthenic Syndrome and a Review of the Literature. *J. Neuromuscul. Dis.* **2023**, *10*, 449–458. https://doi.org/10.3233/JND-221675.
39. Wang, Z.V.; Deng, Y.; Gao, N.; Pedrozo, Z.; Li, D.L.; Morales, C.R.; Criollo, A.; Luo, X.; Tan, W.; Jiang, N.; et al. Spliced X-Box Binding Protein 1 Couples the Unfolded Protein Response to Hexosamine Biosynthetic Pathway. *Cell* **2014**, *156*, 1179–1192. https://doi.org/10.1016/j.cell.2014.01.014.
40. Siwecka, N.; Rozpędek-Kamińska, W.; Wawrzynkiewicz, A.; Pytel, D.; Diehl, J.A.; Majsterek, I. The Structure, Activation and Signaling of IRE1 and Its Role in Determining Cell Fate. *Biomedicines* **2021**, *9*, 156. https://doi.org/10.3390/biomedicines9020156.
41. Le Goupil, S.; Laprade, H.; Aubry, M.; Chevet, E. Exploring the IRE1 Interactome: From Canonical Signaling Functions to Unexpected Roles. *J. Biol. Chem.* **2024**, *300*, 107169. https://doi.org/10.1016/j.jbc.2024.107169.
42. Awasthi, K.; Srivastava, A.; Bhattacharya, S.; Bhattacharya, A. Tissue Specific Expression of Sialic Acid Metabolic Pathway: Role in GNE Myopathy. *J. Muscle Res. Cell Motil.* **2021**, *42*, 99–116. https://doi.org/10.1007/s10974-020-09590-7.
43. Carrillo, N.; Malicdan, M.C.; Huizing, M. GNE Myopathy: Etiology, Diagnosis, and Therapeutic Challenges. *Neurotherapeutics* **2018**, *15*, 900–914. https://doi.org/10.1007/s13311-018-0671-y.
44. Hinderlich, S.; Weidemann, W.; Yardeni, T.; Horstkorte, R.; Huizing, M. UDP-GlcNAc 2-Epimerase/ManNAc Kinase (GNE): A Master Regulator of Sialic Acid Synthesis. *Top Chem. Curr.* **2015**, *366*, 97–138. https://doi.org/10.1007/128_2013_464.
45. Pogoryelova, O.; González Coraspe, J.A.; Nikolenko, N.; Lochmüller, H.; Roos, A. GNE Myopathy: From Clinics and Genetics to Pathology and Research Strategies. *Orphanet J. Rare Dis.* **2018**, *13*, 70. https://doi.org/10.1186/s13023-018-0802-x.
46. Deng, J.; Wang, N.; Wu, Y.; Hao, Z.; Wu, H.; Ma, S.; Liu, J.; Ji, G.; Song, X. Clinical, Pathological and Genetic Characteristics of GNE Myopathy: A Single-Center Observational Study. *BMC Musculoskelet. Disord*. **2025**, *26*, 1049. https://doi.org/10.1186/s12891-025-09282-8.
47. Yoshioka, W.; Noguchi, S.; Nishino, I. Molecular Genetics and Therapeutic Development for GNE Myopathy. *J. Hum. Genet.* **2025**. https://doi.org/10.1038/s10038-025-01398-y.
48. Nishino, I.; Carrillo-Carrasco, N.; Argov, Z. GNE Myopathy: Current Update and Future Therapy. *J. Neurol. Neurosurg. Psychiatry* **2015**, *86*, 385–392. https://doi.org/10.1136/jnnp-2013-307051.
49. Cannata Serio, M.; Graham, L.A.; Ashikov, A.; Larsen, L.E.; Raymond, K.; Timal, S.; Le Meur, G.; Ryan, M.; Czarnowska, E.; Jansen, J.C.; et al. Mutations in the V-ATPase Assembly Factor VMA21 Cause a Congenital Disorder of Glycosylation with Autophagic Liver Disease. *Hepatology* **2020**, *72*, 1968–1986. https://doi.org/10.1002/hep.31218.
50. Hao, C.; Zou, Q.; Bai, X.; Shi, W. Effect of Glycosylation on Protein Folding: From Biological Roles to Chemical Protein Synthesis. *iScience* **2025**, *28*, 112605. https://doi.org/10.1016/j.isci.2025.112605.
51. Florin, A.; Lambert, C.; Sanchez, C.; Zappia, J.; Durieux, N.; Tieppo, A.M.; Mobasheri, A.; Henrotin, Y. The Secretome of Skeletal Muscle Cells: A Systematic Review. *Osteoarthr. Cartil. Open* **2020**, *2*, 100019. https://doi.org/10.1016/j.ocarto.2019.100019.
52. Henze, H.; Hüttner, S.S.; Koch, P.; Schüler, S.C.; Groth, M.; von Eyss, B.; von Maltzahn, J. Denervation Alters the Secretome of Myofibers and Thereby Affects Muscle Stem Cell Lineage Progression and Functionality. *npj Regen. Med.* **2024**, *9*, 10. https://doi.org/10.1038/s41536-024-00353-3.
53. Abrink, M.; Grujic, M.; Pejler, G. Serglycin Is Essential for Maturation of Mast Cell Secretory Granule. *J. Biol. Chem.* **2004**, *279*, 40897–40905. https://doi.org/10.1074/jbc.M405856200.

54. Meen, A.J.; Drevon, C.A.; Pejler, G.; Jenssen, T.G.; Olstad, O.K.; Åbrink, M.; Kolset, S.O. Serglycin Protects against High Fat Diet-Induced Increase in Serum LDL in Mice. *Glycoconj. J.* **2015**, *32*, 703–714. https://doi.org/10.1007/s10719-015-9621-7.
55. Brockington, M.; Yuva, Y.; Prandini, P.; Brown, S.C.; Torelli, S.; Benson, M.A.; Herrmann, R.; Anderson, L.V.B.; Bashir, R.; Burgunder, J.-M.; et al. Mutations in the Fukutin-Related Protein Gene (FKRP) Identify Limb Girdle Muscular Dystrophy 2I as a Milder Allelic Variant of Congenital Muscular Dystrophy MDC1C. *Hum. Mol. Genet.* **2001**, *10*, 2851–2859. https://doi.org/10.1093/hmg/10.25.2851.
56. Okazaki, T.; Matsuura, K.; Kasagi, N.; Adachi, K.; Kai, M.; Okubo, M.; Nishino, I.; Nanba, E.; Maegaki, Y. Duchenne Muscular Dystrophy–like Phenotype in an LGMD2I Patient with Novel FKRP Gene Variants. *Hum. Genome Var.* **2020**, *7*, 12. https://doi.org/10.1038/s41439-020-0099-x.
57. Carmen, L.; Maria, V.; Morales-Medina, J.C.; Vallelunga, A.; Palmieri, B.; Iannitti, T. Role of Proteoglycans and Glycosaminoglycans in Duchenne Muscular Dystrophy. *Glycobiology* **2019**, *29*, 110–123. https://doi.org/10.1093/glycob/cwy058.
58. Noborn, F.; Nilsson, J.; Larson, G. Site-Specific Glycosylation of Proteoglycans: A Revisited Frontier in Proteoglycan Research. *Matrix Biol. J. Int. Soc. Matrix Biol.* **2022**, *111*, 289–306. https://doi.org/10.1016/j.matbio.2022.07.002.
59. Iozzo, R.V.; Schaefer, L. Proteoglycan Form and Function: A Comprehensive Nomenclature of Proteoglycans. *Matrix Biol.* **2015**, *42*, 11–55. https://doi.org/10.1016/j.matbio.2015.02.003.
60. Pobre, K.F.R.; Poet, G.J.; Hendershot, L.M. The Endoplasmic Reticulum (ER) Chaperone BiP Is a Master Regulator of ER Functions: Getting by with a Little Help from ERdj Friends. *J. Biol. Chem.* **2019**, *294*, 2098–2108. https://doi.org/10.1074/jbc.REV118.002804.
61. Adams, B.M.; Canniff, N.P.; Guay, K.P.; Hebert, D.N. The Role of ER Chaperones in Protein Folding and Quality Control. *Prog. Mol. Subcell. Biol.* **2021**, *59*, 27–50. https://doi.org/10.1007/978-3-030-67696-4_3.
62. Ma, M.; Dubey, R.; Jen, A.; Pusapati, G.V.; Singal, B.; Shishkova, E.; Overmyer, K.A.; Cormier-Daire, V.; Fedry, J.; Aravind, L.; et al. Regulated N-Glycosylation Controls Chaperone Function and Receptor Trafficking. *Science* **2024**, *386*, 667–672. https://doi.org/10.1126/science.adp7201.
63. Li, M.; Duan, M.; Yang, Y.; Li, X.; Li, D.; Gao, W.; Ji, X.; Bai, J. Combination of Brefeldin A and Tunicamycin Induces Apoptosis in HepG2 Cells through the Endoplasmic Reticulum Stress-Activated PERK-eIF2α-ATF4-CHOP Signaling Pathway. *Liver Res.* **2025**, *9*, 49–56. https://doi.org/10.1016/j.livres.2025.01.004.
64. Obaseki, I.; Ndolo, C.C.; Adedeji, A.A.; Popoola, H.O.; Kravats, A.N. The Structural and Functional Dynamics of BiP and Grp94: Opportunities for Therapeutic Discovery. *Trends Pharmacol. Sci.* **2025**, *46*, 453–467. https://doi.org/10.1016/j.tips.2025.03.004.
65. Biadsy, S.; Gilad, A.; Madegam, L.A.; Igbaria, A. BIP Orchestrates Bidirectional ER Protein Trafficking via Co-Chaperone Complexes. *Cell. Mol. Biol. Lett.* **2026**, *31*, 34. https://doi.org/10.1186/s11658-026-00875-2.
66. Favero, C.B.; Henshaw, R.N.; Grimsley-Myers, C.M.; Shrestha, A.; Beier, D.R.; Dwyer, N.D. Mutation of the BiP/GRP78 Gene Causes Axon Outgrowth and Fasciculation Defects in the Thalamocortical Connections of the Mammalian Forebrain. *J. Comp. Neurol.* **2013**, *521*, 677–696. https://doi.org/10.1002/cne.23199.
67. Sheetz, J.B.; Chandrasekhar, S.; Rapé, M. Function and Regulation of the Mitochondrial Stress Response. *Nat. Struct. Mol. Biol.* **2026**, *33*, 382–393. https://doi.org/10.1038/s41594-026-01769-9.
68. Suh, J.; Lee, Y.-S. Mitochondria as Secretory Organelles and Therapeutic Cargos. *Exp. Mol. Med.* **2024**, *56*, 66–85. https://doi.org/10.1038/s12276-023-01141-7.
69. Maeda, M.; Arakawa, M.; Saito, K. Disease-Associated Factors at the Endoplasmic Reticulum–Golgi Interface. *Traffic* **2025,** *26*, e70001. https://doi.org/10.1111/tra.70001.
70. McCaughey, J.; Stephens, D.J. ER-to-Golgi Transport: A Sizeable Problem. *Trends Cell Biol.* **2019**, *29*, 940–953. https://doi.org/10.1016/j.tcb.2019.08.007.
71. Iannibelli, E.; Gibertini, S.; Cheli, M.; Blasevich, F.; Cavaliere, A.; Riolo, G.; Ruggieri, A.; Maggi, L. VCP-Related Myopathy: A Case Series and a Review of Literature. *Acta Myol.* **2023**, *42*, 2–13. https://doi.org/10.36185/2532-1900-244.
72. Chen, X.; Shi, C.; He, M.; Xiong, S.; Xia, X. Endoplasmic Reticulum Stress: Molecular Mechanism and Therapeutic Targets. *Signal Transduct. Target. Ther.* **2023**, *8*, 352. https://doi.org/10.1038/s41392-023-01570-w.
73. Herbst, R.; Koneczny, I.; Lochmüller, H.; Strochlic, L. Molecular Mechanisms Underlying Assembly and Maintenance of the Neuromuscular Junction. *Front. Mol. Neurosci.* **2021**, *14*, 797832. https://doi.org/10.3389/fnmol.2021.797832.

74. Samuel, M.A.; Valdez, G.; Tapia, J.C.; Lichtman, J.W.; Sanes, J.R. Agrin and Synaptic Laminin Are Required to Maintain Adult Neuromuscular Junctions. *PLoS ONE* **2012**, *7*, e46663. https://doi.org/10.1371/journal.pone.0046663.
75. Ham, A.S.; Lin, S.; Tse, A.; Thürkauf, M.; McGowan, T.J.; Jörin, L.; Oliveri, F.; Rüegg, M.A. Single-Nuclei Sequencing of Skeletal Muscle Reveals Subsynaptic-Specific Transcripts Involved in Neuromuscular Junction Maintenance. *Nat. Commun.* **2025**, *16*, 2220. https://doi.org/10.1038/s41467-025-57487-1.
76. Ohno, K.; Ohkawara, B.; Shen, X.-M.; Selcen, D.; Engel, A.G. Clinical and Pathologic Features of Congenital Myasthenic Syndromes Caused by 35 Genes—A Comprehensive Review. *Int. J. Mol. Sci.* **2023**, *24*, 3730. https://doi.org/10.3390/ijms24043730.
77. O'Connor, E.; Phan, V.; Cordts, I.; Cairns, G.; Hettwer, S.; Cox, D.; Lochmüller, H.; Roos, A. MYO9A Deficiency in Motor Neurons Is Associated with Reduced Neuromuscular Agrin Secretion. *Hum. Mol. Genet.* **2018**, *27*, 1434–1446. https://doi.org/10.1093/hmg/ddy054.
78. Franco-Juárez, B.; Coronel-Cruz, C.; Hernández-Ochoa, B.; Gómez-Manzo, S.; Cárdenas-Rodríguez, N.; Arreguin-Espinosa, R.; Bandala, C.; Canseco-Ávila, L.M.; Ortega-Cuellar, D. TFEB; Beyond Its Role as an Autophagy and Lysosomes Regulator. *Cells* **2022**, *11*, 3153. https://doi.org/10.3390/cells11193153.
79. Gómez-Virgilio, L.; Silva-Lucero, M.-C.; Flores-Morelos, D.-S.; Gallardo-Nieto, J.; Lopez-Toledo, G.; Abarca-Fernandez, A.-M.; Zacapala-Gómez, A.-E.; Luna-Muñoz, J.; Montiel-Sosa, F.; Soto-Rojas, L.O.; et al. Autophagy: A Key Regulator of Homeostasis and Disease: An Overview of Molecular Mechanisms and Modulators. *Cells* **2022**, *11*, 2262. https://doi.org/10.3390/cells11152262.
80. Fahie, K.; Zachara, N.E. Molecular Functions of Glycoconjugates in Autophagy. *J. Mol. Biol.* **2016**, *428*, 3305–3324, doi:10.1016/j.jmb.2016.06.011.
81. Zhang, R.; Farshadyeganeh, P.; Ohkawara, B.; Nakajima, K.; Takeda, J.-I.; Ito, M.; Zhang, S.; Miyasaka, Y.; Ohno, T.; Mori-Yoshimura, M.; et al. Muscle-Specific Lack of GFPT1 in Knock-in Mice Triggers ER Stress to Alleviate Misfolded Proteins. *Dis. Model. Mech.* **2024**, *17*, dmm.050768. https://doi.org/10.1242/dmm.050768.

Journal of Neuromuscular Diseases 10 (2023) 731–759
DOI 10.3233/JND-221646
IOS Press

Review

Presynaptic Congenital Myasthenic Syndromes: Understanding Clinical Phenotypes through *In vivo* Models

Alessia Pugliese[a,b], Stephen H. Holland[a,c], Carmelo Rodolico[b], Hanns Lochmuller[¨ a,d,e,f,g] and Sally Spendiff[a,*]

[a]*Children's Hospital of Eastern Ontario Research Institute, Ottawa, ON, Canada* [b]*Department of Clinical and Experimental Medicine, University of Messina, Messina, Italy* [c]*Department of Cellular and Molecular Medicine, Faculty of Medicine, University of Ottawa, Ottawa, ON, Canada* [d]*Department of Medicine, Division of Neurology, The Ottawa Hospital, Ottawa, ON, Canada* [e]*Brain and Mind Research Institute, University of Ottawa, Ottawa, ON, Canada* [f]*Department of Neuropediatrics and Muscle Disorders, Medical Center – University of Freiburg, Faculty of Medicine, Freiburg, Germany* [g]*Centro Nacional de Ana´lisis Gen´omico (CNAG-CRG), Center for Genomic Regulation, Barcelona Institute of Science and Technology (BIST), Barcelona, Catalonia, Spain*

Accepted 30 April 2023
Pre-press 19 May 2023
Published 8 September 2023

Abstract. Presynaptic congenital myasthenic syndromes (CMS) are a group of genetic disorders affecting the presynaptic side of the neuromuscular junctions (NMJ). They can result from a dysfunction in acetylcholine (ACh) synthesis or recycling, in its packaging into synaptic vesicles, or its subsequent release into the synaptic cleft. Other proteins involved in presynaptic endplate development and maintenance can also be impaired.

Presynaptic CMS usually presents during the prenatal or neonatal period, with a severe phenotype including congenital arthrogryposis, developmental delay, and apnoeic crisis. However, milder phenotypes with proximal muscle weakness and good response to treatment have been described. Finally, many presynaptic genes are expressed in the brain, justifying the presence of additional central nervous system symptoms.

Several animal models have been developed to study CMS, providing the opportunity to identify disease mechanisms and test treatment options. In this review, we describe presynaptic CMS phenotypes with a focus on *in vivo* models, to better understand CMS pathophysiology and define new causative genes.

Keywords: Congenital myasthenic syndromes, neuromuscular junction, animal models, gene mutations

INTRODUCTION

*Correspondence to:

Congenital myasthenic syndromes (CMS) are a group of genetically inherited diseases, resulting in impaired function of the neuromuscular junction (NMJ). CMS can be classified into presynaptic, synaptic, and postsynaptic defects depending on the localization of the affected protein. A fourth CMS group comprises disorders related to glycosylation [1].

The prevalence of CMS is highly variable worldwide, but it has been estimated at 1.8 to 14.8 per million under those aged 18 years [2–4].

Clinical onset is usually within the first two years oflifewithnon-progressivefluctuatingmuscleweakness and fatigability involving ocular, bulbar, and limb muscles. Less frequently CMS presents at birth with respiratory discomfort, feeding difficulties, poor cry, joint contractures, and other typical symptoms and signs [5]. However, it is not uncommon that some symptoms appear later in life, resulting in an "adult-onset" CMS. This occurs in the case of a few postsynaptic (e.g., slow channel syndrome, *DOK7*, and *RAPSN*) and glycosylation-defect related forms (e.g., *GFPT1*) [6]. Some patients suffer from subtle muscularmanifestationsininfancy,butdonotexhibit a clear distal or proximal muscle weakness until early or late adulthood [7].

CMS diagnosis is based on personal and family history, clinical examination, and neurophysiological studies. A decrement of the compound muscle action potential (CMAP) amplitude is typically detected in response to repetitive nerve stimulation (RNS), and single fibre electromyography (SFEMG) can reveal abnormaljitterandblocking.However,thesefindings are not always observed due to the fluctuating nature of CMS symptoms, so gene sequencing remains crucial in confirming the diagnosis [1].

Presynaptic forms are deemed at around 5%-10% of all CMS and usually present earlier than postsynaptic forms, at birth or during the prenatal period. *CHAT* defects are the most frequent among presynaptic CMS, amounting to 4-5% of all CMS. Each of the other presynaptic CMS represents less than 1% of the total [5]. In pre-synaptic forms the phenotype is more severe including congenital arthrogryposis, joint contractures, developmental delay, and apnoeic crisis that can result in death [5], The abnormal cognitive development may also be impacted by hypoxic brain damage, as suggested by the radiological presence of hypoxic ischaemic encephalopathy in several CMS patients affected by repeated apneas [8]. Moreover, many presynaptic genes are also expressed in thebrain,leadingtoadditionalcentralnervoussystem (CNS) symptoms which are uncommon in postsynaptic CMS (Fig. 1) [9–11]. However, milder cases of presynaptic CMS have been described, presenting with mild proximal weakness and good response to treatment [11].

Presynaptic CMS can result from a dysfunction in acetylcholine (ACh) synthesis or recycling, in its packaging into synaptic vesicles, or its subsequent release into the synaptic cleft [12]. Recently, new proteins have been discovered that are involved in presynaptic endplate development and maintenance, although their function is not yet fully explained [13–15].

Increasingly animal models have been used to study the NMJ, aided by the fact that all mammals and many other research organisms use ACh for neuromuscular transmission. Presynaptic CMS causedbyamutatedpathwaydirectlyassociatedwith ACh can only be modelled in species using ACh as a neurotransmitter. In contrast, other CMS can be evaluated in a wider range of species, resulting in many discoveries with respect to NMJ formation and function.

In Zebrafish, which use ACh for synaptic transmission, morpholino oligonucleotides (MOs) have been used to knock down genes of interest at the NMJ. More recently CRISPR/Cas9 technology has been employed. Mouse models of CMS have also been extensively used to determine pathomechanisms and investigate potential drug treatments. These have been both tissue specific and whole-body knock outs. *Caenorhabditis elegans* (C.

ISSN 2214-3599

elegans) is another animal using ACh as the principal excitatory transmitter at the NMJ with a well-conserved synaptic machinery and a simple genetic system [16]. *Drosophila melanogaster* (D. melanogaster) is an additional good model for studying synaptic transmission. Indeed, many NMJ proteins are conserved between Drosophila and vertebrates, as well as synaptic molecular development. However, flies useglutamateasanexcitatoryneurotransmitter,highlighting the necessity of identifying the right animal model to use [17].

In this review, we provide an update on presynaptic CMS phenotypes with a focus on *in vivo* models whichareimportanttobetterunderstandNMJdisease mechanisms and for defining new causative genes.

733

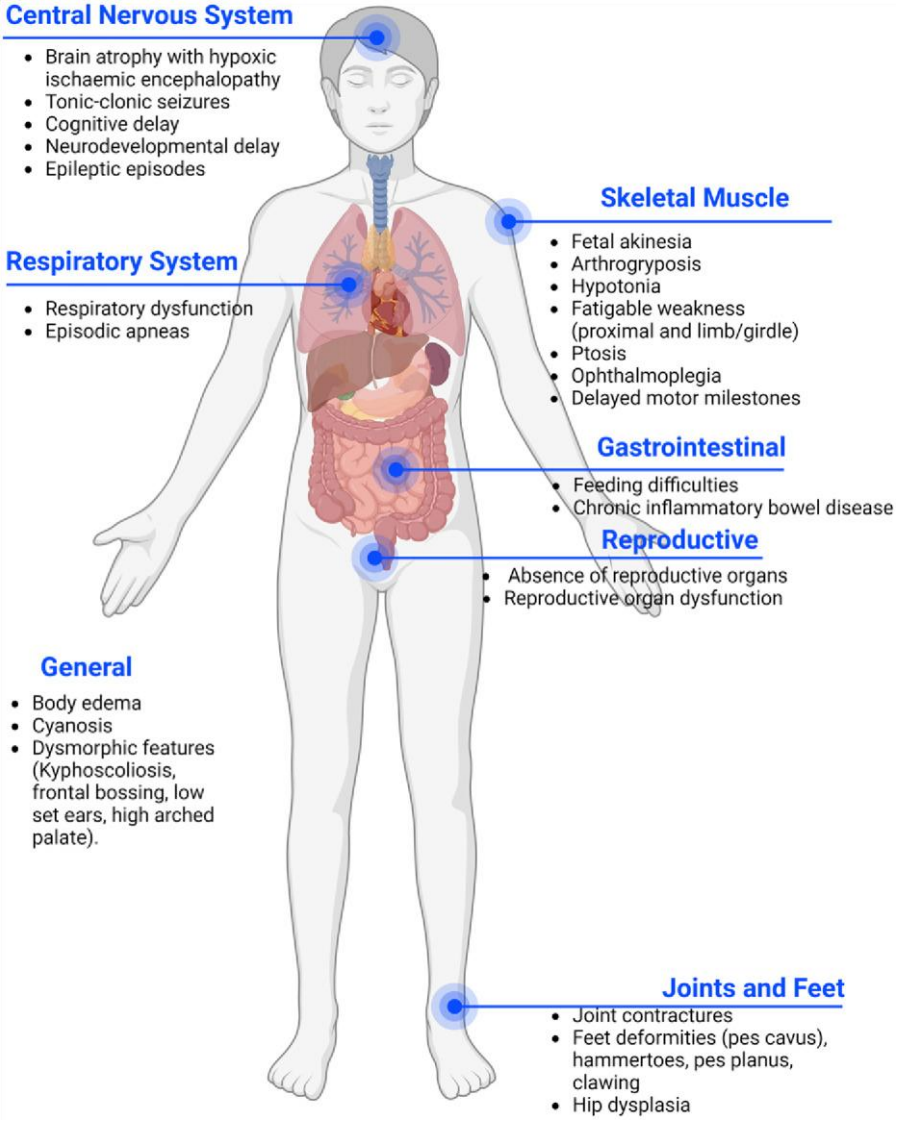

Fig. 1. Common phenotypes of pre-synaptic forms of CMS. In pre-synaptic forms of CMS the phenotype is frequently more severe due to the presence of affected genes in the peripheral and central nervous system. Patients often present with a multi-systemic condition.

We conducted a PubMed literature search, considering papers of any design, except for reviews, published in English from January 2000 to March 2022. Each presynaptic CMS gene was checked as

single searchtermandinassociationwith“congenitalmyasthenicsyndromes”,whiletherelativeencodedprotein was searched in combination with “models”. We selected studies focused on the evaluation of altered protein effects, mutant animal phenotypes, and CMS clinical case reports, assessing their reference lists to identify other relevant articles. Additional information for the characterization of genes and proteins was obtained from https://www.genecards.org/ and https://www.ncbi.nlm.nih.gov/omim/.

We provide details about the function and tissue expression of each gene. Then we proceed to delineate the clinical picture of the related CMS, highlighting how the use of animal models has allowed a better understanding of the pathophysiological mechanisms of the disease.

ACETYLCHOLINE SYNTHESIS AND RECYCLING

SLC5A7

SoluteCarrierFamily5Member7gene(*SLC5A7*), also called Choline Transporter (*CHT*), is located on chromosome 2q12.3, and encodes a high-affinity choline transporter (CHT). CHT is involved in the resynthesis of ACh, taking up the choline from the extracellular space into presynaptic terminals (GC02P107969, GeneCards). (Fig. 2).

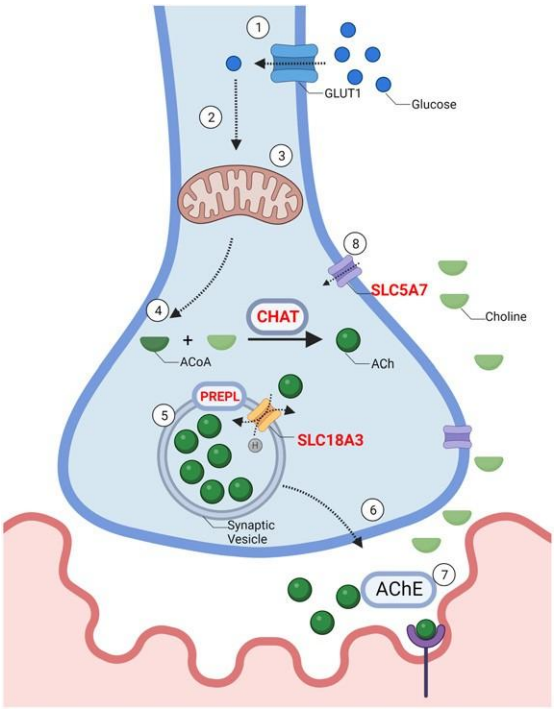

Fig. 2. – The synthesis and recycling of acetylcholine: 1. Synthesis of ACh requires the influx of glucose through a glucose transporter (GLUT) into the cell. 2. Intracellular glucose is then metabolized by glycolysis to produce pyruvate 3. Pyruvate then enters the mitochondria where it is further metabolized to AcetylCoA. 4. Choline acetyltransferase (CHAT) combines Acetyl-CoA with choline to produce acetylcholine (ACh). 5. ACh is packaged into vesicles through Vesicular Acetylcholine Transporter (SLC18A3), a 12-membrane protein located on the synaptic vesicle. Prolyl Endopeptidase *(PREPL)*, plays a role in the packaging ofAChandotherpre-synapticmachinerysuchasSNAREsintothe synaptic vesicle, although the exact mechanism remains unknown. 6. Vesicles travel towards the pre-synaptic membrane and undergo exocytosis. 7. ACh is released from the pre-synaptic membrane through vesicle exocytosis. ACh diffuses across the synaptic cleft and binds to acetylcholine receptors (AChR). Acetylcholine esterase (AChE) breaks down ACh. 8. *SLC5A7* is a Na^+ and Cl^- dependent high-affinity transporter that mediates the uptake of choline at the motor neuron terminal. Genes implicated in CMS are in red.

SLC5A7 CMS is typically inherited in an autosomal recessive manner presenting at birth, however, prenatal signs like antenatal hydramnios, reduced foetal movements, and arthrogryposis have been described [8, 9, 18–20]. Respiratory dysfunction with life-threatening episodic apnoeas is a constant feature, in variable association with hypotonia, fatigable weakness, oculo-bulbar

symptoms and gastrointestinal alterations [8, 9, 18–21]. RNS reveals a decrementalresponse,andbrainMRImayshowbrain atrophy with hypoxic ischaemic encephalopathy [8, 9, 18, 20, 21]. Cognitive defects and neurodevelopmental delay are not unusual features in *SLC5A7* CMS, underlying the link between cortical cholinergic neurotransmission and CHT [9, 20, 21] (Table 1). *SLC5A7* CMS can be referred to as a multisystem disorder, encompassing the central, peripheral, and possibly the autonomic nervous system. This multisystemic involvement was apparent in animal models prior to the first case reports, confirming a causal link between clinical features and the *CHT* mutation.

The presence of *CHT* in both the central [22, 23] and peripheral nervous system was apparent when Ferguson., et al. created *Cht*-knockout (KO) mice (*Cht*$^{-/-}$) which became paralyzed and cyanotic a few minutes after birth and died of hypoxia probably due to failure of diaphragm neurotransmission [24]. When these mice were later transfected with the *Cht* gene under control of the motor neuron promoter Hb9, they were able to move and breathe for about 24 hours [25]. Additionally, intracellular recordings from muscle fibres revealed only initial evoked and spontaneous responses, supporting the hypothesis that *Cht*$^{-/-}$ mice are not able to synthetize ACh after depleting initial stores. The attempt to rescue the phenotype, by limiting the degradation of ACh with AChEI physostigmine and neostigmine, failed in these animals [24]. In humans, the response toAChEIisvariable,resultinginsomeimprovements in most cases, sometimes in addition with ephedrine or salbutamol [8, 9, 20, 21]. However, in one patient, presenting with a delayed motor development and MRI brain atrophy, pyridostigmine was not efficient after 3-days neonatally [21]. This was also the case in an older 14-year-old patient with ocular and bulbar involvement [8]. Finally, three patients died despite treatment with AchEI [19, 20].

Heterozygous *Cht*$^{+/-}$ mice survive and exhibit lower, but functionally acceptable CHT levels comparedwithWT[24].Theypresentnormalperforma nce on multiple sensorimotor, anxiety and cognitive tasks, except under physical or pharmacological stress [26]. Similar results have been obtained by Paolone G. et al., who tested cognitive performance in mice to examine cortical cholinergic neurotransmission.Theypostulatedthepresenceofme chanisms that could compensate for reduced cholinergic activity in *Cht*$^{+/-}$ mice during moderate cognitive challenges, but not in conditions requiring a sudden ACh increase. Some behavioural and mood disorders in humans were correlated with *CHT* gene mutations, especially the p.Ile89Val variant [27]. Indeed, a new mouse model expressing the *Cht* – p.Ile89Val variant

Table 1
Summary of clinical and instrumental features of published patients affected by pre-synaptic CMS

Gene Chromosome Inheritance	Frequency (		Phenotype	Brain MRI	RNS/SFEMG	Muscle biopsy	Genotype	Drugs	Ref.
SLC5A7 2q12.3 AD	14 pts	con	Hypotonia, apneas, swallowing difficulties, developmental delay, ptosis, ophtalmoplegia, muscle atrophy (rare: hydramnios, arthrogriposis, facial dysmorphism, seizures)	brain atrophy (rare: intraventricular and putamen hemorrage)	decremental response to RNS	Myopathic changes, atrophic fibres, targetoid areas	c.282T>A/c.282T>A (p.Ser94Arg/Ser94Arg) c.335T>A/c.335T>A (p.Val112Glu/Val112Glu) c.629C>T/c.629C>T (p.Pro210Leu/Pro210Leu) c.194G>A/c.313C>T ((p.Gly65Glu/Pro105Ser)	some response to pyridostigmine and ephedrine; no response to 3,4-DAP and salbutamol	[8, 9, 18–21]
CHAT 10q11.23 AR	52 pts	con or early infancy	reduced fetal movements, hypotonia, apneas, swallowing and feeding difficulties, developmental delay, fluctuated ptosis, ophthalmoparesis, muscle fatigability	(rare: mild delay in myelination of the centrum semiovale, and corpus callosum atrophy)	decremental response to RNS after prolonged high frequency; increased jitter and blocking at SFEMG	unspecific myopathic changes, type 1 fibre predominance	c.1007T>C/c.1007T>C (p.Ile336Thr/Ile336Thr) c.629T>C/ 631C>G (p.Leu210Pro/Pro211Ala) c.678 684delTGGCACC/ 2078T>G (p.*/Ile693Ser) c.1078G.A/1078G.A (p.Gly360Arg/Gly360Arg)	variable response to pyridostigmine and 3,4-DAP	[11, 30–41]
SLC18A3 10q11.23 AR	4 pts	con	hypotonia, cyanosis, feeding difficulties, global developmental disability, ptosis, ophthalmoplegia, fatigable weakness (rare: arthrogryposis, severe necrotizing enterocolitis)	brain atrophy, demyelination (rare: small hemorrhages in the frontal and parietal lobes)	decremental response to RNS	n.p.	c.557G>C/557G>C (p.Gly186Ala/Gly186Ala) +10q11.22-q11.23del c.1192G>C/1192G>C (p.Asp398His/Asp398His) c.1078G.A/1078G.A (p.Gly360Arg/Gly360Arg)	slight response to pyridostigmine, and 3,4- DAP, distigmine and ephedrine	[10, 47–51]
SNAP25 20p12.12 AD	2 pt	con	fetal hypomotility, cyanosis, fluctuating ptosis, dysarthria, ataxia, fatigable weakness, arthrogryposis and fatal respiratory failure (1 pt)	normal (1 pt), n.p. (1 pt)	decremental response to RNS (1 pt), n.p. (1 pt)	normal (1 pt), mild fibres size variation (1 pt)	c.200T>A (p.Ile67Asn) c.529C>T (p.Gln177X)	no response to pyridostigmine; slight response to 3,4-DAP	[74]

(*Continued*)

Table 1
(*Continued*)

Gene Chromosome Inheritance	Frequency (		Phenotype	Brain MRI	RNS/SFEMG	Muscle biopsy	Genotype	Drugs	Ref.
VAMP1/ SYB1 12p13.21 AR	9 pts	con	hypotonia, feeding difficulties, delayed motor development, ophthalmoparesis, facial and bulbar muscle weakness, generalized muscle weakness, joint contractures	n.p	decremental response to RNS	myopathic features and borderline low complex IV activity, type 2 fibres atrophy	c.200T>A/200T>A (p.Ile67Asn/Ile67Asn) c.146G>C/146G>C (p.Arg49Pro/Arg49Pro) c.51 64delAGGTGGGG GTCCCC/ c.51 64delAGGTGGGG GTCCCC (p.Gly18TrpfsTer5*/Gly 18TrpfsTer5*) c.340delA/340delA (p.Ile114SerfrsTer72 for isoform A, p.Ser114ValfsTer32 for isoform D)	slight response to pyridostigmine and salbutamol	[67–70]
SYT2 1q32.1 AD	10 pts	childhood	ptosis, ophthalmoparesis, limb weakness, muscle fatigue, gait difficulties, foot deformities, reduced or absent deep tendon reflexes	n.p	decremental response to RNS	n.p	c.920A>C (p.Asp307Ala) c.923C>T (p.Pro308Leu)	no response to pyridostigmine; slight response to 3,4-DAP	[81–87]
UNC13A 19 AR	1 pt	con	premature birth, hypotonia, ventilator dependent, facial dysmorphism, ptosis	thin corpus callosum	decrement response to RNS	marked type 2 fibres atrophy	c.304C>T/304C>T (p.Gln102*/Gln102*)	no response to pyridostigmine; modest response to 3,4-DAP	[94]

MYO9A 15q23 AR	3 pts	con	fetal hypomotility, swallowing difficulties, apneas, delayed cognitive functions, ptosis, ophthalmoplegia, muscle weakness	normal	decremental response to RNS; abnormal jitter at SFEMG	n.p.	p.Arg1517His/Arg2283His p.Asp1698Gly/Asp1698Gly	good response to pyridostigmine and 3,4-DAP	[15]
PREPL 2p21 AR	11 pts	con	hypotonia, feeding difficulties, respiratory distress, cognitive impairment, ptosis, bulbar signs, muscle weakness, short stature (rare: absence of uterus and ovaries, microcephaly)	normal	normal response to RNS (rare: decremen-tal response)	irregular intracellular vacuoles and perimysium fibrosis	c.616+1G>T/616+1G>T (p.Glu206Glyfs*22/Glu 206Glyfs*22) c.1528C>T/2094G>T (p.Arg510*/Lys698Asn) c.1529+1G>A/c.1784 delinsAA (p.?/Thr595 Lysfs * 19) c.1282 1285delTTTG/c.1282 _ 1285delTTTG (p.Phe428Argfs*18/Phe428 Argfs*18) c.342delA/342delA (p.Val 115Leufs*39/Val115Leufs*39)	slight response to pyridostigmine	[103–109]
LAMA5 20q13.33 AR	1 pt	con	hypotonia, respiratory failure, scoliosis, chronic inflammatory bowel disease, ptosis, ophthalmoplegia, muscles weakness, dysmorphic features, myopia, tics	mild cerebral atrophy	decremental response to RNS	type I fibres predominance; EM: increased postsynaptic folding, moderate reduction of SVs	p.Arg2659Trp/Arg2659Trp	response to pyridostigmine and 3,4-DAP	[14, 112]
RPH3A 12q24.13 AR/AD?	1 pt	childhood	limb weakness, fatigability, hand tremors, hands incoordination, postural imbalance, nasal speech, learning disabilities	normal	Incremental response to high frequency RNS; abnormal jitter at SFEMG	type I fibres predominance; EM: reduction of SVs, degenerative lamellar bodies	c.806G>A/ c.1390G>T (p.Arg269Gln/p.Val464Leu)	response to albuterol sulfate	[119]

SLC25A1 22q11.21 AR	19 pts	childhood	ptosis, ophthalmoplegia, some dysmorphisms, dysarthria, chewing difficulties, generalized weakness, mild intellectual disability	normal	decremental response to RNS; abnormal jitter and blockings at SFEMG	non-specific myopathic features; enlarged mitochondria and increased in number on EM	c.205G>T/c.205G>T (p.Asp69Tyr/p.Asp69Tyr) c.740G>A/c.740G>A (p.Arg247Gln/p.Arg247Gln) c.628C>T/c.145G>A (p.Arg210X/p.Val49Met)	partial response to pyridostigmine and 3,4-DAP	[122–126]

MRI: magnetic resonance imaging; RNS: repetitive nerve stimulation, SFEMG: single fiber electromyography; AD: autosomal dominant, AR: autosomal recessive; 3,4-DAP: 3,4-diaminopyridine; SVs: synaptic vescicles: con: congenital: pts: patients; n.p.: not performed; ?: inheritance pattern not clear.

hasbeengenerated,resultinginareductionofcholine clearance in the striatum and cortex, decreased ACh release after prolonged neuronal depolarization, and altered attentional performance [28]. These attentional and behavioural deficits reflect cognitive alterations found in humans. Indeed, a few patients have presented with global developmental delay, resulting in speech, learning and social interaction impairment with no awareness of surroundings [20, 21].

Cht+/¯ mice also exhibited diminished parasympathetic heart effects with basal resting tachycardia and hypertension, because of depleted cardiac ACh levels [29]. There is no evidence of cardiac involvement in patients harbouring mutations in *CHT*, but autonomicdysfunctionhasbeennotedwithcoretemperatures as low as 32 ◦C [20].

In contrast to mice, homozygous null alleles of *C. elegans CHT* (*cho-1*) are viable but only release around 40% ACh compared to WT animals. However, this is enough to permit thrashing under normal conditions, but with marked motor alterations when stressed [16] (Table 2).

CHAT

The Choline-O-Acetyltransferase (*CHAT*) gene encodes the homonym enzyme which catalyses ACh synthesis from acetyl CoA and choline at cholinergic synapses. It is expressed both in the central and peripheral nervous system. (GC10P049609, GeneCards) (Fig. 2).

CHAT CMS is the most common presynaptic form, accounting for 4–5% of all CMS cases. It is inherited in an autosomal recessive manner, and also known as CMS with episodic apnoea (CMSEA) [30, 31]. Sudden episodes of respiratory crises and bulbar weakness may be provoked by infection, fever, or other stressful conditions in birth or early infancy, and in several cases this has resulted in death [32–34]. Occasionally EA is accompanied by loss of consciousness and tonic–clonic seizures [35]. Other reported symptoms comprise ptosis, fatigable weakness, proximal muscle weakness, aggravated by exposure to cold, delayed motor milestones and intellectual disability [11, 36–41]. RNS usually detects no decrement at low-frequency stimulation, but it appears after prolonged high-frequency stimulation [11]. AChEI are effective in moderating respiratory crises and improving other symptoms in some cases [11] (Table 1).

Mice with targeted deletion of the *Chat* gene at the NMJ appear normal in a heterozygous state, while homozygous pups die at birth, displaying flaccid paralysis. Both spontaneous and nerve-evoked postsynaptic potentials are absent in mutants, and several morphology and developmental abnormalities have been noted at the NMJ (i.e., marked excess of nerve terminal branching, altered synapse distribution with widened endplate, thinner muscles, and precocious appearance of larger AChR-rich sites at the postsynaptic membrane) [42, 43].

Similar results came from two mutant zebrafish lines, *bajan* and $chata^{tk64}$. *Bajan* zebrafish have a single point mutation (A to C) at the splice acceptor site of Chat intron 2, while $chata^{tk64}$ carry a missense mutation changing a highly conserved serine to an arginine (p.S102R). Both exhibited no coiling movements and reduced touch response in a homozygous state [44, 45]. Spontaneous synaptic currents as well as evoked synaptic responses were markedly decreased [44] (Table 2).

Finally, an example of a naturally occurring *CHAT* mutant animal is the Old Danish Pointing Dog, carrying a valine to methionine substitution at position 29 of the *CHAT* exon 6. Affected dogs can walk and run for only 5–30min before manifesting fore- and hind leg fatigability. Moreover, electrophysiology shows a decrement at 3Hz induced by a long stimulation train [46].

ACETYLCHOLINE PACKAGING INTO SYNAPTIC VESICLES

SLC18A3

Solute Carrier Family 18 Member A3 (*SLC18A3*) mapped to chromosome 10q11.2, encodes for vesicular acetylcholine transporter (VAChT) that mediates ACh internalization into vesicles in the presynaptic terminal (600336, OMIM). Mutations of this gene leads to an autosomal recessive inherited CMS form (Fig. 2).

Clinical onset of *SLC18A3* CMS occurs in the neonatal period, and is often associated with apnoeic episodes, hypotonia, variable degrees of joint contractures, and feeding difficulties [10, 47, 48]. However, four patients also displayed prenatal alterations [49, 50]. Ptosis, ophthalmoplegia, mild facial weakness and generalized fatigable weakness are other common symptoms. Hakoken A.H. et al. described two cases of severe and lethal CMS characterizedbyfoetalakinesia,arthrogryposis,genera lized body edema and dysmorphic features [51].

Table 2
Published literature for animal models available for pre-synaptic CMS genes

Gene	Animal	Technology Used	Model	Phenotype	Strength	Weakness	References
SLC5A7	Mouse	Homologous recombination deletion (exon 2 to intron 4)	*CHT*$^{(-/-)}$	Paralysis at birth, only spontaneous quantal release of ACh. Crossing with HB9-Cre increased survivability to 24hrs	ACh quantal release deficiency	Not viable; paralysis at birth	[16, 22–29]
			CHT$^{(-/+)}$	Improved survivability, cardiac involvement	Improved survival in heterozygotes,	Cardiac involvement noted in model, not observed, or studied in CMS patients	
		CRISPR/Cas9	*CHT*^{I89V}	Developmental and behavioural defects, reduced ACh release and choline clearance	Diminished ACh release in cortex and striatum; neurological deficit observed	Impact on muscle morphology unknown	
	C. elegans	Cas9-sgRNA	*Cho-1*	Viable, reduced ACh release, worsening phenotype when stressed	Reduced ACh release, stressing the model worsens phenotype	Impact on muscle morphology unknown	
CHAT	Mouse	Injection of J1 Embryonic Stem Cell in C57BL/6 blastocyst with loss of Exon 11, 12 and 13	*ChAT*$^{(-/-)}$	Not viable at birth, paralysis, absent spontaneous and induced neurotransmission	Severe phenotype, absent neurotransmission	Not viable; paralysis at birth	[42–46]
			ChAT$^{(-/+)}$	Developmental impairment and behavioural defects, reduced lifespan, reduced muscle strength, motor function decreased	Viable, severe phenotype	Further work required to examine NMJs structure and muscle morphology	
	D. renio	Point mutation (A to C) to the splice acceptor site of ChAT intron 2	*Bajan*	Tail bend, behavioural defects, no evoked touch response, decreased spontaneous synaptic responses	Viable, CMS-like phenotype	NMJ structure and muscle morphology not investigated	
		Missense mutation S102R	*Chata*		Viable, CMS-like phenotype	NMJ structure and muscle morphology not investigated	

(*Continued*)

Table 2
(*Continued*)

Gene	Animal	Technology Used	Model	Phenotype	Strength	Weakness	References

	Canine	None (Spontaneous Mutation)	*Exon 6*	Reduced run distance, stride length and recovery after exercise, decremental response at 3Hz	Exercise-induced muscle fatigue observed with decremental response	Spontaneous mutation, reproducibility challenging	
SLC18A3	Mouse	Homologous recombination Neo/tk knockdown of VAChT	*VAChT*$^{(-/-)}$	Reduced spontaneous and induced ACh release, behavioural defects, loss of muscle strength	Knockdown of SLC18A3; Impaired ACh release, and loss of muscle strength; CMS-like phenotype	No major weakness detected; due to CMS-like phenotype	[52–58, 60–65]
			VAChT$^{(-/+)}$	Slight impairment in spontaneous ACh release, reduced memory output (maze test) and olfactory function	Impaired ACh release, and loss of muscle strength; CMS-like phenotype	Phenotype is mild, not consistent with human CMS patients	
		Cre/LoxP creation of VAChT$_{(six3-Crefl/l)}$ created and crossed with above line	*VAChT*$^{(-/-)}$	Not viable at birth, paralysis, respiratory insufficiencies, cardiac development delay between parasympathetic and sympathetic tone	Severe phenotype observed	Not viable; paralysis at birth, cardiac dysfunction not documented in CMS patients	
		Motor neuron specific Cre/LoxP ablation of VAChT	*VAChT*$^{(-/-)}$	Smaller motor neurons, decreased strength, hypoactive, impaired NMJ function and formation, atrophic muscle, kyphosis	Motor neuron specific, Severe phenotype, with impaired NMJ function, improved lifespan from other VAChT models	Motor neuron specific	
	D. melanogaster	Deletion of Cha, VAChT present in 1st exon of Cha	*Cha*$^{(-/-)}$	Lethal phenotype at larval stage	Severe phenotype, NMJ development not studied	Not viable	
	C. elegans	Mutational screen revealed 19 independent unc-17 mutants	*VAChT*^{G347R}	Reduced growth, poor coordination; other mutations reveal lethality that ablated gene function	Phenotype in some unc-17 mutants	Lethality in some mutations, viable mutations NMJ structure and function not studied	
SYB1/ VAMP1	Mouse	Nonsense mutation truncating SYB1 and VAMP1	VAMP1$^{(lew/lew)}$	Developmental and behavioural defects, muscle wasting, reduced survival (<3 weeks), decreased ACh release and synaptic transmission	Severe phenotype, with impaired NMJ function, and delayed motor development	Reduced lifespan, joint contractures not noted in model	[71–73]
SNAP25	Mouse	Cre/LoxP knockout at	*SNAP25*$^{(-/-)}$	Embryonic lethal,	Severe phenotype,	Not viable	[76–80]

		Exon 4		development delay, impaired NMJ formation, with reduced ACh release	with impaired NMJ function		
			SNAP25$^{(-/+)}$	Viable and fertile, minimal behavioural defects observed	Viable	No significant behavioural defects observed. Severe phenotype reported in SNAP25 CMS patients	
		Missense mutation I67T	*BlindDrunk Mouse*	Ataxic gait, behavioural impairment consistent with a schizophrenia-like symptoms	Neurological phenotype linked to schizophrenia	CMS phenotype not observed	
		B-6-Snap25^{tm3mc2} LoxP sites flanking Exon 5a/5b	*SNAP25*$^{(-/-)}$	Fragmented axonal projections, axonal deterioration over time, behavioural defects	Impaired axonal projections, with deterioration suggesting neurological phenotype	More studies need to be determined to link to a CMS-phenotype	
	Rat	rAAV2/5 Over-expression in dorsal hippocampus	Male Wistar Rats (WT)	Cognitive defects, behavioural impairments	Neurological phenotype observed	Overexpression model with AAV, not observed in patients	
SYT2	Mouse	Homologous recombination inserting LacZ/Neo marker at Exon 2	*SYT2*$^{(-/-)}$	Developmental defects, impaired NMJ form and function, ataxic, seizures, non-viable	Severe phenotype with impairment of NMJ form and function	Non-viable, severe neurological phenotype observed with seizures, not consistent to CMS patients	[88–92]
	D. melanogaster	Mutation of aspartate residues in the C2B domain	*SYT2null*	Decrease in evoked transmitter release	Decreased neurotransmitter release	Further studies are required to investigate CMS-like phenotype	
		L308P mutation in C2B domain	*SYT2*$^{(-/-)}$	Developmental and behavioural defects, homozygous insertion of L308P resulted in lethal at 3 weeks	Severe neurological phenotype	Reduced lifespan	
			SYT2$^{(-/+)}$	Developmental and behavioural defects, increased fatigability, reduced evoked transmitter *release*	Moderate neurological phenotype, CMS-like	CMS like however, NMJ structure not investigated	
	D. renio	Morpholino injection of splice and translation blocking sequences	MO *SYT2*	Loss of synchronous transmission at NMJs, asynchronous transmission not impacted	Impaired synchronous transmission	Mosaic expression of knockdown	

(*Continued*)

Table 2
(*Continued*)

Gene	Animal	Technology Used	Model	Phenotype	Strength	Weakness	References
UNC13A	Mouse	Homologous recombination in embryonic stem cells	MUNC13-1/2/3 $^{(-/-)}$	Paralysis at birth, only spontaneous quantal release of Ach, small NMJs	Severe phenotype observed, NMJ form and function impaired	Not viable	[93, 95, 96]
	C. elegans	Single copy transgenes introduced to EC6699 strain using *mos1*-mediated single copy insertion	MUNC13$^{(-/-)}$	Developmental defects, paralysis due to impaired synaptic transmission	Severe phenotype observed, NMJ form and function impaired	Not viable	
		e1091, an amber mutant obtained by ethyl methansulfonate mutagenesis	MUNC13 mutant	Developmental and behavioural defects, incoordination, impaired neurotransmission	Viable model with impaired neurotransmission	Model requires more studies to confirm CMS-like phenotype	
MYO9A	*D. renio*	Morpholino injection of splice and translation blocking sequences	MO *myo9aa and myo9ab*	Developmental delay, bent tail, behavioural defects, impaired NMJ structure and function	CMS phenotype, impaired NMJ structure and function	Mosaic expression system with morpholino	[15, 97–101]
	Mouse	Mouse Exon 2 flanked with Cre/LoxP	*MYO9A*$^{(-/-)}$	Retarded growth, behavioural defects, severe hydrocephalus, trembling gait, impaired kidney function	Neurological phenotype observed, muscle function impairment	NMJ form and function not studied	
			MYO9A$^{(-/+)}$	Behavioural defects, impaired hippocampal synapse formation, memory and learning impairment	Neurological phenotype observed	NMJ form and function not studied	
PREPL	Mouse	Cre/LoxP targeting Exon 10 of *PREPL*	*PREPL*$^{(-/-)}$	Reduced body weight, behavioural defects, impaired mitochondrial function, hypotonia	Viable, Muscle morphology dysfunction, with behavioural changes	Mitochondrial deficits not confirmed in patients	[110, 111]
LAMA5	*D. renio*	Morpholino injection of splice and translation blocking sequences	MO *LAMA5*	Muscle and nerve structural abnormalities, developmental delay, behavioural and developmental defects	CMS phenotype, impaired NMJ structure and function	Mosaic expression system with morpholino	[113–118]

	Mouse	CRISPR/Cas9 creation of R291L mutant	*LAMA^{pm}*	Die at birth, severe developmental defects, impaired kidney, and lung function	Severe phenotype with developmental defects	Not viable, NMJs not studied	
		Inducible Cre/LoxP (SP-Clama5fl/-) with doxycycline	*SP-CLama5$_{(fl/-)}$*	Lethal shortly after birth, hypoxic, impaired epithelial differentiation and lung development	Severe phenotype, with developmental delay, respiratory issues consistent with patients	Early lethality, more studies required to examine NMJs of this model	
		Chimeric transgene Mr51 and Mr5G2H	*LAMA$^{(-/-)}$*	Embryonic lethal, impaired lung and limb development; Mr5G2H mice were viable but have reduced body size, and kidney function.	Mr5G2H are viable and have impaired development	Not viable; Mr5G2H viable but CMS phenotype not studied, lacks severe CMS phenotype seen in LAMA5-CMS patients	
RPH3A	Mouse	Neomycin cassette flanking between exons of Rph3a, electroporated into ES cells	*Rph 3a^{tm1Sud}/J*	Fertile, Enhanced axonal regeneration; rescues behavioural deficits after spinal cord injury.	Neuronal phenotype observed, mice are fertile	NMJs specifically not investigated, more information is needed to confirm CMS phenotype	[142–146]
	Mouse	syn-PFF injected into C57Bl6 with AAV9-Rph3A overexpression	hSynGFPRph3aWPRE-AAV9	syn-PFF reduced Rph3A interaction with GluN2a-contiaing NMDRs, inducing neurological behavioural dysfunction, rescued with AAV9-Rph3a.	Neuronal phenotype observed, impacting Rph3A	NMJ phenotype not observed, not linked to CMS phenotype	
	Rat	RNAi knockdown in Middle cerebral artery occulusion (MCAO) model	LV-Rph3A-RNAi	Exacerbates cerebral infarction and neuronal death leading to neurological behavioural dysfunction	Neurological phenotype observed	MCAO model investigated, effect on NMJ unknown	
	C. elegans	Null mutation 1500bp deletion including the promoter and 3 exons	Rbf-1	Appeared lethargic, no impact on NMJ morphology, defecation, pharyngeal pumping and mating	Lethargic model, appears weak.	Did not alter NMJ morphology,	

(*Continued*)
Table 2 (*Continued*)

Gene	Animal	Technology Used	Model	Phenotype	Strength	Weakness	References

SLC25A1	*D. renio*	Morpholino injection of splice and translation blocking sequences	MO *SLC25A1*	Motor impairment, altered tail morphology, decreased swim and touch-evoked response, stunted motor neuron branching, with incomplete synapses	Neuromuscular phenotype observed, viable	Mosaic expression system with morpholino	[123, 126, 127]
	Mouse	SLC25A1 overexpression	TRESLC25A1 nTg	Autistic-like phenotype (aberrant behaviours and repetitive jumping), altered synaptic structure and white matter content	Neurological phenotype observed, limited to brain involvement	SLC25A1 overexpression not observed in patients	
		SLC25A1 liver-restricted knockout ($SLC25A1^{tm1a(EUCOMM)Wtsi+tg(Alb-cre)21Mgn}$	*SLC25A1*$^{-/-}$	Viable, normal liver histology, body weight and liver fat content, protected from steatosis, improved blood glucose clearance	Model restricted to liver assessment	NMJ phenotype not observed, not linked to CMS phenotype	
	D. melanogaster	Mutation to sea^{EP}(reduced expression)	*I(3)EP3364*	Increased chromosome aberrations, no functional characteristics noted	Viable model, more studies need to examine impact on NMJ neurotransmission	No phenotype observed	

Cognitive function, especially learning capacity, attention and working memory, may also be affected [10, 47]. A decremental response to RNS is usually detected. Pyridostigmine improves clinical manifestations, and 3,4-Diaminopyridine (3,4-DAP) and ephedrine may be added in some cases [10, 48, 50]. Intriguingly, a mild reduction of left ventricular systolicfunctionwasrescuedaftertreatmentwithAChE I in one patient [10] (Table 1).

One of the first animal models of the VAChT mutation was generated in *Drosophila melanogaster* (common fruit fly). Homozygous mutants were lethal, and those that survived till the larval stage showed reduced motility. Moreover, heterozygous flies exhibited electrophysiological defects in the giant fibre pathway after high-frequency stimulation [52]. More recently, *Drosophila* models have been testedwithanoverexpressionofVAChT,demonstratin gitsnegativeimpactonlongevity,locomotorability in an age-dependent way, learning and memory [53]. Surprisingly, reduced VAChT function produced a similar effect on lifespan and locomotive behavior [54]. There are currently no specific reports on VAChTmutationsandlifeexpectancyofpatients,but clinical and electrophysiological features of affected *Drosophila* resemble those recognized in patients.

The effects of a reduced expression of VAChT in the central and peripheral nervous systems were later confirmed by Prado V.F. et al. in a *Slc18a3* knockdown (KD) mouse model. They detected a reduction in VAChT levels in several central nervous system regions both in heterozygous KD mice and more markedly in homozygous ones. Moreover, miniature end-plate potentials (MEPPs) recorded at NMJs were smaller and less frequent in homozygous mutants.

Homozygous KD mice were significantly limited in physical activity, while both mutant genotypes showed difficulty in learning or remembering features for discriminating a novel object or recognizing a littermate [55]. The reduced cholinergic tone due to a slow refilling of synaptic vesicles in homozygous KD mice was displayed through an alteration in basic cognitive capacity, especially functions requiring a prolonged cholinergic involvement [56].

In addition, homozygous KD mice displayed impaired cardiac function related to autonomic imbalancebetweenparasympatheticandsympathetic tone that was rescued by pyridostigmine [57, 58].

Further proof that VAChT is rate-limiting for neurotransmission is derived from *Slc18a3* KO mice who died of respiratory insufficiency within 2 to 5 minutes following birth. However, small-amplitude and low-frequency MEPPs were detected in embryonic NMJs, probably due to a spontaneous ACh entry into presynaptic vesicles. Indeed, a lack of VAChT leads to the increase of CHAT and CHT expression, and subsequently of cytoplasmic ACh levels. Although, they demonstrated alterations in neuromuscular development like an absence of ACh, proving that passive ACh uptake by vesicles cannot compensateforVAChTdeficiency[59].Similarfeedba ck mechanisms were detected in *C. elegans* by Zhu H. et al [60].

Conversely, heterozygous KO mice presented no locomotor activity dysfunction, no alteration in MEPPs or in NMJ morphology [59].

To avoid the interference from impaired peripheral cholinergic function, Martin-Silva C. et al. generatednovelmutantlineswithintactVAChTexpress ion in the somatomotor cholinergic neurons, but significant reductions in the other cholinergic neurons. This technique allowed them to alter only brain cholinergic activity, resulting in the hyperactive behaviour of mice [61]. Deleting *Slc18a3* from their forebrain impaired spatial memory, cognitive flexibility, and sustainedattention[62,63];andknockingitoutofthe striatum caused different degrees of short-term memory deficit [64]. These studies provide evidence that ACh is fundamental to control locomotor function and to modulate hippocampal memory.

Finally, Cre-loxP technology has allowed for the deletion of Slc18a3 in select groups of motoneurons (*mnVAChT*-KD). Mutant mice have atrophy in muscle fibres innervated by *mnVAChT*-KD and appear hypoactive, leaner and with kyphosis and less muscle strength [65] (Table 2).

Findings from mice models trace once again the humanphenotypefromamotor,cardiacandcognitive point of view. Notably, a compromised cardiac pump functionwasfoundbothinhomozygousKDmiceand in

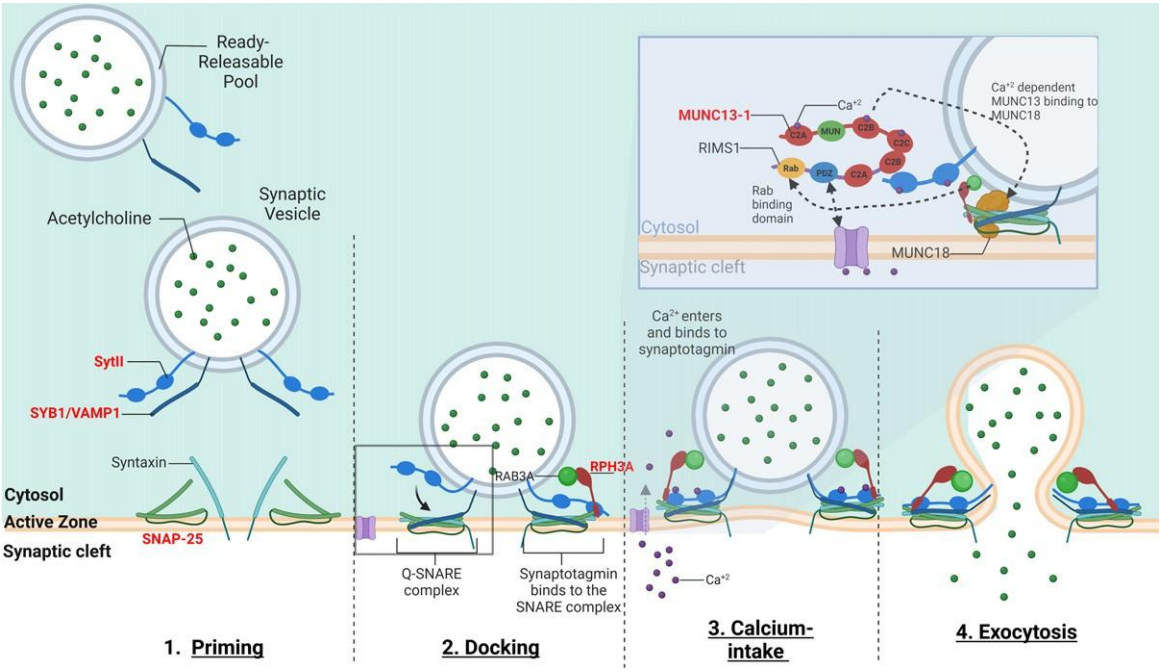

Fig. 3. – The mechanism of calcium-dependent synaptic vesicle exocytosis at the NMJ: The ready releasable pool (RRPs) of synaptic vesicles containing ACh. When activated, the synaptic vesicle moves towards the pre-synaptic membrane terminal where calcium influx releases the synaptic vesicle bound to actin and other cytoskeletal elements (not shown in image). The "Active Zone" is the area at the pre-synaptic terminal membrane where exocytosis occurs. 1. The pool of synaptic vesicles is termed the "readily releasable pool" (RRP) and is necessary to respond to an electrical impulse. Synaptotagmin II (SytII) and Synaptobrevin/VAMP1 (SYB1/VAMP1) proteins attach to the outer synaptic vesicle membrane forming the soluble N-ethylmaleimide-sensitive factor (NSF) attachment protein receptor (SNARE) complex. The cell membrane contains SNAP-25 and syntaxin components essential to the fusion of the vesicle and the cell membrane. 2. Docking – Here as the synaptic vesicle moves closer to the cell membrane, the SNARE complex begins to form 3. When an action potential depolarizes the pre-synaptic membrane, this causes the excitation of voltage-gated calcium channels and calcium entry. Calcium binds to both C2-domains (C2a and C2b) of SytII which induces a simultaneous binding of the vesicle to the cell membrane while completing the formation of the SNARE complex. Calcium induced binding of the SNARE complex requires additional proteins for vesicle exocytosis. MUNC18-1 inhibits the formation of the SNARE complex, locking syntaxin in a closed conformation, upon calcium induction MUNC18-1 interacts with MUNC13-1 opening the syntaxin conformation enabling the formation of the SNARE complex. This change in syntaxin conformation enables the binding of SYB1/VAMP1 initiating the fusion of the synaptic vesicle and cell membrane. In addition, MUNC13-1 contains C1, C2A, C2B, and C2C domains which sequester calcium. MUNC13-1 also contains a central MUN domain. Importantly, Rab3-interacting molecule (RIMS1), which serves as an active zone scaffolding protein has been shown to interact with proteins ELKs and RIM-BPs. RIMS1 also interacts with MUNC13-1 by preventing homodimerization and recruiting MUNC13s towards the active zone. RIMS1 also serves as a key regulator as it acts upon MUNC13 and 18, which are essential in determining the number of release sites and in the fusion of competent vesicles. RIMS1 can interact directly with the voltage-gated calcium channels at the presynaptic membrane, but altering the density of calcium channels present at the active zone, hereby effecting the size of the RRP. 4. The vesicle and cell membrane fuse together, the SNARE complex "zippers" the vesicle tightly to the cell membrane releasing ACh and other proteins into the synaptic cleft. Genes implicated in CMS are in red.

an affected patient, benefiting from AchEI [10]; as wellascompromisedhippocampalandothersuperior functions, that were identified as significant deficits in attention span, working memory, and immediate and delayed visual memory in a formal psychometric assessment of the same patient [10].

ACETYLCHOLINE VESICLES EXOCYTOSIS

VAMP1/SYB1

The vesicle-associated membrane protein (VAMP), also called synaptobrevin (SYB) is part

of the soluble N-ethylmaleimide sensitive factor attachment receptor (SNARE) complex, in association with syntaxin1 and synaptosomal-associated protein 25 kilodalton (kDa). The SNARE complex is involved in the fusion of synaptic vesicles with the presynaptic plasma membrane for the subsequent ACh release into the synaptic cleft [66] (Fig. 3).

SYB1/VAMP1 CMS is an autosomal recessive disorder, occurring at birth. To date, nine patients have been described with a typical phenotype characterized by generalized hypotonia and muscle atrophy, bulbar dysfunction, feeding difficulties, delayed motor milestones, joint contractures or laxity, kyphoscoliosis and respiratory distress, perhaps caused by pulmonary infections [67–69]. Elongated myopathic face with ophthalmoparesis, frontal bossing, low set ears and high arched palate have also been reported [69, 70]. RNS revealed a decremental response in one case, with synaptic facilitation indicating a presynaptic defect [67] and an incremental response in others [68, 70]. Therapy with pyridostigmine led to a variable degree of improvement. In one ofthemostrecentlyreportedpatients,salbutamolwas administered in addition with pyridostigmine with some benefit [69] (Table 1).

Several VAMPs have been targeted in mice and different phenotypes elicited depending on the mutated isoform. Two highly homologous isoforms, *VAMP1/SYB1* and *VAMP2/SYB2*, have been detected in neurons and in nerve terminals of the NMJ [71].

A nonsense mutation in *Vamp1/Syb1* truncated nearly half the protein, resulting in a lethal-wasting mutant phenotype (*lew*) in mice. *Vamp1/Syb1*$^{lew/lew}$ mice displayed altered movements of paws and legs, becoming progressively immobile before death within three weeks [72]. While motor endplates developedwithnodelayin*Vamp1/Syb1*$^{lew/lew}$ mice, spontaneous and evoked synaptic activities were reduced [71]. The minimal registered activity was probably due to the presence of SYB2, which can partially compensate for the absence of SYB1, but its presence in the spinal cord is not enough to guarantee *Vamp1/Syb1*$^{lew/lew}$ mice survival. However, SYB2 plays a critical role in the sensitivity to calcium-triggered vesicle release [71]. Indeed, the complete lack of SYB2 drastically reduced evoked synaptic activity in hippocampal neurons of *Syb2*$^{-/-}$ mouse embryos, while spontaneous miniature excitatory currents had normal amplitude and rise time. Mice died immediately after birth, exhibiting body shape dysmorphism [66].

To examine the link between *Syb1* and *Syb2*, Liu Y. et al. compared *Syb2*$^{-/-}$ to *Syb1*$^{lew/lew}$*Syb2*$^{-/-}$ mice. Both presented with increased intramuscular nerve branching. Moreover, in the latter, evoked synaptic transmission was completely abolished and spontaneous ACh release was insensitive to calcium [73] (Table 2).

Human clinical features are relatively milder than themousemodel.SalpietroV.etal.suggestedthepossibility of a species-specific compensation of vesicle fusion and release at the nerve terminal to explain this difference [68]. Electrophysiological results in mouse models can explain the synaptic facilitation detected in some patients, but there is no evidence of increased intramuscular nerve branching. Since the molecular pathways involving VAMP1 are still not clear, we need research to deeply understand its role at the NMJ.

SNAP25

The Synaptosomal-associated protein 25 kDa (*SNAP25*) gene is located on chromosome 20p12.2 and encodes for a protein that is part of the SNARE complex (SNAP25). SNAP25 and syntaxin1 mediate the fusion of synaptic vesicles to presynaptic plasma membrane where they are docked. (600322, OMIM). (Fig. 3) An obligate alternative splicing of two exon 5 sequences in *SNAP25* can result in two isoforms of SNAP25 (SNAP25A and SNAP25B), which are identical except for 9 residues. In the mouse brain, SNAP25B replaces SNAP25A by the second postnatal week, as the adult-specific isoform [74].

The first report of *SNAP25* CMS dates to 2014, when a *de novo* dominant mutation of the isoform *SNAP25B* (c.200T>A; p.Ile67Asn) was identified in a patient who presented with foetal hypomotility, cyanosis, and joint contractures at birth. During childhood, she exhibited developmental delay with epileptic absence episodes, confirmed by EEG, and

developed eyelid ptosis, fatigable weakness, dysarthria, and ataxic gait. The response to RNS was decremental. Therapy with pyridostigmine was ineffective, while 3,4-DAP along with levetiracetam for seizures, resulted in some improvements [74] (Table 1).

While not in our original literature search time frame (from January 2000 to March 2022), a recent publication has reported another *de novo SNAP25B* mutation (c.529C>T; p.Gln177X). The patient died in the sixth day of life due to respiratory failure. Prenatal ultrasound revealed multiple anomaliesincludingseverepolyhydramniosandmulti ple findings consistent with arthrogryposis such as micrognathia, right clubfoot, left rocker-bottom foot, diffuse skin thickening, and hypomobility [75] (Table 1).

Like other forms of presynaptic CMS, the phenotype observed in the mouse models was more pronouncedthaninthepatient.Heterozygous*Snap25* null mutant mice were phenotypically indistinguishable from WT, while homozygous mice were embryologically lethal with smaller body size and no spontaneous movements. Evoked ACh release was abolished at NMJs, proving that the SNARE complex is crucial for Ca^{2}+-triggered synaptic transmission and explaining the lethality as linked to failure of diaphragm contraction [76].

As well as the peripheral nervous system, SNAP25 is highly expressed by neurons in the central nervous system. Which may explain the presence of central neurologic manifestations such as seizures and ataxic gait in patients.

The *Snap25* mouse model obtained by creating a missense mutation in a highly conserved domain of the SNAP25b isoform has been termed the “blind-drunk mouse”. These mice display ataxic gait with behavioural impairment resembling that of schizophrenia. They also have a lower frequency of evoked cortical excitatory postsynaptic potentials [77].

A brain-specific *Snap25* KO mouse also demonstrated behaviour signs related to schizophrenia. The reduction of *SNAP25* expression in the cortex caused a remarkable elevation of extracellular glutamate levels, resulting in abnormal hyperactivity and stereotypical behavior [78]. Hoerder-Suabedissen et al. produced a transgenic mouse with cell-specific loss of *Snap25* from cortical projection neurons (cKO). cKO mice were viable at birth with normal neuronal development, but axonal projections became fragmented and deteriorated three weeks later [79].

In 2010, McKee A.G. et al. over-expressed *Snap25* in the adult rat dorsal hippocampus by infusion of a recombinant adeno-associated virus vector. They noticed a defect in synaptic function resulting in cognitive deficits, such as delayed acquisition of spatial and fear memory consolidation. Hence, both reduced and excessive Snap25 activity has been implicated in memory and cognitive function impairment [80] (Table 2).

Theonlyreportedpatientdidnotsufferfromcognitive and behavioural alterations. However, we should consider these features as part of *SNAP25* CMS clinical pictures in order to reduce misdiagnoses of this type of CMS.

SYT2

The Synaptotagmin 2 (*SYT2*) gene encodes for a synaptic vesicle membrane protein (SYT2) that works as a calcium sensor in vesicular trafficking and exocytosis (GC01M202559, GeneCards) (Fig. 3).

SYT2 CMS can be inherited in either an autosomal dominant or a recessive manner. The former pattern was described in patients mainly with a childhood onset [81–83], although not exclusively [84]. The latter, was associated with early onset and a more severe phenotype, characterized by reduced foetal movements, hypotonia at birth, joint laxity, and delayed motor milestone [85–87]. Typical manifestations include muscle weakness and fatigability, variable muscle atrophy and reduced or absent deep tendon reflexes, partially reversible after exercise [81]. Ocular involvement has been reported in a few families [82]. Other common features are foot deformities, such as *pes cavus* and hammer toe, and lower limbs sensitivity alterations [81, 82]. Sometimes electromyography of distal muscles detects a slight reinnervation, that is consistent with a motor neuropathy [81, 86]. Electrophysiological studies revealed low-amplitude CMAPs and a

certaindegreeofpostexerciseamplitudefacilitation[81, 83]. Therapy with 3,4-DAP ameliorated both clinical and electrophysiological manifestations, as did pyridostigmine and salbutamol in some patients [82, 84–87] (Table 1).

The role of SYT2 was first examined in *Drosophila*, in which a decrease of evoked transmitter release and its calcium-affinity was obtained through mutating two aspartate residues in the C_2B calcium-bindingpocketofSYT2[88].Morerecently, Shields. et al. reproduced the human substitution of a leucine with a proline in position 308 ($syt^{L\text{-}P}$), in the same domain of *Drosophila* SYT2, via panneuronal expression of *syt* transgenes in the syt^{null} background. SYT2 is substituted by other isoforms in flies, but $syt^{L\text{-}P}$ results in lethality in the absence of WT *syt*. Heterozygous $syt^{L\text{-}P}$ were viable and showed marked fatigability, less motor capacity and reducedevokedtransmitterrelease,similartohumans [89].

Analogous results were obtained from mice with a point mutation in *Syt2*, resulting in a decreased neurotransmitter calcium-dependent release in the Calyx of Held. Mice were viable but infertile, presenting smaller and severely ataxic in a homozygous state [90]. These results were further confirmed in *Syt2* homozygousKOmice,whichdisplayedseveremotor dysfunction two weeks after birth and died after three weeks [91].

Finally, experiments on *syt2* MO KD zebrafish showed a reduction in synchronous release that was responsible for around 90% of the neuromuscular transmission [92] (Table 2).

UNC13A

*UNC13A*encodestheproteinMUNC13-1whichis a protein of the presynaptic active zone in cholinergic neuromuscular synapses and glutamatergic brain synapses that is involved in synaptic vesicle priming [93]. It binds the SNARE protein syntaxin 1B, shiftinginclosedconformationthepositionofMunc18-1, that normally stabilizes syntaxin 1B. In this way, syntaxin 1B is active and contributes to form the SNARE complex for vesicles exocytosis [94] (Fig. 3).

UNC13A CMS has been reported in only one patient with a homozygous nonsense mutation. The patient was born prematurely, presenting with hypotonia, feeding difficulties and respiratory distress with cyanotic episodes. She developed some dysmorphisms (marked frontotemporal narrowing, high-arched palate, small jaw, thoracic kyphoscoliosis, clinodactyly and joint contractures), delay in motor function acquisition, eyelid ptosis and reduced oculomotion. Clinical features comprised microcephalyandcorticalhyperexcitability.EMGreve aled low-amplitude CMAPs at rest, decremental response to low-frequency RNS and an incremental response to high-frequency. Therapy with pyridostigmine and 3,4-DAP slightly improved her symptoms, but the child died around 4 years old [94] (Table 1).

This type of CMS looks like a syndromic disorder, comprising a marked involvement of the central nervous system supported by the fact that MUNC131 has been abundantly shown in rat brain. Two other minor isoforms of the protein are MUNC132 and MUNC13-3 that are expressed in the rostral brainregionandcerebellum,respectively.MUNC131 mice died postnatally because of a deficiency in synaptic vesicle exocytosis in the central nervous system. While Munc13-3 mice presented parallel fibre–Purkinje cell synapses of normal morphology but altered function, with a negative impact on motor learning [93]. Varoqueaux et al. created mice with a double deletion of *Munc13-1/2* and triple deletion of *Munc13-1/2/3* and, once more, the absence of MUNC13-1 resulted in lethality for both. Experiments on embryos, presenting paralyzed, showed morphological alterations in NMJs such as abnormal nerve terminal branching, larger endplates and improper alignment of muscle fibres. Evoked synaptic transmission was reduced while spontaneous release persisted [95].

UNC13A was also evaluated in *C. elegans* as the ortholog *unc-13*, which shares similar C1 and C2B domains that are essential for neurotransmission regulation. Removal of either the C1 or C2B domain enhanced calcium-triggered synaptic transmission,

while deletion of both domains stopped synaptic transmission. Indeed, *unc-13* null mutants were paralyzed, but the rescue of a single copy of *unc-13* or of the protein lacking only C2B domain reverted to normal locomotion [96].

Motor impairments, altered learning, and reduced synaptic transmission from mouse and C. *elegans* models reflect *UNC13A* CMS, resulting in lethality in a homozygous state.

OTHER PRE-SYNAPTIC MECHANISMS

MYO9A

The Myosin IXA (*MYO9A*) gene encodes for an unconventional myosin that is an actin-based motor molecule that inhibits RhoA by stimulating its GTPase activity (MYO9A) (GeneCards, GC15M071822) (Fig. 4A).

To date, three patients of German and Turkish origin have been described in a single publication [15]. They variably presented with ptosis and ophthalmoplegia, bulbar dysfunction, generalized muscle weakness, hypotonia, episodic apnoea and respiratoryfailureatbirth.Duringfollow-up,developmental delayandsomecognitiveabnormalitieswereevident. SFEMG detected abnormal jitter and RNS revealed a decremental response in one patient. The best treatment approach remains ambiguous as the German patientrespondedtopyridostigmineand3,4-DAP,but the Turkish siblings suffered from a respiratory crisis after oral intake of 3.4-DAP and fluoxetine [15] (Table 1).

MYO9A CMS presents a complex clinical picture, probably due to the ubiquitous expression of this protein. Rho activity is involved in morphology and differentiation of ciliated epithelial cells and renal proximal tubules, reflecting different aspects of *MYO9A* mutated animal models.

Myo9a deficient mice developed severe hydrocephalus with enlargement of lateral and third ventricles and stenosis of the Sylvian aqueduct. As a result, they displayed hopping and a trembling gait in adulthood [97]. They also developed bilateral renal disease, characterized by dilated renal calyces and parenchyma fibrosis, leading to polyuria and proteinuria [98]. Folci et al. demonstrated that MYO9A plays a role in hippocampal synapses and cognitive behaviour. *Myo9a* heterozygous KO mice presented with structural and molecular changes in hippocampal synapses, affecting learning and memory tasks as in reported patients [99].

Recently, the function of MYO9A at the mammalian NMJ was examined and while its exact location has still not been determined, several pieces of evidence suggest a presynaptic role [15]. A zebrafish model, in which the *MYO9A* orthologues, *myo9aa* and *myo9ab*, were knocked down using morpholinos developed curly tails, cardiac oedema, and

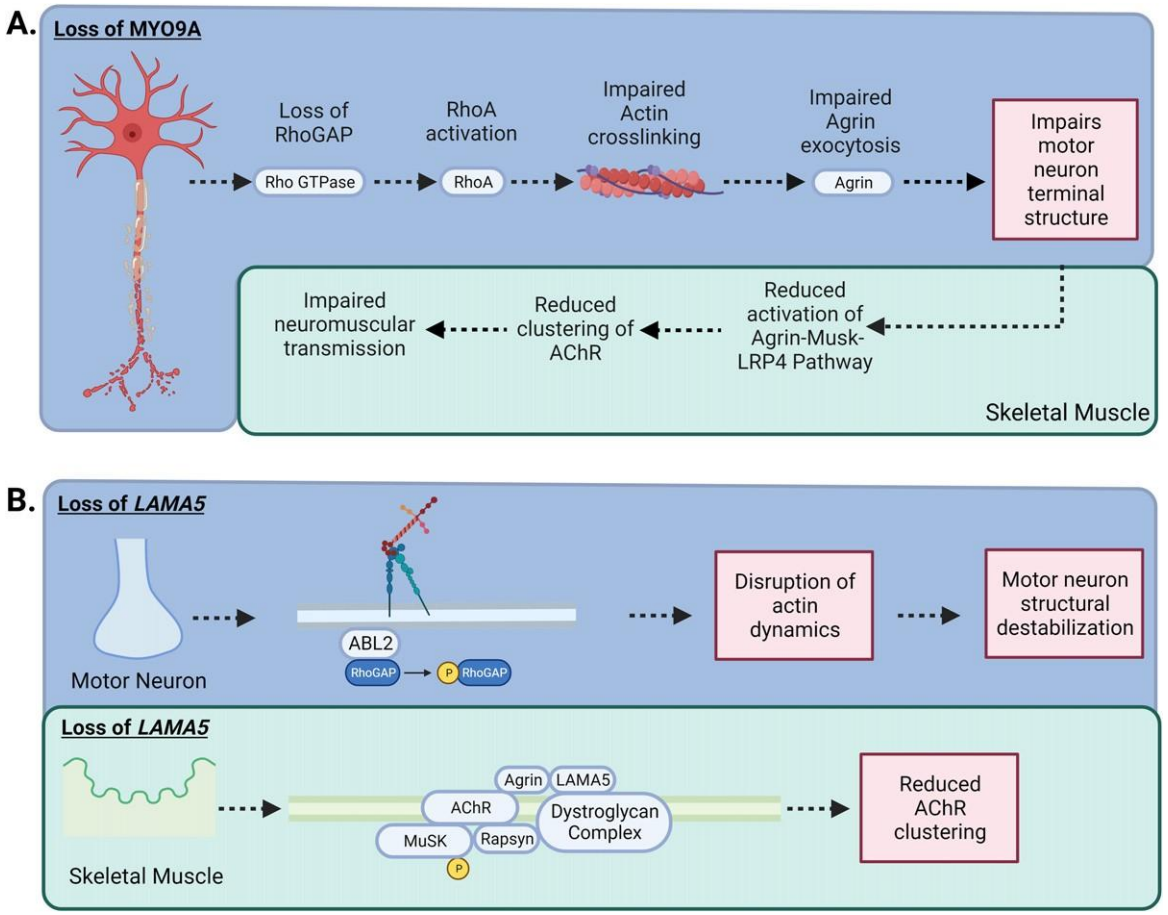

Fig. 4. – MYO9A and LAMA5 in CMS: A) Loss of MYO9A has been shown to impair actin cross-linking, causing an alteration in the growth of axons and terminal structure. In addition, RhoGAP activity is impeded, increasing the activation of the RhoA pathway, impairing the nerve cytoskeleton and intracellular transport resulting in compromised secretion of agrin. A reduction in agrin secretion results in less activation of the Agrin-MuSK-LRP4 AChR clustering pathway. B) Laminins are the most abundant non-collagenous protein in the basal lamina. There are five extracellular matrix heterotrimeric glycoproteins composed of , , and subunits. Laminins are involved in cell signalling, development and maintenance of the NMJ, and regeneration of the nerve terminal. While Laminin 5 (LAMA5) function has not been fully elucidated, CMS patients with mutations in *LAMA5* have a reduction in the number of synaptic vesicles present for release due to the small size in nerve terminals and a reduction in the number of active zones. In addition, specific mutation to the coiled-coil domain *LAMA5* may play a role in preventing interaction with other laminins causing dysfunctional agrin secretion.

abnormal swimming in response to tactile stimulation. The axons were aberrant, branching to the adjacent myotome beyond their target [15].

Based on the results from *Myo9a*-depleted NSC34 cells (mouse motor neuron-derived cells), the same group demonstrated an impaired trafficking and release of proteins in the absence of *Myo9a*. One of these proteins, agrin, is crucial for the proper development and function of the postsynaptic endplate. It was hypothesized that some of the aberrations in the *myo9a* morphant fish were due to its reduction. This theory was confirmed in deficient *myo9aa/ab* zebrafish, obtained through a CRISPR/Cas9 approach where injection of morphants and crispants with agrin improved their locomotion and NMJ morphology [100, 101].

Animal models' motor and behaviour alterations partly match the human phenotype. Patients' hypotonia and muscle weakness assume the same pathophysiological mechanism of zebrafish abnormal swimming. In addition, patients present with cognitive impairment, similar to mice who display learning and memory defects. However, there is no evidence of hydrocephalus in reported

patients, whose brain MRIs are normal, and there is no evidence of renal dysfunction.

PREPL

Prolyl Endopeptidase-Like (PREPL) is a ubiquitous serine protease, highly expressed in the brain, kidney and muscle. Its function remains partly elusive, but it is probably involved in the control of the trans-Golgi network morphology and sorting, as well as in the regulation of synaptic vesicle exocytosis (GC02M044281, GeneCards; 609557, OMIM)
(Fig. 2).

Deletions of *PREPL* in combination with other genes at the 2p21 chromosomal region are associated with different variants of the hypotonia-cystinuria syndrome (HCS), characterized by cystinuria, neonatal hypotonia, eyelid ptosis, occasional bulbar symptoms, and growth hormone deficiency [102]. Some of these features suggest a neuromuscular transmission defect, but the first case diagnosed with a myasthenic syndrome related to PREPL deficiency was reported by Regal L. et al. The patient presented′ with marked hypotonia and feeding difficulties at birth, later associated with ptosis and daily fluctuating proximal muscle weakness. Electrophysiology studies revealed low amplitude MEPPs. Additionally, growth hormone blood levels were deficient. Genetic analysis detected compound heterozygosity for a paternal nonsense mutation in *PREPL* (p.Met270Ter) and a maternal deletion involving *PREPL* and *SLC3A1* (one of the genes causing HCS). The patient improved with pyridostigmine treatment and did not worsen after weaning off the medication [103]. Other patients have been recently reported with similar features and various combinations of facial dysmorphism, developmental delay, hypergonadotropic hypogonadism, and childhood obesity [104–108]. One patient with a splicing mutation in the *PREPL* gene was characterized by the absence of a uterus and ovaries, microcephaly and short neck [109] (Table 1).

PREPL is a unique protein, different from the others in the family, because it plays a role in proteinprotein interactions rather than in peptide proteolysis [110]. It shows homology with prolyl endopeptidase (PREP), whose knock-down in mice produced an impairment in spatial learning and memory, due to its expression in hippocampus and entorhinal cortex [111]. Deletion of *Prepl* in mice led to hypotonia in five-day old pups and impaired growth, as reported in patients. Therefore, it could be also
hypothesizedanunderlyingreducedgrowthhormone signalling, remarking patients' phenotype [110] (Table 2).

LAMA5

Laminin alpha-5 (LAMA5) is part of the laminins family, a group of extracellular matrix glycoproteins that participate in several biological processes. LAMA5 is widely expressed in vertebrate tissues and mediates cellular attachment and migration during embryonic development (GC20M062307, GeneCards) (Fig. 4b).

Currently, the only described *LAMA5* CMS was caused by a homozygous missense mutation, resulting in a deficient number of releasable SVs. Indeed, the mutant *LAMA5* reduces cell adhesion and neurite outgrowth, and influences agrin attachment to the extracellular matrix. Furthermore, the reported mutation impairs the interaction between LAMA5 and the synaptic vesicle glycoprotein 2A (SV2A), which in turn binds to synaptotagmin, regulating the Ca2+dependent SVs exocytosis.

LAMA5 CMS patient presented with a multifaceted phenotype. Clinical features comprised congenital hypotonia and respiratory failure, scoliosis, chronic inflammatory bowel disease, neck and limb muscles weakness. Dysmorphic features, myopia, bilateral ptosis, facial muscles weakness and tics were also observed. RNS showed a marked decremental response and facilitation occurred after maximal muscle activation. The patient responded well to pyridostigmine and 3,4 DAP [14, 112]
(Table 1).

A more complex phenotype occurred in mouse models, which also demonstrated the role of LAMA5 in pulmonary [113, 114] and renal development [115]. For instance, *Lama5* KO mice died at the embryonic stage. Embryos presented with a defective anterior neural tube closure, syndactyly, aberrant genesis of kidneys and an absence of

visceral pleura basement membrane with reduced lobar lung septation [113]. To avoid early lethality, LAMA5 deficiency was restricted to lung epithelial cells but mice still died perinatally of respiratory failure due to marked abnormalities in lung development
[114].

However, a specific neuromuscular phenotype was obtained by creating a muscle specific KO *Lama5* mouse, showing a delayed pre- and postsynaptic differentiation in NMJs [116].

Inaddition,amissensemutationofthe*Lama5*gene was generated in mouse models via CRISPR-Cas9 genomeediting,furtherelucidatingtheimportanceof the role of laminin in tissue development and homeostasis. Mutant mice showed defective foetal growth and developmental abnormalities. Similar alterations occurred in the reported patient, such as elongated face, elevated hard palate, and eye defects, reflecting the role of LAMA5 in embryonic development
[117].

Finally, comparable results were obtained from zebrafish, in which LAMA5 deficiency led to an altered formation of pectoral fins and a lack of fin folds, highlighting its role in basement membrane integrity [118] (Table 2).

RPH3A

Rabphilin 3a (*RPH3A*) encodes for the protein RPH3A, which is involved in docking and fusion steps for neurotransmitter release. Specifically, at the presynaptic level, RPH3A is recruited to the synaptic vesicle membrane binding 14-3-3 protein, Ca2+, phosphatidylinositol 4,5-bisphosphate (PIP2) and SNAP25tomodulatevesicletraffickingandcalciumtri ggered exocytosis (GC12P112570, GeneCards) [119].

An 11-year-old girl with a heterozygous mutation in*RPH3A*wasdescribedbyMaselliR.A.etal.During early childhood, she presented with limb weakness andfatigability,laterfollowedbyhandtremors,hands incoordination,posturalimbalance,andnasalspeech. She also had learning disabilities with no abnormalities at brain MRI and EEG. High frequency RNS revealed and increment of 30% of CMAP areas and SFEMG detected an increased jitter. A favourable response to treatment with albuterol sulfate was shown. The authors demonstrated a synaptic vessicle density reduction, an increase in nonvesicular synaptic membranes, and the presence of degenerative lamellar bodies in the patient NMJ [119] (Table 1).

The exact function of RPH3A in the NMJ has not been completely elucidated. A null mutation in *rbf-1,* the *RPH3A* homolog in *C. elegans*, did not alter NMJ general morphology, nor defecation, pharyngeal pumping, and mating assays. *Rbf-1* mutants appeared lethargic in absence of exogenous stimulation. Indeed, RPH3A alterations seemed synergic with SNARE complex's ones, but *rbf-1* mutants did not enhance the behavioural defects of synaptotagmin mutants. Thus, the role of RPH3A in the Ca^{2}+-sensitiveSVsreleaseisstillcontroversial[120] (Table 2).

PRE- AND POST-SYNAPTIC MECHANISMS

Mitochondrial genes

It has long been thought that mitochondria play a critical role at the NMJ, partly due to their clustering at the synapse. Solute carrier Family 25 Member 1 (*SLC25A1*) encodes the mitochondrial citrate carrier across the inner mitochondrial membrane. (GC22M019407, GeneCards) Hence, *SLC25A1* mutations result in an impaired citrate/isocitrate export from mitochondria, and subsequently increased excretion of 2-hydroxyglutaric acid. This condition was reported in an 18-monthold female manifesting poor sucking, hypotonia, and prolonged apnoeas at birth, followed by psychomotor retardation, epilepsy, sensorineural deafness, and radiological evidence of corpus callosum agenesia and optic nerves hypoplasia [121]. Other patients with a variable associations of speech and motor developmental delay, learning difficulties, fatigable weakness, ptosis, and diplopia were later described, recognizing a link between SLC25A1 and altered NMJ transmission [122–126]. Indeed, SFEMG examination showed increased jitter or jitter with blocking and RNS detected a decremental response with some clinical improvement after therapy with

3,4-DAP or AChEI. Interestingly, reflexes werereducedatrestwithpost-exercisepotentiationin one patient, suggesting a presynaptic alteration [123, 124].

This hypothesis was corroborated by the *SLC25A1* zebrafish orthologues knocking down via antisense MOs injection. The animal model presented a motor impairment similarly to humans, displaying altered tail morphology, swimming, and touchevoked escape responses. Furthermore, histological NMJ evaluation revealed short motor axon terminals with incomplete synapse formation [123]. Indeed, mitochondria are crucial for the presynaptic nerve terminal function since it requires a high energy demand [124] (Table 2) [127–129]. To date the *SLC25A1* mutation is the only mitochondrial mutation described to cause CMS. However, given the importance of mitochondria to neurotransmission it is likely future mutations will be described necessitating the creation of a fifth 'mitochondrial CMS' group.

CONCLUSIONS

Presynaptic CMS are very rare neuromuscular disorders, only comprising 5-10% all CMS types. Most proteins involved in presynaptic function are highly expressed in the central nervous system and other tissues besides the motor endplate, complicating the clinical picture. Some types of CMS classified in other groups, such as postsynaptic or glycosylation defects CMS, result from the alteration of proteins which may partly influence the presynaptic site. A low or no presence of motor neuron axon branches wasdemonstratedatthepresynapticzone,aswellasa reduced quanta number available for release, resulting in a decreased endplate quantal content in two cases of glycosylation CMS [130, 131]. Frequently, CMS phenotypical and genotypical heterogeneity makes diagnosis challenging and delays treatment.

Clinicians can exploit animal models to deeply consider the pathophysiology of CMS, from which the broad spectrum of their clinical features derives. Recent technologies have allowed us to create ever more valid models, limiting off-target effects and providing a reliable substrate to test new drugs.

Many different animals have been used to study the organization and function of the NMJ, including C. elegans, D. melanogaster, zebrafish, and mice. Since the mouse NMJ is large and easily accessible, mouse models are currently the most functional option to investigate histologically and electro-physiologically. Moreover, they allow testing the clinical disease severity by objective measurement of muscle strength and fatigue, repeating the evaluation during the disease course and after treatment [132].

However,thelocalizationofmanypresynapticproteins even in the central nervous system has made presynaptic animal models hard to produce. The central clinical manifestations may cover or alter the NMJ features. Additionally, since most presynaptic proteins are essential for animal survival, specific techniques of NMJ gene modulation are needed. In general, presynaptic gene-KO mice are lethal at the embryonic stage in a homozygous state, preventing the possibility of studying the genetic pathomechanisms. Although, Cre-loxP technology enables gene deletion in select groups of cells such as motoneurons. There are however differences between human and mouse NMJs: anatomically human NMJs are smaller, have a higher folding index and active zone density, lower quantal content, and lower safety factor; finally, protein expression is quite different, influencing NMJ function. Proteomic profile analysis shows no significant variation between the two species. However, the expression profile highlights distinct expression levels for 97% of at least 36 distinct nervous system-related molecular pathways impactingonNMJs.Theyincludesynapticsignalling pathways, particularly, those related to agrin [133, 134].

C. elegans is another useful model to examine neurotransmission mechanisms, in particular at the presynapse, due to the conservation of many pathways between the nematode and mammals. C. elegans is a simple and transparent model to analyse gene and protein expression patterns using fluorescence [135].

Zebrafish is an advantageous model as many pathways of muscle development and differentiation are conserved between zebrafish and mammals.

Zebrafish muscle has similarities to human, sharing some components of the sarcomere and contraction machinery [136]. NMJs are cholinergic with pentameric nicotinic ACh receptors at the postsynaptic membranelikehumans.Inaddition,zebrafishpresent many synaptic molecules with a similar function in mammals. Finally, the transparent nature of this animal is useful for the characterization of genes and proteins' activity *in vivo* [137].

Morpholino oligonucleotides (MOs) are an efficient method of gene-specific antisense knockdown, frequently used in zebrafish. However, the knockdown effectiveness is not always clear and off-target effects may complicate interpretation of findings. MOs could inhibit an irrelevant gene instead of, or in addition to, the intended gene [138]. Moreover, they are a short acting and must be injected at the embryos stage. Recently, crispr-technology has been employed for both short-term observations ("crispants") as well as generating stable zf lines with specifically engineered mutations [139].

However,insomesituationsanimalmodelsmaybe inappropriatetoprovideevidenceoftheentirehuman genotypic heterogeneity. For example, most animal models have been created via a knocking out mechanism mimicking a null gene mutation. However, the majority of patients present with missense mutations which preserves the function of the encoded protein at least in part. Thereby, the distinct phenotypes between humans and animal models depend on both species properties and different types of mutations with their impact on the relative protein structure and function. While many presynaptic CMS causative genes have recently been discovered, we lack reproducible and reliable animal models. However, they remain a valid tool to determine drugs' mechanism of action and response [140].

Finally, the NMJ has also been studied across a wider range of mammalian species such as cat, dog, pig, and sheep, showing that the latter is most similar to humans [141]. Hence, the opportunity to use large animal models for a more accurate NMJ diseases study should be considered.

In conclusion, animal models still present several limitations in reproducing human genotypes and phenotypes and many molecular details about NMJs need to be elucidated. However, a bilateral exchange between clinical and preclinical studies offers the only promising way to increase our recognition of CMS.

ACKNOWLEDGMENTS

All figures were created with BioRender.com.

FUNDING

HL receives support from the Canadian Institutes of Health Research (Foundation Grant FDN-167281, Team Grant ERT-174211), the Canadian Institutes of Health Research and Muscular Dystrophy Canada (NetworkCatalystGrantforNMD4CNG2-170044), the Canada Foundation for Innovation (CFI-JELF 38412), and the Canada Research Chairs program (Canada Research Chair in Neuromuscular Genomics and Health, 950-232279). AP, HL and CR are members of the European Reference Network for rare, neuromuscular diseases ERN EURO-NMD – Project ID No 739543. SH received support from the Bob Korneluk CHEO Trainee Research Grant and Ontario Graduate Scholarship (OGS).

REFERENCES

[1] Engel AG, Shen XM, Selcen D, Sine SM. Congenital myasthenic syndromes: Pathogenesis, diagnosis, and treatment. *Lancet Neurol*. 2015;14(4):420-434. doi:10.1016/S1474-4422(14)70201-7

[2] Mihaylova V, Scola RH, Gervini B, et al. Molecular characterisation of congenital myasthenic syndromes in Southern Brazil. *J Neurol Neurosurg Psychiatry*. 2010;81(9):973-977. doi:10.1136/jnnp.2009.177816

[3] Natera-de Benito D, Topf A, Vilchez JJ, et al. Molecu-¨ lar characterization of congenital myasthenic syndromes in Spain. *Neuromuscular Disorders*. 2017;27(12):10871098. doi:10.1016/j.nmd.2017.08.003

[4] Parr JR, Andrew MJ, Finnis M, Beeson D, Vincent A, Jayawant S. How common is childhood myasthenia? The UK incidence and prevalence of autoimmune and congenital myasthenia. *Arch Dis Child*. 2014;99(6):539-542. doi:10.1136/archdischild-2013-304788

[5] Abicht A, Muller JS, Lochm¨ uller H. Congenital Myas-¨ thenic Syndromes Overview. 2003 May 9 [updated 2021 Dec 23]. In: Adam MP, Ardinger HH, Pagon RA, Wallace

SE, Bean LJH, Gripp KW, Mirzaa GM, Amemiya A, editors. GeneReviews® [Internet]. Seattle (WA): University of Washington, Seattle; 1993–2022. Accessed March 14, 2022. https://pubmed.ncbi.nlm.nih.gov/20301347/

[6] Finsterer J. Congenital myasthenic syndromes. *Orphanet J Rare Dis*. 2019;14(1). doi:10.1186/s13023-0191025-5

[7] Iyadurai SJP. Congenital Myasthenic Syndromes. *Neurol Clin*. 2020;38(3):541-552. doi:10.1016/j.ncl.2020.03.004

[8] McMacken G, Whittaker RG, Evangelista T, Abicht A, Dusl M, Lochmuller H. Congenital myasthenic syndrome¨ with episodic apnoea: clinical, neurophysiological and genetic features in the long-term follow-up of 19 patients. *JNeurol*.2018;265(1):194-203.doi:10.1007/s00415-0178689-3

[9] Bauche S, O'Regan S, Azuma Y, et al. Impaired´ Presynaptic High-Affinity Choline Transporter Causes a Congenital Myasthenic Syndrome with Episodic Apnea. *Am J Hum Genet*. 2016;99(3):753-761. doi:10.1016/j.ajhg.2016.06.033

[10] O'Grady GL, Verschuuren C, Yuen M, et al. Variants in SLC18A3, vesicular acetylcholine transporter, cause congenital myasthenic syndrome. *Neurology*. 2016;87(14): 1442-1448. doi:10.1212/WNL.0000000000003179

[11] MaselliRA,ChenD,MoD,BoweC,FentonG,Wollmann RL. Choline acetyltransferase mutations in myasthenic syndrome due to deficient acetylcholine resynthesis. *Muscle Nerve*. 2003;27(2):180-187. doi:10.1002/mus.10300

[12] Ramdas S, Beeson D. Congenital myasthenic syndromes: where do we go from here? *Neuromuscular Disorders*. 2021;31(10):943-954. doi:10.1016/j.nmd.2021.07.400

[13] Regal L, Shen XM, Selcen D, et al.´ *PREPL Deficiency with or without Cystinuria Causes a Novel Myasthenic Syndrome. Neurology. 2014 Apr 8;82(14):1254-60. Doi: 10.1212/WNL.0000000000000295.*

[14] Maselli RA, Arredondo J, Vazquez J, et al. Presynaptic´ congenital myasthenic syndrome with a homozygous sequence variant in LAMA5 combines myopia, facial tics, and failure of neuromuscular transmission. *Am J Med Genet A*. 2017;173(8):2240-2245. doi:10.1002/ajmg.a.38291

[15] O'Connor E, Topf A, M¨ uller JS, et al. Identification of¨ mutations in the MYO9A gene in patients with congenital myasthenic syndrome. *Brain*. 2016;139(8):2143-2153. doi:10.1093/brain/aww130

[16] Matthies DS, Fleming PA, Wilkes DM, Blakely RD. The Caenorhabditis elegans choline transporter CHO-1 sustains acetylcholine synthesis and motor function in an activity-dependent manner. *J Neurosci*. 2006; 26(23):6200-6212. doi:10.1523/JNEUROSCI.503605.2006

[17] Keshishian H, Broadie K, Chiba A, Bate M. *19%. 1954575 Copyrighl 0 1996 by Annual Reviews Inc. All Righfs Reserved*. www.annualreviews.org

[18] Pardal-Fernandez JM, Carrascosa-Romero MC,´ Alvarez´ S, Medina-Monzon MC, Caama´ no MB, de Cabo C. A new˜ severe mutation in the SLC5A7 gene related to congenital myasthenic syndrome type 20. *Neuromuscular Disorders*. 2018;28(10):881-884. doi:10.1016/j.nmd.2018.06.020

[19] Banerjee M, Arutyunov D, Brandwein D, et al. The novel p.Ser263Phe mutation in the human high-affinity choline transporter1(CHT1/SLC5A7)causesalethalformoffetal akinesia syndrome. *Hum Mutat*. 2019;40(10):1676-1683. doi:10.1002/humu.23828

[20] Rodr´ıguez Cruz PM, Hughes I, Manzur A, et al. Presynaptic congenital myasthenic syndrome due to three novel mutations in SLC5A7 encoding the sodium-dependant high-affinity choline transporter. *Neuromuscular Disorders*. 2021;31(1):21-28. doi:10.1016/j.nmd.2020.10.006

[21] Wang H, Salter CG, Refai O, et al. Choline transporter mutations in severe congenital myasthenic syndrome disrupt transporter localization. *Brain*. 2017;140(11):28382850. doi:10.1093/brain/awx249

[22] AllenDD,SmithQR.*CharacterizationoftheBlood-Brain Barrier Choline Transporter Using the in Situ Rat Brain Perfusion Technique. J Neurochem. 2001 Feb;76(4):103241. Doi: 10.1046/j.1471-4159.2001.00093.x. Erratum in: J Neurochem 2001 Apr;77(2):704.*; 2001.

[23] Murakami H, Sawada N, Koyabu N, Ohtani H, Sawada Y. *Characteristics of Choline Transport across the Blood-Brain Barrier in Mice: Correlation with* in Vitro *Data. Pharm Res. 2000 Dec;17(12):1526-30. Doi: 10.1023/a:1007613326759.*; 2000.

[24] Ferguson SM, Bazalakova M, Savchenko V, Carlos Tapia J, Wright J, Blakely RD. *Lethal Impairment of Cholinergic Neurotransmission in Hemicholinium-3Sensitive Choline Transporter Knockout Mice*.; 2004. www.pnas.orgcgidoi10.1073pnas.0401667101

[25] Lund D, Ruggiero AM, Ferguson SM, et al. Motor neuron-specific overexpression of the presynaptic choline transporter: Impact on motor endurance and evoked muscle activity. *Neuroscience*. 2010;171(4):1041-1053. doi:10.1016/j.neuroscience.2010.09.057

[26] Bazalakova MH, Wright J, Schneble EJ, et al. Deficits in acetylcholine homeostasis, receptors and behaviors in choline transporter heterozygous mice. *Genes Brain Behav*. 2007;6(5):411-424. doi:10.1111/j.1601183X.2006.00269.x

[27] Paolone G, Mallory CS, Koshy Cherian A, Miller TR, Blakely RD, Sarter M. Monitoring cholinergic activity during attentional performance in mice heterozygous for the choline transporter: A model of cholinergic capacity limits. *Neuropharmacology*. 2013;75:274-285. doi:10.1016/j.neuropharm.2013.07.032

[28] Donovan E, Avila C, Klausner S, et al. Disrupted choline clearance and sustained acetylcholine release *in vivo* by a common choline transporter coding variant associated with poor attentional control in humans. *The Journal of Neuroscience*. Published online March 1, 2022:JN-RM1334-21. doi:10.1523/JNEUROSCI.1334-21.2022

[29] English BA, Appalsamy M, Diedrich A, et al. Tachycardia, reduced vagal capacity, and age-dependent

ventricular dysfunction arising from diminished expression of the presynaptic choline transporter. *Am J Physiol Heart Circ Physiol*. 2010;299:799-810. doi:10.1152/ajpheart.00170.2010.-Healthy

[30] Ohno K, Tsujino A, Brengman JM, et al. *Choline Acetyltransferase Mutations Cause Myasthenic Syndrome Associated with Episodic Apnea in Humans*. www.pnas.org

[31] Shen XM, Crawford TO, Brengman J, et al. Functional consequences and structural interpretation of mutations of human choline acetyltransferase. *Hum Mutat*. 2011;32(11):1259-1267. doi:10.1002/humu.21560

[32] Byring RF, Pihko H, Tsujino A, et al. *Congenital Myasthenic Syndrome Associated with Episodic Apnea and Sudden Infant Death*. www.elsevier.com/locate/nmd

[33] Liu Z, Zhang L, Shen D, et al. Compound heterozygous CHAT gene mutations of a large deletion and a missense variant in a Chinese patient with severe congenital myasthenic syndrome with episodic apnea. *Front Pharmacol*. 2019;10(MAR). doi:10.3389/fphar.2019.00259

[34] Zhang Y, Cheng X, Luo C, et al. Congenital Myasthenic Syndrome Caused by a Novel Hemizygous CHAT Mutation. *Front Pediatr*. 2020;8. doi:10.3389/fped.2020.00185

[35] Barisic N, Muller JS, Paucic-Kirincic E, et al. Clinical¨ variability of CMS-EA (congenital myasthenic syndrome with episodic apnea) due to identical CHAT mutations in two infants. *European Journal of Paediatric Neurology*. 2005;9(1):7-12. doi:10.1016/j.ejpn.2004.10.008

[36] Schmidt C, Abicht A, Krampfl K, et al. Congenital myasthenic syndrome due to a novel missense mutation in the gene encoding choline acetyltransferase. doi:10.1016/S0

[37] Kraner S, Laufenberg I, Straßburg HM, Sieb JP, Steinlein OK. *Congenital Myasthenic Syndrome With Episodic Apnea in Patients Homozygous for a CHAT Missense Mutation*. http://archneur.jamanetwork.com/

[38] ScharaU,ChristenHJ,DurmusH,etal.Long-termfollowup in patients with congenital myasthenic syndrome due to CHAT mutations. *European Journal of Paediatric Neurology*. 2010;14(4):326-333. doi:10.1016/j.ejpn.2009.09. 009

[39] Stankiewicz P, Kulkarni S, Dharmadhikari A V., et al. Recurrent deletions and reciprocal duplications of 10q11.21q11.23 including CHAT and SLC18A3 are Likely Mediated by Complex Low-Copy Repeats. *Hum Mutat*. 2012;33(1):165-179. doi:10.1002/humu.21614

[40] Arredondo J, Lara M, Gospe SM, et al. Choline Acetyltransferase Mutations Causing Congenital Myasthenic Syndrome: Molecular Findings and GenotypePhenotypeCorrelations.*HumMutat*.2015;36(9): 881-893. doi:10.1002/humu.22823

[41] Dhasakeerthi T, Aravindhan A, Woodall A, Mills W, Veerapandiyan A. Congenital Myasthenic Syndrome due to a Novel Mutation in CHAT Gene. *J Clin Neuromuscul Dis*. 2021;23(1):54-55. doi:10.1097/CND.0000000000000336

[42] Misgeld T, Burgess RW, Lewis RM, Cunningham JM, Lichtman JW, Sanes JR. Roles of neurotransmitter in synapse formation: development of neuromuscular junctions lacking choline acetyltransferase. *Neuron*. 2002;36(4):635-648. doi:10.1016/s0896-6273(02)010206

[43] Brandon EP, Lin W, D'amour KA, et al. Aberrant patterning of neuromuscular synapses in choline acetyltransferase-deficient mice. *J Neurosci*. 2003;23(3):539-549. doi:10.1523/JNEUROSCI.23-0200539.2003

[44] Wang M, Wen H, Brehm P. Function of neuromuscular synapses in the zebrafish choline- acetyltransferase mutant bajan. *J Neurophysiol*. 2008;100(4):1995-2004. doi:10.1152/jn.90517.2008

[45] Joshi S, Virdi S, Etard C, Geisler R, Strahle U. Muta-¨ tion of a serine near the catalytic site of the choline acetyltransferase a gene almost completely abolishes motility of the zebrafish embryo. *PLoS One*. 2018;13(11). doi:10.1371/journal.pone.0207747

[46] Proschowsky HF, Flagstad A, Cirera S, Joergensen CB, Fredholm M. Identification of a mutation in the CHAT geneofOldDanishPointingDogsaffectedwithcongenital myasthenic syndrome. In: *Journal of Heredity*. Vol 98.; 2007:539-543. doi:10.1093/jhered/esm026

[47] Aran A, Segel R, Kaneshige K, et al. Vesicular acetylcholinetransporterdefectunderliesdevastatingconge nital myasthenia syndrome. *Neurology*. 2017;88(11):10211028. doi:10.1212/WNL.0000000000003720

[48] Lamond A, Buckley D, O'Dea J, Turner L. Variants of SLC18A3 leading to congenital myasthenic syndrome in two children with varying presentations. *BMJ Case Rep*. 2021;14(1). doi:10.1136/bcr-2020-237799

[49] SchwartzM,SternbergD,WhalenS,etal.Howchromosomal deletions can unmask recessive mutations? Deletions in 10q11.2 associated with CHAT or SLC18A3 mutations lead to congenital myasthenic syndrome. *Am J Med Genet A*. 2018;176(1):151-155. doi:10.1002/ajmg.a.38515

[50] Della Marina A, Arlt A, Schara-Schmidt U, et al. Phenotypical and Myopathological Consequences of Compound Heterozygous Missense and Nonsense Variants in SLC18A3. *Cells*. 2021;10(12):3481. doi:10.3390/cells10123481

[51] Hakonen AH, Polvi A, Saloranta C, et al. SLC18A3 variants lead to fetal akinesia deformation sequence early in pregnancy. *Am J Med Genet A*. 2019;179(7):1362-1365. doi:10.1002/ajmg.a.61186

[52] Kitamoto T, Xie X, Wu CF, Salvaterra PM. *Isolation and Characterization of Mutants for the Vesicular Acetylcholine Transporter Gene in Drosophila Melanogaster*. Vol 42.; 2000.

[53] Showell SS, Martinez Y, Gondolfo S, Boppana S, Lawal HO. Overexpression of the vesicular acetylcholine transporter disrupts cognitive performance and causes

age-dependent locomotion decline in Drosophila. *Molecular and Cellular Neuroscience*. 2020;105. doi:10.1016/j.mcn.2020.103483

[54] White D, de Sousa Abreu RP, Blake A, et al. Deficits in the vesicular acetylcholine transporter alter lifespan and behavior in adult Drosophila melanogaster. *Neurochem Int*. 2020;137. doi:10.1016/j.neuint.2020.104744 [55] Prado VF, Martins-Silva C, de Castro BM, et al. Mice Deficient for the Vesicular Acetylcholine Transporter Are Myasthenic and Have Deficits in Object and Social Recognition. *Neuron*. 2006;51(5):601-612. doi:10.1016/j.neuron.2006.08.005

[56] Schmid S, Azzopardi E, De Jaeger X, Prado MAM, Prado VF. VAChT knock-down mice show normal prepulse inhibition but disrupted long-term habituation. *Genes Brain Behav*. 2011;10(4):457-464. doi:10.1111/j.1601183X.2011.00686.x

[57] Lara A, Damasceno DD, Pires R, et al. Dysautonomia Due to Reduced Cholinergic Neurotransmission Causes Cardiac Remodeling and Heart Failure. *Mol Cell Biol*. 2010;30(7):1746-1756. doi:10.1128/mcb.00996-09 [58] Durand MT, Becari C, S V Tezini GC, et al. Autonomic cardiocirculatory control in mice with reduced expression of the vesicular acetylcholine transporter. *Am J Physiol Heart Circ Physiol*. 2015;309:655-662. doi:10.1152/ajpheart.00114.2015.-In

[59] de Castro BM, de Jaeger X, Martins-Silva C, et al. The Vesicular Acetylcholine Transporter Is Required for Neuromuscular Development and Function. *Mol Cell Biol*. 2009;29(19):5238-5250. doi:10.1128/mcb.00245-09

[60] Zhu H, Duerr JS, Varoqui H, McManus JR, Rand JB, Erickson JD. Analysis of Point Mutants in the Caenorhabditis elegans Vesicular Acetylcholine Transporter Reveals Domains Involved in Substrate Translocation. *Journal of Biological Chemistry*. 2001;276(45):41580-41587. doi:10.1074/jbc.M103550200

[61] Martins-Silva C, de Jaeger X, Guzman MS, et al. Novel strains of mice deficient for the vesicular acetylcholine transporter: Insights on transcriptional regulation and control of locomotor behavior. *PLoS One*. 2011;6(3). doi:10.1371/journal.pone.0017611

[62] Martyn AC, De Jaeger X, Magalhaes˜ AC, et al. Elimination of the vesicular acetylcholine transporter in the forebrain causes hyperactivity and deficits in spatial memory and long-term potentiation. *Proc Natl Acad Sci U S A*. 2012;109(43):17651-17656. doi:10.1073/pnas.1215381109

[63] Kolisnyk B, Al-Onaizi MA, Hirata PHF, et al. Forebrain deletion of the vesicular acetylcholine transporter results in deficits in executive function, metabolic, and RNA splicing abnormalities in the prefrontal cortex. *Journal of Neuroscience*. 2013;33(37):14908-14920. doi:10.1523/JNEUROSCI.1933-13.2013

[64] Palmer D, Creighton S, Prado VF, Prado MAM, Choleris E, Winters BD. Mice deficient for striatal Vesicular Acetylcholine Transporter (VAChT) display impaired short-term but normal long-term object recognition memory. *Behavioural Brain Research*. 2016;311:267-278. doi:10.1016/j.bbr.2016.05.050

[65] Joviano-Santos J V., Kljakic O, Magalhaes-Gomes MPS,˜ et al. Motoneuron-specific loss of VAChT mimics neuromuscular defects seen in congenital myasthenic syndrome. *FEBS Journal*. 2021;288(18):5331-5349. doi:10.1111/febs.15825

[66] Schoch S, Deak F, K´ onigstorfer A, et al. SNARE¨ function analyzed in synaptobrevin/VAMP knockout mice. *Science (1979)*. 2001;294(5544):1117-1122. doi:10.1126/science.1064335

[67] Shen XM, Scola RH, Lorenzoni PJ, et al. Novel synaptobrevin-1 mutation causes fatal congenital myasthenic syndrome. *Ann Clin Transl Neurol*. 2017;4(2):130138. doi:10.1002/acn3.387

[68] Salpietro V, Lin W, Delle Vedove A, et al. Homozygous Mutations in VAMP1 Cause a Presynaptic Congenital Myasthenic Syndrome. doi:10.1002/ana [69] Polavarapu K, Vengalil S, Preethish-Kumar V, et al. Recessive VAMP1 mutations associated with severe congenital myasthenic syndromes – A recognizable clinical phenotype. *European Journal of Paediatric Neurology*. 2021;31:54-60. doi:10.1016/j.ejpn.2021.02.005

[70] Al-Muhaizea MA, AlQuait L, AlRasheed A, et al. Pyrostigmine therapy in a patient with VAMP1related congenital myasthenic syndrome. *Neuromuscular Disorders*. 2020;30(7):611-615. doi:10.1016/j.nmd.2020.04.007

[71] Liu Y, Sugiura Y, Lin W. The role of Synaptobrevin1/VAMP1 in Ca2+-triggered neurotransmitter release at the mouse neuromuscular junction. *Journal of Physiology*. 2011;589(7):1603-1618. doi:10.1113/ jphysiol.2010.201939

[72] Nystuen AM, Schwendinger JK, Sachs AJ, Yang AW, Haider NB. A null mutation in VAMP1/synaptobrevin is associated with neurological defects and prewean mortality in the lethal-wasting mouse mutant. *Neurogenetics*. 2007;8(1):1-10. doi:10.1007/s10048-0060068-7

[73] Liu Y, Sugiura Y, Sudhof TC, Lin W. Ablation of¨ all synaptobrevin vSNAREs blocks evoked but not spontaneous neurotransmitter release at neuromuscular synapses. *Journal of Neuroscience*. 2019;39(31):60496066. doi:10.1523/JNEUROSCI.0403-19.2019

[74] Shen XM, Selcen D, Brengman J, Engel AG. *Mutant SNAP25BCausesMyasthenia,CorticalHyperexcitability, Ataxia, and Intellectual Disability*.; 2014. [75] Reynolds HM, Wen T, Farrell A, et al. Rapid genome sequencing identifies a novel de novo SNAP25 variant for neonatal congenital myasthenic syndrome. *Cold Spring Harb Mol Case Stud*. 2022;8(7):a006242. doi:10.1101/mcs.a006242

[76] Washbourne P, Thompson PM, Carta M, et al. Genetic ablation of the t-SNARE SNAP-25 distinguishes mechanisms of neuroexocytosis. *Nat Neurosci*. 2002;5(1):19-26. doi:10.1038/nn783

[77] Jeans AF, Oliver PL, Johnson R, et al. *A Dominant Mutation in Snap25 Causes Impaired Vesicle Trafficking, Sensorimotor Gating, and Ataxia in the Blind-Drunk*

Mouse.; 2007. www.pnas.orgcgidoi10.1073pnas.0610222104

[78] Yang H, Zhang M, Shi J, et al. Brain-Specific SNAP-25 Deletion Leads to Elevated Extracellular Glutamate Level and Schizophrenia-Like Behavior in Mice. *Neural Plast*. 2017;2017. doi:10.1155/2017/4526417

[79] Hoerder-Suabedissen A, Korrell K V., Hayashi S, et al. Cell-specificlossofSNAP25fromcorticalprojectionneurons allows normal development but causes subsequent neurodegeneration. *Cerebral Cortex*. 2019;29(5):21482159. doi:10.1093/cercor/bhy127

[80] McKee AG, Loscher JS, O'Sullivan NC, et al. AAVmediated chronic over-expression of SNAP-25 in adult rat dorsal hippocampus impairs memory-associated synaptic plasticity. *J Neurochem*. 2010;112(4):991-1004. doi:10.1111/j.1471-4159.2009.06516.x

[81] Herrmann DN, Horvath R, Sowden JE, et al. Synaptotagmin 2 mutations cause an autosomal-dominant form of lambert-eaton myasthenic syndrome and nonprogressive motor neuropathy. *Am J Hum Genet*. 2014;95(3):332-339. doi:10.1016/j.ajhg.2014.08.007

[82] Whittaker RG, Herrmann DN, Bansagi B, et al. Electrophysiologic features of SYT2 mutations causing a treatable neuromuscular syndrome. *Neurology*. 2015;85(22):1964-1971. doi:10.1212/WNL.0000000000002185

[83] Fionda L, Turon-Sans J, Fuentes Prior P, et al. A new de novo SYT2 mutation presenting as distal weakness. Neuropathy or neuromuscular junction dysfunction? *Journal of the Peripheral Nervous System*. 2021;26(1):113-117. doi:10.1111/jns.12425

[84] Maselli RA, Wei DT, Hodgson TS, et al. Dominant and recessive congenital myasthenic syndromes caused by SYT2 mutations. *Muscle Nerve*. 2021;64(2):219-224. doi:10.1002/mus.27332

[85] Donkervoort S, Mohassel P, Laugwitz L, et al. Biallelic loss of function variants in SYT2 cause a treatable congenital onset presynaptic myasthenic syndrome. *Am J Med Genet A*. 2020;182(10):2272-2283. doi:10.1002/ajmg.a.61765

[86] Maselli RA, van der Linden H, Ferns M. Recessive congenital myasthenic syndrome caused by a homozygous mutation in SYT2 altering a highly conserved C-terminal amino acid sequence. *Am J Med Genet A*. 2020;182(7):1744-1749. doi:10.1002/ajmg.a.61579

[87] Bauche S, Sureau A, Sternberg D, et al. New recessive´ mutations in SYT2 causing severe presynaptic congenital myasthenic syndromes. *Neurol Genet*. 2020;6(6). doi:10.1212/NXG.0000000000000534

[88] Mackler JM, Drummond JA, Loewen CA, Robinson IM, Reist NE. The C2B Ca2+-binding motif of synaptotagmin is required for synaptic transmission *in vivo*. *Nature*. 2002;418(6895):340-344. doi:10.1038/nature00846 [89] Shields MC, Bowers MR, Fulcer MM, et al. Drosophila studies support a role for a presynaptic synaptotagmin mutation in a human congenital myasthenic syndrome. *PLoS One*. 2017;12(9). doi:10.1371/journal.pone.0184817

[90] Pang ZP, Sun J, Rizo J, Maximov A, Sudhof TC. Genetic¨ analysis of synaptotagmin 2 in spontaneous and Ca 2+-triggered neurotransmitter release. *EMBO Journal*. 2006;25(10):2039-2050. doi:10.1038/sj.emboj.7601103

[91] Pang ZP, Melicoff E, Padgett D, et al. Synaptotagmin-2 is essential for survival and contributes to Ca 2+triggering of neurotransmitter release in central and neuromuscular synapses. *Journal of Neuroscience*. 2006;26(52):1349313504. doi:10.1523/JNEUROSCI.3519-06.2006

[92] Wen H, Linhoff MW, McGinley MJ, et al. Distinct roles for two synaptotagmin isoforms in synchronous and asynchronous transmitter release at zebrafish neuromuscular junction. *Proc Natl Acad Sci U S A*. 2010;107(31):1390613911. doi:10.1073/pnas.1008598107

[93] Augustin I, Korte S, Rickmann M, et al. *The CerebellumSpecific Munc13 Isoform Munc13-3 Regulates Cerebellar Synaptic Transmission and Motor Learning in Mice*.; 2001.

[94] Engel AG, Selcen D, Shen XM, Milone M, Harper CM. Loss of MUNC13-1 function causes microcephaly, cortical hyperexcitability, and fatal myasthenia. *Neurol Genet*. 2016;2(5). doi:10.1212/NXG.0000000000000105

[95] Varoqueaux F, Sons MS, Plomp JJ, Brose N. Aberrant Morphology and Residual Transmitter Release at the Munc13-Deficient Mouse Neuromuscular Synapse. *Mol Cell Biol*. 2005;25(14):5973-5984. doi:10.1128/mcb.25.14.5973-5984.2005

[96] Michelassi F, Liu H, Hu Z, Dittman JS. A C1-C2 Module in Munc13 Inhibits Calcium-Dependent Neurotransmitter Release. doi:10.1016/j.neuron

[97] Abouhamed M, Grobe K, Leefa Chong San I v, et al. Myosin IXa Regulates Epithelial Differentiation and Its Deficiency Results in Hydrocephalus. *Mol Biol Cell*. 2009;20:5074-5085. doi:10.1091/mbc.E09

[98] Thelen S, Abouhamed M, Ciarimboli G, Edemir B, Bahler¨ M. Rho GAP myosin IXa is a regulator of kidney tubule function. *Am J Physiol Renal Physiol*. 2015;309:501-513. doi:10.1152/ajprenal.00220.2014.-Mammalian

[99] Folci A, Murru L, Vezzoli E, et al. Myosin IXa binds AMPAR and regulates synaptic structure, LTP, and cognitive function. *Front Mol Neurosci*. 2016;9(JAN). doi:10.3389/fnmol.2016.00001

[100] O'Connor E, Phan V, Cordts I, et al. MYO9A deficiency in motor neurons is associated with reduced neuromuscular agrin secretion. *Hum Mol Genet*. 2018;27(8):1434-1446. doi:10.1093/hmg/ddy054

[101] O'connor E, Cairns G, Spendiff S, et al. Modulation of agrin and RhoA pathways ameliorates movement defects and synapse morphology in MYO9A-depleted Zebrafish. *Cells*. 2019;8(8). doi:10.3390/cells8080848

[102] Boonen K, Regal L, Jaeken J, Creemers JWM.´ *PREPL, a Prolyl Endopeptidase-Like Enzyme by Name Only?Lessons from Patients*. Vol 10.; 2011.

[103] Regal L, Shen XM, Selcen D, et al.´ *Supplemental Data at Neurology.Org PREPL Deficiency with or without Cystinuria Causes a Novel Myasthenic Syndrome*.; 2014.

[104] Regal L, M´ a˚rtensson E, Maystadt I, et al. PREPL deficiency: Delineation of the phenotype and development of a functional blood assay. *Genetics in Medicine*. 2018;20(1):109-118. doi:10.1038/gim.2017.74 [105] Zhang P, Wu B, Lu Y, et al. First maternal uniparental disomy for chromosome 2 with PREPL novel frameshift mutation of congenital myasthenic syndrome 22 in an infant. *Mol Genet Genomic Med*. 2020;8(3). doi:10.1002/mgg3.1144

[106] Silva S, Miyake N, Tapia C, Matsumoto N. The second point mutation in PREPL: A case report and literature review. *J Hum Genet*. 2018;63(5):677-681. doi:10.1038/s10038-018-0426-y

[107] Laugwitz L, Redler S, Buchert R, et al. Isolated PREPL deficiency associated with congenital myasthenic syndrome-22. Klin Padiatr. 2018 Sep;230(5):281-283. 20. doi:doi: 10.1055/a-0605-3659

[108] Shchagina O, Bessonova L, Bychkov I, Beskorovainaya T, Poliakov A. A family case of congenital myasthenic syndrome-22inducedbydifferentcombinationsofmolecular causes in siblings. *Genes (Basel)*. 2020;11(7):1-6. doi:10.3390/genes11070821

[109] Yang Q, Hua R, Qian J, et al. PREPL Deficiency: A Homozygous Splice Site PREPL Mutation in a Patient With Congenital Myasthenic Syndrome and Absence of Ovaries and Hypoplasia of Uterus. *Front Genet*. 2020;11. doi:10.3389/fgene.2020.00198

[110] Lone AM, Leidl M, McFedries AK, Horner JW, Creemers J, Saghatelian A. Deletion of prepl causes growth impairment and hypotonia in mice. *PLoS One*. 2014;9(2). doi:10.1371/journal.pone.0089160

[111] D'Agostino G, Kim JD, Liu ZW, et al. Prolyl endopeptidase-deficient mice have reduced synaptic spine density in the CA1 region of the hippocampus, impaired LTP, and spatial learning and memory. *Cerebral Cortex*. 2013;23(8):2007-2014. doi:10.1093/cercor/bhs199

[112] Maselli RA, Arredondo J, Vazquez J, et al. A presynaptic´ congenital myasthenic syndrome attributed to a homozygous sequence variant in LAMA5. *Ann N Y Acad Sci*. 2018;1413(1):119-125. doi:10.1111/nyas.13585 [113] Nguyen NM, Miner JH, Pierce RA, Senior RM. Laminin 5 is required for lobar septation and visceral pleural basement membrane formation in the developing mouse lung. *Dev Biol*. 2002;246(2):231-244. doi:10.1006/dbio.2002.0658

[114] Nguyen NM, Kelley DG, Schlueter JA, Meyer MJ, Senior RM, Miner JH. Epithelial laminin 5 is necessary for distal epithelial cell maturation, VEGF production, and alveolization in the developing murine lung. *Dev Biol*. 2005;282(1):111-125. doi:10.1016/j.ydbio.2005.02.031

[115] Kikkawa Y, Miner JH. Molecular dissection of laminin 5 *in vivo* reveals separable domain-specific roles in embryonic development and kidney function. *Dev Biol*. 2006;296(1):265-277. doi:10.1016/j.ydbio.2006.04. 463

[116] Nishimune H, Valdez G, Jarad G, et al. Laminins promote postsynaptic maturation by an autocrine mechanism at the neuromuscular junction. *Journal of Cell Biology*. 2008;182(6):1201-1215. doi:10.1083/jcb.200805095 [117] Jones LK, Lam R, McKee KK, et al. A mutation affecting laminin alpha 5 polymerisation gives rise to a syndromic developmental disorder. *Development (Cambridge)*. 2020;147(21). doi:10.1242/dev.189183

[118] Webb AE, Sanderford J, Frank D, Talbot WS, Driever W, Kimelman D. Laminin 5 is essential for the formation of the zebrafish fins. *Dev Biol*. 2007;311(2):369-382. doi:10.1016/j.ydbio.2007.08.034

[119] Maselli RA, Vazquez J, Schrumpf L, et al. Presynap-´ tic congenital myasthenic syndrome with altered synaptic vesicle homeostasis linked to compound heterozygous sequence variants in RPH3A. *Mol Genet Genomic Med*. 2018;6(3):434-440. doi:10.1002/mgg3.370

[120] Staunton J, Ganetzky B, Nonet ML. *Rabphilin Potentiates Soluble N-Ethylmaleimide Sensitive Factor Attachment Protein Receptor Function Independently of Rab3*.; 2001.

[121] Edvardson S, Porcelli V, Jalas C, et al. Agenesis of corpus callosum and optic nerve hypoplasia due to mutations in SLC25A1encodingthemitochondrialcitratetransporter.*J Med Genet*. 2013;50(4):240-245. doi:10.1136/jmedgenet2012-101485

[122] Nota B, Struys EA, Pop A, et al. Deficiency in SLC25A1, encoding the mitochondrial citrate carrier, causes combined D-2- and L-2-hydroxyglutaric aciduria. *Am J Hum Genet*. 2013;92(4):627-631. doi:10.1016/j.ajhg.2013.03.009

[123] Chaouch A, Porcelli V, Cox D, et al. Mutations in the mitochondrialcitratecarrierSLC25A1areassociatedwith impairedneuromusculartransmission.*JNeuromusculDis*. 2014;1(1):75-90. doi:10.3233/JND-140021

[124] Balaraju S, Topf A, McMacken G, et al. Congenital myas-¨ thenicsyndromewithmildintellectualdisabilitycausedby arecurrentSLC25A1variant.*EuropeanJournalofHuman Genetics*. 2020;28(3):373-377. doi:10.1038/s41431-0190506-2

[125] Al-Futaisi A, Ahmad F, Al-Kasbi G, Al-Thihli K, Koul R, Al-Maawali A. Missense mutations in SLC25A1 are associated with congenital myasthenic syndrome type 23. *Clin Genet*. 2020;97(4):666-667. doi:10.1111/cge.13678 [126] Li W, Zhang M, Zhang L, et al. A case report of an intermediate phenotype between congenital myasthenic syndrome and D-2- And L-2-hydroxyglutaric aciduria due to novel SLC25A1 variants. *BMC Neurol*. 2020;20(1). doi:10.1186/s12883-020-01854-6

[127] Rigby MJ, Orefice NS, Lawton AJ, et al. Increased expression of SLC25A1/CIC causes an autistic-like phenotype with altered neuron morphology. *Brain*. 2022;145(2):500516. doi:10.1093/brain/awab295

[128] TanM,MosaoaR,GrahamGT,etal.Inhibitionofthemitocho ndrialcitratecarrier,Slc25a1,revertssteatosis,glucose

intolerance, and inflammation in preclinical models of NAFLD/NASH. *Cell Death Differ*. 2020;27(7):21432157. doi:10.1038/s41418-020-0491-6

[129] Morciano P, Carrisi C, Capobianco L, et al. A conserved role for the mitochondrial citrate transporter Sea/SLC25A1 in the maintenance of chromosome integrity. *Hum Mol Genet*. 2009;18(21):4180-4188. doi:10.1093/hmg/ddp370

[130] Nicolau S, Liewluck T, Shen XM, Selcen D, Engel AG, Milone M. A homozygous mutation in GMPPB leads to centronuclear myopathy with combined pre- and postsynaptic defects of neuromuscular transmission. *Neuromuscular Disorders*. 2019;29(8):614-617. doi:10.1016/j.nmd.2019.07.001

[131] Senderek J, Muller JS, Dusl M, et al. Hexosamine¨ biosynthetic pathway mutations cause neuromuscular transmission defect. *Am J Hum Genet*. 2011;88(2):162172. doi:10.1016/j.ajhg.2011.01.008

[132] Webster RG. Animal models of the neuromuscular junction, vitally informative for understanding function and the molecular mechanisms of congenital myasthenic syndromes. *Int J Mol Sci*. 2018;19(5). doi:10.3390/ijms19051326

[133] Jones RA, Harrison C, Eaton SL, et al. Cellular and Molecular Anatomy of the Human Neuromuscular Junction. *Cell Rep*. 2017;21(9):2348-2356. doi:10.1016/j.celrep.2017.11.008

[134] SlaterCR.*ReliabilityofNeuromuscularTransmissionand How It Is Maintained*.

[135] Wang ZW. Origin of quantal size variation and high-frequency miniature postsynaptic currents at the Caenorhabditis elegans neuromuscular junction. *J Neurosci Res*. 2010;88(16):3425-3432. doi:10.1002/jnr.22468 [136] Maves L. Recent advances using zebrafish animal models for muscle disease drug discovery. *Expert Opin Drug Discov*. 2014;9(9):1033-1045. doi:10.1517/17460441.2014.927435

[137] Bayes´ A, Collins MO, Reig-Viader R, et al. Evolution of˜ complexity in the zebrafish synapse proteome. *Nat Commun*. 2017;8. doi:10.1038/ncomms14613

[138] Eisen JS, Smith JC. Controlling morpholino experiments: Don't stop making antisense. *Development*. 2008;135(10):1735-1743. doi:10.1242/dev.001115

[139] Albadri S, del Bene F, Revenu C. Genome editing using CRISPR/Cas9-based knock-in approaches in zebrafish. *Methods*. 2017;121-122:77-85. doi:10.1016/j.ymeth.2017.03.005

[140] Fralish Z, Lotz EM, Chavez T, Khodabukus A, Bursac N. NeuromuscularDevelopmentandDisease:LearningFrom in vitro and *in vivo* Models. *Front Cell Dev Biol*. 2021;9. doi:10.3389/fcell.2021.764732

[141] Boehm I, Alhindi A, Leite AS, et al. Comparative anatomy of the mammalian neuromuscular junction. *J Anat*. 2020;237(5):827-836. doi:10.1111/joa.13260 [142] Sekine Y, Kannan R, Wang X, Strittmatter SM. Rabphilin3A reduces integrin-dependent growth cone signaling to restrict axon regeneration after trauma. *Exp Neurol*. 2022;353:114070.

[143] Schluter OM, Schnell E, Verhage M, et al. Rabphilin¨ Knock-Out Mice Reveal That Rabphilin Is Not Required for Rab3 Function in Regulating Neurotransmitter Release. *The Journal of Neuroscience.* 1999;19(14):58345846.

[144] Ferrari E, Scheggia D, Zianni E, et al. Rabphilin-3A as a novel target to reverse -synuclein-induced synaptic loss in Parkinson's disease. *Pharmacol Res*. 2022;183. doi:10.1016/j.phrs.2022.106375

[145] Zhu X, Li H, You W, et al. Role of Rph3A in brain injury induced by experimental cerebral ischemia-reperfusion model in rats. *CNS Neurosci Ther*. 2022;28(7):1124-1138. doi:10.1111/cns.13850

[146] Feng WJ, Liang T, Yu JW, et al. RAB-27 and its effector RBF-1 regulate the tethering and docking steps of DCV exocytosis in C. elegans. *Sci China Life Sci*. 2012;55(3):228-235. doi:10.1007/s11427-012-4296-9